Vol. 6 No.2 2021
ISSN:1390-9347

Bionatura

Latin American journal of Biotechnology and Life Sciences

Scientific open access information

World, Science, and Education in the post-COVID era

Scopus

UNIVERSIDAD YACHAY TECH
clinicalbiotec.com

UCO
Universidad Católica de Oriente

CENTRO DE BIOTECNOLOGÍA Y BIOMEDICINA
CBB
CENTRO DE BIOTECTOLOGÍA Y BIOMEDICINA

http://www.revistabionatura.com/ https://www.facebook.com/bionaturajournal/ https://twitter.com/rbionatura

El Centro de Biotecnología de la ESPOL, CIBE

Genera, aplica, transfiere y difunde las soluciones biotecnológicas que demanda el sector agroindustrial de la costa ecuatoriana.

Sus fortalezas se enfocan en servicios de análisis o de investigación aplicada que puedan proveer soluciones a problemas particulares de la agricultura.

Tipos de ensayos

- Clínica de plantas.
- Servicios analíticos.
- Servicios de bioensayos.

Servicios más requeridos

- Diagnóstico de enfermedades en cultivos agrícolas.
- Estudio de sensibilidad de Sigatoka Negra a fungicidas.
- Cuantificación de fitohormonas, perfil de ácidos grasos por CG-EM.
- Cuantificación de polifenoles y flavonoides, actividad antioxidante.
- Extensión agrícola.

Productos que puede evaluar

- Cultivos agrícolas con presencia de enfermedades causadas por patógenos (bacterias, virus y hongos).
- Bioproductos o bioinsumos con impacto en el rendimiento de cultivos.
- Fungicidas o productos similares para el control de Sigatoka Negra.

Nuestra visión es ser el líder nacional en biotecnología en beneficio del desarrollo de la sociedad ecuatoriana.

Docencia, investigación, extensión y proyección social al servicio del territorio

UCO
Universidad Católica de Oriente
Vigilada Mineducación

Fortalezas **institucionales**

- Biotecnología
- Limnología
- Derechos Humanos – Posconflicto
- Internacionalización
- Inclusión Social
  - SER Servicio Educativo Rural
  - Educación de Alfabetización
- MIS – Instituto de formación para el trabajo y el desarrollo humano
- Formación humanística "Ruta Humanística en el currículo - Cátedra abierta Madre de la Sabiduría"
- Investigación y desarrollo tecnológico
- Comprometida con la calidad
- Centro de Estudios Territoriales
- Biodiversidad
  - Herbario
  - Ictiología
  - Litoteca

Áreas del **conocimiento**

- Ciencias Agropecuarias
- Ciencias de la Educación
- Ciencias de la Salud
- Ciencias Económicas y Administrativas
- Ciencias Sociales
- Derecho
- Ingenierías
- Teología y Humanidades

- 26 programas de pregrado
- 16 programas de posgrado
  - 1 doctorado
  - 8 maestrías
  - 7 especializaciones

www.uco.edu.co Universidad catolicadeoriente @uconia

Contacto institucional Universidad Católica de Oriente
Sector 3, Cra. 46 No. 40B 50 - **PBX:** (57)(4) 569 90 90. Ext. 694
Fax: (57)(4) 531 09 72 - **Email:** uco@uco.edu.co

Vol. 6 No. 2 2021

Bionatura

La Revista Bionatura publica trimestral en español o inglés trabajos inéditos de investigaciones básicas y aplicadas en el campo de la Biotecnología, la Inmunología, la Bioquímica, Ensayos Clínicos y otras disciplinas afines a las ciencias biologícas, dirigidas a la obtención de nuevos conocimientos, evaluación y desarrollo de nuevas tecnologías, productos y procedimientos de trabajo con un impacto a nivel mundial.

Equipo editorial

Editor Jefe / Chief Editor

Dr. Nelson Santiago Vispo. Ph.D. Research / Full Professor. Yachay Tech University, Ecuador. Member of the European Association of Science Editors (EASE) and Council of Science Editors (USA).

Principal Editorial Board / Consejo Editorial Principal

Dr. Fernando Albericio. Ph.D. Full Professor. University of KwaZulu-Natal. Durban, South Africa.
Dr. Spiros N. Agathos, Ph.D. Full Professor. Université Catholique de Louvain - UCLouvain. Louvain-la-Neuve, Belgium.
Dra. Hortensia María Rodríguez Cabrera. Ph.D. Full Professor and Dean, School of Chemical Sciences and Engineering Yachay Tech University, Ecuador.
Dr. Frank Alexis. Research / Full Professor. Vice Chancellor Of Research and Innovation. Yachay Tech University, Ecuador.

Consejo Editorial / Editorial Board

Dr. Gerardo Ferbeyre. Full Professor. Département de biochimie.Faculté de Médecine. Université de Montréal, Canadá.
Dr Frank Camacho Casanova. Ph.D , Facultad de Ciencias Biológicas. Universidad de Concepción . Chile.
Dr. Eduardo López Collazo. Director IdiPAZ Institute of Biomedical Research, La Paz Hospital, España.
Dr.Yovani Marrero-Ponce. Ph.D. Full Professor. Universidad San Francisco de Quito (USFQ), Quito, Ecuador.
Dr. Manuel Limonta. Prof. PhD. Director: Regional Office for Latin American and the Caribbean International Council for Science (ICSU). Doctor honoris causa Autonomous Metropolitan University of México City (UAM). Dr. Honoris Causa - Universidad Central Ecuador.
Dr. Dagoberto Castro – Restrepo. Prof. PhD. Research and Development Director. Universidad Catolica del Oriente. Rio Negro. Colombia
Dr. Michael Szardenings. PhD. Ligand Development Unit.Fraunhofer Institute for Cell Therapy and Immunology.Germany.
Dra. Luciana Dente. Research Professor University of Pisa, Italy.
Dr. Costantino Vetriani. Research / Full Professor. Rutgers, The State University of New Jersey. USA.
Dr. Si Amar Dahoumane.PhD. Research / Professor. Yachay Tech University, Ecuador.
Dr. Amit Chandra, MD, MSC, FACEP Global Health Specialist, Emergency PhysicianMillennium Challenge Corporation, London School of Economics and Political Science.
Dr. Silvio e. Perea. PhD. Head of the Molecular Oncology Laboratory. Centro de Ingeniería Genética y Biotecnología. Cuba.
Dra. Daynet Sosa del Castillo. PhD. Directora del Centro de Investigaciones Biotecnológicas del Ecuador. CIBE-ESPOL.
Dra. Consuelo Macías Abraham. Especialista de II Grado en Inmunología, Investigadora y Profesora Titular, Doctora en Ciencias Médicas y Miembro Titular de la Academia de Ciencias de Cuba. Directora del Instituto de Hematología e Inmunología (IHI), de La Habana, Cuba.
Dr. René Delgado. PhD. IFAL / Presidente Sociedad Cubana de Farmacología. Cuba.
Dr. Ramón Guimil. Senior Director. Oligonucleotide Chemistry bei Synthetic Genomics, Estados Unidos.
Dr. Eduardo Penton. MD, PhD, Investigador Titular. Centro de Ingeniería Genética y Biotecnología, Cuba.
Dr. Julio Raúl Fernández Massó, PhD, Investigador Titular. Centro de Ingeniería Genética y Biotecnología, Cuba
Dra. Lisset Hermida. Investigadora Titular. Centro de Ingeniería Genética y Biotecnología, Cuba.
Dr. Tirso Pons. Staff Scientist. Structural Biology and Biocomputing Programme (CNIO), España.
Dr. Che Serguera. French Institute of Health and Medical Research. MIRCen, CEA, Fontenay-aux-Roses Paris, France.
Dr. Jorge Roberto Toledo. Profesor Asociado. Universidad de Concepción, Chile.
Dr. Oliberto Sánchez. Profesor Asociado. Universidad de Concepción, Chile.
Dr. Aminael Sánchez Rodríguez. PhD. Director del departamento de Ciencias Biológicas, Universidad Técnica Particular de Loja, Ecuador.
Dra. Maritza Pupo. Profesora investigador. Facultad de Biología. Universidad de la Habana, Cuba.
Dr. Fidel Ovidio Castro. Founder, Profesor investigador. Tecelvet, Chile.
Dra. Olga Moreno. Partner, Head Patent Division. Jarry IP SpA, Chile.
Dr. Carlos Borroto. Asesor de Transferencia de Tecnología. Dirección General at Centro de Investigaciones Científicas de Yucatán (CICY), México.
Dr. Javier Menéndez. Manager Specialist Process and Product 5cP. Sanofi Pasteur, Canadá.
Dr. Pedro Valiente. Profesor investigador. Facultad de Biología. Universidad de la Habana, Cuba.
Dr. Diógenes Infante. Prometeo / SENESCYT. Especialista de primer nivel en Biotecnología. Universidad de Yachay Tech, Ecuador.
Dra. Georgina Michelena. Profesora Investigador. Organización de las Naciones Unidas. (ONU), Suiza.
Dr. Francisco Barona, Profesor Asociado. Langebio Institute, México
Dr. Gustavo de la Riva. Profesor Investigador Titular. Instituto Tecnológico Superior de Irapuato, México.
Dr. Manuel Mansur. New Product Introduction Scientist (NPI) at Elanco Animal Health Ireland, Irlanda.
Dr. Rolando Pajón. Associate Scientist, Meningococcal Pathogenesis and Vaccine Researc. Center for Immunobiology and Vaccine Development, UCSF Benioff Children's Hospital Oakland", Estados Unidos.
Dra. Ileana Rosado Ruiz-Apodaca. Profesor / Investigador. Universidad de Guayaquil, Ecuador.
Dr. Carlos Eduardo Giraldo Sánchez. PhD, Profesor / Investigador. Universidad Católica de Oriente. Rionegro-Antioquia/Colombia.
Dr. Mario Alberto Quijano Abril. PhD, Profesor / Investigador. Universidad Católica de Oriente. Rionegro-Antioquia/Colombia.
Dr. Felipe Rojas Rodas. PhD, Profesor / Investigador. Universidad Católica de Oriente.Rionegro-Antioquia/Colombia.
Dra. Isabel Cristina Zapata Vahos, Profesor / Investigador. Universidad Católica de Oriente.Rionegro-Antioquia/Colombia.
Dr. Felipe Rafael Garcés Fiallos, PhD. Profesor / Investigador. Vicerrectorado de Investigación, Gestión Social del Conocimiento y Posgrado Universidad de Guayaquil (UG), Ecuador.
Dra. Celia Fernandez Ortega. PhD. Investigadora Titular. Centro de Ingeniería Genética y Biotecnología, Editora ejecutiva Biotecnologia Aplicada. Cuba.
Dra. Ligia Isabel Ayala Navarrete.PhD. Profesor / Investigador. Universidad de las Fuerzas Armadas - ESPE. Ecuador.
Dr. Nalini kanta Sahoo, PhD. Professor & Head Department Marri Laxman Reddy Institute of Pharmacy. Hyderabad, Andhra Pradesh, India.
Dr. Saman Esmaeilnejad. PhD. Department of medical sciences, Tarbiat Modares University, Tehran, Iran.
Dr. Olukayode Karunwi. PhD. Research / Professor. Clemson University. Clemson, United States.

Associate Editor / Editor Asociado

Victor Santiago Padilla.

Redacción y Edición / Copyediting and corrections

Mg. Frey A. Narváez-Villa. Jefe del Fondo Editorial Universidad Católica de Oriente. Rionegro-Antioquia/Colombia.
MSc. José Enrique Alfonso Manzanet.

Diseño y Realización gráfica / Graphic design and production

DI. José Manuel Oubiña González.

Relaciones Publicas / Public relations

Camila Barranco Rodriguez.

Asistente de publicación / Publication assistant

Evelyn Padilla Rodriguez.

latindex

Index in directory of open access journals

Instrucciones para los Autores

Los Trabajos serán Inéditos: Una vez aprobados, no podrán someterse a la consideración de otra revista, con vistas a una publicación múltiple, sin la debida autorización del Comité Editorial de la Revista. La extensión máxima será 8 cuartillas para los trabajos originales, 12 las revisiones y 4 las comunicaciones breves e informes de casos, incluidas las tablas y figuras. Los artículos se presentarán impresos (dos ejemplares). Todas las páginas se numerarán con arábigos y consecutivamente a partir de la primera. Estos deben acompañarse de una versión digital (correo electrónico o CD) en lenguaje Microsoft Word, sin sangrías, tabuladores o cualquier otro atributo de diseño (títulos centrados, justificaciones, espacios entre párrafos, etc.). Siempre se ha de adjuntar la carta del consejo científico que avala la publicación y una declaración jurada de los autores.

Referencias Bibliográficas. Se numerarán según el orden de mención en el texto y deberán identificarse mediante arábigos en forma exponencial. Los trabajos originales no sobrepasarán las 20 citas; las revisiones, de 25 a 50 y las comunicaciones breves e informes de casos.

En las Referencias en caso de que las publicaciones revisadas esten online se debe proveer un enlace consistente para su localización en Internet. Actualmente, no todos los documentos tienen DOI, pero si lo tienen se debe incluir como parte de la referencias. Si no tuviese DOI, incluir la URL.

Tablas, modelos y anexos: Se presentarán en hojas aparte (no se intercalarán en el artículo) y en forma vertical numeradas consecutivamente y mencionadas en el texto. Las tablas se ajustarán al formato de la publicación se podrán modificar si presentan dificultades técnicas.

Figuras: Las fotografías, gráficos, dibujos, esquemas, mapas, salidas de computadora, otras representaciones gráficas y fórmulas no lineales, se denominarán figuras y tendrán numeración arábiga consecutiva. Se presentarán impresas en el artículo en páginas independientes y en formato digital con una resolución de 300 dpi. Todas se mencionarán en el texto. Los pies de figuras se colocarán en página aparte. El total de las figuras y tablas ascenderá a 5 para los trabajos originales y de revisión y 3 para las comunicaciones breves e informes de casos.

Abreviaturas y siglas: Las precederá su nombre completo la primera vez que aparezcan en el texto. No figurarán en títulos ni resúmenes. Se emplearán las de uso internacional.

Sistema Internacional de Unidades (SI): Todos los resultados de laboratorio clínico se informarán en unidades del SI o permitidas por este. Si se desea añadir las unidades tradicionales, se escribirán entre paréntesis. Ejemplo: glicemia: 5,55 mmol/L (100 mg/100 mL).

Para facilitar la elaboración de los originales, se orienta a los autores consultar los requisitos uniformes antes señalados disponibles en: http://www. fisterra.com/recursos_web/ mbelvancouver. htm#ilustraciones%20 (figura)

Los trabajos que no se ajusten a estas instrucciones, se devolverán a los autores. Los aceptados se procesarán según las normas establecidas por el Comité Editorial. El arbitraje se realizará por pares y a doble ciego en un período no mayor de 60 días. Los autores podrán disponer de no más de 45 días para enviar el artículo con correcciones, se aceptan hasta tres reenvíos. El Consejo de Redacción se reserva el derecho de introducir modificaciones de estilo y /o acotar los textos que lo precisen, comprometiéndose a respetar el contenido original.

El Comité Editorial de la Revista se reserva todos los derechos sobre los trabajos originales publicados en esta.

Bionatura

La **Revista Bionatura** es un medio especializado, interinstitucional e interdisciplinario, para la divulgación de desarrollos científicos y técnicos, innovaciones tecnológicas, y en general, los diversos tópicos relativos a los sectores involucrados en la biotecnología, tanto en Ecuador como en el exterior; así mismo, la revista se constituye en un mecanismo eficaz de comunicación entre los diferentes profesionales de la biotecnología.

Es una publicación sin ánimo de lucro. Los ingresos obtenidos por publicidad o servicios prestados serán destinados para su funcionamiento y desarrollo de su calidad de edición. (http://revistabionatura.com/media-kit.html)

Es una revista trimestral, especializada en temas concernientes al desarrollo teórico, aplicado y de mercado en la biotecnología.

Publica artículos originales de investigación y otros tipos de artículos científicos a consideración de su consejo editorial, previo proceso de evaluación por pares (peer review) sin tener en cuenta el país de origen.

Los idiomas de publicación son el Español e Inglés.

Los autores mantienen sus derechos sobre los artículos sin restricciones y opera bajo la política de Acceso Abierto a la Información, bajo la licencia de Creative Commons 4.0 CC BY-NC-SA (Reconocimiento-No Comercial-Compartir igual).

Esta revista utiliza Open Journal Systems, que es un gestor de revistas de acceso abierto y un software desarrollado, financiado y distribuido de forma gratuita por el proyecto Public Knowledge Project sujeto a la Licencia General Pública de GNU.

Nuestros contactos deben ser dirigidos a:
Revista Bionatura: editor@revistabionatura.com

ISSN: 1390-9347 (Versión impresa)
Formato: 21 x 29,7 cm
ISSN: 1390-9355 (Versión electrónica)
Sitio web: **http://www.revistabionatura.com**

Publicación periódica trimestral
Esta revista utiliza el sistema peer review para la evaluación de los manuscritos enviados.

Instrucciones a los autores en:
http://revistabionatura.com/instrucciones.html

Asistente de publicación / Publication assistant
Evelyn Padilla Rodriguez (sales@revistabionatura.com)

ÍNDICE / INDEX

EDITORIAL

LETTER TO EDITOR / CARTA AL EDITOR

RESEARCH / INVESTIGACIÓN

Jordy José Cevallos-Chávez

EDITORIAL

World, Science, and Education in the post-covid era

Hortensia Rodriguez [1], Nelson Santiago Vispo[2]

DOI. 10.21931/RB/2021.06.02.1

The current Covid-19 pandemic, produced by a mutant strain of coronavirus, SARS-CoV-2, has generated throughout the world, in the 21st century, a severe economic, social, and health crisis never saw before. It began in China at the end of December 2019, in Hubei (Wuhan city), where 27 cases of pneumonia of unknown etiology were reported, with seven severe patients. The first case was described on December 8, 2019,[1], and by March 2020, the WHO declares the global pandemic, which denotes its rapid global expansion[2].

The global response to this emergency presented apparent differences regarding speed and effectiveness relative to the level of scientific-technological capacities of each country and the development of its entrepreneurship and innovation ecosystems. An interesting aspect to highlight is the speed with which researchers and entrepreneurs from various work areas focused on the challenges posed by the health emergency. The development of rapid tests for COVID-19 detection, or the design and manufacture of vaccines, were some of the notable examples. Once again, it is shown that having talent and support is a considerable asset for countries[3].

Right from the start of the pandemic, many international biomedical information centers and publishers agreed to make public worldwide all medical or applied research information on this viremia so it can be used to offer the best medical response in the shortest time possible. Publishing houses have sped up the editorial peer review processes and made them open. In this sense, having a free flow of scientific information is the best treatment to face any epidemic and respond in the shortest possible time[4].

Governments should be asking themselves, when the pandemic subsides, what should we do now? Most stakeholders consider the knowledge about the disease in this pandemic to be an open-access common resource, a public good that should be freely available. How would this change when we do not have a crisis? So, is it acceptable to hold back the progress of science? Furthermore, who has the right to make these decisions? It would be governments supported by science. The research community's strategies to combat COVID-19 give us a proof of concept of what is possible.

It is possible to wonder if commercial publishers should rule: be the primary decision-makers and gatekeepers of access to knowledge. More importantly, it is possible to question what kind of scholarly publishing system we want (collectively as a society) and design it accordingly[5].

Scholars agree that durable and robust trust networks are essential for setting priorities, making effective decisions in rapidly changing environments, solving problems, and building resilient institutions to manage shared resources in general and infrastructure for scholarly dissemination in particular. This collaborative culture in the hard sciences should not be the only one to be assumed and should be extended to any knowledge generation in everyday use.

In this current action situation, the accumulated experiences of past epidemics, the demands for access to research led by the WHO and governments, and the interest of scientists have been the driving force for joint action by publishers to release information and has allowed rapid diagnostic and therapeutic advance as weapons against COVID. All these dynamics have set new guidelines and regulations in open access to information.

In the educational field, this emergency has led to the massive closure of classroom activities in schools to prevent the spread of the virus and mitigate its impact. In this context, the coronavirus has instantly changed how education is delivered, turning every home into a classroom after the necessary regulations. Thereby, the health emergency has exacerbated the disparities that already existed in education. The prolonged closure of schools could reverse the advances of the last five decades, especially in terms of girls' and adolescents' education and young women.

In few weeks, the way students learn changed, and precisely these transformations give us a glimpse of the equity flaws that our educational system continues to present, even in the most privileged circles. The World Economic Forum[3] suggests that this pandemic becomes an opportunity to remind us of the skills that our students need just in a crisis like these, thus being informed decision-making, creative problem solving, and, above all, adaptability. Resilience must also be built into our education systems to ensure that those skills remain a priority for all students.

After more than a long year of the pandemic, it is time for governments to focus on strategies that mitigate the impact of the covid on education. It may not be easy, but the path is laid out with at least four strong recommendations. 1) Focus on reopening schools safely, consulting, and considering all stakeholders, including parents and health sector workers. 2) Prioritize education in budget decisions.3) Education initiatives must reach those most at risk of being left behind, such as people in emergencies or crises, minority groups, the displaced, and people with disabilities. 4) Promote the leap towards progressive systems that provide quality education for all.

With the unexpected emergence and rapid spread of the pandemic, it has been confirmed that local strategic capabilities are crucial. However, at the same time, it has highlighted the imperative need for solidarity and co-responsibility if we are to emerge victorious from the pandemic.

Facing the pandemic has also become a substantial educational equity challenge that can have consequences that alter students' lives in general, without a doubt affecting the most vulnerable. Therefore, governments must promote educational development strategies that minimize the gap that this pandemic has generated.

Although we are apparently on the verge of ending the coronavirus crisis, thanks to the development and implementation of vaccines, we are at a point of no return to our old nor-

[1] Escuela de Ciencias Químicas e Ingeniería, Universidad Yachay Tech, Ecuador.
[2] Escuela de Ciencias Biológicas e Ingeniería, Universidad Yachay Tech, Ecuador.

Corresponding author: hmrodriguez@yachaytech.edu.ec

Photo by Vlad Tchompalov on Unsplash

mality. The pandemic irreversibly changed us, so the current challenge is to get all of us on the bandwagon of technological development, education and even eliminate the digital gap that discriminates against full access to opportunities.

Covid 19 is as close as humans can get to a wake-up call. The pandemic exposed how, and vulnerable our world economy is and how flawed and monetary biased our priorities are. However, on the plus side, it has also highlighted the scientific community's role in guiding governments and the importance of investing in science. It taught selflessness to prioritize isolation and confinement since stopping the disease is more critical when weighted against the psychosocial and economic effect this represents[6]. Finally, we have learned the importance of paradigm shifts in terms of the imperative need for scientific discoveries to be at the service of humanity and not as a private business.

Bibliographic references

1. Secretaria General de Sanidad. Actualización n°13. Numonía por nuevo conavirus (2019-nCov) en Wuhan, provincia de Hubei, (China). Cent. Coord. Alertas y Emergencias Sanit. 1–6 (2020).
2. Organización Mundial de la Salud. Alocución de apertura del Director General de la OMS en la rueda de prensa sobre la COVID-19 celebrada el 11 de marzo de 2020. Discursos del Director General de la OMS 1 https://www.who.int/es/director-general/speeches/detail/who-director-general-s-opening-remarks-at-the-media-briefing-on-covid-19---11-march-2020 (2020).
3. Foro Económico Mundial. El Foro Económico Mundial. https://es-.weforum.org/ (2020).
4. Open Access to COVID-19 and related research. https://www.openaccess.nl/en/open-access-to-covid-19-and-related-research.
5. Tavernier, W. COVID-19 demonstrates the value of open access what happens next? College and Research Libraries News vol. 81 226–230 (2020).
6. Omar Domínguez-Amorocho, Luz Mery Contreras-Ramos, Laura Patricia Amaya Díaz. Cuarentena y COVID-19, una percepción más allá de la infección. Revista Bionatura vol. 6 1679 (2021).

LETTER TO EDITOR / CARTA AL EDITOR

Cuarentena y COVID-19, una percepción más allá de la infección

Temporal prediction of the number of deaths from traffic accidents in the United States

Omar Domínguez-Amorocho[1*], Luz Mery Contreras-Ramos[2], Laura Patricia Amaya Díaz[3]

DOI. 10.21931/RB/2021.06.02.2

El síndrome respiratorio agudo severo (SARS), cuyo agente causal es el Coronavirus SARS-CoV, surgió en 2003, sin embargo, a finales del 2019, se observó que un nuevo Coronavirus (SARS-CoV-2) causaba una enfermedad similar a la influenza, denominada COVID-19 (acrónimo del inglés *coronavirus disease* 2019), la cual, presentaba desde síntomas respiratorios leves hasta lesiones pulmonares graves, y en algunos casos, cursando con insuficiencia multiorgánica y muerte[1,2,3].

Durante la ola pandémica, la mayoría de los países han adoptado medidas de distanciamiento social y se han impuesto estrategias de "cuarentena" en un intento por reducir la propagación de la COVID-19, incluidos el toque de queda, restricciones en reuniones o eventos masivos, la cancelación de eventos sociales y públicos planificados, cierre de sistemas de transporte público y algunas restricciones de viaje.

El aislamiento social asociado a la pandemia por COVID-19 ha demostrado ser un factor generador de eventos a nivel de salud mental y física, entre ellos, trastornos de estrés agudo, irritabilidad, insomnio, angustia emocional y trastornos del estado de ánimo (incluidos síntomas depresivos, miedo y pánico, ansiedad y estrés debido a preocupaciones financieras, frustración y aburrimiento, soledad, falta de suministros y falta de comunicación)[4,5,6]. Otros factores estresantes asociados con procesos prolongados de aislamiento social, como los experimentados en América Latina, pueden incluir una disponibilidad irregular o menor de suministros habituales, como alimentos y medicamentos y la restricción de las actividades diarias[5].

Diversas evidencias vinculan el aislamiento social con las consecuencias adversas para la salud, incluida la depresión, la mala calidad del sueño, el deterioro cognitivo acelerado, Además, cuanto más tiempo se limita a una persona a la cuarentena, más pobres son los resultados de salud mental; específicamente, se pueden observar síntomas de trastorno de estrés postraumático (TEPT), conducta de evitación y enojo[5].

Las personas que carecen de conexiones sociales o informan frecuentes sentimientos de soledad tienden a sufrir tasas más altas de morbilidad y mortalidad[7,8,9], riesgo y prevalencia de infecciones[10,11,12] y deterioro cognitivo[13], una condición observada de manera particular en adultos mayores[14]. Los riesgos para la salud asociados con el aislamiento social incluso se han comparado en magnitud con los peligros conocidos por el tabaquismo y la obesidad[15] aunque no han sido estudiados de manera equivalente, también es muy importante resaltar, la asociación que existe entre el aislamiento social y la adquisición o agudización de dichas condiciones[16,17].

Tanto la soledad como el aislamiento social han sido asociados también con comportamientos menos saludables como el tabaquismo, la inactividad física y trastornos del sueño[18,19], estos factores, se encuentran directamente asociados a procesos biológicos relevantes para la salud, como son las variaciones en la presión arterial, incremento en marcadores séricos inflamatorios, alteraciones en el metabolismo de lípidos y compromiso inmunológico[15,20,21] e incluso niveles de asociación con riesgo de muerte prematura[22].

Diversos estudios han intentado comprender las vías psicológicas, conductuales y biológicas por las cuales el aislamiento social y la soledad conducen a una reducción en la calidad de vida en términos de la salud y una disminución de la longevidad[23-27], incluso, la evidencia actual indica que el mayor riesgo de mortalidad por falta de relaciones sociales es mayor que el de la obesidad[28,29].

Si bien se acepta generalmente que los efectos negativos para la salud del aislamiento social son directos e indirectos (mediados por comportamientos de salud riesgosos), y aunque la literatura de investigación proporciona varias vías y mecanismos conductuales, psicológicos y fisiológicos a través de los cuales el aislamiento social puede influir o afectar la salud[30-32], no está claro y / o no se ha investigado cuál de ellos es más decisivo, en qué circunstancias y en qué poblaciones y entornos culturales. Algunos estudios sugieren que los riesgos para la salud del aislamiento social representan efectos a largo plazo[33-35].

Es importante resaltar que los procesos de aislamiento preventivo obligatorio o "cuarentenas" han mostrado ser eficientes y necesarios en la prevención y control del avance de diversas enfermedades infecciosas, siendo particularmente una herramienta efectiva, para el control de la pandemia de COVID-19, demostrando variaciones importantes de la transmisión de SARS-CoV-2 y del número de muertes asociado a periodos de mantenimiento o relajación de estas medidas[36-38]. Por otro lado, el impacto social de la pandemia de COVID-19 ha sido amplio y muy desafiante. La cuarentena y el distanciamiento social son medidas necesarias para evitar la propagación del virus, pero también conducen a niveles elevados de soledad y aislamiento social, que a su vez repercuten directamente sobre la salud física y mental[39-42], además de generar una afectación importante de otros aspectos como la economía y la cultura.

Como conclusión, no es posible definir las ventajas o desventajas de los procesos de aislamiento obligatorio desde la perspectiva multidimensional de la salud. Partiendo de los diferentes estudios que han sido publicados en los últimos meses, la pandemia de COVID-19 ha planteado y seguirá planteando una serie de retos que permitirán rediseñar las estrategias de distanciamiento social y aislamiento como medida de control de la propagación de la infección, del mismo modo, permitirá analizar esos otros factores relacionados con la salud física y mental, los cuales, comienzan a tomar más relevancia y en algunas sociedades se han hecho mucho más evidentes durante este prolongado y sin precedente periodo de cuarentena[43-45].

La cuarentena y el distanciamiento social son medidas necesarias para evitar la propagación del virus, pero también

[1] Facultad de Ciencias de La Salud, Universidad de Santander UDES, Bucaramanga, Colombia.
[2] Facultad de Enfermería, Universidad Cooperativa de Colombia, Bucaramanga, Colombia.
[3] Facultad de Ciencias Sociales, políticas y humanidades, Universidad de Santander UDES, Bucaramanga, Colombia.

Corresponding author: o.dominguez@mail.udes.edu.co.

conducen a niveles elevados de soledad y aislamiento social, que a su vez repercuten directamente sobre la salud física y mental de los individuos.

Fuentes de financiación

Universidad de Santander UDES, Universidad Cooperativa de Colombia.

"Los autores declaran que no tienen intereses contrapuestos"

Referencias bibliográficas

1. Guan ZY, Ni Y. Hu, WH. Liang, C. Q. Ou, J. X. He et al. Clinical characteristics of coronavirus disease 2019 in China. N. Engl. J. Med. 2020; 382:1708–1720. doi:10.1056/NEJMoa2002032pmid:32109013
2. Zhu ND, Zhang W, Wang X, Li B, Yang J, Song et al. A novel coronavirus from patients with pneumonia in China, 2019. N. Engl. J. Med. 2020; 382:727–733. doi:10.1056/NEJMoa2001017pmid:31978945
3. Jiang S, L Du, Z Shi. An emerging coronavirus causing pneumonia outbreak in Wuhan, China: Calling for developing therapeutic and prophylactic strategies. Emerg. Microbes Infect. 9 2020; 275–277. doi:10.1080/22221751.2020.1723441pmid:32005086
4. Pfefferbaum B, North CS. Mental Health and the Covid-19 Pandemic. N Engl J Med. 2020 Aug 6;383(6):510-512. doi: 10.1056/NEJMp2008017. Epub 2020 Apr 13.
5. Brooks SK, Webster RK, Smith LE, Woodland L, Wessely S, Greenberg N, & Rubin, G. J. The psychological impact of quarantine and how to reduce it: Rapid review of the evidence. Lancet. 2020; 395: 912–920. https://doi.org/10.1016/S0140- 6736(20)30460- 8
6. Desclaux A, Badji D, Ndione A. G, & Sow K. Accepted monitoring or endured quarantine? Ebola contacts' perceptions in Senegal. Social Science in Medicine. 2017; 178: 38–45. https://doi.org/10.1016/j.socscimed.2017.02.0
7. Shaukat N, Ali DM, & Razzak J. Physical and mental health impacts of COVID-19 on healthcare workers: a scoping review. International journal of emergency medicine. 2020; 13(1): 40. https://doi.org/10.1186/s12245-020-00299-5
8. Xiong J, Lipsitz O, Nasri F, Lui L, Gill H, Phan L, Chen-Li D, Iacobucci M, Ho R, Majeed A, & McIntyre, R. S. Impact of COVID-19 pandemic on mental health in the general population: A systemati review. Journal of affective disorders. 2020; 277:55–64. https://doi.org/10.1016/j.jad.2020.08.001
9. Uchino BN. Social support and health: A review of physiological processes potentially underlying links to disease outcomes. Journal of Behavioral Medicine. 2006; 29:377– 387. doi:10.1007/s10865-006-9056-5
10. Malcolm M, Frost H, & Cowie J. Loneliness and social isolation causal association with health-related lifestyle risk in older adults: a systematic review and meta-analysis protocol. Systematic reviews. 2019; 8(1):48. https://doi.org/10.1186/s13643-019-0968-x
11. Cohen S, Doyle WJ, Skoner DP, Rabin BS, Gwaltney JM Jr. Social ties and susceptibility to the common cold. JAMA. 1997 Jun 25; 277(24):1940-4
12. Pressman SD, Cohen S, Miller GE, Barkin A, Rabin BS& Treanor JJ. Loneliness, social network size, and immune response to influenza vaccination in college freshmen. Health Psychol. 2005; 24: 297–306. (doi:10.1037/0278-6133.24.3.297).
13. Wilson RS, Krueger KR, Arnold SE, Schneider JA, Kelly JF, Barnes LL, Tang Y, Bennett DA. Loneliness and risk of Alzheimer disease. Arch Gen Psychiatry. 2007 Feb; 64(2):234-40.
14. Yu B, Steptoe A, Chen Y, Jia X. Social isolation, rather than loneliness, is associated with cognitive decline in older adults: the China Health and Retirement Longitudinal Study. Psychol Med. 2020 Apr 27:1-8. doi: 10.1017/S0033291720001014. Epub ahead of print. PMID: 32338228.
15. Kraav S, Awoyemi O, Junttila N, Vornanen R, Kauhanen J, Toikko T, Tolmunen T. The effects of loneliness and social isolation on all-cause, injury, cancer, and CVD mortality in a cohort of middle-aged finnish men. A prospective study. Aging and Mental 2020. Health, doi:10.1080/13607863.2020.1830945
16. Jung FU, & Luck-Sikorski C. Overweight and Lonely? A Representative Study on Loneliness in Obese People and Its Determinants. Obesity facts. 2019; 12(4):440–447. https://doi.org/10.1159/000500095
17. Zachary Z, Brianna F, Brianna L, Garrett P, Alyssa D, & Mikayla K. Self-quarantine and weight gain related risk factors during the COVID-19 pandemic. Obesity research & clinical practice. 2020;14(3): 210–216. https://doi.org/10.1016/j.orcp.2020.05.004
18. López-Moreno M, López MTI, Miguel M, & Garcés-Rimón M. Physical and psychological effects related to food habits and lifestyle changes derived from covid-19 home confinement in the spanish population. Nutrients. 2020; 12(11): 1-17. doi:10.3390/nu12113445.
19. Grossman ES, Hoffman YSG, Palgi Y, & Shrira A. COVID-19 related loneliness and sleep problems in older adults: Worries and resilience as potential moderators. Personality and Individual Differences. 2021; 168 doi:10.1016/j.paid.2020.110371
20. Hodgson S, Watts I, Fraser S, Roderick P, & Dambha-Miller H. Loneliness, social isolation, cardiovascular disease and mortality: A synthesis of the literature and conceptual framework. Journal of the Royal Society of Medicine. 2020; 113(5): 185-192. doi:10.1177/0141076820918236.
21. Smith K, Gavey S, Rlddell NE, Kontari P, & Victor C. The association between loneliness, social isolation and inflammation: A systematic review and meta-analysis. Neuroscience & Biobehavioral Reviews. 2020; 112: 519-541. https://doi.org/10.1016/j.neubiorev.2020.02.002

22. Alcaraz K, Katherine S Eddens, Jennifer L Blase, W Ryan Diver, Alpa V Patel, Lauren R Teras, Victoria L Stevens, Eric J Jacobs, Susan M Gapstur, Social Isolation and Mortality in US Black and White Men and Women, American Journal of Epidemiology, Volume 188, Issue 1, January 2019, Pages 102–109, https://doi.org/10.1093/aje/kwy231
23. Cacioppo JT, Cacioppo S, Capitanio JP, & Cole SW. The neuroendocrinology of social isolation. Annual Review of Psychology. 2015; 66:9.1–9.35. doi:10.1146/annurevpsych-010814-015240
24. Shankar A, McMunn A, Banks J, & Steptoe A. Loneliness, social isolation, and behavioral and biological health indicators in older adults. Health Psychology. 2011; 30:377–385. doi:10.1037/a0022826
25. Thoits PA. Mechanisms linking social ties and support to physical and mental health. Journal of Health and Social Behavior. 2011; 52:145–161
26. Hawkley LC, & Cacioppo JT. Loneliness and pathways to disease. Brain, Behavior, and Immunity. 2003;17(Suppl. 1):S98–105.
27. Hawkley LC, & Cacioppo JT. Loneliness matters: A theoretical and empirical review of consequences and mechanisms. Annals of Behavioral Medicine. 2010; 40:218–227. doi:10.1007/s12160-010-9210-8
28. Flegal KM, Kit BK, Orpana H, & Graubard BI. Association of all-cause mortality with overweight and obesity using standard body mass index categories: A systematic review and meta-analysis. Journal of the American Medical Association. 2013; 309:71–82. doi:10.1001/jama.2012.113905
29. Holt-Lunstad J, Smith TB, Baker M, Harris T, & Stephenson D. Loneliness and social isolation as risk factors for mortality: a meta-analytic review. Perspectives on Psychological Science. 2015;10(2): 227–237. doi:10.1177/1745691614568352
30. Na L, Hample D. Psychological pathways from social integration to health: An examination of different demographic groups in Canada.Soc Sci Med. 2016 Feb; 151():196-205.
31. Bhatti AB, Haq AU. The Pathophysiology of Perceived Social Isolation: Effects on Health and Mortality. Cureus. 2017 Jan 24; 9(1):e994.
32. Cacioppo JT, Cacioppo S. Social Relationships and Health: The Toxic Effects of Perceived Social Isolation. Soc Personal Psychol Compass. 2014 Feb 1; 8(2):58-72.
33. Matthews T, Danese A, Wertz J, Ambler A, Kelly M, Diver A, Caspi A, Moffitt TE, Arseneault L. Social isolation and mental health at primary and secondary school entry: a longitudinal cohort study. J Am Acad Child Adolesc Psychiatry. 2015 Mar; 54(3):225-32
34. Garre-Olmo J, Turró-Garriga O, Martí-Lluch R, Zacarías-Pons L, Alves-Cabratosa L, Serrano-Sarbosa D. on behalf of the Girona Healthy Region Study Group. Changes in lifestyle resulting from confinement due to COVID-19 and depressive symptomatology: A cross-sectional a population-based study. Comprehensive Psychiatry, 2021; 104 doi:10.1016/j.comppsych.2020.152214
35. Jurblum M, Ng CH, & Castle DJ. (). Psychological consequences of social isolation and quarantine: Issues related to COVID-19 restrictions. Australian Journal of General Practice. 2020; 49(12):778-783. doi:10.31128/AJGP-06-20-5481
36. te Vrugt, M., Bickmann, J. & Wittkowski, R. Effects of social distancing and isolation on epidemic spreading modeled via dynamical density functional theory. Nat Commun 11, 5576 (2020). https://doi.org/10.1038/s41467-020-19024-0
37. Girum, T., Lentiro, K., Geremew, M. et al. Global strategies and effectiveness for COVID-19 prevention through contact tracing, screening, quarantine, and isolation: a systematic review. Trop Med Health 48, 91 (2020). https://doi.org/10.1186/s41182-020-00285-w
38. Candido D., Claro I., de Jesus J., Souza W. et Al. Evolution and epidemic spread of SARS-CoV-2 in Brazil. Science (2020); 369: 1255-1260 DOI: 10.1126/science.abd2161
39. Hwang, T. J., Rabheru, K., Peisah, C., Reichman, W., & Ikeda, M. (2020). Loneliness and social isolation during the COVID-19 pandemic. International psychogeriatrics, 32(10), 1217–1220. https://doi.org/10.1017/S1041610220000988
40. Ma, J., Hua, T., Zeng, K. et al. Influence of social isolation caused by coronavirus disease 2019 (COVID-19) on the psychological characteristics of hospitalized schizophrenia patients: a case-control study. Transl Psychiatry 10, 411 (2020). https://doi.org/10.1038/s41398-020-01098-5
41. Banerjee D, Rai M. Social isolation in Covid-19: The impact of loneliness. International Journal of Social Psychiatry. 2020;66(6):525-527. doi:10.1177/0020764020922269
42. Pereira, M., Oliveira, LC., Costa, FT., Bezerra, CM., Pereira, MD., dos Santos CKA., Dantas EHM. The COVID-19 pandemic, social isolation, consequences on mental health and coping strategies: an integrative review. Research, Society and Development, [S. l.], v. 9, n. 7, p. e652974548, 2020. DOI: 10.33448/rsd-v9i7.4548.
43. Duarte, Michael de Quadros, Santo, Manuela Almeida da Silva, Lima, Carolina Palmeiro, Giordani, Jaqueline Portella, & Trentini, Clarissa Marceli. (2020). Covid-19 and the impacts on mental health: a sample from Rio Grande do Sul, Brazil. Ciência & Saúde Coletiva, 25(9), 3401-3411. Epub August 28, 2020.https://doi.org/10.1590/1413-81232020259.16472020
44. Castro-de-Araujo, Luís Fernando Silva, & Machado, Daiane Borges. (2020). Impact of COVID-19 on mental health in a Low and Middle-Income Country. Ciência & Saúde Coletiva, 25(Suppl. 1), 2457-2460. Epub June 05, 2020.https://dx.doi.org/10.1590/1413-81232020256.1.10932020
45. Dalal, P. K., Roy, D., Choudhary, P., Kar, S. K., & Tripathi, A. (2020). Emerging mental health issues during the COVID-19 pandemic: An Indian perspective. Indian journal of psychiatry, 62(Suppl 3), S354–S364. https://doi.org/10.4103/psychiatry.IndianJPsychiatry_372_20

LETTER TO EDITOR / CARTA AL EDITOR

Hepatobiliary involvement in COVID-19 patients

Mohammad Amin Akbarzadeh[1], Mohammad-Salar Hosseini[2*]

DOI. 10.21931/RB/2021.06.02.3

As the new data emerges from the studies regarding COVID-19 infection, various complications are detected among the infected patients. Unlike its name, the severe acute respiratory syndrome coronavirus 2 (SARS-CoV-2) is not limited to the respiratory system[1]. Some studies have suggested the impact of COVID-19 on liver function[2,3]. Since the liver plays essential intoxication, enzyme activation, storage, and synthesis of necessary proteins, lipids, and carbohydrates, the potential liver complications may affect the body beyond ordinary expectations.

A chief hepatic injury is almost always determined by the elevated levels of liver enzymes, like alanine aminotransferase (ALT), aspartate aminotransferase (AST), and gamma-glutamyltransferase (GGT). According to a study on 1099 patients with laboratory-confirmed SARS-CoV-2 infection, 22.2% and 21.3% of the patients with available data had elevated AST and ALT levels (>40 U/L), where only 23 patients had pre-existing liver conditions[4]. In another study, reporting clinical characteristics of 99 COVID-19 cases, 43 patients showed degrees of liver dysfunction with elevated levels of AST (>40 U/L) or ALT (>50 U/L)[5]. Also, another study showed that patients might even develop liver injury before demonstrating any changes in the blood level of AST and ALT[6]. Likewise, several findings suggest a potential association between the severity of the disease and elevation of liver enzymes[7]. Even a recently published retrospective cohort of 1827 COVID-19 patients showed that over 61% of the patients had abnormal serum levels of AST[8]. More importantly, the study showed that the abnormal liver test could be associated with poor prognosis and clinical outcomes.

The presence of liver damage among COVID-19 patients could be explained through many underlying mechanisms. First of all, like other viral infections, hepatocellular damage can be caused directly by the SARS-CoV-2, as its presence is reported from various systems, including the hepatic system. The virus uses angiotensin-converting enzyme 2 (ACE2) receptors as an entry gate to cells, and cells with ACE2 receptor expression are potential parts of the route underlying the pathophysiology of the infection[9-11]. Cholangiocytes express ACE2 molecules, and several reports suggest that this expression may have a role in complications such as cholestasis, provoke immune-related responses, which in severe conditions may lead to cytokine storm, and lead to liver injuries and significant hepatobiliary complications[12].

The infection could affect the protein synthesis function of the liver. Besides, due to the lack of an effective and definite treatment regimen for managing COVID-19 patients, repurposing different drugs and using various treatment protocols has become quite common[13]. Since the liver plays the leading role in metabolizing chemicals and toxic compounds, consuming drugs without a definite knowledge of their side effects could place the liver in a devastating state, especially when the body power of endurance is remarkably reduced dealing with the bother of infection. Therefore, drug-induced hepatotoxicity should be taken into account seriously, and administration of various drugs – precisely, the herbal compounds – should be monitored more cautiously[14-16].

Signs, symptoms, and conditions like abnormal liver function tests, elevated levels of bilirubin, and acute hepatitis can be presented in patients due to various reasons[17,18]. Considering the significantly high prevalence of hepatic complications in COVID-19 patients, different clinical features should be interpreted considering a possible presence of SARS-CoV-2 infection. This is especially important in patients with pre-existing liver conditions, such as patients with cirrhosis, chronic cholestatic liver disease (e.g., primary sclerosing cholangitis, primary biliary cholangitis), liver transplantation recipients, liver cancer, etc. There may also be a potential association between COVID-19 infection and comorbidities related to liver dysfunction, notably metabolic disorders (e.g., diabetes mellitus), fatty liver diseases, and viral hepatitis[7,19]. Chronic viral hepatitis may enhance the viral replication of the hepatocytes, which can contribute to the severe manifestation of COVID-19 infection.

Hepatobiliary involvement in COVID-19 patients

Recent studies have shown a possible association between COVID-19 infection and liver-related complications. ALT and AST are the most utilized biomarkers which need to be monitored closely in all populations to avoid missing the potential relations with the pathophysiology of the SARS-CoV-2 infection. Further studies with a focus on evaluating the chief liver functions are strongly recommended. Most of the available findings only cover the blood levels of AST and ALT. Further studies should consider other liver enzymes, ultrasound, and even biopsy to determine the particular affection of the liver during this infection. Additional studies considering different ranges of liver enzymes may help us develop a prognostic scale for COVID-19 patients, which could be determinative in managing these patients. Also, assessing the patients with COVID-19 and viral hepatitis is mandatory, as so little information is available on the prognosis of patients with this co-infection. SARS-CoV-2 infection is a multi-system disease, and since the hepatic injury could cause permanent damages and even increase the risk of mortality independently, liver-related complications of COVID-19 should be observed strictly.

[1] Research Center for Evidence-Based Medicine and Student Research Committee, Tabriz University of Medical Sciences, Tabriz, Iran.
[2] Liver and Gastrointestinal Diseases Research Center, Student Research Committee and Emergency Medicine Research Team, Tabriz University of Medical Sciences, Tabriz, Iran.

Corresponding author: hosseini.msalar@gmail.com

Funding information

Not Applicable.

Competing interest

The authors declare that they have no competing interests.

Keywords

Digestive system diseases, hepatic insufficiency, liver, SARS-CoV-2, COVID-19

Bibliographic references

1. Abobaker A, Raba AA, Alzwi A. Extrapulmonary and atypical clinical presentations of COVID-19. Journal of medical virology. 2020;92:2458-64.
2. Phipps MM, Barraza LH, LaSota ED, Sobieszczyk ME, Pereira MR, Zheng EX, et al. Acute liver injury in COVID-19: prevalence and association with clinical outcomes in a large US cohort. Hepatology. 2020;72:807-17.
3. Tian D, Ye Q. Hepatic complications of COVID-19 and its treatment. Journal of medical virology. 2020;92:1818-24.
4. Guan W-j, Ni Z-y, Hu Y, Liang W-h, Ou C-q, He J-x, et al. Clinical Characteristics of Coronavirus Disease 2019 in China. New England Journal of Medicine. 2020;382:1708-20.
5. Chen N, Zhou M, Dong X, Qu J, Gong F, Han Y, et al. Epidemiological and clinical characteristics of 99 cases of 2019 novel coronavirus pneumonia in Wuhan, China: a descriptive study. The Lancet. 2020;395:507-13.
6. Pan L, Mu M, Yang P, Sun Y, Wang R, Yan J, et al. Clinical Characteristics of COVID-19 Patients With Digestive Symptoms in Hubei, China: A Descriptive, Cross-Sectional, Multicenter Study. The American journal of gastroenterology. 2020;115:766-73.
7. Zhang C, Shi L, Wang F-S. Liver injury in COVID-19: management and challenges. The lancet Gastroenterology & hepatology. 2020;5:428-30.
8. Hundt MA, Deng Y, Ciarleglio MM, Nathanson MH, Lim JK. Abnormal Liver Tests in COVID-19: A Retrospective Observational Cohort Study of 1,827 Patients in a Major U.S. Hospital Network. Hepatology. 2020;72:1169-76.
9. Gu J, Han B, Wang J. COVID-19: gastrointestinal manifestations and potential fecal–oral transmission. Gastroenterology. 2020;158:1518-9.
10. Gao F, Zheng KI, Fan Y-C, Targher G, Byrne CD, Zheng M-H. ACE2: A Linkage for the Interplay Between COVID-19 and Decompensated Cirrhosis. The American Journal of Gastroenterology. 2020.
11. Zippi M, Hong W, Traversa G, Maccioni F, De Biase D, Gallo C, et al. Involvement of the exocrine pancreas during COVID-19 infection and possible pathogenetic hypothesis: a concise review. Infez Med. 2020;28:507-15.
12. Zhao B, Ni C, Gao R, Wang Y, Yang L, Wei J, et al. Recapitulation of SARS-CoV-2 infection and cholangiocyte damage with human liver ductal organoids. Protein & cell. 2020;11:771-5.
13. Senanayake SL. Drug repurposing strategies for COVID-19. In: Future Science; 2020. (ISBN No. 2631-3316)
14. Boeckmans J, Rodrigues RM, Demuyser T, Piérard D, Vanhaecke T, Rogiers V. COVID-19 and drug-induced liver injury: a problem of plenty or a petty point? Archives of toxicology. 2020;94:1367-9.
15. Falcão MB, de Goes Cavalcanti LP, Filgueiras Filho NM, de Brito CAA. Case report: hepatotoxicity associated with the use of hydroxychloroquine in a patient with COVID-19. The American journal of tropical medicine and hygiene. 2020;102:1214-6.
16. Leegwater E, Strik A, Wilms EB, Bosma LB, Burger DM, Ottens TH, et al. Drug-induced liver injury in a COVID-19 patient: potential interaction of remdesivir with P-glycoprotein inhibitors. Clinical Infectious Diseases. 2020.
17. Paliogiannis P, Zinellu A. Bilirubin levels in patients with mild and severe Covid-19: A pooled analysis. Liver International. 2020;40:1787-8.
18. Qin C, Wei Y, Lyu X, Zhao B, Feng Y, Li T, et al. High aspartate aminotransferase to alanine aminotransferase ratio on admission as risk factor for poor prognosis in COVID-19 patients. Scientific reports. 2020;10:1-10.
19. Marhl M, Grubelnik V, Magdič M, Markovič R. Diabetes and metabolic syndrome as risk factors for COVID-19. Diabetes & Metabolic Syndrome: Clinical Research & Reviews. 2020;14:671-7.


UNIVERSIDAD
YACHAY
TECH
SOMOS LA PRIMERA UNIVERSIDAD
DEL ECUADOR
CON MAYOR RELEVANCIA EN
PUBLICACIONES
CIENTÍFICAS
FUENTE: www.natureindex.com/country-outputs/Ecuador

RESEARCH / INVESTIGACIÓN

Soluble production of a full-length human papillomavirus type 16 L1 protein by *Escherichia coli*

Yunier Serrano, Susana Miraidys Brito, Elsa Pimienta, Alina Falero, Karen Marrero
DOI. 10.21931/RB/2021.06.02.4

Abstract: Persistent infection with human papillomavirus type 16 (HPV16) causes the development of cervical cancer. *Escherichia coli* is a cost-effective host successfully used to develop a second-generation vaccine against HPV, based on the purification of soluble truncated L1 protein variants. Previous attempts to produce soluble full-length HPV16-L1 protein by *E. coli* have failed. This study was aimed at cloning a Cuban HPV16-L1 gene in *E. coli* and assessing its expression as a soluble full-length L1 protein by manipulating culture conditions. The L1 gene was amplified from a Cuban patient's cervical sample and cloned into pET28a and pBAD/Myc-HisA vectors. Production and solubility of L1 protein were evaluated in *E. coli* TOP10 harboring pBADHPV16-L1 plasmid and *E. coli* BL21-(DE3), Rosetta-(DE3)/pLysS, and SHuffle® T7 Express *lysY* strains harboring pETHPV16-L1 plasmid, grown under arabinose (0.2%)- or isopropyl β-D-1-thiogalactopyranoside (IPTG, 100 μM)-induction or Super Broth-based auto-induction for 24 and 48 h. The recombinant plasmids pETHPV16-L1 and pBADHPV16-L1 were constructed. The HPV16-L1 protein was produced insoluble to high levels in conventionally IPTG-induced *E. coli*-pETHPV16-L1 cells. However, under auto-induction, soluble full-length HPV16-L1 protein was successfully produced at similar levels by *E. coli* BL21 (DE3), Rosetta (DE3) pLysS and SHuffle® T7 Express *lysY* cells, reaching up to 7.2 ± 0.5% and 14.3 ± 1.6% of the total proteins in the soluble fraction after growing for 24 and 48 h, respectively. It is concluded that the auto-induction procedure at 18 °C with 30 μM IPTG and 100 rev/min promotes soluble full-length HPV16-L1 protein production by *E. coli*.

Key words: Human papillomavirus type 16, *Escherichia coli*, L1 protein.

Introduction

Human papillomavirus (HPV) are non-enveloped double-stranded DNA viruses[1], of which more than 200 types have been described as pathogens in humans[2]. HPVs are classified into high-risk (H) and low risk (LR) according to their oncogenic potential[2]. The persistent infection of approximately 15 high-risk HPV types causes almost all cervical cancer cases (CC) and immediate precursor lesions[3]. Of these genotypes, HPV16 and HPV18 account for approximately 70% of global CC cases[4]. As a whole, the CC is the third most common carcinoma among women[5]. In particular, HPV16 is the most prevalent high-risk genotype globally[6,7], and studies have shown that it is related to a large proportion of other HPV-associated cancers worldwide[7].

The papillomaviruses consist of L1 and L2 structural proteins, being L1 protein the preferred target for HPV vaccine development due to its self-assembling into virus-like particles (VLPs) mimic the structure of native virions[4,8]. The L1-VLPs retain the vast majority of the natural virus's neutralizing epitopes and can induce high titers of neutralizing antibodies[4]. There are currently three HPV-VLP-based prophylactic vaccines available: Cervarix, Gardasil-4, and Gardasil-9 3. Clinical trials have shown that these vaccines induced neutralizing and protective antibodies to prevent HPV-associated infections[7]. However, the vaccines' high production and delivery costs are significant barriers to global implementation, mainly in low-incoming countries where cervical cancer results in higher mortality[9]. In Cuba, the CC constitutes the fourth cause of cancer deaths in women[10], being the HPV16 the most frequently found genotype[5]. The molecular epidemiologic results support the national implementation of vaccination against HPV in our country[5,11], unfeasible at present due to the high costs of current vaccines. Thus, there is a pressing need for more cost-effective vaccines[1].

The bacterium *Escherichia coli* constitutes the most attractive host for recombinant protein production due to their low cost, high productivity, and rapid production rates[12,13]. Using this host, a VLP-based vaccine was recently licensed in China[14]. L1 proteins in this vaccine (including HPV16-L1 protein) were produced in truncated form and purified from *E. coli* soluble fraction[3,15]. However, soluble full-length HPV16-L1 protein production in *E. coli* has not yet been achieved since L1 protein is mainly detected in the cells induced by the cells' insoluble fractions IPTG[16]. The auto-induction culture is a strategy that allows accumulating soluble recombinant protein in *E. coli* cytoplasm[17-19], as well as the employ of low temperature and low inductor concentration[19-21]. Therefore, it would be attractive to produce high amounts of soluble full-length HPV16-L1 protein, considering that L1 protein purification from soluble fraction may be a cost-effective alternative since refolding of purified protein is avoided[3]. Thus, the present study aimed to assess soluble full-length L1 protein production from a wild type HPV16-L1 gene in *E. coli* by manipulating culture conditions.

Materials and methods

Reagents, *E. coli* Strains, and Plasmids

Restriction enzymes, T4 DNA ligase and Pfu DNA polymerase, PCR reagents, 1kb DNA Step Ladder, Broad Range Protein Molecular Weight Markers, Wizard® Minipreps DNA purification system, and Wizard® Gel and PCR Clean-Up System were purchased from Promega (USA). Agar, tryptone, yeast extract, and sodium chloride were from OXOID (England). Kanamycin, ampicillin, and chloramphenicol antibiotics were from AppliChem (Germany). IPTG, the auto-induction medium components, and all chemicals used in SDS-PAGE and *Wes-*

Unit for Biological Products Research, Division of Research, Development & Innovation, National Center for Scientific Research, La Habana, Cuba.

Corresponding author: madukachinonye@yahoo.com

tern Blot were from Merck (Germany). The *E. coli* strains and plasmids used in this study are listed in Table 1.

All DNA manipulations, including restriction digestions, ligations, and agarose gel electrophoresis, were performed according to standard procedures[24]. Preparation of *E. coli* competent cells and plasmid transformation protocols were adapted from Li *et al.*[25].

Amplification of HPV16-L1 gene and cloning into pUC18*Not*I plasmid

The HPV16-L1 gene (1527 bp) was amplified by Polymerase Chain Reaction (PCR) using total DNA isolated from an HPV16-diagnosed biopsy sample from a Cuban patient[26] and the primer pairs 5'- CCATGGGTCTTTGGCTGCCTAGTG -3' and 5'- AGATCTCTTACAGCTTACGTTTTTTGCGTT -3'. The amplified gene was flanked by NcoI and BglII sites (underlined) at the 5' and 3' ends, respectively, and it was cloned into HincII-digested pUC18*Not*I vector generating the pUCHPV16-L1 plasmid in *E. coli* Mach1. Restriction analysis and nucleotide sequencing (Macrogen, Republic of Korea) were used to confirm the HPV16-L1 gene presence in recombinant clones.

Construction of *E. coli* HPV16-L1 expression plasmids

The wild type HPV16-L1 gene (1518 bp) encoding full-length L1protein from pUCHPV16-L1 was sub-cloned into pET28a (+) and pBAD/Myc-HisA expression vectors as a NcoI-BglII fragment, obtaining the pETHPV16-L1 and pBADHPV16-L1 recombinant plasmids, respectively. These plasmids were characterized by restriction, then pBADHPV16-L1 was introduced into *E. coli* TOP10, while the pETHPV16-L1 plasmid was transformed into *E. coli* BL21(DE3), Rosetta (DE3)pLysS, and SHuffle® T7 Express *lysY*. pBAD/Myc-HisA and pET28a(+) vectors were introduced into *E. coli* TOP10 and *E. coli* BL21(DE3), respectively, as expression controls.

SDS-PAGE and *Western Blot* analysis

For determination of molecular weight, identity testing, and solubility of HPV16-L1 protein, 10% (w/v) sodium dodecyl sulfate-polyacrylamide gel electrophoresis (10 % SDS-PAGE) under reduced conditions[27] was used, followed by staining with Coomassie brilliant blue R250. For Western Blot, all samples were diluted 1:20, except the *E. coli* TOP10 lysates and elec-

E. coli strains	Relevant characteristics	Source/Reference
Mach1	F⁻ Φ80*lacZ*ΔM15 Δ*lac*X74 *hsd*R(rK⁻, mK⁺) Δ*rec*A1398 *end*A1 *ton*A	Invitrogen®
BL21(DE3)	*E. coli B F⁻ ompT gal dcm lon hsdSB(rB⁻ mB⁻) λ (DE3)*	Novagen®[C2J]
TOP 10	*F⁻ mcrA Δ(mrr-hsdRMS-mcrBC) φ80lacZΔM15 ΔlacX74 recA1 araD139 Δ(araA-leu)7697 galU galK rpsL endA1 nupG.*	Invitrogen®
Rosetta(DE3)pLyS	*F⁻ ompT gal dcm lon hsdSB(rB⁻ mB⁻) λ (DE3)*pLysSRARE (Cam^R)	Novagen®
SHuffle®T7 Express *lysY*	MiniF lysY (CamR) / fhuA2 lacZ::T7 gene1 [lon] ompT ahpC gal2x-λatt::pNEB3-r1-cDsbC (Spec^R, lacI^q) ΔtrxB sulA11 R(mcr-73::miniTn10--TetS)2 [dcm]R(zgb-210::Tn10 --TetS) endA1 Δgor Δ(mcrC-mrr)114::IS10	NEB[23]
Plasmids	**Relevant characteristics**	**Source/Reference**
pUC18*Not*I	High copy number cloning vector for general molecular biology works, Amp^R	Invitrogen®
pUCHPV16-L1	pUC18*Not*I with HPV16-L1 gene into HincII site.	This study
pBAD/Myc-HisA	Expression vector with the ara*BAD* promoter, Amp^R	Invitrogen®
pBADHPV16-L1	pBAD/Myc-HisA with HPV16-L1 gene into NcoI-BglII sites	This study
pET28a(+)	Expression vector with the *T7/lac* promoter, Kan^R	Novagen®
pETHPV16-L1	pET28a (+)with HPV16-L1 gene into NcoI - BamHI sites.	This study

Table 1. Bacteria and plasmids used in this study.

troblotted into a nitrocellulose membrane (Sigma, USA). The HPV16-L1 protein was detected with the MAB885 (CamVir-1) antibody (1:50 000, Merck, Germany). Blots were then treated with goat anti-mouse IgG peroxidase (HP) conjugated (1:64 000, Cuba) and revealed with 3, 3'- diaminobenzidine tetrahydrochloride substrate (Sigma, Germany). The intensity of protein bands from the SDS-PAGE gel was calculated using ImageJ software[19].

Evaluation of HPV16-L1 protein production by *E. coli* BL21 (DE3) and TOP 10 in test tubes

E. coli TOP10 cells harboring pBAD/Myc-HisA or pBAD-HPV16-L1 and *E. coli* BL21(DE3) cells harboring pET28a (+) or pETHPV16-L1 plasmids were inoculated into 5 mL Super Broth medium (SB) (32 g/L of tryptone, 24 g/L of yeast extract, 5 g/L of NaCl, pH 7.2) containing appropriate antibiotics and incubated at 37°C and 200 rev/min for 16 h. These overnight cultures were diluted 100 times in test tubes containing 5 ml of fresh SB medium. The cells were incubated at 37°C until they reached an optical density at 600 nm ($OD_{600\,nm}$) of 0.4–0.6. Then, the expression of L1 gene was induced by the addition of 0.1 mM IPTG or 0.2% (w/v) of L(+)-arabinose. After incubation for an additional 3 h at 37 °C, cells were harvested by centrifugation and suspended in 1x PBS (137 mM NaCl, 2.7 mM KCl, 10 mM Na_2HPO_4, 2 mM KH2PO4, pH 7.4) at an OD_{600nm} = 6.5. The 80 µL of cell suspension was immediately mixed with 20µl of SDS-sample buffer (0.25 M Tris-HCl, pH 6.8, 2% SDS, 5% 2-mercaptoethanol, and 5% glycerol) and boiled at 95 °C for 10 min.

Evaluation of HPV16-L1 protein production by *E. coli* under conventional induction with IPTG in shake flasks

For L1 protein production by *E. coli* BL21(DE3), Rosetta, and SHuffle containing pETHPV16-L1 plasmid, a single colony from each strain was grown overnight in 5 ml of SB medium-plus kanamycin (50 µg/ml) at 30 °C and 200 rev/min. Overnight cultures were diluted 100 times in fresh SB medium and incubated at 27°C and 200 rev/min until they reached an OD_{600}=0.4-0.6. *E. coli* cells were then induced with 0.1 mM IPTG for 4 h under the same conditions. *E. coli* BL21 (DE3) harboring pET28a(+) vector was included as the negative control. Sample preparation was carried out as before for HPV16-L1 protein production in test tubes.

Evaluation of HPV16-L1 protein production by *E. coli* under auto-induction in shake flasks

Production of L1 protein by *E. coli* BL21(DE3), Rosetta, and Shuffle strains carrying the pETHPV16-L1 plasmid and *E. coli* BL21 (DE3) strain harboring pET28a(+) vector were also assayed in an SB-based auto-induction medium[28], using 30 µM IPTG instead of lactose as auto-inducer. Thus, a single colony of each strain was pre-cultured overnight into test tubes containing 5 ml of SB medium with kanamycin (50 µg/ml) at 30 °C and 200 rev/min for 16 h. Then, 2 ml of the grown-culture were transferred into a 2 L- flask containing 200 ml of auto-induction medium supplemented with the same antibiotic. The cultures were incubated at 18 °C and 100 rev/min for 24 or 48h. Sample preparation was carried out as before for HPV16-L1 protein production in test tubes.

Evaluation of HPV16-L1 protein solubility in *E. coli* under different culture conditions

For assessing HPV16-L1 protein solubility from conventionally-induced cells or auto-induced cells; *E. coli* BL21(DE3), Rosetta, and SHuffle harboring pETHPV16-L1 plasmid were harvested by centrifugation at 10 000 rev/min, 10 min, 4°C (5810R, Eppendorf AG, Germany), washed twice with 50 mL of 1 x PBS and suspended in 40 ml of 1 x PBS. Then, bacterial cells were lysed using an Emulsiflex C3 cell disrupter (Avastin, Germany), and 80 µL of each cell lysate was saved as the whole cell's protein (WCP). The samples' remainder was centrifuged (10,000 rev/min, 10 min) to separate soluble fractions (SF).

Bioinformatic tools

Gene Runner 3.05 Version was used for PCR primer design, and vector NTI Suite 7 was employed for plasmids restriction analyses.

Statistical analysis

All experiments were performed at least three times. Determination of statistical differences was performed with Prism 6 (Graphpad Software, Inc., San Diego, CA, USA) using one-way analysis of variance (ANOVA) with Tukey's multiple comparison test. Error bars presented as the means ± *standard deviation* (S.D.).

Results

Cloning of HPV16-L1 gene and construction of pETHPV16-L1 and pBADHPV16-L1 expression plasmids

PCR amplification using total DNA isolated from a Cuban patient's cervical sample showed a fragment of ~1.5 kb (Figure 1A), close to the expected value (1527 bp). The amplified L1 gene codes for a 57 kDa full-length HPV16-L1 protein. The amplified fragment was then cloned into the pUC18*Not*I vector obtaining the pUCHPV16-L1 recombinant plasmid, which was subsequently sequenced. Analysis of cloned-L1 gene nucleotide sequence by Blastn showed it was 99% identical to the L1 gene from the HPV16 reference strain (accession number: K027118). Nucleotide sequencing identified guanine (G) at 604 positions instead of cytosine (C) in the L1 gene of the HPV16 reference strain, thus resulting in a change of CAT codon histidine-202 in the L1 gene of HPV16 reference strain by GAT codon for aspartate-202 in the cloned L1 gene. The second GGT codon, coding for glycine-2, was identified in the cloned L1 gene resulting from the insertion of the NcoI site required for subsequent sub-cloning into pET28a (+) and pBADMyc-HisA expression vectors.

After HPV16-L1 gene sequencing, it was subcloned into pBAD/Myc-HisA and pET28a(+) vectors obtaining the pBAD-HPV16-L1 and pETHPV16-L1 expression plasmids. L1 presence in recombinant plasmids was verified by double restriction with NcoI and HindIII enzymes and by single restriction with BamHI enzyme. Said digestions yielded DNA fragments with sizes close to the theoretical ones and showed that L1 gene was correctly inserted under ara*BAD* (Figure 1 B, lanes 2-3) and T7/*lac* promoter control (Figure 1 C, lanes 2-3).

HPV16-L1 protein production by *E. coli* BL21 (DE3) and TOP 10 strains

The IPTG-induced *E. coli* BL21 (DE3)/pETHPV16-L1 cells produced HPV16-L1 protein as an intense band of about 57 kDa (Figure 2A, lane 2), which was recognized, along with other smaller species, by the HPV16-L1 specific monoclonal antibody CamVir (Figure 2B, lane 2). In contrast, arabinose-induced *E. coli* TOP 10 cells produced low levels of HPV16-L1 protein (Figure 2A, lane 4), only detected by Western blotting with CamVir antibody (Figure 2B, lane 4).

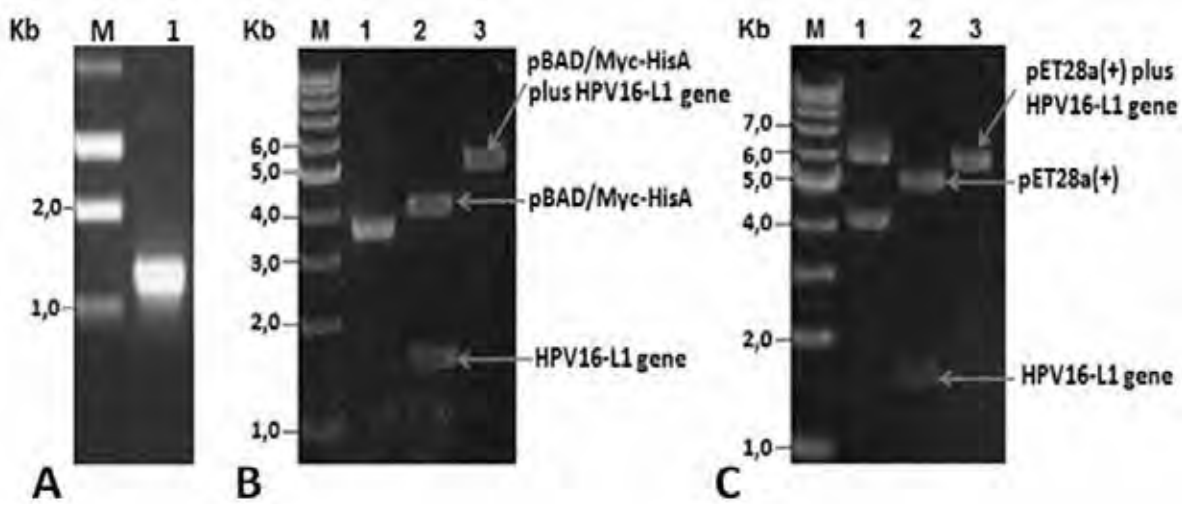

Figure 1. A) PCR product analyses. Lane M: 1Kb DNA Step ladder (Promega), 1: Amplified wild-type HPV16-L1 gene. B) pBAD-HPV16-L1 plasmid restriction analyses. Lane 1: undigested pBADHPV16-L1 plasmid, lane 2: NcoI-HindIII digested pBADHPV16-L1 plasmid, lane 3: BamHI digested pBADHPV16-L1 plasmid. C) pETHPV16-L1 plasmid restriction analyses. Lane 1: undigested pETHPV16-L1 plasmid, lane 2: NcoI-HindIII digested pETHPV16-L1 plasmid, lane 3: BamHI digested pETHPV16-L1 plasmid.

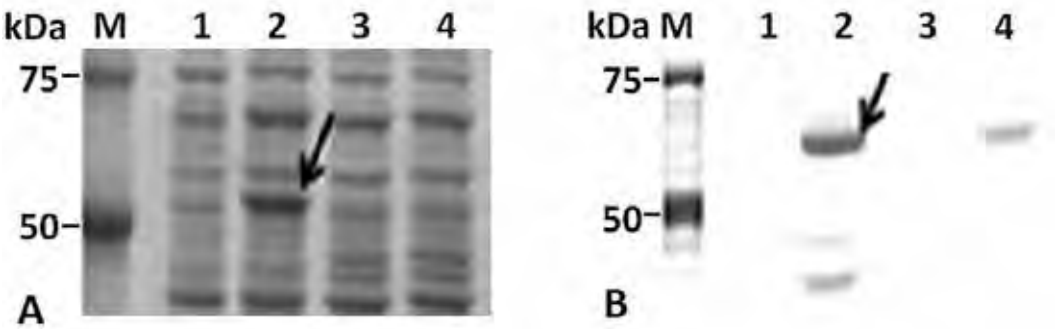

Figure 2. HPV16-L1 protein production by *E. coli* from pBAD/Myc-HisA or pET28a-derived plasmids. A): 10% (w/v) SDS-PAGE and B): *Western Blot* with CamVir-1 antibody of IPTG- or arabinose-induced-cells. Lane M: Broad Range Molecular Weight Marker (Promega), lane 1 and 2: *E. coli* BL21(DE3) harboring pET28a(+) and pETHPV16-L1 plasmids, respectively. Lane 3 and 4: *E. coli* TOP10 harboring pBAD/Myc-HisA and pBADHPV16-L1 plasmids, respectively.

HPV16-L1 protein production by IPTG-induced or auto-induced-grown *E. coli* BL21 (DE3), Rosetta, and SHuffle strains in shake flasks

HPV16-L1 protein production was evaluated in BL21 (DE3), Rosetta, and Shuffle strain transformed with pETHPV16-L1 plasmid under IPTG auto-induction. *E. coli* BL21 (DE3), Rosetta, and SHuffle cells produced HPV16-L1 protein as an intense band of about 57 kDa under IPTG-induction (Figure 3A, lanes 2, 3, and 4) as well as under auto-induction for 24 h (Figure 3D; lanes 2, 3 and 4) and 48 h (Figure 3G; lanes 2, 3 and 4). The overproduced protein under all tested culture conditions, as well as smaller species, reacted with the HPV16-L1 specific CamVir antibody (Figure 3B, E and H; lanes 2, 3 and 4). The BL21(DE3) lysates carrying the pET28a (+) vector showed a weak band (Figure 3A, D and G: lane 2) that CamVir did not recognize (Figure 3B, E and H: lane 2).

Conventionally-IPTG-induced cells produced similar amounts of L1 protein (Figure 3C). However, under auto-induction conditions for 24 h, BL21(DE3) produced the highest amount of L1 protein concerning Rosetta ($p<0.0001$) and SHuffle (Figure 3F; $p<0.01$). For 48 h, BL21(DE3) also produced the highest amount of L1 protein compared to Rosetta ($p<0.0001$) and SHuffle (Figure 3I; $p<0.05$). The L1 protein level was higher in SHuffle regarding Rosetta at 48h (Figure 3I; $p<0.01$).

Solubility of HPV16-L1 protein produced by IPTG-induced- or auto-induced-grown *E. coli* BL21 (DE3), Rosetta, and SHuffle strains in shake flasks

The HPV16-L1 protein's accumulation was undetected in the soluble fractions of the conventionally-IPTG-induced cells from the three *E. coli* evaluated strains (Figure 4A and B: lanes 2, 4, and 6). By contrast, in auto-induced cells, the soluble L1 protein was detected (Figure. 4 D and G: lanes 2, 4, and 6) at similar levels by the three *E. coli* strains (Figure 4F and I). The percentage of HPV16-L1 protein concerning the total proteins in auto-induced cells during 24 and 48 h was 7.2 ± 0.5% and 14.3 ± 1.6%, respectively. Moreover, part of L1 protein was produced insoluble in BL21 auto-induced for 24 h (Figure 4 D and E: lanes 1 and 2), as well as in BL21(DE3) and SHuffle auto-induced for 48 h (Figure 4G and H: lanes 1,2,5 and 6). However, in Rosetta grown for 24 h or 48 h, practically all the produced L1 protein accumulated in the soluble fraction (Figure 4 D and G: lanes 3 and 4).

Discussion

The effectiveness of commercially available anti-HPV VLPs-based vaccines has promoted a considerable interest in developing vaccine candidates from cheaper hosts[8,29]. VLP-ba-

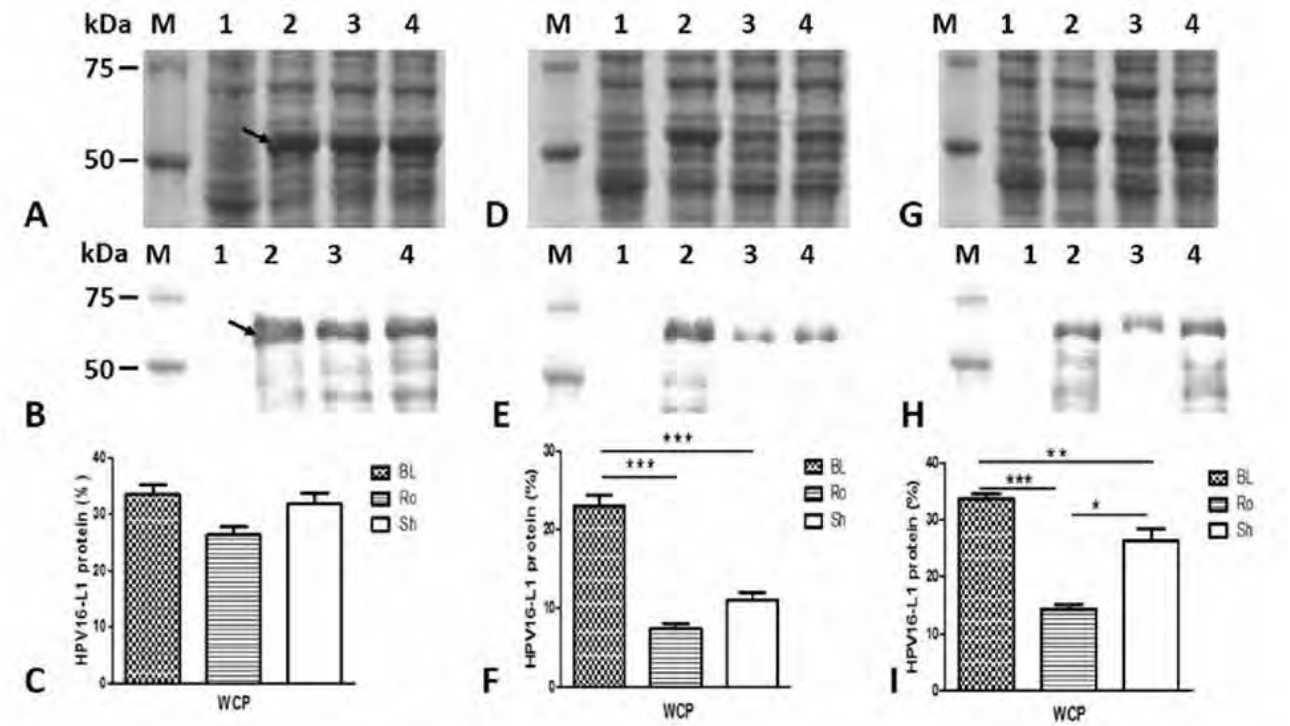

Figure 3. Production of HPV16-L1 protein by *E. coli* BL21(DE3), Rosetta, and SHuffle strains harboring pETHPV16-L1 plasmid grown under different conditions. A, D, and G: 10 % (w/v) SDS-PAGE of 4h-IPTG-induced, 24h-auto-induced, and 48h-auto-induced cells, respectively. B, E, and H: *Western Blot* with CamVir -1 antibody (1: 50 000) of 4h-IPTG-induced, 24h-auto-induced, and 48h-auto-induced cells, respectively. Lane M: Broad Range Protein Molecular Weight Markers (Promega), lane 1: BL21(-DE3)/pET28a(+) vector, Lane 2: BL21(DE3)/pETHPV16-L1, Lane 3: Rosetta /pETHPV16-L1, Lane 4: SHuffle /pETHPV16-L1. Arrows indicate L1 protein. C, F and I: Densitometric analyses of SDS-PAGE scanned gels. Statistical analyses were performed by one-way ANOVA followed by Tukey's multiple comparisons test. Significant differences were considered at $P< 0.05$, $P < 0.01$ and $P<0.0001$. The data are presented as means ± SD (N = 3). BL: BL21(DE3), Ro: Rosetta, and Sh: SHuffle.

sed vaccines derived from *E. coli* are more cost-effective than those prepared from insect cells or yeasts at an industrial scale. [(1)] A VLP-based vaccine assembled from soluble N-terminal truncated variants of L1 protein in *E. coli* was developed[3,15] and recently licensed in China[14], showing this host's potential for producing L1 proteins. In the present study, a wild-type full-length HPV16-L1 gene was amplified by PCR from total DNA extracted from a biopsy sample of an HPV16-diagnosed patient with cervical cancer amplified gene was cloned and verified by sequencing. The cloned HPV16-L1 gene matches the European variant (Accession K02718) with the highest sequence homology level (99 %). There was only one nucleotide difference between the K02718 (C) and the cloned sequence (G) at position 604, changing the codon CAT for histidine-202 in the reference sequence to GAT codon encoding aspartate-202 in the amplified product, which otherwise is required for VLPs assembly in recombinant systems[30].

Successful expression and solubility of recombinant proteins depend on, among the main factors: the choice of the expression vector, expression host, medium composition, and induction conditions[13,20]. Thus, it was assessed the production level and solubility of full-length HPV16-L1 protein in *E. coli* TOP 10 transformed with the pBADHPV16-L1 plasmid and *E. coli* BL21(DE3), Rosetta and SHuffle transformed with pETHPV16-L1 plasmid by conventional induction with L(+)-Arabinose or IPTG, as well as SB-based auto-induction. L1 protein was efficiently produced in BL21(DE3) induced with IPTG employing the pET vector series previously used to produce the HPV16-L1 protein in *E. coli* host by other researchers[31]. The smaller species recognized by CamVir-1 antibody in BL21(-DE3) cell lysates agrees with previous reports on HPV16-L1 protein fragmentation from wild-type L1 gene expressed in insect cells[30], *Saccharomyces cerevisiae*[32] and *E. coli* cells[8,31].

In contrast to BL21 (DE3)/pETHPV16-L1, the *E. coli* TOP10/*pBAD* expression system did not efficiently produce L1 protein. The arabinose-regulated promoter has been widely used for protein expression in *E. coli*[18] to promote high amounts of soluble recombinant proteins[33]. However, in our study, L1 protein was barely detected by Western Blot, which could be related to L1 gene expression's lesser efficiency from the pBAD vector series. Our results showed that the produced protein corresponds to the L1 protein from HPV16 and that the BL21(DE3)/pET expression system is better than TOP10/pBAD system for the production of L1 protein from the wild-type HPV16-L1 gene.

Once we verified the production of the L1 protein by BL21(DE3) /pET expression system, we proceeded to assay its production in *E. coli* BL21(DE3), Rosetta, and SHuffle carrying the pETHPV16-L1 plasmid under induction with IPTG or SB-based auto-induction. The results obtained showed that the HPV16-L1 protein was produced at similar levels in conventionally-induced cells. In contrast, the L1 protein production levels in auto-induced cells were significantly different. BL21(DE3) produced the highest amount of HPV16-L1 protein, followed by SHuffle and Rosetta. These results are consistent with Zarschler et al., who found a slightly higher production of single-domain antibodies in BL21(DE3) than SHuffle using the pET system after induced with IPTG[34]. The behavior in the production levels of HPV16-L1 protein in SHuffle and Rosetta concerning BL21 (DE3) may be related to constitutive lysozy-

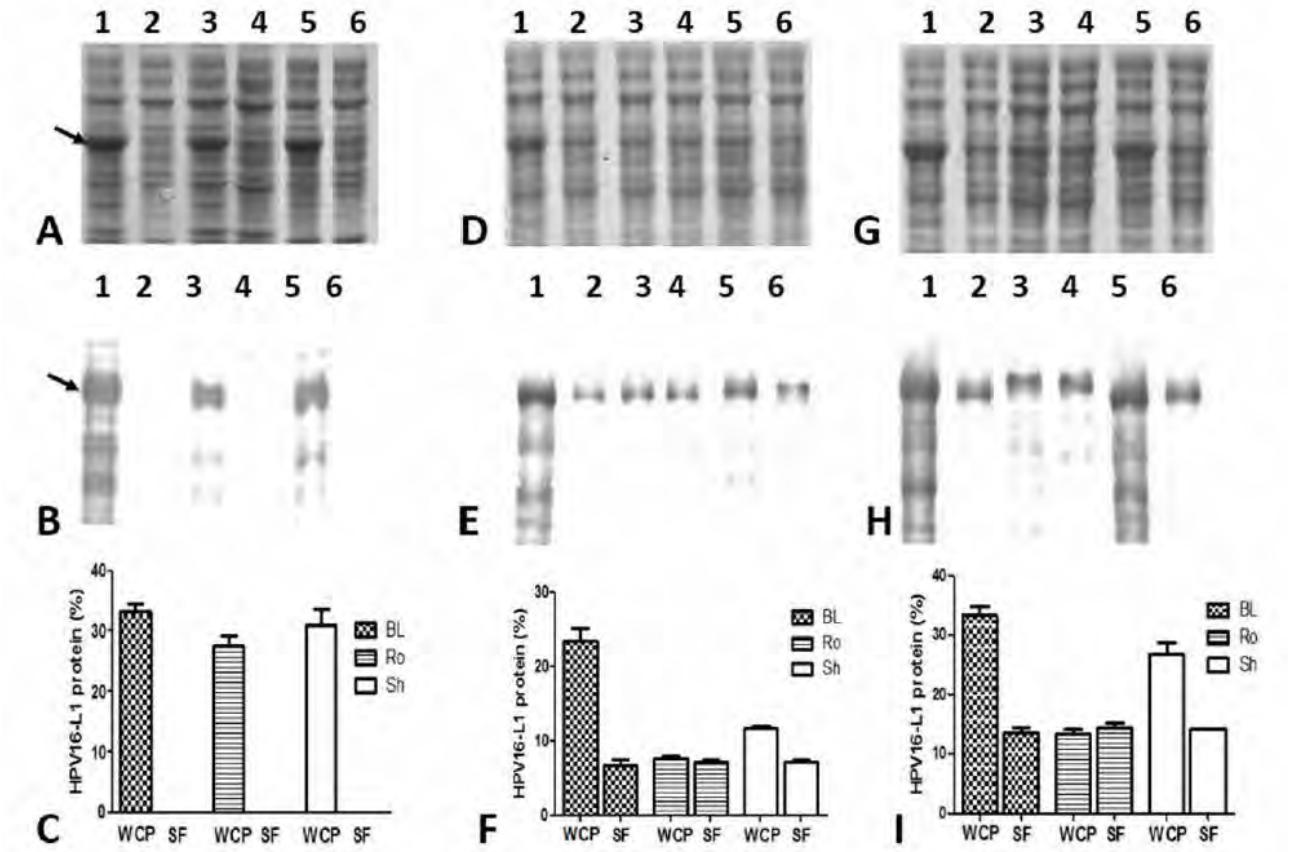

Figure 4. Solubility of HPV16-L1 protein in *E. coli* BL21(DE3), Rosetta, and SHuffle strains harboring pETHPV16-L1 plasmid grown under different conditions. A, D, and G: 10 % SDS-PAGE of 4h-IPTG-induced, 24h-auto-induced, and 48h-auto-induced cells, respectively. B, E, and H: *Western Blot* with CamVir-1 antibody (1: 50 000) of 4h-IPTG-induced, 24h-auto-induced, and 48h-auto-induced cells, respectively. Lane 1: BL21(DE3) whole cell lysate, 2: BL21(DE3) soluble fraction, 3: Rosetta whole cell lysate, 4: Rosetta soluble fraction, 5: SHuffle whole cell lysate, 6: SHuffle soluble fraction. Arrows indicate L1 protein. * Whole Cell Protein (WCP), Soluble Fraction (SF). C, F and I: Densitometric analyses of SDS-PAGE scanned gels. Soluble HPV16-L1 protein percent among different strains was not different, by one-way ANOVA followed by the Tukey's multi comparisons test. Data presented as means ± SD (N = 3). BL: BL21(DE3), Ro: Rosetta, and Sh: SHuffle.

me production and accumulation within cells. The lysozyme is a natural inhibitor of T7 RNA polymerase (T7 RNAP)[20], which is supplied by pLysS plasmid (10-12 copies per cell)[23] in Rosetta[35] or by miniF plasmid (1-2 copies per cell)[36] in SHuffle[37]. It is possible that, during long time-culture (like auto-induction) of lysozyme expressing cells, the lysozyme produced reaches high levels and decreases the T7 RNAP availability, affecting the L1 protein yield in those cells.

The solubility of L1 protein produced by conventionally-induced cells or auto- induced cells was also analyzed. The soluble HPV-L1 protein production might be advantageous for developing a successful and efficient *E. coli*-based HPV-LI VLPs vaccine[3], due to the soluble protein may preserve the protective conformational epitopes[3,15]. In this regard, soluble full-length L1 protein has not been detected by SDS-PAGE from IPTG-induced *E. coli* cell[31]. Likewise, in our study, the L1 protein was found insoluble in conventionally-induced cells, which differs from the soluble production of HPV11-L1 protein from a wild-type L1 gene using the pET vector series[38]. By contrast, HPV16-L1 protein solubility was enhanced in auto-induced cells, which is in line with previous reports about using auto-induction as a strategy to promote soluble recombinant protein production in *E. coli*[17-19]. This strategy successfully increased the solubility of recombinant proteins produced insoluble under IPTG-induction in *E. coli*, such as human tissue plasminogen (tPA)[17,28] and streptococcal cysteine protease[39]. Long *et al.* reported soluble production of full-length tPA in *E. coli*, showing that auto-induction is a reliable strategy to reach at least 50% of tPA expression in the soluble fraction *E. coli*17. Three years later, Fathi-Roudsari *et al.* optimized the expression conditions for the tPA protein (truncated variant) *E. coli* by decreasing temperature and using an SB-based auto-induction medium, resulting in at least three times higher levels of active reteplase production in oxidative cytoplasm of Rosetta-gami[19]. Like Fathi-Roudsari *et al.*, we used an SB-based auto-induction medium and 18 ^{0}C grown temperature instead of using lactose; a low IPTG concentration (30 µM) was used, which previously has been used efficiently in auto-induction[40]. Our results are also consistent with the positive effect of decreasing inducer's concentration and induction temperature on the recombinant protein solubility in the *E. coli* cytoplasm[19-21]. Thus, a decrease in temperature during induction causes a reduction in the recombinant protein synthesis rate and a reduction in hydrophobic interactions and consequently prevents the formation of inclusion bodies[20]. Fathi-Roudsari *et al.* found that decreasing the temperature to 25 and 18 °C increased active reteplase level by 20 and 60%, respectively[19].

On the other hand, the amount of L1 protein accumulated in BL21(DE3), Rosetta, and SHuffle's soluble fraction was similar, suggesting that soluble L1 protein production depends more on culture conditions than the genetic background of each strain (Table 1)[20,23,35]. Gu et al. produced soluble truncated

HPV16-L1 protein with a purity of about 10% under conventional induction with IPTG[41], a level similar to those achieved in the current study (7.2 and 14 % 24 and 48 h of autoinduction, respectively).

Our results demonstrated that a slow expression procedure that combines growth at a low temperature, a low IPTG concentration, and a low agitation speed under auto-induction conditions promotes soluble HPV16-L1 protein accumulation. These constitute the first report describing the successful production of soluble full-length HPV16-L1 protein from a wild-type L1 gene in *E. coli* using an auto-induction strategy. This could be valuable for using prokaryotic auto-induction expression systems to produce HPV16-L1 antigen for vaccine development, omitting the *in vitro* refolding step for its purification. Purification of the soluble full-length HPV16-L1 protein for structural and immunogenicity analyses is currently underway.

In short, a Cuban wild type full-length HPV16-L1 gene was successfully cloned and expressed in *E. coli* BL21(DE3), Rosetta (DE3) pLysS, and SHuffle® T7 Express *lys*Y employing the pET system. *E. coli* culture under auto-induction at 18°C, with 30μM IPTG and a low agitation (100 rev/min) promotes soluble production of full-length HPV16-L1 protein. development of this bacterial system could be used for purifying HPV16-L1 protein from soluble fraction and evaluating its capacity to form VLPs, which could be used as vaccine candidate antigen.

Conclusions

The auto-induction procedure at 18 °C with 30 μM IPTG and 100 rev/min promotes soluble full-length HPV16-L1 protein production by *E. coli*.

Acknowledgment

We thank Dr. Juan Carlos Piña for providing us with the genomic DNA for HPV16L1 gene amplification.

Conflict of Interest

The authors declare that they have no conflict of interest.

Bibliographic references

1. Huang X, Wang X, Zhang J, Xia N, Zhao Q. Escherichia coli - derived virus-like particles in vaccine Development. npj Vaccines. 2017; 2(3):1-9.
2. Harlé A, Guillet J, Thomas J, Sastre-Garau X, Rouyer M, Ramacci C, et al. Evaluation and validation of HPV real-time PCR assay for the detection of HPV DNA in oral cytobrush and FFPE samples. Scientific Reports. 2018; 8:11313.
3. Wei M, Wang D, Li Z, Song S, Kong X, Mo X, et al. N-terminal truncations on L1 proteins of human papillomaviruses promote their soluble expression in Escherichia coli and self-assembly in vitro. Emerg Microbes Infect. 2018; 7(1):160.
4. Zhang Y, He Y, Li L, Liang S, Yan M, Ren D, et al. development and characterization of an HPV18 detection kit using two novel HPV18 type-specific monoclonal antibodies. Diagnostic Pathology. 2018; 13:55.
5. Soto Y, Torres G, Kourí V, Limia CM, Goicolea A, Capó V, et al. Molecular epidemiology of human papillomavirus infections in cervical samples from cuban women older than 30 years. J Low Genit Tract Dis. 2014; 18(3):210-217.
6. Javanmard D, Namaei M H, Haghighi F, Ziaee M, Behavan M, Mirzaei J, et al. The Frequency and Typing of Human Papilloma Virus Among Women with Normal and Abnormal Cytology in Southern Khorasan, Eastern Iran. Jundishapur J Microbiol. 2017; 10(4): e43213.
7. Maleki Z. Human papilloma virus vaccination: Review article and an update. World J Obstet Gynecol. 2016; 5(1): 1627.
8. Bang HB, Lee YH, Lee YJ, Jeong KJ. High-Level Production of Human Papillomavirus (HPV) Type 16 L1 in Escherichia coli. J Microbiol Biotechnol. 2016; 26(2):356-63.
9. Bruni L, Diaz M, Barrionuevo-Rosas L, Herrero R, Bray F, Bosch FX, et al. Global estimates of human papillomavirus vaccination coverage by region and income level: a pooled analysis. Lancet Glob Health. 2016; 4(7):e453–63.
10. Bruni L, Albero G, Serrano B, Mena M, Gómez D, Muñoz J, Bosch FX, de Sanjosé S. ICO/IARCInformation Centre on HPV and Cancer (HPV Information Centre). Human Papillomavirus and RelatedDiseases in Cuba. Summary Report 17 June 2019. Available from: https://hpvcentre.net/statistics/reports/CUB.pdf
11. Guilarte E, SotoY, Kourí V, Limia CM, Sánchez ML, Rodríguez AE, et al. Circulation of human Papillomavirus and Chlamydia trachomatis in women. MEDICC Rev. 2020;22(1):17–27.
12. Baeshen MN, Al-Hejin AM, Bora RS, Ahmed MM, Ramadan HA, Saini KS, et al. Production of Biopharmaceuticals in E. coli: Current Scenario and Future Perspectives. J Microbiol Biotechnol. 2015; 25 (7): 953-62.
13. Uhoraningoga A, Kinsella GK, Henehan GT, Ryan BJ. The Goldilocks Approach: A Review of Employing Design of Experiments in Prokaryotic Recombinant Protein Production. Bioengineering (Basel). 2018; 5(4):89.
14. Qian C, Liu X, Xu Q, Wang Z, Chen J, Li T, Zheng Q, et al. Recent Progress on the Versatility of Virus-Like Particles. Vaccines. 2020; 8(139):1-14.
15. Gu Y, Wei M, Wang D, Li Z, Xie M, Pan H, et al. Characterization of an Escherichia coli-derived human papillomavirus type 16 and 18 bivalent vaccine.Vaccine. 2017; 35(35 Pt B):4637-4645.
16. Kelsall SR, Kulski JK. Expression of the major capsid protein of human papillomavirus type 16 in Escherichia coli. J Virol Methods. 1995; 53(1):75-90.
17. Long X, Gou Y, Luo M, Zhang S, Zhang H, Bai L, et al. Soluble expression, purification, and characterization of active recombinant human tissue plasminogen activator by auto-induction in E. coli. BMC Biotechnology. 2015;15:13.
18. Jia B, Jeon CO. 2016. High-thoughput recombinant protein expression in Escherichia coli: current status and future perspectives. Open Biol. 2016; 6: 160196.
19. Fathi-Roudsari M, Maghsoudi N, Maghsoudi A, Niazi S, Soleiman M. Auto-induction for high level production of biologically active reteplase in Escherichia coli. Protein Expr Purif. 2018; 151:18-22.
20. Hayat SMG, Farahani N, Golichenari B, Sahebkar A. Recombinant Protein Expression in Escherichia coli (E.coli): What We Need to Know?.Curr Pharm Des. 2018; 24(6):718-725.
21. Yousefi M, Farajnia S, Mokhtarzadeh A, Akbari B, Ahdi Khosroshahi S, Mamipour M, et al. Soluble Expression of Humanized Anti-CD20 Single Chain Antibody in Escherichia coli by Cytoplasmic Chaperones Co-expression. Avicenna Journal of Medical Biotechnology. 2018; 10(3):141-146.
22. Srimeenakshi S, Murthy M, Selvakumar K, et al. An Overview of the Parameters for Recombinant Protein Expression in Escherichia Coli. J Cell Sci Ther. 2015; 6: 221. doi:10.4172/2157-7013.1000221.
23. Rosano GL, Ceccarelli EA. Recombinant protein expression in Escherichia coli: advances and challenges. Front Microbiol. 2014; 5:172.
24. Zhou Y, Zhang Y, He W, Wang J, Peng F, Huang L, et al. Rapid Regeneration and Reuse of Silica Columns from PCR Purification and Gel Extraction Kits. Sci Rep. 2018; 8(1):12870.
25. Li X, Sui X, Zhang Y, Sun Y, Zhao Y, Zhai Y, et al. An improved calcium chloride method preparation and transformation of competent cells. African Journal of Biotechnology. 2010; 9(50): 8549-8554.
26. Piña JC, Crespo G, Fando RA, Casanova G, Curbelo M, Guerra MM. Identificación molecular de genotipos papilomavirus humanos en pacientes con cáncer de cuello uterino. AMC. 2016; 20(3): 288-298.

27. Laemmli UK. Cleavage of structural proteins during the assembly of the head of bacteriophage T4. Nature. 1970; 227(5259):680-685.
28. Studier FW. Protein production by autoinduction in high density shaking cultures. ProteinExpr. Purif. 2005; 41: 207–234.
29. Guan J, Bywaters SM, Brendle SA, Ashley RE, Makhov AM, Conway JF, et al. Cryoelectron Microscopy Maps of Human Papillomavirus 16 Reveal L2 Densities and Heparin Binding Site. Structure. 2017; 25(2):253-263.
30. Kirnbauer R, Taub J, Greenstone H, Roden R, Dürst M, Gissmann L, et al. 1993. Efficient self-assembly of human papillomavirus type 16 L1 and L1-L2 into virus-like particles. J. Virol.1993; 67:6929-6936.
31. Zhang W, Carmichael J, Ferguson J, Inglis S, Ashafian H, Stanley M. Expression of human papillomavirus type 16 L1 protein in Escherichia coli: denaturation, renaturation, and self-assembly of virus-like particles in vitro.Virology.1998; 243(2):423-31.
32. Patel MC, Patkar KK, Basu A, Mohandas KM, Mukhopadhyaya R. Production of immunogenic human papillomavirus-16 major capsid protein derived virus like particles.Indian J Med Res. 2009; 130(3):213-8.
33. Kaur J, Kumar A, Kaur J. Strategies for optimization of heterologous protein expression in E. coli: Roadblocks and reinforcements. International Journal of Biological Macromolecules 2018; 106 (2018): 803–822.
34. Zarschler K, Witecy S, Kapplusch F, Foerster C, Stephan H. High-yield production of functional soluble single-domain antibodies in the cytoplasm of Escherichia coli. Microb Cell Fact. 2013; 12:97.
35. Novy R., Drott D., Yaeger K., Mierendorf R. (2001). Overcoming the codon bias of E. coli for enhanced protein expression. Innovations 12 1–3.
36. Nozaki S, Niki H, Ogawa T. Replication initiator DnaA of Escherichia coli changes its assembly form on the replication origin during the cell cycle. J Bacteriol. 2009; 191(15):4807-14.
37. Samuelson JC, Davis TB, Raleigh EA, Southworth MW, Inventors; Nyland Biolabs, Inc., Ipswich, assignee: Expression of toxic genes in vivo in a non-natural host. United States patent US 8.492,117 B2 . 2013 Jul 23.
38. Li M, Cripe TP, Estes PA, Lyon MK, Rose RC, Garcea RL. Expression of the human papillomavirus type 11 L1 capsid protein in Escherichia coli: characterization of protein domains involved in DNA binding and capsid assembly. J Virol. 1997; 71(4):2988–2995.
39. Lane MD, Seelig B. Highly efficient recombinant production and purification of streptococcal cysteine protease streptopain with increased enzymatic activity. Protein Expr Purif. 2016; 121:66–72.
40. Faust G, Stand A, & Weuster- Botz D. (2015). IPTG can replace lactose in auto- induction media to enhance protein expression in batch- cultured Escherichia coli. Engineering in Life Sciences, 15(8), 824-829.
41. Gu Y, Li S, Wei M, Xian Y, Luo W, Xia N, Inventors; Xiamen (CN), assignee: Truncated L1 protein of human papillomavirus type 16. US 2010/0255031 Al. 2010 Oct 7.

Received: 28 November 2020
Accepted: 10 January 2021

RESEARCH / INVESTIGACIÓN

Benthic polychaete off Tanintharyi Island, Myeik Archipelago

Zarni Ko Ko[1] and Hnin Pwint Htwe[2]

DOI. 10.21931/RB/2021.06.02.5

Abstract: The survey examined shallow to deep-sea benthic data on benthic fauna from the Myanmar coastal region's northern sector. Benthic samples were collected from 17 stations (26-1500m depth) off Taninthayi Island during the Mayanmar ecosystem survey of the R/V Dr. Fridtjof Nansen Research Vessel. Polychaete (25 taxa in total) had a higher proportion than other groups of benthic fauna. The range of species diversity and evenness were insignificantly different, but species richness differed. The highest species diversity, species evenness, and richness were showed in shallow areas (26 m depth).

Key words: Diversity indices, Polychaetes, Taninthayi Island, Myeik Archipelago.

Introduction

Polychaete is part of the old, a group that is longer than full and non-vertebrate. The polychaetes are multi-segment annelids with parapodia; setae are present in distinct fascicles. They are dioecious and have simple existing ducts from the gonads. They are usually marine, rarely fresh-water, and only rarely terrestrial or parasitic in their habitat. Any of these features needed not is present, and none of them is essential for the recognition of an animal as a polychaete.

Polychaetes are the dominant macrofaunal taxa in all marine silt from the intertidal region down to the deep ocean. They constitute more of the entire microbenthic creatures in terms of the number of species and individuals. The lion's share of the species is minimal and short-lived, showing a tall auxiliary generation. Consequently, they are a primary connection in marine nourishment networks and highlight necessarily within the diets of numerous bottom-feeding angles.

Being small-sized life forms, they play a pivotal part in biology and Environmental Impact Assessment (EIA) ponders. As numerous polychaetes are inactive, changes in their wealth and differences have been utilized in natural checking, especially in evaluating the estuaries' wellbeing.

The present survey area, Tanintharyi Island, Myeik Archipelago, is located in the Southern part of the Myanmar Coastal Region. This benthic survey was the preliminary survey of the R/V Dr. Fridtjof Nansen Research Vessel in the Myanmar Coastal Region. Myeik coastal area is rich in many economically important fish, shrimps, oysters, clams, and mussels. Man eats the flesh of many species.

Benthic animals are four groups, namely polychaetes, crustaceans, echinoderms, and mollusks. So, the R/V Dr. Fridtjof Nansen Research Vessel was conducted in Tanintharyi Island, Myeik Archipelago. Cherry Aung[1] initiated the earliest study of marine benthos of the Myanmar Coast. She studied the subtidal benthos of Myanmar shelf waters. In 2011, Si Thu Hein[2] study polychaetes from three Intertidal Mud Flat stations of Myeik Coastal Areas.

And then War War Soe[3] also conducted soft-bottom intertidal macrobenthos from along the Coastal Areas of Myeik Archipelago. Moreover, Hlaing Hlaing Htoon[4] reported the Dawei point of the Tahnintharyi Coastal Region. This survey's objectives are (a) to identify what types of polychaetes are found in present survey areas and (b) to analyze the diversity indices of polychaetes of Tanintharyi Island.

Materials and methods

The study area, Tanintharyi Island, Kyunsu Township, Tanintharyi Region, is located between Lat. 12°50′ N & 10°10′ N and Long. 98°15′ E & 97°50′ E. Samples of polychaetes were taken in June 2015 onboard the R/V Dr. Fridtjof Nansen Research Vessel on the parts of northern Myeik Archipelago. On 17 transactions, bottom sediments were sampled at depths of 26m, 43m,44m, 46m, 53m, 60m, 100m, 106m, 220m, 245m, 249m, 252m, 295m, 341m, 500m, 1000m, and 1500m (Table 1). The samples were taken with wire mounted Van Vee Grab, washed with sea-water in these two drawers, which included 5 mm sieve and 0.5 or 0.3 mm sieve and preserved by 4-8 % formalin or 96 % ethanol with 1 spoon of borax powder and put them into the 1-liter bottles. Species diversity indices for each sample were calculated using Shannon and Weaver[5], Pielou[6], and Margalef' s[7]. H' =-Pi*lnPi, E' =H'/lnS, D' =S-1/ln N Where, H' is the index of species diversity, Pi is the population abundance of i^{th} species calculated by ni/N, ni is the number of individual of the i^{th} species, N is the total number of individuals in a station, E' is the index of species evenness, S is the total number of species and D' is the index of species richness.

Results and Discussion

A total of 25 genera of Polychaetes were recorded in the present study; 1 genus from Ampharetidae, 1 genus from Hesionidae, 3 genera from Capitellidae, 1 genus from Sabellariidae, 2 genera from Eunicidae, 1 genus from Lumbrineridae, 1 genus from Glycerida, 1 genus from Nephtyidae, 1 genus from Nereidae, 1 genus from Phyllodocidae, 2 genera from Polynoidae, 1 genus from Sabellidae, 1 genus from Sabellaridae, 1 genus from Maldanidae, 1 genus from Orbiniidae, 1 genus from Paraonidae, 1 genus from Poecilochaetidae, 2 genera from Spionidae, 1 genus from Flabelligeridae, 1 genus from Terebellidae were described.

About 25 polychaete species were identified from the studied areas, of which 19 taxa were identified from the shallowest water (26m depth), 4, 4, 1, 2, and 3 taxa of polychaetes from depths 44m, 46m, 53m, 60m, 66m respectively. And only 3 taxa of polychaetes were also identified form eleven sampling sites of deepwater, off Tanintharyi Island, Myeik Archipelago (Table 2). In 2013, 120 species of polychaetes were recorded in soft-bottom intertidal zones of Myeik coastal areas by War War Soe[3]. Moreover, 31 species of polychaete were ob-

[1] Lecturer, Department of Marine Science, Mawlamyine University, Mon State, Myanmar.
[2] MRes , Department of Marine Science, Myeik University, Myeik Taninthayi Region, Myanmar.

Corresponding author: zni1446@gmail.com

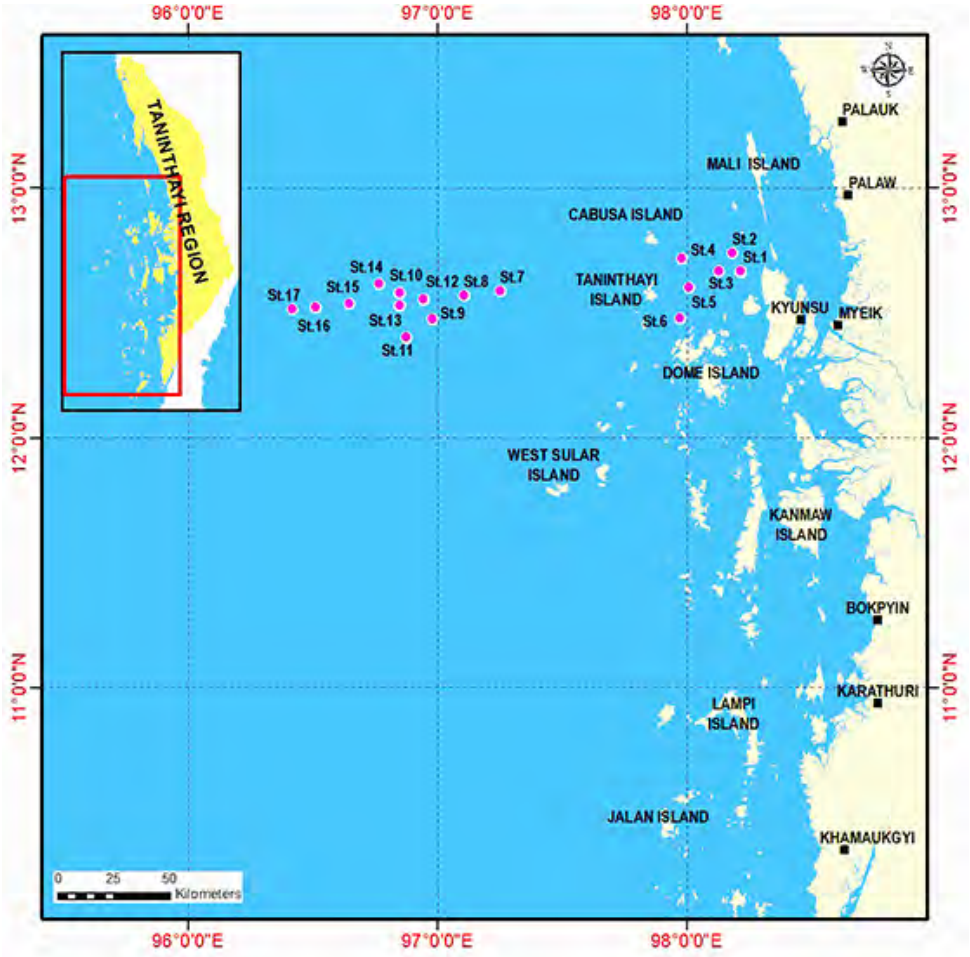

Figure 1. Showing the sampling sites of the Taninthayi Island, Tanintharyi Coastal Region.

Sites	Depth	Coordinates	
		Latitude (N)	Longitude (E)
1	26m	12.6685	98.2115
2	44m	12.7392	98.1797
3	46m	12.6686	98.1233
4	53m	12.7182	97.9778
5	60m	12.6005	98.0052
6	66m	12.3254	97.8215
7	100m	12.5859	97.2501
8	106m	12.5703	97.104
9	220m	12.4747	96.9776
10	245m	12.5807	96.8462
11	249m	12.401	96.8741
12	252m	12.5564	96.9414
13	295m	12.5799	96.8469
14	341m	12.6166	96.7655
15	500m	12.536	96.6453
16	1000m	12.5232	96.5123
17	15000m	12.5155	96.4173

Table 1. Sampling sites of the station Taninthayi Island, Tanintharyi Coastal Region.

Sr. No.	Species name	Depth in meter																
		26	44	46	53	60	66	100	106	220	245	249	252	295	341	500	1000	1500
1.	*Ampharete*	+	-	-	-	-	-	-	-	-	-	-	-	-	-	-	-	-
2.	*Leocrates*	+	-	-	-	-	-	-	-	-	-	-	-	-	-	-	-	-
3.	*Capitella*	-	-	+	-	-	-	-	-	-	-	-	-	-	-	-	-	-
4.	*Heteromastus*	+	-	+	-	+	-	-	-	-	-	-	-	-	-	-	-	-
5.	*Notomastus*	+	+	+	+	-	-	-	-	-	-	-	-	-	-	+	-	-
6.	*Lygdamis*	+	-	-	-	-	-	-	-	-	-	-	-	-	-	-	-	-
7.	*Eunice*	-	-	-	-	-	+	-	-	-	-	-	-	-	-	-	-	-
8.	*Marphysa*	+	-	-	-	-	+	-	-	-	-	-	-	-	-	-	-	-
9.	*Lumbrinereis*	+	-	-	-	+	-	-	-	-	-	-	-	-	-	-	-	-
10.	*Glycera*	+	-	-	-	-	-	-	-	-	-	-	-	-	-	-	-	-
11.	*Nephtys*	-	-	-	-	-	+	-	-	-	-	-	-	-	-	-	-	-
12.	*Nereis*	-	-	+	-	-	-	-	-	-	-	-	-	-	-	-	-	-
13.	*Phyllodoce*	+	-	-	-	-	-	-	-	-	-	-	-	-	-	-	-	-
14.	*Harmothoe*	+	-	-	-	-	-	-	-	-	-	-	-	-	-	-	-	-
15.	*Lepidonotus*	+	-	-	-	-	-	-	-	-	-	-	-	-	-	-	-	-
16.	*Potamilla*	+	-	-	-	-	-	-	-	-	-	-	-	-	-	-	-	-
17.	*Idanthyrsus*	+	-	-	-	-	-	-	-	-	-	-	-	-	-	-	-	-
18.	*Maldane*	+	+	-	-	-	-	-	-	-	-	-	-	-	-	-	-	-
19.	*Scoloplos*	+	+	-	-	-	-	-	-	-	-	-	-	-	-	-	-	-
20.	*Paraonis*	-	-	-	-	-	-	-	-	-	-	-	-	-	-	-	+	-
21.	*Poecilochaetus*	+	-	-	-	-	-	-	-	-	-	-	-	-	-	-	-	-
22.	*Prionospio*	-	+	-	-	-	-	-	-	-	-	-	-	-	-	-	-	-
23.	*Spio*	+	-	-	-	-	-	-	+	-	-	-	-	-	-	-	-	-
24.	*Diplocirrus*	+	-	-	-	-	-	-	-	-	-	-	-	-	-	-	-	-
25.	*Streblosoma*	+	-	-	-	-	-	-	-	-	-	-	-	-	-	-	-	-

Table 2. Distribution of polychaetes at all sites of Tanintharyi Island, Tanintharyi Coastal Region.

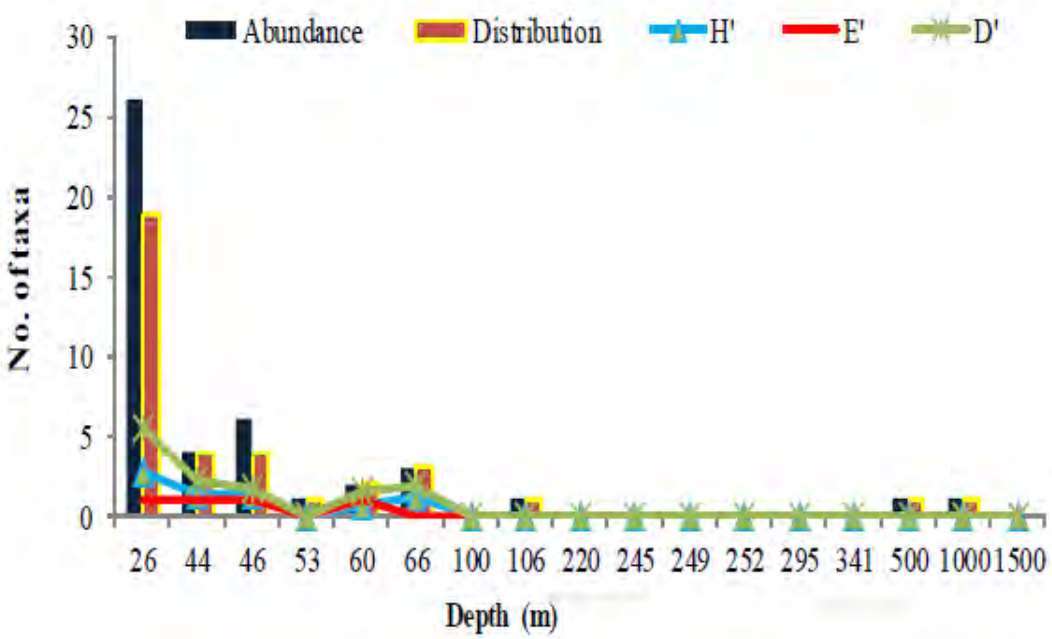

Figure 2. Composition, Abundance, Species Diversity, Eveness and Richness of polychaete in Tanintharyi Island.

served around the Dawei point, Tanintharyi Coastal Region[4].

In the present survey, *Notomastus* was commonly found at 26m, 44m, 46m, 53m, and 500m depths in shallow and depth-water. *Heteromastus* was also found commonly at 26m, 46m, and 60m depths, respectively. *Paraonis* was only occurred at deepwater of 1000m depth. At survey depths; 100m depth (site 7), 220m depth (site 9), 245m depth (site 10), 249m depth (site 11), 252m depth (site 12), 295m depth (site 13), and 341m depth (site 14) were no observed any polychaete taxa. Depth wise taxa composition in Tanintharyi Island was shown in Table 2 and Figure 3.

In the present study, Shannon diversity values for polychaetes were in the range of 0-2.79. The *H′* for polychaetes in Myeik Archipelago and Dawei point was the range in 2.26-3.62 and1.83- 2.62,[3,4] respectively. The range of evenness (*E′*), richness (*D′*) for polychaetes was 0-1 and 0-5.52, respectively. In Myeik Archipelago, *E′* value was the range in 0.74-0.88, and *D′* was War War Soe3 reported 2.62-10.55. Moreover, in Dawei's point, the values *E′* and *D′* were ranged in 0.77-0.88, and 2.33-6.16 was noticed[4].

Low diversity and a higher population density of a few organisms denote stress conditions, which practically eliminate many species but promote a few survival. Contrary to this, high diversity and lesser relative dominance of individual species characterize areas of relative environmental stability[8]. In the present study, benthic production in terms of abundance and number of polychaete genera low in deepwater stations. Low diversity and lower benthic fauna at depth water stations indi-

cate stress conditions because of destructive fishing activities (trawling and purse seining) and dredging. Besides, fishers' fishing activities, especially those living in a coastal area, can damage the bottom communities.

In the present study, high species diversity, species richness, species evenness of polychaetes were noticed at shallow water sites, low species diversity, low richness, and low evenness of polychaetes were noticed in depth beyond 66m. Species diversity index varied between 0.69 and 2.79. Sites 8, 15, and 16 showed the least species diversity of all sites that present only one genus. At stations 4 and 5, only 2 genera were occurred, showing the low richness of 1.44. In the other stations, the index varied from 0 to 5.52. On comparing for species, evenness distribution high values were observed at stations 2, 4, and 5. The study of polychaetes in the area showed a wide variation in distribution, abundance, and composition. This decrease in species richness and diversity of benthic fauna cannot be due to the lack of food, and the only factor that appears to be limiting is dissolved oxygen[9].

The study of benthos in the area showed a wide variation in distribution, abundance, and composition. This may be probably due to various biological and physicochemical environmental factors. Wide fluctuation in salinity and the nature of substratum and organic enrichment in the sediment are the critical factors restricting the abundance of benthos (Sheeba[8]). The studies by Rosenberg[10] and Jones and Candy[11] suggested that the benthic fauna of dredged areas differs from that of non dredged areas concerning species composition, abundance, and diversity.

Sr. No.	Species name	Depth in meter																
		26	44	46	53	60	66	100	106	220	245	249	252	295	341	500	1000	1500
1.	*Ampharete*	1	-	-	-	-	-	-	-	-	-	-	-	-	-	-	-	-
2.	*Leocrates*	2	-	-	-	-	-	-	-	-	-	-	-	-	-	-	-	-
3.	*Capitella*	-	-	1	-	-	-	-	-	-	-	-	-	-	-	-	-	-
4.	*Heteromastus*	1	-	2	-	1	-	-	-	-	-	-	-	-	-	-	-	-
5.	*Notomastus*	1	1	2	1	-	-	-	-	-	-	-	-	-	-	1	-	-
6.	*Lygdamis*	1	-	-	-	-	-	-	-	-	-	-	-	-	-	-	-	-
7.	*Eunice*	-	-	-	-	-	1	-	-	-	-	-	-	-	-	-	-	-
8.	*Marphysa*	1	-	-	-	-	1	-	-	-	-	-	-	-	-	-	-	-
9.	*Lumbrinereis*	1	-	-	-	1	-	-	-	-	-	-	-	-	-	-	-	-
10.	*Glycera*	1	-	-	-	-	-	-	-	-	-	-	-	-	-	-	-	-
11.	*Nephtys*	-	-	-	-	-	1	-	-	-	-	-	-	-	-	-	-	-
12.	*Nereis*	-	-	1	-	-	-	-	-	-	-	-	-	-	-	-	-	-
13.	*Phyllodoce*	1	-	-	-	-	-	-	-	-	-	-	-	-	-	-	-	-
14.	*Harmothoe*	1	-	-	-	-	-	-	-	-	-	-	-	-	-	-	-	-
15.	*Lepidonotus*	1	-	-	-	-	-	-	-	-	-	-	-	-	-	-	-	-
16.	*Potamilla*	3	-	-	-	-	-	-	-	-	-	-	-	-	-	-	-	-
17.	*Idanthyrsus*	1	-	-	-	-	-	-	-	-	-	-	-	-	-	-	-	-
18.	*Maldane*	1	1	-	-	-	-	-	-	-	-	-	-	-	-	-	-	-
19.	*Scoloplos*	2	1	-	-	-	-	-	-	-	-	-	-	-	-	-	-	-
20.	*Paraonis*	-	-	-	-	-	-	-	-	-	-	-	-	-	-	-	1	-
21.	*Poecilochaetus*	1	-	-	-	-	-	-	-	-	-	-	-	-	-	-	-	-
22.	*Prionospio*	-	1	-	-	-	-	-	-	-	-	-	-	-	-	-	-	-
23.	*Spio*	4	-	-	-	-	-	-	1	-	-	-	-	-	-	-	-	-
24.	*Diplocirrus*	1	-	-	-	-	-	-	-	-	-	-	-	-	-	-	-	-
25.	*Streblosoma*	1	-	-	-	-	-	-	-	-	-	-	-	-	-	-	-	-

Table 3. Abundance of polychaetes at all sites of Tanintharyi Island, Tanintharyi Coastal Region.

Sites	Depth (m)	No. of taxa	Abundance	Diversity (*H'*)	Evenness (*E'*)	Richness (*D'*)
1	26	19	26	2.79	0.95	5.52
2	44	4	4	1.39	1.00	2.17
3	46	4	6	1.30	0.94	1.67
4	53	1	1	0	0	0
5	60	2	2	0.69	1.00	1.44
6	66	3	3	1.10	0.91	1.82
7	100	0	0	0	0	0
8	106	1	1	0	0	0
9	220	0	0	0	0	0
10	245	0	0	0	0	0
11	249	0	0	0	0	0
12	252	0	0	0	0	0
13	295	0	0	0	0	0
14	341	0	0	0	0	0
15	500	1	1	0	0	0
16	1000	1	1	0	0	0
17	1500	0	0	0	0	0

Table 4. Composition, Abundance, Species Diversity, Evenness, and Richness of polychaete inTanintharyi Island, Tanintharyi Coastal Region.

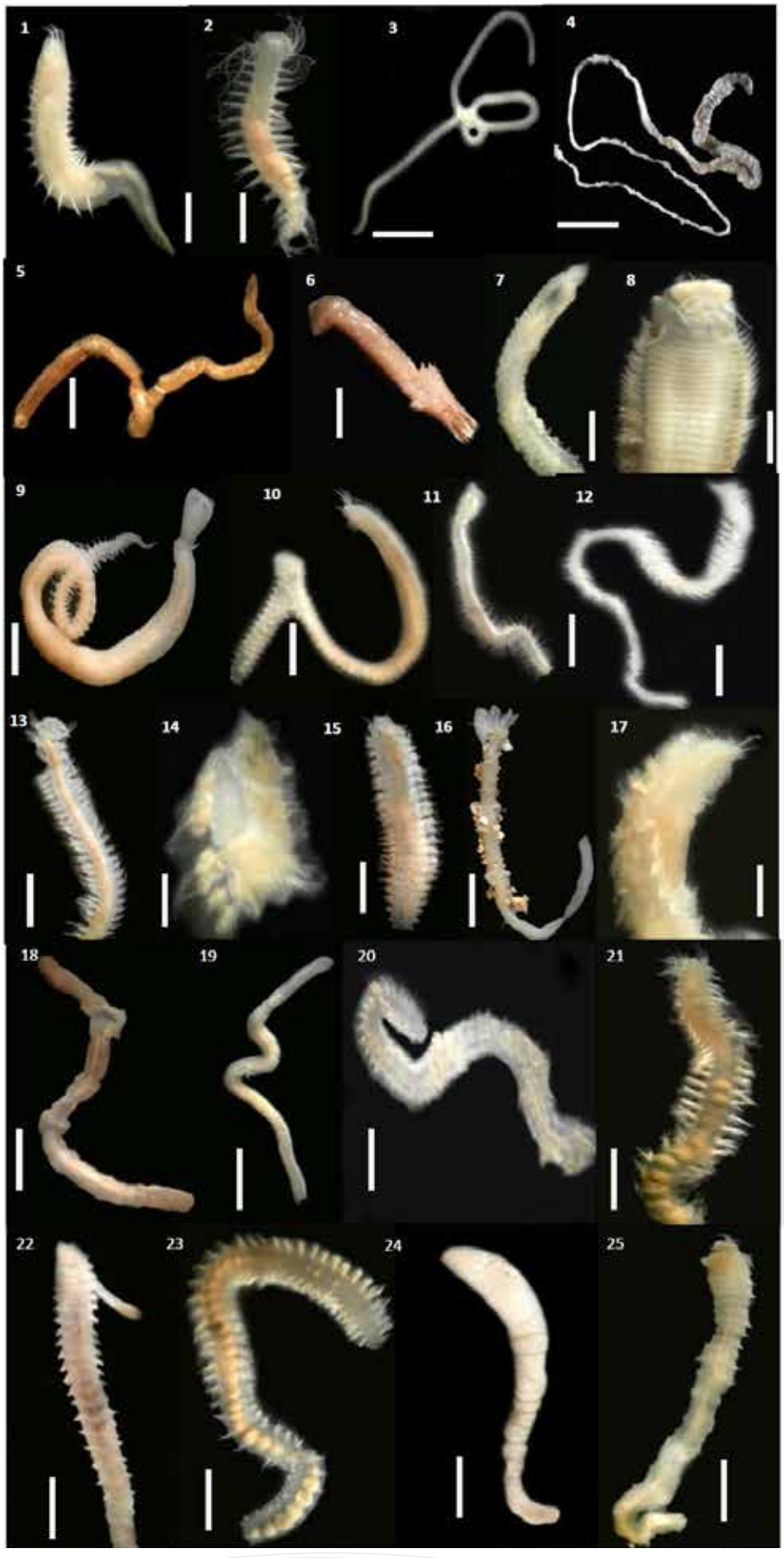

Figure 3. *Polychaetes:* 1) *Ampharete*, 2) *Leocrates*, 3) *Capitella*, 4) *Heteromastus*, 5) *Notomastus*, 6) *Lygdamis*, 7) *Eunice*, 8) *Marphysa*, 9) *Lumbrineris*, 10) *Glycera*, 11) *Nephtys*, 12) *Nereis*, 13) *Phyllodoce*, 14) *Harmothoe*, 15) *Lepidonotus*, 16) *Potamila*, 17) *Idanthyrsus* 18) *Maldane*, 19) *Scoloplos*, 20) *Paraonis*, 21) *Poecilochaetus*, 22) *Prionospio*, 23) *Spio*, 24) *Diplocirrus*, 25) Streblosoma. Scale bars= 1.5 mm

Conclusions

The recorded specimens comprised 25 taxa of polychaetes and some taxa of arthropods. Echinoderm and mollusks were removed because most are dead shells. Among the benthic fauna, polychaetes were the most dominant taxa from the present survey. Site 1 (26m depth) showed the highest abundance of benthic fauna (polychaetes) in terms of number and genera. In the present study, benthic production in terms of abundance and the number of genera low in deepwater stations. It can be stated that low diversity and a lower number of benthic fauna at deepwater stations indicate stress conditions because of destructive fishing activities and dredging. This study supports as baseline data for future monitoring programs in the area.

Acknowledgment

I am thankful to Dr Aung Myat Kyaw Sein, Acting Rector of Mawlamyine University, Dr. San San Aye, Pro-Rector of Mawlamyine University, for their encouragement and supports in preparing this work. I am very grateful to Dr. San Tha Tun, Professor, and Head of the Department of Marine Science, Mawlamyine University, for his valuable suggestions and constructive criticisms on this study. I am really thanks to Hnin Pwint Htwe, Mres, Department of Marine Science, Myeik University, for their assistance during identification and many helps in research works. Thanks are also due to many of Dr Naung Naung Oo and other colleagues in Department of Marine Science, Myeik University and Mawlamyine Unversity for their assistance and encouragement during this research work. Finally, I would like to thank my beloved parents and my dear brother for their physical, moral and financial supports throughout this study.

Bibliographic references

1. Cherry Aung. (2002). Distribution and abundance of meiofauna in shallow water of North Andaman Sea around Myanmar coast. Unpublished Departmental Research Paper. Department of Marine Science, Mawlamyine University, Myanmar.
2. Si Thu Hein. (2011). Study on polychaete diversity in some intertidal mud flat of Myeik area. Unpublished MRes Thesis. Department of Marine Science, Myeik University, Myeik, Myanmar.
3. War War Soe. (2013). Ecology of soft-bottom macrobenthic faunal communities in the intertidal zone of Myeik coastal areas. Unpublished PhD Dissertation. Department of Marine Science, Mawlamyine University, Mawlamyine, Myanmar.
4. Hlaing Hlaing Htoon (2016). A study on the intertidal benthos around the Dawei point with reference to the polychaetes. Unpublished PhD Dissertation. Department of Marine Science, Mawlamyine University, Mawlamyine, Myanmar.
5. Shannon, C. E. and Wiener, W. 1963. The mathematical theory of communication. University of Illinoise. Urban press, Illinoise, USA. 117 pp.
6. Pielou, E. C. 1975. Ecological diversity. John Wiley & Sons, INC, New York. 165 pp.
7. Margalef, R. 1958. Perspectives in ecological theory. University of Chicago press, USA. 111 pp.
8. Sheeba, P. 2000. Distribution of benthic infauna in the Cochin backwaters in relation to environment parameters. Unpublished PhD Thesis. Cochin University of Science and Technology.
9. Joydas, T. V. 2002. Macrobenthos of the shelf waters of the west coast of India. Unpublished PhD Thesis. Cochin University of Science and Technology.
10. Rosenberg, R. 1977. Effects of dredging operations on estuarine benthic macrofauna. Mar Pollu. Bull. 8 102-105.
11. Jones, G. and Candy, S. 1981. Effects of dreding on the macrobenthic infauna of Bontany Bay. Aug. J. Mar. Freshwater Res. 32: 379-398.

Received: 10 November 2020
Accepted: 10 February 2021

RESEARCH / INVESTIGACIÓN

Assessing sugarcane brown rust resistance using Image analysis

Yaquelin Puchades-Izaguirre[1], Mónica Tamayo-Isaac[1], Wilfre Abiche-Maceo[1], Reynaldo Rodríguez-Gross[1], María La O-Hechavarría[2], Mérida L. Rodríguez-Regal[2]

DOI. 10.21931/RB/2021.06.02.6

Abstract: Image analysis provides an accurate and precise method of pest evaluation. This work's objective was to compare the usefulness of the ImageJ® 1.43u image processor and visual estimation as methods to characterize brown rust lesions and estimate the resistance of new sugarcane cultivars. For this, leaves images of 10 cultivars were captured, and the parameters quantity, most regular size of the pustules, and leaf area affected were determined. The data were correlated with the eight control (standard) genotypes' evaluations to obtain a classification of disease resistance. The results showed that the software's determinations were the most accurate, although all the methods were reliable for rating the reaction to brown rust. Therefore, it is proposed to move away from visual disease assessment toward a system based on digital image analysis.

Key words: Sugarcane, brown rust resistance, Image analysis.

Introduction

In-plant pathology, accurate assessments of pest severity are essential to breed resistant and less susceptible plant cultivars, classify or rate cultivar resistance, correlate lesions with yield losses, calculate damage thresholds, determine the efficacy of pesticides and perform reproducible experiments. Although visual disease estimates provide a relatively quick and easy method, they are prone to inaccuracy, leading to incorrect conclusions[1].

Image analysis provides a more accurate and precise method of disease evaluation than visual estimation. Many software can be used for processing and provide a measure of severity, for example, ImageJ® and MATLAB. These are mainly used to compute the affected leaf area and the characteristics of the symptoms (size, quantity, etc.)[2].

The ImageJ® 1.43u program[3] is a Java-based open-source image analysis and processing tool that contains numerous features applicable to the measurement of disease severity. It has been used 9) to quantify the development of the Aspergillus *oryzae fungus*[4]; in the classification of insects[5]; for morphological and morphometric characterization of *Puccinia kuehnii* (Krüger)[6], and in the identification of the symptoms of ringspot and orange rust of sugar cane[7,8].

Brown rust from sugarcane is a disease widely distributed in most of the sugarcane areas of the world[9,10]. It is caused by the fungus *Puccinia melanocephala* Sydow & P. Sydow and is considered among the most important to the crop[11]. It is characterized by linear pustules, reddish to dark brown, on the underside of the leaf, and the percentage of affected leaf area varies depending on the resistance that cultivars offer to the pathogen[12].

In Cuba, disease resistance is a criterion for the selection of new sugarcane cultivars. From the above derives the importance of keeping the strategies of its evaluation updated. The evaluation methodology was recently modified, and a new scale containing new quantitative criteria (area with pustules and more frequent length of the pustules) was proposed[13]. The present work's objective was to compare the utility of the ImageJ® 1.43u image processor and visual estimation as methods to characterize brown rust lesions and to estimate the resistance of new sugar cane cultivars.

Methods

Field experiment: The trial was established in September 2018 with 10 cultivars of the 2007 series (C07-593, C07-594, C07-595, C07-596, C07-597, C07-598, C07-599, C07- 600, C07-601 and C07-602) and controls representing different categories of brown rust infection: PR980 (highly resistant, AR), Ja64-11 (resistant, R), SP70-1284 (moderately resistant, MR) , C88-380 (moderately susceptible, MS), C334-64 (MS), C323-68 (susceptible, S), My5514 (S), Ja60-5 (highly susceptible, AS), and B4362 (very highly susceptible, MAS)[13]. Controls are rating from 1 to 7 according to the different categories of brown rust infection from the most resistant to the most susceptible.

An experimental random block design with three replicates was used. Each experimental plot consisted of one row of 6 m in length with 1,6 m row spacing. As barriers of the experiments and every two cultivars, B4362 was planted to increase and homogenize the inoculum pressure.

Data collection

Evaluations were carried out between 3 and 5 months of age in the crop's plant cane cycle. In each plot, 2 cm^2 images were taken of the middle third of the leaf +3 of 10 sugarcane stems (Figure 1) with a conventional digital camera. The variables: quantity (CPUST) and most frequent length of the brown rust pustules (LPUST) were determined by visual estimation and ImageJ® 1.43u software. Figure 2 presents an example of image processing and determination of study variables.

Data analysis

The differences between the values of the CPUST and LPUST variables obtained through visual estimation and the ImageJ® 1.43u software were determined using factorial variance analysis and Tukey's multiple comparison test ($p < 0.05$).

The percentage of affected leaf area (PAPUST) was calculated using the equation:

Pustules / cm^2 (%) = PAPUST = (CPUST * LPUST * 0.38) / 2[13]. Additionally, this variable was recorded directly by computation in the ImageJ® 1.43u software (Figure 2). The results of the PAPUST variable obtained from: (i) calculation with the visual estimation variables, (ii) calculation with the variables

[1] Experiment Station for Sugarcane Research Oriente-Sur (ETICA Oriente Sur), Institute for Sugarcane Research (INICA), Santiago de Cuba, Cuba.
[2] Institute for Sugarcane Research (INICA), Carretera CUJAE, La Habana, Cuba.

Corresponding author: yaquelin.puchades@inicasc.azcuba.cu.

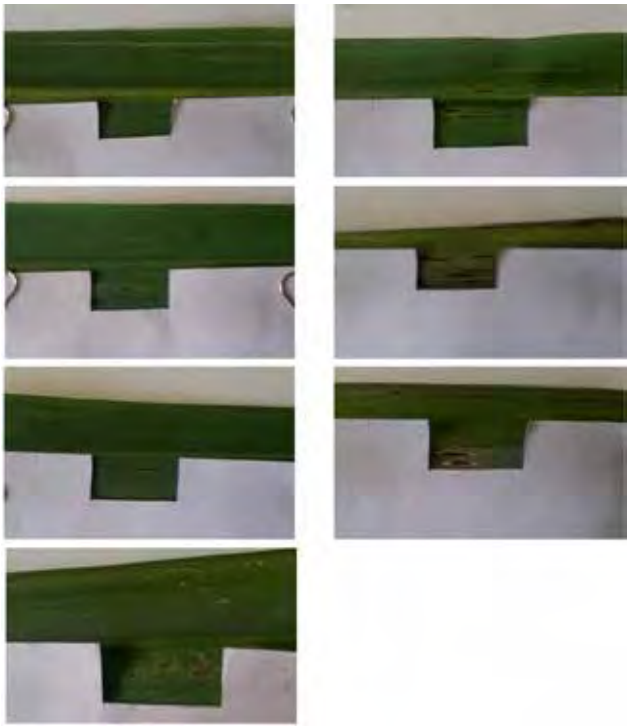

Figure 1. Images of 2 cm^2 of the middle third of the +3 leaf of different sugarcane cultivars affected by brown rust. Sample images from our dataset.

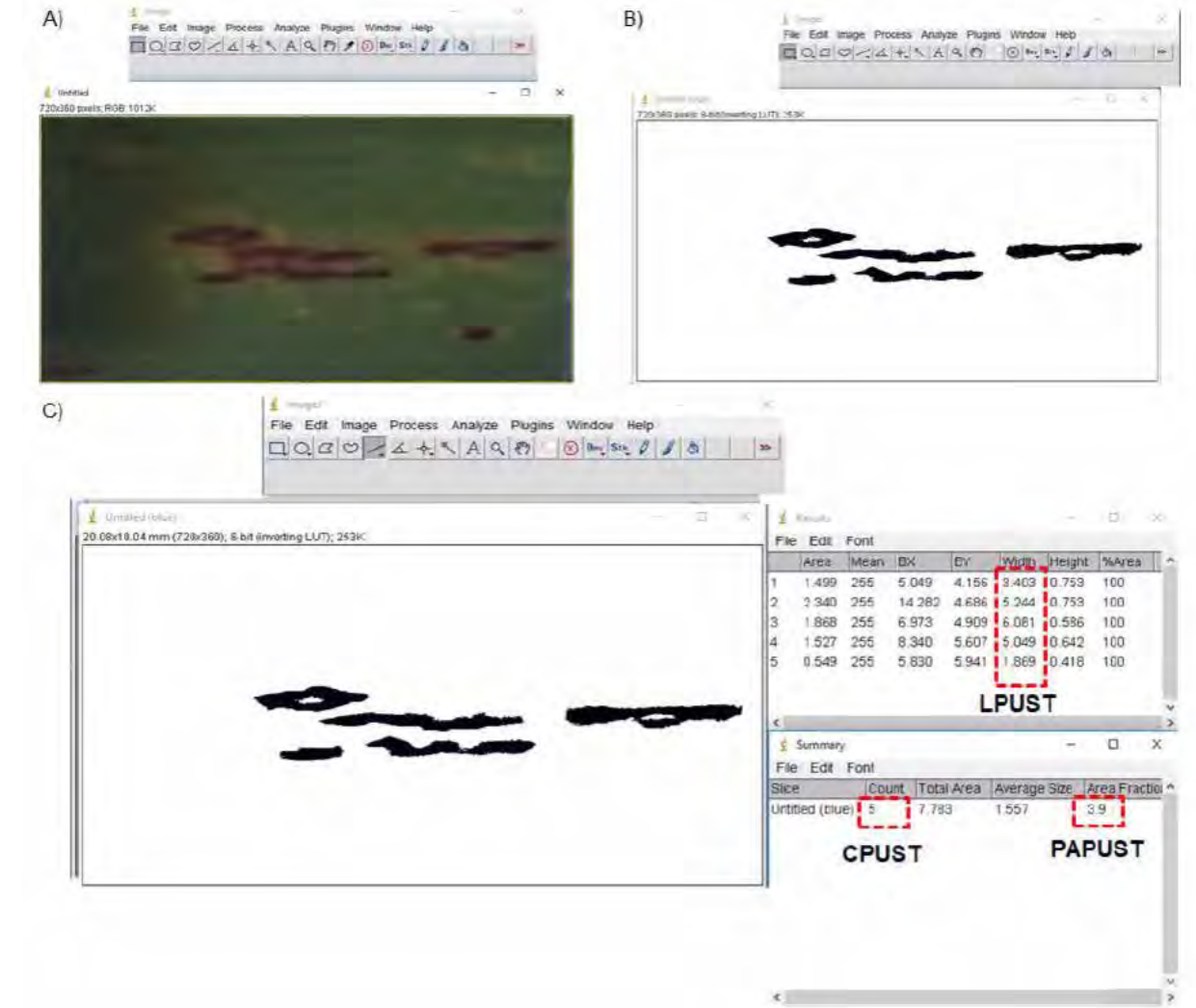

Figure 2. Example of image processing in ImageJ® 1.43u to determine the study variables (CPUST, LPUST y PAPUST). A) 2 cm^2 original image, B) binary processed image, C) determination of variables quantity (CPUST), most frequent length of the pustules (LPUST) and percentage of affected leaf area (PAPUST).

estimated by ImageJ® 1.43u, and (iii) direct computation of PAPUST by ImageJ® 1.43u were compared. The precision of the methods was estimated using the standard deviation, standard error, and repeatability statistics parameters.

The relationship between the percentage affected leaf area and the different rating degrees was verified by linear regression for the controls. The reliability of the results was determined using Pearson correlation between the means reported in the new methodology for brown rust evaluation[13] and those accounted for by the different methods used in the present work. The ratings of the new cultivars were calculated from the linear equations obtained in regression[14].

Results and Discussion

The variance analysis verified that there are very significant differences between the values of the variables LPUST and CPUST obtained both by visual estimation and by image analysis. The differences between cultivars are determined by their differential response to brown rust (Table 1).

The individual analysis observed fewer differences between the methods in determining the LPUST variable (Table 2). However, image processing measurements were more accurate based on a statistical analysis of standard deviation and standard error.

The comparison between the percentages of affected leaf area (PAPUST) calculated according different methods established very significant differences between cultivars and methods (Table 3). The determination of this variable is of great importance, and it is the basis of the new cultivar classification system due to the differential reaction of the sugarcane cultivars to brown rust.

More significant variability was observed in the PAPUST determinations made by visual estimation. The data offered directly by the ImageJ® 1.43u was more precise but very similar to that obtained when the CPUST and LPUST resulting of the software were used for the calculation. Repeatability confirmed the greater robustness of the determinations offered by ImageJ® 1.43u (Table 4).

The use of linear regression detected in all methods a significant relationship between the percentage of affected leaf area and the rating degrees assigned to the control cultivars (Table 5). The mathematical models obtained explained between 74 and 71% of the total variation of the data.

The correlation between the means of the percentage of leaf area affected by brown rust of the control cultivars, reported in the new methodology for brown rust evaluation[13] and those accounted by the different methods used in the present work, revealed the existence of a significant association in all cases (Table 6). This indicated that the results are consistent or coherent with each other. The determination coefficients (r2) for the image processing methods were higher than the visual estimate.

The resistance classification obtained by each method showed very similar results (Table 7). All new cultivars showed an intermediate reaction (moderately resistant or moderately susceptible) to brown rust, which indicates that they should be selected for extension in commercial areas for their agro-industrial potential managed appropriately in areas of the low incidence of the disease.

The results derived from this work demonstrate that the visual estimation presents a high degree of variation in evaluating the lesions caused by brown rust in sugarcane cultivars. This method used on a large scale is very time consuming, subjective and error-prone[15]. Automated analysis of digital images can overcome these problems without differing results.

Identifying new cultivars by their resistance to diseases is an essential step in any genetic improvement program. With this consideration, the application of image processing is a promising approach to overcome the drawbacks of visual estimation[16]. This method, accompanied by a suitable analysis algorithm, is objective and allows non-invasive measurements directly in greenhouses and fields.

To estimate the precision of the experiments, the repeatability statistic (h2) was included because it considers the variability by the treatments (methods) and not the variation of the experimental error. Traditionally, the coefficient of variation has been used to decide whether an experiment is reliable or not; however, it is closely related to the environmental mean and does not allow determining whether the differences are determined by genotype or experimental error[17,18].

The use of the Pearson's coefficient as an indicator of the experiment's quality was essential in deciding whether the data obtained is reliable and consequently whether or not to accept their validity. Similarly, linear equations allowed the estimation of varietal resistance. Australia uses a similar method to assign a reliability category to disease resistance trials in the sugarcane breeding program, thereby ensuring accuracy in the classification of new cultivars[14].

The modifications to the methodology for evaluating resistance to brown rust proposed in the genetic improvement program for sugarcane in Cuba included incorporating quantitative indicators in the measurement of symptoms of a disease to ensure the reliability of the results[13]. The present work verifies that, regardless of the method used to estimate the lesions, the cultivar classification results are consistent with each other, although with greater precision in those obtained through image processing.

Effect	DF†	LPUST‡		CPUST‡‡	
		MS§		MS§	
Cultivar (C)	17	23.47	**	194.89	**
Methods (M)	1	10.10	**	250.37	**
C x M	17	3.97	**	94.37	**
Observations	9	1.56	ns§§	26.05	*
Error	315	1.08		11.59	

† DF= degree of freedom

§ MS= medium square

‡ LPUST= most frequent length of the pustules

‡‡ CPUST= quantity of the pustules

** significant differences p<0.01,

§§ ns= non-significant differences

Table 1. Effect of determinations by visual estimation and image analysis on the quantity and most frequent length of the pustules in 18 sugarcane cultivar affected by brown rust.

Cultivar	CPUST‡‡				LPUST‡			
	Est-visual§		ImageJ§§		Est-visual§		ImageJ§§	
C07-593	0.02	b	3.10	a	0.50	b	1.64	a
C07-594	0.30	ns	0.90	ns	0.40	b	1.70	a
C07-595	0.02	b	1.80	a	0.50	b	1.29	a
C07-596	11.30	a	3.50	b	1.00	ns	1.27	ns
C07-597	0.02	b	6.20	a	0.02	b	0.93	a
C07-598	6.00	a	0.30	b	1.40	ns	0.87	ns
C07-599	0.01	ns	0.40	ns	0.10	ns	0.12	ns
C07-600	5.70	ns	4.10	ns	2.50	ns	2.50	ns
C07-601	0.10	ns	0.60	ns	0.02	ns	0.61	ns
C07-602	0.10	b	6.20	a	0.02	b	1.84	a
Controls								
B4362	18.50	ns	10.50	ns	6.50	ns	4.70	ns
C323-68	9.20	a	2.00	b	2.00	ns	1.73	ns
C334-64	8.80	ns	6.00	ns	1.90	ns	1.43	ns
C88-380	9.33	a	0.78	b	2.33	ns	1.66	ns
Ja60-5	10.78	a	4.50	b	2.89	ns	2.58	ns
Ja64-11	0.10	ns	0.10	ns	0.10	ns	0.13	ns
SP70-1284	4.60	ns	3.60	ns	2.00	ns	2.31	ns
My5514	6.50	b	3.80	b	1.40	b	3.52	a
PR980	0.00	ns	0.00	ns	0.00	ns	0.00	ns
Average	**4.53**		**3.26**		**1.71**		**1.16**	
Est. Desv	**5.57**		**4.46**		**1.51**		**1.61**	
Error	**0.42**		**0.33**		**0.12**		**0.11**	

Table 2. Average values of quantity (CPUST) and most frequent length of the pustules (LPUST) in 18 sugarcane cultivar affected by brown rust.

Different letters represent significant differences at $p < 0.05$ probability level.
§ Est-visual= visual estimation
§§ ImageJ= obtained directly as a feature of ImageJ® 1.43u software
‡ LPUST= most frequent length of the pustules
‡‡ CPUST= quantity of the pustules

Effect	PAPUST †		
	DF ‡	SM §	
Cultivar (C)	17	186.86	**
Methods (M)	2	97.76	**
C x M	34	30.57	**
Observations	9	8.68	**
Error	477	3.20	

Table 3. Effect of the determinations by visual estimation and image analysis on the variable percentage of leaf area affected (PAPUST) by brown rust in 18 sugarcane cultivars.

† PAPUST= percentage of affected leaf area
‡ DF= degree of freedom
§ MS= medium square
** significant differences $p<0.01$

Parameters	PAPUST†		
	C-Est-visual††	C-ImageJ§	ImageJ§§
Mean	2.17	1.6	1.52
Est. Dev	4.35	2.68	2.47
Error	0.33	0.2	0.18
Repeatability (h^2)	0.62	0.65	0.74

Table 4. Mean values, standard deviation and standard error of the variable percentage of leaf area (PAPUST) affected by brown rust of different methods used in its determination.

† PAPUST= percentage of affected leaf area
†† C-Est-visual= calculated using variables CPUST and LPUST recorded by visual estimation
§ C-ImageJ= calculated using variables CPUST and LPUST estimated by ImageJ® 1.43u.
§§ ImageJ= computed by ImageJ® 1.43u software.

Methods	Equation	r	r^2	p
Visual ††	PAPUST=2.8060 * Degree – 6.442	0.84	0.71	<0.05
C-ImageJ§	PAPUST=1.0546 * Degree – 2.355	0.85	0.72	<0.05
ImageJ§§	PAPUST=1.1458 * Degree - 2.638	0.86	0.74	<0.05

†† visual= percentage of affected leaf area was calculated using variables CPUST and LPUST recorded by visual estimation
§ C-ImageJ= percentage of affected leaf area was calculated using variables CPUST and LPUST estimated by ImageJ® 1.43u.
§§ ImageJ= percentage of affected leaf area was computed by ImageJ® 1.43u software.

Table 5. Linear models associated with the determination of the rating degree of the brown rust resistance in sugarcane cultivar.

Methods	r	r^2	EE r	p
Visual ††	0.95	0.90	0.13	<0.01
C-ImageJ§	0.97	0.95	0.12	<0.01
ImageJ§§	0.98	0.96	0.11	<0.01

†† visual= percentage of affected leaf area was calculated using variables CPUST and LPUST recorded by visual estimation
§ C-ImageJ= percentage of affected leaf area was calculated using variables CPUST and LPUST estimated by ImageJ® 1.43u.
§§ ImageJ= percentage of affected leaf area was computed by ImageJ® 1.43u software.
r= Pearson's correlation coefficient
r^2= determination coefficient
EE r= standard error
p= statistical significance

Table 6. Pearson's correlation coefficient between the percentage of leaf area affected by brown rust of the control cultivars reported in the new methodology (13) and those estimated by different methods.

Cultivar	Rating Degrees-Reaction					
	Visual ††		C-ImageJ§		ImageJ§§	
C07-593	3	MR	4	MS	4	MS
C07-594	3	MR	3	MR	3	MR
C07-595	3	MR	3	MR	3	MR
C07-596	4	MS	4	MS	3	MR
C07-597	3	MR	4	MS	4	MS
C07-598	3	MR	3	MR	3	MR
C07-599	3	MR	3	MR	3	MR
C07-600	4	MS	4	MS	4	MS
C07-601	3	MR	3	MR	3	MR
C07-602	3	MR	4	MS	4	MS

†† visual= percentage of affected leaf area was calculated using variables CPUST and LPUST recorded by visual estimation
§ C-ImageJ= percentage of affected leaf area was calculated using variables CPUST and LPUST estimated by ImageJ® 1.43u.
§§ ImageJ= percentage of affected leaf area was computed by ImageJ® 1.43u software.
MR= moderately resistant
MS= moderately susceptible

Table 7. Rating degrees and reaction to brown rust of 10 sugarcane cultivars estimated by different methods.

Conclusions

Image analysis has been employed in a novel manner to assess brown rust - sugarcane pathosystem to accurately compute characteristic disease lesion and classify new cultivars' resistance with more precision than visual estimation. Although the accuracy of visual scoring methods can be improved through scorer training and standard area diagrams and scales, a degree of variation and inaccuracy remains. Inaccuracies in disease assessment can lead to erroneous conclusions drawn; thus, any steps to improve accuracy should be taken. Therefore, it is proposed to move away from visual disease assessment toward a system based on digital image analysis, as outlined here. The method is simple to implement and is not computationally complex.

Acknowledgment

The authors are grateful for the financing support and facilities provided by the Oriente Sur Experiment Station (ETICA Oriente Sur) of the Institute for Sugarcane Research (INICA) for the realization of this research that is part of the project entitled "Updating of methodological procedures for pest resistance evaluation in sugarcane cultivars " ((PROY- 0097-003-002-044).]

Bibliographic references

1. Parker, S. R., Shaw, M. W., Royale, D. J. Measurements of spatial patterns of disease in winter wheat crops and the implications for sampling. Plant Pathol., 1997; 46:470-480. doi: 10.1046/j.1365-3059.1997.d01-38.x
2. Bock, C. H., Poole, G. H., Parker, P. E., Gottwald, T. R. Plant disease severity estimated visually, by digital photography and image analysis, and by hyperspectral imaging. Crit. Rev. Plant Sci., 2010; 29:59-107. doi: 10.1080/07352681003617285
3. Schneider, C.A., Rasband, W.S., Eliceiri, K.W. NIH Image to ImageJ 25 Years of Image Analysis. Nature Methods, 2012; 9: 671-675. doi: 10.1038/nmeth.2089.
4. Barry, D.J., Chan, C. Williams, G.A. Morphological quantification of filamentous fungal development using membrane immobilization and automatic image analysis. Journal of Industrial Microbiology & Biotechnology, 2009; 36(6): 787-800. doi: 10.1007/s10295-009-0552-9.
5. Gimmen, J. Garcia, S. Generating Color Vignettes and Metadata for Insect Auto-Classification. In: Proceedings of The National Conference on Undergraduate Research (NCUR). Weber State University, Ogden Utah, University of Guam, Mangilao, GU 96923, USA, March 29 – 31, 2012: 505-509. http://ncurproceedings.org/ojs/index.php/NCUR2012/article/download/126/77
6. Tamayo, M., Puchades, Y., Hechavarría, M., Rodríguez, R., Chacón, V., Alfonso, I. Caracterización morfológica y morfométrica del organismo causal de la roya naranja de la caña de azúcar. Cuba & Caña, 2014; 1: 12-16.
7. Aday, O. C., González, R., Díaz-Mujica, F. R., Reyes, C., Gil, Y., Reyes, S., Barroso, J. Aplicación del software ImageJ® 1.43u en la caracterización de los síntomas de la mancha anular de la caña de azúcar. Centro Agrícola, 2017; 44(2): 83-88. http://cagricola.uclv.edu.cu
8. Aday, O. C., Alfonso, I., Rodríguez, E., Díaz-Mujica, F. R., Gil, Y., Váldes, B. L., Barroso, J. Caracterización de los síntomas de la roya naranja (Puccinia kuehnii (W. Kruger) E. J. Butler) en cuatro cultivares de caña de azúcar en Cuba. Centro Agrícola, 2017;44(2): 61-67. http://cagricola.uclv.edu.cu
9. Rott, P., J. Girard, J.C. Comstook. Impact of pathogen genetics on breeding for resistance to sugarcane diseases. Proc. Int. Soc. Sugar Cane Technol., 2013; 28: 1–11. http://www.issct.org/proceedings/2013.html
10. Huang, Y.K., W.F. Li, Zhang, R.Y., Wang, X.Y. Color Illustration of Diagnosis and Control for Modern Sugarcane Diseases, Pests, and Weeds. China Agriculture Press and Springer Nature Singapore Pte Ltd., 2018; 18–20. https://doi.org/10.1007/978-981-13-1319-6
11. Peixoto Jr., R.F.; Figueira, A.V.O.; Landell, M.G.A.; Nunes, D.S.; Pinto, L.R.; Sanguino, A. Development and characterization of microsatellite markers for Puccinia melanocephala, causal agent of sugarcane brown rust. Proc. Int. Soc. Sugar Cane Technol., 2013; 28: 1-4. http://www.issct.org/proceedings/2013.html
12. Raid, R.N., Comstock, J.C. Common rust. In: A guide to sugarcane diseases. Rott, P., Bailey, R.A., Comstock, J.C., Croft, B.J., Saumtally, A.S. (Eds) CIRAD and ISSCT CIRAD publications, Montpellier, France, pp 85-88.
13. Montalván, J., Alfonso, I., Rodríguez, E., Puchades, Y., Rodríguez, J., Aday, O., Carvajal, O., Delgado, J. Evaluación de la resistencia a roya parda de la caña de azúcar en Cuba. Centro Agrícola, 2018; 45(2): 47-54. http://cagricola.uclv.edu.cu
14. Stringer, J., Croft, B., Bhuiyan, S., Deomano, E., Magarey, R., Cox, M., Xu, X. A new method of statistical analysis for disease screening trials. Proc. Aust. Soc. Sugar Cane Technol., 2012; 34: 6 p. https://espace.library.uq.edu.au/view/UQ:f30daf2
15. Stewart, E. L., McDonald, B. A. Measuring quantitative virulence in the wheat pathogen Zymoseptoria tritici using high-throughput automated image analysis. Phytopathology, 2014; 104:985-992. doi: 10.1094/PHYTO-11-13-0328-R.
16. Thomas, S., Behmann, J., Steier, A., Kraska, T., Muller, O., Rascher, U., Mahlein, A. K. 2018. Quantitative assessment of disease severity and rating of barley cultivars based on hyperspectral imaging in a non-invasive, automated phenotyping platform. Plant methods, 2018; 14, 45. doi:10.1186/s13007-018-0313-8
17. Yan, W., Holland, J. B. A heritability-adjusted GGE Biplot for test environmental evaluation. Euphytica, 2010; 171:355-369. doi: 10.1007/s10681-009-0030-5
18. Gordón-Mendoza, R., Camargo-Buitrago, I. Selección de estadísticos para la estimación de la precisión experimental en ensayos de maíz. Agron. Mesoam., 2015; 26(1):55-63. doi 10.15517/am.v26i1.16920

Received: 30 November 2020
Accepted: 15 january 2021

RESEARCH / INVESTIGACIÓN

Injury patterns among road traffic accidents: a hospital-based study in Ecuador

Aline Siteneski[1,2*], Leonardo D. Jalca Cantos[2], Emily P. Calderón Delgado[2], Ruth M. Yaguache Celi[2], César A. Silva Saltos[2], Angel Zamora[2], Mónica Mastarreno[2], Diego Portalanza[3]

DOI. 10.21931/RB/2021.06.02.7

Abstract: Traffic accidents are serious public health problems, account for profound economic costs to individuals, families, and societies. The social impacts range from physiological to economic causes, which could be a serious negative effect, especially in undeveloped countries. To further elucidate this problem, the prevalence of injuries caused by traffic accidents in a Santa Ana Health Centre, Portoviejo, Ecuador, was studied. This registry-based retrospective study analyzed data on Santa Ana, from Enero 2016 to Diciembre 2019, and the medical records of patients who had been admitted were extracted and analyzed. Passengers cars, motorcycles, and bicycles involved in collisions were included, and the information collected was relating to sex, age, and type of injuries. In total, 75%±6.34 patients victims of road traffic injuries were males, and their mean age was 20 and 49 years. There was a cooperative agreement between total injury occurrence (%) and type of vehicle. Bus and car accidents had lower relation (R^2 = 0.44, 078) (p = 0.063, 0.005) with total occurrence. The highest relation was found in motorbikes (R^2 = 0.98 p = 2e-05), since it's the primary or most popular means of transportation in the city. The best of our knowledge is the first study to reporting data on road traffic injuries in the Province of Manabí, the third-largest province in extension in Ecuador. Additional studies with larger populations are thus necessary to construct a robust data system in undeveloped countries that can facilitate the flow of reliable information about road traffic injuries.

Key words: Road traffic injuries, Traumatic brain injury Polytrauma, Ecuador.

Introduction

Traffic accidents are serious public health problems, account for profound economic costs to individuals, families, and societies[1]. The estimated global annual rate of road traffic deaths of about 17.4 per 100000 population[2]. in low-and-middle-income countries, despite owning just about 54% of the world's motor vehicles, is predicted to move from the current eighth to the sixth leading cause of death by the year 2030[3]. It is suggested that for every one road traffic accident-related death, an additional 20–50 more individuals suffer some disability[4,5]. Road traffic injuries are also the leading cause of years of potential life lost, according to the global burden of disease study[6,7]. The severity is represented through the dates of 2016 when motor vehicle collision was responsible for 1.35 million fatalities globally, and these numbers are continuously increasing[8].

Data showed that almost 50% of global road traffic deaths occur among vulnerable road users, as motorcyclists represent 23 %, followed by pedestrians 22 %, and cyclists 4 %[9]. Additionally, it is worth mentioning that early mortality and disability are attributable to young adults (between 15–44 years). More than 460.000 young people under 30 years die in road traffic crashes each year, about 1262 a day and, more than 75 percent of the deaths occur mostly among low- and middle-income countries[10]. Any complications resulting from road traffic injuries contribute to the lengthened hospital occupancy, increasing costs, and mortality. Polytraumatizm is one of these complications, with rates descript up to 60%[11,12]. Immobilization, limited immunologic response, emergency interventions, and frequent mechanical ventilation are the causes of this high complication rate; abrupt and primary trauma deaths are determined by significant brain injuries or significant blood loss (hemorrhagic shock). In contrast, late mortality is caused by minor brain damages and host defense failure[3–15]. Both poly traumatism and traumatic brain injuries are increasing as motor vehicles are more widely used in developing countries[16,17].

In low-and middle-income countries, the scarcity of adequate medical care, rehabilitation services, and protection mechanisms aggravate problems. Road traffic injuries can include pedestrian, bicycle, or motor vehicle as a motorcycle, bus, or car whose collision involves at least one moving vehicle that occurred or originated on a road or street open to public traffic and resulted in one or more people being killed or injured[18,19]. The resultant misfortune deaths or disabilities can take a heavy toll on families and friends, who frequently are obliged to dispense from work to dedicate themselves to the patient's care[5]. Similarly, all patients and families suffer adverse financial debts because of the costly rehabilitation services and reduced income, physical discomfort, social and emotional strains[20,21]. It is worth stating that due to the high costs associated with road traffic injuries related to patients' incapacity, governments have been adopting public politics to reduce these events. Equally, the road safety management, safer roads and mobility, safer vehicles, safer road users, and postcrash care[22,23].

According to the World Health Organization (WHO), there is a need for more research on epidemiologic accident patterns in low and middle or low-income countries to determine the problem's dimensions and identify vulnerable individuals. The health sector needs to expand its traditional caregiving role and be involved in areas relevant to promoting road safety, such as data collection, support, policy development, and capacity development[2,9,10]. Determining the type of injury, the vehicle involved, and the risk group through the system by collecting information may be valuable key elements not identifying and assessing preventive actions. Those measures have critical clinical implications concerning these patients' care prevent traffic fatalities in middle or low-income countries[1,24,25]. In Ecuador, according to the National Traffic Agency (NTA), the

[1] Research Institute, Technical University of Manabí, Portoviejo, Ecuador.
[2] Faculty of Health Sciences, Medicine Career, Technical University of Manabí, Portoviejo, Ecuador.
[3] Federal University of Santa Maria, Department of Physics, Climate Research group, Brazil.

Corresponding author: aline.siteneski@gmail.com

annual record of misfortunes has been decreased in the last four years, but for Manabí Province, this number was increased[26,27]. In this sense, the present work's objective investigated road traffic injuries in the Santa Ana health Centre in Ecuador.

Methods

Patients and variable description

The observational study was a retrospective analysis of the data from a health center-based database of Santa Ana in Ecuador, belonging to Portoviejo city, Manabí (Figure 1). The data from Santa Ana were recorded from 2016 until 2019 by the Technical University of Manabí (UTM) medicine students, all traffic accident injuries were registered. The inclusion criteria for the study were no fatal patients. Collected information on the variables were type and injury mechanisms: polytrauma, brain injuries, gender, age, and type of vehicle involved (motorcycle, bicycle, car, or bus) during 4 years (2016-2019).

Variable analysis

To understand the relation between the obtained data, an exploratory data analysis (EDA) was performed. First, we plotted boxplots for all types of vehicles (TOV) (bike, bus, car, and motorbike) and injuries (TOI) brain injury (TB), polytrauma (POL), upper limb fracture (ULF), lower limb fracture (LLF), spinal, chest and abdomen injury (SCA), facial injuries (FI), superficial injuries (SI) and dislocations (DIS) for4 years (2016-19). Second, we divided TOV and TOI into years to understand year-to-year variations. A boxplot is a standardized way of displaying the data set based on a five-number summary: the

Figure 1. The figure represents the study area in Santa Ana, Manabí Province, in Portoviejo, Ecuador.

minimum, the maximum, the sample median, and the first and third quartiles[28,29]. We use the interquartile range (IQR) to compare variables using the following equation (Eq 1)

$$IQR = Q3 - Q1 = q_n(0.75) - q_n(0.25) \quad (1)$$

Were *IQR* is the interquartile range, *Q3* is the third quartile, *Q1* is the first quartile, q_n *(0.75)* is the upper quartile, and q_n *(0.25)* is the lower quartile. Third, to show the spread of positive and negative values from TOI, a diverging chart was performed based on the total number of years. Preparation of the data as follows:

a) Compute normalized values, to create central, positive and negative divergence (Eq. 2):

$$N_v = \frac{Q - Q_{mean}}{Sd_{Q_i}} \quad (2)$$

Were N_v being the normalized values, *Q* are single value observation, Q_{mean} is the value mean, *Sd* is the standard deviation, and Q_i are the total observations[30]. Fourth, density histograms were plotted to represent the visualization of the variations within TOV and TOI. For this, using equispaced breaks (x=observed values) and estimated density values (y= relative frequencies) as follows (Eq. 3)

$$\sum_i f(x_i)(b_{i+1} - b_i) \quad (3)$$

The number of breaks and *f(x)*[31] is the estimated density value[32]. Finally, to represent gender and age groups differences, we used a population pyramid[33] in which ages were divided into groups (1 – 4 years, 5- 9 years, 10 – 14 years, 15 – 19 years, 20 – 49 years, 50 – 64 year and > 65) using ranges from the Ecuadorian Nacional Survey Institute (INEC)[34]. Finally, the total relative frequency was correlated with the type of vehicle using linear regression; for this, we calculate the coefficient of determination (R^2), slope, and intercept.

$$R^2 = \frac{n(\sum xy) - (\sum x)(\sum y)}{\sqrt{[n\sum x^2 - (\sum x)^2][\, n\sum y^2 - (\sum y)^2 \quad]}} \quad (4)$$

R2 is the coefficient of determination, x is the frequency value for total injuries per type of vehicle, and y is the vehicle's total frequency. All plots and calculations were performed using RStudio version 1.2.5033[35,36] using stats package. Density histograms and boxplots were plotted using the ggplot2 package for R[37].

Compliance with ethical standards

Personal identifiers had already been removed from the study. Because of this study's anonymous and retrospective nature, the need for informed consent was waived by the Ethics Committee that approved the study Protocol.

Results

Type of injuries comparisons between the four years

The highest traffic accident injury incidence during the studied period (2016-2019) is shown in figure 2a and 2b. In the first year, 45% of the patients suffered a traumatic brain injury (considered mild, moderate, and severe), poly traumatism (estimated as mild, moderate, and severe), which represented 35%, and 10% cases of lower extremity fracture (equivalent to the tibia, fibula, malleoli, patella, pelvis, anterior cruciate ligament, and metatarsus), open upper extremity wound (associated with the radius and ulna), open upper extremity wound (radius and ulna), lower extremity (considering tibia and metatarsus) corresponding to 5% in each of the cases respectively. In the second year of study, poly traumatism corresponding to 32.26%, traumatic brain injury corresponding to 25.81%, fracture of the lower extremity equivalent to 21.51%, 5.38% upper extremity (associated with carpus, radius, ulna, humerus and clavicle), FI corresponding to 4.30% (related to fracture of the upper jaw, eye injury, eyebrow injury, fracture of the bones of the face and nose) and fracture of the spine, chest, and abdomen representing 4.30%, open lower extremity wound equivalent to 3.23%, superficial injury (corresponding to multiple lacerations) with 2.15% and dislocation (upper and lower limb) with 1.08%. In the third year of the study, we found a high multiple trauma percentage (48.75%) and traumatic brain injury (21.25%), followed by LLF (12.50%), upper limb (8.75%), open lower limb, and FI (3.75% each group) and dislocation (1.25%). Finally, in 2019, we found traumatic brain injury and polytrauma (18, 25% respectively) as the leading cause of injury, followed by superficial injury (22%) LLF (14%) ULF (8 %), spine injury, chest and abdomen (6%), face injury (3%), and dislocation (5%).

Type of vehicle comparisons between the years of the studied period

Four motor vehicle types were recorded (motorcycle, bicycle, car, and bus) associated with road traffic accidents. (Figures 3a and 3b). In 2016, it was observed that the frequencies of victims were high in motorcyclists (represented 75% of the cases), followed by car users (25%). Later, in 2017, road traffic accidents represented by motorcycles, cars, and buses were 78.49%, 17.20%, and 4.30%, respectively. Statistics for 2018 shown that 85% of accidents were motorcycles, 13.75% automobiles, and 1.25% bicycles. Decisively, in 2019 was observed 83% of motorcyclists, followed by 11% cars, buses (5%), and cyclists (2%).

Age and sex comparisons

From 2016 to 2019, the prevalence of road traffic injuries was recorded mainly in men and was gradually increased over the years, reaching its highest record in 2017 (75% in the first year, 81.72%, 80 and 75.38% respectively, of the total data of 258 investigated patients). The predominant age of the victims was between 20 and 49 years.

Type of vehicle and trauma relation

The Odds Ratio (OD) represent the type of injury and type of vehicle were descript in table 1 OR were > 1 showing a positive association between motorcycles or cars and all kinds of injuries. Total cases per type of trauma were represented in Figure 4. There was a cooperative agreement between total injury occurrence (%) and vehicle type (Figure 5). Bus and car accidents had lower relation (R^2 = 0.44, 078) (p = 0.063, 0.005) with total occurrence. The highest relation was found in motorbikes (R^2 = 0.98 p = 2e-05), since it's the primary or most popular means of transportation in the city.

Discussion

The present study found that road traffic accidents were more frequent in motorcyclists of young men. Besides, we

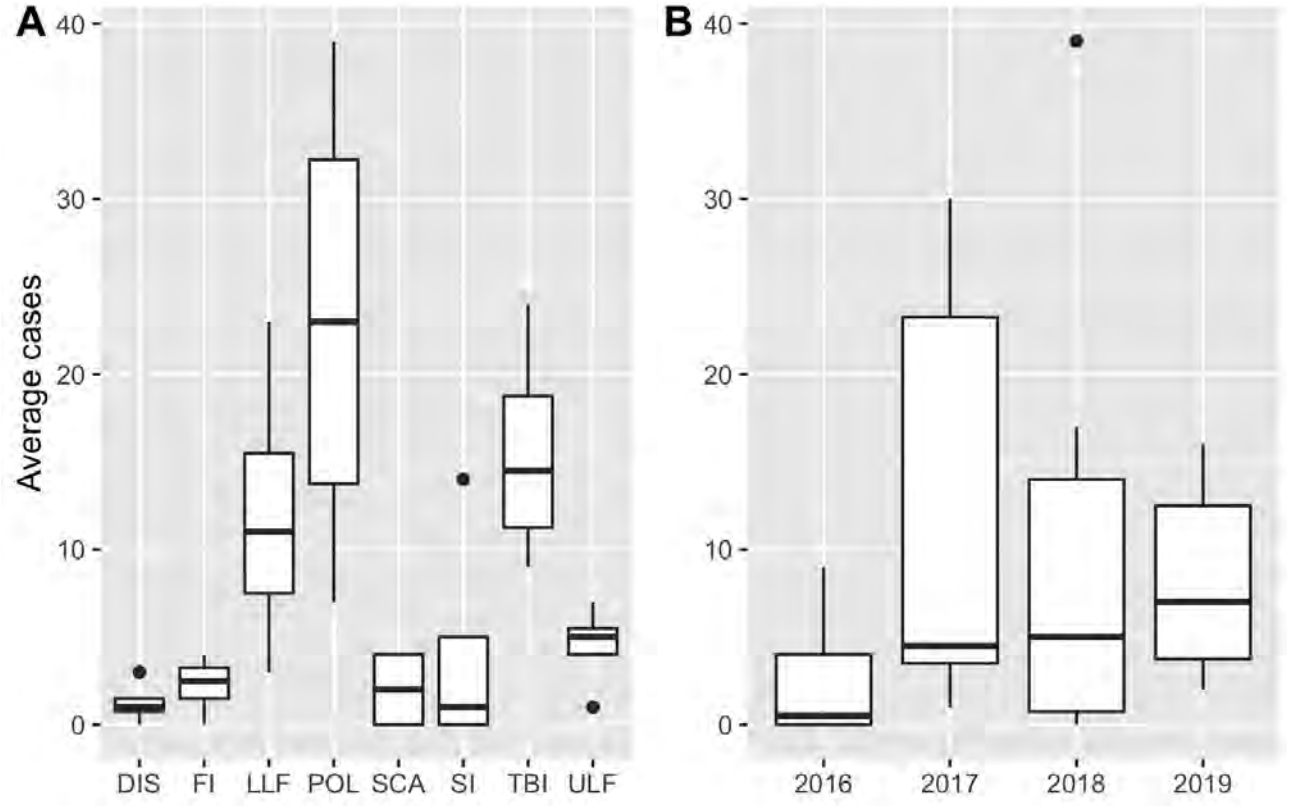

Figure 2. Prevalence of cases per type of vehicle and average of occurrence over time. The number of cases per type of injury (TOI) (a) and yearly average of occurrence (b) boxplot. Boxes represent values between the 25th and 75th percentile. Lines represent the median, and the dots represent the outliers.

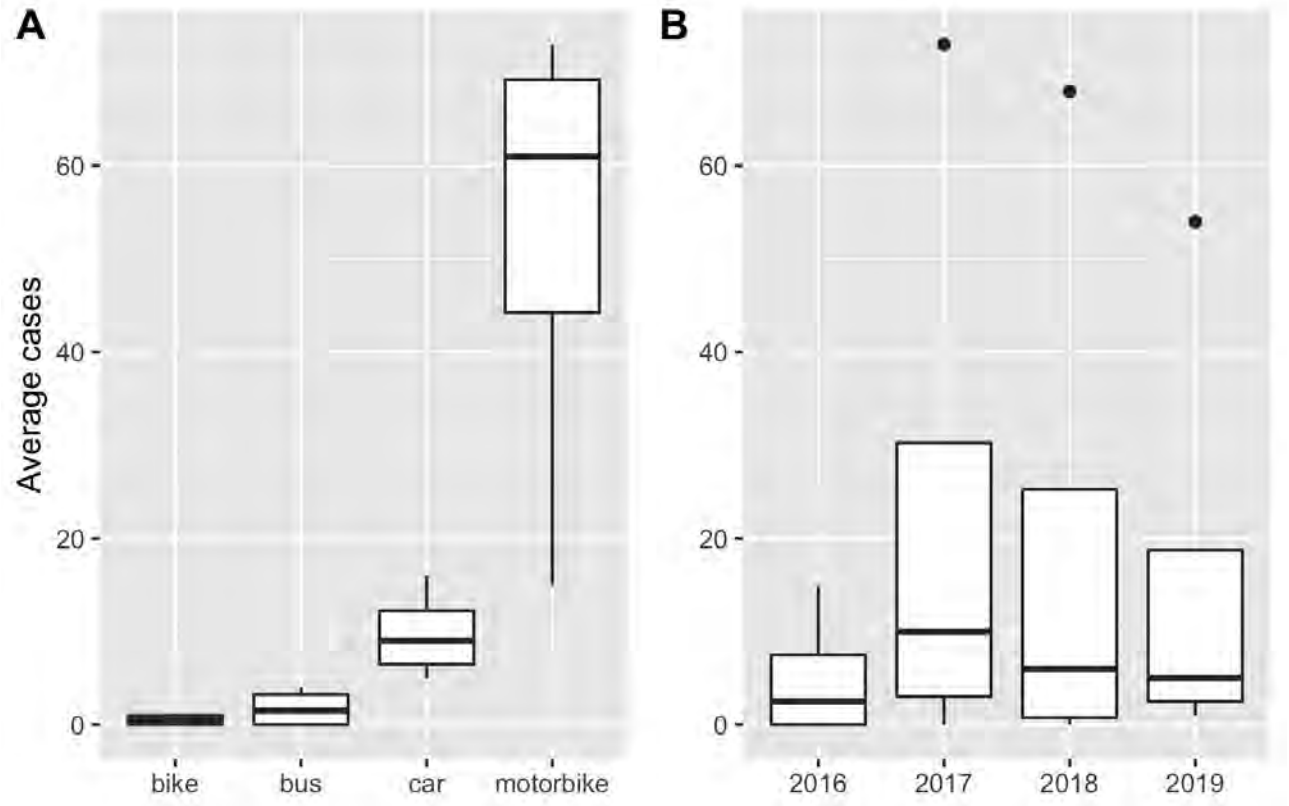

Figure 3. Prevalence of cases per type of vehicle and average of occurrence over time. The number of cases per type of vehicle (TOV) (a) and yearly average of occurrence (b) boxplot. Boxes represent values between the 25th and 75th. Lines represent the median and the dots represent the outliers.

	OR	C.I (lower)	C.I (upper)	*p value*
FI	0.1610	0.0047	1.8363	0.2451
LLF	0.4932	0.0915	2.9647	0.3995
POL	0.5969	0.1170	3.4318	0.6760
SCA	0.1783	0.0051	2.0553	0.2500
TBI	0.1153	0.0182	0.7683	0.0252
ULF	0.1966	0.0244	1.4923	0.1010
DIS	0.2902	0.0435	2.0914	0.2828
Car	0.2116	0.0328	1.2039	0.0694
Motorbike	0.1917	0.0342	0.9496	0.0381
	RR	**C.I (lower)**	**C.I (upper)**	***p value***
FI	0.2121	0.0272	1.6564	0.2451
LLF	0.6282	0.2392	1.6498	0.3995
POL	0.7241	0.2912	1.8007	0.6760
SCA	0.2333	0.0301	1.8066	0.2500
TBI	0.1768	0.0532	0.5873	0.0252
ULF	0.2800	0.0716	1.0945	0.1010
DIS	0.3758	0.1188	1.4325	0.2828
Car	0.3684	0.1514	0.8964	0.0694
Motorbike	0.3500	0.1745	0.7022	0.0381

Table 1. Odds and risk ratios for the type of injury and type of vehicle.

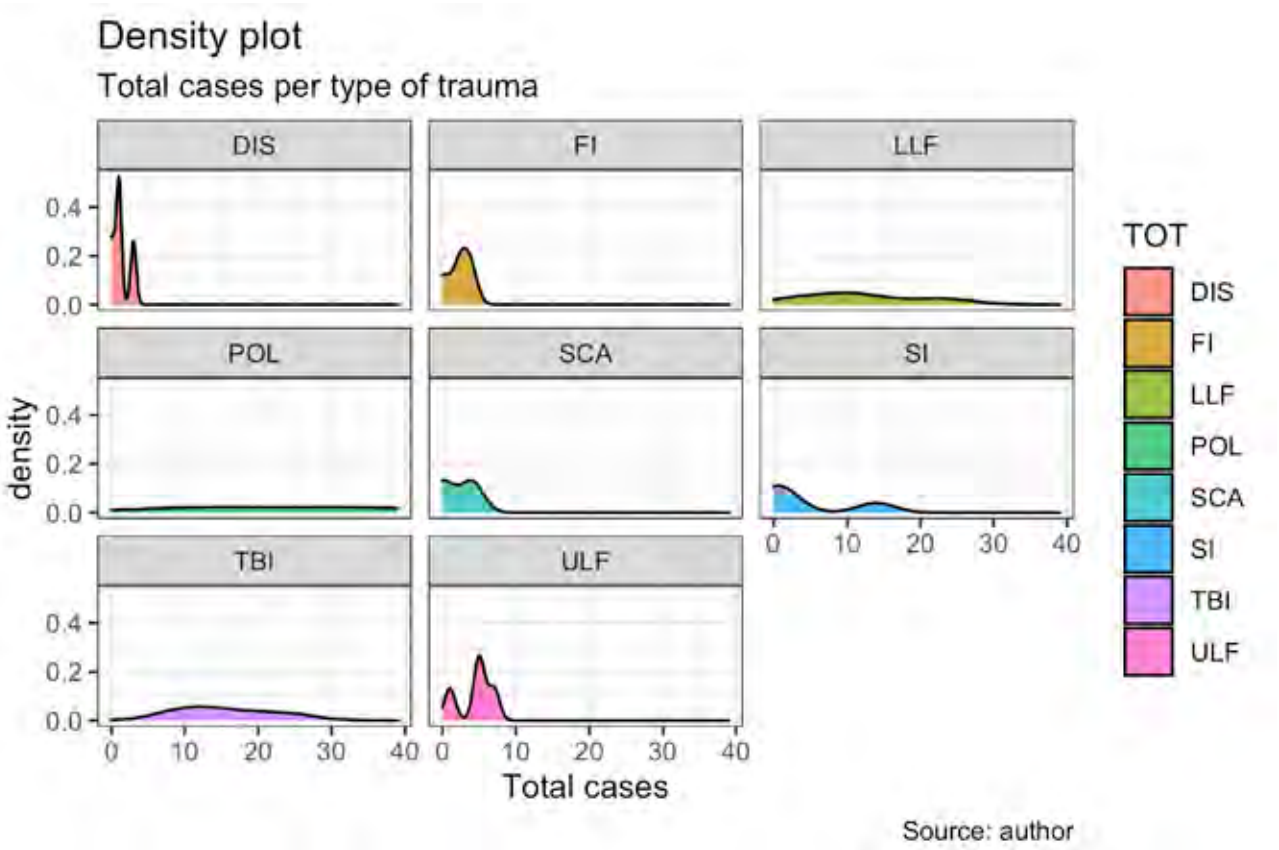

Figure 4. Density histogram represents the type of trauma for all years of study. (a)Type of trauma density histogram; (brain injury (TB), polytrauma (POL), upper limb fracture (ULF), LLF (lower limb fracture), spinal, chest, and abdomen injury (SCA), FI (face injury), superficial injuries (SI) and dislocations (DIS) for all years, (b) Normalised diverging bars for total counts (incidents) for TOI. *relative values.

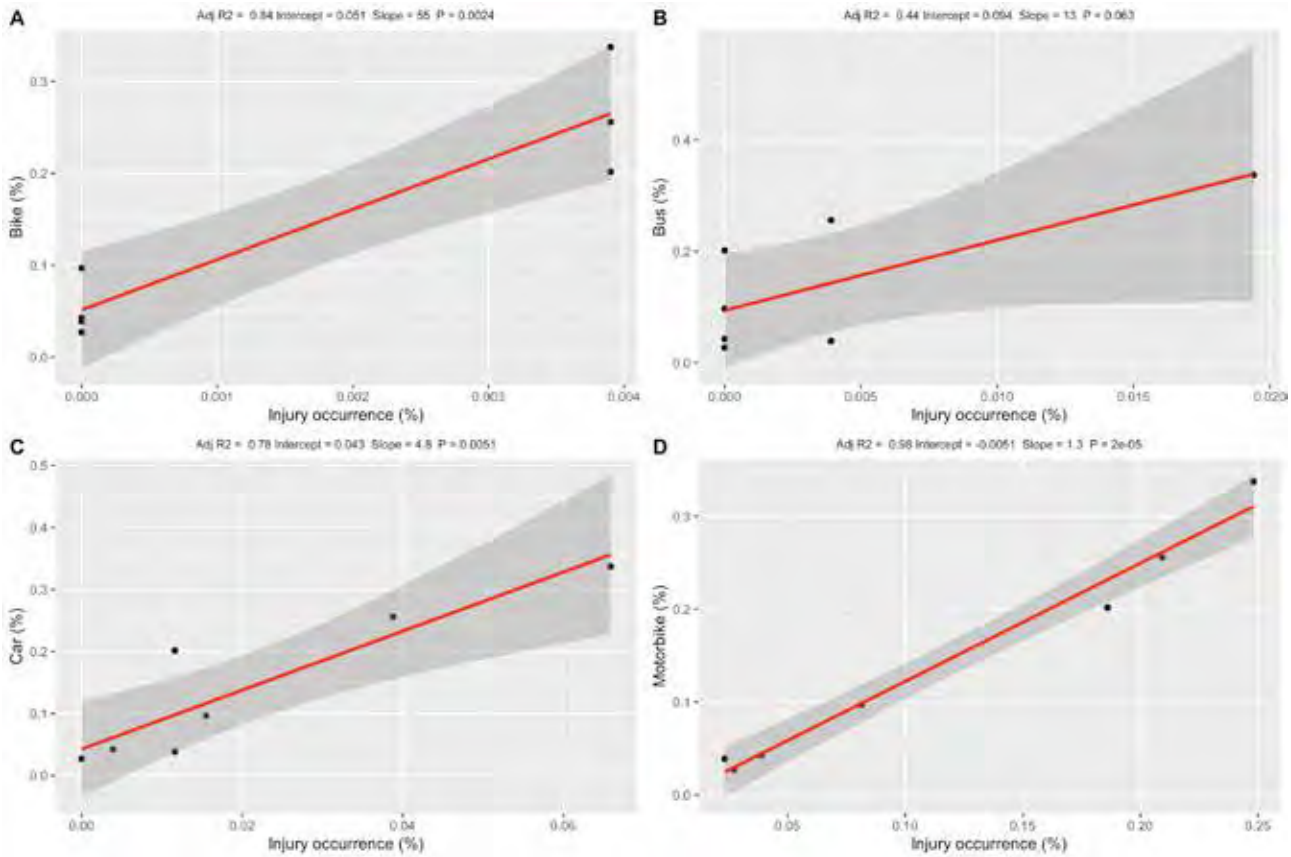

Figure 5. General linear regressions indexes for total injury occurrence and a) bike, b) bus, c) car, and d) motorbike accidents.

showed that the most affected age group was 20 to 49 years old, while also the more common type of lesion was poly traumatism followed by traumatic brain injuries. The number of road traffic accidents in Ecuador, specially Manabí province, increased during the study period (four years) 38. In the world, road traffic injuries are reported as the leading cause of death among young people aged 15–29 years and are among the top three causes of mortality among people aged 15–44 years 39, 40. To the best of our knowledge, it is the first to report data on road traffic injuries in the province of Manabí, third-largest province in extension in Ecuador.

Several lines of evidence have indicated that motorcycles are considered the most dangerous form of motorized transportations, and the risk of its accidents is further heightened by poor road conditions coupled with busy roads. Even though motorcycles are one of the private transport used extensively in many countries because of their affordability, motorcycles are the most unsafe form of motor-powered transportation[41]. Considering its easy maneuverability and speed, victims of motorcycle crash undergo more movement and impact and sustain more severe injuries. In our study motorcyclists, were most vulnerable to road traffic injuries; young patients constituted the vast majority of injured motorcyclists. Nearly half of all global road traffic deaths are among pedestrians and motorcyclists, mostly occurring on urban roads[10]. Pedestrians are the most vulnerable road users, making up to 22% of the annual global road traffic deaths in low and middle-income countries, followed by motorcyclists, pedal cyclists, and car occupants[4]. In a country like Ecuador, where a substantial portion of road users are motorcyclists, our results reinforce the importance of the vital necessity to implement effective local policies to reduce injury risk associated with motorcycles. Education campaigns promoting safe riding habits and behavior and helmets must be implemented to reduce motorcycle casualties[24,41]. Introducing and enforcing the use of motorcycle helmets can reduce death risk by 40 percent and the risk of severe head injuries by more than 70 percent[42], so the use of helmets has the potential to reduce road traffic injuries and deaths substantially and the associated personal and societal costs.

Although an increase of technological advancements and road improvements has been made to avoid motors vehicle accidents and reduce occupants' injury severity of occupants[43], we found that car accident were the second cause of road traffic injuries in Santa Ana Health Centre Ecuador. Motor vehicle collision is predicted to become the fifth most common cause of fatalities globally by 2030[5] and the first cause of death in developed countries[44], while in low and middle-income countries, most of the victims are cyclists and motorcyclists[39,44]. Therefore, it is recommended that all countries more significant efforts to decrease car fatalities. In the years between our study periods, laws requiring seatbelt usage in rear seats and strengthened fines for drunk driving were established to reduce car accidents in Ecuador. The use of a safety seat belt might be responsible for reducing car accidents for an extended period. Road traffic law in Ecuador was revised so that rear-seat passengers were required to wear a seatbelt, in addition to four-wheeled vehicle drivers and front-seat passengers. Previous studies showed the advantage of wearing a rear seatbelt in dropping the risk of motor vehicle crash-related mortalities and injuries[45].

Interestingly, a systematic review of 15 randomized controlled trials on the efficacy of safety education agendas indicated the scarcity of good evidence in low and middle-income countries of the effectiveness of traffic education. Highlight the importance of effective enforcement of traffic regulations

could provide economic benefits, combining the strategy of education with legislation and enforcement[16,20]. Moreover, vehicle crashworthiness improvements have increased the collision survivability of motor vehicle passengers, and the focus of recent automobile designs is to avoid crashes altogether[43].

Imprudence at the individual level, like speeding, driving while impaired, driving while distracted, inexperienced or young, and using substances, favors road traffic accident injuries[46]. In the present study, most frequently, road traffic injuries were observed in 20 to 49 years old persons. Precisely the age of more production in work when these people in consequence of road traffic accident injuries could become disabled and these results corroborate previous studies in other countries[47]. With this, patients and families suffer adverse financial debts because of the expensive rehabilitation services and reduced income, physical pain, social and psychological stresses, besides the absence from work[48]. Furthermore, due to the high costs associated with road traffic injuries related to patients' incapacity, public policies were used to define the costs in terms of years of life saved or disability-adjusted life years averted[49].

WHO considers a very cost-effective intervention if it generates a healthy life year for less than the gross domestic product per capita, cost-effective if it produces a healthy life year for less than three times the gross domestic product per capita and non-cost-effective if it produces a healthy life year for more than three times the gross domestic product per capita[50]. Our data reinforce the importance of adequate public policies to prevent road traffic injuries in an underdeveloped country such as Ecuador. Interventions focus should address setting more strict blood alcohol concentration limits, enforcing seat belts for drivers and passengers, and helmets for motorcyclists and bicyclists[45]. Polytraumatizm is a severe consequence with rates up to 60% mortality[12]. Immobilization, limited immunologic response, emergency interventions, and the frequent need for mechanical ventilation are descript as causes for this high complication rate[13], mostly due to central nervous system damage or exsanguination, have been descript of causes of death[17]. Fractures of the diaphysis and the distal third of the femur and the proximal tibia are also frequent in poly traumatized patients. Open fractures of the lower limbs are more severe since they are associated with a more extensive soft tissue injury and other simultaneous injuries, and that lower extremity fracture was found ourselves as the third most common cause of road traffic injuries in Santa Ana Health Centre. Despite these findings, our 4 years of data (2016-2019) revealed that a reduction in the total number of accidents might be attributed to factors, such as education, law enforcement, improvement of public policies, safety belts use, or shortening of the duration between the emergency call and hospital arrival, etc. These measures may be responsible for the reduction of road traffic injuries that we found.

The present study has considerable limitations; for example, we did not include all injury cases in the Manabí Province; instead, a small health center in the capital was chosen. It is an area of great agricultural importance with a high circulation rate; our data can serve as a source for future studies. Indeed, we did not consider the information on crashes, such as collision details (a type of car, collision direction, and velocity), seatbelt use, and airbag deployment, and this database was hospital-based, cases of pronounced instant death at collision scene were omitted. This may be considered in future studies making connections between accident data collected by the police Department and medical data based on hospital records. This strategy would make the data more reliable. However, we believe our analyses provided representative results. Interestingly, a study evaluated deaths in Manabí Province, where 7% of fatalities were caused by road traffic accidents in 2016, lower rates than in other provinces. It is worth highlighting that unclear or missing data were excluded before analysis in the present study; thus, the analyzed data had a high-reliability level.

Consequently, further studies about road traffic injuries are warranted at both the national and local levels to establish the mortality and morbidity estimates, reliable information and data on modifiable risk factors, costs associated, age- and gender-specific, joint injury severity gashes correlated with fatality. Finally, our findings described here highlight the ability of data collections in a small health center. Establishing robust yet straightforward data systems in middle and low-income countries can facilitate the flow of continuous, reliable, and systematic information on key variables to all stakeholders[24, 51].

Conclusiones

Altogether, the results provided suggest a reducing total road traffic injuries over the years. We showed more frequently in motorcycle young men (between 20 to 49 years old), suffered road traffic injuries, while also a more common type of lesion was poly traumatism followed by traumatic brain injuries. Additional studies are thus warranted to establish a causal relationship between these effects. These results also highlight the importance of considering modifiable risk factors and public policy interventions as the basis for the prevention of road traffic injuries.

Acknowledgments and funding

This study was aid by the Research Institute of the Technical University of Manabí. Authors are thankful to the students of medicine that performed data-collection and the Faculty of Health Sciences, Medical career to provide facilities. The authors would like to thank the Santa Ana Health Centre for using the data records required to perform this work.

Conflict of interest

The authors declare that they have no conflict of interest.

Referencias bibliográficas

1. Bachani AM, Paichadze N, Bentley JA, Tumwesigye NM, Bishai D, Atuyambe L, Wegener S, Guwatudde D, Kobusingye, Hyder AA. Postgraduate training for trauma prevention, injury surveillance and research, Uganda. Bull World Health Organ. 2018; 96:423-427.
2. Rohrer WM. Road Traffic Accidents as Public Health Challenge in the Gulf Cooperation Council (GCC) Region. Public Heal - Open J. 2016; 1(3):e6-e7.
3. WHO. Global Status Report on Road Safety 2018: Summary. Geneva: World Health Organization. 2018 (WHO/NMH/NVI/18.20). Licence: CC BY-NC-SA 3.0 IGO). 2018. [Accessed 20 April 2020]
4. Sidawi B, al Majil A. Editorial on Impacts on Traffic Safety. International Journal of Transportation Science and Technology. 2012; 1(4):1-3.
5. Peden M. Global collaboration on road traffic injury prevention. Int J Inj Contr Saf Promot. 2005; 12(2):85-91.
6. Global, regional, and national incidence, prevalence, and years lived with disability for 354 diseases and injuries for 195 countries and territories, 1990–2017: a systematic analysis for the Global Burden of Disease Study 2017. Global Burden of Disease Collaborative Network. Lancet. 2017; 392:10159.

7. Zhang K, Batterman S. Air pollution and health risks due to vehicle traffic. Sci Total Environ. 2013; 450-451, 307–316.
8. Whiteford HA, Degenhardt L, Rehm J, Baxter AJ, Ferrari AJ, Erskine HE, et al. Global burden of disease attributable to mental and substance use disorders: Findings from the Global Burden of Disease Study 2010. Lancet. 2013; 382 (9904): 1575-1586.
9. WHO. Global status report on road safety 2015. Inj Prev. 2015. [Accessed 2 April 2020]
10. WHO. WHO: Road traffic injuries. World Health Organization. 2018. [Accessed 2 Mayo 2020]
11. Sierink JC, Saltzherr TP, Wirtz MR, Streekstra GJ, Beenen LFM, Goslings JC. Radiation exposure before and after the introductionof a dedicated total-body CT protocolin multitrauma patients. Emerg Radiol. 2013; 20 (6): 507–512.
12. Saltzherr TP, Visser A, Ponsen KJ, Luitse JS, Goslings JC. Complications in multitrauma patients in a dutch Level 1 trauma center. J Trauma - Inj Infect Crit Care. 2010; 69 (5): 1143-1146.
13. Keel M, Trentz O. Pathophysiology of polytrauma. Injury. 2005; 36(6):691-709.
14. Mauritz W, Brazinova A, Majdan M, Leitgeb J. Epidemiology of traumatic brain injury in Austria. Wien Klin Wochenschr. 2014; 126: 42-52.
15. International Society for the Study of Trauma and Dissociation. Guidelines for Treating Dissociative Identity Disorder in Adults. J Trauma Dissociation. 2011; 12: 115-187.
16. Maas AI, Stocchetti N, Bullock R. Moderate and severe traumatic brain injury in adults. The Lancet Neurology. 2008; 7(8):728-41.
17. Probst C, Zelle BA, Sittaro NA, Lohse R, Krettek C, Pape HC. Late death after multiple severe trauma: When does it occur and what are the causes? J Trauma - Inj Infect Crit Care. 2009; 66 (4):121-1217.
18. Lagarde M, Palmer N. The impact of health financing strategies on access to health services in low and middle income countries. Cochrane Database Syst Rev. 2018; 2018(4):CD006092.
19. Verguet S, Jamison DT. Health Policy Analysis: Applications of Extended Cost-Effectiveness Analysis Methodology in Disease Control Priorities, Third Edition. In: Disease Control Priorities. Improving Health and Reducing Poverty. 2017; 3a ed (9): 157-166.
20. Yan LL, Li C, Chen J, Miranda JJ, Luo R, Bettger J, Zhu Y, Feigin V, O'Donnell M, Zhao D, Wu Y. Prevention, management, and rehabilitation of stroke in low- and middle-income countries. Neurol. Sci. 2016; 2(2) 21–30
21. Naghavi M, Abolhassani F, Pourmalek F, Lakeh M, Jafari N, Vaseghi S, et al. The burden of disease and injury in Iran 2003. Popul Health Metr. 2009; 15:7-9.
22. Belin MÅ, Tillgren P, Vedung E. Vision Zero - a road safety policy innovation. Int J Inj Contr Saf Promot. 2012; 19 (2): 171-179.
23. Collaboration UNRS. Global plan for the Decade of Action for Road Safety 2011–2020. Geneva WHO. 2011; (3):1-16.
24. Hyder AA, Allen KA, Peters DH, Chandran A, Bishai D. Large-scale road safety programmes in low- and middle-income countries: An opportunity to generate evidence. Glob Public Health. 2013; 8 (5): 504-518.
25. Slyunkina ES, Kliavin VE, Gritsenko EA, Petruhin AB, Zambon F, He H, et al. Activities of the Bloomberg Philanthropies Global Road Safety Programme (formerly RS10) in Russia: Promising results from a sub-national project. Injury. 2013; 44: 64 - 69.
26. Agencia Nacional de Tránsito. Descargables - Accidentes2015 - Agencia Nacional de Tránsito del Ecuador - ANT. Agencia Nacional de Tránsito. 2015.
27. Estadística de transporte terrestre y seguridad vial. Estadísticas sobre Siniestros de Tránsito - Agencia Nacional de Tránsito del Ecuador - ANT. Estadísticas de transporte terrestre y seguridad vial. 2019.
28. Hubert M, Vandervieren E. An adjusted boxplot for skewed distributions. Comput Stat Data Anal. 2008; 52 (12): 5186-5201.
29. Gooch JW. Boxplot. In: Encyclopedic Dictionary of Polymers. 2011.
30. Rangel A, Clithero JA. Value normalization in decision making: Theory and evidence. Current Opinion in Neurobiology. 2012; 22(6):970-81.
31. Tabelow K, Clayden JD, Lafaye de Micheaux P, Polzehl J, Schmid VJ, Whitcher B. Image analysis and statistical inference in neuroimaging with R. Neuroimage. 2011; 55 (4), 1686-1693.
32. Venables WN, Ripley BD. Modern Applied Statistics with S. 2002. Springer-Verlag Nueva York 44a ed: 498p.
33. Aldrich J, Rodríguez H. Population Pyramid. In: Building SPSS Graphs to Understand Data. 2014. California: Sage publications, 392p.
34. Moncayo J, García J. INEC. Compendio Estadístico 2014 Ecuador. Inec: 290p.
35. Rstudio Team. RStudio: Integrated Development for R. [Online] RStudio, Inc., Boston, MA. 2016.
36. RStudio Team. RStudio. Boston: Integrated Development for R. RStudio. 2017.
37. Wickham H. ggplot2 - Elegant Graphics for Data Analysis, Second Edition. Media. 2016; 2a ed: 260 p.
38. Agencia Nacional de Tránsito. Siniestros Por Provincia a Nivel Nacional- Diciembre 2018. 2018;11.
39. World Health Organization. Global status report on road safety. World Health Organisation; 2015. [Accessed 20 junio 2020]
40. Rosli N, Ambak K, Daniel BD, Sanik ME. Structural equation modelling in behavioral intention to use safety helmet reminder system. In: MATEC Web of Conferences. 2016; 47: 1-7.
41. Esmaeilikia M, Radun I, Grzebieta R, Olivier J. Bicycle helmets and risky behaviour: A systematic review. Transp Res Part F Traffic Psychol Behav. 2019; 60: 299-310.
42. Liu BC, Ivers R, Norton R, Boufous S, Blows S, Lo SK. Helmets for preventing injury in motorcycle riders. Cochrane Database of Systematic Reviews. 2008; 23;(1):CD004333.
43. Jermakian JS, Bao S, Buonarosa ML, Sayer JR, Farmer CM. Effects of an integrated collision warning system on teenage driver behavior. J Safety Res. 2017; 61: 65-75.
44. Rogé J, El Zufari V, Vienne F, Ndiaye D. Safety messages and visibility of vulnerable road users for drivers. Saf Sci. 2015; 79: 29:38.
45. Ng CP, Law TH, Wong SV, Kulanthaya S. Factors related to seatbelt-wearing among rear-seat passengers in Malaysia. Accid Anal Prev. 2013; 50: 351-360.
46. Kleiman MAR, Jones T, Miller C, Halperin R. Driving While Stoned: Issues and Policy Options. SSRN Electron J. 2018; 11 (2): 12.
47. Choquehuanca-Vilca V, Cárdenas-García F, Collazos-Carhuay J, Mendoza-Valladolid W. Epidemiological profile of road traffic accidents in Peru, 2005-2009. Rev Peru Med Exp Salud Publica. 2010; 27(2): 162-69.
48. Mock C, Arreola-Risa C, Quansah R. Strengthening care for injured persons in less developed countries: a case study of Ghana and Mexico. Injury control and safety promotion. 2003; 10(1-2):45-51.
49. Ditsuwan V, Lennert Veerman J, Bertram M, Vos T. Cost-effectiveness of interventions for reducing road traffic injuries related to driving under the influence of alcohol. Value Heal. 2013; 16(1):23-30.
50. Hutubessy R, Chisholm D, Tan-Torres Edejer T, Adam T, Baltussen R, Evans D, et al. Generalized cost-effectiveness analysis for national-level priority-setting in the health sector. Cost Eff Resour Alloc. 2003; 19;1(1):8.
51. Razzak JA, Sasser SM, Kellermann AL. Injury prevention and other international public health initiatives. Emergency Medicine Clinics of North America. 2005; 23(1):85-98.

Received: 12 December 2020
Accepted: 20 January 2021

RESEARCH / INVESTIGACIÓN

Biocompatible thermo-responsive N-vinylcaprolactam based hydrogels for controlled drug delivery systems

J. Fernanda Romero[1], Antonio Díaz-Barrios[1*], Gema González[2]

DOI. 10.21931/RB/2021.06.02.8

Abstract: The treatment of several diseases requires drugs commonly administered orally or intravenously. Said administration has several drawbacks, such as low control of the necessary drug levels in plasma, making the treatment ineffective and, furthermore, side effects and low compatibility with the patient. Recently, the use of stimuli-responsive hydrogels in controlled Drug Delivery Systems (DDSs) has been considered an excellent alternative because of its inherent biocompatibility, responsiveness to physiological changes in the body, and diversity of both natural and synthetic material options. The present work focuses mainly on the synthesis, characterization, and drug release capacity of poly (N-vinyl caprolactam) (PVCL) and poly (N-vinyl caprolactam) microgels crosslinked with various concentrations of poly (ethylene glycol) diacrylate (PEGDA), which show temperature stimuli-responsiveness near the physiological temperature of the human body. For that reason, changes in the average hydrodynamic particle diameter at different temperatures are estimated and correlated with the drug release rate. The model drug chosen for releasing studies is colchicine, a potential drug for gout disease treatment, currently in disuse because of its low therapeutic index. It is expected that the use of the control release procedure by drug encapsulation in this polymer overcomes this drawback. The synthesis of PVCL homopolymer and three VCL-co-PEGDA hydrogels varying the PEGDA crosslinker concentration was successfully carried out by emulsion polymerization. Their characterization was performed by DLS and FTIR spectroscopy. Polymerization yields were estimated by total solids analysis, and UV-VIS determined the cloud points. Finally, the drug loading and release over time were monitored by HPLC and UV-VIS spectroscopy showing that drug release profiles obtained corresponded to a sustained drug delivery system.

Key words: Thermo-responsive polymers, lower critical solution temperature (LCST), nanogels, drug delivery system, colchicine.

Introduction

The hydrogel's swelling behavior allows the hydrogel to absorb a water volume, which penetrates the gel matrix, causing gel-solvent interactions to be stronger than gel-gel interactions. Nevertheless, it does not mean that the water explicitly dissolves the polymer[1–4]. Dušek and Patterson[5] argued that it is possible to control the swelling property reversibly with external condition changes, such as physical or chemical stimuli. Recently, thermo-responsive gels are one of the most studied hydrogels due to their physiological importance, since they can take advantage of the temperature difference between the environment, the human body (37°C), the presence of fever (>37.5°C), or the presence of an intratumoral environment (40–44°C)[6,7]. For these reasons, they have an excellent performance for cancer therapy[7], transdermal drug therapy[8], and oral drug delivery[9]. Thermo-sensitive hydrogels exhibit a phase transition when there is a change in temperature, so gel volume increases or decreases depending on having an Upper Critical Solution Temperature (UCST) or Lower Critical Solution Temperature (LCST)[10,11].

In particular, LCST hydrogels present an interesting phase separation when heating the system above a specific temperature named LCST (Figure 1). Below LCST, the polymer chains interact with water by H-bonding, so the hydrogen bond energy predominates in the system, and the polymer is miscible in the water showing a swollen state (single-phase). Upon heating, the hydrogen bond interactions become weaker, while polymer-polymer hydrophobic interactions become more robust due to the molecular agitation, and polymer phases out of the solution. That phase transition is visually perceptible because the solution passes from transparent to turbid. In this way, LCST polymers are excellent candidates to design polymeric particles for controlled, targeted, and sustained drug delivery on the nanometric scale, also called nanocarriers[12]. The release mechanism for drug delivery consists of (1) the encapsulation at temperatures below LCST and (2) the delivery when the polymer shrinks at a temperature above LCST.

One of the synthetic LCST hydrogels most studied is the poly (N-isopropyl acrylamide) (PNIPAM), a vinyl polymer with secondary amide pendant groups that shows an LCST around 32°C. However, this polymer induces cellular cytotoxicity at 37°C, and the secondary amide group can produce toxic amines if hydrolysis occurs. Consequently, it is not biocompatible[13]. Thus, it has been a challenge to develop a biocompatible thermo-responsive hydrogel, and poly(N-vinyl caprolactam) (PVCL) based polymers are considered an excellent alternative to PNIPAM for controlled and biocompatible drug delivery systems.

PVCL shows a similar LCST near 32°C[14,15]. Additionally, Vihola *et al.*[13] demonstrated that cell cultures successfully tolerated PVCL polymer after three hours of incubation, at concentrations in the range of 0.1–10.0 mg/ml, at room temperature and physiological temperature (37°C). Therefore, PVCL is biocompatible[13–16].

Many researchers have been developing hydrogels based on PVCL because of the reversible volume transition from micro- to nano-scale[12,17–20].

This work aims to synthesize PVCL-based polymers to obtain suitable nanocarriers for drug delivery applications.

[1] School of Chemical Sciences and Engineering, Yachay Tech University, Urcuquí, Ecuador.
[2] School of Physical Sciences and Nanotechnology, Yachay Tech University, Urcuquí, Ecuador y Centro de Ing. Materiales y Nanotecnología, Instituto Venezolano de Investigaciones Científica, Caracas, Venezuela.

Corresponding author: diazakk@gmail.com

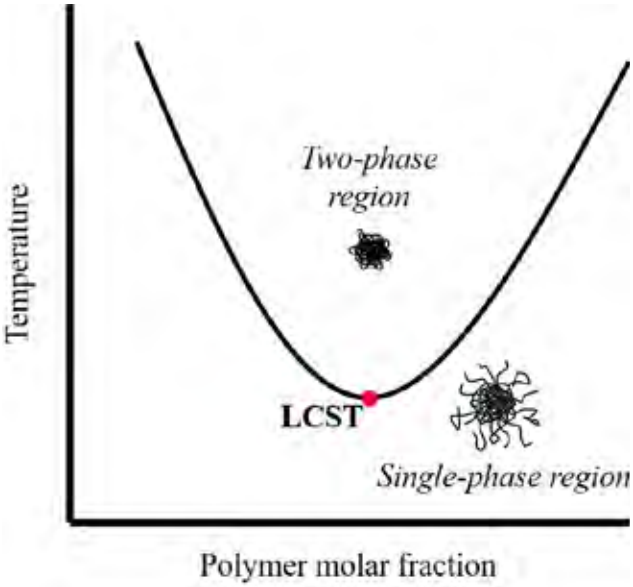

Figure 1. Phase diagram of LCST thermo-responsive hydrogels.

PEGDA is the chosen crosslinker due to its biocompatibility, hydrophilicity, and ability to prevent protein adsorption and cell adhesion[21-23]. In the present work, the model drug for drug release studies is colchicine due to the critical application for gout treatment and its low therapeutic index[24], which motivates to overcome this limitation.

Methods

Materials

Monomers

N-vinyl caprolactam (VCL; Sigma Aldrich, 98%), and Poly(ethylene glycol) diacrylate (PEGDA; Sigma Aldrich, Mn 250 g/mol). Initiator: ammonium persulfate (APS; FMC Corporation,>99%). Emulsifier: sodium dodecyl sulfate (SDS; STEOL®CS-230 Stepan). Buffer: sodium hydrogen carbonate (Sigma-Aldrich, ≥99.7%) used as provided. Colchicine (Sigma Aldrich ≥ 95%), potassium dihydrogen phosphate (Fisher Scientific, 99.6%), and methanol (LiChrosolv®, HPLC grade) were also used as provided. All aqueous solutions were prepared with double deionized water (DDI) produced by aDirect-Q®3 UV Water Purification System.

Synthesis of hydrogels

Four thermo-responsive microgels, one PVCL homopolymer, and three poly(N- Vinylcaprolactam -co-PEGDA) copolymers were synthesized by emulsion polymerization of VCL and PEGDA in a flat bottom flask equipped with a reflux condenser, using PEGDA as a crosslinker, SDS as an emulsifier, APS as initiator, and sodium hydrogen carbonate as a buffer (Figure 2).

Once the monomers, emulsifier, and buffer were loaded, the system was heated to 70°C and stirred at 350 rpm. Then, the initiator was added, and after a short period, the reaction system became turbid, showing that polymerization began. The reaction was allowed to continue for 7h with stirring at 70°C . Once polymerization finished, the reaction was allowed to cool down to room temperature and stirring continued for 12h to avoid agglomeration. The final products were dialyzed against DDI water at least three times a day to remove unreacted reagents and impurities until the solvent showed conductivity of DDI (1.7µS). Recipes and reaction conditions are resumed in Table 1.

Code	*PEGDA (wt % VCL)*	Rx conversión (%)
PVCL	–	71.8 ± 1.1
VCL-PEGDA2	2	55.8 ± 0.3
VCL-PEGDA4	4	75.0 ± 2.4
VCL-PEGDA8	8	63.8 ± 0.6

Reaction conditions: $rpm = 350$; $t = 7\ h$; $T = 70\ °C$.
The concentration of VCL was 2.0 wt %.
The concentration of the initiator was 0.7 wt % VCL.
The concentration of buffer and emulsifier were 1.7 wt % VCL.

Table 1. Polymerization conditions and reaction conversion.

Total Solids (TS) Analysis

The concentration of hydrogels was estimated by Total Solids (TS) analysis by weighing the solid present in a known volume of a purified hydrogel. The analysis was carried out by weighing a Petri dish, filling it with a known hydrogels volume, and evaporating the water in a drying oven at 105°C for 2h to constant weight. Finally, the Petri dish was weighted, and concentration (C) of purified hydrogels was calculated by Equation (1), Where mi is the weight of the empty Petri dish, mf is the weight of Petri dish with residual gel, and V is the volume of hydrogel added.

$$C(\%\ wt) = \left(\frac{m_f - m_i}{v}\right) \cdot 100 \qquad (1)$$

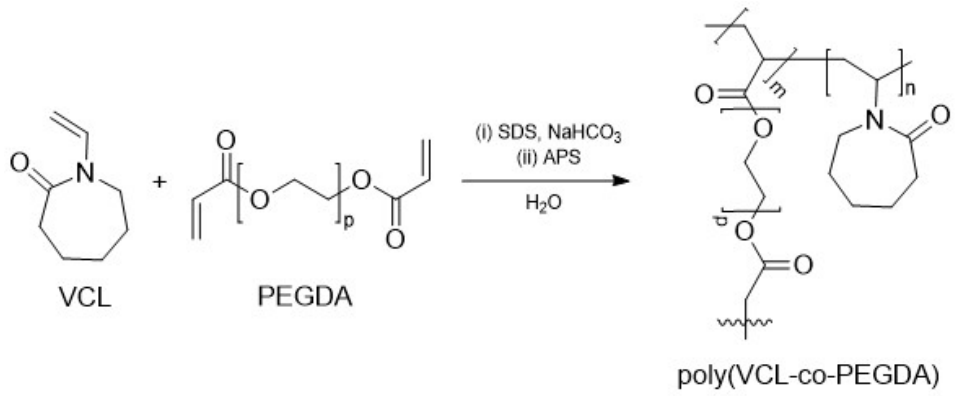

Figure 2. Scheme of VCL-PEGDAx synthesis reaction.

The yield of polymerization was calculated gravimetrically by Equation (2), where C_{TS} is the concentration of hydrogels obtained from total solids (TS) analysis, and $C_{TS,\ theoretical}$ is the theoretical total solids of hydrogels.

$$\%yield = \left(\frac{C_{TS}}{C_{TS,theoretical}}\right) \cdot 100 \qquad (2)$$

Characterization and Methods

Dialysis

Purification of hydrogels and drug uptake/delivery systems were carried out by dialysis against DDI water using *Carolina ™ Dialysis Tubing* (MWCO: 12.000 - 14.000 Daltons) as a dialysis membrane.

ATR-FTIR Spectroscopy

An Attenuated Total Reflectance Fourier Transformed Infrared (ATR-FTIR) *Agilent Cary* 630 spectrometer was used to characterize the obtained polymers. Measurements were carried out for PVCL, VCL-PEGDAx hydrogels, VCL and PEGDA dried samples.

Cloud Point Determination

The cloud point (or LCST) of hydrogels was determined by a *ZUZI® 4211/50* spectrophotometer monitoring the hydrogel's light transmittance upon cooling the hydrogels from 40°C until room temperature. The measurements were performed at 650 nm to avoid the absorbance of light by the polymeric gels. The temperature was recorded with a digital thermometer.

Particle Size Determination

The mean particle diameters of hydrogels' aqueous dispersion were measured by Dynamic Light Scattering (DLS) method using a *BI-90 Plus Brookhaven Instrument Corporation* particle size analyzer. The device was equipped with a standard solid state laser light source (35 mW and 659 nm).

All measurements were carried out five-times at two temperatures (RT and T >LCST) to give an average hydrodynamic diameter and size distribution. The plastic cuvette was filled with approximately 1 mL of the hydrogels previously purified by dialysis. The mean particle diameter and polydispersity index (PDI) parameters were calculated using *ZetaPlus Particle Sizing Software*. Two Nanosphere™ size standards were used: (1) 90 nm (*Duke Scientific Corporation*), and (2) 20 nm (*Thermo Scientific*).

High-Pressure Liquid Chromatography (HPLC)

An *UltiMate 3000* HPLC apparatus equipped with an autosampler, a quaternary pump, a column compartment, and a UV-VIS detector was used as a drug uptake/release analytical method. The analysis was carried out using a reverse-phase *Hypersil GOLD™ (150 mm 4.6 mm, 5 µ particle size)* C-18 column. The mobile phase was prepared by mixing potassium dihydrogen phosphate (450 mL, 6.8 g/L) and methanol (530 mL).25 The mixture was cooled to room temperature and made up to 1000 ml with methanol. Then, the pH was adjusted to 5.5 with diluted phosphoric acid. The final mixture was filtered through *Titan 47 mm Membrane Disc* filters. The mobile phase flow rate was 1.0 mL/min, and the injection volume was 20 µL. The column temperature was kept at 30 °C, and detection was carried out at 254 nm.

Standard solutions and calibration curves

A standard stock solution of colchicine (1000 µg/mL) was prepared. From this stock solution, standards with concentrations of 2, 5, 15, 16, 20, 40, 65, 100 µg/mL were also prepared. Two calibration curves were constructed over the concentration ranges of 2-20 and 5-100 µg/mL, both with five concentration levels. *Chromeleon™ Chromatography Data System Software* was used to obtain the corresponding calibration curves.

Drug Uptake Studies

The method was to take 9 mL of the hydrogel, placed it in a 50 mL glass recipient, and dry at 50 °C. The dried hydrogel was allowed to swell in 5 mL of drug solution (1000 µg/mL). The mixture was sonicated for 20 min at RT and allowed to stand for 48 h to reach equilibrium. Then, the mixture was subjected to dialysis overnight to remove the non-loaded drug from the system. Posteriorly, the dialysate solution was recollected, filtrated with 0.45 µm syringe filters, and quantified by the analytical method previously described. Thus, the % of drug loading (DL) and encapsulation efficiency (EE) was determined using Equation (3) and Equation (4), respectively, where is the mass of hydrogel in the encapsulation process, is the encapsulated drug, and is the total amount of drug initially added.

$$\%\ DL = \left(\frac{m_{actual\ loading}}{m_{hydrogel}}\right) \cdot 100 \qquad (3)$$

$$\%\ EE = \left(\frac{m_{actual\ loading}}{m_{theoretical\ leading}}\right) \cdot 100 \qquad (4)$$

Drug Release Studies

The previously dialyzed solutions were placed in a dialysis membrane and again dialyzed to release the drug against DDI water (35 mL) at approximately 38°C; this is above the LCST. At regular intervals of time, dialysates containing the released drug were collected in test tubes. After every sample collection, the solvent was refreshed. Finally, all recollected samples were filtered with 0.45 µm syringe filters and quantified by the previously described HPLC analytical method.

Results and Discussion

One PVCL homopolymer and three poly(VCL-co-PEGDA) water-soluble hydrogels were synthesized by emulsion polymerization with different crosslinker amounts (2, 4, 8 wt. %) relative to the VCL monomer. During the reactions, the appearance of turbidity was observed with the APS initiator's addition, showing that polymerization started. After 7h of reaction, the polymers were cooled down, and turbidity slowly disappeared. The transition to transparency from turbidity confirmed that volume phase transition had occurred, and the resulting polymer materials were thermo-responsible[26].

Once polymerization had been finished, the hydrogels were purified by dialysis to remove unreacted reagents until dialysate showed conductivity of DDI water (1.7 µS), approximately. The polymerization reactions show relatively good yields as can be appreciated in Table 1

ATR-FTIR Studies

The chemical structure of the poly (VCL-co-PEGDA) hydrogels was confirmed by ATR-FTIR spectroscopy. The characteristic peaks of VCL monomer, PEGDA crosslinker, and VCL-PEGDAx (x = % crosslinker amount) hydrogels are listed in Table 2.

	Shift (cm^{-1})					
	=C-H	C=C	C=O (amide)	C=C (oop)	C=O (esther)	O-H
VCL	3160	1659	1621	992	–	–
PEGDA	–	1636	–	–	1719	–
PVCL	–	–	1610	–	–	3428
VCL-PEGDA2	–	–	1612	–	1727	3426
VCL-PEGDA4	–	–	1610	–	1730	3429
VCL-PEGDA8	–	–	1611	–	1729	3429

Table 2. ATR-FTIR Peak assignments for VCL, PEGDA, PVCL and for VCL-PEGDAx copolymers.

	LCST ($\pm 0.1°C$)
PVCL	32.0
VCL-PEGDA2	32.7
VCL-PEGDA4	32.6
VCL-PEGDA8	32.3

Table 3. Lower Critical Solution Temperature (LCST) values for PVCL and VCL-PEGDAx polymers.

	mean particle size (nm)	
	at T<LCST	at T>LCST
PVCL	31.8 ± 0.2	16.6 ± 1.9
VCL-PEGDA2	142.5 ± 13.7	8.3 ± 0.8
VCL-PEGDA4	1339.7 ± 73.9	4.0 ± 0.3
VCL-PEGDA8	361.9 ± 7.6	2.3 ± 0.2

Table 4. Mean particle size of PVCL and VCL-PEGDAx polymers at T < LCST and at T > LCST.

In the FTIR spectrum of the monomer VCL (Figure 3a), it can be observed the characteristic vinyl peaks of =C-H stretching at 3160 and C=C stretching at 1659 . The characteristic peak of carbonyl (C=O) stretching for an amide group is generally found at 1700-1640 . Cyclic amides (lactams) decrease the C=O frequency for increasing ring size. Indeed, in the monomer spectrum, C=O is shown at a lower frequency (1621) due to the 7-membered lactam

Figure 3b shows the characteristic peaks of the crosslinker PEGDA. In general, the C=O stretching band of an ester group appears at 1750-1735 . Conjugation of the carbonyl group with , unsaturations shifts the stretching C=O vibration by about 15 to 25 to lower frequencies, and C=C vibration to lower frequency, too. Thus, the C=O band of the ester groups is found at 1719 and C=C stretching band at 1636

The FTIR spectra of VCL based hydrogels are shown in Figure 3c. PVCL corresponds to N-vinyl caprolactam (VCL) homopolymer, while VCL-PEGDAx (x=2,4,8) corresponds to the copolymer of VCL and PEGDA with 2, 4, and 8 % of PEGDA.

The FTIR spectra of PVCL homopolymer and VCL-PEGDAx (x=2,4,8) polymers are shown in Figure 3c. The Four spectra showed the absence of C=C stretching (1659), =CH stretching (3100), and C=C out-of-plane bending (992) in comparison to the monomer VCL spectrum, indicating that polymerization occurred. The intense C=O stretching band of the VCL amide group is shown at ~1610 , and the C-N stretching at ~1477 in all spectra. Both peaks showed a displacement to lower frequencies compared to monomer VCL that might be due to the changes in the molecules' conformation and interaction of molecules upon polymerization. , The C=O (ester) stretching band at ~1730 , and its displacement to higher frequency indicates the absence of conjugation, and that it could be associated with the presence of crosslinking on VCL-PEGDA hydrogels.

Thermo-responsiveness Studies

During the synthesis process, copolymers showed a phase transition from turbid to transparent solutions when cooling down. For this reason, turbidity measurements were carried out to estimate the cloud point temperatures (also called LCST) of hydrogels at 650 nm. Figure 4 shows the transmittance curves of PVCL and VCL-PEGDAx hydrogels, and Table 3 resumes the LCST values of hydrogels.

According to the literature, the LCST can be defined as the temperature at which the polymer solution becomes turbid, so it has a transmittance closer to 0%. For poly(N-vinyl caprolactam) (PVCL), the LCST value is reported between and is slightly affected by the concentration. On the other hand, polyethylene glycol (PEG) derivatives present LCST values around in water. However, it can be said that the use of PEGDA, a derivative of PEG, as crosslinker influences LCST values[27,28] as observed in the present work.

Thus, PVCL showed a sharp phase transition at LCST value, which is in good agreement with the literature[12]. VCL-PEGDA2 showed a similar phase transition behavior but slightly higher LCST value at, while VCL-PEGDA4 and VCL-PEGDA8 showed a continuous phase transition over a broad temperature range from 29 to 32 °C and the LCST values, according to the 0% transmission criteria are and , respectively.

Particle Size Studies

The thermal-responsiveness studies demonstrated that PVCL and VCL-PEGDAx hydrogels show a phase transition LCST when the aqueous solution's temperature is around 32 °C. Thus, above LCST the polymer collapses going out of phase and this has been attributed to polymer-polymer hydrophobic interactions overcoming hydrogen bonding in the polymer-solvent interactions. On the other side, below LCST, VCL-based hydrogels swell, and this can be attributed to hydrogen bonding governing the polymer-solvent interactions[6,29]. Sample VCL-PEGA4 presents a considerable size, which might be associated with aggregation phenomena.

Table 4 shows the mean particle size of PVCL and VCL-PEGDAx polymers at temperatures below and over LCST. As shown below, LCST the gels showed random values of average particle size concerning crosslinker concentration; however, these values are much higher than particle size values above LCST. In general, a decrease in particle size for PVCL and VCL-PEGDAx hydrogels is observed when the temperature rises above the previously determined LCST, which supports the phase transition from swollen to a collapsed state. The mean particle size above LCST does show some differences within the same order of magnitude, and the observed trend is a decrease in mean particle size when the PEGDA crosslinker amount is increased. It has been reported that PEGDA acts as a polymer surfactant stabilizer[22] and causes that polymer-poly-

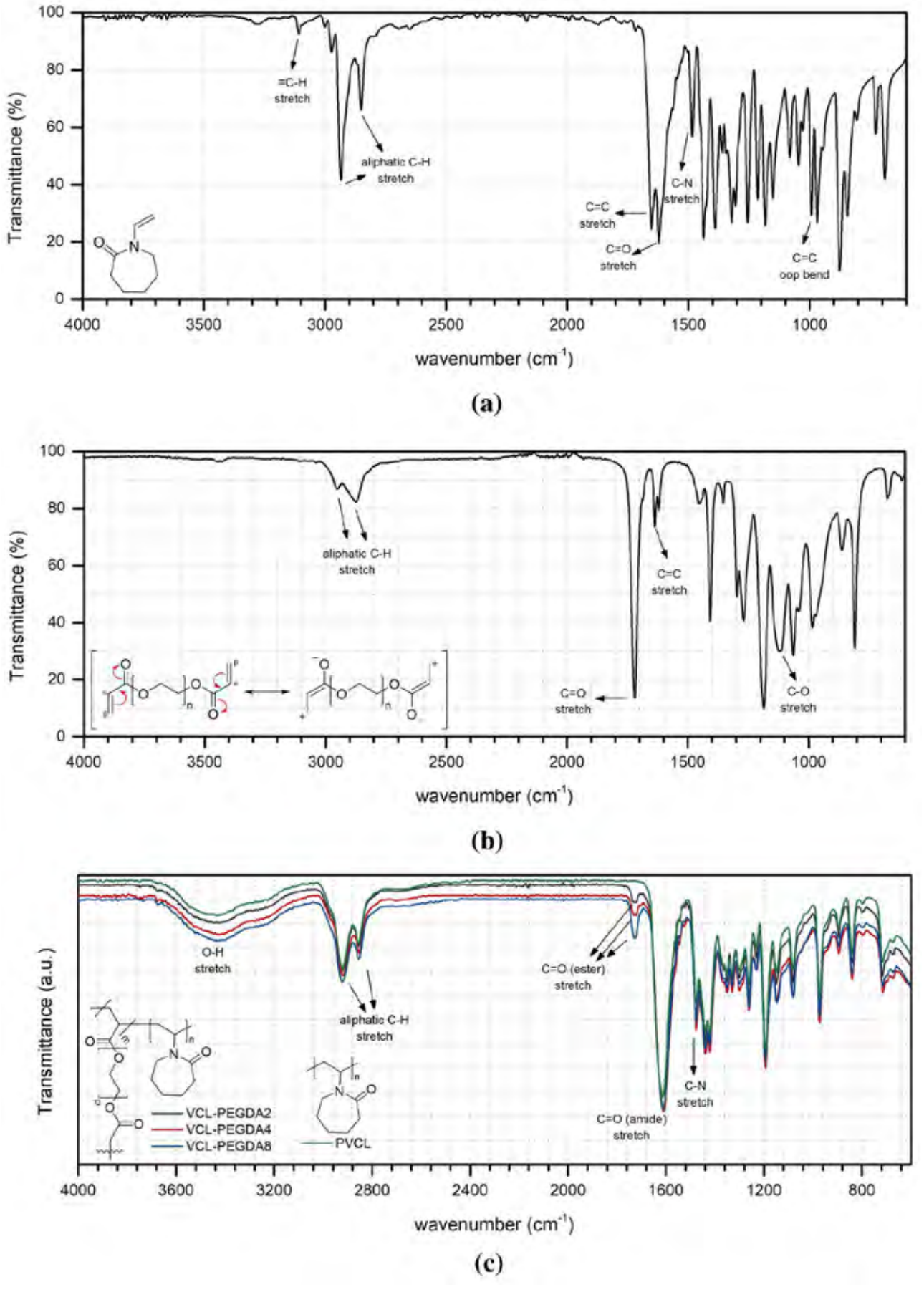

Figure 3. ATR-FTIR spectra of (a) VCL, (b) PEGDA, and (c) VCL-PEGDAx.

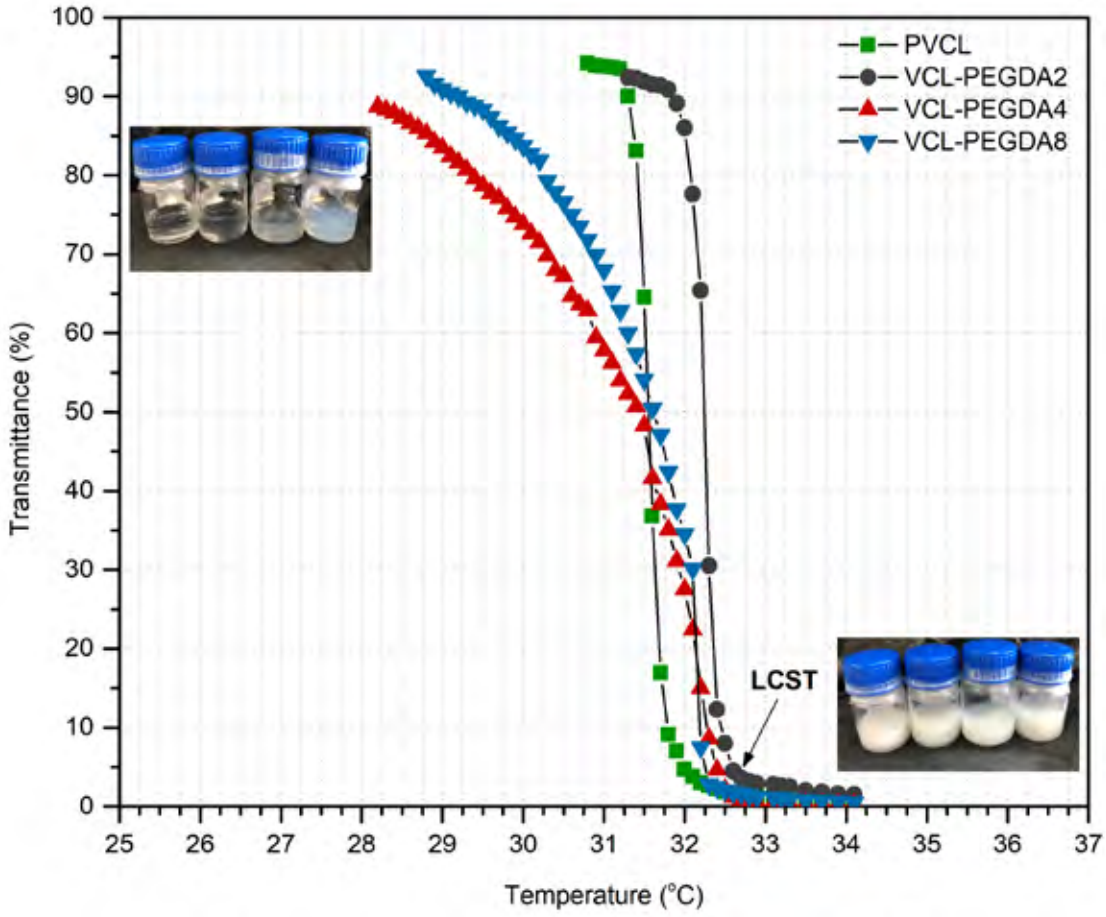

Figure 4. Transmittance curves as a function of temperature for VCL-PEGDAx.

mer interactions overcome polymer-solvent interactions. Therefore, the presence of PEGDA, due to this stabilization effect, might contribute to the decrease in the mean particle size of VCL-PEGDA copolymers.

Uptake and Release Studies

Colchicine loading and encapsulation efficiency of PVCL and VCL-PEGDAx hydrogels are shown in Table 5. As can be observed, the drug loading did not change meaningfully by the crosslinker addition, ranging from (1.1 ± 0.2) % to (1.7 ± 0.2) %. On the other hand, the encapsulation efficiency tends to decrease when the crosslinked amount increases.

	% *DL*	% *EE*
PVCL	1.4 ± 0.2	37.5 ± 10.8
VCL-PEGDA2	1.7 ± 0.2	37.3 ± 10.9
VCL-PEGDA4	1.2 ± 0.2	35.0 ± 11.0
VCL-PEGDA8	1.1 ± 0.2	30.3 ± 11.4

Table 5. Drug Loading (% DL) and Encapsulation Efficiency (% EE) of VCL-PEGDAx hydrogels.

The drug release profiles for the colchicine-loaded PVCL and VCL-PEGDAx hydrogels are shown in Figure 5. In general, a sustained release was obtained for all VCL-PEGDA hydrogels used in this study. They showed a gentle slope at the beginning, followed by a plateau whose appearance and maximum value depends on the hydrogel composition.

Thus, the maximum % of cumulative release appears to be a function or crosslinker content in the hydrogel and follows this order: VCL-PEGDA8 > VCL-PEGDA4 > VCL-PEGDA2, corresponding to PEGDA crosslinker content of 8, 4, and 2 wt. %, respectively. As previously commented, this trend can be associated with more collapse polymer and smaller gel average particle size with higher polymer PEGDA crosslinker content. This is in agreement with the polymeric surfactant stabilization effect previously mentioned[22]. PVCL as a homopolymer with a different chemical structure does not show a large particle size contraction, however it has a good drug release comparable to gel VCL-PEGDA4 and above gel VCL-PEGDA2.

It has been stated that smart hydrogels are recommended in the following situations: (a) a sustained constant concentration of the drug in the body is desired, (b) the bio-active compound has a very short half-time, (c) the drug has strong side-effects or stability problems, (d) it is necessary to achieve better patient compliance, and (e) the drug has to be taken in frequent dosage[30]. The design of the hydrogels prepared in this study fulfills the requirement of a sustained release of the colchicine as a drug with a low therapeutic index[24]. Similar drug release profiles have been observed for other PVCL-based hydrogels[9,17,29,31].

Conclusions

Four thermo-responsive polymeric hydrogels were synthesized through emulsion homopolymerization of N-vinyl caprolactam and copolymerization of VCL and PEGDA, the latter acting as the crosslinker. FTIR results confirmed the chemical structures of the above-mentioned polymeric hydrogels. The cloud point determination of all four VCL based hydrogels

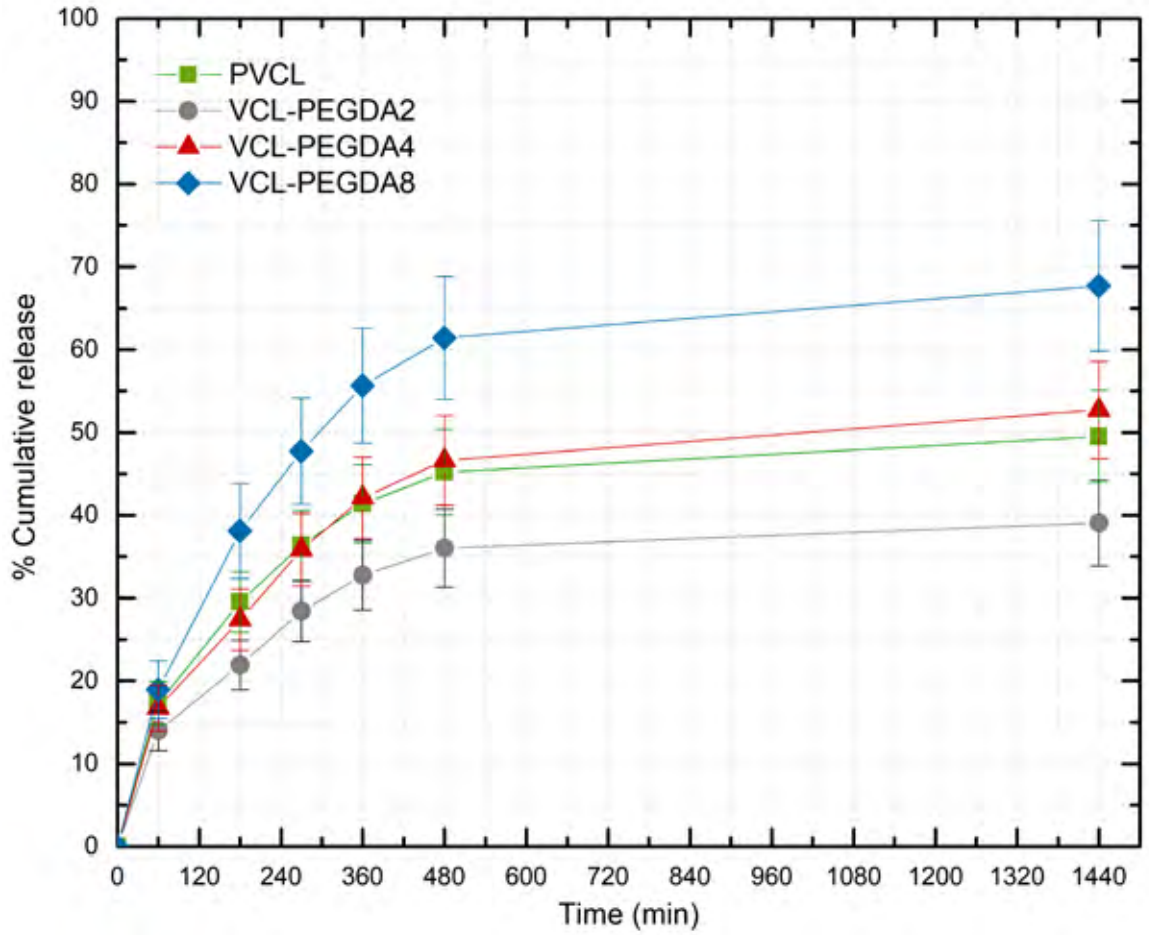

Figure 5. Cumulative release (%) of colchicine at T = 38 °C.

showed values around 32°C, related to their LCST, and confirmed their thermo-responsive behavior. As shown by the cloud point values, the phase transition is slightly affected by the crosslinker amount in the polymeric hydrogel. For PVCL and low crosslinked VCL-PEGDA2 a sharp phase transition is observed, while for the higher content of PEGDA, VCL-PEGDA4, and VCL-PEGDA8, continuous phase transition over a wide temperature range is observed.

A sustained release was observed for PVCL and VCL-PEGDAx hydrogels. The hydrogel containing the lower amount of PEGDA showed a better drug loading capacity, while the increment of PEGDA crosslinker contributes to a better drug release profile. The maximum % of cumulative colchicine release appears to be a function of crosslinker content in the hydrogel and follows the following order: VCL-PEGDA8 > VCL-PEGDA4 > VCL-PEGDA2. This trend can be associated with a more collapsed gel state and smaller mean particle size with higher PEGDA crosslinker content in the polymer. Similar drug release profiles have been observed for other PVCL based hydrogels reported in the literature[9,29,31,32].

Acknowledgment

We thank the School of Chemical Sciences and Engineering at Yachay Tech University for providing laboratory facilities. Also, we acknowledge the helpful assistance of Paulina Romero and Salomé Galeas during DSL measurements at Escuela Politécnica Nacional de Quito. We are grateful to Floralba López, Hortensia Rodríguez, and Kamil Makowski for material provision and useful discussions, to Ruth Oropeza and Terencio Thibault for HPLC and UV-VIS measurements, respectively.

Bibliographic references

1. Soni KS, Desale SS, Bronich TK. Nanogels: An overview of properties, biomedical applications and obstacles to clinical translation. J Control Release [Internet]. 2016;240:109–26. Available from:
2. Ahmed EM. Hydrogel: Preparation, characterization, and applications: A review. J Adv Res [Internet]. 2015;6(2):105–21. Available from: http://www.sciencedirect.com/science/article/pii/S2090123213000969
3. Jagur-Grodzinski J. Polymeric gels and hydrogels for biomedical and pharmaceutical applications. Polym Adv Technol. 2009;21:27–47.
4. Wack H. Method and Model for the Analysis of Gel-Blocking Effects during the Swelling of Polymeric Hydrogels. Ind Eng Chem Res - IND ENG CHEM RES. 2006;46.
5. Dušek K, Patterson D. Transition in swollen polymer networks induced by intramolecular condensation. J Polym Sci B Polym Phys. 1968 Jul;6(7):1209–16.
6. Teotia AK, Sami H, Kumar A. 1 - Thermo-responsive polymers: structure and design of smart materials. In: Zhang Z, editor. Switchable and Responsive Surfaces and Materials for Biomedical Applications [Internet]. Oxford: Woodhead Publishing; 2015. p. 3–43. Available from: http://www.sciencedirect.com/science/article/pii/B9780857097132000018
7. Alsuraifi A, Curtis A, Lamprou DA, Hoskins C. Stimuli Responsive Polymeric Systems for Cancer Therapy. Pharmaceutics [Internet]. 2018 Aug 22;10(3):136. Available from: https://www.ncbi.nlm.nih.gov/pubmed/30131473
8. Chatterjee S, Hui PC, Kan C, Wang W. Dual-responsive (pH/temperature) Pluronic F-127 hydrogel drug delivery system for textile-based transdermal therapy. Sci Rep [Internet]. 2019;9(1):11658.doi.org/10.1038/s41598-019-48254-6

9. Vihola H, Laukkanen A, Tenhu H, Hirvonen J. Drug release characteristics of physically crosslinked thermosensitive poly(N-vinylcaprolactam) hydrogel particles. J Pharm Sci [Internet]. 2008;97(11):4783–93. Available from: http://www.sciencedirect.com/science/article/pii/S0022354916327782
10. Shin J, Braun P V, Lee W. Fast response photonic crystal pH sensor based on templated photo-polymerized hydrogel inverse opal. Sensors Actuators B Chem [Internet]. 2010;150(1):183–90. Available from: http://www.sciencedirect.com/science/article/pii/S0925400510005939
11. Mohammed M, Yusoh K, Shariffuddin J. Poly(N-vinyl caprolactam) thermoresponsive polymer in novel drug delivery systems: A review. Mater Express. 2018;8:21–34.
12. Cortez-Lemus NA, Licea-Claverie A. Poly(N-vinylcaprolactam), a comprehensive review on a thermoresponsive polymer becoming popular. Prog Polym Sci [Internet]. 2016;53:1–51. Available from: http://www.sciencedirect.com/science/article/pii/S007967001500091X
13. Vihola H, Laukkanen A, Valtola L, Tenhu H, Hirvonen J. Cytotoxicity of thermosensitive polymers poly(N-isopropylacrylamide), poly(N-vinylcaprolactam) and amphiphilically modified poly(N-vinylcaprolactam). Biomaterials [Internet]. 2005;26(16):3055–64. Available from: http://www.sciencedirect.com/science/article/pii/S0142961204008051
14. Dalton M, Halligan S, Killion J, Murray K, Geever L. Smart Thermosensitive Poly (N-vinylcaprolactam) Based Hydrogels for Biomedical Applications. Adv Environ Biol. 2014;8:1–6.
15. Sun S, Wu P. Infrared Spectroscopic Insight into Hydration Behavior of Poly(N-vinylcaprolactam) in Water. J Phys Chem B [Internet]. 2011 Oct 13;115(40):11609–18. Available from: https://doi.org/10.1021/jp2071056
16. Lau ACW, Wu C. Thermally Sensitive and Biocompatible Poly(N-vinylcaprolactam): Synthesis and Characterization of High Molar Mass Linear Chains. Macromolecules [Internet]. 1999 Feb 1;32(3):581–4. Available from: https://doi.org/10.1021/ma980850n
17. Rao KM, Mallikarjuna B, Rao KSVK, Siraj S, Rao KC, Subha MCS. Novel thermo/pH sensitive nanogels composed from poly(N-vinylcaprolactam) for controlled release of an anticancer drug. Colloids Surfaces B Biointerfaces [Internet]. 2013;102:891–7. Available from: http://www.sciencedirect.com/science/article/pii/S0927776512005218
18. Maudens P, Meyer S, Seemayer CA, Jordan O, Allémann E. Self-assembled thermoresponsive nanostructures of hyaluronic acid conjugates for osteoarthritis therapy. Nanoscale [Internet]. 2018;10(4):1845–54. Available from: http://dx.doi.org/10.1039/C7NR07614B
19. Panja S, Dey G, Bharti R, Kumari K, Maiti TK, Mandal M, et al. Tailor-Made Temperature-Sensitive Micelle for Targeted and On-Demand Release of Anticancer Drugs. ACS Appl Mater Interfaces [Internet]. 2016 May 18;8(19):12063–74. Available from: https://doi.org/10.1021/acsami.6b03820
20. Sudhakar K, Rao KM, Subha MCS, Rao KC, Sadiku ER. Temperature-responsive poly(N-vinylcaprolactam-co-hydroxyethyl methacrylate) nanogels for controlled release studies of curcumin. Des Monomers Polym [Internet]. 2015;18(8):705–13. Available from: https://doi.org/10.1080/15685551.2015.1070497
21. Son KH, Lee JW. Synthesis and Characterization of Poly(Ethylene Glycol) Based Thermo-Responsive Hydrogels for Cell Sheet Engineering. Materials (Basel) [Internet]. 2016;9(10). Available from: https://www.mdpi.com/1996-1944/9/10/854
22. Imaz A, Forcada J. N-vinylcaprolactam-based microgels: Effect of the concentration and type of crosslinker. J Polym Sci Part A Polym Chem [Internet]. 2008;46(8):2766–75. Available from: https://onlinelibrary.wiley.com/doi/abs/10.1002/pola.22609
23. Imaz A, Forcada J. N-vinylcaprolactam-based microgels: Synthesis and characterization. J Polym Sci Part A Polym Chem [Internet]. 2008;46(7):2510–24. Available from: https://onlinelibrary.wiley.com/doi/abs/10.1002/pola.22583
24. Niel E, Scherrmann J-M. Colchicine today. Jt Bone Spine [Internet]. 2006;73(6):672–8. Available from: http://www.sciencedirect.com/science/article/pii/S1297319X06001837
25. Gowda BG. High-performance liquid chromatographic determination of colchicine in pharmaceutical formulations and biological fluids. Int J Pharm Pharm Sci. 2014;6:335–7.
26. Gola A, Niżniowska A, Musiał W. The Influence of Initiator Concentration on Selected Properties on Poly-N-Vinylcaprolactam Nanoparticles. Nanomater (Basel, Switzerland) [Internet]. 2019 Nov 7;9(11):1577. Available from: https://www.ncbi.nlm.nih.gov/pubmed/31703338
27. Bordat A, Boissenot T, Nicolas J, Tsapis N. Thermoresponsive polymer nanocarriers for biomedical applications. Adv Drug Deliv Rev [Internet]. 2019;138:167–92. Available from: http://www.sciencedirect.com/science/article/pii/S0169409X18302539
28. Liu F, Kozlovskaya V, Kharlampieva E. Poly(N -vinylcaprolactam): From Polymer Synthesis to Smart Self-assemblies: Chemistry, Properties and Applications. In 2018. p. 93–120.
29. Wang Y, Nie J, Chang B, Sun Y, Yang W. Poly(vinylcaprolactam)-Based Biodegradable Multiresponsive Microgels for Drug Delivery. Biomacromolecules [Internet]. 2013 Sep 9;14(9):3034–46. Available from: https://doi.org/10.1021/bm401131w
30. Bajpai AK, Shukla SK, Bhanu S, Kankane S. Responsive polymers in controlled drug delivery. Prog Polym Sci [Internet]. 2008;33(11):1088–118. Available from: http://www.sciencedirect.com/science/article/pii/S0079670008000609
31. Madhusudana Rao K, Krishna Rao KSV, Sudhakar P, Chowdoji Rao K, Subha MCS. Synthesis and characterization of biodegradable poly (vinyl caprolactam) grafted on to sodium alginate and its microgels for controlled release studies of an anticancer drug. J Appl Pharm Sci. 2013;3(6):61–9.
32. Madhusudana Rao K, Mallikarjuna B, Krishna Rao KSV, Siraj S, Chowdoji Rao K, Subha MCS. Novel thermo/pH sensitive nanogels composed from poly(N-vinylcaprolactam) for controlled release of an anticancer drug. Colloids Surfaces B Biointerfaces [Internet]. 2013;102:891–7. Available from: http://dx.doi.org/10.1016/j.colsurfb.2012.09.009

Received: 8 November 2020
Accepted: 18 January 2021

RESEARCH / INVESTIGACIÓN

The effect of consuming Pokea clam meat on nitric oxide plasma levels in hypertensive patients in Sampara District, Konawe District

I Putu Sudayasa[1], Suryani As'ad[1], Rosdiana Natsir[1], Venny Hadju[1], Mochammad Hatta[1], Muh. Nasrum Massi[1], Burhanuddin Bahar[1], Sri Rahmadhani[1], Yusminah Hala[2], La Ode Alifariki[3*]

DOI. 10.21931/RB/2020.06.02.9

Abstract: The high number of vitamins and minerals in Pokea meat encouraged us to determine the effect of consuming Pokea meat on Nitric Oxide Plasma levels in patients with hypertension and normotension. This study aimed to analyze Pokea meat consumption (Batissa violacea var. celebensis von Martens) on plasma oxide (NO) levels in hypertensive patients in Sampara, Konawe District. This research uses an observational analytic method with a case-control study design through molecular biology approach. The sample comprises 60 people consisting of 30 case samples and 30 control samples using the purposive sampling technique. Laboratory examination data is on NO plasma levels. Statistical analysis used data analysis use-dependent t-test. The distribution of Pokea meat consumption variables in the Hypertension group respondents had a mean value of 35.14 ± 17.66, while in the Non-Hypertension group of respondents was 41.10 ± 19.82. In the variable nitric oxide, the Hypertension group had a mean and standard deviation of 69.48 ± 42.78 µmol / L while the Non-Hypertension group had a mean and standard deviation of 262.8 ± 39.90 µmol / L. The statistical test analysis results showed an effect of Pokea consumption on plasma NO levels (p = 0,000). Pokea Consumption Influences NO Plasma Levels in Hypertension Patients, and there are also differences in NO Plasma Levels in Patients with Hypertension and non-hypertension in Sampara District, Konawe District, Southeast Sulawesi.

Key words: Hypertension, nitric oxide plasma, Pokea clam, sampara.

Introduction

Pokea clams or Batissa violacea var. celebensis von Martens (1897) are bivalves belonging to the Corbiculidae family and are a type of freshwater clam fish located in the Southeast Sulawesi region[1]. Pokea is scattered in several large islands in Indonesia such as (West Papua, Sumatra, Sulawesi, Java), while in Sulawesi, particularly in Southeast Sulawesi's waters, especially in large rivers such as Pohara River, Lasolo River, Roraya River, Laeya River[2].

In 100-gram clam meat contains Clam meat is rich in omega-3 and omega-6 fatty acids and contains 59 kilocalories of energy[3]. The amount of protein in shellfish is an average of 8 grams. This protein plays an essential role in the formation of enzymes in the body, the formation of organ cells and muscles, the formation of hormones, repair damaged cells in the body, regulate metabolism, form the immune system, and as a source of energy[3,4].

Yenni and colleagues' research regarding the proximate analysis of Pokea clam meat showed 50.48% protein content, 6.86% fat, 29.13% carbohydrate, and 5.53% fiber, and 2.70% water. Pokea meat contains the highest protein content of more than 50%, the moderate fat content of more than 5%, and more than 20% of carbohydrate content based on its dry weight. The nutritional content of Pokea is equivalent to several types of mollusks, which are empirically believed to be aphrodisiacs, increase reproductive vitality, treat fever, jaundice, and reduce blood pressure overcome hypertension[5].

Suryana, in her study, found a significant difference in respondents' Nitric Oxide levels in the Non-Hypertension and Hypertension groups with a value of $p < \alpha$ ($p = 0.023$). The mean value of Nitric Oxide levels in the Hypertension group was lower than Non-Hypertension. Likewise, Tadei and colleagues' results also show that the mechanism of blood vessel endothelial dysfunction is associated with a decrease in plasma NO levels[6].

Hypertension is ranked first among the 10 highest non-communicable diseases compared to acute respiratory infections in Southeast Sulawesi. Specifically, in the City of Kendari, hypertension ranks the third most disease[7].

The high number of vitamins and minerals in Pokea meat encouraged us to determine the effect of consuming Pokea meat on Nitric Oxide Plasma levels in patients with hypertension and normotension.

Methods

This study is an observational analytic with a case-control design conducted in March-August 2019, in the Sampara District area. Using a purposive sampling technique, 60 respondents were selected, consisting of 30 case samples and 30 control samples. Sources of data regarding hypertension patients were obtained from the Sampara Health Center. Blood pressure confirmation is measured with a Sphygmomanometer. The research instrument was a Pokea meat consumption questionnaire, Semi-Quantitative Food Frequency Questionnaire (FFQ-SQ). Nitric Oxide Plasma levels are measured through venous blood collection and examined at the Hasanuddin University clinical laboratory approved by the Medical Faculty of Hasanuddin University (230/UN4.6.4.5.31/PP36/2019). Data analysis used a dependent t-test. Based on the Kolmogorov Smirnov test using SPSS V. 16.00, the data were normally distributed.

[1] Postgraduate Study Program in Medicine, Postgraduate Program at Hasanuddin University, Makassar, South Sulawesi, Indonesia.
[2] Postgraduate School of Negeri Makassar University, Makassar, South Sulawesi, Indonesia.
[3] Department of Epidemiology, Faculty of Medicine, University of Halu Oleo, Kendari, Indonesia.

Corresponding author: ners_riki@yahoo.co.id

Results

Analysis of general characteristics of respondents

Distribution of respondent characteristics based on gender, age group, level of education, occupation, ethnicity, residence, as listed in Table 1.

Table 1 shows the frequency distribution based on respondents' characteristics that the most gender in the Hypertension group was 19 women (40.4%), and in the Non-Hypertension group, the most female sex was 28 people (50.6%).

The most dominant age group in the Hypertension group is 40-46 years, as many as 8 people, and in the Non-Hypertension group, most at 40-46 years, as many as 10 people. Most types of work are housewives with 15 people and 26 people in the Non-Hypertension group. In the education category, the highest number of respondents in the Hypertension group was SMA, as many as 15 people in the Non-Hypertension group as many as 13 people are in SMA level of education.

Based on ethnicity, the most respondents were Tolaki tribe, with 27 people in the Hypertension group and 29 people in the Non-Hypertension group. Respondents in the Hypertension group mostly lived in Andepali and Andadowi villages with 10 people, while respondents in the Non-Hypertension group mostly lived in Andepali Village with 19 people. The respondents' general characteristics will have the distribution of particular characteristics from the examination of lipid profiles, plasma NO levels, and eNOS gene expression.

Analysis of Special Characteristics of Respondents

Specific characteristics regarding the results of examining Pokea meat consumption, plasma NO levels, as listed in Table 2.

Table 2 shows the distribution of Pokea meat consumption variables where respondents in the Hypertension group had a mean value of 35.14 ± 17.66, while in the Non-Hypertension group, it was 41.10 ± 19.82. The results also showed the amount of Pokea meat consumption in the Hypertension group was 13.25 gr at the minimum number and 67.86 at the

Characteristics	Incidence of Hypertension			
	Hypertension		Non-Hypertension	
	n	%	n	%
Gender				
Male	11	84,6	2	15,4
Female	19	40,4	28	59,6
Age (Years old)				
33-39	4	36,4	7	63,6
40-46	8	44,4	10	55,6
47-53	4	44,4	5	55,6
≥ 54	3	100	0	0,0
Occupation				
Housewife	15	36,6	26	63,4
Entrepreneur	8	100	0	0,0
Farmer	3	50	3	50
Student	2	100	0	0,0
Government Employee	2	66,7	1	33,3
Education				
Elementary	5	38,5	8	61,5
Junior High School	5	41,7	7	58,3
Senior High School	15	536	13	46,4
Scholar	5	71,4	2	28,6
Ethnic Group				
Tolaki	27	48,2	29	51,8
Bugis	1	100	0	0,0
Muna	2	100	0	0,0
Java	0	0,0	1	100
Address				
Andepali	10	34,5	19	65,5
Andadowi	10	47,6	11	52,4
Totombe Jaya	2	100	0	0,0
Polua	5	100	0	0,0
Bao-Bao	1	100	0	0,0

Table 1. Frequency Distribution of Respondent Characteristics.

maximum, while in the Non-Hypertension group, it was 13.25 for the minimum and 78.57 for the maximum.

Nitric oxide levels in the Hypertension group had Mean and Standard Deviations of 69.48 ± 42.78 µmol / L while those in the Non-Hypertension group had mean and standard deviations of 262.8 ± 39.90 µmol / L. The minimum and maximum values of nitric oxide levels in the Hypertension group were 16.16 ± 255.46 µmol / L while in the Non-Hypertension group with values 87.83 ± 309.55 µmol / L.

Table 3 shows the effect of Pokea meat consumption on nitric oxide levels with a mean value of 69,481 and p of 0,000.

Figure 1 shows the differences in nitric oxide levels (NO) in the Hypertension and Non-Hypertension groups, where the levels of nitric oxide (NO) in the Hypertension group are lower than those in the hypertension respondents.

Discussion

Distribution of consumption of Pokea meat, nitric oxide plasma levels

During the initial interview with respondents (Hypertension and Not-Hypertension), it was revealed that 66.7% consumed Pokea meat 1-3 times and> 3 times a day as much as 33.3% of respondents. We also found that the Non-Hypertension group had a higher Pokea meat consumption pattern of 41.10 grams per day than the Hypertension group with a consumption pattern of 35.14 grams per day.

Based on the results of our observations on the community in the village of Andepali, Sampara District, Konawe District, 85% of respondents found that they often consumed Pokea meat in the last three months. with a proportion of 58% of respondents stating that they eat Pokea clam meat as much as 1-3 a day and as many as 57% consume Pokea with a portion of ½ -1 cup. Around 46% of the community obtains Pokea from the market or traveling vendors, and the others 78% process Pokea directly. In general, the type of processed Pokea consumed is in the form of satay Pokea (39%) and boiled Pokea (8%). The community manages Pokea meat by boiling 67%, processing it by frying 43%, sautéing 33%[8].

Research conducted by Rasyid, et al. on the chemical composition of Pokea meat in the Sampara area, Konawe Regency, Southeast Sulawesi obtained results from t-test analysis of the essential amino acids content of fresh and boiled Pokea meat; the only lysine was significantly different. The study also found non-essential amino acids, glutamic acid, serine, glycine, and cysteine, which differed significantly in composition in Pokea meat[9].

The total amount of amino acids in Pokea meat is relati-

Variable	Group	Mean	SD	Min	Max
Consuming Pokea meat (gr/day)	Hypertension	35.14	17.66	13.25	67.86
	Non Hypertension	41.10	19.82	13.25	78.57
Nitric Oxide Level (µmol / L)	Hypertension	69,48	42,78	16,16	255,46
	Non Hypertension	262,8	39,90	87,83	309,55

Table 2. Distribution of Pokea meat consumption pattern and plasma Nitric Oxide levels in Hypertension and Non-Hypertension.

Variable	n	Mean	Std. Deviation	p-value
Consuming Pokea Meat	30	34,14	17,66	
Nitric Oxide (NO) Level	30	69,481	42,784	0.000

Table 3. Analysis of the Effects of Pokea meat consumption on plasma Nitric Oxide levels in hypertensive patients.

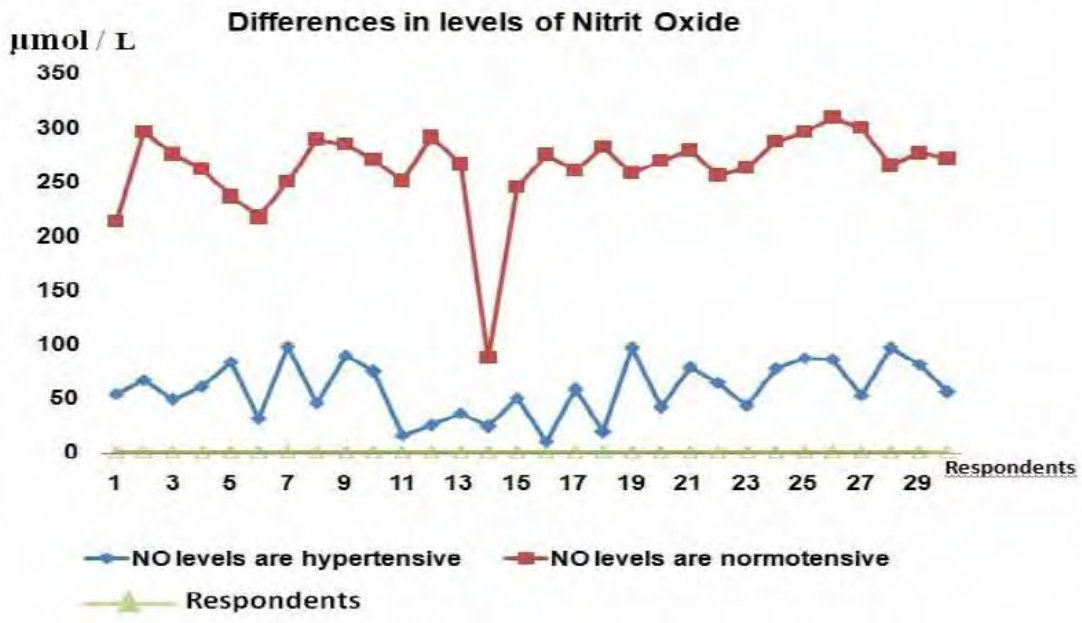

Figure 1. Differences in levels of Nitric Oxide Plasma in patients with hypertension and not hypertension.

vely the same after boiling, while non-essential amino acids decreased significantly by 29.43%. In fresh meat and boiled Pokea identified as many as 25 types of fatty acids. The content of fatty acids in Pokea skin after boiling is relatively stable. Based on n6 / n3 and PUFA / SFA ratio, the ratio of fresh, boiled, and dry Pokea peels can be said to be healthy and safe for consumption. Identifying the extract is correct because it is proven to provide positive reaction results containing protein and carbohydrates[9].

Consumption of foods high in saturated fatty acids increases cholesterol levels in the blood and leads to atherosclerosis, affect the decrease in Nitric Oxide levels, leading to hypertension. Initially, LDL will be oxidized by superoxide produced by NAD (P) H macrophages oxidize. Ox-LDL stimulates several redox-sensitive processes that harm endothelial function. Through inhibition of eNOS activity and NO inactivation, ox-LDL may reduce NO bioavailability[10].

There was a difference between hypertension and non-hypertension groups in the variable level of oxide, where the non-hypertensive group was significantly higher than the hypertension group. This study's results are supported by previous research, which shows significant differences in respondent's Nitric Oxide levels in the Non-Hypertension and Hypertension groups with a value of p <α (p = 0.023). The mean value of Nitric Oxide levels in the Hypertension group was lower than Non-Hypertension[11]. Similarly, studies also show that the mechanism of vascular endothelial dysfunction is associated with a decrease in plasma NO levels[6].

NO levels are synthesized by nitric oxide synthase (NOS) from L-arginine. After being synthesized, NO undergoes diffusion from endothelial cells into vascular smooth muscle cells and causes an increase in intracellular cyclic guanosine monophosphate (cGMP). This increase in cGMP will trigger the relaxation of vascular smooth muscle[12].

Nitric oxide (NO) is an Endothelial Derived Releasing Factor (EDRF) that acts as a vasodilator and lubricant to prevent the attachment of Low-Density Lipoprotein (LDL) and blood cells. Based on this study's results, in patients with hypertension, it was found that NO levels were lower compared to patients without hypertension.

These results are consistent with the theory that NO plays a role in regulating blood pressure and decreasing NO's availability as an essential factor during endothelial cell aging[13].

Analysis of the Effect of Consuming Pokea on Nitric Oxide Plasma Levels

In figure 1 visible difference in levels of nitric oxide (NO) in the hypertension and non-hypertensive groups where the levels of nitric oxide (NO) in the Hypertension group are lower than those of the hypertensive respondents. This is influenced by the production of depressed NO levels in hypertensive respondents.

NO levels play a role in blood vessel walls, precisely in endothelium vasodilation, platelet activity inhibition, and smooth muscle cells' proliferation and migration[14]. If NO homo-sensitivity is disrupted by high-fat food in the blood, vasodilation will be disrupted so that the diameter of the endothelium cannot widen, causing a rise in blood pressure.

In the analysis of Pokea meat consumption on nitric oxide levels, it was found that there was an effect with a p-value of 0,000, while the expression of the endothelial Nitric oxide synthase (eNOS) gene also affected, with a p-value of 0,000.

This study seems to be in line with research (Suryana, 2017), which shows that there are significant differences in respondent's Nitric Oxide levels in the Non-Hypertension and Hypertension groups with a value of p <α (p = 0.023).

The mean value of Nitric Oxide levels in the Hypertension group was lower than Non-Hypertension. This is following several other studies that show that in patients with primary hypertension, endothelial-dependent vasodilation occurs due to decreased availability of Nitric Oxide[15].

We found higher levels of nitric oxide in people who were not hypertensive, although the average value of nitric oxide levels in hypertensive patients was above the expected value of 69,481 µmol / L; however, many hypertension respondents were below average values (25–45 µmol / L), whereas in the group of not hypertension, the average value of NO was 262.8 µmol / L.

According to the results of the study in Padang City, showed that the majority of respondents had low levels of physical activity and lowed NO plasma with an average of 26.3 ± 15.2 µmol / L. Respondents with mild physical activity had low plasma NO levels (61.7%) compared to normal plasma NO levels (38.3%). There is a significant relationship between physical activity and plasma NO levels (p = 0.007)[16].

The enzyme eNOS (nitric oxide synthase enzyme) is expressed by the NOS3 gene (nitric oxide synthase-3). This enzyme plays a role in NO production, which has a vasodilating effect on blood vessels. At present, three NOS3 gene polymorphisms have been identified associated with the incidence of essential hypertension, namely Glu298Asp, -786T> C, and intron 4a4b[17].

Individual carriers of NOS3 gene polymorphism show decreased eNOS expression so that it can reduce NO production. NO, together with Angiotensin II, which acts as vasoconstriction, collaborates in regulating blood pressure balance. Increased Angiotensin II and decreased NO activity because continuous vasoconstriction means increased vascular resistance and blood pressure, ultimately causes hypertension[18].

A study conducted by Sulastri et al. in the Minangkabau ethnic community showed that the Glu298Asp allele eNOS3 gene polymorphism was not related to hypertension incidence Minangkabau ethnic group. NO plasma levels in patients with hypertension are at the lowest normal levels. Omega-3 plasma is associated with plasma NO levels only in hypertensive patients with GT heterozygous alleles[19].

According to the results of Sulastri et al.'s research, this supports the recommendation of omega-3 consumption in hypertensive patients with heterozygous GT alleles to increase plasma NO levels. In contrast, it is expected for normotensive sufferers to reduce the intake of saturated fatty acids because it can suppress plasma NO levels[19].

Nitric oxide is a compound that can convey signals to the smooth muscle in blood vessels to relax, causing blood vessel dilation (vasodilation), which results in a decrease in blood pressure. Existence of Nitric Oxide (NO) is an Endothelial Derived Releasing Factor (EDRF) that acts as a vasodilator and lubricant to prevent the attachment of Low-Density Lipoprotein (LDL) and blood cells. Nitric oxide is produced by endothelial cells from the amino origin L-arginine in a catalyzed reaction by the enzyme Nitric Oxide Synthase (NOS). Nitric oxide can cause guanylyl cyclase in vascular smooth muscle to be inactive, resulting in the accumulation of mono phosphoinositide (cGMP) guanosine and relaxation[15].

Nitric Oxide, also known as nitrogen monoxide, is a crucial intermediate in the body's chemical cycle. In humans, Nitric Oxide compounds are chemical compounds that are important for transporting electrical signals in cells and function in physiological and pathological processes. Likewise, this com-

pound can cause blood vessel dilation, or in medical terms, it is called a potent vasodilator to reduce blood pressure[20].

Nitric Oxide (NO) plays a role in the regulation and maintenance of blood vessel pressure. NO is produced by endothelial cells and has vasodilation and antiproliferation effects on vascular smooth muscle cells. The release of NO will trigger vascular smooth muscle relaxation. A decrease in NO can occur due to a decrease in the enzyme Nitric Oxide Synthase (NOS). Decreased NOS activity causes vasoconstriction and hypertension[12].

Sulastri et al.'s research results, in 2011, in the Minangkabau ethnic community, showed NO plasma levels of hypertension subjects 26.91 ± 15.40 µM / L and norm tension 25.79 ± 15.04 µM / L. Thymine substitution to cytosine at position 786 was found as much as 1.5% in the hypertension group and 9.2% in the norm tension group. Low plasma NO levels (67.2%) were found in subjects with TC heterozygous alleles. There was a significant correlation between antioxidant consumption (vitamin E) and plasma NO levels in hypertensive subjects with TC heterozygous alleles (p = 0.03). Consumption of vitamin E and carotenoids can increase plasma NO levels only in patients with hypertension and normotension who have eNOS3 gene polymorphisms with TC heterozygous alleles[19].

In patients with hypertension, besides the ability of the eNOS3 gene to synthesize NO decreases, an unbalanced diet will worsen NO production, but diets containing high antioxidants can increase the synthesis of NO plasma. One type of food that has been reported to contain high antioxidants is Pokea.

Conclusions

Consumption of Pokea Influences NO Plasma Levels in Hypertension Patients and there are also differences in NO Plasma Levels in Patients with Hypertension and non-hypertension in Sampara District, Konawe District, South-east Sulawesi.

Acknowledgment

The author would like to thank the parties who have contributed to the implementation of this research, especially the Dean of the UHO Faculty of Medicine, Chair of the UHO LPPM

Bibliographic references

1. Bahtiar. Studi Bioekologi dan Dinamika populasi Pokea (Batissa violacea var. celebensis von Martens, 1897) yang Tereksploitasi Sebagai Dasar Pengelolaan di Sungai Pohara Sulawesi Tenggara. Institut Pertanian Bogor; 2012.
2. Bahtiar. Pertumbuhan, Kematian dan Tingkat Eksploitasi Kerang Pokea (Batissa violacea var. celebensis, vonMarten 1897) pada Segmen Muara Sungai Lasolo Sulawesi Tenggara. Mar Fish. 2016;7(2):137–47.
3. Tari AA, Duan FK, Amalo D. Analisis Kandungan Gizi Jenis-Jenis Kerang yang Biasa Dikonsumsi Masyarakat Nembe Desa Oeseli Kecamatan Rote Barat Daya Kabupaten Rote Ndao NTT. J Biotropikal Sains. 2018;15(2):1–9.
4. Kamelia, Lisya Tri Insani, Rismawati DCS. Pemanfaatan Kerang Pisau (Solen lamarckii)Sebagai Bahanolahan Kuliner di Pantai Kejawanan Cirebon. In: Seminar Nasional Pendidikan Sains. 2019. p. 76–81.
5. Sudayasa P, Ruslan N, Kurniati I. Pengaruh Konsumsi Daging Kerang Pokea (Batissa violacea celebensis) Terhadap Tekanan Darah Pada Masyarakat Pesisir Pohara. 2017;515–22.
6. Taddei, S., Virdis A, Ghiadomi L, Sudano I SA. Effects of Antihypertensive Drugs On Endothelial Dysfunction. Drugas. 2012;62:265–84.
7. Tenggara DKPS. Profil Kesehatan Sulawesi Tenggara 2016. Data & Informasi Dinas Kesehatan Sulawesi Tenggara, editor. Kendari; 2017.
8. Sudayasa, I Putu, Hartati B. Family Nutrition Improvement Effort Though Nutrition Management of Pokea Clam Based on Enviromental Health. J Pengabdi Kpd Masy (Indonesian J Community Engag. 2019;5(2):222–36.
9. Rasyid, S.A., Bintang, M., Priosoeryanto, B.P., Nurlila, R.U., Surya R. Analysis Chemical Compound of Pokea (Batissa violacea celebensis Martens 1897) the Origin of Konawe Regency Southeast Sulawesi. Indian J Public Heal Res Dev. 2018;9(6):345–50.
10. Amelia, R., Oenziel, F., & Nasrul E. Pengaruh Diet Tinggi Asam LemakTerhadap FungsiEndotel Pembuluh darah Tikus Jantan Strain Wistar. Universitas Andalas Padang; 2011.
11. Suryana. Asupan Lemak dan Kadar Nitrit Oxide Pada Penderita Hipertensi Primer dan Normotensi. Politeknik Negeri Jember; 2017.
12. Kaplan NM. Hypertension with pregnancy and pill, In Kaplan NM, editor, Clinical Hypertension. Williams &Wilkins: Baltimore, USA; 2015.
13. Smith, A.R., Hagen T. Vascular endothelial dysfunction in aging: loss of Akt-dependent endothelial nitric oxide synthase phosphorylation and partial restoration by (R)-alpha-lipoic acid. Biochem Soc Trans. 2013;31:1447–9.
14. Sandoo A, Veldhuijzen van Zanten JJC., Metsios GS, Carroll D, Kitas GD. The Endothelium and Its Role in Regulating Vascular Tone. Open Cardiovasc Med J. 2015;4(1):302–12.
15. Sunarti, Husain,A., Hakimi,M,. Sofro A. Hubungan Antara Homosistein dan Nitrit Oksid Pada Hipertensi Esensial di Jawa Tengah, Indonesia. Ber Kedokt Masy. 2017;23(2):58–63.
16. Isral G, Afriwardi A, Sulastri D. Hubungan Aktivitas Fisik dengan Kadar Nitric Oxide (NO) Plasma pada Masyarakat di Kota Padang. J Kesehat Andalas. 2014 May 1;3.
17. Shankarishan P, Borah PK, Ahmed G MJ. Endothelial nitric oxide synthase gene polymorphisms and the risk of hypertension in an indian population. Biomed Res Int. 2014;1(1):1–11.
18. Hernayanti, Moeljopawiro S SA. Efek polimorfisme gen nitrit oksida sintase 3 (NOS3) terhadap kadar nitrit oksida dan tekanan darah pada individu terpapar plumbum. J Mns dan Lingkung. 2012;19(2):160–8.
19. Feryadi, R., Sulastri, D., Kadri H. Hubungan Kadar Profil Lipid dengan Kejadian Hipertensi pada Masyarakat Etnik Minangkabau di Kota Padang Tahun 2012. J Kesehat Andalas. 2014;3(2):1–2.
20. Hermann M, Flammer A TFL. "Nitric oxide in hypertension. J Clin Hypertens. 2016;8(12):17–29.

Received: 30 November 2020
Accepted: 20 January 2021

RESEARCH / INVESTIGACIÓN

Induction of apoptosis by Kola nut extract as a recent and promising treatment strategy for Leukemia

Hamdah Alsaeedi[1,2], Rowaid Qahwaji[1], Talal Qadah[1*]

DOI. 10.21931/RB/2021.06.02.10

Abstract: Kola nut extracts have recently been reported to contain chemopreventive compounds providing several pharmacological benefits. This study investigated Kola nut extracts' anti-cancer activity on human immortalized myelogenous leukemia cell line K562 through apoptosis and cell cycle arrest. Fresh Kola nuts were prepared as powder and dissolved in DMSO. Different concentrations (50, 100, 150, 200, and 250 µg/ml) of working solutions were prepared. The K562 cells were treated with the different concentrations of Kola nut extract or vehicle control (10% DMSO) followed by incubation at 37°C for 24, 48, and 72 hours, respectively. Treatment activity was investigated in K562 cells; by Resazurin, and FITC/Propidium Iodide and 7-AAD stained cells to evaluate apoptotic cells and the cell cycle's progression. Inhibition of leukemia cell proliferation was observed. The extract effectively induced cell death, early and late apoptosis by approximately 30% after 24 and 48 hours incubation, and an increase in the rate of dead cells by 50% was observed after 72 hours of incubation. Also, cell growth reduction was seen at high dose concentrations (150 and 200 µg/ml), as evident by cell count once treated with Kola nut extract. The total number of apoptotic cells increased from 5.8% of the control group to 27.4% at 250 µg/ml concentration. Moreover, Kola nut extracts' effects on K562 cells increased gradually in a dose and time-dependent manner. It was observed that Kola nut extracts could arrest the cell cycle in the G2/M phase as an increase in the number of cells by 29.8% and 14.6 % were observed from 9.8% and 5.2% after 24 and 48 hours of incubation, respectively. This increase was detected in a dose and time-dependent manner. Kola nut extracts can be used as a novel anti-cancer agent in Leukemia treatment as it has shown significant therapeutic potential and therefore provides new insights in understanding the mechanisms of its action.

Key words: Kola nut extracts, Leukemia, K562 cell line, Apoptosis, Cancer.

Introduction

Leukemia is defined as blood cancer as it originates from blood-forming tissues such as bone marrow; therefore, large quantities of abnormal blood cells are made before its circulation. Clinical symptoms vary between leukemia types based on its stage, genetic and environmental factors involved in the pathophysiological process[1]. Leukemia is divided into two main categories depending on the affected cell lines, including myeloid and lymphoid Leukemia. Further classification is done based on the onset of disease, including the acute or chronic stage. This all together characterizes Leukemia into four major types, which include Acute Myeloid Leukemia (AML), Chronic Myeloid Leukemia (CML), Acute Lymphocytic Leukemia (ALL), and Chronic Lymphocytic Leukemia (CLL)[2]. The CML is responsible for 15-20% of the total adult leukemia cases[3]. The Philadelphia chromosome's presence is a common hallmark linked to CML disorder that results from the fusion of two genes, i.e., Abelson murine leukemia (ABL1) gene located on chromosome 9 with breakpoint cluster region or BCR gene present on chromosome 22. The output product of this fusion is a protein termed BCR-ABL1 with oncogenic properties. Independent of a ligand's presence, this BCR-ABL1 tyrosine kinase remains constitutively active, causing stimulation of multiple downstream signaling pathways like RAS, JUN kinase, STAT, RAF, and MYC that enhance the growth and replication process[4]. The exact basis of most leukemia cases is yet to be discovered. However, environmental or inherited factors such as smoking, chemicals (i.e., benzene), ionizing radiation, previous exposure to chemotherapy, and Down-syndrome have been linked to it[5]. In addition to this, DNA mutations that activate oncogenes or inhibit the tumor suppressor gene can promote Leukemia by causing impaired cell death regulation, division, or differentiation[6].

Multiple treatment options are available for Leukemia, such as chemotherapy, ionizing radiation, and hematopoietic stem cell transplantation[7]. Several side effects are associated with chemotherapy including cytotoxicity[8], hair loss, coagulopathies, dry skin, brain abnormalities, and weekend immune system[9-12]. Another complication associated with chemotherapy is that patient develops resistance against chemotherapy through different pathways[13]. Hematopoietic stem cell transplantation is an alternative strategy for treating different diseases such as Leukemia and Lymphomas as these hematopoietic stem cells can differentiate into any mature blood cell types, and they also possess the ability of self-renewal[14]. However, it is quite expensive and associated with several complications like hemorrhagic cystitis, bacteremia, mucositis, and graft versus host disease[15,16]. Ocular effects, post-transplant immunosuppression, organ toxicity, and congestive heart failure are some of the other complications commonly seen[16]. All these can result in cancer relapse after few months of transplantation[16]. Therefore, efforts have been made to find alternative treatment options with less toxicity and better prognosis.

One approach is to trigger the intrinsic apoptotic pathways, which will promote the cell death of leukemic cells[17] as dysfunction in apoptotic pathway and lack of cell differentiation are among the hallmarks of leukemia[18]. Another therapeutic approach was to use interferon-alpha to induces immune cells of the host, including B lymphocytes, T lymphocytes, antigen-presenting dendritic cells, and natural killer cells to manage CML[19], thereby INF α activates the immune response, modulates hematopoiesis and interleukin signaling to produce a cytogenetic response[20]. However, different side effects such as muscle aches, autoimmune hemolytic anemia (AIHA), immune-mediated renal disease, underactive thyroid function,

[1] Department of Medical Laboratory Technology, Faculty of Applied Medical Sciences, King Abdulaziz University. Jeddah, Saudi Arabia.
[2] Clinical Laboratory Department, College of Applied Medical Sciences, Shaqra University. Shaqra, Saudi Arabia.

Corresponding author: thqadah@kau.edu.sa

chronic fatigue, neurotoxicity, and many others are associated with interferon therapy[19]. Nowadays, treatment with tyrosine kinase inhibitors (TKIs) is the norm. While selecting a particular TKI as a treatment option, various parameters such as patient's age, comorbidities, cost TKI resistance, and the toxicity profile of TKI in question need to be considered carefully and with proper monitoring[4].

One treatment regimen includes medicinal plants as an anti-cancer agent as these plants produce a wide range of chemical compounds, although not useful for the plant yet having anti-cancer ability against various human cancer[21]. According to an estimate, about 60% of drugs commonly used as anti-cancer agents have been acquired from natural sources, among which plants are major contributors[22]. Around more than 3000 plants have been recorded to possess ant cancerous characteristics; therefore, these medicinal plants are used as an alternative treatment strategy in different countries. This alternative approach to prevent or delay cancer development is called chemoprevention, which utilizes medicinal herbs and food[23-25]. Among such medicinal plants include Kola nuts of the *Sterculiaceae* family of plants. These plants are native to African tropical rainforests and are a rich source of caffeine; therefore, these nuts are used in several beverage preparations. These nuts are also chewed by a person or in a different social gathering in several West African cultures. Commonly used Kola nuts species include Cola acuminate/Cola nitida and bitter Cola (Gracina Kola)[26,27]. Although it has many benefits, excessive consumption can cause anxiety, hypertension, neuro stimulatory effect, and irritation of the gastrointestinal tract[28-30], which may be due to caffeine's excessive content in these nuts[31,32]. These Kola nuts possess antimicrobial activity in a range of 8-24 nm compared to Gentamicin and nystatin, and they have been used to treat fever, malaria, scabies, ringworm, gonorrhea, and dysentery[33].

Apart from these, the presence of anti-androgenic and anti-estrogenic components of Kola nuts compelled the researchers to study Kola nut extract's pharmacological effect when applied on solid tumors such as breast and prostate cancer cell lines[34,35]. The results reveal Kola nut extracts' selective toxicity against MDA-MB-468 and MCF-7 breast cancer cell lines, and DU145 and LNCaP prostate cancer cell line[34,35]. This proved that Kola nuts have anti-cancer activity, and its extract can be used for inhibiting cancer cell growth. These results increased Endrini and his colleagues' interest in finding the apoptotic mechanism underlying the Kola nut extracts in MCF-7 breast cancer cell line[36]. The MCF-7 cell lines were treated with 60-80 µg/ml of Kola nut extracts for 24 hours, and analyzed the treated cells by flow cytometry. He observed an increased number of apoptotic cells in MCF-7 cell line. This means that the Kola nut extract influence the cell cycle (S and G2/M phases) and can promote MCF-7 cell lines apoptosis. The K562 cell line was initially established from patients with chronic myelogenous Leukemia (CML) and expressed as the typical hallmark of CML[37]. Further, the molecular level reveals that it is positive for the Philadelphia (Ph) chromosome made by Bcr/Abl fusion gene through a reciprocal translocation between chromosomes 9 and 22[37]. These cell lines were also selected because they were highly undistinguishable with a dynamic proliferative capacity and inhibition of apoptosis[38].

Although treatment of CML cases with current chemical approaches is considered adequate, specific adverse reactions associated with this treatment option such as pleural effusion, vascular pathology, musculoskeletal and gastrointestinal symptoms have been reported[39,40]. Therefore, this study aimed to investigate the potential anti-cancer effect of herbal products, namely Kola nut extract, on the human immortalized myelogenous leukemia cell line K562 through analyzing apoptotic activity and cell cycle arrest. It can be taken as an experimental trial to overcome adverse reactions associated with chemical treatment as well as to widen treatment options for patients suffering from Myelocytic Leukemia.

Materials and methods

Kola nut extract preparation

A stock of Kola Nut extracts powder was dissolved in sterile Dimethyl sulfoxide (DMSO) (10%) and aliquoted into an Eppendorf tube covered with aluminum foil in a final concentration of 2.8 mg/ml. The aliquots stocks were kept at –20°C for further use. Different working concentration points (50, 100, 150, 200, and 250 µg/ml) were adopted for the prepared stock solution's experimental procedure. Besides, the required volume of extract to obtain a final concentration was calculated.

Annexin V

For apoptosis detection, double-staining of the cells with Annexin V-Propidium iodide (PI) were used. 400 µL of 1X Annexin V binding buffer per sample was used. The initial 10X buffer was diluted with deionized distilled water in a 1:10 ratio and set aside on ice. For Annexin V incubation reagent, 100 µl reagent (10 µl of 10X binding buffer, 10 µl propidium iodide (PI), 1 µl Annexin V-FITC and 79 µl deionized distilled water) was utilized per sample with cells density of 1 x 10^6. Individual samples (seeding cells at 1 x 10^6) were then stained with 7-Amino- Actinomycin D (7-AAD) stain, which was prepared by incubated 7-Amino- Actinomycin D (7-AAD) (20 µg/ml) with RNase (20 µg/ml) at 37°C for 30 minutes.

Culturing and treatment of K562 cells

K562 cells were cultured in 6 wells plate at the desired density of 15 x 10^4 cells in 3ml /well, treated with the targeted concentrations of Kola nut extract (0, 50, 100, 150, and 200 µg/ml) or vehicle control (10% DMSO), and then incubated for 24, 48 and 72 hours, respectively at 37°C. After incubations, the cell suspension was gently mixed and carefully loaded into hemocytometer chambers to count the cells. Additionally, the average cell count was determined, and the procedure was repeated to ensure accuracy.

The proliferation of cytotoxic assays

Trypan blue assay

50 µl of aliquoted of cells suspension was gradually mixed with 50 µl of trypan blue stain in (1.5 ml) Eppendorf tube and kept at room temperature for 5 minutes. 20 µl of the stained cells were then picked and loaded onto chambers of hemocytometer, and then the live and dead cells were separately quantified in four corner squares using the L rule of both chambers. The average cell count was determined, and to ensure the accuracy of the method, the procedure was repeated. The findings represent as percentages of live or dead cells were then calculated.

Proliferation assay 96 wells plate

The cytotoxic potential of Kola nut extract against myeloid leukemia cell line (K562) was determined using Resazurin cell viability assay kit after the experimental treatments in triplica-

te wells and incubation period of 24, 48, and 72 hours at 37°C. Results of cell viability were carried out by the colorimetric method and calculated by Subtracted background absorbance (culture medium without cells at 600 nm from resolution and absorbance at 570 nm).

Flowcytometry of annexin V/PI stained cells for apoptotic assay

Treated cells with different concentrations and at different time intervals were pelleted and incubated in 100 µl prepared Annexin V incubation reagents in the dark for 15 minutes at room temperature and then immediately re-suspended in 400 µl of prepared 1X binding buffer. At the same time, apoptotic cells were detected on a BD FACSAriaIII Flow cytometer (Becton Dickinson) within one hour; to obtain the maximal signal. Additionally, results were analyzed using BD FACSDiva software, which sorted cells into intact or viable cells (Annexin negative/PI negative), early apoptotic cells (Annexin positive/ PI negative), late apoptotic cells (Annexin positive /PI-positive), and necrotic cells (Annexin negative/PI-positive).

Cell cycle assay

Flow cytometry of 7-AAD stained cells was used to detect cell cycle progression. The cells were pelleted and fixed with ice-cold 80% ethanol by dropwise 2 ml from a Pasteur pipette immediately mixed on vortex and then stored at –20°C for a week. Following the fixative time, the preserved cells were pelleted and incubated with prepared 7-Amino- Actinomycin D (7-AAD) at 37°C for 15 minutes. Similarly, as the apoptotic assay, the cell cycle analysis was done on a BD FACSAria III Flow cytometer, and the results were analyzed using BD FACSDiva software through collected 250,000 events per sample in population 2.

Statistical evaluation

Results were analyzed by excel software by formulated precise illustrative figures and tables to compare cellular proliferation and death rates for two groups of experimental leukemic cell lines; control and test.

Results

Kola Nut Extract Inhibits Cell Proliferation of K562 Cell Line and Decreases the Cell Viability

To study Kola nut extracts' effect on cell viability, we performed resazurin cell viability assay and live/dead trypan blue assays. Our results showed that Kola nut extract's anti-proliferative ability against the K562 leukemic cell line increases cell death rate. These effects were investigated at three incubation periods of 24, 48, and 72. (Figure 1). Positive anti-proliferative activities were visible in 48 and 72 hours of incubation, from the lowest concentration of the treatment (50 µg/ml) and steadily up to the highest concentration (200 µg/ml). Although the maximum inhibitory effect on K562 proliferation was not exceeding 30%, the rate of dead K562 cells was sharply raised to approximately 50% after 72 hours incubation, which is greater than that of 24 and 48 hours incubation period (Figure 2). The cell growth rate was also significantly reduced at concentrations of 150 and 200 µg/ml), results not shown. Therefore, from the results above, the inhibitory rate of K562 cell proliferation treated by Kola nut was increased in a dose and time-dependent manner. Moreover, Kola nut extract proved a high possible activity was inducing apoptosis and leukemia inhibition in K562 cell proliferation.

Kola Nut Extract Induces Variable Forms of Cell Death in K562 Cell Lines

By using flow cytometer technique with FITC annexin V and PI staining of K562 cell line treated with Kola nut extract with indicated doses (50,150, 250 µg/ml) and time intervals (24 and 48 hours), we observed that kola nuts successfully induced cell death; apoptosis (early and late) and necrosis; after 24 (figure 3), and 48 hours (figure 4) incubation period. The results revealed an increase in total apoptotic cells from 5.8% (control) to 27.4% (250 µg/ml) compared to the rate of necrosis (not higher than 7%). Also, 4-time increases in the percentage of late apoptotic cells were observed compared to early apoptotic cells (a maximum of 5% early apoptotic and 22.4% late apoptotic). The percentage of cells declined by approximately 23% (from 91% to 68% live cells population).

After 48 hours of incubation, the Kola nut extract's apparent effect was observed with all designed concentrations and quite a high efficiency compared with 24 hours, as seen in figure 4 and table 1. The K562 cells showed a relatively similar dose-dependent decrease in the population of live cells (from 93% to 71%) as after 24 hours, where the percentage of total apoptotic cells increased by about 22% compared with untreated control cells. In both 24 and 48 incubation periods, Kola nut's ability to induce necrosis was also observed; however, it was neglected compared to the apoptotic population.

Kola Nut Extracts Arrest the Cell Cycle in G2/M phase of the Cell Cycle

While studying the impact of Kola nut extract on the distribution of cell cycle phases, different Kola nut extract (from 0 to 250 µg/ml) were applied following two incubation periods of 24 and 48 hours. The results are shown in figure 3 (After 24 hours incubation), and figure 4 (After 48 hours incubation) showed the dose-dependent impact of Kola nut extract on the distribution of cell cycle phases.

As seen in table 2, the cells treated with Kola nut extract showed rise in the G2/M phase percentage from approximately 9.8% to the maximum of 29.8% from 5.2% to 14.6% following 24 and 48 hours, respectively. Alternatively, a noticeable decline in the overall G0/G1 and S phases was observed by approximately 27% and 19%, respectively, following the treatment of indicated doses of Kola nut extract.

Discussion

Treating CML patients with TKI is accepted as a practical option with an increased survival rate in most patient populations; however, specific adverse effects are associated with this treatment option. Studies report toxicities and different adverse events such as pleural effusion, vascular events, and arterial hypertension associated with TKIs. The estimated treatment cost per patient in European countries is reported to be ~30 000-40 000 € per year[39]. Also, indefinite treatment with TKI might be needed for some patients even after attaining a deep molecular remission[41]. Due to these complications, efforts were made to find an alternative route more inclined toward naturally available options with minimal adverse effects and more cost-effective. For that reason, our study was designed to evaluate the response of the human immortalized myelogenous leukemia cell line K562 against Kola nut extract at different doses and incubation periods. As the work to study Kola nut extracts' pharmacological action on breast and prostate cancer cell lines has already been re-

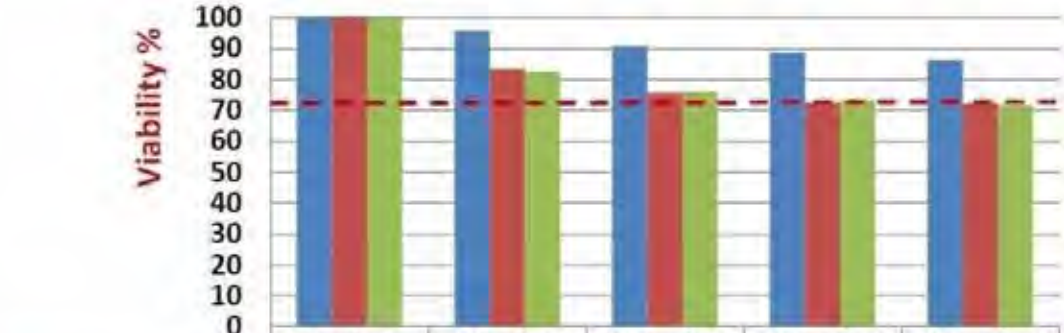

	Control	50µg/mL	100µg/mL	150µg/mL	200µg/mL
Viability % (24 hrs)	100	95.68	90.87	88.73	86.23
Viability % (48 hrs)	100	83.48	75.71	72.55	72.20
Viability % (72 hrs)	100	82.54	75.90	73.28	71.79

Figure 1. Anti-proliferative Kola nut extract activity against K562 cells after 24-, 48-, and 72-hours incubation. The resazurin cell viability assay was used to indicate an anti-proliferative effect on the seeding of 5 x 103 K562 cells. The control represents untreated K562 cells. Several treatment concentration points were used (50, 100, 150, and 200 µg/ml). The results are based on a single experiment, and RPMI/ DMSO media was used as a blank. The red line indicated the maximum inhibitory effect obtained by Kola nut treatment after 24-, 48-, and 72-hours incubation.

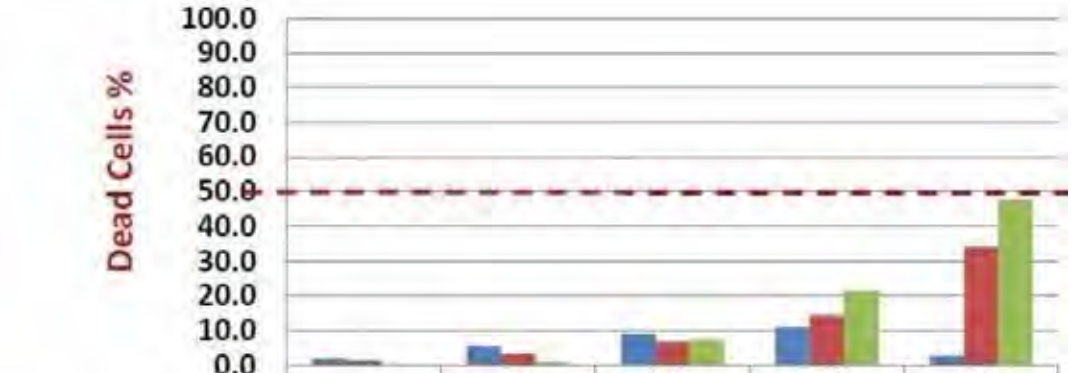

	Control	50 µg/mL	100 µg/mL	150 µg/mL	200 µg/mL
Death Rate - 24 hrs	2.0	5.6	9.0	10.9	2.8
Death Rate - 48 hrs	1.4	3.1	6.8	14.4	34.1
Death Rate - 72 hrs	0.3	0.9	7.4	21.5	47.7

Figure 2. Death rate obtained by Kola nut extract against K562 cells after 24-, 48-, and 72-hours incubation. The trypan blue assay was used to investigate Kola nut's possibility to induce cell death on seeding of 15 x 104 K562 cells. The control represents untreated K562 cells. Several treatment concentration points were used (50, 100, 150, and 200 µg/ml). The results are based on a single experiment. The red line indicated the maximum cellular death rate obtained by Kola nut treatment after 24-, 48-, and 72-hours incubation.

Time (hours)	24 hours				48 hours			
Apoptosis (%)	Kola nut dose (mg/ml)							
	0	50	150	250	0	50	150	250
Live (%)	90.9	88.3	67.3	68.6	93.3	91.4	71.9	71.2
Early apoptotic (%)	0.7	0.9	3.2	5	2.2	3	2.3	2.2
Late apoptotic (%)	5.1	6.8	22.2	22.4	3.3	4.3	24.4	25.2
Necrotic (%)	3.3	4	7.3	4	0.7	1.4	1.3	1.4
Total Apoptotic (%)	5.8	7.7	25.4	27.4	5.5	7.3	26.7	27.4

Table 1. Effect of Dose and Time Course –Dependence of Kola Nut Extract on Induction of Apoptosis and Necrosis in K562 Cells.

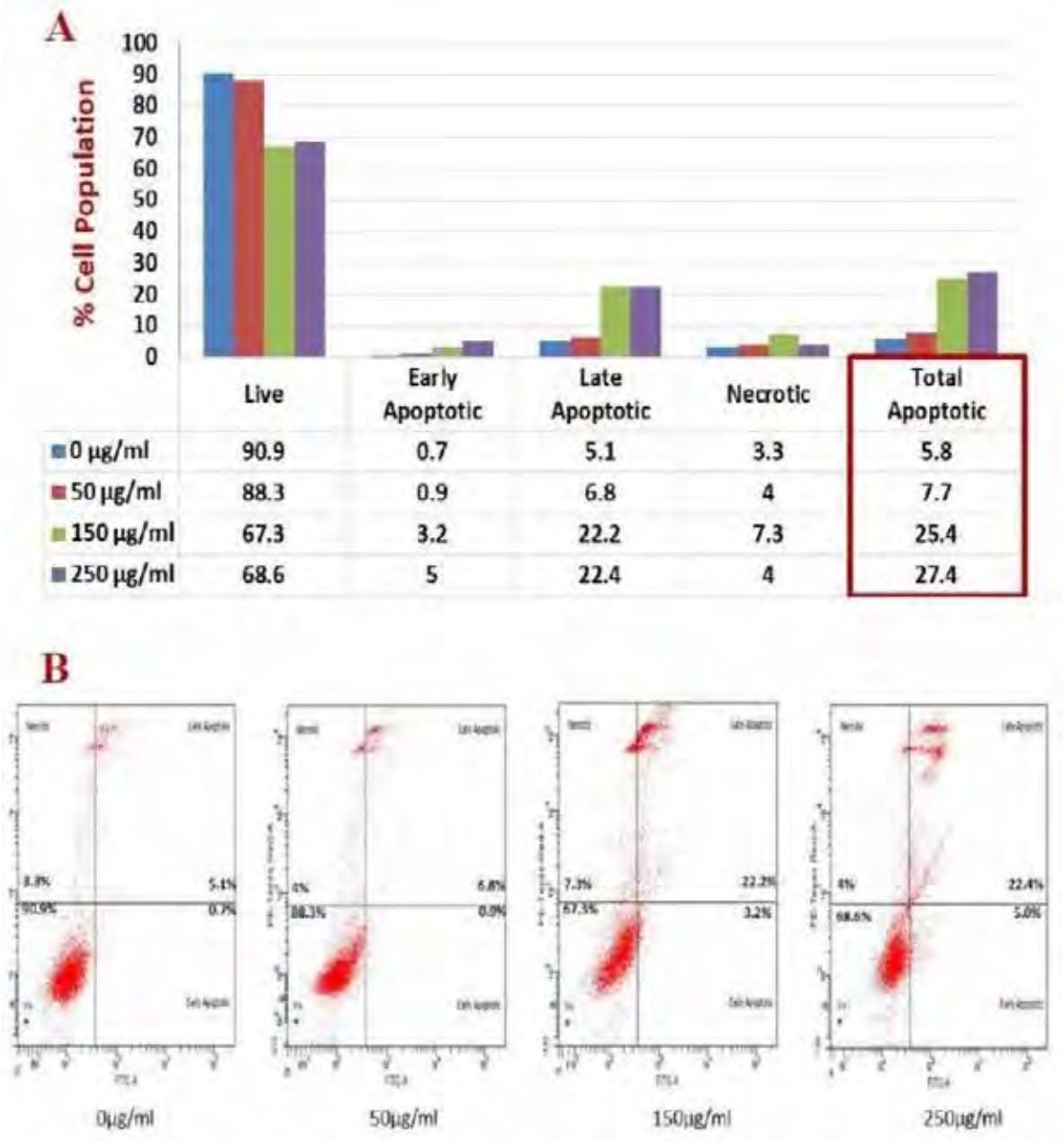

Figure 3. The illustrative chart (A) and flow cytometer scatter plot (B) showed the activity of Kola nut extract to induce apoptosis/necrosis on K562 cells that incubated for 24 hours, stained with Annexin V/PI, and analyzed by flow cytometer. Total apoptosis represents both early and late apoptotic forms.

Time (hours)	24 hours				48 hours			
Cell Cycle Phase (%)	Kola nut dose (mg/ml)							
	0	50	150	250	0	50	150	250
Apoptotic	0.8	3.2	8.2	7.5	1.7	5.2	10.9	22.8
G0 / G1	45.3	23.1	17.7	17.5	48.4	43.7	22.1	29.6
S	39.7	27.2	26.7	18.7	41.8	37.7	31	24.6
G2 / M	9.8	29.8	28.4	24.7	5.2	4.1	14.6	12.1

Table 2. K562 Cell Cycle Distribution (G0/G1, S and G2) After Followed Dose and Time Course Incubation with Kola Nut Extract Treatment.

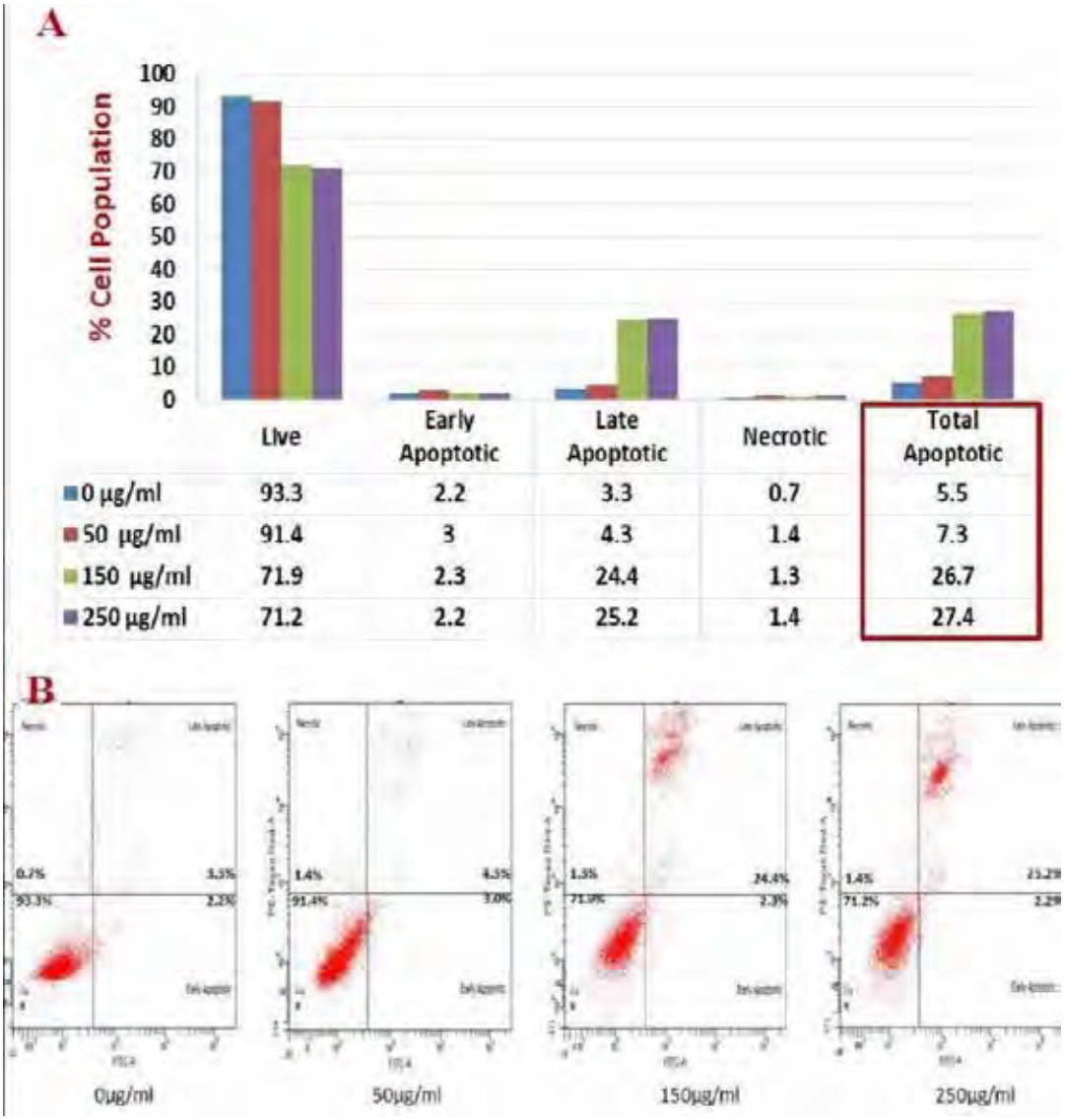

Figure 4. The illustrative chart (A) and flow cytometer scatter plot (B) showed the activity of Kola nut extract to induce apoptosis/necrosis on K562 cells that incubated for 48 hours, stained with Annexin V/PI stain, and analyzed by flow cytometer. Total apoptosis represents both early and late apoptotic forms.

ported in the literature[34-36]. Our work proved that the Kola nut extract could inhibit the growth of human myelogenous Leukemia and reduce cell viability in a dose and time-dependent manner. Fontenot and his colleagues (2007) initially screened the cytotoxicity of several extracts (hexane, ether, acetone, methanol, and distal water) of Kola nut on the viability of the estrogen-responsive breast cancer cells (MCF-7) that showed diverse effects of each extract at 100 ppm after 24 hours; in proliferation assay, they detected that the acetone extract induced more significant than 50% of cell death. Contrarily, the other extracts showed a growth stimulator to MCF-7 cell line, especially ether extract, while in exclusion trypan blue assay, the affected extracts acetone and ether showed a reduction in the viable cells number as compared to control cells. These findings are consistent with the present study, which displayed a decline in the number of the K562 cells treated with Kola nut extract.

Additionally, Fontenot and his colleagues (2007) have found out that the ether extract of Kola nut can impede the growth of the androgen-dependent (LNCaP) prostate tumor cell model due to the strong affinity for the androgenic receptor. Those findings indicate that the different extractable bioactive compounds of Kola nut may have chemopreventive activities, which are selectively toxic to cancerous cells[34-36]. In consideration of this, the apoptotic assay was performed on K562 cell lines treated with Kola nut extracts, and the results revealed that Kola nut extract could stimulate different forms of cell death: early and late apoptosis and necrosis with the percentages of late apoptotic cells more noticeable than other forms of cell death. Late apoptotic cells or secondary necrotic cells arise from early apoptotic cells that develop due to their unrecognizable signals by the phagocytic cells[42,43]. This is because the impairment of phagocytosis makes the early apoptotic cells accumulate and progress to late apoptotic cells or secondary necrotic cells[42,43]. The late apoptotic cells also indicate that they carry a remaining early hallmark of apoptosis signal, Annexin-V binding protein, which is produced when the phosphatidylserine of cell membrane undergoes exposure to internal cells stimulus[44]. Besides, the stimulus of Kola nut extract may affect a time-dependent manner as several hours are needed for late apoptosis enhancement[45].

Other than the possible type of cell death inducement, the mechanism of target action on cell cycle distribution has been

studied. It is well-known that the impaired cell cycle is a hallmark of cancer cells[18,46]. As evident from this study, Kola nut extract arrested the cell cycle in G2/M phase, with increased cells in this phase and reduced the number of cells in G0/G1 and S phases. Interestingly, the G2/M phase has a checkpoint that signifies as a potential target for cancer therapy, which prevents the cells that have damaged DNA in the late S or G2 phase to enter the mitotic phase, to re- repairing and thus, retarded the proliferation of cell through halting the cell cycle progression[47]. Thus, the promoted cell cycle arrest thought to provide evidence that the Kola nut extract could regulate the proliferation of the cells, although a previous study showed that Kola nut extract treatment caused dysregulation of cell cycle in breast cancer cell line MCF-7; after 24 hours at two indicted doses (80 and 60 µg/ml); however, their results revealed that the Kola nut extract has an obvious effect on both the S and G2/M phases by reducing the percentages of cells involved in each phase; while, the G2/M phase was increased in the present study[36].

Conclusions

Kola nut extracts can be used as an anti-cancer agent against CML *in vitro* as it has shown a tremendous therapeutic potentiality and therefore providing new insights in understanding the mechanisms of its action against CML. However, an experimental plan for using the Kola nut extracts against a cell line of acute myeloblastic leukemia origin representing a study limitation in our current work may give a better picture and understanding of the anti-cancer activity of this promising therapeutic agent.

Acknowledgment

King Abdulaziz City funded this work for Science and Technology (KACST) (Grant no. 1-17-00-009-0020). The authors, therefore, acknowledge with thanks KACST for financial support.

Conflict of Interest

All authors declare that they have no conflict of interest associated with this publication.

Bibliographic references

1. Davis AS, Viera AJ, Mead MD. Leukemia: an overview for primary care. American family physician. 2014;89(9):731-8.
2. Arber DA, Orazi A, Hasserjian R, Thiele J, Borowitz MJ, Le Beau MM, et al. The 2016 revision to the World Health Organization classification of myeloid neoplasms and acute leukemia. Blood. 2016;127(20):2391-405.
3. Soverini S, De Benedittis C, Mancini M, Martinelli G. Best practices in chronic myeloid leukemia monitoring and management. The Oncologist. 2016;21(5):626.
4. Jabbour E, Kantarjian H. Chronic myeloid leukemia: 2018 update on diagnosis, therapy and monitoring. American journal of hematology. 2018;93(3):442-59.
5. Hutter JJ. Childhood leukemia. Pediatr Rev. 2010;31(6):234-41.
6. Radivoyevitch T, Sachs R, Gale R, Molenaar R, Brenner D, Hill B, et al. Defining AML and MDS second cancer risk dynamics after diagnoses of first cancers treated or not with radiation. Leukemia. 2016;30(2):285-94.
7. Gatenby RA. A change of strategy in the war on cancer. Nature. 2009;459(7246):508-9.
8. Corrie PG. Cytotoxic chemotherapy: clinical aspects. Medicine. 2008;36(1):24-8.
9. Staat K, Segatore M. The phenomenon of chemo brain. Clinical journal of oncology nursing. 2005;9(6):713.
10. Rodgers GM, Becker PS, Blinder M, Cella D, Chanan-Khan A, Cleeland C, et al. Cancer-and chemotherapy-induced anemia. Journal of the National Comprehensive Cancer Network. 2012;10(5):628-53.
11. Al-Mohanna H, Al-Khenaizan S. Permanent alopecia following cranial irradiation in a child. Journal of cutaneous medicine and surgery. 2010;14(3):141-3.
12. Elad S, Zadik Y, Hewson I, Hovan A, Correa MEP, Logan R, et al. A systematic review of viral infections associated with oral involvement in cancer patients: a spotlight on Herpesviridea. Supportive care in cancer. 2010;18(8):993-1006.
13. Chorawala M, Oza P, Shah G. Mechanisms of anti-cancer drugs resistance: an overview. Int J Pharm Sci Drug Res. 2012;4(1):1-9.
14. Hatzimichael E, Tuthill M. Hematopoietic stem cell transplantation. Stem cells and cloning: advances and applications. 2010;3:105.
15. Kasteng F, Sobocki P, Svedman C, Lundkvist J. Economic evaluations of Leukemia: a review of the literature. International journal of technology assessment in health care. 2007;23(1):43.
16. Mohty B, Mohty M. Long-term complications and side effects after allogeneic hematopoietic stem cell transplantation: an update. Blood cancer journal. 2011;1(4):e16-e.
17. Samudio I, Konopleva M, Carter B, Andreeff M. Apoptosis in leukemias: regulation and therapeutic targeting. Acute Myelogenous Leukemia: Springer; 2009. p. 197-217.
18. Hanahan D, Weinberg RA. Hallmarks of cancer: the next generation. cell. 2011;144(5):646-74.
19. Talpaz M, Hehlmann R, Quintás-Cardama A, Mercer J, Cortes J. Re-emergence of interferon-- in the treatment of chronic myeloid leukemia. Leukemia. 2013;27(4):803-12.
20. Woessner DW, Lim CS, Deininger MW. Development of an effective therapy for chronic myelogenous Leukemia. Cancer J. 2011;17(6):477-86.
21. Kooti W, Servatyari K, Behzadifar M, Asadi-Samani M, Sadeghi F, Nouri B, et al. Effective medicinal plant in cancer treatment, part 2: review study. Journal of evidence-based complementary & alternative medicine. 2017;22(4):982-95.
22. Solowey E, Lichtenstein M, Sallon S, Paavilainen H, Solowey E, Lorberboum-Galski H. Evaluating medicinal plants for anti-cancer activity. The Scientific World Journal. 2014;2014.
23. Jo E-H, Hong H-D, Ahn N-C, Jung J-W, Yang S-R, Park J-S, et al. Modulations of the Bcl-2/Bax family were involved in the chemopreventive effects of licorice root (Glycyrrhiza uralensis Fisch) in MCF-7 human breast cancer cell. Journal of agricultural and food chemistry. 2004;52(6):1715-9.
24. Rech Franke SI, Guecheva TN, Henriques JAP, Prá D. Orange juice and cancer chemoprevention. Nutrition and cancer. 2013;65(7):943-53.
25. Steward W, Brown K. Cancer chemoprevention: a rapidly evolving field. British journal of cancer. 2013;109(1):1-7.
26. Dah-Nouvlessounon D, Adjanohoun A, Sina H, Noumavo PA, Diarrasouba N, Parkouda C, et al. Nutritional and anti-nutrient composition of three kola nuts (Cola nitida, Cola acuminata and Garcinia kola) produced in Benin. Food and Nutrition Sciences. 2015;6(15):1395.
27. Atawodi SE-o, Pfundstein B, Haubner R, Spiegelhalder B, Bartsch H, Owen RW. Content of polyphenolic compounds in the Nigerian stimulants Cola nitida ssp. alba, Cola nitida ssp. rubra A. Chev, and Cola acuminata Schott & Endl and their antioxidant capacity. Journal of agricultural and food chemistry. 2007;55(24):9824-8.
28. Ishidate Jr M, Sofuni T, Yoshikawa K, Hayashi M, Nohmi T, Sawada M, et al. Primary mutagenicity screening of food additives currently used in Japan. Food and chemical toxicology. 1984;22(8):623-36.
29. Ibu J, Iyama A, Ijije C, Ishmael D, Ibeshim M, Nwokediuko S. The effect of Cola acuminata and Cola nitida on gastric acid secretion. Scandinavian Journal of Gastroenterology. 1986;21(sup124):39-45.

30. Tende J, Ezekiel I, Dare S, Okpanachi A, Kemuma S, Goji A. Study of the effect of aqueous extract of kolanut (Cola nitida) on gastric acid secretion and ulcer in white wistar rats. British Journal of Pharmacology and Toxicology. 2011;2(3):132-4.
31. Okoli B, Abdullahi K, Myina O, Iwu G. Caffeine content of three Nigerian cola. Journal of Emerging Trends in Engineering and Applied Sciences. 2012;3(5):830-3.
32. Gaspar S, Ramos F. Caffeine: consumption and health effects. Encyclopedia of Food and Health. 2016:573-8.
33. Adam SI, Yahya AA, Salih WM, Abdelgadir WS. Antimicrobial activity of the masticatory Cola acuminata Nut (Gooro). Current Research Journal of Biological Sciences. 2011;3(4):357-62.
34. Fontenot K, Naragoni S, Claville M, Gray W. Characterization of Bizzy Nut extracts in estrogen-responsive MCF-7 breast cancer cells. Toxicology and applied pharmacology. 2007;220(1):25-32.
35. Solipuram R, Koppula S, Hurst A, Harris K, Naragoni S, Fontenot K, et al. Molecular and biochemical effects of a kola nut extract on androgen receptor-mediated pathways. Journal of toxicology. 2009;2009.
36. Endrini S, Jaksa S, Marsiati H, Othman F, Rahmat A. Effects of cola nut (Cola nitida) on the apoptotic cell of human breast carcinoma cell lines. Journal of Medicinal Plants Research. 2011;5(11):2393-7.
37. Lozzio CB, Lozzio BB. Human chronic myelogenous leukemia cell-line with positive Philadelphia chromosome. 1975.
38. Koeffler H, Golde D. Human myeloid leukemia cell lines: a review. 1980.
39. Saussele S, Richter J, Hochhaus A, Mahon F. The concept of treatment-free remission in chronic myeloid Leukemia. Leukemia. 2016;30(8):1638-47.
40. Francis J, Palaniappan M, Dubashi B, Pradhan SC, Chandrasekaran A. Adverse drug reactions of imatinib in patients with chronic myeloid Leukemia: A single-center surveillance study. J Pharmacol Pharmacother. 2015;6(1):30-3.
41. García-Gutiérrez V, Hernández-Boluda JC. Tyrosine kinase inhibitors available for chronic myeloid Leukemia: Efficacy and safety. Frontiers in Oncology. 2019;9:603.
42. Ravichandran KS, Lorenz U. Engulfment of apoptotic cells: signals for a good meal. Nature Reviews Immunology. 2007;7(12):964-74.
43. Poon IKH, Hulett MD, Parish CR. Molecular mechanisms of late apoptotic/necrotic cell clearance. Cell Death & Differentiation. 2010;17(3):381-97.
44. Smith BA, Smith BD. Biomarkers and molecular probes for cell death imaging and targeted therapeutics. Bioconjugate chemistry. 2012;23(10):1989-2006.
45. Ziegler U, Groscurth P. Morphological Features of Cell Death. Physiology. 2004;19(3):124-8.
46. Malumbres M, Barbacid M. Cell cycle, CDKs and cancer: a changing paradigm. Nature Reviews Cancer. 2009;9(3):153-66.
47. Wang Y, Ji P, Liu J, Broaddus RR, Xue F, Zhang W. Centrosome-associated regulators of the G2/M checkpoint as targets for cancer therapy. Molecular Cancer. 2009;8(1):8.

Received: 15 November 2020
Accepted: 15 February 2021

RESEARCH / INVESTIGACIÓN

Gestión de la calidad en tiempos de Covid-19: Nueva metodología de trabajo en Investigaciones Agropecuaria del Centro de Ingeniería Genética y Biotecnología, Cuba

The Quality Management Systems in Covid-19 Times: New approaches to research projects at the Center for Genetic Engineering and Biotechnology, Cuba

I. Menéndez[1], A. Rodríguez[1], A. Hernández[1], A. Mena[2], MP. Estrada[1]

DOI. 10.21931/RB/2021.06.02.11

Resumen: Los Sistemas de Gestión de Calidad (SGC) se utilizan en las empresas biotecnológicas especialmente en las áreas de investigaciones para gestionar los proyectos. La pandemia de la Covid-19 ha provocado un impacto en la manera de aplicar los SGC. Este reporte resume los cambios en la gestión de los proyectos en el área de las Investigaciones Agropecuarias del CIGB. Se diseñó una nueva metodología de trabajo, encaminada a potenciar la introducción de los cultivos transgénicos en la producción de alimentos, en tiempos de Covid. Como resultado principal, la reorganización en el trabajo bajo las normas de los SGC, permitió que los proyectos de mayor relevancia económica para el país cumplimentaran los objetivos estratégicos propuestos.

Palabras clave: Covid-19, Sistemas de Gestión de Calidad, Biotecnología.

Abstract: Quality Management Systems (QMS) are essential tools for biotechnological enterprises, especially in investigation areas, in which QMS are used to manage the research projects. The worldwide COVID 19 pandemics generated the search for more consistent QMS strategies. This work aims to summarize new approaches for the management of research projects at the Center for Genetic Engineering and Biotechnology (CIGB). A novel methodology was designed to introduce transgenic crops for food production. The QMS remodelling permitted that the most relevant CIGB research projects fulfil the proposed goals.

Key words: Quality Management Systems, transgenic crops, Covid-19, Biotechnology.

Introducción

La producción de alimentos en Cuba deviene prioridad y constituye hoy más que nunca un asunto de soberanía nacional[1]. En el escenario actual, en que la pandemia de la Covid-19, obligó a cerrar fronteras, el comercio se paralizó y se arrecian las medidas del bloqueo económico contra el país establecido por EE.UU., se hace imprescindible generalizar e innovar a grandes escalas los resultados científicos relacionados con la esfera de la agricultura y de esta forma sustituir las importaciones que garantizan la adecuada alimentación de la población cubana.

Como parte de la política estatal, el Centro de Ingeniería Genética y Biotecnología de Cuba (CIGB) que realiza investigación, desarrollo, producción y comercializa el resultado de su labor, tiene un área dedicada a las Investigaciones Agropecuarias (IAP) que desarrolla productos aplicados a la investigación de genes para la defensa de las plantas frente a plagas, al mejoramiento genético de especies vegetales de interés agrícola, así como a la investigación de biocatalizadores para la conversión del azúcar de caña[2] en productos de alto valor agregado entre otros proyectos científicos de la biotecnología aplicada a las plantas, animales y la industria[3,4].

La utilización de los productos transgénicos, hoy en el mundo, se ha convertido en una estrategia de importancia para el desarrollo sostenible de la producción de alimentos en muchos países. Es una herramienta útil para la creación de cultivos resistentes a plagas, virus o variaciones genéticas que permiten el incremento de la productividad en campo. El CIGB cuenta con más de 30 años de experiencia en las investigaciones relacionadas con los Organismos Genéticamente Modificados (OMG)[5] y ha trabajado siempre dentro del marco legal que regula y controla el empleo de estos OMG en el país y en el mundo (aprobación del decreto ley 4/2000).

Los Sistemas de Gestión de Calidad (SGC) son muy utilizados en las empresas biotecnológicas, especialmente en las áreas de investigaciones para gestionar sus proyectos. Los SGC se caracterizan por su eficacia para la gestión de procesos, mejoras de productos y servicios y satisfacción de sus clientes. El área de IAP del CIGB en su gestión ha hecho uso de las Tecnologías de la información y las comunicaciones (TIC) y el establecimiento de las Buenas Prácticas de Laboratorio (BPL, Normas ISO 9001)[4]. Sin embargo, la aparición de la pandemia, ha provocó la adopción de nuevas estrategias y metodologías de trabajo para el cumplimiento de los objetivos y tareas de los proyectos donde el empleo de las TIC, ha jugado un papel protagónico. A su vez, se desarrollaron nuevas estrategias de trabajo, tales como: a) cambiar el nivel de prioridad en favor de los proyectos más avanzados, que estaban relacionados directamente con la producción de alimentos; b) fomentar la introducción de productos biotecnológicos OMG de manera ordenada y controlada en los programas de desarrollo agrícolas[6]. Estos cambios llevaron a potenciar la introducción de los cultivos transgénicos en la producción de alimentos[7] del país como una alternativa, para mejorar la eficiencia económica de estas producciones. Este reporte resume los cambios en la Gestión de los Proyectos en el área de IAP del CIGB, que demostraron un mejor aprovechamiento de la fuerza de trabajo y avance de los proyectos en tiempos de Covid-19.

[1] Agricultural Research, Center for Genetic Engineering and Biotechnology, Cuba.
[2] Quality Management Systems, Center for Genetic Engineering and Biotechnology, Cuba.

Corresponding author: ivon.menendez@cigb.edu.cu

Materiales y métodos

Reorganización del personal en los laboratorios

Como se muestra en la figura 1, a partir del mes marzo en que comenzó la pandemia en Cuba, se observa que el personal de los laboratorios disminuyó aproximadamente a un 40 % con respecto a meses anteriores. Se asumió como prioridad los proyectos estratégicos para el área y para el centro. El resto del personal se mantuvo en la modalidad de teletrabajo (Figura 1).

Actualización de la Carpeta de Proyecto

Cada Jefe de Proyecto en la modalidad de teletrabajo actualizó y confeccionó, toda la documentación necesaria para el seguimiento y cumplimiento de los objetivos y tareas específicas de sus proyectos. (Carpeta de proyecto). Toda la documentación fue revisada y aprobada por la Dirección de Gestión de la calidad y asuntos regulatorios, por vía electrónica. Se realizaron video- conferencias con los jefes de los proyectos para la discusión de la actualización de los objetivos anuales bajo las nuevas condiciones y de la misma forma fueron chequeados los resultados semestrales de cada proyecto con la Dirección del área y la Dirección General del CIGB.

Cumplimiento de la normas establecidas por BPL

Se mantuvo la revisión de los libros de trabajo, como está establecido cada cuatro meses, por parte de los jefes de proyecto y por la responsable de BPL. Las inspecciones de los laboratorios se realizaron de manera coordinada y se programaron de manera que solo permaneciera en los laboratorios, el personal necesario. Los recursos materiales, fueron utilizados de forma racional, para lograr el ahorro al máximo de los mismos. Se cumplió con las normas establecidas por las BPL como en períodos anteriores por todo personal que se encontraba trabajando.

Cumplimiento de las normas de Bioseguridad

Todo el personal se mantuvo trabajando en el CIGB bajo los protocolos de Bioseguridad establecidos. Se exigió en todo momento el uso obligatorio del nasobuco dentro y fuera del centro, la desinfección de las manos a la entrada del centro y a la entrada de los pisos en el edificio central, la presencia de los pasos podálicos en cada área de la instalación, la desinfección de las superficies y el distanciamiento físico fueron las más generalizadas. Además, se establecieron las medidas de bioseguridad en todos los laboratorios donde se está trabajando los proyectos relacionados con las investigaciones sobre Covid-19.

Cumplimiento de los objetivos por proyecto en tiempos de Covid-19

En la figura 2 se muestra el porciento de cumplimiento de los objetivos de los proyectos en el año 2019 y en el 2020. Al comparar ambos años se aprecia una disminución del cumplimiento de los objetivos con respecto al 2019. Sin embargo, se logró un aumento en el número de publicaciones y patentes, que refleja el impacto positivo del teletrabajo en tiempos de Covid-19. (Figura 2).

Impacto de las nuevas estrategias en la gestión organizativa

La situación de confinamiento provocada por Covid-19 también ha tenido un impacto en la gestión organizativa de la institución. El teletrabajo, como una medida de distanciamiento necesaria adoptada por el gobierno cubano, impone nuevas formas de relacionarse con la información[8]. Por ejemplo, se ha hecho necesario mejorar las condiciones de conectividad que garanticen el intercambio de información y los protocolos de seguridad informática. Por otra parte, desde que se establece dentro de los marcos legales para la institución, hay una mejoría en los índices de ausentismo y de aprovechamiento de la jornada laboral. Todo esto contribuye al incremento de la productividad y, por ende, lograr los resultados esperados.

Otras de las estrategias que incide directamente en la gestión organizativa fue la reprogramación de los objetivos planificados en los proyectos del área. Este cambio en las prioridades de trabajo se centró en desarrollar los proyectos más avanzados, que estaban relacionados directamente con la producción de alimentos; y en la realización de publicaciones científicas, por ende, propicia un aumento de la visibilidad de todos los resultados obtenidos hasta la fecha[9,10].

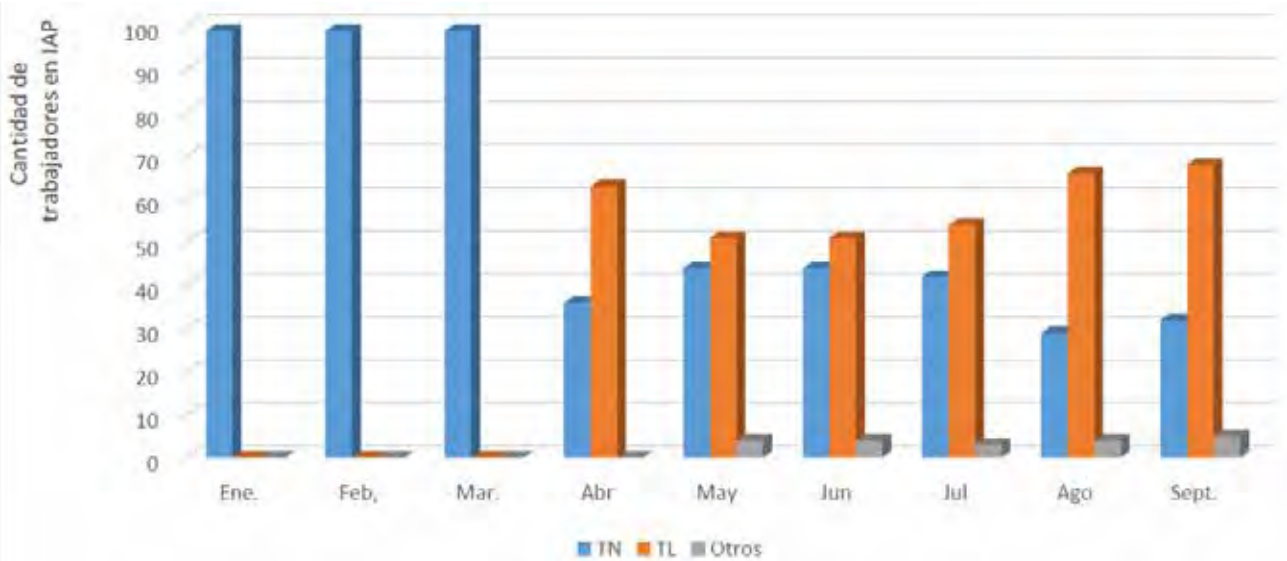

Figure 1. Distribución de la fuerza de trabajo en los primeros 9 meses del año 2020 en IAP. TN: trabajo normal, TL: tele trabajo.

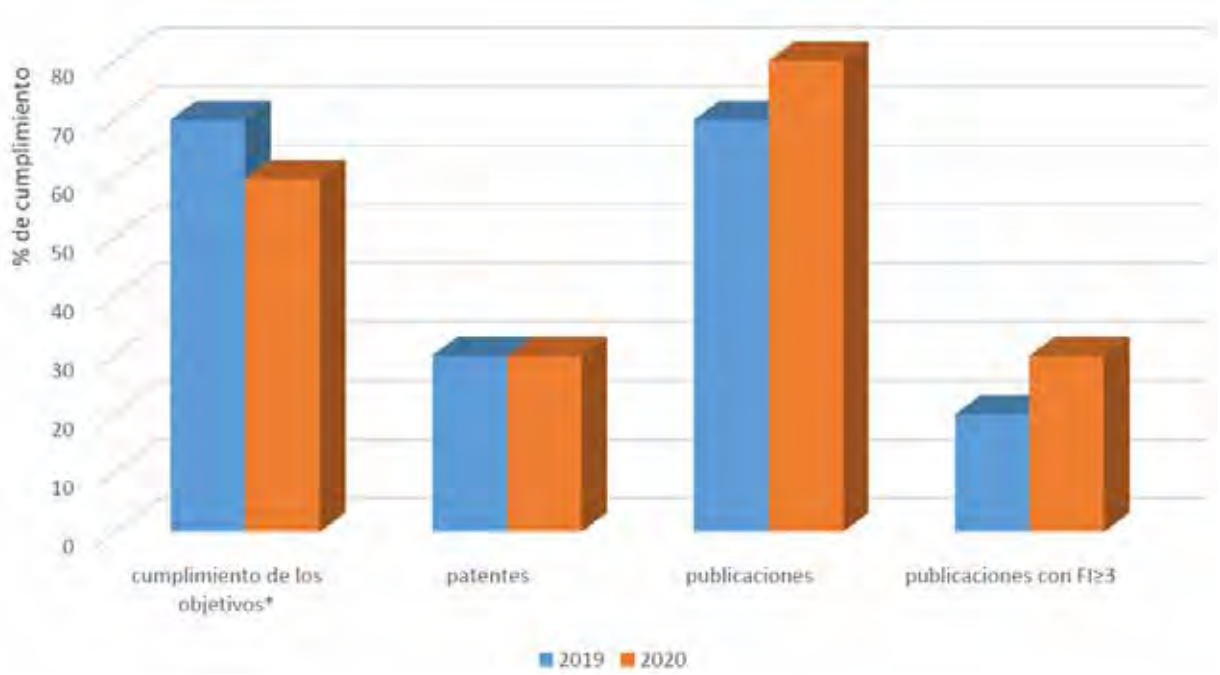

Figure 2. Principales resultados de los proyectos en los años 2019 y 2020 en IAP.*Objetivos trazados en cada proyecto de investigación.

Conclusiones

Gracias a la restructuración oportuna de la metodología de trabajo del área de IAP en tiempos de Covid-19, se ha logrado cumplimentar con éxitos, los objetivos estratégicos de los proyectos de mayor relevancia económica para el centro y para el país. Esta metodología fue una solución efectiva para mantener la seguridad de todo nuestro personal en tiempos de pandemia.

Referencias bibliográficas

1. Costa A, Sousa R, Sorzano A. Soberanía y seguridad alimentaria en Cuba: políticas públicas necesarias para reducir la dependencia alimentaria. Agrisost. 2013;19(3):1-14.
2. González-Fernández N. First International Conference Bioprocess Cuba 2017. Biotecnol Apl. Published online 2017:4501-4504.
3. Menéndez I, Hermida L, Hernández A, et al. Characterization nanoparticles-based vaccines and vaccine candidates: a Transmission Electron Microscopy study Caracterización por Microscopía Electrónica de Transmisión de vacunas y candidatos vacunales basados en nanopartículas. Bionatura. 2016;1(2).
4. Menéndez I, Orquín A, García MP. Gestión de Calidad en Centro de Ingeniería Genética. Aenor. Published online 2017. https://portal.aenormas.aenor.com/revista/325/casos-practicos-cigb.html
5. Blanco Miranda Y. Nuevo decreto-ley regula uso de los organimos geneticamente modificados en la agricultura. Juv Técnica.
6. Chavez Fernandez L. Prevén mayor uso de organismos genéticamente modificados en la agricultura cubana. Agencia Cuba Not. Published online 2021.
7. Morejon-Pereda M, Herrera-Altuve JA, Ayra-Pardo C, et al. Alternativas en la nutrición del maíz transgénico FR-Bt1 de (Zea mays L.): respuesta en crecimiento, desarrollo y producción. Cultiv Trop. 2017;38(4):146-155.
8. Martí-Noguera JJ. Sociedad digital: gestión organizacional tras el COVID-19. Rev Venez Gerenc. 2020;25(9).
9. Rodríguez-Mallon A, Encinosa Guzmán P, Bello Soto Y, et al. A chemical conjugate of the tick P0 peptide is efficacious against Amblyomma mixtum. Transbound Emerg Dis. Published online 2020:175-177.
10. Rodríguez Mallón A, Javier González L, Encinosa Guzmán P, et al. Functional and Mass Spectrometric Evaluation of an Anti-Tick Antigen Based on the P0 Peptide Conjugated to Bm86 Protein. Pathogens. Published online 2020:513.

Received: 28 diciembre 2021
Accepted: 10 febrero 2021

RESEARCH / INVESTIGACIÓN

Differences of sodium consumption pattern hypertension sufferer in coastal and highland communities in Wakatobi islands

La Ode Alifariki[1], Tukatman Tukatman[2], Bangu Bangu[2], HeriviyatnoJulika Siagian[2*]
DOI. 10.21931/RB/2021.01.02.12

Abstract: Available data indicate that food sodium (such as salt) is directly related to blood pressure (BP). The research aims to look at the different sodium consumption patterns of hypertension sufferers in two different coastal areas and highland areas in the Wakatobi Islands. The type of research is observational analytic research using a cross-sectional design. This study has been carried out in the District of Wangi-Wangi, especially in the MolaSamaturu villages and Waginopo Village in October 2019. The number of research samples is 100 people (50 respondents in Mola Samaturu Village and 50 people in Waginopo Village). The results showed the differences between sodium consumption patterns in hypertensive sufferers in Mola Samaturu Village and Waginopo Village with a p-value = 0,000 <α 0.05. Sodium consumption patterns in coastal communities are higher than in highlands community.

Key words: Hypertension, sodium consumption pattern, Wakatobi islands.

Introduction

Hypertension is a significant risk factor for cardiovascular and cerebral vascular disease, also kidney failure. It is known that the amount of salt intake in meals plays a role in the pathogenesis of primary hypertension[1-3]. Increased sensitivity of blood pressure toward excess sodium affects 50% of patients with primary hypertension[4,5]. Salt dietary intake causes enhancement of blood pressure associated with kidney and cardiovascular diseases, including left ventricular hypertrophy and microalbuminuria[6].

Sodium is the most cation in an extracellular fluid where 35-40% (60 mmol per kg of body weight) is in the skeleton, and a small portion (about 10-14 mmol / L) is in the intracellular fluid7. Under normal circumstances, sodium excretion in the kidneys is regulated to maintain a balance between intake and output, with extracellular fluid volume remains stable[8]. More than 90% of the extracellular fluid's osmotic pressure is determined by salt, specifically in sodium chloride (NaCl) and sodium bicarbonate (NaHCO3), thereby changing the osmotic pressure in the extracellular fluid represents changing sodium concentration[9].

Increased sodium intake causes fluid retention of the body, which increases blood volume by pulling intra-cellular fluid into extracellular so that the heart should pump forcefully to drive large volumes of blood through narrowing of the intravascular space, which results in hypertension[10,11]. This was proven in a study conducted by Abdurrachim, Hariyawati, and Suryani[12] that there was a significant relationship between sodium intake with blood pressure in the elderly at TresnaWerdhanursing Home and BinaLaras Budi Luhur nursing home, Banjarbaru City.

Blood pressure is the bloodstream pressure in blood vessels and circulates in all tissues of the human body[13,14]. Blood pressure consists of 2 parts of systolic pressure and diastolic pressure[15,16]. Systolic blood pressure is defined as the pressure during heart contractions, while diastolic blood pressure is defined as blood pressure when the heart relaxes[14].

The sodium content in foods dramatically varies and depends on the food source (e.g., animal foods source naturally contain more sodium) and the level of change that food itself goes through. Foods that are naturally low in sodium are fruits, vegetables, oils, and cereals, with the contents range from 20 mg up to 100 g[7].

The Food and Agriculture Organization (FAO) and WHO recommends that the amount of salt consumption in the community is less than 5 gram a day because of the adverse effects of excessive salt consumption on health, especially on blood pressure and cardiovascular disease[4,17].Based on data from National Basic Health Research in 2013, it was found that the prevalence of risky food consumption patterns, especially salty foods, was 26.2%, and Southeast Sulawesi was 11.5%[18].

Geographically, the Wangi-Wangi Islands' position is surrounded by the sea of Banda, where most of the people in the community earn a livelihood as seaweed farmers and fishers even though there are some villages that quite far from the coast with livelihoods as land farmers. This geographical position gives a plus and minus effect on the health of the Wangi-Wangi community, especially those living in coastal areas exposed to high salt or sodium consumption patterns.

According to Bustan, more people living in urban areas suffer from hypertension than people living in villages; furthermore, based on the geographical location where coastal areas have more hypertension than highland areas[19]. Research conducted by Setiawati on the coast of Manado Tua Island obtained a significant relationship between sodium intake and the incidence of hypertension[20].

Based on the phenomenon, this study aims to determine differences in sodium consumption patterns of hypertensive patients in coastal and highland communities in the Wakatobi Islands.

Methods

The type of study is observational analytic research using a cross-sectional design. This research has been conducted in the District of Wangi-Wangi, specifically atMolaSamaturuvillage and Waginopo Village, in October 2019. The study population comprises all people with hypertension who live in MolaSamaturu Village (124 people) and Waginopo Village (116 people), with 240 people in October 2019. The number

[1] Epidemiology Department, College of Medicine, Halu Oleo University, Kendari, Indonesia.
[2] Nursing Department, College of Science and Technology, Sembilanbelas November University, Kolaka, Indonesia.

Corresponding author: heriviyatno.j.siagian@gmail.com

of research samples was 100 people (50 respondents in MolaSamaturu Village and 50 people in Waginopo Village). The blood pressure variable is obtained by measuring using a blood pressure meter with hypertension criteria for hypertension sufferers is 140/90 mmHg (first-degree hypertension, second-degree hypertension, and third-degree hypertension). The sodium consumption pattern variable is obtained by measuring the consumption pattern using the Food Frequency Questionnaire (FFQ) then analyzed using a Nutri survey with a safe sodium consumption pattern standard (<2000 mg/day). The statistical test uses an independent t-test with a value of $\alpha = 0.05$.

Results

Table 1 shows respondents' characteristics with hypertension based on age range mostly in the MolaSamaturu village as 30% with age range 30-35 years old. In the Waginopo village, mostly in the age range 42-47 years old is 44%. By gender characteristics, mostly in MolaSamaturu Village with a percentage of 46% men and Waginopo Village the most were 44% men. By type of occupation, in MolaSamaturu village, 62% of respondents are fishermen, and Waginopo Village, most of the respondents, are farmers as much as 50%. Characteristics of respondents based on BMI show the most respondents in the MolaSamaturu village is in normal BMI (18.5-25.0) as much as

Characteristics	MolaSamaturu Village		Waginopo Village	
	Frequency(n)	Percentage (%)	Frequency (n)	Percentage (%)
Range of Age				
24-29	12	24	4	8
30-35	15	30	2	4
36-41	8	16	10	20
42-47	11	22	22	44
48-53	4	8	12	24
Gender				
Male	23	46	15	30
Female	22	44	35	70
Occupation				
Farmer	0	0	25	50
Housewife	13	26	10	20
Fisherman	31	62	2	4
Laborer	4	8	10	20
Government Employees	2	4	3	6
BMI				
Thin (17,0-18,4)	7	14	3	6
Normal (18,5-25,0)	37	74	37	74
Obesity(25,1- 27,0)	10	20	12	24

Table 1. Respondents characteristics.

74%, either in the Waginopo village, most of the respondents is in the normal BMI with the percentage of 74%.

Based on table 2, respondents' characteristics in the category of hypertension in the MolaSamaturu village mostly in the stage I category with percentage is 50%, the same in Waginopo village that mostly is in the stage I as many as 66%. For the sodium consumption pattern variable, MolaSamaturu village with 68% is in ≥ 2000 mg/day category, while in Waginopo village mostly in < 2000 mg/day category with 76% of respondents (Table 2).

Table 3 shows that the mean systolic and diastolic blood pressure values of respondents in Mola Samaturu were higher than respondents in Waginopo Village, as well as sodium consumption, higher in Mola Samaturu Village, higher than respondents in Waginopo Village.

Table 4 shows a difference between Sodium consumption pattern hypertension sufferers in MolaSamaturu village and Waginopo village with p value= 0.000< α 0.05 (table 4).

Discussion

Sample testing is based on the relationship between hypertension as a dependent variable with seafood consumption as an independent variable along with other risk factors causing hypertension, such as age, gender, alcohol consumption, smoking, history of DM, family history of DM, history of dyslipidemia, and history dyslipidemia in families not examined in this study.

This research shows that hypertension is more in coastal areas (MolaSamaturu Village) compared to highland areas (Waginopo Village). Sodium is a mineral found in the body and many foods source. Sodium is an essential nutrient for maintaining blood volume, regulating water balance in cells, and maintaining nerve function. The kidney controls sodium balance by increasing or decreasing the excretion of sodium in the urine. Another theory states that kidney disorders cannot correctly excrete sodium (Na) in average amounts; the conse-

Characteristics	MolaSamaturu village		Waginopo village	
Category of Hypertension	Frequency (n)	Percentage (%)	Frequency (n)	Percentage (%)
Hypertension stage I	25	50	33	66
Hypertension stage II	13	26	14	28
Hypertension stage III	12	24	3	6
Sodium Consumption Pattern				
≥ 2000 mg/day	34	68	12	24
< 2000 mg/day	16	32	38	76

Table 2. Distribution of variables .

Variable	Mola Samaturu village		Waginopo village	
	mean	min-max	mean	min-max
Diastolic blood pressure	96.6	80-120	95.8	80-120
Systolic blood pressure	163.5	140-210	156.0	140-200
Sodium Consumption Pattern	3020.08	1256-9887	1983.98	897-7600

Table 3. Distribution of mean score, minimum-maximum blood pressure, and sodium consumption pattern hypertension sufferer.

Sodium Consumption Pattern	n	Mean Rank	p value
≥ 2000 mg/day	46	37.8	0.000
< 2000 mg/day	54	61.3	

Table 4. Distribution of mean score, minimum-maximum blood pressure, and sodium consumption pattern hypertension sufferer.

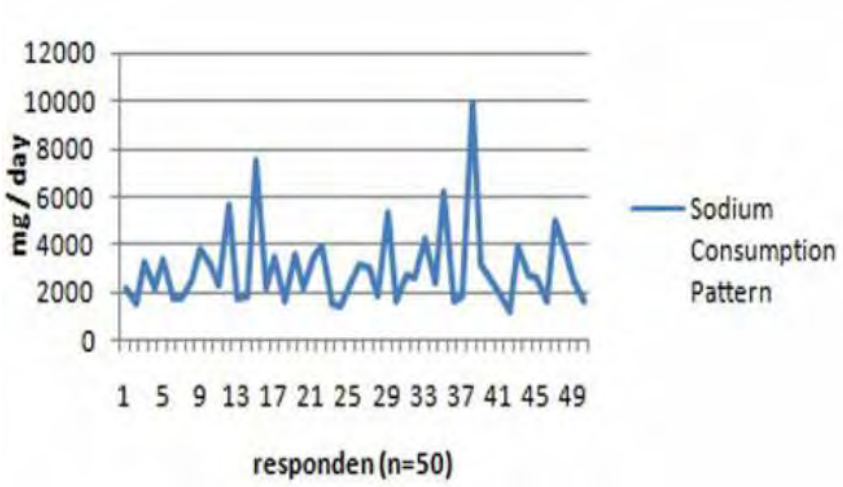

Figure 1. Sodium consumption pattern in Molasamaturu Village.

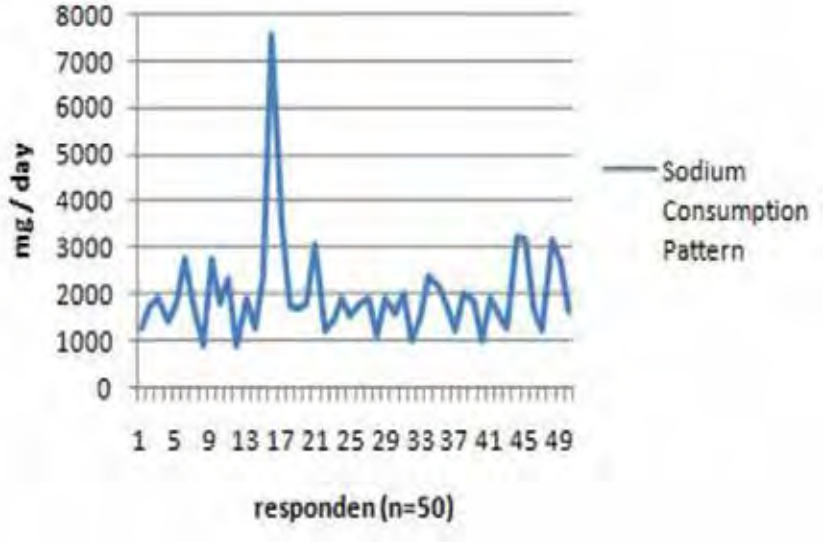

Figure 2. Sodium consumption pattern in WaginopoVillage.

quences are sodium (Na) in intravascular volume increase so that hypertension occurs[21].

The distribution of stage II and III hypertension sufferers shows that higher in coastal communities than in the highlands; this can be attributed to the excessive sodium consumption behavior found in seafood. The recommended daily sodium consumption is around 2400 mg, which can be achieved from salt around 2000 mg while another 400 mg is found in the food consumed[22].

The food consumption pattern of highland communities, especially in the Waginopo area, shows the same thing with coastal communities in frequency. However, there are significant differences in the types of food that characterize coastal communities, such as shellfish, crabs, and others that contain high sodium.This is in line with previous research, which states that the consumption patterns of coastal communities have a frequency of eating 3 times a day with staple foods, namely rice, animal consumption patterns are relatively high, especially seafood and fish ponds, while the pattern of fruit consumption is still relatively low frequency 0 in a day with a percentage of 75%[23].

In 1904, Ambard and Beaujard revealed salt intake correlates to BP as the first study on hypertension diet conducted on 6 patients with hypertension for 3 weeks using three types of salt and protein. The amount of salt in the body is measured by salt in food and urine per day. The amount of salt in the intake is small, the patient will experience a negative sodium balance, and blood pressure decreases. Otherwise, if the amount of salt in the intake is high, the amount of salt will be excreted a little so that sodium balance is achieved, and blood pressure will increase even though the amount of protein intake is small. Based on the result, the conclusion was the salt affects blood pressure. They were conducting the restriction on salt intake and success to reduce blood pressure[24].

This study's analysis results indicate that the highest sodium intake is in the coastal area, where sodium intake is excessive with a percentage of 68%. In contrast, in the highlands region, the highest sodium intake category is the sodium intake category, with a percentage of 76%. Factors that influence the high consumption of salt or sodium in coastal communities in the MolaSamaturu village are raw eating habits of shellfish, sea urchins, and salted fish. From the survey results, people in coastal areas consume high sodium foods daily, especially salted fish in hurricane season becomes the primary alternative for a food source in the coastal community. Another case is the community in Waginopo Village, which rarely consumes seafood from shellfish and salted fish. Some respondents even said that dried fish was not salted but only dried and then processed and consumed.

Research on the relationship of seafood with the incidence of hypertension has been done by Masengi *et al.*[25], which states a significant relationship between seafood consumption with the incidence of hypertension ($p = 0.001$).

Statistically, there was a significant difference ($p = 0.00$) for sodium intake in coastal areas and highlands areas where sodium intake was higher in coastal areas than in the highland

area. This study is in line with Sundari *et al.*[26], where sodium intake significantly affects essential hypertension, p-value—in line with research Rusliafa *et al.*[27] states that there are differences in hypertension incidence in coastal and highland areas, namely eating pattern (sodium intake p = 0.026).

Several studies have been conducted in some areas worldwide regarding daily salt intake related to blood pressure. A survey of salt intake in the newfound land area revealed the differences between the center of the island (inland) and the coastal community, where the typical salt intake is varying between 6.7 and 7.3 g/day compared to 8.4 and 8.8 g/day[28]. Parallel changes in the incidence of hypertension lead to differences in salt intake in several regions. The incidence of hypertension in the inland community was 15%, aged between 55 to 75 years old, lower than the coastal community with a percentage around 27%. Similar results were found among the Solomon Islanders[29]. In those tribes, had a salt intake below 2 g/day, only 1% of the population having raised in BP which lived away from the coast. About 3% of the Inland community population experienced elevating BP with salt intakes around 3 and 8 g/day. While people who lived on the coastal area had a salt intake between 9 to 15 g/day, indicating an increase of BP around 8% of the population. Migratory, in his study, found a relationship between daily salt intake and BP.The similarities in the results of this study are probably caused by the same characteristics of coastal and mountainous communities in consuming their daily food.

Conclusions

There is a difference between sodium consumption patterns in hypertensive sufferers in *Mola Samaturu* Village and *Waginopo* Village with a p-value = 0,000 <α 0.05. Sodium consumption patterns in coastal communities are higher than in highlands community. This is due to the ease of getting foods that contain high sodium compared to highland areas. Further studies may find out the possibility of food modification that can reduce sodium levels, especially in coastal areas.

Acknowledgment

The author would like to thank the parties who have contributed to the implementation of this research, especially the Dean of the UHO Faculty of Medicine, Chair of the UHO LPPM.

Bibliographic references

1. La Ode Alifariki SK. Epidemiologi Hipertensi: Sebuah Tinjauan Berbasis Riset. Penerbit LeutikaPrio; 2019.
2. Alifariki LO. Analisis Faktor Determinan Proksi Kejadian Hipertensi di Poliklinik Interna BLUD RSU Provinsi Sulawesi Tenggara. Medula. 2015;3(1):214–23.
3. Sudayasa IP, Alifariki LO, Rahmawati, Hafizah I, Jamaludin, Milasari N, et al. Determinant juvenile blood pressure factors in coastal areas of Sampara district in Southeast Sulawesi. Enferm Clin. 2020;
4. Ozkayar N, Dede F, Ates I, Akyel F, Yildirim T, Altun B. The relationship between dietary salt intake and ambulatory blood pressure variability in non-diabetic hypertensive patients. Nefrologia. 2016;36(6):694–700.
5. Elliott P, Stamler J, Nichols R, Dyer AR, Stamler R, Kesteloot H, et al. Intersalt revisited: further analyses of 24 hour sodium excretion and blood pressure within and across populations. Intersalt Cooperative Research Group. BMJ. 1996 May;312(7041):1249–53.
6. Tuomilehto J, Jousilahti P, Rastenyte D, Moltchanov V, Tanskanen A, Pietinen P, et al. Urinary sodium excretion and cardiovascular mortality in Finland: a prospective study. Lancet (London, England). 2001 Mar;357(9259):848–51.
7. Strazzullo P, Leclercq C. Sodium. Adv Nutr. 2014 Mar;5(2):188–90.
8. Kimble et al. Applied Therapeutic The Clinical Use of Drugs, Ninth Edition. In: David B. Troy, editor. Ninth Edit. Philadelphia, Pennsylvania, USA: 5 Lippincott Williams & Wilkins; 2009. p. 69–6, 69–13, 69–15, 69–16, 69–18, 69–29.
9. Nurpalah R RN. Gambaran Kadar Natrium (Na) pada pasien Hipertensi dengan rentang Usia 31-55 tahun. J Kesehat Bakti Tunas Husada. 2014;11(1).
10. Centers for Disease Control. The Role of Potassium and Sodium in Your Diet. Division for Heart Disease and Stroke Prevention; 2018.
11. Farquhar WB, Edwards DG, Jurkovitz CT, Weintraub WS. Dietary sodium and health: more than just blood pressure. J Am Coll Cardiol. 2015 Mar;65(10):1042–50.
12. Rivanli, Engka JNA, Sapulete IM. Hubungan kadar natrium dengan tekanan darah pada remaja. J e-Biomedik. 2016;4(2).
13. Joyner MJ, Casey DP. Regulation of increased blood flow (hyperemia) to muscles during exercise: a hierarchy of competing physiological needs. Physiol Rev. 2015 Apr;95(2):549–601.
14. Rafsanjani MS, Asriati A, Kholidha, Andi Noor AL. Hubungan Kadar High Density Lipoprotein (HDL) Dengan Kejadian Hipertensi. J Profesi Med J Kedokt dan Kesehat. 2019;13(2).
15. Frese EM, Fick A, Sadowsky HS. Blood pressure measurement guidelines for physical therapists. Cardiopulm Phys Ther J. 2011 Jun;22(2):5–12.
16. Magfirah AL. Pengaruh Terapi Berkebun Terhadap Perubahan Tekanan Darah Pada Lansia dengan Hipertensi di PSTW Minaula Kendari. J Islam Nurs. 2018;3(2):7–15.
17. Organization WH. Reducing salt intake in populations: report of a WHO forum and technical meeting, 5-7 October 2006, Paris, France. 2007;
18. Kemenkes RI, Kementerian Kesehatan RI. Profil Kesehatan Indonesia. Jakarta: Depkes RI; 2018.
19. Bustam M. Epidemiologi Penyakit Tidak Menular. Jakarta: EGC; 2007.
20. Rampengan, Sukarno M. Perbandingan Tekanan Darah Antara Penduduk Yang Tinggal di Dataran Tinggi dan Dataran Rendah. J e biomedik. 2018;4(2):1–8.
21. Khomsan dkk, Baliwati, Y.F., Khomsan, A., Dwiriani CM 2004. Pengantar Pangan dan Gizi. Jakarta: Penebar Swadaya; 2004.
22. Falefi R dkk. Hubungan Konsumsi Makanan Laut Dengan Kejadian Hipertensi Pada Masyarakat Pesisir Di Wilayah Kerja Puskesmas Mangkang Kota Semarang. J Kesehat Masy. 2019;7(4):743–8.
23. Hamidah I. Studi Tentang Pola Konsumsi Masyarakat Pesisir Indramayu. J Biol Dan Pendidik Biol. 2017;1(2):46–51.
24. Ambard L. Causes de l'hypertension arterielle. Arch Gen Med. 1904;1:520–33.
25. Masengi S, Palar S, Rotty L. Pengaruh Konsumsi Makanan Laut Terhadap Kejadian Hipertensi Di Desa Malalayang Dua. J e-Biomedik. 2013;1(1):726–32.
26. Sundari dkk. Faktor Risiko Non Genetik dan Polimorfisme Promoter Region Gen CYP11B2 Varian T(-344)C Aldosterone Synthase pada Pasien Hipertensi Esensial di Wilayah Pantai dan Pegunungan. Universitas Brawijaya Malang; 2013.
27. Rusliafa J, Amiruddin R, Noor NB. Komparatif Kejadian Hipertensi Pada Wilayah Pesisir Pantai Dan Pegunungan Di Kota Kendari Tahun 2014. 2014.
28. Fodor JG, Abbott EC, Rusted IE. An epidemiologic study of hypertension in Newfoundland. Can Med Assoc J. 1973;108(11):1365.
29. Page LB, Damon A, Moellering Jr RC. Antecedents of cardiovascular disease in six Solomon Islands societies. Circulation. 1974;49(6):1132–46.

Received: 12 December 2020
Accepted: 10 February 2021

RESEARCH / INVESTIGACIÓN

Identification of maize kernel resistance proteins against *Aspergillus flavus* by a statistical approach: A predictive model of resistance capacity

Leandro Balzano[1], Jesús Alezones[2], Nardy Diez García[3]

DOI. 10.21931/RB/2021.06.02.13

Abstract: Although kernel infection by *Aspergillus flavus* and pre-harvest aflatoxin contamination of *Zea mays* grain is a significant crop production problem, not only in Venezuela but also around the world, little progress has been made in identifying proteins and metabolic pathways associated with this pathogen resistance. Usually, a protein with a two-fold expression between control and condition is considered a biomarker of some phenomena, but we think it is essential to evaluate its contribution to resistance. That is why we decided to determine the behavior's resistance capacity in terms of expression levels of an identified protein of maize kernels infected with *A. flavus* by using a multivariate approach. In this work, we identify 47 of 66 differentially expressed spots with a remarkable contribution to resistance against the fungus *Aspergillus flavus*. We finally test this approach to know if it can be used as a predictive resistance model and probe it by including theoretical and experimental protein expression profiles of other inoculated maize lines.

Key words: Host resistance, resistance-associated proteins, *Zea mays*, *Aspergillus flavus*, comparative proteomics, resistance predictive model.

Introduction

The latest statistics released by the Food and Agriculture Organization of the United Nations (FAO), indicate that by the year 2011, maize was the second most produced and demanded vegetable item in the world, after sugar cane[1]. Fungi are the world's primary cause of maize crop loss because of their economic implications, which represents a substantial phytosanitary problem to be solved. In Venezuela, the major maize crop pathogen is *Aspergillus flavus*, with 35-45% of incidence. It is the cause of around 80% percent of kernel losses because it reduces not only the grain nutritional value, but also its presence usually causes the accumulation of highly toxic and carcinogenic secondary metabolites named aflatoxins[2–6].

In general, plants can respond to invasion by pathogens through the activation of a variety of defense strategies, which are induced by complex interactions between biochemical pathways in a coordinated manner[7,8]. Defense responses generally include several cellular changes due to variations of protein expressions involved in cellular metabolism, as the production of structural carbohydrates, structural proteins, signal transcription and translation, transporters, intracellular traffic, and production of antimicrobial compounds, among other processes[9,10]. However, there is not much research focused on the response mechanisms of maize against fungal infection. Despite being a long-term method, recurrent selection can decrease or even eliminate fungicide dependent cultures. Besides, it is a low cost method, so it is widely used in developing countries[11,12].

Resistant plant selection is made a long time ago and tries to relate phenotypical characteristics with genotypical ones. Kernel screening (KSA) assay is a resistance-evaluation method that consists of maize grain exposition to a pathogen concentration to determine its capacity to inhibit pathogen proliferation[13]. In this work, we modified this method to increase the *A. flavus* spores concentration to 4x10^6 spores/mL of *A. flavus*. We evaluated the kernel differential-expression proteins between high-production *A. flavus*-infection-susceptible and *A. flavus*-infection-resistant maize lines to determine plant resistance mechanisms. We extracted maize grain proteins using two different pH buffers, quantified them, and verified their integrity. Then we obtained two-dimensional patterns and compared them, detecting multiple protein-expression variations.

All the information obtained allowed the generation of similarity matrices that were used to study the relationships among maize genotypes investigated using different techniques of classification/ordination such as principal components analysis[14,15], Neighbor-joining clustering algorithm[16,17] and principal coordinates analysis[18]. The combination of these techniques allows two crucial facts: 1.- determining the proteins differential pattern expression that majorly contributes with resistance capacity by the interpretation of the variables responsible for the classification or ordination, which were identified by MALDI-TOF mass spectrometry, to construct a resistance response model of a maize-grain cell against *A. flavus* and 2.- developing a methodological strategy of data processing that is capable of predict the resistance level of other maize lines.

Materials and methods

Maize lines and fungal selection

We pre-selected eleven high-production maize lines developed initially by the International Maize and Wheat Improvement Center (CIMMYT) and adapted to Venezuelan lands, based on two characteristics, 1.- its high productivity and 2.- its resistance capacity against *A. flavus* determined by modified KSA assay[13]. After that, we selected four lines based on the grain color, two highly resistant (one white grain and one yellow grain) and two highly susceptible (one white grain and one yellow grain). We inoculated the seeds with 4x106 spores/mL of *A. flavus* and incubated each grain line for 7 days, at 30ºC and 90-100% humidity resistance-capacity evaluation (figure 1), and 20 h for protein-expression profile evaluations.

[1] University of Florida, Department of Microbiology and Cell Science, Gainesville, United States.
[2] Fundación para la Investigación Agrícola DANAC, Estado Yaracuy, Venezuela.
[3] Centro de Investigación Biotecnológicas del Ecuador (CIBE), Facultad de Ciencias de la Vida, Escuela Superior Politécnica del Litoral, ESPOL, Guayaquil, Ecuador.

Corresponding author: ndiez@espol.edu.ec

A. flavus Ospino 1-B was the fungal strain used due to its high colonization power. It was grown on agar plates at 30 °C until the mycelium had covered all the plates, and the spores were collected by shaking the plate in sterile water. The spores were then counted in a Neubauer chamber to inoculate maize grains with the mentioned spore quantity.

Protein extraction

For protein extraction, each plant's whole grain was pulverized with liquid nitrogen, and aliquots of 100 mg were homogenized in 1 mL of extraction buffer mixed with 1X protease inhibitor mix (GE healthcare). Two different protein extraction buffers (pH=2.8 or pH=7.5) were used according to the protocol described by Campo *et al.*[19]. These aliquots were incubated for 1h with continuous slow stirring and then were centrifuged at 16.000 g for 5 min at 4°C. The supernatants' proteins were incubated at -20°C overnight, with two volumes of methanol, so the final alcohol concentration in the mixture was 70%. Then, all tubes were centrifuged at 16.000g for 5 min at 4°C, the supernatants were discarded and the pellets were washed twice with 70% ethanol at 4°C, after which, the tubes were centrifuged again, the supernatants were discarded, and all the precipitates were saved at -70°C until use. The protein pools were resuspended in 50 µL DeStreak buffer (GE Healthcare), quantified by the Bradford QuickStart® method (Bio-Rad), and SDS-PAGE verified their integrity. We carried out three independent infection experiments, with three protein extractions of the pulverized plant material, in order to explore the protein level variations associated with the biological material and the experimental techniques.

Two-dimensional gel electrophoresis

Nonlinear pH 3-10 isoelectric focusing dry strip gels (GE Healthcare) were rehydrated overnight in 250 µL rehydration solution (8M urea, 1% CHAPS, 20mM DTT, and 0.2% of 3-10 non/linear carrier ampholytes), along with 30 µg (analytical) or 100 µg (preparative) of proteins. Isoelectric focusing was performed at 20°C in an Ettam IPGphor (GE Healthcare), following the standard protocol recommended by the fabricant: gradual increase until 200V for 20 min, gradual increase until 450V for 15 min, gradual increase until 750V for 15 min, gradual increase until 2000V for 30 min, all gradual increases were performed being careful not to overcome 25 milliamperes. After isoelectric focusing, gel strips were equilibrated for 15 min in a buffer containing 50 mM Tris-HCl (pH 8.8), 6 M urea, 30% glycerol, 2% SDS containing 10 mg/mL DTT, followed for 15 min with the same buffer but containing 5 mg/mL iodoacetamide instead of DTT. For the second dimension, strips were loaded onto SDS polyacrylamide gels (12% acrylamide separating gel, 8x7x0.1 cm, width x height x thickness), then the top of the gel was sealed with 1% agarose solution, and finally, we ran two-dimentional gel electrophoresis at 200V for about 35 min, until the front run was about to go out of the gel. All gels were silver-stained with PlusOne Silver staining kit (GE Healthcare) which is compatible with mass espectrometry. Gel were digitized with an HP scanner and analyzed with the Phoretix 2D v-2004 (nonlinear Dynamics Ltd.) program.

Comparative analysis of protein expression profiles

The protein expression profiles obtained from all maize lines were compared in two different analyses, white lines, and

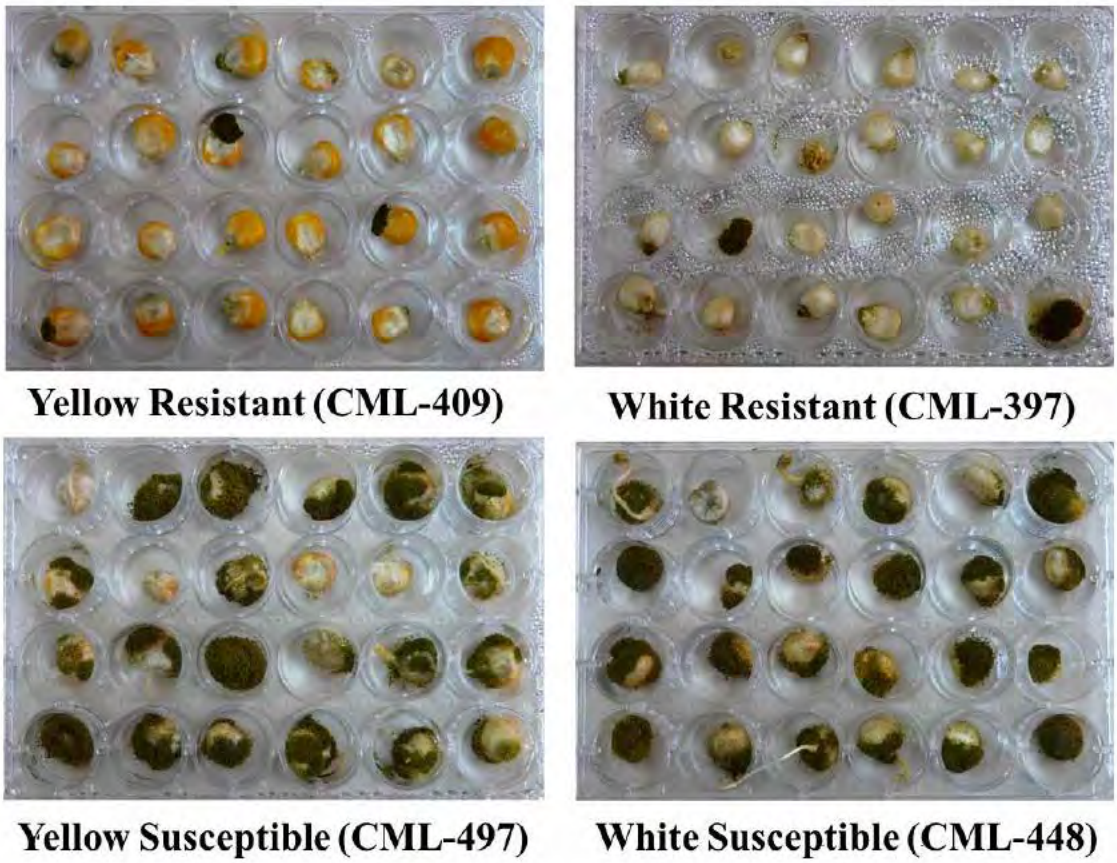

Figure 1. Characteristics of the chosen high-production maize lines in terms of their resistance or susceptibility to *A. flavus*. Kernel screening assay of the selected maize lines showing its resistance or susceptibility against *A. flavus* 4x10^6 spores /mL defined by fungus proliferation ratio in 7 days of infection.

yellow ones, between each other. We decided to compare just the profiles obtained from *A. flavus*-inoculated susceptible maize grain lines with those obtained from *A. flavus*-inoculated resistant maize grain lines. The two-fold differential-expression proteins detected by the Phoretix 2D program (Nonlinear Dynamics Ltd.) were selected for peptide sequencing.

Protein identification and database search

Proteins were identified by peptide mass fingerprinting using MALDI-TOF mass spectrometry (MS) performed with a PrOTOF 2000 (Perkin-Elmer Inc.) instrument, previously calibrated with trypsin-digested bovine serum albumin. For the analysis, 1µL of tryptic peptides were mixed with 1 µL of the matrix (α-cyano-4-hydroxycinnamic acid, 5mg/mL) and loaded on a stainless steel MALDI plate. Protein identification was carried out using MASCOT (Matrix Science Ltd.) or Protein Prospector software (v5.10.1, UCSF Mass Spectrometry Facility, University of California). Nonredundant NCBI (National Center for Biotechnology Information), MSDB, and Swiss-Prot (European Bioinformatics Institute Heidelberg, Germany) databases[20,21] were used for the search. The search parameters applied were described by Lee *et al.*[22]; they are a mass tolerance of 50 ppm with one incomplete cleavage allowed; alkylation of cysteine by carbamidomethylation was the only fixed modification; the variable modifications considered were acetylation of the *N*-terminus, oxidation of methionine, and the pyroGlu formation of *N*-terminal Gln.

Resistance response models

With all the available information and the additional one gathered in this work, we propose a whole maize cell resistance response model after 20 h of infection by *A. flavus*. This model was accomplished using bioinformatics interphases indexed in http://www.bioprofiling.de/index.html, which employs the information stored in NCBI and SwissProt databases[20,21]. These tools can be applied in just one plant, *Arabidopsis thaliana*, so the only way to use it was, placing this plant's accession number of homolog proteins instead of maize-identified proteins.

Statistical analysis for biomarkers determination and resistance prediction-method generation

The data of the 2D gels spots areas were used to determine the proteome-differences under the same conditions of infection, useful information to determine the differential-expression proteins more closely associated with maize-grain resistance cells against the fungus. We applied principal coordinates analysis (PCoA) to the binomial-transformed and mathematically size-adjusted by generalized Procrustes data matrices and projected on the principal coordinate plane to determine levels of resistance of the lines under study, given by its plane location. Cluster analysis was performed to evaluate the relationship between the proteins present in all the lines under study. We also applied Principal Components Analysis (PCA) to all original data matrices previously grouped by color and resistance capacity, eliminating extraction buffer variable by generalized Procrustes, to determine the spots that majorly contribute to resistance characteristic. We finally evaluated the statistical resistance-predictive method applied by using experimental and theoretical lines with characteristics of both resistant lines and evaluating them by principal coordinates analysis. All analysis was realized with the software InfoStat[23].

Results and Discussion

Maize lines selection

Guided by the mentioned characteristics, we pre-selected 11 maize lines (Table 1), and then we selected 4 maize lines from this initial selection: 2 resistant and 2 susceptible to *A. flavus* infection. White grain lines were selected with a close relationship between them, both having the same germplasm source, known as Tuxpeño 1. In contrast, yellow grain lines were deliberately selected with different germplasm sources (CML-409 is derived from "Antigua Veracruz" population, while CML-497 is derived from RCY source). The maize-grain-lines-resistance levels were confirmed by KSA assay (figure 1), modified as mentioned.

N°	Maize line	Color	Characteristic	Adjusted means	Real means
1	CML-493	Yellow	Resistant	1,21	0,84
2	**CML-397**	**White**	**Resistant**	**1,23**	**0,91**
3	CML-274	White	Resistant	1,29	0,69
4	CML-46	White	Resistant	1,30	0,91
5	**CML-409**	**Yellow**	**Resistant**	**1,31**	**1,22**
6	CML-176	White	Witness	1,46	1,35
7	CML-159	White	Susceptible	1,72	2,06
8	CML-247	White	Susceptible	1,77	2,69
9	**CML-497**	**Yellow**	**Susceptible**	**1,80**	**2,95**
10	**CML-448**	**White**	**Susceptible**	**1,80**	**3,43**
11	CML-7	White	Susceptible	1,86	3,19

The adjustment was made to compare the results of all lines that were not obtained simultaneously. All values were adjusted to guarantee data normality by the function $\sqrt[2.55]{Colonization(Z)+3}$, where Z is the real mean value obtained. In the cases of equal adjusted mean values, resistance is determined by real mean values.

In bold letters, we show the four selected maize lines for protein identification through comparative proteomics.

Table 1. Modified KSA assay results of pre-selected maize lines against A. flavus grain infection. These results are ordered by resistance capacity 7 days post-infection. Adjusted values by a mean test (5%) of three replicates.

Although CML-493 was the most resistant maize line, it was not used because it is a quality protein maize (QPM) line, and we neither used CML-7 maize line even though it was the most susceptible line, because its yield in tons per hectare in Venezuela is far lower than the one of CML-448 maize line.

Evaluation of studied maize lines proteomes

We decided to study the relationship between the four evaluated proteomes and determine if there is any proteome expression-pattern difference in the proteins with both types of lines, yellow and white. For this, we used a data matrix using only proteins present in at least one of the white lines and one of the yellow maize lines, resulting in 224 spots. Generalized Procrustes adjusted this data matrix to eliminate the extraction method factor and maintaining only the factors, grain color, and resistance capacity. We made a cluster analysis of the adjusted matrix, using calculating the square Euclidean distance and Ward. We demonstrate that the proteomes obtained from the two resistant lines, under infection conditions for 20 hours, are more similar than those with their same color-susceptible lines. Furthermore, the relationship between resistant lines is stronger than the relationship between susceptible lines. This demonstrates that, under infection, both resistant lines show a similar response mechanism (Figure 2).

Determination of major resistance-contributing proteins

Using these 224 spots matrices, we made a PCA to determine the proteins (variables) that majorly contribute to each maize line's centroids position and, consequently, to resistance capacity. In this way, we determined that 66 proteins majorly contribute to resistance (figure 3). In this figure, we show the 66 proteins spot number, separated by colors where spots in green are the spots that majorly contribute to the YR line position, in blue are the spots that majorly contribute to the WR line position, and in red are the spots that majorly contribute to the position of both resistant lines. We then decided to identify these significant resistance-contributing proteins.

Protein identification by peptide-mass fingerprinting and sequencing

MALDI-TOF MS. carried out identification of the two-fold up or down-regulated proteins. Selected spots were subjected to in-gel tryptic digestion. MALDI-TOF MS analysis and mass spectra were searched against the protein sequence databases. 47 of the 66 selected spots were identified by peptide mass fingerprinting (PMF) (Table 2). Two to three peptides were sequenced from each spot for protein identification. Nineteen proteins remained unidentified, some of them because the homology score was too low to consider it as that protein, others because they did not show significant homology to any known protein sequence. This is an exciting matter for further investigations. We consider it essential to remark some of the identified proteins, like NADPH HC toxin reductase (NHCTR), whose function is to inactivate HC toxin, a cyclic tetrapeptide *Helminthosporium carbonum*, by carbonyl group reduction[24]. Hm1 was the first considered resistance gene cloned and evaluated, proving the toxin's encoded protein activity[25]. HC toxin is a potent histone deacetylase inhibitor[26]. Histone deacetylase eliminates histones, acetyl groups, transforming the lysine and arginine amino groups into amides, diminishing their DNA affinity, allowing separation and posterior transcription. Thus, HC toxin inhibits the separation between histones and DNA, inhibiting protein transcription, probably resistance proteins[27]. At the transcriptional level, we determined an overexpression in the resistant lines after infection, exceptionally the white resistant (WR) line that reaches higher relative-expression values. Besides, there are no significant changes in the white susceptible (WS) line after infection, and we could not detect any expres-

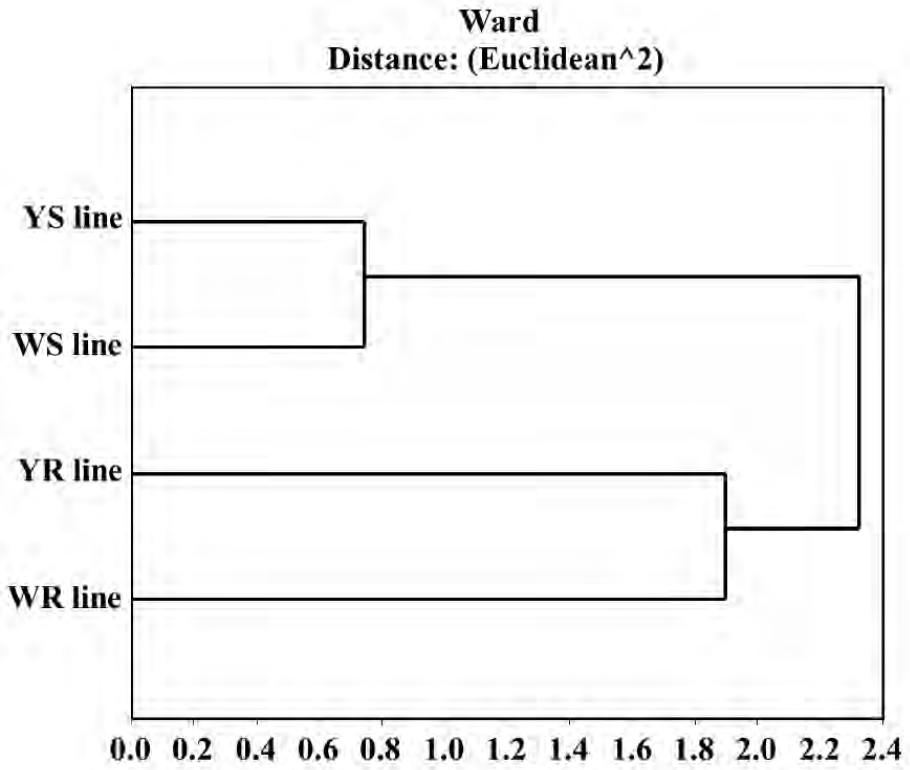

Figure 2. Cluster diagram of the four studied lines inoculated (20h) with A. flavus. This was made using the 224 spots detected in at least one yellow line and one white line. It shows a stronger relationship between the resistant lines' proteome with each other than between maize-grain color. Results obtained with InfoStat v 2012.

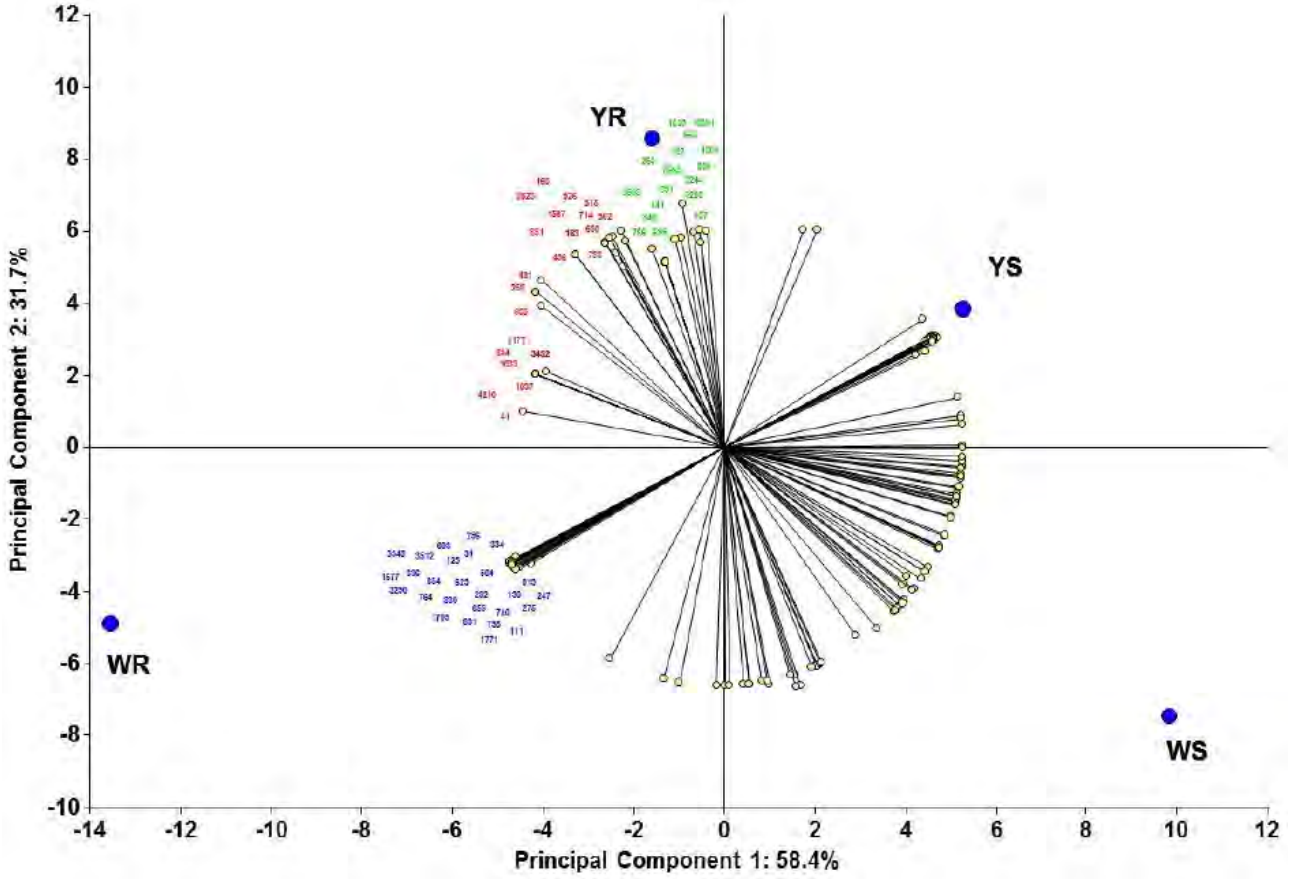

Figure 3. Principal components analysis to determine resistance-contributing proteins. Statistical analysis made using InfoStat v2012[23].

sion level in the yellow susceptible (YS) line (data not shown or see supplementary data or figure S1). This protein showed an overexpression on white-grains resistant-maize line with respect to the susceptible one at the translational level and was not detected in yellow lines.

NADPH HC toxin reductase overexpression in WR line was detected in this work, a fascinating result, because it is known that this enzyme responds almost exclusively to the fungus *Helminthosporium carbonum*, due to a coevolution phenomenon between the two organisms[28]. This result indicates that *A. flavus* somehow stimulates maize grains response mechanisms, similar to those activated by *H. carbonum*, perhaps because of a similar infection mechanism. In *H. carbonum*, the toxin synthesis depends on a complex locus of five genes that encodes, among other things, promoter proteins and HC-toxin synthase (Genbank: M98024.2)[29]. We compared the HC-toxin synthase sequence of *H. carbonum* with *A. flavus* (taxid:5059) and found a mRNA sequence coding for a protein with 97% of homology NRRL3357, nonribosomal peptide synthase Pes1 (XM_002380451.1). This suggests the existence of a similar toxin-synthesis mechanism between the two fungi, which provokes an overexpression of NADPH HC toxin reductase. This work is the first report of overexpression of this enzyme caused by *A. flavus*.

We also detected four proteins involved in the shikimate pathway, phospho-2-dehydro-3-deoxyheptonate aldolase 2 (PDDA2), myb-like transcription factor (myb-P), chalcone synthase (ChS), and α-1,4-glucan-protein synthase (α-GS), which describe their importance in the resistance phenomena. Several proteins involved in the catabolism, phosphoglycerate kinase (PGK), xylose isomerase (XI), soluble inorganic pyrophosphatase (SIPP), glyceraldehyde 3-phosphate dehydrogenase cyt 1 (GAPDHc1), fructose bisphosphate aldolase (FBA), are required for energy production due to the high demand to face the pathogen.

Additionally, we detected chaperone proteins, motor proteins, ATP synthesis proteins and transmembrane transporters, and some hypothetical and unknown functional proteins.

Response model of a maize-kernel cell against *A. flavus* at 20 hours infection

All the information gathered was used to develop a response model that describes the processes that we consider provide the highest corn-kernels resistance-levels against *A. flavus*. The ORFs whose role is not confirmed yet, were not included in the response model. Figure 4 shows the model which summarizes what occurs within the cell, including proteins reported in other studies[19,30–37]. It can be noted that an immediate response mechanism takes place (left side of the model), where an overexpression of several proteins responsible for reactive-oxygen species (ROS) production occurs. These ROS are involved both in the direct attack and in cell damaged wall repair, but they are highly toxic for host cells, because they cause membrane pores, protein damage and conglomeration among other events. Therefore, the activation of proteins related to ROS degradation can be expected as was observed. Chaperone proteins that protect the native proteins folding were also detected, and the subexpression of proteins related to the degradation of other proteins indicates that in resistant-plants maize-grains, the protection of proteins already synthesized is favored instead of protein degradation and resynthesis, which supposes lower energy cost. We found that energy is not wasted unnecessarily. However, energy requirements increase proportionally because of infection, which sti-

Spot N°	Protein name	Mass (kDa)/pI		Score	Coverage (%)	Acc. N°	Specie	Resistant vs. Susceptible	
		Theoretical	Experimental					Yellows	Whites
926	A49-like RNA polymerase I associated factor family	8.9/ 49.070	7.96/ 30.573	68 (a)	33	EU968493.1	*Zea mays*	0	+2.644±0.18
496	Acetolactate synthase1	5.8/59.730	5.9/63.590	68 (a)	19	NP_001151761	*Zea mays*	+2.746±0.26	+1.422±0.03
275	Alcohol deshydrogenase 1	6.3/ 40.904	6.43/ 43.156	96 (a)	37	AAF43977	*Zea mays*	+2.01±0.06	+2.21±0.08
3244	Aldose reductase	6.2/ 31.131	7.95/ 58.066	149 (c)	30	ACG28331.1	*Zea mays*	+2.5280.06	0
3285	Aldose reductase	6.2/ 31.131	8.1/ 28.106	209 (c)	44	ACG28331.1	*Zea mays*	+5.292±0.23	0
830	Alpha-1,4-glucan-protein synthase	5.8/41.691	5.7/38.194	55 (a)	14	NP_001105598	*Zea mays*	R	R
831	Alpha-1,4-glucan-protein synthase	5.8/41.691	5.7/38.840	62 (a)	23	NP_001105598	*Zea mays*	0	R
714	Aquaporin PIP1-5	8.3/30.933	8.2/34.743	58 (a)	25	NP_001105131	*Zea mays*	+2.134±0.18	0
658	ATP synthase β chain	5.9/59.057	5.2/51.793	58 (a)	17	NP_001151807	*Zea mays*	+1.082±0.16	+2.032±0.12
137	ATP synthase CF0 A subunit	5.3/27.334	5.4/28140	56 (a)	28	NP_043019.1	*Zea mays*	-1.017±0.19	-2.25±0.26
111	Chalcone synthase C2	6.7/41.588	6.4/41.547	66 (a)	21	NP_001142246	*Zea mays*	-1.166±0.04	-2.208±0.03
818	DIBOA-glucoside dioxygenase BX6	6.2/41.628	6.1/40.240	80 (a)	26	NP_001105100	*Zea mays*	+3.761±0.10	+2.005±0.01
296	Fructose-bisphosphate aldolase, cytoplasmic isozyme	7.5/39.036	7.6/41.348	61 (a)	21	NP_001105336	*Zea mays*	0	+2.677±0.13
629	Glutathione transferase	6.2/ 25.119	6.3/ 25.602	78 (a)	47	CAA73369	*Zea mays*	-4.242±0.61	+2.698±0.31
258	Glyceraldehyde-3- phosphate dehydrogenase, cytosolic 1	6.5/36.600	6.4/36.347	52 (a)	18	NP_001105413	*Zea mays*	+2.123±0.02	+3.005±0.43
31	Heat shock protein 70	5.3/63.193	5.2/69.705	42 (a)	15	CAA27330	*Zea mays*	-2.008±0.16	+2.288±0.04
41	Heat shock protein 82	5.0/82.125	5.1/75.398	68 (a)	21	NP_001135416.2	*Zea mays*	-2.946±0.13	0
125	thioredoxin peroxidase (Hypotetical protein OsI_01349)	6.11/ 24.167	5.9/ 28.858	38 (a)	26	EEC70391.1	*Oryza sativa* (indaca)	+4.194±0.66	+3.507±0.60
8665	Hypothetical protein Loc100276485	5.5/49.741	5.6/24731	47 (a)	21	NP_001143735.1	*Zea mays*	-2.189±0.08	-4.218±0.11
421	Kinesin heavy chain	8.09/ 17.317	8.15/ 15.427	46 (a)	35	AAK91823.1	*Zea mays*	+2.538±0.04	0
3508	Kinesin heavy chain	8.09/ 17.317	8.35/ 15.141	44 (a)	33	AAK91823.1	*Zea mays*	+3.129±0.04	+1.538±0.18
3512	Kinesin heavy chain	8.09/ 17.317	7.95/ 15.281	53 (a)	32	AAK91823.1	*Zea mays*	+6.934±0.24	0
334	Lon protease homolog 2, peroxisomal	7.7/97900	7.6/100.212	58 (a)	18	NP_001105903	*Zea mays*	+1.683±0.04	-2.032±0.04
336	Lon protease homolog 2, peroxisomal	7.7/97900	7.7/100.212	65 (a)	20	NP_001105903	*Zea mays*	+1.281±0.05	-2.968±0.31
603	Myb-related protein P	9.9/17.332	9.3/17.817	49 (a)	32	P27898-2	*Zea mays*	+3.856±0.28	+5.255±0.62
733	NADPH adrenodoxin oxidoreductase	7.31/ 54.533	7.10/ 50.178	46 (a)	36	ACG45856	*Zea mays*	0	-2.046±0.06
247	NADPH HC toxin reductase	5.45/ 27.100	7.25/ 26.588	33 (a)	34	AAM78363	*Zea mays*	0	+2.890±0.07
654	NADPH-dependent oxidoreductase	7.6/ 40.581	6.3/ 25.135	44 (a)	34	NP_001149289.1	*Zea mays*	-1.099±0.09	+2.182 ±0.80
653	Phospho-2-dehydro-3-deoxyheptonate aldolase 2	6.2/ 21.892	5.35/ 26.287	76 (a)	25	EU974270	*Zea mays*	-1.223±0.26	+2.252±0.38
504	Phosphoglycerate kinase	5.65/ 42.470	5.50/ 45.746	40 (a)	35	NP_001142404	*Zea mays*	+1.466± 0.14	+3.241± 0.38
740	Phosphoglycerate kinase	5.65/ 42.470	5.30/ 46.061	43 (a)	37	NP_001142404	*Zea mays*	+1.180± 0.01	+2.380±0.26
1567	Proteasome subunit alpha type 3	5.9/ 27.535	5.73/ 27.816	48 (a)	35	ACG48183	*Zea mays*	-5.920±0.87	S
441	Serine acetyltransferase 1	6.4/33.902	7.9/37.418	33 (a)	18	ACG35209.1	*Zea mays*	-1.623±0.10	-2.032±0.09
657	Soluble inorganic pyrophosphatase	5.3/24.524	5.5/25.133	55 (a)	25	NP_001104889	*Zea mays*	-1.676±0.16	-2.92±0.11

Table 2. Summary of the proteins identified by MS from fungal-infected grains by both buffers.

663	Soluble inorganic pyrophosphatase	5.3/24.524	5.6/24.561	55 (a)	23	NP_001104889	*Zea mays*	-1.307±0.07	-4.355±0.05
764	Superoxide dismutase [Cu-Zn] 4AP	6.640/ 15.071	5.60/ 17.071	165 (c)	28	P23346.2	*Zea mays*	0	+3.944±0.21
766	Superoxide dismutase [Cu-Zn] 4AP	6.640/ 15.071	6.03/ 17.488	631 (c)	35	P23346.2	*Zea mays*	-38.253±2.98	+4.370±0.40
263	Uncharacterized protein LOC100191853	6.43/ 39.826	6.62/ 35.839	53 (b)	39	NP_001130749	*Zea mays*	+13.731±1.34	+2.638±0.26
292	Uncharacterized protein LOC100216703	9.1/ 39.743	9.1/ 45.311	35 (a)	33	NP_001136580	*Zea mays*	0	+3.642±0.06
819	Uncharacterized protein LOC100273276	5.4/ 43.226	5.4/ 42.889	61 (a)	37	NP_001141189	*Zea mays*	-16.559±1.27	+1.276±0.14
655	Uncharacterized protein LOC100383799	9.08/ 39.744	6.4/ 25.091	55 (a)	61	NM_001176433.1	*Zea mays*	0	+3.0±0.16
502	Unknown protein ACL54769.1	5.8/40.462	5.6/41.564	67 (a)	23	ACL54769	*Zea mays*	+3.635±0.24	+1.633±0.04
691	T-complex protein 1 subunit delta (TcP1Sδ).	6.78 / 57.733	5.8/ 58.243	869 (c)	43	ACN26238.1	*Zea mays*	-46.14±1.56	-4.91±0.09
695	Xylose isomerase	5.4 / 54.381	5.73/ 52.663	37 (a)	32	ACG35698	*Zea mays*	-3.202±0.07	-2.552±0.63
130	Ypt homolog1	5.60/ 23.311	5.10/ 27.228	44 (a)	42	NM_001112076.1	*Zea mays*	0	+2.178±0.06
840	Ypt homolog2	5.80/ 22.400	5.69/ 26.010	37 (a)	61	NP_001105441.1	*Zea mays*	+1.371±0.27	+4.044±0.06
758	Zein-beta precursor	8.1/19.916	7.5/17.563	39 (a)	38	NP_001105739.1	*Zea mays*	R	+2.968±0.22

Table 2. Summary of the proteins identified by MS from fungal-infected grains by both buffers.

mulates an increase of catabolic-proteins expression and an increase of ATP synthesis in chloroplasts and mitochondria, and an energy waste necessary for proteins synthesis involved in defense against ROS species, as well as of proteins involved in synthesis of molecules used for direct attack and in cell wall-repair and reinforcement, both in affected cells and in neighbor ones, which stops the infection advance. Our study differs from others where the point of view is from the fungus and not from the maize's response[38,39].

Statistical analysis for correlating proteome with resistance capacity

All original data matrices of the proteins with differential expression patterns were analized to correlate spots present in both yellow and white grain maize obtained by both buffers, so we regrouped all information, making irrelevant the extraction buffers just focus on grain color and resistance capacity. This was accomplished by transformation to presence/absence (binomial), and we applied generalized Procrustes methodology. Distance matrices generated were submitted to PCoA (figure 5). In this figure we noted that due to the matrices characteristics, 266-483 variables (spots) depending on the evaluated matrix and only in 4 cases (white resistant line proteome, white susceptible line proteome, yellow resistant line proteome, and yellow susceptible line proteome) PCoA could collect 97.6% of the information in the two firs axis, noticing that in axis X is the information concerning the grain color and in Y axis, the resistance capacity (figure 5). We can also observe that due to their distances from the centroid to the Y axis, WS (CML-448) and WR (CML-397) are the most susceptible and the most resistant lines, respectively, which corroborates the results of the modified KSA assay (table 1).

We think that the PCoA generates a statistical plane used as a predictive model of resistance capacity against *A. flavus*.

Testing the predictive statistical model of resistance

To evaluate the proposed statistical predictive model, we perform a principal coordinates analysis including not only the studied maize lines proteomes behavior, but also by creating two theoretical maize lines, a theoretical white resistant line (ThWR) which has the spot behavior of WR plus the protein patterns identified in YR that could bring resistance but absent in the WR line (figure 6A); and a theoretical yellow resistant line (ThYR), which has the spot behavior of YR plus the protein patterns identified in WR, that could bring resistance but absent in the YR line (figure 6B). Specifically, for the ThWR we added to its theoretical proteome, the behavior of the two isoforms of aldose reductase, Hypothetical protein Loc100273276 and aquaporin PIP1-5 obtained from yellow lines. For the ThYR case we added to the theoretical proteome, the behavior of NADPH HC toxin reductase, Phospho-2-dehydro-3-deoxyheptonate aldolase 2, the isoforms of Lon protease homolog 2, peroxisomal, NADPH adrenodoxin oxidoreductase Fructose bisphosphate aldolase, the isoforms of Phosphoglycerate kinase, ATP synthase β chain and the HSP70 obtained from the white lines. Statistical analysis demonstrates two important aspects; in first place, the metabolic model of maize kernel-cell response to the infection of *A. flavus* is very accurate, and in the second place, they corroborate the predictive power of the model developed in this work. Although ThWR receives no statistical gain in resistance when we incorporate the factors absent from it but present in YR, it demonstrates the predictive power of statistical analysis developed since the ThWR is located towards the white lines. For the case of the ThYR, we can see that the line remains located on the side of the yellow lines, which confirms the capacity of the predictive statistical model. Furthermore, by ThYR location in coordinates plane, we can infer that this hypothetical line would be more resistant than its original line (YR), which corroborates the contribution of the protein's behavior obtained from WR to resistance.

We decided to make a final test of the model incorporating the proteome behavior obtained from the other two pre-selected maize lines (CML-46 and CML-247) at the same time (figure 7). In these results, we can see that both lines locate not

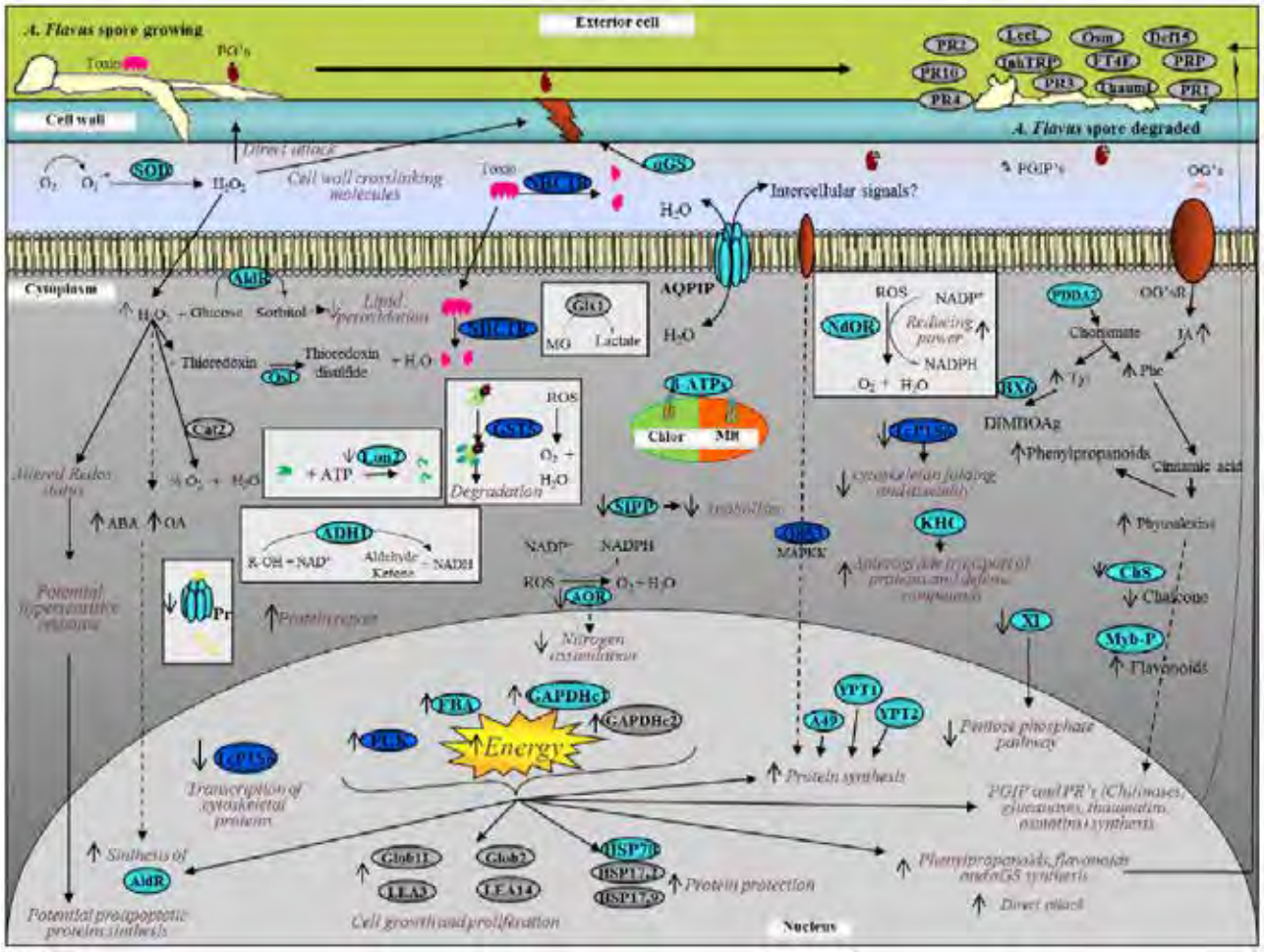

Figure 4. Response model of maize kernel cell against *A. Flavus* at 20 hours post-infection. The model was constructed using the characteristics that we consider to provide the highest maize kernel cells resistance against infection with *A. flavus*. In gray, we show the most relevant proteins reported; in light blue, proteins with only their translational behavior; and in dark blue, proteins with transcriptional and translational behavior.

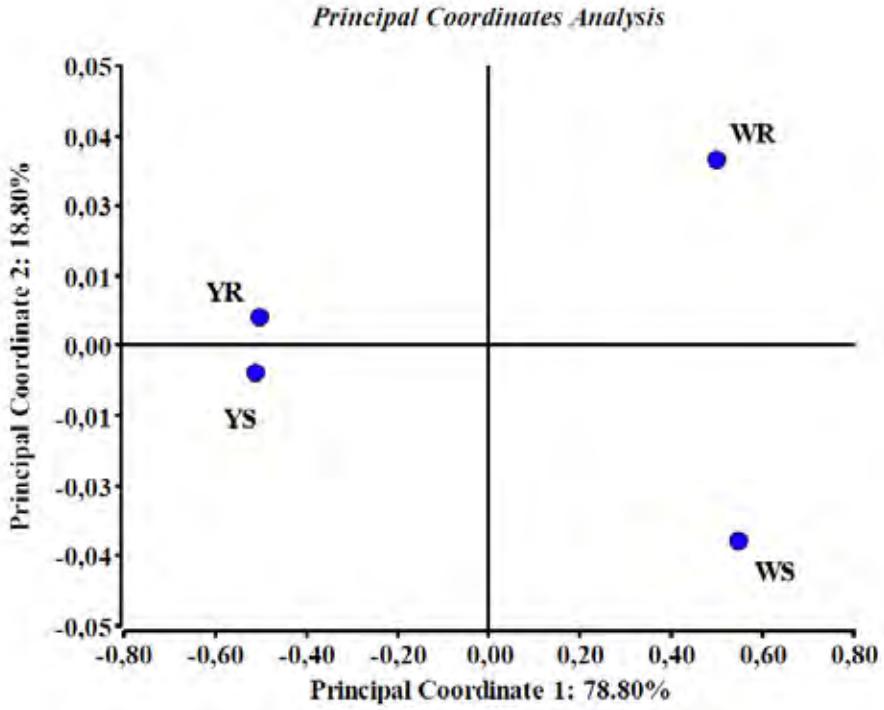

Figure 5. Principal coordinate analysis of the studied maize lines proteomic expression patterns. Points are centroids of each studied maize line. Note that in axis X is the information concerning the grain color and in Yaxis, the resistance capacity. Results obtained with InfoStat v 2012[23].

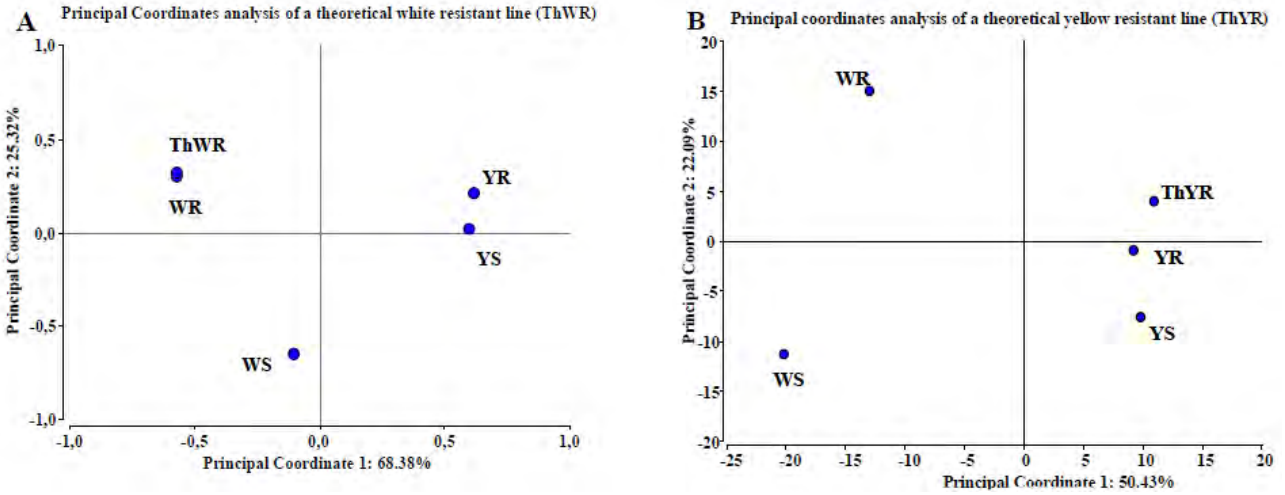

Figure 6. Test of PCoA predictive model using theoretical white (A) and yellow (B) maize lines. In (A) we observe no gain of resistance of the ThWR line than WR line; the analysis collects 93.7% of the information. In (B) we observe a real gain of resistance capacity of ThYR line compared to YR line when we include the behavior of some proteins from WR line that are absent in YR. The analysis collects 72.52% of the information. Results obtained with InfoStat v 2012[23].

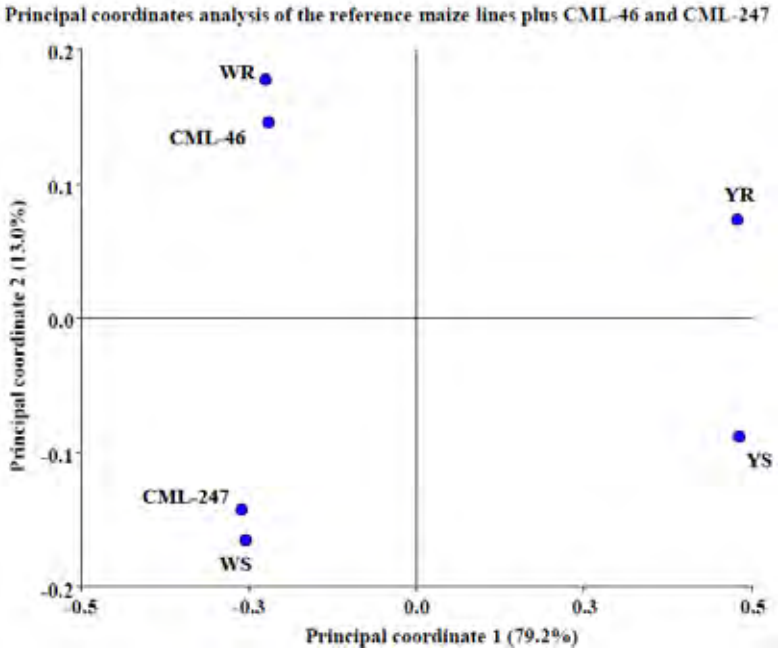

Figure 7. Test of PCoA predictive model using two more maize lines proteomic behavior. We observe that both lines locate not only on the white side of the coordinates plane but also on the coordinates plane, corroborating the statistical analysis predictive capacity. In two planes, the analysis collects 92.2% of the information. Results obtained with InfoStat v 2012[23].

only on the white side of the coordinates plane, but also their position concerning Y axis, which is the axis that collects the information relative to resistance capacity. This corroborates the statistical analysis predictive capacity and demonstrates its strong relationship with KSA results (table 1). KSA results reported CML-46 line to be slightly more resistant than YR (CML-409), but not as much as WR (CML-397) line, and on the other hand, CML- 247 was reported to be more susceptible than YS (CML-497) but less than WS (CML-448). These are the same results obtained by proteomics and PCoA analysis developed in this work.

Conclusions

This work exhibits a global view of the interrelations between the maize-kernel cell-proteins that occurs in response to infection with *A. flavus*, in an easy-to-understand response model of an individual cell. Besides, with the statistical analysis developed, it was possible to determine which proteins contribute to resistance capacity. Principal coordinates analysis allowed us to generate a statistical plane that can be used as a predictive method of other maize lines' resistance capacity. Cluster analysis showed that the proteomes obtained from the two resistant lines under infection conditions are more similar between each other than between susceptible lines. Furthermore, this relation is closer than the relationship between susceptible lines. This demonstrates that under infection, both resistant lines show a similar response mechanism. This work is the first known report of overexpression of NADPH HC toxin reductase stimulated by *A. flavus* infection. The presence of a similar enzyme to HC toxin synthetase from *H. carbonum* in the genome of *A. flavus*, detected by sequence homology, suggests the existence of a similar toxin and corroborates this result. We finally present an overview of the response mechanism of maize kernels to infection with A. flavus, and propose the use of these statistical methods of resistance capacity determination, using proteins expression pattern for a recurrent selection process to choose the most resistant maize lines after each sowing event, always preserving the required productivity levels.

Acknowledgment

This work was supported by the BID-FONACIT II project Nº N-100001-D. We also thank the Fundación DANAC, for the assistance with material and equipment to accomplish several KSA assays.

Bibliographic references

1. FAOSTAT Database [Internet]. [cited 2012 May 1]. Available from: http://faostat.fao.org/site/339/default.aspx
2. Malaguti G. Section 3: Enfermedades del maíz en Venezuela. In: Fontana H, González C, editors. El maíz en Venezuela. Caracas: Fundación Polar publications; 2000. p. 245–50.
3. Medina-Martínez MS, Martínez AJ. Mold occurrence and aflatoxin B1 and fumonisin B1 determination in corn samples in Venezuela. J Agric Food Chem. 2000;48(7):2833–6.
4. Mazzani C, Borges O, Luzón O, Barrientos V, Quijada P. Incidencia de Aspergillus flavus, Fusarium moniliforme, aflatoxinas y fumonisinas en ensayos de híbridos de maíz en Venezuela. Fitopatol Venez. 1999;12(9):13.
5. Paliwal RL. El Maíz en los trópicos: Mejoramiento y producción. Introducción al maíz y su importancia. Files deposit of the food and agriculture organization of the United Nations (FAO); 2001.
6. Pingali PL, Heisey PW. Cereal-crop productivity in developing countries: past trends and future prospects. In: Alston J, Pardey P, Taylor, editors. Agricultural science policy: Changing global agendas [Internet]. Baltimore and London: The International Food Policy Research Institute / The John Hopkins University Press; 2001. p. 56–82. Available from: http://www.cimmyt.org
7. Miché L, Battistoni F, Gemmer S, Belghazi M, Reinhold-Hurek B. Upregulation of jasmonate-inducible defense proteins and differential colonization of roots of Oryza sativa cultivars with the endophyte Azoarcus sp. Mol Plant Microbe Interact. 2006;19(5):502–11.
8. Schenk PM, Kazan K, Wilson I, Anderson JP, Richmond T, Somerville SC, et al. Coordinated plant defense responses in Arabidopsis revealed by microarray analysis. Proc Natl Acad Sci. 2000;97(21):11655–60.
9. Hajduch M, Ganapathy A, Stein JW, Thelen JJ. A systematic proteomic study of seed filling in soybean. Establishment of high-resolution two-dimensional reference maps, expression profiles, and an interactive proteome database. Plant Physiol. 2005;137(4):1397–419.
10. Kaku H, Nishizawa Y, Ishii-Minami N, Akimoto-Tomiyama C, Dohmae N, Takio K, et al. Plant cells recognize chitin fragments for defense signaling through a plasma membrane receptor. Proc Natl Acad Sci. 2006;103(29):11086–91.
11. Paliwal RL. El Maíz en los trópicos: Mejoramiento y producción. Enfermedades del maíz. Files deposit of the food and agriculture organization of the United Nations (FAO); 2001.
12. Tubajika KM, Damann KE. Sources of resistance to aflatoxin production in maize. J Agric Food Chem. 2001;49(5):2652–6.
13. Brown RL, Cleveland TE, Payne GA, Woloshuk CP, Campbell KW, White DG. Determination of resistance to aflatoxin production in maize kernels and detection of fungal colonization using an Aspergillus flavus transformant expressing Escherichia coli - -glucuronidase. Phytopathology. 1995;85(9):983–9.
14. Anderson TW. Asymptotic theory for principal component analysis. Ann Math Stat. 1963;34(1):122–48.
15. Krzanowski WJ. Between-groups comparison of principal components. J Am Stat Assoc. 1979;74(367):703–7.
16. Saitou N, Nei M. The neighbor-joining method: a new method for reconstructing phylogenetic trees. Mol Biol Evol. 1987;4(4):406–25.
17. Sneath PH, Sokal RR. Numerical taxonomy. The principles and practice of numerical classification. San Francisco, USA: Freeman W.H. and Co.; 1973. 573 p.
18. Gower JC. Some distance properties of latent root and vector methods used in multivariate analysis. Biometrika. 1966;53(3–4):325–38.
19. Campo S, Carrascal M, Coca M, Abián J, San Segundo B. The defense response of germinating maize embryos against fungal infection: a proteomics approach. Proteomics. 2004;4(2):383–96.
20. BioProfiling.de [Internet]. [cited 2011 Aug 1]. Available from: http://www.bioprofiling.de/index.html
21. European Bioinformatics Institute [Internet]. [cited 2011 Oct 1]. Available from: http://www.ebi.ac.uk/
22. Lee D-G, Ahsan N, Lee S-H, Kang KY, Bahk JD, Lee I-J, et al. A proteomic approach in analyzing heat- responsive proteins in rice leaves. Proteomics. 2007;7(18):3369–83.
23. Di Rienzo JA, Casanoves F, Balzarini M, González L, Robledo C. InfoStat version 2012 [Internet]. Argentina: Universidad Nacional de Córdoba; 2012. Available from: http://www.infostat.com.ar/
24. Han F, Kleinhofs A, Kilian A, Ullrich SE. Cloning and mapping of a putative barley NADPH-dependent HC-toxin reductase. Mol Plant Microbe Interact. 1997;10(2):234–9.
25. Meeley RB, Walton JD. Enzymatic detoxification of HC-toxin, the host-selective cyclic peptide from Cochliobolus carbonum. Plant Physiol. 1991;97(3):1080–6.
26. Brosch G, Ransom R, Lechner T, Walton JD, Loidl P. Inhibition of maize histone deacetylases by HC toxin, the host-selective toxin of Cochliobolus carbonum. Plant Cell. 1995;7(11):1941–50.
27. Choudhary C, Kumar C, Gnad F, Nielsen ML, Rehman M, Walther TC, et al. Lysine acetylation targets protein complexes and co-regulates major cellular functions. Science. 2009;325(5942):834–40.
28. Haubruck H, Prange R, Vorgias C, Gallwitz D. The ras- related mouse ypt1 protein can functionally replace the YPT1 gene product in yeast. EMBO J. 1989;8(5):1427–32.
29. Walton JD. HC-toxin. Phytochemistry. 2006;67(14):1406–13.
30. Baker RL, Brown RL, Chen Z-Y, Cleveland TE, Fakhoury AM. A maize lectin-like protein with antifungal activity against Aspergillus flavus. J Food Prot. 2009;72(1):120–7.
31. Baker RL, Brown RL, Chen Z-Y, Cleveland TE, Fakhoury AM. A maize trypsin inhibitor (ZmTIp) with limited activity against Aspergillus flavus. J Food Prot. 2009;72(1):185–8.
32. Bravo JM, Campo S, Murillo I, Coca M, San Segundo B. Fungus-and wound-induced accumulation of mRNA containing a class II chitinase of the pathogenesis-related protein 4 (PR-4) family of maize. Plant Mol Biol. 2003;52(4):745–59.
33. Chen Z-Y, Brown RL, Damann KE, Cleveland TE. Identification of unique or elevated levels of kernel proteins in aflatoxin-resistant maize genotypes through proteome analysis. Phytopathology. 2002;92(10):1084–94.
34. Chen Z-Y, Brown RL, Rajasekaran K, Damann KE, Cleveland TE. Identification of a maize kernel pathogenesis-related protein and evidence for its involvement in resistance to Aspergillus flavus infection and aflatoxin production. Phytopathology. 2006;96(1):87–95.
35. Jia J, Fu J, Zheng J, Zhou X, Huai J, Wang J, et al. Annotation and expression profile analysis of 2073 full- length cDNAs from stress- induced maize (Zea mays L.) seedlings. Plant J. 2006;48(5):710–27.
36. Sekhon RS, Kuldau G, Mansfield M, Chopra S. Characterization of Fusarium-induced expression of flavonoids and PR genes in maize. Physiol Mol Plant Pathol. 2006;69(1–3):109–17.
37. Sels J, Mathys J, De Coninck BM, Cammue BP, De Bolle MF. Plant pathogenesis-related (PR) proteins: a focus on PR peptides. Plant Physiol Biochem. 2008;46(11):941–50.
38. Fountain JC, Koh J, Yang L, Pandey MK, Nayak SN, Bajaj P, et al. Proteome analysis of Aspergillus flavus isolate-specific responses to oxidative stress in relationship to aflatoxin production capability. Sci Rep. 2018;8(1):1–14.
39. Chen Z-Y, Rajasekaran K, Brown RL, Sayler RJ, Bhatnagar D. Discovery and confirmation of genes/proteins associated with maize aflatoxin resistance. World Mycotoxin J. 2015;8(2):211–24.

Received: 23 November 2020
Accepted: 20 January 2021

RESEARCH / INVESTIGACIÓN

Assimilation of natural Radionuclides in the wheat plant from cultivated soil

Suad A. Alsaedi[1], Naseer A. Alsaadie[1*], Raghad S. Mouhamad[1], Nibras A. Yass[2]
DOI. 10.21931/RB/2021.06.02.14

Abstract: The intake of naturally nuclides ^{238}U, ^{232}Th, and ^{40}K by wheat crop from two different fertilization soils of Iraq was studied under natural farm conditions. The overall mean of soil to wheat cereal transfer factors (TF) was studied and observed to be in the range of 0.6×10^{-3} to 0.70×10^{-3} for ^{238}U, 0.11×10^{-3} to 0.13×10^{-3} for ^{232}Th and 0.054 to 0.055 for ^{40}K. The calculated values of TF for wheat grain denote that 40K are the significant radionuclides that are transferred in grain. This evaluation is most important for the production of foodstuffs with low contents of radionuclides. The assimilation of radionuclides by consuming wheat cereals from the farms studied gives a small fraction to the total annual ingestion dose received by a person due to naturally existent radioactivity material in the environment. This study proves that the natural radioactivity and Ingestion effective dose was lower than the safe, which the total of the dose received from ^{238}U and ^{232}Th due to consumption of wheat grains alone from fertilized field 0.056 and 0.045 mSv y^{-1} from the unfertilized field total ingestion dose, the dose received from ^{40}K due to the consumption from the unfertilized and fertilized field was 0.0102 and 0.0137 respectively. The dose values were less than the limit value of 0.30 mSv y^{-1}. Therefore, the consumption of these foods has no health risks. This process may help to obtain basics on radiological health regulations. The activity concentration of natural radionuclides ^{238}U, ^{232}Th, and ^{40}K in fertilized and unfertilized soil and wheat plants growing into is statistically significant at 1% level of significance using an independent t-test.

Key words: Gamma spectrometry, soils, wheat, radiation exposure.

Introduction

Soil–plant–man is one of the main paths for transferring radionuclides to human being[1]. These naturally occurring radionuclide may get carried to plants and the nutrients during elements uptake, accumulate in different parts and even reach the edible portions. When consumed through man and animal as nutrition, these crops or their parts would cause contribute irradiation. Food is one of man's unique needs, and the numerous world population has become a menace to global food safety. Therefore, the requirement to increase agricultural food production arises to ensure food security for the growing world population. Due to this critical need of man, Mineral fertilizers are chemical compounds that provide necessary elements and nutrients to the plants are substantial and more used inputs in agriculture, helping contribute to global food security, farmer sustenance, and essential human nutrition. Besides, to increase the amount, quality of land and enhance crop productivity[2,3]. Like the remnant of the world, Iraq's population is increasing, and there is also the need to increase the availability of food by increasing the rate of food production via the application of chemical fertilizers. The primary raw materials for producing chemical fertilizers must therefore supply the essential nutrients necessary for plant growth. The essential nutrients are Nitrogen, phosphorus, and potassium. Natural radioactivity of mainly Uranium-238(^{238}U), Thorium-232 (^{232}Th), and Potassium-40 (^{40}K) seen in phosphate fertilizers emanate from the phosphate ore (due to geological reasons), which is the primary raw material used for phosphate fertilizer production. The application of phosphate fertilizer globally for increased crop production and land reclamation has risen to more than 30 million tons annually[4]. The data on plant uptake of radionuclides under natural field conditions, especially from background areas, are scarce. The soil properties such as pH, clay minerals, Ca, K, organic matter contents, and fertilizer application can strongly affect the retention, uptake, and distribution of radionuclides in plants. As a result, it may be rather difficult to predict the rates of uptake of radionuclide in a particular site. Uranium, thorium, and potassium concentrations are often higher in phosphate-rich soils. The range and average concentration of radionuclides ^{235}U, ^{238}U, ^{40}K and ^{226}Ra Bq kg^{-1} in phosphate fertilizers around the world was 1.6-53 (15 ± 1), 26-1145 (220 ± 20), 23-12324 (4860 ± 250) and 4-393 (87 ± 8)[5]. The content of the radioactive elements ^{238}U, ^{235}U, ^{232}Th in the local Triple Super Phosphate (TSP) fertilizer used in Iraqi agricultural soils was 6.46, 0.068, and 4.35 mg kg^{-1}, and local NPK fertilizer was 1.83, 0.015, and 0.838 mg kg^{-1}[6]. Application of certain fertilizers with higher concentrations of these radionuclides—for example, common mineral fertilizer superphosphate—can potentially result in accumulation of ^{238}U, ^{232}Th, and ^{40}K in food crops grown in the amended soils[7-9].

All types of food, including wheat, have a detectable amount of radioactivity successfully transferred to the human body through the route of ingestion. We also know that food activity is closely related to agricultural soil activity where food crops were grown under these conditions. Among various earth samples, the soils of wheat have been chosen for radioactivity studies because this crop is trendy, widespread, and considered a strategic crop. Currently, there is not much information on radioactivity concentration in food, especially a wheat plant, Which is one of the most important crops in Iraq, as Iraq's arable land is estimated at 8 million hectares, comprising less than 15% of the country's total area is mostly concentrated in the north and northeast and the valleys of the Tigris and Euphrates rivers. However, only 4 to 5 million hectares are being cultivated. , where crops are grown. Cereal production (mostly wheat, barley, and corn) is the principal agricultural activity in Iraq, accounting for 70 to 85% of cultivated area. The main varieties cultivated in Iraq are Alnoor, Ebaa 99/95, Wahat Al Iraq, Al Hashemeia, Sham 6, Dour 29, Al Rasheed, Al Hadbaa Al Fateh. The average yield in Iraq is 1.1 T/ha by adding compound fertilizers amount 140 kg/ha while the world avera-

[1] Agriculture Research Directorate, Ministry of Science and Technology, Baghdad, Iraq.
[2] Iraqi University, Faculty of Arts, Department of Geography, Iraq.

Corresponding author: naseeralsaadie61@gmail.com

ge is about 2.8 T/ha[10], there is only a limited number of studies that evaluate soil and fertilizers. We decided to measure the concentration of natural radionuclides in wheat plant widely cultivated in fertilized and unfertilized soil for these reasons. This study aims to determine if natural radioactivity in wheat plants from soil to assess soil radioactivity's impact on crops the health implication on the man who is the final consumer.

Materials and methods

Soil and wheat samples were carried on from 20 agricultural fields surrounding Kut city (Capital of Wasit Governorate–Iraq) and provided the population with a part of wheat harvest used in the mills to produce flour for daily consumption (Fig. 1). Two types of cultivated fields of the study area were studied, one field was fertilized with 300 kg/ha of ammonium phosphate fertilizer before sowing the seeds, and the other was unfertilized. The fields measuring about 200 m^2 were divided into small sub-sections of 20 m^2 each. The soil was sampled from each sub-section, including the surface layer, and to a depth of 10 cm as wheat has an adventitious root system, spreads in the upper layer of the soil, and does not go deep. The soil samples from 3 to 4 points in a single sub-section were mixed, dried, sieved, and homogenized to obtain a composite sample representative of that section. Three a portion of about 1 kg soil was taken from this complex sample for further analysis, and their average activity has been reported as one sample. Likewise, around 20–30 utterly mature wheat crops were taken from every sub-section of the selected fields and separated into the grain.

Soil samples and grain (wheat plant samples) were dried for 48 hours in an oven at 100°C. Soil samples were grounded to pass an 80 mesh (0.5 mm opening) sieve. Plant samples, on the other hand, were also ground to pass 100 mesh sieve. Ground samples were kept in tightly closed jars for radioassay and other relevant analysis. Radio assays were performed using gamma-ray spectroscopy, a high purity germanium radiation detector (HPGe) with 40% efficiency, linked to a multi-channel analyzer (MCA) 8192 channel. Results obtained were analyzed using the analytical program Giene-2000. Calibration of the Gama Spectrometer was performed using a standard analog radiometric source from ^{152}Eu, ^{60}CO.

Gamma rays resulting from the decay of natural uranium, thorium, and potassium were determined based on published reports of the United Nations Scientific Committee such as ^{40}K, ^{226}Ra, ^{214}B ^{212}Pb, as well as the industrial element ^{137}Cs. The data on radioactivity concentration in soil and grains obtained from one field were subjected to Student's t-test with the other field one to test the significance of the differences in their mean values at a 99% confidence level.

Results and Discussion

The specific activity due to ^{238}U, ^{232}Th, and ^{40}K in the soils collected from all the fields has been measured as shown in Table (1). The mean radionuclide contents of the two types of soil show fertilization variations and reliance on them as one of the impact factors, which is well reflected in the current study. The use of ammonium phosphate fertilizers made from the original rock-phosphate mineral in the wasit field does change the soil's radioactivity content appreciably as the difference between the average values of the fertilized and unfertilized fields is statistically significant. Previously reports by 11,12 on natural radioactivity content in soils of Iraq also confirm these results. The natural radioactivity contents obtained in the present study are within the range for acceptable limits background activity reported for soils worldwide[13].

The mean activity concentration of ^{238}U, ^{232}Th, and ^{40}K in fertilized soil Cultivated with the wheat plant is 27.3, 19.1, and 364 $Bqkg^{-1}$, respectively, and for unfertilized soil is 19.2, 13.3, and 275 $Bgkg^{-1}$, respectively. The T values of 5.33, 5.79, and 5.66 for ^{238}U, ^{232}Th, and ^{40}K, respectively, being more significant than the critical T value at an alpha of 0.01 level of significance, shows that the difference in activity concentration of naturally occurring radioactive materials in fertilized and unfertilized soil is statistically significant; thus the difference between the mean activity concentration of natural radionuclides ^{238}U, ^{232}Th and ^{40}K in fertilized and unfertilized soil may be due to increment in the rate of used fertilizers, especially phosphate fertilizer and this could also mean that agricultural fertilizers do have a significant impact on the transfer of natural radionuclides to the soil.

A comparison showed that the fertilized soil contains a little higher concentrations of natural radionuclides than the

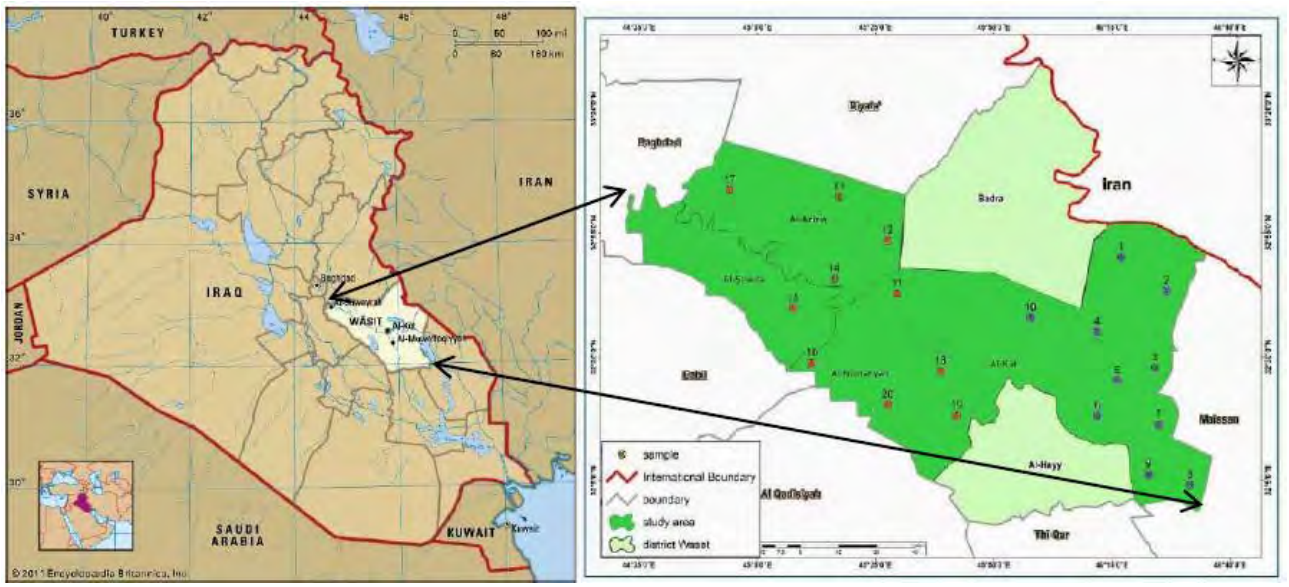

Figure 1. Area of study and sampling station.

Soil	^{238}U	^{232}Th	^{40}K
Unfertilized Wasit field (no. of samples = 10) Rang Mean	 10.9 – 32.7 19.2±1.95	 6.03 – 17.4 13.3±1.05	 231 – 290 275±21.8
fertilized Wasit field (no. of samples = 10) Rang Mean	 11.2 – 36.1 27.3±4.40	 8.46 – 24.8 19.1±2.66	 293 – 386 364±25.5
T value (Independent t-test) Critical value of $t_{(df=19,\ \alpha=0.99)}$	5.33 2.54	5.79 2.54	5.66 2.54
Reference value	35	30	400

Table 1. Activity concentration of ^{238}U, ^{232}Th, and ^{40}K (Bq kg^{-1}) in soil (± Uncertainty).

unfertilized soil; the concentration of ^{238}U, ^{232}Th, and ^{40}K in fertilized soils is one time more than that in the soils from unfertilized.

The concentration of ^{238}U, ^{232}Th, and ^{40}K in the cereal is the edible portion of the wheat plant, immediately consumed by people, and can indicate ingestion dose to population. The concentrations of natural radionuclides analyzed of wheat grains planting in the fertilized, and unfertilized field are shown in (table 2). The range of specific activity concentration for ^{238}U, ^{232}Th, and ^{40}K varied from 10.2 to 14.7 with average (13.4 mBq kg^{-1}), 1.6 to 2.09 with average (1.73 mBq kg^{-1}) and 9.21 to 17.4 with average (14.9 Bq kg^{-1}) respectively, in wheat grains planting at Unfertilized Wasit province field, and 14.6 to 18.2 (16.5 mBq kg^{-1}), 1.64 to 2.55 (2.04 mBq kg^{-1}) and 12.0 to 36.2 (20.1Bq kg^{-1}) respectively, for wheat crop grains planting in fertilized Wasit province.

T-test results (Table 2.) indicated that the difference between the overall mean of all studied radionuclide concentrations one by one into the grain of wheat cultivated through the two fields soil (Unfertilized and Fertilized) by conventional criteria, this difference is considered to be extremely statistically significant. The percentage of activity concentration ^{238}U, ^{232}Th, and ^{40}K increased in the wheat grain of location fertilized field by 23, 18, and 35%, respectively, compared to their content in the unfertilized location.

The mean values of activity concentrations of ^{238}U, ^{232}Th, and ^{40}K for the wheat grain samples in this study were too much lower than the accepted values referred by the United Nations Scientific Committee on the Effects of Radiation Sources[13]. The obtained results of activity concentrations of the impressive natural radionuclides had this order $^{40}K > ^{238}U > ^{232}Th$; the mean concentration was highest for ^{40}k because ^{40}K is an essential element of living organisms; therefore, the ^{40}K radioactivity cannot be avoided. This result is following the information presented by (14,15). The study carried out by (16) found that the specific activity in wheat flour samples are available in Iraqi markets were varied from (1.09±0.087) to (12.5±2.03) Bq kg^{-1} for ^{238}U, ^{232}Th From (0.126±0.066) to (4.30±0.388) Bq kg^{-1} and ^{40}K from (41.8±5.88) to (264.729 ± 3.843) Bq kg^{-1}. A pot experiment was carried out, and Jew's-mallow (*Corchorus olitorius*) is hugely a popular national Egyptian vegetable food that the Egyptians highly consume either as fresh or cooked food. Was cultivated on soil with fertilizers (NPK) and unfertilized by (17) were found that the average value of the specific activity of ^{226}Ra, ^{238}U, ^{232}Th, and ^{40}K in Bq kg^{-1} for Jew's-mallow plant fertilized was 0.501, 0.055, 0.136, and 11.4 respectively, and Non-Fertilized it was 0.29, 0.050, 0.130 and 9.83 respectively.

The food chain implants the primary path of the radionuclides entry into the human body; thus, the intake estimation of these radionuclides is fundamental. Among all parameters applied to assessing the concentrations of the radionuclide in plants, transfer factor from soil to plant (TF) is one of the most substantial parameters utilized in models to estimate the effects of radioactive contamination on the environment. This parameter reflects radionuclide uptake through roots and can be realized as the ratio of radioactivity unit per dry crop mass to that of unit per dry soil mass[18]. Some factors that affect the natural radionuclides transfer from soil to plants, such as fertilization, plant species, and the soil properties[19], transfer factors (TF) were calculated as the ratio of the radionuclide concentration in the plant (Bq/kg plant) to its concentration in soil (Bq/kg soil). The soil to grains transfer factor for radionuclides studied are given in (Table 3) and compared with the default values suggested by IAEA[18].

The overall mean transfer factor (TFs) of ^{238}U, ^{232}Th, and ^{40}K from unfertilized soil to grain wheat was 0.70×10^{-3}, 0.13×10^{-3}, and 0.054 respectively, compared with 0.60×10^{-3}, 0.11

Location	^{238}U mBq kg^{-1}	^{232}Th mBq kg^{-1}	^{40}K Bq kg^{-1}
Unfertilized Wasit field (no. of samples = 10) Rang Mean	 10.2 – 14.7 13.4^{a} ±2.29	 1.60 – 2.09 1.73^{a} ±0.0.208	 9.21 – 17.4 14.9^{a} ±2.83
fertilized Wasit field (no. of samples = 10) Rang Mean	 14.6 – 18.2 16.5^{b}±3.08	 1.64 – 2.55 2.04^{b} ±0.338	 12.0 – 36.2 20.1^{b} ±4.52
T value (Independent t-test) Critical value of $t_{(df=19,\ \alpha=0.99)}$	2.55 2.54	2.92 2.54	3.65 2.54
Reference value [14]	20	3	–

Table 2. Activity concentration of ^{238}U, ^{232}Th, and ^{40}K in wheat grains (± Uncertainty).

Location	^{238}U mBq kg^{-1}	^{232}Th mBq kg^{-1}	^{40}K Bq kg^{-1}
Unfertilized Wasit wheat field (no. of samples = 10) Mean	0.70×10^{-3}	0.13×10^{-3}	0.054
fertilized Wasit field (no. of samples = 10) Mean	0.60×10^{-3}	0.11×10^{-3}	0.055
Reference value	2×10^{-3}	5×10^{-4}	7.8×10^{-1}

Table 3. Transfer factor for ^{238}U, ^{232}Th, and ^{40}K in wheat grain.

$\times 10^{-3}$ and 0.055 respectively, for the fertilized field. This finding indicated that the mean value of ^{238}U uptake is greater than that of ^{232}Th. These differences can be associated with the difference in solubility of elements with oxidation state +II. Uranium exhibits higher solubility than thorium in water[20], reported that thorium is less mobile than uranium, which is consistent with our TF observation of ^{232}Th and ^{238}U; generally, ^{40}K exhibits a higher TF value in grain than that of ^{238}U and ^{232}Th because K is a significant nutrient needed by the plant in large quantities[21]. The experimental values of the transfer factor of natural radionuclide in wheat grains grown from both types of fields unfertilized and fertilized are close to the default value suggested by the IAEA. Also, the results showed that radionuclide concentrations in grain are not linearly related to soil concentrations; these results are in agreement with that reported by (22), the nearly comparable values of transfer factors for radionuclides despite their different concentration levels in soil is a result of very complex behavior of elements in the soil[23]. have reported that the degree of accumulation of natural radioactive elements is affected by the metal-selective function of plants during the uptake of elements to maintain the mechanism of homeostasis in a typical environment.

People are risky to natural radiation from external sources, including radionuclides in the earth, cosmic radiation, and internal radiation from radionuclides integrated into the body and from the significant ways of radionuclide intake ingestion of food and water. An appointed denomination of exposure to internal radiation radionuclides of (uranium and thorium) decay series and ^{40}K existing in food consumed by people leads to ingestion. The Ingestion effective dose ($D_{G,r}$) related to intake of ^{238}U, ^{233}Th, and ^{40}K in foodstuff samples is reflected as a radiological hazard for human health. The annual effective ingestion dose to man due to the consumption of wheat grains can be estimated to utilize the formula is below[24,25].

$$D_{G,r} = \sum_f (U_f \times A_{f,r}) \times g_{T,r}$$

Where $D_{G,r}$ is the annual ingestion dose (mSv y^{-1}), f indicates a food type, the coefficients U_f and $A_{f,r}$ represent the annual intake of grain wheat (kg y^{-1}), and the specific activity of the radionuclide (r) of interest (Bq Kg^{-1}), respectively, and $g_{G,r}$ is the conversion coefficient of dose for ingestion of radionuclide r (Sv Bq^{-1}) in tissue grain (G). For the public, the adult conversion coefficient of dose $g_{G,r}$ for ^{238}U, ^{232}Th, and ^{40}K are 2.8×10^{-7}, 2.2×10^{-7}, and 6.2×10^{-9} Sv Bq^{-1}, respectively[24]. The annual intake values of wheat for adults were taken as 110 kg y^{-1} [26].

The effective ingestion dose in (mSv y^{-1}) for adults due to specific activity of ^{238}U, ^{232}Th, and ^{40}K in wheat grain samples is calculated using Eq. above shows in (Figure 1). The overall mean summation of the Ingestion effective dose was varied from (0.041, 0.004, and 0.010) mSv y^{-1}, respectively, to (0.051, 0.005, and 0.014) mSv y^{-1}, for wheat grains from the unfertilized and fertilized field. Figure 2 shows the comparison between the average of the ingestion effective dose for ^{238}U, ^{232}Th, and ^{40}K in wheat grain samples which obtain the average of ingestion effective dose due to ^{238}U was higher than due to ^{232}Th and ^{40}K because of the increased dose conversion coefficient for ingestion of radionuclide, the total of the dose received from ^{238}U and ^{232}Th due to consumption of wheat grains alone from the fertilized field (0.056 mSv) shall constitute 19.6% of the unfertilized field total ingestion dose (0.045 mSv). The individual and sum total of the dose received from these radionuclides' contributions in wheat grains from two field ingestion doses are lower than the reference value 1 mSv y^{-1} recommended by (27).

Conclusions

Cereals like wheat constitute a significant part of man's daily diet; wheat is mainly used for food and used as feed/fodder. A gamma spectrometer was used to estimate the concentration of natural radionuclide activity in the soil and grain wheat from unfertilized and fertilized fields collected from the Wasit province. The specific activities of the radionuclides ^{238}U, ^{232}Th, and ^{40}K in the soil, at all the investigated unfertilized locations, were in the range from 10.9 to 32.7, 1.2 to 36.1 and 23.0 to 290 Bq kg^{-1}, respectively, and 11.2 to 36.1, 8.46 to 24.8 and 293 to 386 Bq kg^{-1}, respectively, for fertilized location, radionuclides concentration and the two locations above in grain wheat were in the range of 10.2 to14.7 mBq kg^{-1}, 1.64 to 2.09 mBq kg^{-1} and 9.21 to 17.4 Bq kg^{-1} and 14.6- 18.2 mBq kg^{-1}, 1.64 - 2.55 mBq kg^{-1} and 12.0–36.2 Bq kg^{-1}, respectively. Thus, the application of soil fertilizer to increase yield increases the concentration of radionuclide biological activity. The site-specific TF calculated values for grain wheat indicate that ^{40}K are the main radionuclides transferred in cereals. The site-specific TF obtained for a radionuclide serves as a useful tool to obtain precise and realistic dose estimate through terrestrial food chain models; the computed annual dose due to intake of uranium, thorium, radium, and potassium through the wheat grains grown in the agricultural fields under the present study is a small fraction of the reported global annual ingestion dose. The findings have been shown that consumed grain wheat is safe from any radiation risk. The current study suggests that other staple foodstuffs are needed to have a similar study to create baseline data of consumed foodstuffs to prepare a radiological map of Iraq.

Author Contributions

Conceptualization, Suaad A. Alsaedi; methodology, Naseer A. Al-Saadie; formal analysis, Suaad A. Alsaedi; investigation, Nibras A. Yass ; resources, Naseer A. Al-Saadie; writing—original draft preparation, Nibras A. Yass; writing—review and

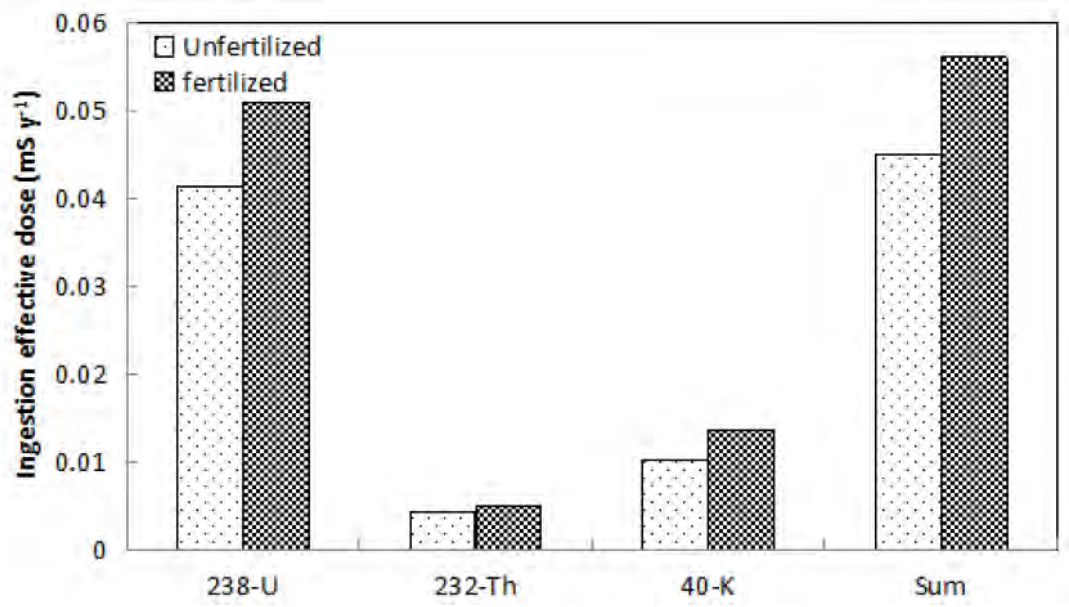

Figure 2. Dose acquired by intake of wheat grains.

editing, Suaad A. Alsaedi; visualization, Raghad S. Mouhamad; project administration, Raghad S. Mouhamad.

All authors have read and agreed to the published version of the manuscript.

Funding

This research received no external funding.

Bibliographic references

1. International Atomic Energy Agency. (1982). Generic Models and Parameters for Assessing the Environmental Transfer of Radionuclides from Routine Releases, Exposure of Critical Groups. Safety Series No. 57, IAEA, Vienna.
2. Esraa Hamad Raheem. (2015). Activity Concentration of Natural Radioactivity and Dose Assessment for Brands of Chemical Fertilizers used in Iraq. International Journal of Current Engineering and Technology, 5(6):3823-3828.
3. Food and Agriculture Organization of the United Nations (FAO). (2019). The International Code of Conduct for the Sustainable Use and Management of Fertilizers. Rome. ISBN 978-92-5-131705-1.
4. Hazim Louis Mansour and Yousif Muhsin Zayir Al-Bakhat. (2018). Measurement of Radioactivity Levels and Assessment of Radiation Hazards for Plants Species Grown at Scrap Yard (B) at Al-Tuwaitha Nuclear Site (Iraq). Nuclear Science, 2(4):94-98.
5. UNSCEAR. 2008. Sources and effects of ionizing radiation. Report to General Assembly with Scientific Annexes. New York, United Nation Publication.
6. Naseer A. Alsaadie; Suhailah. K. Saihood; Yasir. A. Hamad. (2018). Statistical evaluation of successive mineral fertilization used on accumulation of some heavy and radioactive element in soil and plant. 14th Arab Conference on the Peaceful Uses of Atomic Energy, Sharm Elshrikh, Republic of Egypt, 16-20 December.
7. Ononugbo C. P.; Azikiwe1 O. and Avwiri G. O. (2019). Uptake and Distribution of Natural Radionuclides in Cassava Crops from Nigerian Government Farms. Journal of Scientific Research & Reports, 23(5): 1-15.
8. Theophilus Adjirackor; Emmanuel O. D. and Frederic Sam. 2017. Naturally occurring radionuclide transfer from soil to vegetables in some farmlands in Ghana and statistical analysis. Radiation Protection Environment , 40(1):34-43.
9. Ali A. Abojassim; Heiyam N. Hady and Zahrah B. Mohammed. (2016). Natural radioactivity levels in some vegetables and fruits commonly used in Najaf Governorate, Iraq. J. Bioen. Food Sci., 3(3):113-123.
10. FAW. (2014). World wheat production. International Food and Agriculture Organization statistics.
11. Auday Albayati; Bashair Mohammed and Raad Mahmoud Nasif. (2016). Determination of Radionuclide's Concentrations in Soil Around of Al-Tuwaitha Nuclear Research Center in Iraq by Using Gamma Spectroscopy Analysis System. Journal of Chemical, Biological and Physical Sciences, 6(3):996-1005.
12. Ayham Assie; Abdul-Jabbar A. Oudah; Awatif S. Jassim and Asia H. Al-Mashhadani. (2016). Determination of natural radioactivity by gamma spectroscopy in Balad soil, Iraq. Advances in Applied Science Research, 7(1):35-41.
13. United Nations Scientific Committee on the Effects of Atomic Radiation Sources. (2000). Effects and Risks of Ionizing Radiation, Report to the General assembly with Scientific Annexes. United Nations, New York: United Nations Scientific Committee on the Effects of Atomic Radiation Sources.
14. Abdulridha S. Younis and Nada F. Tawfiq. (2019). Assessment of Natural Radioactivity Level and Annual Effective Dose of Amber Rice Samples Cultivated in the South of Iraq. The 2nd International Conference on Renewable Energy and Environment Engineering, E3S Web of Conferences 122, 05004.
15. Gooniband Shooshtari M.; Deevband M. R.; Kardan M. R.; Fathabadi N.; Salehi A. A.; Naddafi K.; Yunesian M.; Nabizadeh Nodehi R.; Karimi M. and Hosseini S. S. (2017). Analytical study of 226Ra activity concentration in market consuming foodstuffs of Ramsar. Journal of Environmental Health Science and Engineering, 15(19):1-7.
16. Ali Abid Abojassim, Husain Hamad Al-Gazaly and Suha Hade Kadhim. (2014). 238U, 232Th and 40K in wheat flour samples of Iraq markets. Ukrainian Food Journal, 3(3):333-340.
17. Salama, M. A., Yousef, Kh.M. and Mostafa, A.Z. (2019). Detection of Natural Radionuclides Concentration in Corchorus Olitorius and Soil as Affected by Different Fertilizers. Arab J. Nucl. Sci. Appl., 52(1):33-43.

18. International Atomic Energy Agency (IAEA). (1994). Handbook of parameter values for the prediction of radionuclide transfer in temperate environments Technical reports series no. 364 IAEA, Vienna.
19. Elsaman R.; Ali G.A.M.; Uosif M. A. M .; El-Taher A. and Chong K.F. (2020). Transfer factor of natural radionuclides from clay loam soil to sesame and Cowpea: radiological hazards. International Journal of Radiation Research, 18(1):157-166.
20. Focazio M. J., Focazio, Z., Szabo T. F., Kraemer A. H., Mullin T. H. and Barringer V. DePaul. 2001. Occurrence of selected radionuclides in ground water used for drinking water in the United States: A targeted reconnaissance survey, 1998 US Department of the Interior, US Geological Survey.
21. Abdul Majeed M. Al Mutairi and Norlaili A Kabir. 2020. Natural Radionuclides in Soil and Root Vegetables in Malaysia: Transfer Factors and Dose Estimates. Radiation Protection Dosimetry, 188(1):47–55.
22. Jelena Mrdakovic Popic, Deborah H. Oughton and Lindis Skipperud. 2020. Transfer of naturally occurring radionuclides from soil to wild forest flora in an area with enhanced legacy and natural radioactivity in Norway. Environmental Science, 22:350-363.
23. Chonlada Raikham and Papaporn Jantawongrit. (2020). Using of Organic or Inorganic Fertilizers to Grow Thai Jasmine Rice 105 in Soil with Natural Radioactivity (226Ra, 232Th and 40K); Transfer of Radioactivity to Roots. Science Technology and Engineering Journal (STEJ), 6(1):57-66.
24. International Atomic Energy Agency (IAEA). (1989). Measurement of Radionuclides in Food and the Environment, reports no. 295 IAEA, Vienna.
25. Abdalrahman Alsalihi1 and Riyadh Abualhiall. (2019). Estimation of Radiation Doses, Hazard Indices and Excess Life Time Cancer Risk in Dry Legumes Consumed in Basrah Governorate/Iraq. Journal of Pharmaceutical Science and Research, 11(4):1340-1346.
26. The Iraqi Ministry of Trade. Ration Card System (RCS). (2017). Available from: http://www.mot.gov.iq/.
27. International Commission on Radiological Protection. (1996). Age-Dependent Doses to Members of the Public from Intake of Radionuclides: Part 5 Compilations of Ingestion and Inhalation Dose Coefficients (ICRP Publication 72)". Pergamon Press, Oxford.

Received: 20 November 2020
Accepted: 25 January 2021

RESEARCH / INVESTIGACIÓN

Upregulation of miR-206 is a potential diagnostic biomarker in breast cancer

Faezeh Karami[1*], Narges Maleki[1,2], Arefeh Khazraei Monfared[1], Sayeh Jafari Marandi[1]

DOI. 10.21931/RB/2021.06.02.15

Abstract: Breast cancer is one of the most common malignancies, and like most cancers, most cases are caused by somatic mutations. Due to estrogen's role in the growth, differentiation, and division of breast and endometrial cancer cells, tamoxifen is used as an estrogen receptor antagonist in breast cancer cells with estrogen receptor (ER +) has a special place, which unfortunately in one-third of the Cases are resisted. This study aimed to investigate the effect of tamoxifen-treated tumor-derived exosomes on the expression pattern of Twist and Bcl-2 oncogenic genes in fibroblast cells. MCF-7 breast cancer cell line and fibroblast cells were purchased and cultured in a complete culture medium. After the appropriate number of cells was reached, they were treated with the appropriate concentration of tamoxifen. Cellular supernatant was then gathered in flasks, and exosomes were extracted from them. After extracting RNA from exosomes and cDNA synthesis, the expression level of miR-206, Twist-1, and Bcl-2 genes were evaluated using the Real-Time PCR method. The electronic microscope results confirmed the correctness of the exosomes isolated from the tumor cell culture medium. It has also been shown that tamoxifen treatment increases the expression of miR-206 in exosomes derived from breast tumor cells. The control group which has been kept untreated induced the expression level of Twist-1 and Bcl-2 genes time-dependently. However, when tamoxifen-treated tumor-derived exosomes treated the target cells, the expression level of oncogenic miRs Twist-1 and Bcl-2 were declined over time. Overall, this study showed that tamoxifen treatment on breast cancer cells could apply its antioncogenic effects on tumor stromal cells, such as fibroblasts, by altering the expression levels of exosomal microRNAs in tumor cells.

Key words: Breast cancer, tamoxifen, fibroblast, exosome, miR-206.

Introduction

Breast cancer is one of the most common malignancies, and like most cancers, most cases are caused by somatic mutations. Today, breast cancer is the most common cancer among women globally, and the resulting death rate is the highest in cancer deaths among women[1]. Tamoxifen is a non-steroidal anti-estrogenic drug introduced in the United Kingdom in 1960 as a contraceptive drug and was approved by the Food and Drug Administration in 1977 as a treatment for metastatic breast cancer. The adjuvant therapy title for breast cancer is used in people at risk[2]. As a treatment for breast cancer, tamoxifen slows or stops the growth of cancer cells that need estrogen to grow or spread, and as a complementary treatment, it helps prevent the spread and recurrence of breast cancer[3]. The exact mechanism of action of the drug is unclear. Tamoxifen may act by blocking estrogen receptors in tumor cells that need estrogen to grow. The estrogen receptor- tamoxifen complex may be transported into the nucleus of a tumor cell, inhibiting DNA production[4].

Exosomes are vesicles at the nanometers that are actively secreted by almost all types of cells, including fibroblasts, endothelial cells, epithelial cells, nerve cells, immune cells, and cancer transmit signals between cells. This suggests that exosomes play several roles in regulating physiological responses[5]. The pathophysiological effects of exosomes on diseases, especially cancers, have recently been identified. According to research, tumor-derived exosomes play a role in the spread of cancer malignancy by increasing cancer cells' proliferation, creating a pre-metastatic site, and regulating drug resistance. Clinically, exosomes' performance as diagnostic biomarkers, therapeutic targets, or even as carriers of anticancer drugs has been emphasized due to their unique biological and pathophysiological characteristics[6].

MiRNAs are small molecules that play a crucial role in physiological, pathological, angiogenesis, apoptosis, and cancerous processes. Today, miRNA is used as a biomarker to diagnose and treat cancer to prevent cancer patients' difficult stages of treatment. A miRNA is a short ribonucleic acid (RNA) found in eukaryotic cells. A miRNA molecule has a small number of nucleotides than other RNAs (it has an average of 22 nucleotides). MiRNAs are post-transcription regulatory elements that bind to a complementary sequence on the target mRNA, resulting in suppressing the transcription, degrading the target, and ultimately silencing the gene. The human genome encodes more than 2,000 types of miRNAs that may make up 60% of genes and are abundant in various human cells[7]. The TWIST1 gene encodes a transcription factor[8], and the BCL2 gene encodes an anti-apoptotic protein[9]. Based on what has been previously saying and the hypothesis that tumor cell secretions could cause malignancy in the fibroblast cells of the tumor microenvironment, so in the present study, we sought to investigate the effect of tumor cell-derived exosomes on the expression level of Twist-1 and Bcl-2 oncogenes as well as miR-206 in tumor cells.

Materials and methods

Cell Purchase and preparation

MCF-7 breast cancer cell line with NCBI CODE 135 was purchased from Iran Genetic Resources Center, and fibroblast cells were purchased from Tarbiat Modares University. The cells were stored in a fully cultured medium with FBS, and were kept in an incubator with CO2 Saturation Rate: 5% and a temperature of 37°C.

Tamoxifen treatment

Based on the results of the previous experiments[10], ta-

[1] Department of Cellular and Molecular Biology, Faculty of Biological Sciences, Islamic Azad University-Tehran North Branch, Tehran, Iran.
[2] Gynecology and Reproductive Biology Department, Kowsar poly-clinic, Tehran, Iran.

Corresponding author: karami_faezeh@yahoo.com

moxifen IC50 was a concentration between 54µM (equivalent to 20µg/ml) and 68µM (equivalent to 25µg/ml). Hence, the concentration of 60Mµ (as a concentration close to IC50) was considered for this study's treatment.

Exosome Isolation

To isolate the exosomes from the culture medium of MCF-7 cells, centrifugation at 3000g was performed for 10minutes, and an exoquick solution (system biosciences) was added to the liquid. The microtubes were incubated at 4°C for 20min and then centrifuged again at 1500g for 15min. 50 microliters of PBS were added to the resulting precipitate. Eventually, the microtubes were stored at -20°C. The exosome isolation from the supernatant was performed on both treated and control cell groups. The exosomes' extraction was confirmed by microscopic examination, and the size and morphology of the exosomes were evaluated by a digital electron microscope (Digital FESEM, KYKY-EM3200, China).

Labeling Exosomes

The isolated exosomes were labeled using PKH26 (PKH26 Red fluorescent - Mini26-1, Sigma) dye. Initially, one milliliter of Diluent C was added to one milliliter of the exosomes. After pipetting, one milliliter of diluted dye was added to the microtube. After incubation at room temperature for 5 min, two milliliters of Diluent C were added to the microtubules to stop labeling. In the next step, 1.5ml of exoquick, exosome separation solution, was added with a ratio of 3 to 1 (relative to the content of microtubes), and after incubation for 20 minutes at 4°C, centrifugation at 15000g was done for 20 minutes. The sediment was then dissolved in 30 microliters of PBS. Fibroblast cells were treated with these labeled exosomes and incubated at room temperature for 12 hours. Due to miRNAs' presence in exosomes, the exosomal transfer of miR-206 to fibroblast cells was investigated. In this regard, fibroblast cells were treated with 100µg/ml tumor-derived exosomes and 50µg/ml alpha-amanitin to evaluate the miR-206 transfer rate fibroblast cells at 0, 24, and 48 hours after treatment. The reason for using alpha-amanitine is to inhibit any transcription activity that can be induced by exosomal treatment in cells.

RNA Isolation

Initially, 50 microliters of trizol (Invitrogen) were added to the cells. They were then incubated at room temperature for 5 min, and then 15µl of chloroform were added to them, and the microtubes were incubated at room temperature for 2-3 min. The sample microtubes were centrifuged at 12000g for 10minutes. At this stage, the upper solution was transferred to a new microtube as RNA. One milliliter of ethanol 75% was added and then pipetted. Finally, the microtubes were stored at -80°C. The extracted RNA's quantitative assay was performed using spectrophotometry (NanoDrop Technologies, Wilmington, DE, USA).

Evaluating the expression level of TWIST1, BCL2, and miR-206 genes: For cDNA synthesis, TWIST1 and BCL2 genes were used (1st strand cDNA Synthesis kit - Thermo Fisher Scientific). Moreover, oligo dT, primer, and random hexamer were all added with one ratio, and the synthesis was continued according to the manufacturer's guidelines. Thermofisher kit and the Aligo dT (Exiqon) kit were used to evaluate the expression of miR-206. The sequence of primers used for each gene in the Real-time PCR reaction is listed in Table 1. The temperature cycle was similar for all three genes and began with an initial eruption at 95 C for 5 min, then with 40 cycles, each involving refraction at 95 C for 5 s. The connection process was maintained at 65-62. C for 20 s and the expansion at 72. C for 30 s. Data analysis was performed using the CT comparison method. Compared to the endogenous U6 snRNA expression levels and expression of other genes, normalization of miRNA expression levels was normalized and compared by GAPDH gene. Data analysis was performed using ABI step one Real-Time PCR Software v2.0.2 software (Applied Biosystems, UK) and statistical analysis using Excel software (Microsoft, 2010) and GraphPad software.

Statistical analysis: The data obtained from the present study were analyzed using SPSS v.20 software and one-way and Tukey variance statistical tests, and P <0.05 was considered significantly meaningful.

Results

Exosome confirmation

To investigate the exosomes' molecular content derived from breast tumor cells, the exosomes were first isolated from the tumor cells' culture medium by the method mentioned above. The first is to confirm these exosomes by any appropriate methods that assess the exosome's size and morphology. The size and morphology of the exosomes were evaluated by electron microscopy. The results showed that the isolated exosomes had a spherical appearance with a size range of 30 to 150 nm (Figure 1).

gene	Primer sequence
GAPDH	Forward: 5-ACCCACTCCTCCACCTTTGA-3
	Reverse: 5-CTGTTGCTGTAGCCAAATTCGT-3
BCL-2	Forward: 5-GATGTGATGCCTCTGCGAAG-3
	Reverse: 5-CATGCTGATGTCTCTGGAATCT-3
Twist-1	Forward: 5-GGCCGGAGACCTAGATG-3
	Reverse: 5-ACGGGCCTGTCTCGCTTTCT-3
U6snRNA	Forward: 5-CTCGCTTCGGCAGCACATATACT-3
	Reverse: 5-ACGCTTCACGAATTTGCGTGTC-3

Table 1. The sequence of primers used in the real-time PCR reaction.

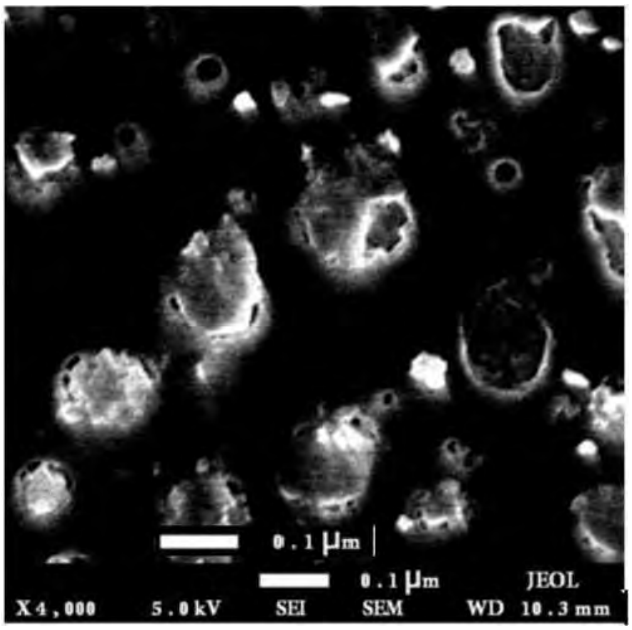

Figure 1. Examination of exosomes isolated by electron microscopy. The exosomes' examination using electron microscopy showed the spherical appearance and size of 30-150 nm of the exosomes.

Cellular uptake of PKH26-labeled fluorescent colored tumor exosomes to fibroblast cells

To determine tumor cell-derived exosomes' ability to enter fibroblast cells, fPKH26-labeled fluorescent colored tumor exosomes were incubated with fibroblast cells for 12 hours. Fluorescent microscopic analysis showed that PKH26-labeled fluorescence-labeled exosomes are located in the cytoplasm of fibroblast cells (Figure 2). This indicates the ability of fibroblast cells to absorb exosomes derived from tumor cells.

Effects of exosomal treatment on fibroblast cells and the transfer of exosomal miR-206 to fibroblast cells

As seen in Figure 3, levels of miR-206 transcripts in fibroblast cells treated by exosomes and alpha-amanitin showed a significant increase over time.

Examination of miR-206 expression levels in breast cancer cell-derived exosomes in the presence and absence of tamoxifen

MiR-206 expression levels in tumor cell-derived exosomes treated by tamoxifen have higher expressions than those of the control group (Figure 4). This result suggests that tamoxifen treatment may alter the expression level of miR-206 in tumor cell-derived exosomes.

Effect of breast tumor-derived exosomes on the expression level of Twist-1 and Bcl-2 genes in fibroblastic cells

Tamoxifen-Treated tumor-derived exosomes induce the Twist-1 gene expression time-dependently; However, tumor-derived exosomes that had been left untreated reduced the gene expression of Twist-1 over time (Figure 5).

Regarding the Bcl-2 oncogene, the results showed that when tumor cells were treated with tamoxifen, exosomes derived from these types of cells reduced Bcl-2 expression over time. However, exosomes derived from tumor cells that did not receive medication had an increasing effect on the expression of the Bcl-2 gene (Figure 6).

Discussion

Past studies have shown that exosomes are rich in microRNAs[11], so it seems that the exosomal transfer of miRNAs from tumor cells could be a factor in cell malignancy. It can also be inferred that pharmacological agents can alter tumor exosomes' molecular contents and prevent tumor formation. The present study showed that tamoxifen treatment increased miR-206 expression in tumor cell-derived exosomes. Previous studies have shown that miR-206 acts as a suppressor for tumors by directly targeting transcripts of the Twist-1 gene in breast cancer's pathogenesis and that its expression is inversely related to tumor development[12]. Afterward, this paper examined the exosomal transfer of miRNA-206 to fibroblast cells that had been treated with tumor exosomes (treated with tamoxifen). This study hypothesized that tamoxifen treatment on the tumor cell could alter the selected miRNA expression pattern in tumor cell exosomes. So, in this study, the expression level of miR-206 in cell-derived exosomes was also as-

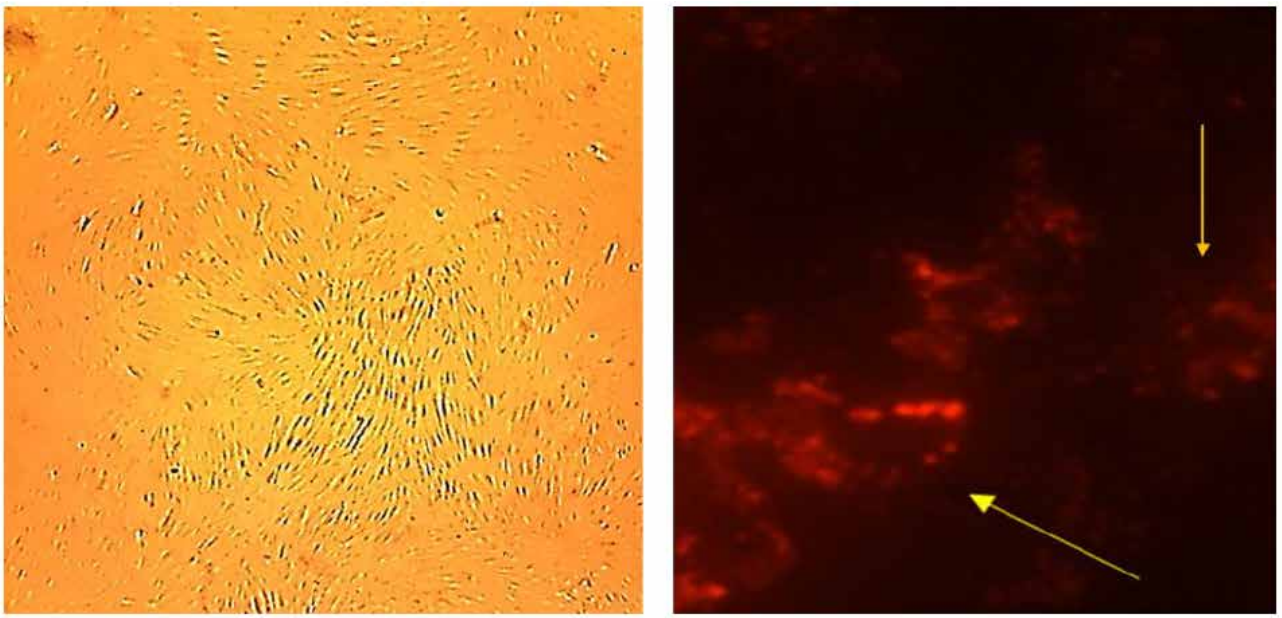

Figure 2. Left: Morphological view of fibroblastic cells with spindle-shaped appearance (magnification x90). Right: PKH26-labeled tumor exosomes located in the cytoplasm of fibroblast cells.

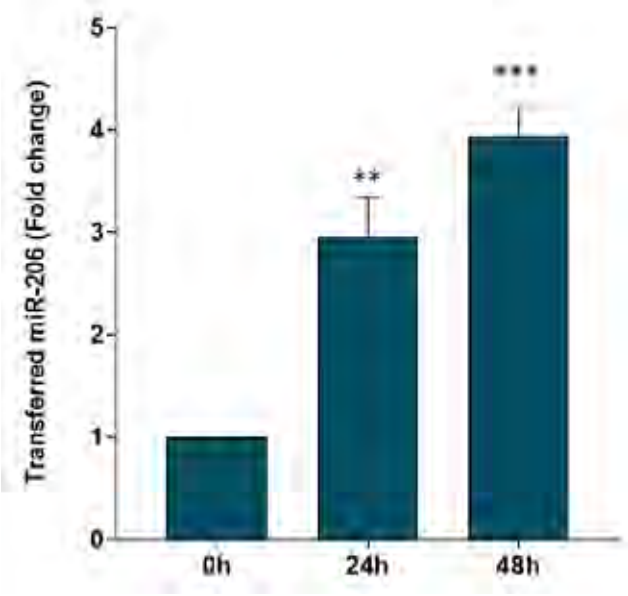

Figure 3. The expression level of miR-206 being treated by tamoxifen. Examining the miR-206 expression level at 0, 24, and 48 hours showed that the gene expression level increased significantly in a time-dependent manner.

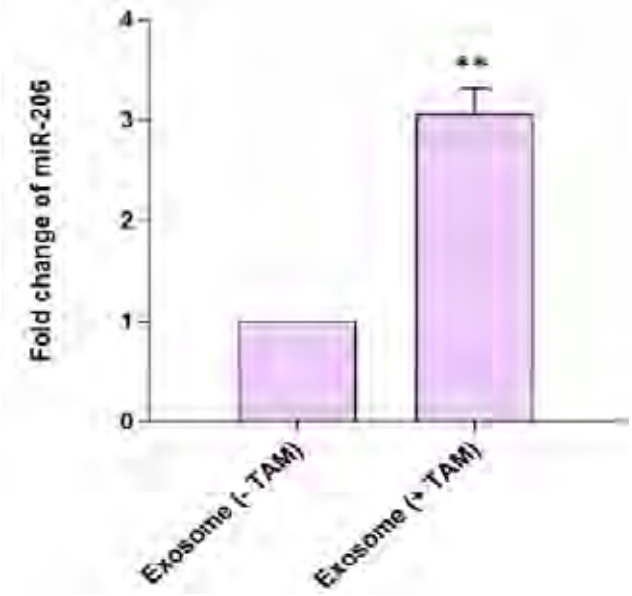

Figure 4. Expression levels of miR-206 in tumor cell-derived exosomes treated by tamoxifen compared with the control group. This gene expression in exosomes derived from tamoxifen-treated cells is significantly higher than those of the control group.

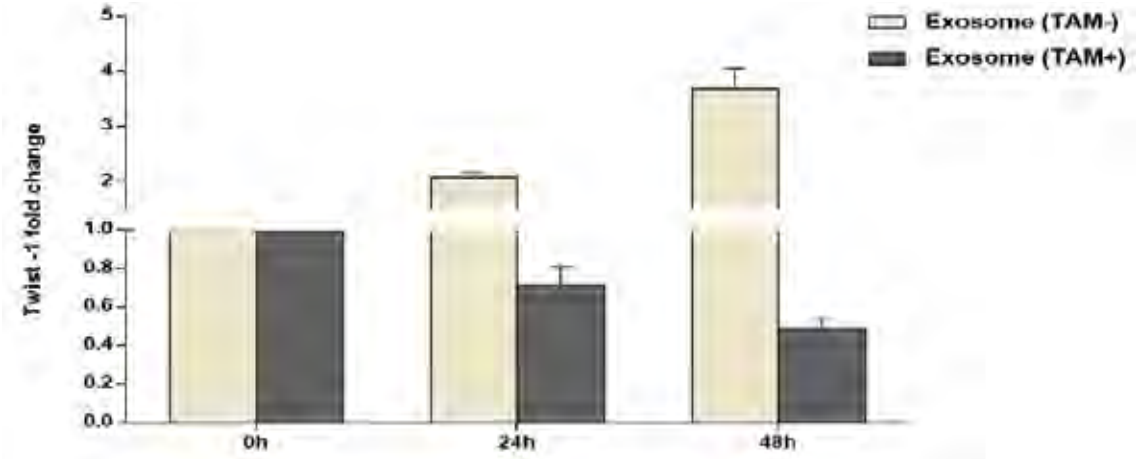

Figure 5. The expression level of miR-206 being treated by tamoxifen. Examining the miR-206 expression level at 0, 24, and 48 hours showed that the gene expression level increased significantly in a time-dependent manner.

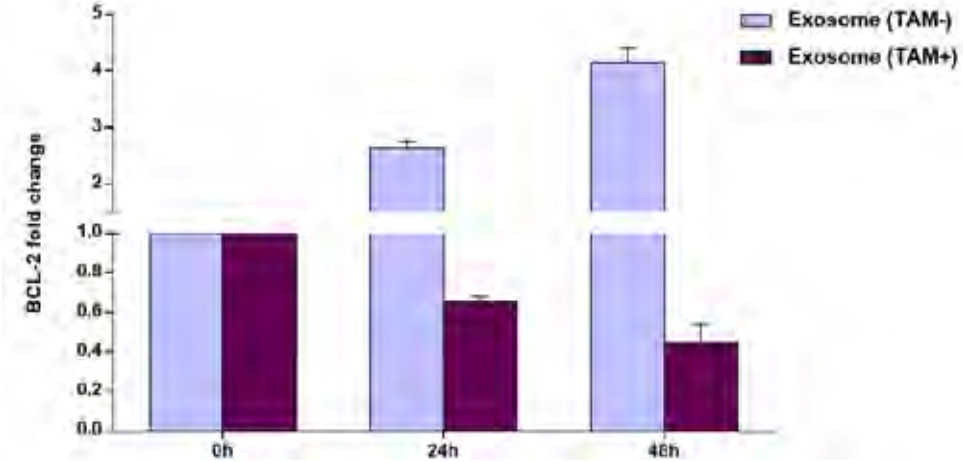

Figure 6. The inhibitory effect of tamoxifen-treated tumor-derived exosomes versus the progressive effect of untreated treated tumor-derived exosomes on the expression of the BCL-2 gene over time. The GAPDH is used for normalization. The expression of the BCL-2 gene being treated with the drug exosome (+) has a down-regulation and has increased over time, while the expression of the BCL-2 gene in drug (-) treated exosome cells has increased over time.

sessed. MCF-7 breast tumor cell line was categorized into two groups: the experiment group that received tamoxifen and the control group that did not receive medication. Subsequently, the experiment group was treated with tamoxifen. Expression levels of miR-206 in tumor cell-derived exosomes treated with tamoxifen showed higher expression than in control cell-derived exosomes. This result suggests that tamoxifen treatment may alter the expression of miR-206 in tumor cell-derived exosomes.

In the tumor microenvironment, tumor cell secretions can cause malignancy to their microbial fibroblasts; so, in the present study, we scrutinized the effect of tumor cell-derived exosomes on the expression of Twist-1 and Bcl-2 oncogenes. Much to our surprise, untreated tumor-derived exosomes induced the expression of the Twist-1 gene time-dependently, while the experiment group reduced the expression of Twist-1 over time. Therefore, given the more significant presence of miR-206 in tamoxifen-treated tumor-derived exosomes, it is concluded that the transferring of the miR-206 was the underlying reason for the decrease in the expression level of Twist-1 over 48 hours of assessment. The Bcl-2 oncogene followed precisely the same expression pattern as Twist-1. In other words, untreated tumor-derived exosomes induced the expression of the BCL-2 gene time-dependently, while the experiment group reduced the expression of BCL-2 over time. Overall, the present study suggests that miR-206 exosomal transferring from mammary tumor cells treated with tamoxifen may have inhibitory effects on oncogenesis through diminishing the activity and expression of Twist-1 and Bcl-2 genes in fibroblast cells.

They are comparing gene expression profiles[13]. It is reported that increased Twist-1 gene expression was associated with invasion and metastasis of breast cancer. Suppression of Twist-1 expression by siRNA in metastatic breast carcinoma cells specifically inhibits cells' ability to metastasize from the mammary gland to the lung. The expression of Twist-1 in epithelial cell lines leads to loss of cell-to-cell junction through E-cadherin, activation of mesenchymal markers, and induction of cell movement; Twist-1 binds to E-box elements in the promoter region of E-cadherin, the transcription expression of which suppresses cell-to-cell junction. Based on these findings and knowing the function of Twist-1 as a significant regulator in fetal formation, the researchers hypothesized that Twist-1 would help metastasis by increasing the EMT stage in cancer progression[14]. Therefore, a decrease in the expression of Twist-1 under the influence of miRNA-206 can indicate the function of the miRNA-206 as a tumor suppressor.

On the other hand, the high expression of miR-206 in exosomes derived from tamoxifen-treated cells suggests how this drug's use may affect the expression of Twist-1 and Bcl-2. In fact, with the use of tamoxifen, the expression of miR-206 in the exosomes increases, which in turn reduces the expression of Twist-1 and Bcl-2, resulting in a decrease in cancer cell metastasis. In 2016, Zhong et al. examined the expression profile in drug-resistant breast cancer cells and their exosomes using microsurgery. Their results showed that most miRNAs in exosomes had low expression over cells. However, some miRNAs were more expressed in exosomes, indicating that some miRNAs were concentrated in exosomes. They found 22 miRNAs overexpressed in exosomes and cancer cells themselves, and 12 miRNAs increased that expression after chemotherapy[13].

The present experiment results generally showed that when breast cancer cells were treated with tamoxifen, the miR-206 content in these cells' exosomes was higher than that of cancer cells without drug treatment. Since exosomes are a rich and protective source for miRNAs and transfer miRNAs between cells in the tumor microenvironment, treatment of tumor exosomes on fibroblast cells causes miRs' transferring. Untreated tumor-derived exosomes increased the expression of Twist-1 and Bcl-2 genes in a time-dependent manner in fibroblast cells. This could be the reason for the malignancy of fibroblastic cells in the vicinity of tumor cells. In contrast, tamoxifen-treated tumor-derived exosomes reduced the expression of Twist-1 and Bcl-2 genes over time in fibroblast cells. This may be because the therapeutic effect of tamoxifen in breast cancer patients is due to its effect on exosomal miRNAs' expression, such as miR-206, and its consequent reduction in tumor progression.

Conclusions

The present experiment results generally showed that when breast cancer cells were treated with tamoxifen, the miR-206 content in these cells' exosomes was higher than that of cancer cells without drug treatment. Since exosomes are a rich and protective source for miRNAs and transfer miRNAs between cells in the tumor microenvironment, treatment of tumor exosomes on fibroblast cells causes miRs' transferring. Untreated tumor-derived exosomes increased the expression of Twist-1 and Bcl-2 genes in a time-dependent manner in fibroblast cells. This could be the reason for the malignancy of fibroblastic cells in the vicinity of tumor cells. In contrast, tamoxifen-treated tumor-derived exosomes reduced the expression of Twist-1 and Bcl-2 genes over time in fibroblast cells. This may be because the therapeutic effect of tamoxifen in breast cancer patients is due to its effect on exosomal miRNAs' expression, such as miR-206, and its consequent reduction in tumor progression.

Conflict of interests

No. The authors declare that they have no competing interests.

Availability of data and materials

The data used in this study are available from the corresponding author on request.

Authors' contributions

Faezeh Karami and Sadegh Babashah contributed equally to this work as Corresponding authors. The corresponding authors of this article justify that ALL the mentioned individuals in this article are members of this research team and had had substantial contributions to conception and design, acquisition of data, analysis, and interpretation of data, drafting the article, revising it, and Final approval of the version to be published.

Consent for publication

All the authors confirm that the manuscript represents their honest work.

Bibliographic references

1. Torre, L. A., Bray, F., Siegel, R. L., Ferlay, J., Lortet - Tieulent, J., & Jemal, A. (2015). Global cancer statistics, 2012. CA: a cancer journal for clinicians, 65(2), 87-108.
2. Lu, W. J., Desta, Z., & Flockhart, D. A. (2012). Tamoxifen metabolites as active inhibitors of aromatase in the treatment of breast cancer. Breast cancer research and treatment, 131(2), 473-481.
3. Brauch, H., Schroth, W., Goetz, M. P., Mürdter, T. E., Winter, S., Ingle, J. N., Schwab, M., & Eichelbaum, M. (2013). Tamoxifen use in postmenopausal breast cancer: CYP2D6 matters. Journal of Clinical Oncology, 31(2), 176.

4. Manna, S., & Holz, M. K. (2016). Tamoxifen action in ER-negative breast cancer. Signal transduction insights, 5, STI. S29901.
5. Kowal, J., Tkach, M., & Théry, C. (2014). Biogenesis and secretion of exosomes. Current opinion in cell biology, 29, 116-125.
6. Raposo, G., & Stoorvogel, W. (2013). Extracellular vesicles: exosomes, microvesicles, and friends. J Cell Biol, 200(4), 373-383.
7. Reddy, K. B. (2015). MicroRNA (miRNA) in cancer. Cancer cell international, 15(1), 38.
8. Xu, Y., Qin, L., Sun, T., Wu, H., He, T., Yang, Z., Mo, Q., Liao, L., & Xu, J. (2017). Twist1 promotes breast cancer invasion and metastasis by silencing Foxa1 expression. Oncogene, 36(8), 1157.
9. Delbridge, A. R., Grabow, S., Strasser, A., & Vaux, D. L. (2016). Thirty years of BCL-2: translating cell death discoveries into novel cancer therapies. Nature Reviews Cancer, 16(2), 99.
10. Moheghi, N., Afshari, J. T., & Brook, A. (2011). The cytotoxic effect of zingiber afficinale in breast cancer (MCF7) cell line. The Horizon of Medical Sciences, 17(3), 28-34.
11. Hannafon, B., Gin, A., Behbod, F., & Ding, W. (2019). Abstract P6-05-09: Exosome microRNA contents are altered during breast cancer progression. In: AACR.
12. Moyret-Lalle, C., Ruiz, E., & Puisieux, A. (2014). Epithelial-mesenchymal transition transcription factors and miRNAs: "Plastic surgeons" of breast cancer. World journal of clinical oncology, 5(3), 311.
13. Zhong, S., Chen, X., Wang, D., Zhang, X., Shen, H., Yang, S., Lv, M., Tang, J., & Zhao, J. (2016). MicroRNA expression profiles of drug-resistance breast cancer cells and their exosomes. Oncotarget, 7(15), 19601.
14. Qin, L., Liu, Z., Chen, H., & Xu, J. (2009). The steroid receptor coactivator-1 regulates twist expression and promotes breast cancer metastasis. Cancer research, 69(9), 3819-3827.

Received: 15 December 2020
Accepted: 14 February 2021

RESEARCH / INVESTIGACIÓN

Size variation of morphological traits in *Bosmina freyi* and its relation with environmental variables in a tropical eutrophic reservoir

Yury Catalina López-Cardona[1], Edison Parra-García[1], Jaime Palacio-Baena[2], Silvia Lucía Villabona-González[3]

DOI. 10.21931/RB/2021.06.02.16

Abstract: We assessed the size variation of morphological traits in *Bosmina freyi* regarding changes in environmental variables, the biomass of invertebrate predators, and algal food availability in two depths of the photic zone, the riverine zone, and near the dam zone (lacustrine zone) in The Riogrande II reservoir. In 200 individuals of *B. freyi*, using the software TpsDig2 we measured the body size, mucron and antennule lengths, and the antennule aperture percentage. Using the Mann-Whitney U test, we assessed the differences between these traits considering the zones and the photic depths; however, we used a canonical discriminant analysis with morphologic traits and environmental variables. Measured morphological traits showed a heterogeneous distribution between sampled zones and depths ($p < 0.05$). The highest values mucron and antennule lengths and the smallest antennule aperture angle were observed on small body size individuals, associated with physical, chemical, and biological characteristics in the riverine zone and the subsurface. Size structure distribution in *B. freyi* was related to changes in water temperature, trophic state, depredation, availability, and quality of food, of which implications related to the zooplankton community structure, predator-prey relations, and energy flow in the reservoir.

Key words: Cladocera, predation, size structure, trophic state.

Introduction

Cladocera is a zooplankton assemblage that occupies an intermediate position in the aquatic food chain[1] because they ingest protozoa[2], algae, bacteria, and detritus lentic systems, and simultaneously they constitute one of the chosen prey for invertebrates and vertebrates[3].

Some species of this group have a wide variation in size structure due to genetic factors[4] and environmental factors as temperature[5], food availability[6], pH[7], and acidification[1].

Bosmina genera is a group of small cladoceran filter feeders[8] with variations in body size, shape, and length of antennules and mucron[1,5,9].

According to Masson S (2004)[10] in Canadian lakes, increasing chlorophyll-a concentrations favors small individuals' predominance. Other authors detail that some changes in *Bosmina* size are because the predation pressure by Copepoda, Rotifera[11,12] and macroinvertebrates of *Chaoborus* genera[1,4,8,9,13], indicate that predation by invertebrates induces an increase of size and the development of defense structures as the elongation of mucron and antennules in *Bosmina*.

Bosmina freyi[14] contributes more than 60% of the total zooplankton biomass in The Riogrande II reservoir[15] due to its broad trophic plasticity[16] and resistance to high turbidity conditions[17]. This species was reported for the first time in 2004 in South-America[18], for Colombia in 2010 (Elmoor-Loureiro, com. pers.), and consequently, there is a lack of information about the structure of morphological traits.

We hypothesized that if the size distribution of morphological traits of *Bosmina freyi* in the vertical and longitudinal axis in The Riogrande II reservoir changes concerning environmental variables and the presence of invertebrate predators, so in the reservoir zone with the highest trophic state and warmer water, individuals of small size will dominate and in zones with high invertebrate predators biomass, individuals will have a mucron and antennule with a longer length and an antennule closed-angle.

Methods

The Riogrande II reservoir is located in the northeastern of Colombia in The Río Grande II basin at 2200 m.a.s.l (6º 33' 50"- 6º 28' 07" N and 75º 32' 30"- 75º 26' 10" O). Has a total volume up to landfill level (2270 m.a.s.l) of 240 million of m^3 and an average area of 1214 ha. This waterbody receives water from the Grande and Chico rivers and the Las Ánimas creek[19]. This system is mainly used for hydroelectric generation and potable water supply[20]. The Riogrande II reservoir has higher turbidity and a greater degree of eutrophication at riverine zones, mainly in the Chico River zone, due to sediment washing process in the basin and the domestic, industrial, agricultural, and livestock wastewater discharge from the closer cities (Entrerríos and San Pedro de los Milagros) located in the two principal rivers[21].

This research was conducted as part of the "*Estudio de la problemática ambiental de tres embalses de Empresas Públicas de Medellín para la gestión integral y adecuada del recurso hídrico*", we carried out five sampled areas in The Riogrande II reservoir, in the subsurface and the photic zone edge (Figure 1) in September 2011. The highest dominance of *Bosmina freyi* happened in this period[15].

Physical, chemical and biologic variables data information (chlorophyll-a and plankton biomass) were took from the "Estudio de la problemática ambiental de tres embalses de Empresas Públicas de Medellín para la gestión integral y adecuada del recurso hídrico"[15,22-24].

Methods for zooplankton sample collection and the estimation of Carlson index of trophic state (TSI) modified by (25) are described in (14).

We took 20 specimens of *B. freyi* (n = 200 individuals), and we used a photographic camera adapted to an optical microscope and were individually photographed to determine morphological traits using TpsDig2 (Figure 2). Lengths were measured in µm and the antennule angle in the opening percentage, assuming that a right angle (90°) has an aperture of 100%.

[1] Grupo de Investigación en Limnología Básica y Experimental y Biología y Taxonomía Marina, Universidad de Antioquia, Medellín, Colombia.
[2] Grupo de Investigación en Gestión y Modelación Ambiental, Universidad de Antioquia, Medellín, Colombia.
[3] Grupo de Investigación en Limnología y Recursos Hídricos, Universidad Católica de Oriente, Rionegro, Colombia.

Corresponding author: yurylopezbio@gmail.com

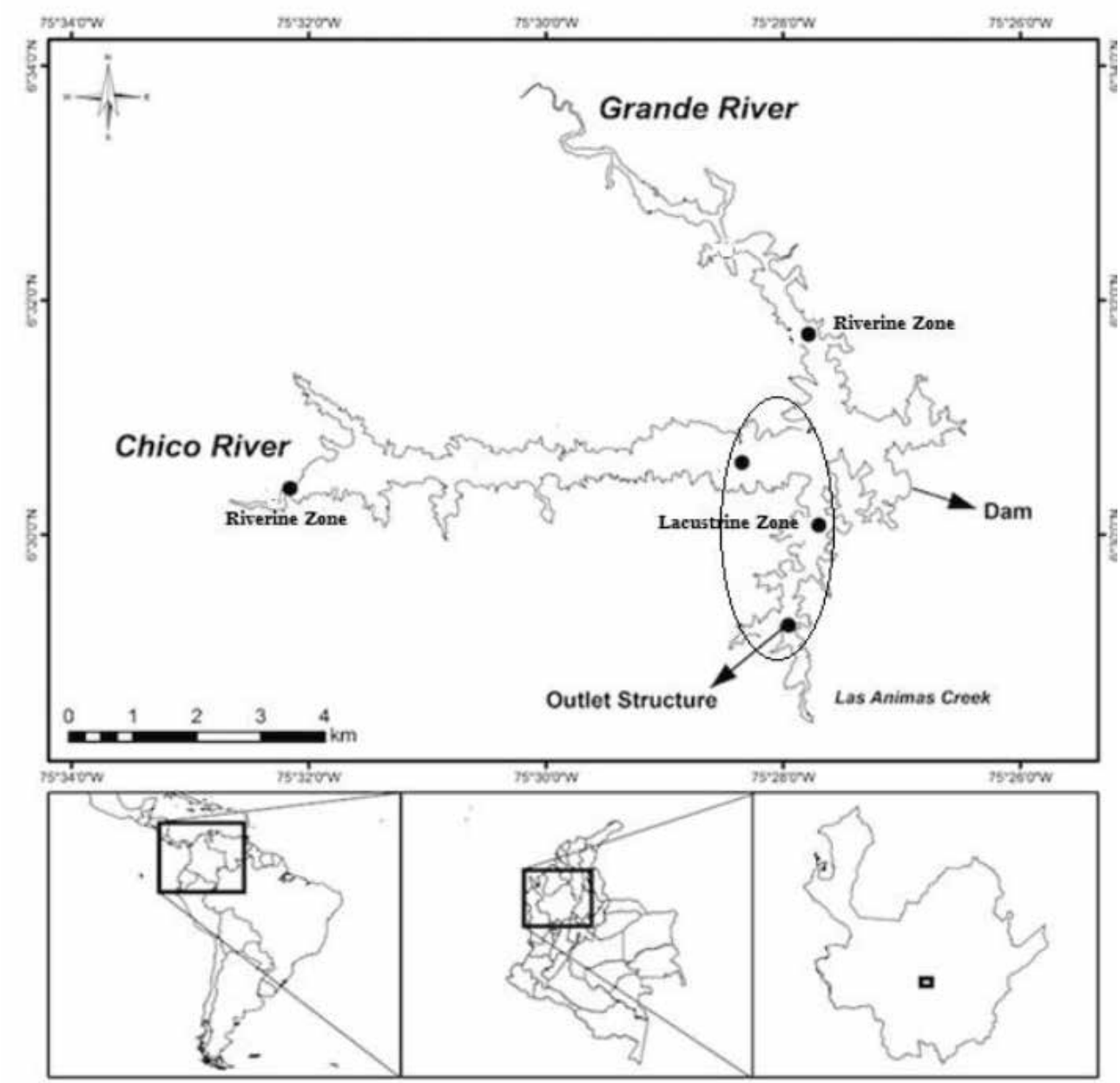

Figure 1. Study area and location of sampling stations.

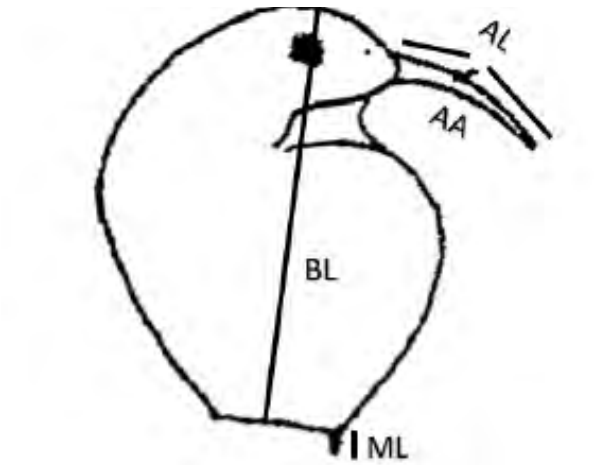

Figure 2. Body length (BL), mucron length (ML), antennule total length (AL) and antennule angle (AA) of *Bosmina freyi* (Modified from (5))

Data analysis

We used a Mann–Whitney U test because data did not fulfill the normality of residuals and homogeneity of variances. The last is to assess the significance of the differences between individuals' morphological traits from the zones and depths.

We also made a Generalized Discriminant Analysis using the measured morphological traits and the environmental variables. We calculated the scores and canonical vectors for graphic representation of the essential canonical discriminant functions in terms of explained variance, allowing a simple interpretation in the canonical space of differentiation among morphological traits of *B. freyi* and the environmental matrix[26]. Data analyses were made using R Wizard V 2.3 Software[27].

Results

The riverine zone had the highest temperature degree, greater eutrophication, and higher phytoplankton biomass

(chlorophyll-a), rotifers (Asplanchna girodi De Geurne, 1888), and copepods predators (*Mesocyclops longisetus* Thiébaud, 1912; *Metacyclops leptopus* Kiefer, 1927; and *M. mendocinus* Wierzejski, 1892) biomass. Meanwhile, the lacustrine zone recorded the highest transparency, dissolved oxygen concentration, and *Cryptomonas sp.* biomass (Table 1).

B. freyi body length varied over the range of 202.64 and 457.02 µm (average = 294.7 µm), mucron length between 14.87 and 29.94 µm (average = 22.47 µm), antennule length between 94.21 and 170.25 µm (average = 134.11 µm) and the antennule opening angle ranged between 72.48 and 88.21% (average = 81.05%).

According to the Mann-Whitney U test, mucron and antennule lengths and the opening angle were significantly different among sampling zones and depths (Figure 3, a & b). Meanwhile, body length was significantly different among depths; it exhibited a significantly higher value in the specimens from the photic zone boundary (Figure 3 b). While mucron and antennule lengths were higher in individuals from the riverine zone and the subsurface concerning those from the lacustrine zone and the photic zone boundary, antennule aperture showed an opposite behavior.

A variance of 100% explains canonical discriminant analysis among zones and depths in the first axis. In both cases, classification and cross-validation values were 100%, clearly discriminating between riverine zones and lacustrine zone, as well as the subsurface and the photic zone boundary.

While individuals of *B. freyi* with higher mucron and antennule lengths are related with the riverine zone (warmer waters, as well as a greater degree of eutrophication and higher phytoplankton and predatory copepods biomass), in the lacustrine zone (more oxygenated and clear waters), specimens showed a tendency to present higher body size and an antennule more separated from the body (Figure 4 a & 5).

Depths were discriminated mainly by the presence of individuals with a higher mucron and antennule lengths in the subsurface, related to a higher temperature and greater dissolved oxygen availability. By contrast, individuals with higher body size and antennule aperture were mainly associated with the photic zone boundary, with higher predatory copepods and rotifers biomass, as well as phytoplankton and *Cryptomonas sp.* biomass (Figure 4 b & 5).

Discussion

Melão, M. G. (1999)[28] mentioned that temperature increase is a factor that directly affect organism's life cycle and population attributes, causing a time decrease in the organism's growth and an increase in population growth rates, which favors large populations with small size individuals[29], such as we observed in this study in the riverine zone and in the reservoir subsurface, where occurred the highest number of individuals with youth traits and higher mucron and antennule lengths[30].

Higher values of Carlson Index (TSI) and chlorophyll-*a* concentration in the riverine zone also favor small individuals due to a continuous energy source to maintain high metabolic rates[31]. So, *B. freyi* population size structure in the reservoir seems to behave similarly to the general pattern of cladoceran size structure, in which smaller species are correlated to conditions of a more significant trophic state[32].

It has been reported that biotic variables have an indirect influence on mucron and antennule sizes and a direct effect on spatial and temporal population's dynamic, affecting the presence of predators and establishing food restrictions[33]. This situation implies changes in size structure and the lengths of species attributes[1], as evidenced by this study.

The highest biomass of predatory copepods and rotifers in the riverine zone matched with has been reported in some studies about the influence of predation by invertebrates on morphological traits of *Bosmina* genera[9,34,35]. Significantly[36], claim that copepods can consume Bosminidae species with sizes less than 400 µm. Nevertheless, the highest mucron and antennule size could reduce predation rates of small individuals of *B. freyi* by copepods, as it happens with other cladoceran species[37].

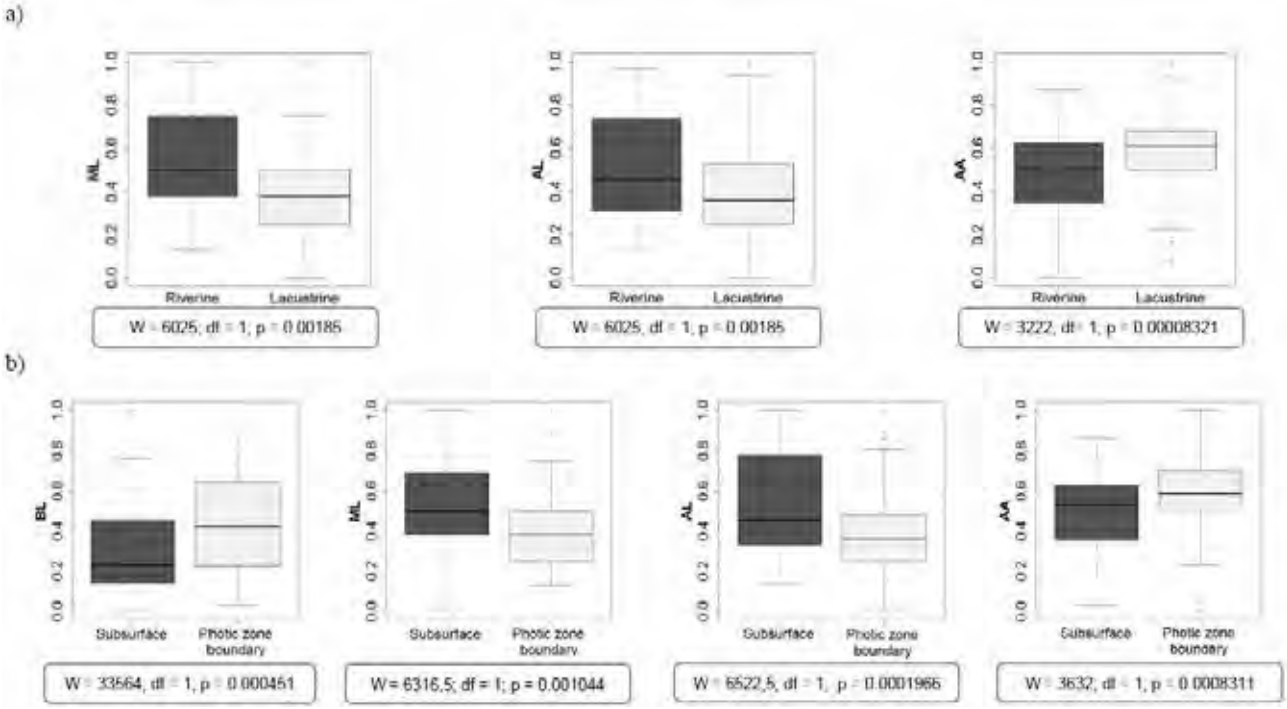

Figure 3. Morphological traits distribution BL, ML, AL, and AA into two zones (a) and depths (b) in the photic zone of The Riogrande II reservoir, September 2011.

Variable		Zone	
		Riverine	Lacustrine
Transparency (m)	Minimum	0.76	1.35
	Maximum	1.14	1.76
	Average	0.95	1.51
	C.V (%)	20.13	12.05
Water temperature (°C)	Minimum	20.66	19.85
	Maximum	24.30	21.60
	Average	21.90	20.60
	C.V (%)	6.50	2.72
Trophic State Index (TSI)	Minimum	57.61	52.68
	Maximum	64.23	58.36
	Average	60.92	56.03
	C.V (%)	5.47	4.35
Dissolved oxygen ($mg.L^{-1}$)	Minimum	5.98	5.42
	Maximum	7.61	8.83
	Average	6.68	7.20
	C.V (%)	10.38	13.90
Chlorophyll-*a* ($\mu g.L^{-1}$)	Minimum	14.87	14.95
	Maximum	26.31	22.11
	Average	21.57	18.01
	C.V (%)	19.50	15.18
Predatory rotifers biomass ($\mu g.L^{-1}$)	Minimum	0.00	0.60
	Maximum	13.51	9.29
	Average	4.85	3.71
	C.V (%)	126.09	82.24
Predatory copepods biomass ($\mu g.L^{-1}$)	Minimum	0.25	0.53
	Maximum	10.65	2.32
	Average	4.07	1.18
	C.V (%)	111.52	59.26
Cryptomonas sp. biomass ($\mu g.L^{-1}$)	Minimum	0.40	0.14
	Maximum	665.42	203.57
	Average	69.53	19.51
	C.V (%)	152.21	164.50

Table 1. Physical, chemical, and biological variables in The Riogrande II reservoir's photic zone, September 2011. C.V (%) = Coefficient of Variation.

Antennule aperture may also be a defense mechanism against predators, and it depends on the predator attack mechanism. Some authors such as (38, 39) consider that a curved antennule (lower aperture) as that of the individuals detected in the riverine zone, protects the ventral part of cladocerans from some predators of genus *Mesocyclops* and especially from *Asplanchna girodi*, a rotifer species that dominated the biomass of rotifers in The Riogrande II reservoir during the study made by (15).

The highest biomass of the smaller organisms of *B. freyi*, of the predatory copepods and rotifers, may also be due to the highest primary production in the riverine zone[40] because the highest availability of resources may determine its presence in the longitudinal axis of the reservoir through the tributaries, especially the Chico River[39].

In the vertical axis, the size distribution of *B. freyi* structures could be attributed to vertical migration, common in the zooplanktonic community, particularly in *Bosmina* genera[41]. In The Riogrande II reservoir[15] found a gradient in the vertical distribution of the zooplankton biomass. While smaller species seem to prefer superficial layers of the reservoir, the largest ones tend to be located in the deepest layers of the photic zone, probably as a strategy to avoid predation and selective removal of bigger species subsurface. This could resemble the vertical distribution of sizes in *B. freyi* population in which the individuals of larger size and smaller antennule and mucron length were mainly concentrated in the deepest layer of the photic zone.

Predatory copepods and rotifers agglomerated in this layer, and probably, as the individuals of *B. freyi* with a larger size (higher than 400 µm), they avoid predation/or are selectively removed from the subsurface[15].

The highest abundance of more significant individuals and smaller mucron and antennule lengths tended to coincide with the increase of Cryptomonas sp biomass in the zone near the dam (lacustrine zone), the photic zone boundary. The last implies that maybe these genera of algae constitute an essential resource for adults of *B. freyi*[30] in the reservoir[24] said that nanoplanktonic and mixotrophic species of Cryptophyta are a persistent component of zooplankton diet from The Riogrande II reservoir; apparently, it favors its growth and reproduction rates because it provides enough organic carbon, nitrates, and phosphates. Furthermore, it is very feasible that *B. freyi* complements its diet with detritus[42] and that alimentary strategy becomes more critical on small individuals of *B. freyi* together with the dissolved substances and organisms of picoplankton ingestion (< 2 µm).

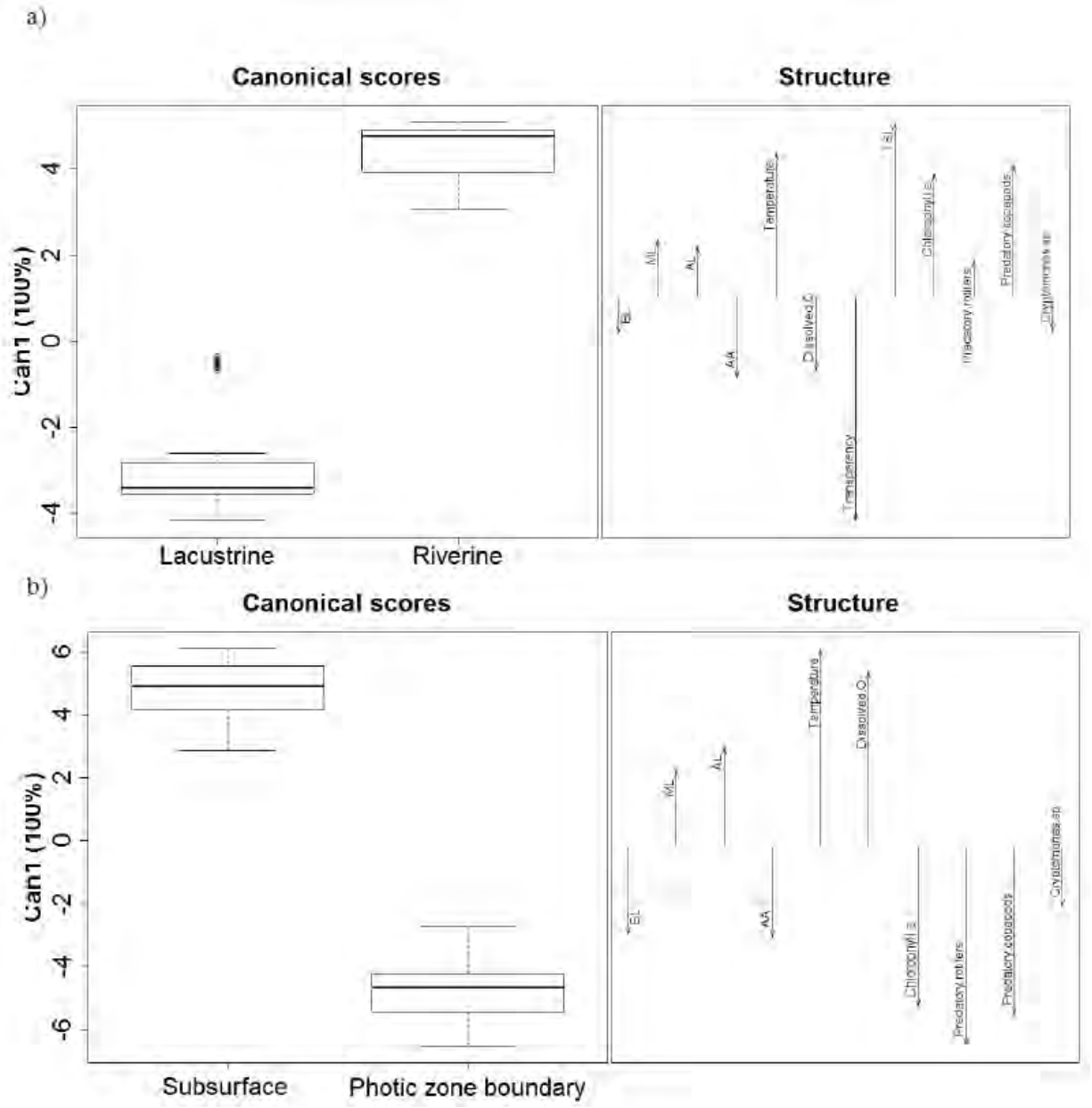

Figure 4. Canonical Discriminant Analysis applied to *B. freyi* morphological traits, environmental variables and phytoplankton, and zooplankton biomass. Linear regression model for zones (a) and depths (b) in the photic zone of The Riogrande II reservoir, September 2011.

Conclusions

Results showed that the distribution in the size structure in *B. freyi* is related to changes in biotic and abiotic variables. So, high temperatures and a greater nutrients concentration favored the growth of small individuals' populations, mainly in the reservoir's riverine zones.

Small sizes individuals seem to be protected from predation by other zooplankters as rotifers and copepods by a high mucron and antennule length, as well as by a closed antennule. By contrast, individuals from *B. freyi* with a bigger size and adult features just like predatory rotifers and copepods seem to avoid predation pressure, probably from visual predators as vertebrates, remaining mainly in the deepest zone of the photic layer. Furthermore, these cladocerans coexist with the highest densities of *Cryptomonas sp.*, one of the most nutritious resources for *Bosmina* in the reservoir.

Consequently, the distribution of the size structure of *B. freyi* affects the structure of the zooplanktonic community, the predator-prey trophic relationships, and the flow of energy and matter in the reservoir. Nevertheless, factors do not involve here, as competence and seasonality may also be determinants and affect the population attributes of *B. freyi*.

Acknowledgments

Thanks to the program "Estudio de la problemática ambiental de tres embalses de Empresas Públicas de Medellín para la gestión integral y adecuada del recurso hídrico", for the provision of information; and to the research groups Limnobase-Biotamar and GAIA from the Universidad de Antioquia for their support. Thanks to Isabel Cristina Gil for the paper translation.

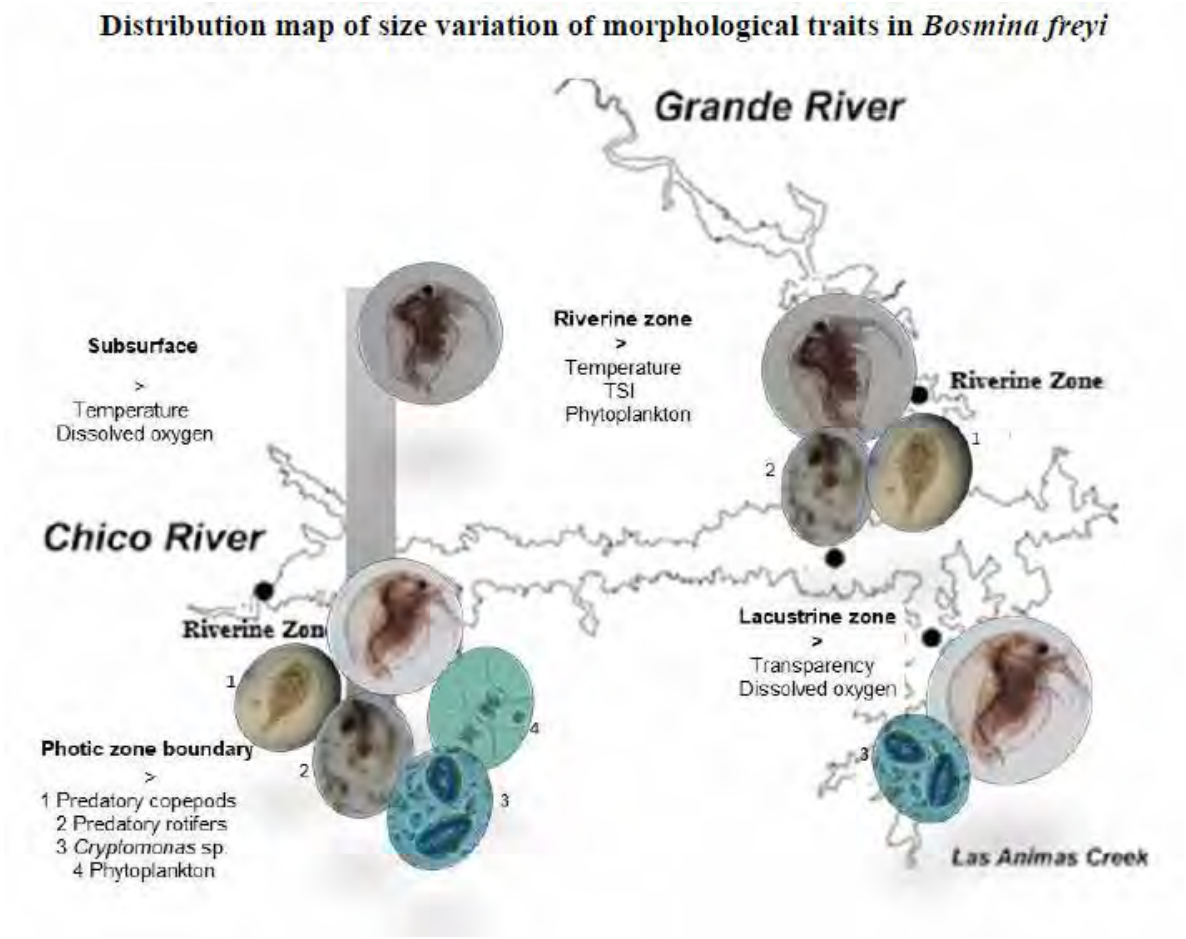

Figure 5. Distribution map of size variation of morphological traits in *Bosmina freyi* in The Riogrande II reservoir.

Referencias bibliográficas

1. Labaj, A.L., Korosi, J.B., Kurek, J., Jeziorski, A., Keller, W.B. and Smol, J.P. (2016). Response of Bosmina size structure to the acidification and recovery of lakes near Sudburdy, Canada. Journal of. Limnology, 75(s2): 22–29. http://doi.org/10.4081/jlimnol.2016.1183
2. Demott, W.R. (1982). Feeding selectivities and relative ingestion rates of Daphnia and Bosmina. Limnology Oceanography, 27(3): 518–527.
3. De Bernardi, R. and Peters, R. (1987). Why Daphnia? In Peters, R. and De Bernardi, R., ed. Daphnia. Memorie Dell'Istituto Italiano Di Idrobiologia, 45, pp. 1-9.
4. Black, R.W. (1980). The Nature and Causes of Cyclomorphosis in a Species of the Bosmina longirostris Complex. Ecology, 61(5): 1122–1132. http://www.jstor.org/stable/1936832.
5. Kappes, H. and Sinsch, U. (2002). Morphological variation in Bosmina longirostris (OF Muller, 1785) (Crustacea: Cladocera): consequence of cyclomorphosis or indication of cryptic species? Journal of Zoological Systematics and Evolutionary Research, 40, 113–122.
6. Kappes, H. and Sinsch, U. (2002b). Temperature and predator induced phenotypic plasticity in Bosmina cornuta and B. pellucida (Crustacea: Cladocera): Freshwater Biology, 47, 1944–1955.
7. Korosi, J.B., Paterson, A.M., Desellas, A.M. and Smol, J.P. (2008). Linking mean body size of pelagic Cladocera to environmental variables in Precambrian Shield lakes: a paleolimnological approach. Journal of Limnology, 67, 22-34.
8. Korosi, J.B., Kurek, J. and Smol, J. (2013). A review on utilizing Bosmina size structure archived in lake sediments to infer historic shifts in predation regimes. Journal of Plankton Research, 35 (2): 444–460. http://doi.org/10.1093/plankt/fbt007
9. hang, K. and Hanazato, T. (2003). Seasonal and reciprocal succession and cyclomorphosis of two Bosmina species (Cladocera, Crustacea) coexisting in a lake : their relationship with invertebrate predators. Journal of Plankton Research, 25 (2): 141–150. Retrieved from: http://plankt.oxfordjournals.org/
10. Masson, S., Pinel-Alloul, B. and Dutilleul, P. (2004). Spatial heterogeneity of zooplankton biomass and size structure in southern Québec lakes: variation among lakes and within lake among epi-, meta- and hypolimnion strata. Journal of Plankton Research, 26, 1441–14458.
11. Guiset, A. (1977). Stomach contents in Asplanchna and Ploesoma. Archiv für Hydrobiologie- BeiheftErgebnisse der Limnologie, 8, 126-129.
12. Salt, G.W. (1977). An analysis of the diets of five sympatric species of Asplachna. Archiv für Hydrobiologie–BeiheftErgebnisse der Limnologie, 8, 123-125.
13. Alexander, M. and Hotchkiss, S. (2010). Bosmina remains in lake sediment as indicators of zooplankton community composition. Journal of Paleolimnology, 43, 51–59. http://doi.org/10.1007/s10933-009-9312-0
14. De Melo, R. D., and Hebert, P. D. (1994). A taxonomic reevaluation of North American Bosminidae. Canadian Journal of Zoology, 72(10), 1808-1825.
15. Villabona-González, S.L., Ramírez-Restrepo, J.J., Palacio-Baena, J.A. and Costa-Bonecker, C. (2015). Respuesta de la biomasa zooplanctónica a los gradientes de estado trófico y precipitación de un embalse tropical. Revista de la Academia Colombiana de Ciencias Exactas, Físicas y Naturales, 39(152): 374-388.
16. Kerner, M., Ertl, S. and Spitzy, A. (2004). Trophic diversity within the planktonic food web of the Elbe Estuary determined on isolated individual species by 13C analysis. Journal of Plankton Research, 26(9): 1039-1048.

17. Popp, A., Hoagland, K. and Hergenrader, G. (1996). Zooplankton community response to reservoir aging. Hydrobiologia, 339, 13-21.
18. Elmoor-Loureiro, L.M.A., Mendonça-Galvão, L. and Padovesi-Fonseca, C. (2004). New cladoceran records from lake Paranoá, central Brazil. Brazilian Journal of Biology, 64(3A): 415-422.
19. Villabona-González, S.L., Buitrago-Amariles, R.F., Ramírez-Restrepo, J.J. and Palacio-Baena, J.A. (2014). Biomasa de rotíferos de dos embalses con diferentes estados tróficos (Antioquia, Colombia) y su relación con algunas variables limnológicas. Actualidades Biológicas, 36(101): 149-162.
20. Empresas Públicas De Medellín. 1994. Proyecto de aprovechamiento múltiple de Riogrande. Declaración de impacto ambiental., Medellín, Colombia.
21. Zabala, A.M. (2013). Evaluación del estado trófico del embalse Riogrande II (Antioquia, Colombia) a través del comportamiento espacial y temporal de los nutrientes. Trabajo de grado, Universidad de Antioquia, Medellín, Colombia, 112 p.
22. Palacio-Baena, J., Herrera-Loaiza, N., López-Muñoz, M., Palacio-Betancourt, H. and Rodríguez, M. (2013). Limnoecología de los embalses Riogrande II, La Fe y Porce II. In: Palacio J., ed. Informe técnico embalse Riogrande II "Estudio de la problemática ambiental de tres embalses de Empresas Públicas de Medellín para la gestión integral y adecuada del recurso hídrico". Universidad de Antioquia, Universidad Nacional sede Medellín, Empresas Públicas de Medellín, pp. 444-528.
23. Toro, M., Moreno, A., Chalarca, D. and Grajales, H. (2013). Dinámica ambiental de los nutrientes (especies químicas del nitrógeno, fósforo y sílice) en los embalses La Fe, Riogrande II y Porce II a través de modelos conceptuales y matemáticos, como herramienta de gestión de la calidad de agua en los tres sistemas. In: Palacio J. ed. Informe técnico embalse Riogrande II "Estudio de la problemática ambiental de tres embalses de Empresas Públicas de Medellín para la gestión integral y adecuada del recurso hídrico". Universidad de Antioquia, Universidad Nacional sede Medellín, Empresas Públicas de Medellín, pp. 242-297.
24. López-Muñoz, M., Ramírez-Restrepo, J., Palacio-Baena, J., Echenique, R., Mattos-Bicudo, C. and Parra-García, E. (2016). Biomasa del fitoplancton eucariota y su disponibilidad para la red trófica del embalse Riogrande II (Antioquia, Colombia): Revista de la Academia Colombiana de Ciencias Exactas, Físicas y Naturales, 40 (155): 244-253.
25. Toledo, A.P., Talarico, M., Chinez, S.J. and Agudo, E.G. (1983). A aplicação de modelos simplificados para a avaliação de procesos de eutrofização em lagos e reservatórios tropicais. XIX Congreso interamericano de Engenharia e ambiental. Camboriú, Brasil.
26. Friendly, M. (2007). HE plots for multivariate general linear models. Journal of Computational and Graphical Statistics, 16, 421-444.
27. Guisande, C., Heine, J., González-Dacosta, J. and García-Roselló, E. (2014) Rwizard Software. University of Vigo. Vigo, Spain.
28. Melão, M. G. (1999). Desenvolvimento e aspectos reprodutivos de cladóceros e copépodos de águas continentais brasileiras. In: Pompêo, M., ed. Perspectivas da Limnologia no Brasil. São Luís: Gráfica e Editora União, pp. 45–57.
29. Gillooly, J. (2000). Effect of body size and temperature on generation time in zooplankton. Journal of Plankton Research, 22, 241–251.
30. Lagergren, R., Svensson, J.E. and Stenson, J.A. (2007). Models of ontogenetic allometry in cladoceran morphology studies. Hidrobiologia, 594, 109–116. http://doi.org/10.1007/s10750-007-9085-2
31. Hall, D.J., Threlkeld, S.T., Burns, C.W. and Crowley, P.H. (1976). The size-efficiency hypothesis and the size structure of zooplankton communities. Annual Review of Ecology and Systematics, 7, 177-208.
32. Corgosinho, P. and Pinto-Coelho, R. (2006). Zooplankton biomass, abundance and allometric patterns along an eutrophic gradient at Furnas Reservoir (Minas Gerais , Brazil): Acta Limnologica Brasiliensia, 182, 213–224.
33. Hart, R. and Bychek, E. (2011). Body size in freshwater planktonic crustaceans: an overview of extrinsic determinants and modifying influences of biotic interactions. Hidrobiologia, 668, 61–108. http://doi.org/10.1007/s10750-0100400-y
34. Conde-Porcuna, J.M., Morales-Baquero, R. and Cruz-Pizarro, L. (1993). Effectiveness of the caudal spine as a defense mechanism in Keratella cochlearis. Hydrobiologia, 255/256, 283-287
35. Kappes, H., Mechenich, C. and Sinsch, U. (2000). Long-term dynamics of Asplanchna priodonta in LakeWindsborn with comments on the diet. Hydrobiologia, 432, 91–100.
36. Wong, C.K. and Sprules, W.G. (1985). Size-selective feeding by the predatory copepod Epischura lacustris Forbes. Canadian Journal of Fisheries and Aquatic Sciences, 42, 189-193.
37. Branstrator, D.K. (1998). Predicting diet composition from body length in the zooplankton predator Leptodora kindtii. Limnology and Oceanography, 43, 530–535.
38. Sakamoto, M. and Hanazato, T. (2008). Antennule shape and body size of Bosmina: key factors determining its vulnerability to predacious Copepoda. Limnology, 9, 27-34. http://doi.org/10.1007/s10201-007-0231-3
39. Giraldo, M. (2010). Composición de la dieta del rotífero Asplanchna girodi (De Guerne, 1888) y su variación temporal y espacial en el embalse Riogrande II (Antioquia, Colombia): Trabajo de grado, Universidad de Antioquia, Medellín, Colombia, 80 p.
40. Bonecker, C., Azevedo, F. and Simões, N. (2012). Zooplankton body-size structure and biomass in tropical floodplain lakes: relationship with planktivorous fishes. Acta Limnologica Brasiliensia, 23(3): 217–228. http://doi.org/10.1590/S2179975X2012005000005
41. Gavilán-Díaz, R. (1990). Flutuações Nictemerais dos Fatores Ecológicos na Represa de Barra Bonita-Médio Tietê-SP. Dissertação de Mestre, Universidade Federal de São Carlos, Brasil, 157 p.
42. Parra-García, E. A., Rivera-Parra, N., Picazo, A., and Camacho, A. (2020): Detrital food chain as a possible mechanism to support the trophic structure of the planktonic community in the photic zone of a tropical reservoir. Limnetica, 39(1): 511-524.

Received: 14 November 2020
Accepted: 14 February 2021

RESEARCH / INVESTIGACIÓN

Evaluación de la eficiencia de extractos naturales en el proceso de coagulación floculación de aguas crudas, con fines de potabilización

Evaluation of the efficiency of natural extracts in the coagulation floculation process of raw water, for purification purposes

Carlos Augusto Benjumea-Hoyos, Manuela Toro Martínez, Valerya Luna Marin
DOI. 10.21931/RB/2021.06.02.17

Resumen: El presente estudio permitió por medio de ensayos de jarras, evaluar la eficiencia de los extractos naturales de *Zea mays* (Maíz), *Aloe vera* (Sábila) y *Citrus sinensis* (Naranja) para disminuir los valores de turbidez en aguas crudas con fines de potabilización y su efecto en el pH y la conductividad. Esto con el fin de investigar alternativas viables que permitan mejorar la calidad del agua cruda y que sean de fácil acceso para comunidades marginales; el uso de extractos naturales en el proceso de potabilización de aguas y en específico en la remoción de turbidez permite evaluar la capacidad de estos en relación con los compuestos químicos convencionales utilizados en dicho proceso. En este sentido, se obtuvo una remoción en la turbidez del 85% con los extractos de maíz y sábila; y del 69% con el extracto de naranja. Los resultados obtenidos dejan ver los beneficios de utilizar extractos naturales en los procesos de tratamiento de aguas, el fácil acceso a la materia prima requerida, su bajo costo, producción mínima de lodos inocuos debido a la no presencia de sales metálicas y su aporte a reducir el uso de coagulantes químicos, serían aportes importantes en la disminución de impactos ambientales asociados a los riesgos que este tipo de lodos convencionales podrían provocar.

Palabras clave: Coagulación, floculación, extractos naturales, turbidez, pH, conductividad, calidad del agua, potabilización.

Abstract: The present study allowed, through jar tests, to evaluate the efficiency of the natural extracts of *Zea mays* (Corn), *Aloe vera* (Aloe vera), and *Citrus sinensis* (Orange) to reduce the turbidity values in raw water for purification purposes and its effect on pH and conductivity. This is to investigate viable alternatives that improve the quality of raw water and are easily accessible to marginal communities; the use of natural extracts in the water purification process and specifically in the removal of turbidity allows evaluating their capacity concerning the conventional chemical compounds used in the process. In this sense, a turbidity removal of 85% was obtained with the extracts of corn and aloe; and 69% with the orange extract. The results obtained show the benefits of using natural extracts in drinking water treatment processes, the easy access to the required raw material, its low cost, minimum production of harmless sludge and its contribution to reducing chemical coagulants' use would be contributions significant in reducing environmental impacts associated with the risks that this type of conventional sludge could cause.

Key words: Coagulation, flocculation, natural extracts, turbidity, pH, conductivity, purification.

Introducción

Según UNICEF (2019)[1], con base en la problemática del acceso al agua potable, se estima que 1 de cada 10 personas todavía carecen de servicios básicos, incluidos los 144 millones que beben agua de superficie que no ha recibido tratamiento. Además, evidencia que 8 de cada 10 personas que viven en zonas rurales carecen de acceso al agua potable, y en 1 de cada 4 países con estimaciones para diferentes grupos de riqueza, la cobertura de los servicios básicos era más desfavorecida para personas de escasos recursos económicos, como consecuencia de la mala gobernabilidad y gobernanza del agua en todo el mundo[2]. A lo anterior se le suma la alta demanda de agua que aumentará entre un 20 y 30 % en 2050 respecto al nivel actual, por el crecimiento poblacional, desarrollo económico y los modos de consumo[3].

En el caso de Colombia a pesar de que los servicios públicos constituyen un derecho humano fundamental que debe proveerse de manera obligatoria a la comunidad en las cantidades mínimas[4], esto no se ha podido satisfacer en todo el territorio Nacional, lo cual hace más evidente la falta de gobernabilidad y gestión[5]. En Consecuencia, 28.1 millones de personas en la zona urbana cuentan con agua potable, es decir 86.11% de la población total y alrededor de 3.8 millones de personas reciben agua no apta para consumo humano, haciendo referencia a un 11.56% de la población total del país[6]. Los municipios con menor cobertura de agua potable presentan consecuencias mortales en la población por lo que por cada 100.000 nacidos hay 96 muertes maternas asociadas a la falta de cobertura de acueducto y alcantarillado, además, 11 de cada 100.000 menores de 5 años mueren a causa de enfermedades diarreicas[7].

Los cuerpos de agua cruda contienen partículas coloidales que generan turbidez debido a sedimentos y nutrientes, los cuales no precipitan completamente de manera natural y, por ende, deben ser removidos[8,9]. Por tal motivo, la clarificación del agua, que se entiende como el retiro de materiales sólidos y coloidales, es fundamental en el proceso de potabilización, que incluye las fases de coagulación-floculación en el cual las partículas presentes se aglomeran formando pequeños gránulos con un peso específico mayor; de esta forma las partículas sedimentan y ocurre la remoción de los materiales en suspensión, lo que permite que el agua alcance características físicas y químicas idóneas como un paso en su tratamiento, con el fin de lograr que esta cumpla las normas y estándares de salud pública[10].

[1] Universidad Católica de Oriente, Grupo de investigación Limnología y Recursos Hídricos, Rionegro, Colombia.

Corresponding author: yaquelin.puchades@inicasc.azcuba.cu.

Generalmente en las plantas de potabilización se utilizan coagulantes inorgánicos, muchos de ellos como el sulfato de aluminio y cloruro férrico, entre otros, que se han utilizado para eliminar las impurezas y las partículas coloidales presentes en los cuerpos de agua debido a su rendimiento y disponibilidad[11]. Sin embargo, existe evidencia que relaciona a los coagulantes a base de aluminio, con el desarrollo de enfermedades como el Alzheimer en los seres humanos[12-15], así mismo con la producción de grandes cantidades de sedimentos que, al ser vertidos en las fuentes de agua, se convierten en un problema ambiental debido a que en altas dosis pueden llegar a ser tóxico[16].

Ante esta problemática, se hace necesaria la búsqueda de alternativas que puedan sustituir total o parcialmente las sales de hierro y aluminio, así como los polímeros orgánicos sintéticos[17]. En varios países de Latinoamérica, desde los años 70 en adelante se propuso la utilización de los coagulantes naturales, donde la mayoría de estos se derivan de semillas, hojas, cortezas o savia, raíces y frutos de árboles y plantas, además se pueden extraer de microorganismos, animales y tejidos vegetales[18] con el propósito de reducir el consumo de reactivos químicos.

De acuerdo con lo anterior, en la literatura se han encontrado antecedentes sobre el uso de coagulantes naturales en Colombia para ser usados en los procesos de clarificación de agua[19] tales como el cactus Opuntia ficus, samán o árbol de lluvia Pithecellobium[20] moringa oleifera, entre otros[21-23]. Esto se ha estudiado principalmente en regiones del caribe, debido a que demuestran que no es posible acceder al agua potable en las comunidades de escasos recursos económicos y, en especial la población rural[24].

Ante este panorama surge la necesidad de evaluar mediante este trabajo el poder coagulante de *Citrus sinensis*, *Zea mays* y *Aloe vera*, en el proceso de clarificación en el agua cruda.

Materiales y métodos

Área de estudio

Los ensayos se realizaron en el laboratorio de monitoreo ambiental de la Universidad Católica de Oriente ubicada en el municipio de Rionegro-Antioquia. Las muestras de agua fueron obtenidas de la quebrada el Águila con coordenadas geográficas latitud 6°9'6.00" N, longitud 75°21'59.45" O, la cual es afluente del Río Negro (figura 1).

A las muestras se les ajustó su turbidez inicial, bajo parámetros similares a los empleados por Caicedo (2017)[25], en un modelo de solución de mezcla de fondo a una relación de 1/1 de limo propio de la zona de estudio y agua cruda de la quebrada, preparando la solución en un recipiente plástico previamente lavado y realizando un mezclado de manera manual. La mezcla se dejó reposar con el fin de lograr el asentamiento de los sólidos sedimentables, y al mismo tiempo se permitió el aumento de la turbidez hasta garantizar rangos de 255 a 309 NTU. Se determinaron las variables fisicoquímicas de la mezcla como pH (Unidades de pH), conductividad (µS/cm) y concentración de cloruro de sodio NaCl (mg/L) con un multiparamétrico marca HACH hq40d, modelo MULTI 340i y la turbidez con un turbidímetro marca HACH 2100q, método nefelométrico (método 2130B), ambos calibrados con soluciones estandarizadas.

En la preparación de los extractos naturales, se inició con el tratamiento del material vegetal. Para el caso de *Citrus sinensis* (Naranja) se recolectaron las cascaras y se eliminó el bagazo (Mesocarpio), se dejó secar durante 24 horas para lograr una humedad de alrededor del 10%, luego se trituró en trozos de 0.5 mm aproximadamente de manera manual y mecánica; se realizó el mismo proceso con el *Zea mays* (Maíz) a diferencia de que la materia prima de este último se obtiene seca.

Finalmente, para el material vegetal de *Aloe vera* (Sábila) se utilizó solo el cristal interno que esta contiene, dado que este representa hasta un 80% del peso total de la planta[26]. Con el fin de evitar la pérdida de las propiedades originales del *Aloe vera*, no se procedió a un secado, sino que se sometió a un macerado hasta lograr un cambio de estado de sólido a semilíquido.

Para la extracción del componente activo, se preparó una solución al 5% (p/v) bajo precipitación con 100 ml de alcohol etílico (90% v/v) por cada 5 gramos de material vegetal obtenido, dicha solución se mezcló con agitadores magnéticos durante 30 min y un tiempo de sedimentación de 1 hora. Posteriormente se separó el sólido y liquido de la solución con una bomba de vació y filtros de papel. La porción sólida obtenida se llevó a secado en horno a 70°C, solo para el caso de la naranja y el maíz.

Seguidamente, se procedió a la preparación del extracto natural para ser utilizado como coagulante. Para ello, se prepararon disoluciones al 5 % (p/v) compuestas por 5 gramos de los sólidos secos por cada 100 ml de una solución salina de NaCl a concentraciones de 0.125 M, 0.25 M y 0.5 M. Dichas

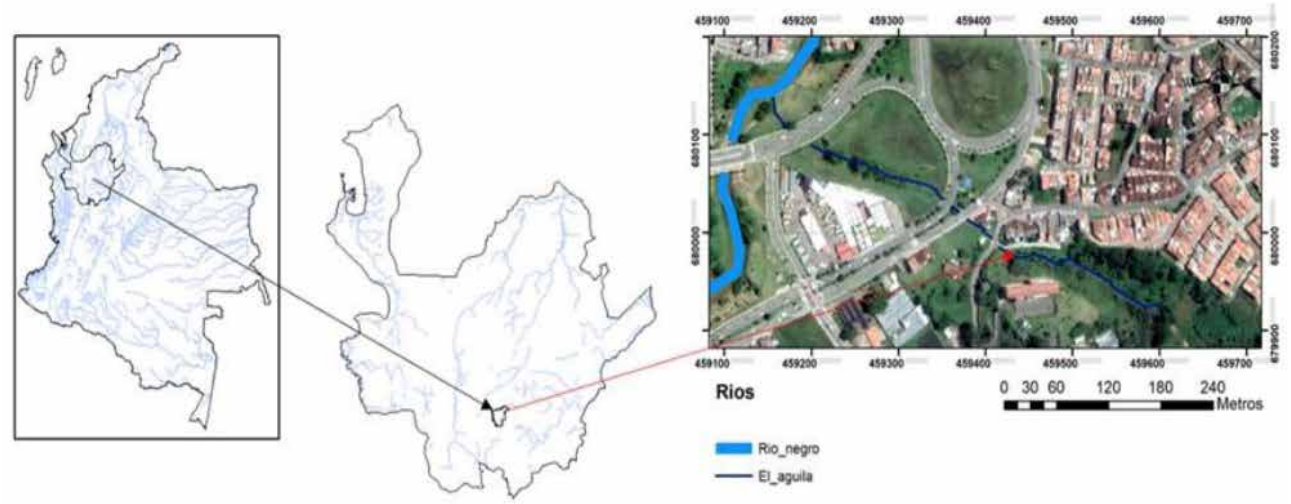

Figure 1. Localización punto de muestreo Quebrada El Águila, Rionegro-Antioquia. Fuente: Autores.

disoluciones se mezclaron durante 30 minutos con agitadores magnéticos, y una vez transcurrido este tiempo se filtraron con la bomba de vació y papel filtro. El líquido filtrado constituye el extracto crudo salino (ECS) en sus tres distintas concentraciones[27,28].

Los ECS fueron utilizados en los ensayos de actividad coagulante, con ayuda del método conocido como test de jarras según lo establecido por la ASTM (2003)[29] y lo propuesto por Norma Técnica Colombiana NTC 3903 en cuanto al procedimiento para el ensayo de coagulación-floculación en un recipiente con agua o método de jarras de manera individual. El procedimiento se realizó con cinco beacker de 1000 ml a los cuales se les adiciono el agua cruda, dejando uno como blanco (Control) al cual no se le adiciono ningún extracto; los otros cuatro se dosificaron con 7 ,10,12 y 15ml respectivamente. Las anteriores soluciones se sometieron a una mezcla rápida a 150 revoluciones por minuto (rpm) durante 3 min, seguida de una mezcla lenta a 25 rpm durante 20 min, por último, se finalizó con la fase de sedimentación durante 20 min y se midieron nuevamente las variables fisicoquímicas de cada uno de los beackers.

Para determinar el efecto de diferentes tipos de coagulantes (*Citrus siniensis*, *Zea mays* y *Aloe vera*) sobre las variables pH, conductividad y porcentaje de remoción de turbiedad se hizo uso de un diseño unifactorial con tres réplicas para cada uno de los tratamientos utilizados.

Con el fin de establecer diferencias estadísticas significativas entre los tratamientos se hizo uso de un análisis de varianza ANOVA con un 95% de confianza seguido de un análisis post-hoc Tukey-HSD con la misma confianza. Los supuestos de normalidad de los residuales se verificaron por medio de la prueba de Kolmogorov-Smirnov[30] y Shapiro & Wilk (1965)[31] y la homocedasticidad de los residuales por medio de la prueba de Levene (1960)[32]. Los resultados se presentaron a partir de una gráfica de interacción de medias entre uno o dos factores. Todo el componente estadístico se desarrolló en el software RWizard 4.2[33].

Teniendo en cuenta lo establecido en la metodología, la cual se encuentra enfocada en evaluar la actividad coagulante de los extractos naturales en base salina (ECS), los tratamientos analizados como Control, a los cuales no se les realizo adición de extracto coagulante, no se consideraron dentro del tratamiento estadístico debido a que estos presentaron una remoción de turbidez por sedimentación natural , la cual fue sobrepasada visualmente por la actividad coagulante de los extractos, posterior a los 10 primeros minutos de comenzada la metodología establecida con el test de jarras.

Resultados

La tabla 1 presenta la caracterización de las variables fisicoquímicas evaluadas en el agua cruda realizada durante el presente estudio. Se estableció un intervalo de oscilación para cada variable teniendo en cuanta las repeticiones realizadas.

Con la finalidad de encontrar el mejor extracto por su acción coagulante, se estimó de manera individual para cada uno cuál fue su mejor tratamiento con base a la concentración salina de NaCl de este.

El análisis de varianza ANOVA permitió conocer la relación del factor concentración (mg/L) de NaCl, sobre la variable respuesta porcentaje de remoción de turbidez con cada uno de los tres extractos coagulantes utilizados, esta se realizó con una confiabilidad del 95%. Se tuvo en cuenta el valor de P, que para los tres extractos presento valores menores de 0.05 indicando que existen diferencias significativas entre los tratamientos evaluados en cuanto a el porcentaje de remoción de turbidez final obtenida.

El porcentaje de remoción de turbidez en relación con el extracto aplicado se muestra en la figura 2, donde teniendo en cuenta la turbiedad inicial del agua cruda, se observó y determino que los tratamientos con mayor eficiencia por extracto fueron a una concentración de 0.5 molar de NaCl, obteniendo un porcentaje de remoción de turbidez de hasta un 85% para el caso del maíz y la sábila, mientras que para el extracto de la naranja se alcanzó una de remoción de hasta un 69%.

Lo anterior constituyen los resultados principales de la presente investigación, por lo cual se analizarán seguidamente solo los tratamientos que presentaron mayor eficiencia en la remoción de turbidez en cada caso, para ser relacionados con las variables fisicoquímicas después del proceso de coagulación.

Con el fin de determinar la dosis óptima de coagulante para cada extracto, se evaluó el porcentaje de remoción de turbidez por dosis adicionada en los mejores tratamientos.

Por medio nuevamente de análisis de varianza ANOVA, se encontró que los valores de P para todos los extractos fueron mayores de 0.05 lo que indica que no existen diferencias significativas entre la remoción de turbidez con respecto a la dosis de coagulante adicionada.

En la figura 3, se identifica que para el tratamiento con maíz a una concentración de 0.5 molar de NaCl, la eficiencia más alta se presentó con un porcentaje de remoción de turbidez de un 85% con dosis de 7 y 12 ml, pasando de valores de turbidez de 269 NTU a 40.6 y 41.2 NTU; respectivamente. Mientras que con las dosis de 10 y 15 ml se lograron remociones de un 83,5% con valores finales de turbidez de 44.3 y 46.9 NTU, respectivamente. Para los tratamientos con sábila a concentración de 0.5 molar de NaCl las dosis con mejor efecto fueron las de 10, 12 y 15 ml con remoción hasta de un 85%, pasando de una turbidez inicial de 300 NTU a 47.4, 48.9 y 46 NTU respectivamente, mientras que la dosis de 7 ml mostro una disminución de la turbidez hasta 71.3 NTU. Posteriormente se encontró que, para el extracto realizado con naranja, se presentó una remoción de hasta un 69% con la dosis de 15 ml pasando de una turbidez inicial de 296 NTU a 87.8 NTU, mientras que las de 10 ml y 12 ml muestran remociones similares de hasta un 66% pasando a remover la turbiedad hasta 96.4 NTU y 97.8 NTU respectivamente. Finalmente, la menor remoción fue con 7 ml, disminuyendo la capacidad del coagulante hasta remociones de un 63% finalizando con una turbidez de 107 NTU.Se evaluó de manera general el efecto independiente de las variables fisicoquímicas en el diseño metodológico, con el fin de determinar cuál de las ellas tenía un efecto mayor en relación con el porcentaje de remoción de turbidez.

PARÁMETRO	UNIDAD	RANGO
Turbidez	NTU	255 a 309
pH	Unidades de pH	6.52 a 8.38
Conductividad	µS/cm	54.1 a 101.9
NaCl	mg/L	26.5 a 53

Tabla 1. Rango de oscilación de las variables fisicoquímicas de la muestra de agua.

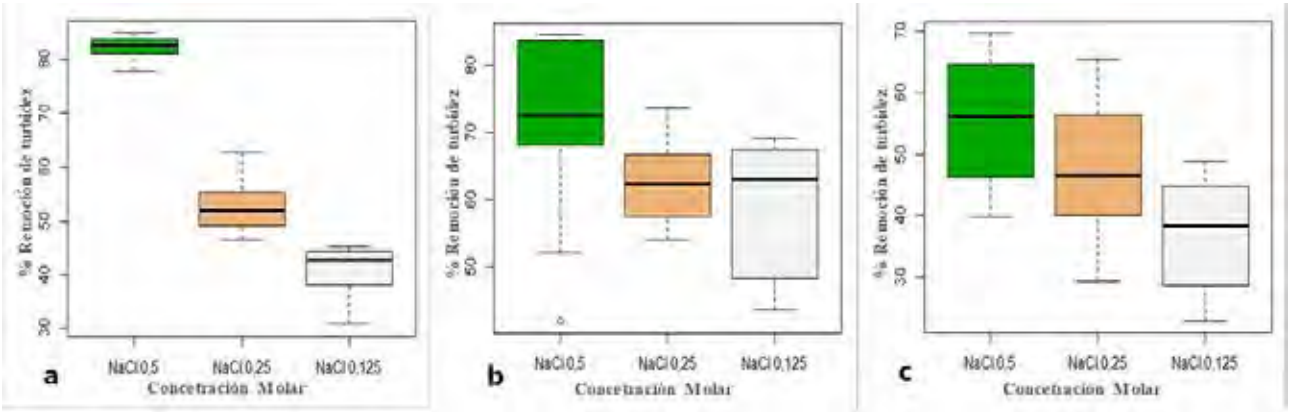

Figure 2. Porcentaje de Remoción de turbidez con extracto de Zea mays "maíz" (a), Aloe vera "sábila" (b) y Citrus sinensis "naranja" (c).

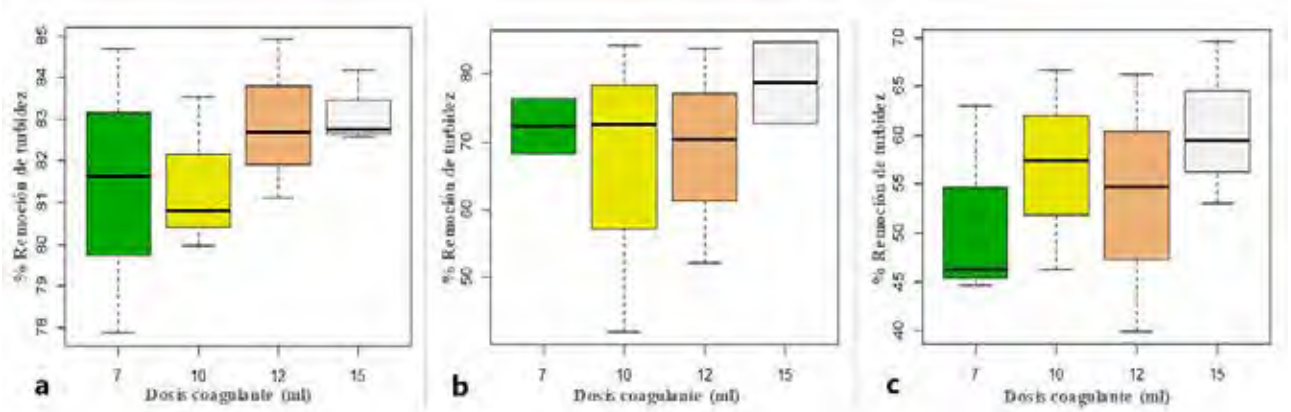

Figure 3. Porcentaje de remoción de turbidez por dosis de coagulante de extractos de Zea mays "maíz" (a), Aloe vera "sábila" (b) y Citrus sinensis "naranja" (c).

El análisis arrojo un efecto del 62% del pH y del 38% de la conductividad (µS/cm) en los tratamientos con coagulantes naturales en el agua cruda con rangos de turbidez inicial de 255 – 309 NTU.

En la figura 4 se presenta el efecto del pH teniendo como factor principal las dosis de coagulantes adicionadas para el tratamiento óptimo por extracto determinado; dicha variable no presenta diferencias significativas entre tratamiento, lo que se logra visualizar dado el entrecruzamiento del error estándar (líneas verticales). Se observa que para el maíz la muestra presento un valor inicial de pH 6.95 finalizando con un valor de 7.01 en todos los tratamientos. Con la sábila el valor inicial de pH fue de 6.52 concluyendo con valores de pH 6.93, 6.79, 6.67 y 6.70 para los tratamientos con dosis de 7, 10, 12 y 15 ml respectivamente; en tanto con la naranja este presento un valor inicial de pH de 6.12 variando de 7.32, 7.19, 7.15 y 7.06 con respecto a las dosis de 7, 10, 12 y 15 ml respectivamente.

En cuanto a la variabilidad de la conductividad, se puede observar en la figura 5 su relación con la dosis de coagulante adicionada y su efecto con respecto al porcentaje de remoción de turbidez en cada uno de los tratamientos. La relación entre la conductividad (µS/cm) y la concentración salina de NaCl fue directamente proporcional, las cuales presentaron un aumento progresivo en correlación con la dosis de coagulante adicionado, obteniéndose valores de hasta 1063 uS/cm para el maíz, 603.8 uS/cm para sábila y 1246 uS/cm con la naranja para la dosis de 15 ml, los cuales fueron los valores más altos, teniéndose que para las dosis más bajas esto disminuyo proporcionalmente.

Discusión

Se encontró cómo dosis óptima de ECS para el maíz el tratamiento de 7ml, para el caso de la sábila de 10 ml y para la naranja de 15 ml, todas a una concentración de 0.5 molar de NaCl; esto debido a que no se presentaron diferencias significativas con las demás dosis y que además se obtuvo la mayor eficiencia en remoción de turbidez, lo cual beneficia, entre otras cosas la baja cantidad de coagulante requerido en el proceso y el poco efecto en las variables fisicoquímicas evaluadas, principalmente el pH.

Con respecto a la actividad coagulante del extracto de maíz para disminuir la turbidez, según Shogren (2009)[34] el componente activo que le da la capacidad coagulante-floculante en el tratamiento de aguas es el almidón, el cual es un polímero natural que cuenta además con una alta biodegradabilidad; con dicho componente activo se ha logrado en algunos casos remociones de hasta un 90% de turbidez y color en fuentes hídricas superficiales[10]. Lo anterior, con base a los resultados obtenidos para el tratamiento más eficiente con el maíz en relación con la remoción de turbidez y la dosis optima de coagulante, coincide con lo reportado Jiménez y Piscal (2015)[35], quienes consiguieron una remoción del 86.77%, y afirman que los altos valores de turbidez permiten que el almidón contenido en el maíz funcione como catalizador y logre que más partículas coloidales se adhieran para formar flocs de mayor peso, promoviendo la remoción de turbidez en aguas crudas. Por su parte Aguirre *et al.* (2018)[28] lograron obtener una remoción del 68% y Sotheeswaran *et al.* (2011)[36] obtuvieron una eficiencia del 19%; estos resultados demuestran la influencia de las diferentes metodologías aplicadas para la extracción del componente activo.

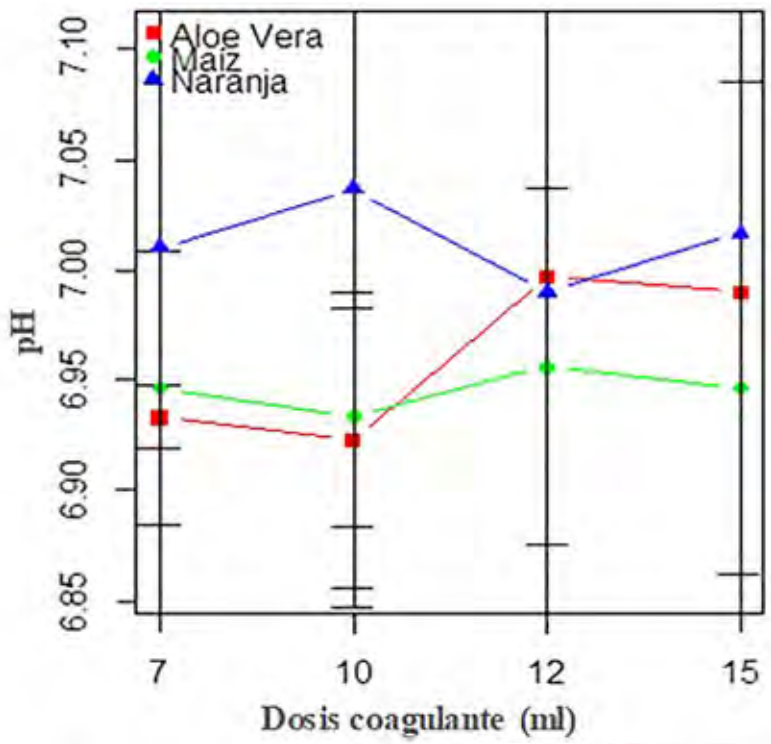

Figure 4. Variación del pH con respecto a la dosis y el extracto natural.

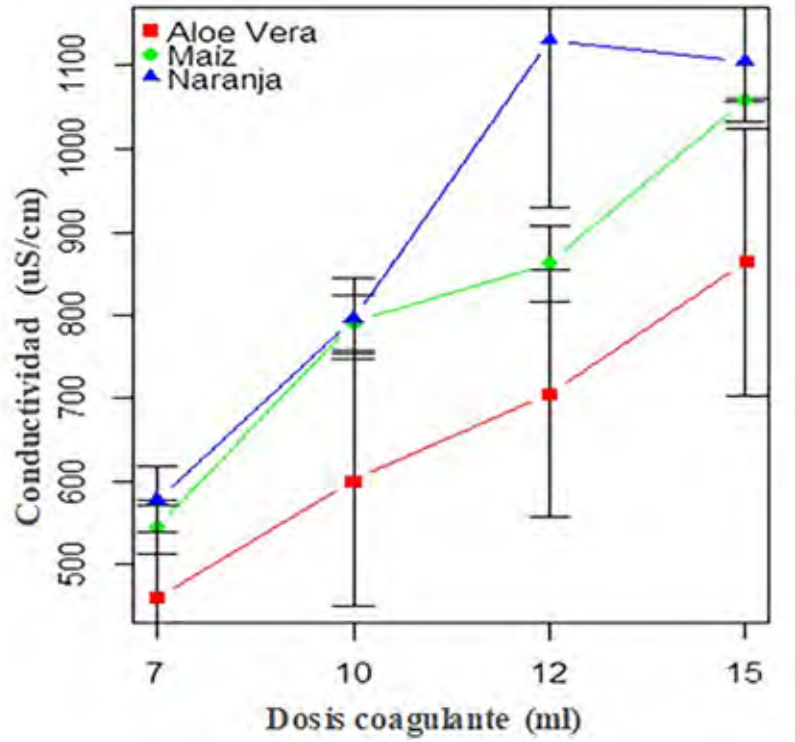

Figure 5. Variación de la conductividad (µS/cm) con respecto a la dosis y el extracto natural para los mejores tratamientos.

Por otra parte, la diferencia de cargas iónicas entre el almidón presente en el maíz y la poca variabilidad del pH de la muestra en relación con la dosis de coagulante aplicado en el presente estudio, generaron un equilibrio químico entre las partículas, lo que favoreció la eficiencia de remoción de turbidez y lo que se puede asociar, inclusive, a que se ha demostrado una afinidad entre dichas variables, donde se afirma que a menores dosis de coagulante y pH por debajo de la neutralidad se favorece el proceso de coagulación[37].

La actividad coagulante del extracto de sábila y el de la naranja se encuentra ligada a la pectina[38], esta se encuentra asociada a la capacidad de gelificación natural de los compuestos que a su vez permite que sea soluble en agua y a que sea eficiente para ser utilizada en procesos de tratamientos de coagulación de aguas crudas[39], donde además su capacidad coagulante se encuentra estrechamente relacionada con la disponibilidad de cationes bivalentes[40].

En relación con lo obtenido con el extracto de sábila y la dosis optima de coagulante determinada para dicho tratamiento, se observa un comportamiento similar a lo reportado por Diestra y Ramos (2019)[41] los cuales obtuvieron una remoción de turbidez con extractos de sábila desde un 80.98% hasta un 88.5% con tiempos de floculación de 25 minutos, coincidiendo con lo realizado en el presente estudio, lo que además confirma

que dicho tiempo es óptimo y evita que los flocs se destabilicen y comiencen nuevamente a aumentar los valores de turbidez. Lo primero, también se relaciona con lo propuesto por Munavalli (2017)[42] quien alcanzo remociones entre un 75% a un 81% en aguas con turbidez entre 70-90 NTU, lo que puede deberse a lo afirmado por Morales (2018)[43] donde se logró demostrar que a mayor cantidad de extracto de sábila se pueden obtener mejores resultados en la remoción de turbidez, lo que permite inferir que en el presente estudio un aumento en la concentración del extracto podría presentar remociones incluso mayores al 90%.

Cabe resaltar que, en lo realizado por Mendoza, *et al.* (2014)[44], donde se trabajó el extracto en solución acuosa (agua destilada) solo se logró una remoción del 22.5% confirmando que el extracto de Alo vera en solución salina logra una mayor destabilizacion de los coloides y es más efectiva para ser utilizada en los tratamientos de coagulación y floculación del agua.

Es importante mencionar que el pH en el tratamiento con extracto de sábila no presento variaciones significativas entre el pH y las dosis adicionadas, manteniendo un rango entre 6.9 a 7.0 unidades de pH (remoción hasta del 85%), este resultado es comparable con lo establecido por Guo (2008)[45], quien afirma que a pH entre 3 a 11 la sábila presenta una aplicabilidad en gran cantidad de procedimientos en el ámbito del tratamiento de aguas, permitiendo porcentajes de remoción de turbidez de hasta un 92%, lo cual se puede comparar con los resultados de Babora , *et al.* (2014)[46] quienes obtuvieron que a pH altos se logran remociones de hasta un 72%.

El porcentaje de remoción máxima con el extracto de naranja fue de 69%, que en comparación con lo reportado por Ticona (2018)[47], quien realizo igualmente una extracción en base salina, logro una remoción de hasta un 81.99%, cabe señalar que dicho trabajo fue realizado con valores de turbidez inicial de 13.6 NTU, lo que permite inferir sobre cómo se puede lograr mejorar los efectos de dicho extracto en relación con la turbidez inicial y la salinidad, relacionándolo con lo que obtuvo Campo, *et al.* (2018)[48] de extracto de naranja en solución acuosa que removió solo un 39% y un 79% en combinación de quitosano. Por otra parte Contreras, *et al.* (2015)[49], determinaron que la actividad coagulante también se puede relacionar con el ácido galacturónico, el cual también se encuentra presente en la pectina de los extractos de naranja[50] y permite una mayor absorción química entre partículas suspendidas en el agua. Por su parte Miller, *et al.* (2008)[51] lograron reducción de turbidez del 50% en combinación con otros azucares como la galactosa, mientras que Carpio (2007)[52] logro una biosorción de Plomo (Pb) usando extractos de naranja con una eficiencia de hasta un 95%.

La estabilidad del pH luego del proceso de coagulación con el extracto de naranja y sus valores tendientes a la neutralidad contrastan con lo reportado por Chávez (2009)[50], quién encontró un mayor rendimiento de la pectina (propia del extracto de naranja) a valores de pH entre 1,5 y 2.

Lo obtenido en el presente estudio, presenta entonces, un beneficio en cuanto al tratamiento de aguas crudas, puesto que las cascaras utilizadas para la extracción de coagulante, se encontraban en etapa madura, lo cual en relación con los antecedentes químicos de la naranja se asocia con un aumento de las azucares presentes en la misma y una disminución en la acidez natural de dicho fruto[53].

La conductividad del agua posterior al tratamiento de coagulación con los extractos de maíz, sábila y naranja, presentaron un aumento directamente proporcional a la dosis aplicada de coagulante, esto debido a que la solución se preparó en base salina con cloruro de sodio (NaCl), que permite una mayor actividad coagulante debido a su capacidad electrolítica[24]. Dicha solución permitió separar las moléculas en iones de Na+ y Cl-, logrando conducir más electricidad y al mismo tiempo permitir la precipitación de otros iones que pueden causar efectos adversos en el tratamiento de agua[54].

En la resolución 2115 de 2007[55] se establecen los límites máximos permisibles de turbidez (< 2 NTU), conductividad (1000 µS/cm) y pH (entre 6.5 y 9,0) para agua de consumo humano. La conductividad en las dosis optimas de coagulante natural determinadas por su capacidad de remoción de turbidez para el maíz y sábila fueron respectivamente 512 y 371 (µS/cm) lo que les da un valor agregado para ser utilizados en el tratamiento del agua, mientras que para el caso de la naranja la dosis optima presento un valor superior al de la norma (1246 µS/cm), por lo tanto se debe considerar su uso, debido a que se requeriría un tratamiento previo antes de ser puesta a disposición para consumo o considerar el aumento de las proporciones iniciales del componente activo adicionado en las soluciones para impedir los excesivo valores en la conductividad.

Con los valores de turbidez obtenidos luego de la aplicación de los coagulantes naturales en el agua cruda, no se logra llegar hasta los valores requeridos para consumo humano, pero cabe resaltar que este tratamiento se realiza previo a los procesos de filtración, donde probablemente se lograría obtener los valores demandados en la norma con relación a dicha variable.

Por otra parte, los extractos no alteraron significativamente los valores iniciales de pH, estos resultados también han sido obtenidos en trabajos donde se toma como beneficio la estabilidad de dicha variable, para ser utilizados como coadyuvantes en el tratamiento de coagulación, como lo encontró Kopytko, *et al.* (2014)[56], donde se logró reducir en un 20% la cantidad de sulfato de aluminio requerido para tratamiento del agua, a lo que además se le suma la actividad antimicrobiana que los extractos a base del gel o cristal de la hoja de *Aloe vera* presentan para remover bacterias presentes en el agua[57]. Shahriari , *et al.* (2011)[58] utilizaron extractos de almidón con cloruro férrico para remover turbidez en agua preparada, logrando remociones de hasta un 92.4% y tal como encontraron Laines , *et al.* (2008)[59] que se pueden utilizar extractos a base de almidón y sulfato de aluminio para ser utilizados inclusive en la remoción de turbidez de lixiviados, logrando remociones de hasta un 98.6%.

En contraste con los coagulantes químicos convencionales especialmente los utilizados a base de aluminio y hierro, han demostrado que al ser adicionados en el proceso de coagulación, generan variaciones en el pH óptimo (6,5 a 9,0 unidades de pH), lo que dificultan el tratamiento del agua[60] acidificándola debido a la reacción que ocurre con la alcalinidad[37], además, pueden generar efectos secundarios en otras variables fisicoquímicas como la turbidez y alcalinidad[61], por lo que se establece que si dicha variable se encuentra en un rango de 6 y 8 unidades de pH las sales de aluminio se solubilizan más fácilmente, mientras que las sales de hierro permiten se utilizadas en un rango de pH mayor entre 5.5 y 8.5 unidades de pH; este último compuesto permiten la formación de floc con mayor peso disminuyendo el tiempo de sedimentación pero son poco utilizadas por adicionar color al agua[62].

Finalmente, en relación con lo obtenido en el presente trabajo y los posibles usos de los extractos naturales como coadyuvantes en el tratamiento de aguas con sulfato de aluminio y cloruro férrico, los cuales se encuentran actualmente regulados por normativa colombiana[55] y teniendo en cuenta los estudios realizados por World Health Organization (2003)[12] y Llopis y Ballester (2002)[61] donde demuestran que la exposición al aluminio puede generar daños irreversibles en el sistema inmune humano e incluso permitir el desarrollo de enfermedades asociadas a daños cerebrales que afectan las capacidades psíquicas y cognitivas, se resalta el aporte que se puede dar al utilizar extractos

de fuentes vegetales e incluso animales, enfocado en soluciones para Colombia así como lo explica Castellanos (2017)[64], los que además tienen un grado de toxicidad bajo, buena biodegradabilidad y poca variabilidad del pH[37], presentan un rango de dosis efectiva más amplio para la floculación de varias suspensiones coloidales y producen lodos inocuos y una menor cantidad de los mismo[14,16].

Conclusiones

La presente investigación permitió realizar el proceso de coagulación-floculación con extractos de origen natural mediante la metodología del test de jarras, con lo cual se logró generar un equilibrio químico que permitió desestabilizar las cargas iónicas de los coloides favoreciendo la formación de flocs, obteniendo en este proceso una reducción de hasta el 85% en términos de turbiedad.

La metodología empleada para la extracción de coagulantes naturales de *Zea mays* (Maíz), *Aloe Vera* (Sábila) y *Citrus Sinensis* (Naranja) permitió demostrar la efectividad de los mismos en la remoción de turbidez con dosis bajas de coagulante aplicado, siendo también significativo el hecho de que el pH del agua no se vio afectado. Aunque la remoción dada no logra satisfacer lo establecido en la normatividad colombiana de agua potable solo con el proceso de coagulación-floculación y sedimentación; no obstante, los valores ideales de turbidez podrían ser alcanzados mediante los procesos siguientes en el tren de tratamiento mediante los procesos de filtración. Adicionalmente se puede considerar el aumento del potencial de los extractos naturales al ser utilizados como coadyudantes con los coagulantes químicos comerciales. Es importante mencionar lo establecido en los objetivos de desarrollo sostenible, específicamente para Colombia en el ámbito de garantizar agua potable en el territorio nacional, por lo tanto, la alternativa estudiada puede ser tenida en cuanta como una adaptación para mitigar los problemas de salud pública y calidad de vida que se presentan actualmente.

Agradecimientos

Los autores agradecen el apoyo durante todo el proceso del proyecto al Grupo de investigación Limnología y Recursos Hídricos y sus semilleros asociados; y a la Universidad Católica de Oriente.

Conflicto de interés

Los autores declaran no tener conflicto de intereses.

Referencias bibliográficas

1. UNICEF. (2019). Agua, Saneamiento e higiene. UNICEF/UN0215532/Rich.
2. Echeverría, J., & Anaya-Morales, S. (2018). El derecho humano al agua potable en Colombia: Decisiones del estado y de los particulares. Pontificia Universidad Javeriana.
3. UNESCO. (2019). Informe Mundial de las Naciones Unidas sobre el Desarrollo de los Recursos Hídricos. Ginebra.
4. Motta, R. (2011). El derecho al agua potable en la jurisprudencia colombiana. Revista Republicana.
5. Zamudio, C. (2012). Gobernabilidad sobre el recurso hídrico en Colombia: entre avances y retos. Revista Gest. Ambient., 15, 3, 99-11.
6. MINVIVIENDA. (2018). Plan director agua y saneamiento básico visión estratégica 2018 - 2030. Bogotá D.C
7. IDEAM. (2019). Estudio Nacional del agua 2018. Ideam, 452 pp.
8. Fuentes, L., Contreras, W., Perozo, R., Mendoza, I., & Villegas, Z. (2008). Uso del quitosano obtenido de Litopenaeus schmitti (Decapoda, Penaeidae) en el tratamiento de agua para consumo humano. Multicias, vol 8.
9. Luna J y Benjumea Hoyos C. (2019). Evaluation of the decomposition of digital images, for indirect estimation of turbidity in water samples. Revista Bionatura 4(2) 861-871.
10. Rodriguez, J., Rojas, A., Lugo, L., & Malaver, C. (2007). Evaluación del Proceso de la Coagulación para el Diseño de una Planta Potabilizadora. Umbral Científico, 8-16.
11. Shak, K., & Wu, T. (2014). Coagulation-flocculation treatment of high-strengthatgroindustrial wastewater using natural Cassia obtusifolia seed gum; treat mentefficiencies and flocs characterization.
12. World Health Organization. (- 2003)- . Aluminium in drinking-water: background document for development of WHO Guidelines for drinking-water quality. World Health Organization. https://apps.who.int/iris/handle/10665/75362.
13. Binayke, R. A., & Jadhav, M. V. (2013). Application of Natural Coagulants in Water Purification. International Journal of Advanced Technology in Civil Engineering, 2, 118-123.
14. Guzmán, L., Villabona, Á., Tejada, C., & García, R. (2013). Reducción De La Turbidez Del Agua Usando Coagulantes Naturales: Una Revisión. Revista U.D.C.A Actualidad & Divulgación Científica, vol. 16. scielo.
15. WWAP. (2019). Informe Mundial de las Naciones Unidas sobre el Desarrollo de los Recursos Hídricos 2019: No dejar a nadie atrás. París: Programa Mundial de Evaluación de los Recursos Hídricos de la UNESCO.
16. Cabrera, N., Hernández, A., Simancas, E., Ayala, J., & Almanza, K. (2017). Coagulantes naturales extraídos de Ipomoea incarnata en el tratamiento de aguas residuales industriales en Cartagena de Indias. Cartagena: Sci. Tech., vol. 22.
17. Arias, A., Hernández, J., Castro, A., & Sánchez, N. (2017). Tratamiento De Aguas Residuales De Una Central De Sacrificio: Uso Del Polvo De La Semilla De La M. Oleífera Como Coagulante Natural. Biotecnol. en el Sector Agropecuario. y Agroindustrial, vol. 15.
18. Tarón, A., Guzmán, L., & Barros, I. (2017). Evaluación de la Cassia fistula como coagulante natural en el tratamiento primario de aguas residuales. ORINOQUIA, vol. 21.
19. Murillo Castaño, D. M. (2011). Análisis de la influencia de dos materias primas coagulantes en el aluminio residual del agua tratada. Pereira: Doctoral dissertation, Universidad Tecnológica de Pereira. Facultad de Tecnologías. Química Industrial.
20. Hildebrando Ramírez Arcila, J. J. (2015). Agentes naturales como alternativa para el tratamiento del agua. Universidad Militar Nueva Granada, 13-18.
21. Turriago, F. A., & Melo, G. R. (2012). Evaluación de la eficiencia de la utilización de semillas de moringa oleífera como una alternativa de biorremediación en la purificación de aguas superficiales del caño cola de pato ubicado en el sector rural del municipio de Acacias. Villavicencio: Universidad nacional abierta y a distancia UNAD.
22. Sandoval A, M. M., & Laines C, J. R. (2013). Moringa oleifera una alternativa para sustituir coagulantes metálicos en el tratamiento de aguas superficiales. Ingeniería, 17, 93-101.
23. Jodi, M. L., Birnin-Yauri, U. A., Yahaya, Y., & Sokoto, M. A. (2012). The use of some plants in water purification. Global Advanced Research Journal of Chemistry and Material Science, 4, 71-75.
24. Bravo G, M. A. (2017). Coagulantes y floculantes naturales usados en la reducción de turbidez, sólidos suspendidos, colorantes y metales pesados en aguas residuales. Bogotá D.C: Universidad Distrital Francisco José De Caldas.
25. Caicedo, J. V. (2017). Evaluación de la eficiencia como coagulante de la semilla de soja molida, soja deslipidificada y la torta de soja, frente al sulfato de aluminio en procesos de clarificación de aguas. Universidad Distrital Francisco José De Caldas, 7-8.
26. Domínguez F, R., Arzate, I., Chanona, J., Welti, J., Alvarado, J., Calderón, G., . . . Gutiérrez, G. (2012). El ger de Aloe vera: estructura, composición química, procesamiento, actividad biológica e importancia en la industria farmacéutica y alimentaria. Revista Mexicana de Ingeniería Química, 11, 23-43.

27. Garcia, B. (2007). Metodología de extracción in situ de coagulantes naturales para la clarificación de agua superficial. Aplicación en países en vías de desarrollo. Universidad politécnica de valencia, 23-30.
28. Aguirre, S. E., Piraneque, N. V., & Cruz, R. K. (2018). Sustancias naturales: Alternativa para el tratamiento de agua del río Magdalena Palermo Colombia. Scielo, 29, n. 3.
29. ASTM, D.-8. (2003). Standard Practice for Coagulation-Flocculation Jar Test of Water, ASTM International. West Conshohocken: ASTM International.
30. Lilliefors, H. W. (1967). On the Kolmogorov-Smirnov test for normality with mean and variance unknown. Journal of the American statistical Association, 62(318), 399-402.
31. Shapiro, S. S., & Wilk, M. (1965). An analysis of variance test for normality (complete samples). Biometrika, 591-611.
32. Levene, Howard (1960). Robust tests for equality of variances. En Ingram Olkin, Harold Hotelling, et al., ed. Stanford University Press. pp. 278-292.
33. Guisande C., Heine J., González-DaCosta J. & García-Roselló E. (2014). RWizard Software. University of Vigo. Vigo, Spain.
34. Shogren, R. L. (2009). Flocculation of kaolin by waxy maize starch phosphates. Carbohydrate Polymers, (76) 639–644.
35. Jiménez Benavides, D. L., & Piscal, B. V. (2015). Estudio y evaluación del almidón de maíz como alternativa natural en el proceso de coagulación de agua para consumo humano. San Juan de Pasto: Universidad de Nariño.
36. Sotheeswaran, S., Nand, V., Matakite, M., & Kanayathu, K. (2011). Moringa oleifera and other local seeds in water purification in developing countries. Chemistry and Environment, 15.
37. Trujillo, D., Duque, L. F., Arcila, J. S., Rincón, A., Pacheco, S., & Herrera, O. F. (2014). Turbidity removal in a water sample from a natural source via coagulation/flocculation using plantain starch.
38. Hernández Curbelo, C., Moreno Quintero, M. E., Hernández Ramírez, D., & Crespo Zafra, L. M. (2016). Acid hydrolysis of Aloe Vera (Sábila) bagasse for obtaining pectin. Centro Azúcar, 44.
39. Sánchez F., S. A., & Unitiveros B., G. (2004). Determinación de la actividad floculante de la pectina en soluciones de Hierro (III) y Cromo (III). Sociedad Química del Perú, 4, 201-208.
40. Perazzo C, F. G., Goulart, C., Figueiredo, D., Oliveira, C., & Silva, J. (2008). Economic and Environmental Impact of Using Exogenous Enzymes on Poultry Feeding. International Journal of Poultry Science, 7, 311-314.
41. Diestra R, F. S., & Ramos P, I. V. (2019). Efecto de la concentración de Aloe Vera (Sábila) y tiempo de floculación en la remoción de sólidos suspendidos y materia orgánica biodegradable de aguas residuales municipales sector el Cerillo, Santiago de Chuco. Trujillo - Perú: Biblioteca Digital - Dirección de Sistemas de Informática y Comunicación.
42. Munavalli, G. (2017). Use of Aloe Vera as Coagulant aid in Turbidity Removal. Engineering Research and Technology, 10, 1.
43. Morales O, J. A. (2018). Determinación del poder coagulante de la sábila para la remoción de turbidez en el proceso de tratamiento de agua para consumo humano. Oxapampa: Universidad Nacional Daniel Alcides Carrión.
44. Mendoza, I., Fuentes, L., & Díaz, A. (2014). Aloe barbadensis (Miller) como coagulante natural en la potabilización de aguas con baja turbidez. Zulia-Venezuela: LIANCOL.
45. Guo, H. (2008). Study on the Natural Macromolecular Flocculant of Aloe. Aloe trade.
46. Babora B, R., Freire, R., & Oliveira B, W. (2014). Remoción de turbidez de agua usando Aloe vera como coagulante natural. Forum Ambiental, 10, 1-11.
47. Ticona, V. E. (2018). Estudio de la determinación de la actividad floculante en agua provenientes del río Chilo conteniendo As, Pb y Cr tratados con pectina obtenidos a partir de la cáscara de naranja, limón y mandarina. Arequipa- Perú: Universidad Nacional San Agustín de Arequipa.
48. Campo Vera, Y., Delgado, M. A., Roa, Y., Mora, G., & Carreño Ortiz, J. (2018). Preliminary evaluation of the effect of chitosan and orange peel in the coagulation-flocculation of wastewater. U.D.C.A Actualidad & Divulgación Científica, 21, 565-572.
49. Contreras L, K. P., Mendoza A, Y., Mendoza S, J. G., Verbel O, R., & Mendoza O, G. P. (2015). El Nopal (Opuntia ficus-indica) como coagulante natural complementario en la clarificación de agua. Producción más limpia, 10, 40-50.
50. Chávez Milla, J. M. (2009). Extraction of pectin from peel "criolla orange" (Citrlls aurantium L.) from Rodríguez de Mendoza Province. Investigaciones Amazonenses, 3, 24-26.
51. Miller, S. M., Fugate, E. J., Craver O, V., Smith, J. A., & Zimmerman, J. B. (2008). Toward Understanding the efficacy and Mechanism of Opuntia spp. as a Natural Coagulant for Potential Application in Water Treatment. Environmental Science & Technology, 42, 4274-4279.
52. Carpio M, J. C. (2007). Biosorción de plomo (II) por cáscara de naranja "citrus cinensis" pretratada. ResearchGate, Lima- Perú.
53. Agustí M. (2003). Citricultura. Madrid-México: Mundi-Prensa Libros.
54. Arango-Ruiz, Á. (2012). Effects of the pH and the conductivity on the electrocoagulation of waste water from dairy industries.
55. MINVIVIENDA (2007). Resolución nº 2115 de 22 junio de 2007. Por medio de la cual se señalan características, instrumentos básicos y frecuencias del sistema de control y vigilancia para la calidad del agua para consumo humano.
56. Kopytko, M. I., Villamizar R, E. P., & Picón R, Y. (2014). Application of Natural Product (Aloe Vera) in coagulation-Flocculation procedures for Water Treatability Study. International Journal of Engineering Science and Innovative Technology, III.
57. Musmeci, R., & Lezcano, M. T. (2013). Acción antimicrobiana del gel de aloe vera sobre staphylococcus aureus, escherichia coli, pseudomonas aeruginosa y candida albicans. Revista sobre Estudios e Investigaciones del Saber Académico, 23-27.
58. Shahriari, T., Nabi Bidhendi, G., & Shahriari, S. (2011). Evaluating the Efficiency of Plantago Ovata and Starch in Water turbidity removal. International Journal of Environmental Research and Public Health, 6, 259-264.
59. Laines C, J. R., Goñi A, J. A., Schroeder A, R. H., & Camacho C, W. (2008). Mezcla con potencial coagulante para tratamiento de lixiviados de un relleno sanitario. Interciencia, 33, 22-28.
60. Cogollo, J. M. (2011). Water clarification using polymerized coagulants: Aluminum Hydroxychloride case. Dyna, 78, 18-27.
61. Llopis S, L., & Ballester D, F. (2002). Revisión de los estudios sobre exposición al aluminio y enfermedad de Alzheimer. Salud Pública, 76, 645-658.
62. Restrepo, H. A. (2009). Evaluación del proceso de coagulación-Floculación de una planta de tratamiento de agua potable. Medellín: Universidad Nacional de Colombia.
63. Castellanos P, F. L. (2017). Revision of the use of natural coagulants in the process of water clarification in Colombia. Bogotá D.C: Universidad Militar Nueva Granada.
64. Tukey, J. (1949). Comparing Individual Means in the Analysis of Variance. Biometrics, 5 (2), 99-114.

Received: 15 febrero 2021
Accepted: 15 marzo 2021

RESEARCH / INVESTIGACIÓN

COVID-19 data analysis using HJ-Biplot method: A study case

Franklin Tenesaca-Chillogallo, Isidro R. Amaro
DOI. 10.21931/RB/2021.06.02.18

Abstract: COVID-19 is a new viral disease declared as a pandemic by the World Health Organization in 2020. This highly infectious disease, caused by the virus Severe Acute Respiratory Syndrome Coronavirus 2 (SARS-CoV-2), has shown a different impact on young individuals, old individuals, and people with other health conditions. In this study, we aim to identify the different relationships between COVID-19 with other health complications. Additionally, our purpose is to ordinate the ages of individuals according to COVID-19 affection. For this, we apply the HJ-Biplot along with Cluster multivariate analysis techniques to a data set of patients diagnosed with COVID-19, Pneumonia, smoking Habits, Diabetes, Obesity, Chronic Obstructive Pulmonary Disease, Asthma, Immunosuppression, Hypertension, Cardiovascular Problems, Chronic Renal Insufficiency, and other health problems. The data set that we use in this work was obtained from the Mexico Government website. This exploratory research illustrates that COVID-19 disease presents different relationships with other health problems and individuals. For example, this viral disease is highly correlated with Hypertension, Diabetes, smoking habits, and Obesity health conditions. Other high correlations are found among Chronic Obstructive Pulmonary Disease, Cardiovascular problems, Pneumonia, Chronic Renal Insufficiency, Hypertension, and Diabetes. Also, the ordination of individuals according to COVID-19 affection shows us that 60 to 89 years old people are highly affected by this disease. Furthermore, we identify the formation of two clusters of individuals. On the one hand, the first Cluster is formed by old individuals highly affected by many diseases. On the other hand, the second Cluster is formed mainly by young individuals lowly affected by this study's health problems. Identifying COVID-19 correlated health conditions and the age of the most affected individuals is crucial to the correct handle of the pandemic.

Key words: Cluster, COVID-19, health condition, HJ-Biplot, ordination.

Introduction

Coronavirus disease 2019 (COVID-19) is a new viral disease that has started spreading from China to the rest of the world since the end of 2019, causing more than 962,600 deaths in approximately 215 countries and territories, as of September 20, 2020[1,2]. This viral disease, caused by the virus Severe Acute Respiratory Syndrome Coronavirus 2 (SARS-CoV-2) has been declared a pandemic by the World Health Organization in February 2020[2]. In this study, our purpose is to understand how health conditions such as Pneumonia, smoking Habits, Diabetes, Obesity, Chronic Obstructive Pulmonary Disease, Asthma, Immunosuppression, Hypertension, Cardiovascular Problems, Chronic Renal Insufficiency are related to COVID-19 disease. Also, we aim to ordinate the ages of individuals according to the impact of COVID-19 disease.

Previous studies performed using data sets from hospitals in Atlanta City and the Shanghai Municipality in the United States and China agrees that old age is a factor risk for COVID-19 condition[3–5].

As a methodology, we use the HJ-Biplot Multivariate Analysis Method. This technique provides a two-dimensional space, representing most of the information from the initial data set. The Biplot graph shows the relationship among variables, individuals, and the interactions among variables and individuals in the same reference system. Also, we use Cluster Analysis to discriminate groups of individuals.

The results exposed in this explanatory research may help policymakers in the government make better decisions regarding the management of the health crisis due to the COVID-19 pandemic. This, since we explicitly mention the characteristics of people most affected by this disease. This study case is of particular interest to Mexico since the mortality rate (deaths per 100 confirmed cases) in this country is 10.6%, the highest rate globally as of September 2020[6].

The paper is organized as follows. In section Materials and Methods, we describe the data and the multivariate methods used in this study. In section Results and Discussion, we present and interpret the results of applying the HJ-Biplot and Cluster methods on the data set. Finally, in section Conclusions, we state the reasoned judgments obtained from this study.

Materials and methods

Data General Description

The data set used in this study was obtained from the online page of the Government of Mexico[7]. This data source provides public information regarding COVID-19 spread in Mexico. In the original data set, 35 variables collect general information of 595917 individuals such as age, gender, nationality, previous diseases, previous contact with infected people, the Mexican province of residence, etc.

In this study, we consider only the variables that are related to diseases and other health conditions. In total, we use 12 variables, which are explained in Table 1. At the same time, we considered 12 groups of age to the analysis; the groups' characteristics are explained in Table 2.

Table 3 shows the number of positive infected people in each group for each variable. However, we see that these values change enormously along rows, and therefore multivariate analysis techniques would not allow us to interpret the data correctly. This problem is fixed by creating a relative data set, i.e., each element in the new Relative Data Set shows the proportion between the number of positive cases and the number of patients for each group and variable. The data set containing the relative values is shown in Table 4.

[1] Universidad Católica de Oriente, Grupo de investigación Limnología y Recursos Hídricos, Rionegro, Colombia.

Corresponding author: yaquelin.puchades@inicasc.azcuba.cu.

Variable	Description
PNEUM	Pneumonia
COV19	COVID-19
SMOK	Smoking habits
DIAB	Diabetes
OBES	Obesity
COPD	Chronic obstructive pulmonary disease
ASTH	Asthma
INMUS	Immunosuppression
HYPERT	Hypertension
CARDV	Cardiovascular problems
CRIN	Chronic Renal Insufficiency
OTHER	Other Health complications

Table 1. Variables Description.

Groups	The Age range of patients
G1	0 - 9
G2	10 - 19
G3	20 - 29
G4	30 - 39
G5	40 - 49
G6	50 - 59
G7	60 - 69
G8	70 - 79
G9	80 - 89
G10	90 - 99
G11	100 - 109
G12	110 - 120

Table 2. Groups Description.

GROUP	PNEUM	COV19	SMOK	DIAB	OBES	COPD	ASTH	INMUS	HYPERT	CARDV	CRIN	OTHER	Total
G1	2015	2425	69	62	180	21	349	493	79	284	57	839	12860
G2	913	1840	432	138	885	24	729	449	143	131	167	545	16050
G3	4381	30733	8398	3167	9330	171	3205	752	2059	582	762	1597	85967
G4	9542	51499	12538	4646	20233	366	4451	1230	7012	1057	1241	2976	127045
G5	14674	52188	9369	12719	22562	784	5906	1505	16277	1651	1527	3241	114720
G6	18226	43380	6524	18583	17495	1445	2281	1528	22491	2203	2269	2695	81251
G7	16091	26797	3944	15529	9168	1959	1131	1286	18706	2371	2297	1934	45973
G8	10209	13832	2272	8689	3912	2080	495	746	11914	2083	1414	1257	23104
G9	4575	5234	930	3051	1197	1333	204	284	5199	1205	593	701	9730
G10	772	821	152	391	120	318	37	55	885	241	93	134	1844
G11	34	36	5	11	5	13	2	3	23	5	6	4	97
G12	1	5	1	1	2	0	0	0	1	0	0	0	18

Table 3. Absolute values Table.

GROUP	PNEUM	COV19	SMOK	DIAB	OBES	COPD	ASTH	INMUS	HYPERT	CARDV	CRIN	OTHER
G1	15,67	18,86	0,54	0,48	1,4	0,16	2,71	3,83	0,61	2,21	0,44	6,52
G2	5,68	30,14	2,69	0,86	5,51	0,15	4,54	2,8	0,89	0,82	1,04	3,39
G3	5,1	35,75	9,77	1,36	10,85	0,2	3,73	0,87	2,4	0,68	0,89	1,86
G4	7,51	40,54	9,87	3,66	15,93	0,29	3,5	0,97	5,52	0,83	0,98	2,34
G5	12,79	45,49	8,17	11,09	19,67	0,68	3,4	1,31	14,19	1,44	1,33	2,83
G6	21,64	51,48	7,75	22,06	20,77	1,72	2,71	1,81	26,7	2,62	2,69	3,2
G7	35	58,29	8,58	33,78	19,94	4,26	2,46	2,8	40,69	5,16	5	4,21
G8	44,19	59,87	9,83	37,61	16,93	9	2,14	3,23	51,57	9,02	6,12	5,44
G9	47,02	53,79	9,56	31,36	12,3	13,7	2,1	2,92	53,43	12,38	6,09	7,2
G10	41,87	44,52	8,24	21,2	6,51	17,25	2,01	2,98	47,99	13,07	5,01	7,27
G11	35,05	37,11	5,15	11,34	5,15	13,4	2,06	3,09	23,71	5,15	6,19	4,12
G12	5,56	27,78	5,56	5,56	11,11	0	0	0	5,56	0	0	0

Table 4. Relative values Table.

HJ-Biplot Method

Biplot is a multivariate analysis technique developed by Gabriel 1971[8]. This method permits the representation of X ($I*J$ data matrix) in a low dimensional space facilitating its interpretation. This procedure is accomplished by the simultaneous representation of row and column markers *a1,a2,...al* and *b1,b2,...bl* respectively. These row and column markers are obtained with help of the Singular Value Decomposition (SVD) of the data matrix X. Thus, we write:

$$X = UDV^T, \quad (1)$$

Where U is the matrix whose columns are the eigenvectors of XX^T,D is the matrix whose diagonal elements contain the singular values of X in decreasing order, and V is the matrix whose columns are the eigenvectors of X^TX. Then, we choose A(*I*S matrix*) and B(*S*J matrix*) such that:

$$X = AB = UDV^T, \quad (2)$$

And the X_{ij} element of X is approximately the inner product of the *i*-th row marker and the *j*-th column marker. The most used biplots are GH-Biplot where $A = U$ and, $B^T = VD$ and JK-Biplot where $A = UD$ and $B^T = V$. Galindo 19869 proposed a new biplot, known as the HJ-Biplot where A= UD and BT=V. In this case, the inner product of the *i*-th row marker and the *j*-th column marker do not coincide with the X_{ij} element of X.

In the current project, we use the HJ-Biplot method with Singular Value Decomposition. In this reference system, rows and columns in X are illustrated with the highest quality of representation. In the HJ-Biplot case, the properties of row markers are similar to those in the JK-Biplot, and the properties of the column markers are similar to those in the GH-Biplot[10,11].

Properties of the HJ-Biplot

1. Both Row and Column markers are represented simultaneously in a Euclidean space with the same highest representation quality.
2. The scalar product of the columns of X is equal to the scalar product of the column markers.
3. The scalar product of the rows in X is equal to the scalar product of the row markers.

$$X^TX = (UDV^T)^T(UDV^T) = BB^T. \quad (3)$$

4. The length of the vector representing the variable X_j is proportional to the variance of that variable.

$$XX^T = (UDV^T)(UDV^T)^T = AA^T. \quad (4)$$

5. The cosine of the angle between two vectors b_j and b_j representing the variables X_i and X_j respectively is proportional to the correlation between those variables.

6. The Mahalanobis distances between individuals are interpreted as inverse similarities. Hence, these distances are approximated by the row markers' Euclidean distances (representing the groups of age). Hence, where Σ is an estimate of the corresponding variance-covariance matrix.

$$(x_i - x_j)^T \hat{\Sigma} (x_i - x_j) \approx (a_i - a_j)^T (a_i - a_j), \quad (5)$$

7. The projections of row markers (points) onto the column markers (arrows) allow individuals' ordination regarding its value in the variables.

Graphical interpretation of HJ-Biplot

For column markers

The length of a column marker (vector) b_j representing the variable X_j is proportional to the variance of that variable; in this sense, longer column vectors show greater variance than shorter column vectors. Also, the cosine of the angle between the column vectors b_j and b_j approximate the correlation between the variables X_i and X_j. Therefore, vectors forming angles less than 90o justify a high positive correlation between the represented variables; 90o or close angles show that there is no correlation; 180o or close angles evidence a high negative correlation between variables X_i and X_j.

For row markers

The distance between row markers (points) represents an inverse similarity because closer individuals are more similar than the distant ones. This property allows the formation of clusters of individuals in our graph.

For projections of row markers onto column markers

The order of the projections of row markers (points) onto column markers (arrows) approximates each individual's value onto that variable. Hence, the values of the individuals whose projections fall near to the origin are close to the mean value of that variable. The values of the individuals whose projections fall away from the origin and in the same direction of the column marker are large. The values of the individuals whose projections fall away from the origin but on the other direction of the column marker are small.

Since biplots' characteristics allow researchers in different fields to interpret high dimensional sets of data, it has been used in enology, mycology, image analysis, genetics, hydrology, botany, decision theory, library science, and ecology. Specifically, the HJ-Biplot method has been applied in immunology, entomology, enology, geology, marine biology, and sociology. A more exhaustive review of HJ-Biplot applications can be found in Nieto 2014[11]. Some recent applications of the HJ-Biplot method are found in Serafim 2013[10]; Gallego-Álvarez 2015[12]; Delgado-Álvarez 2015[13]; Patino-Alonso 2015[14]; Hernández-Suárez 2016[15]; Ruiz 2018[16]; Oliveira-Da Silva 2019[17]; and Jaramillo-Feijoo 2020[18].

Hierarchical clustering

Cluster analysis is a set of numeric techniques that create clusters or groups of elements with similar characteristics[19]. In hierarchical clustering, the elements are grouped following some steps that may start from a cluster for each of the classified elements and end up with a single cluster containing all the elements. Hierarchical methods are classified as agglomerative and divisive techniques. Some agglomerative hierarchical clustering methods are average linkage, complete linkage, single linkage, ward linkage, weighted linkage, median linkage, and centroid linkage, all operating similarly[20,21]. Each of these techniques has a cophenetic matrix and a dendrogram (or tree diagram) associated. One way to compare these methods' performance is by contrasting the cophenetic correlation coefficient (CPCC) obtained from each matrix. In this sense, the best hierarchical clustering method is the one with the highest CPCC. Previous studies have shown that the average and centroid linkage methods with Euclidean distance measure are the best techniques for hierarchical agglomerative clustering[21].

Another relevant aspect of hierarchical clustering is the number of clusters to be chosen. In this regard, the number of clusters is determined using the dendrogram. Hence, we place a line at a certain height of the dendrogram identifying the number of clusters formed below. To place the line (or best cut) at the most convenient height on the dendrogram, some researchers have proposed methods such as the static tree cut, dynamic tree cut, and others[20-23]. However, there is not a fixed criterion regarding which method gives the appropriate number of clusters. Oldham 2006 has shown that the static tree cut method is the most helpful technique in a hierarchical configuration[24]. The static tree cut technique proposes the line's placement on the dendrogram at the most significant space between two fusion levels (the heights in the dendrogram where the clusters form)[20]. In our dendrogram, we place the line approximately at the height of 4.5. This, since between the two fusion levels close to the heights 4 and 5, there are no changes in the number of clusters. In this way, we differentiate 2 clusters. Further applications of clusters are detailed in Everitt 2011[20]. Some recent uses of cluster analysis are found in Serafim 2013[10]; Patino-Alonso 2015[14]; Jaramillo-Feijo 2020[18]; and Zhang 2020[25].

Results and Discussion

In this exploratory study, we have started with a data set of 35 variables and 595917 individuals. Then, we have focused on 12 variables related to diseases and health conditions, including COVID-19. Also, we have classified the individuals into 12 different groups according to age. Both variables and group details are shown in Tables 1 and 2, respectively. After that, we have created a table of relative values (Table 4) used in the MultBiplot statistical software[26]. The results of this application are presented and discussed below.

In Table 5, we present the eigenvalues, inertias, and cumulative inertias for our HJ-Biplot. We see that our matrix X is well represented by the first two axes accounting for 82.17% of the total inertia.

In Figure 1, we have the HJ-Biplot representation of the groups and variables on the same reference system through the row and column markers. In this two-dimensional plot, we consider the relative values (Table 4) instead of the absolute ones (Table 3). Moreover, we discriminate the groups of individuals with two clusters using the average linkage hierarchical clustering method (CPCC = 0.7729) which has proven to be better than centroid linkage (CPCC = 0.7694), complete linkage (CPCC = 0.7663), median linkage (CPCC = 0.7556), ward linkage (CPCC = 0.7534), weighted linkage (CPCC = 0.7253),

and single linkage (CPCC = 0.6729) methods. The number of clusters is obtained with the use of the static tree cut method. Hence, in Figure 2, we see the dendrogram with the corresponding best cut (red line) at the height of 4.5, evidencing the formation of two clusters.

We consider that a marker has a sufficiently high quality of representation on this graph if its value is more significant than half of the value of the best-represented column or row marker[27]. From this perspective, in Table 6, we have the quality of representation of each axis's variables. On the one hand, we see that the correctly interpreted variables are PNEUM, COV19, SMOK, DIAB, OBES, COPD, INMUS, HYPERT, CARDV, CRIN, and OTHER since they meet our criteria for a sufficiently high quality of representation. On the other hand, the variable ASTH does not achieve a sufficiently high quality of representation, and therefore we cannot interpret this variable in our two-dimensional space.

Also, in Table 7, we show the quality of representation of each group on the plot. Following the same criteria as before we see that all groups have a high quality of representation on this plot. This leads us to a correct interpretation of all groups in two dimensions.

By the HJ-Biplot properties mentioned above, the variables represented by vectors forming angles close to 0° among them are positively highly correlated. For example, the variable COV19 has a strong positive correlation with HYPERT, DIAB, SMOK, and OBES. Similarly, we find other correlated variables such as INMUS and OTHER; SMOK and OBES; COPD, CARDV, PNEUM, CRIN, HYPERT, and DIAB. Whereas the variables forming angles close to 180° are negatively highly correlated. For instance, INMUS and OBES. Meanwhile, the variables represented by vectors forming angles close to 90° among them are minor or uncorrelated. For instance, the variable COV19 has a small or no correlation with the variables INMUS and OTHER. Other examples of uncorrelated variables are INMUS and DIAB; COPD and OBES; COPD and SMOK; CARDV and OBES; CARDV and SMOK; PNEUM and OBES; PNEUM and SMOK; CRIN and OBES; CRIN and SMOK; HYPERT and OBES. Recall that the variable ASTH cannot be correctly interpreted in this biplot.

Also, by the previously mentioned properties, the vectors' length representing the variables approximate its variance. Therefore, INMUS, OTHER, COPD, CARDV, PNEUM, CRIN, HYPERT, DIAB, COV19, SMOK, and OBES have similar variances.

The arrangement of groups (individuals) in the factorial plane is also interpreted, given the HJ-Biplot properties. Figure 1 evidences the presence of two clusters. Cluster 1 (right side of the graph) comprises older adults G6, G7, G8, G9, G10, and G11. Cluster 2 (left side of the graph) comprises young indivi-

Axis	Eigenvalue	Inertia	Cumulative Inertia
1	77.51	58.73	58.73
2	30.94	23.44	82.18
3	13.00	9.85	92.02
4	6.40	4.85	96.87
5	2.84	2.15	99.03
6	0.67	0.51	99.53
7	0.55	0.42	99.95
8	0.06	0.04	99.99
9	0.01	0.01	100.00
10	0.00	0.00	100.00
11	0.00	0.00	100.00
12	0.00	0.00	100.00

Table 5. Eigenvalues, Inertias, and Cumulative Inertias of HJ-Biplot.

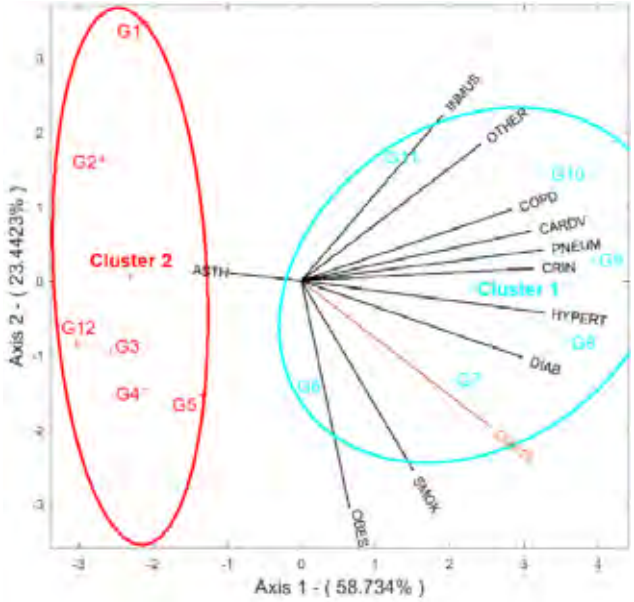

Figure 1. HJ-Biplot of groups and variables.

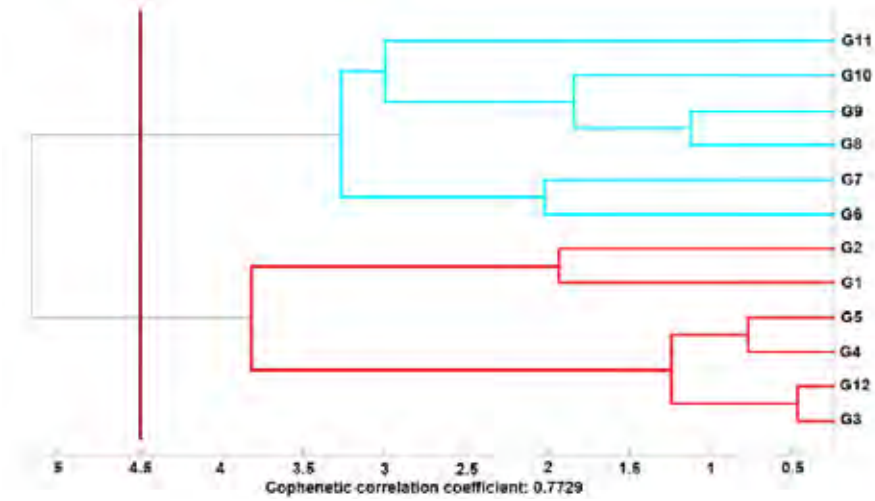

Figure 2. Dendrogram of the hierarchical Cluster with average linkage.

Variables	Axis 1 (%)	Axis 2 (%)	Total (%)
PNEUM	97.1	1.6	98.7
COV19	59.0	35.1	94.1
SMOK	20.7	59.3	80.0
DIAB	81.4	9.7	91.1
OBES	3.8	85.0	88.8
COPD	73.5	8.4	81.9
ASTH	8.6	0.1	8.7
INMUS	33.2	45.4	78.6
HYPERT	96.9	1.6	98.5
CARDV	87.5	4.1	91.6
CRIN	89.6	0.2	89.8
OTHER	53.3	30.8	84.1

Table 6. Quality of representation for variables.

Groups	Axis 1 (%)	Axis 2 (%)	Total (%)
G1	24.9	67.0	91.9
G2	58.8	21.8	80.6
G3	70.9	9.7	80.6
G4	58.8	27.8	86.6
G5	37.0	48.7	85.7
G6	0	76.2	76.2
G7	56.2	24.6	80.8
G8	91.8	4.8	96.6
G9	97.1	0.4	97.5
G10	72.9	14.6	87.5
G11	17.0	45.2	62.2
G12	48.8	3.8	52.6

Table 7. Quality of representation for groups.

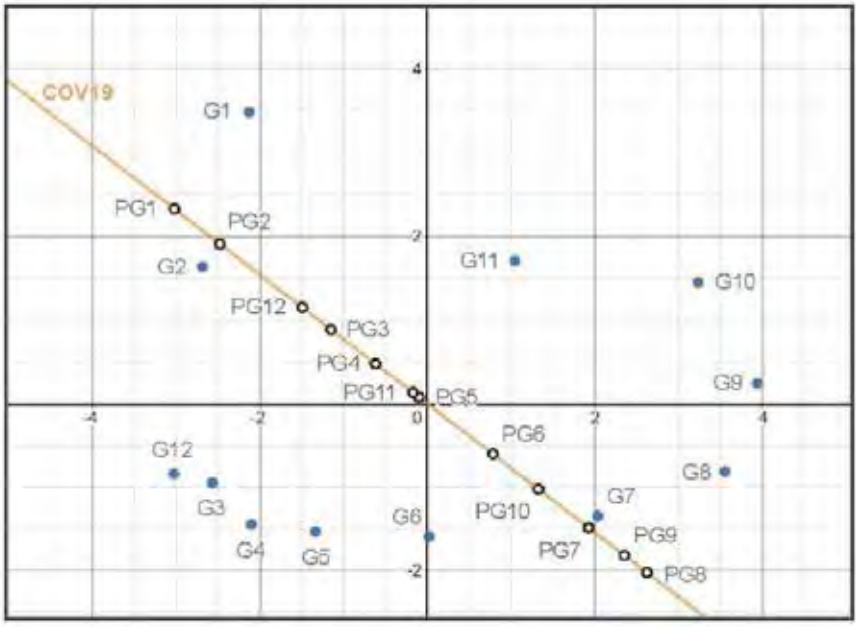

Figure 3. Projections of groups onto the variable COV19.

duals G1, G2, G3, and G4. The groups G3, G4, and G5 are closer than other groups indicating a similar behavior regarding the studied variables.

In Figure 3, we see the projections of the groups (individuals) onto the vector of the variable COV19, which is one of the main motivations for our study. In this graph, the projections are labeled with the group's name, preceded by the letter "P" (for example, PG1 is the projection of G1 onto the column marker COV19). We observe an ordination of the projections onto the variable COV19 according to the values these groups have in that variable. On the one hand, we observe that most of the proportion of patients affected by COVID-19 are in the groups G7, G8, and G9, i.e., 60 to 89 years old. On the other hand, the minor proportion of people affected by this disease are in the groups: G1 and G2, i.e., they are 0 to 19 years old. The groups G1, G2, G12, G3, G4, and G5 have low values on the variables COPD, CARDV, PNEUM, CRIN, HYPERT, DIAB, and COV19. While the groups G7, G8, G9, and G10 have high values on the same variables. These results are concordant with other investigations reported in Killerby 2020[3]; Li 2020[4]; The Novel Coronavirus Pneumonia Emergency Response Epidemiology Team 2020[5]. A similar analysis can be performed with the rest of the groups and variables plotted in our graph.

Conclusions

The HJ-Biplot application to our data set is helpful because of its visual interpretability. This feature allows the visual exploration and analysis of correlations among the variables associated with diseases and other health conditions and reflects the information of these variables in relation to each group. It also makes an ordination of groups according to its value in each variable. Moreover, the quality of representation of column and row markers on this biplot is high. This, since all groups and 11 out of 12 variables are highly represented on this graph.

We find that patients affected by the COVID-19 disease share some common characteristics. For example, we see that people that get sick with the COVID-19 disease are also affected by Hypertension, Diabetes, smoking habits, and the Obesity health condition. Additionally, the age of the patients plays

an important role, being it another critical characteristic. In this sense, the groups' ordination over the variable of COVID-19 shows that the most affected patients are 60 to 89 years old and that the less affected individuals are 0 to 19 years old. Furthermore, the configuration of groups on this biplot shows two main clusters. We see that most of the first Cluster groups represent older people while most of the second Cluster groups represent young patients.

There are other relations among variables and among groups and other interactions among variables and groups that result from this study. These relationships are interpreted similarly. For instance, in this two-dimensional space, we find a correlation among variables representing Chronic Obstructive Pulmonary Disease, Cardiovascular problems, Pneumonia disease, Chronic Renal Insufficiency, Hypertension, and Diabetes. Also, regarding the ordination of groups over the variables, we see that most of the groups representing young people have low values on the previously indicated variables, while groups representing older adults have high values on the same variables. In general, these findings suggest that older individuals are more related to the diseases and health conditions mentioned earlier than younger people.

The results presented in this explanatory paper state a precedent for future investigations from a medical approach. Specifically, it is necessary to investigate the implications of the different grades of correlation among variables, groups, and between variables and groups. Another improvement for this paper could be acquired by using variables representing other relevant health conditions.

Bibliographic references

1. Worldometer. Coronavirus Cases [Internet]. Worldometer. 2020 [cited 2020 Sep 20]. p. 1–22. Available from: https://www.worldometers.info/coronavirus/?
2. World Health Organization. Report of the WHO-China Joint Mission on Coronavirus Disease 2019 (COVID-19) [Internet]. Vol. 1, The WHO-China Joint Mission on Coronavirus Disease 2019. 2020. Available from: https://www.who.int/docs/default-source/coronaviruse/who-china-joint-mission-on-covid-19-final-report.pdf
3. Killerby ME, Link-Gelles R, Haight SC, Schrodt CA, England L, Gomes DJ, et al. Characteristics Associated with Hospitalization Among Patients with COVID-19-Metropolitan Atlanta, Georgia, March-April 2020 [Internet]. Metropolitan Atlanta, Georgia; 2020 Jun [cited 2020 Aug 11]. Available from: https://www.cdc.gov/coronavirus/2019-ncov/hcp/infection-control-
4. Li X, Xu S, Yu M, Wang K, Tao Y, Zhou Y, et al. Risk factors for severity and mortality in adult COVID-19 inpatients in Wuhan. J Allergy Clin Immunol [Internet]. 2020 July 1 [cited 2020 August 11];146(1):110–8. Available from: https://www.sciencedirect.com/science/article/pii/S0091674920304954
5. The Novel Coronavirus Pneumonia Emergency Response Epidemiology Team. The Epidemiological Characteristics of an Outbreak of 2019 Novel Coronavirus Diseases (COVID-19) — China, 2020. China CDC Wkly [Internet]. 2020 Feb 1 [cited 2020 Sep 20];2(8):113–22. Available from: http://weekly.chinacdc.cn/en/article/doi/10.46234/ccdcw2020.032
6. Johns Hopkins University. Mortality Analyses - Johns Hopkins Coronavirus Resource Center [Internet]. 2020 [cited 2020 Aug 2]. Available from: https://coronavirus.jhu.edu/data/mortality
7. Gobierno de México. Datos Abiertos de México - Información referente a casos COVID-19 en México - Bases de datos COVID-19 [Internet]. 2020 [cited 2020 Aug 2]. Available from: https://datos.gob.mx/busca/dataset/informacion-referente-a-casos-covid-19-en-mexico/resource/e8c7079c-dc2a-4b6e-8035-08042ed37165?inner_span=True
8. Gabriel KR. The biplot graphic display of matrices with application to principal component analysis. Biometrika [Internet]. 1971 Dec 1 [cited 2020 Sep 14];58(3):453–67. Available from: https://academic.oup.com/biomet/article/58/3/453/233361
9. Galindo M. Una alternativa de representación simultánea: HJ-Biplot [Internet]. 1986 [cited 2020 Aug 25]. p. 13–23. Available from: https://www.researchgate.net/publication/39430983_Una_alternativa_de_representacion_simultanea_HJ-Biplot
10. Serafim A, Company R, Lopes B, Silva N, Castela E, Bebianno MJ, et al. Profile analysis of mothers susceptible to contaminant exposure in the Algarve region: Application of the HJ-BIPLOT method. Biometrical Lett [Internet]. 2013 Aug 19 [cited 2020 Sep 14];49(1):57–66. Available from: https://content.sciendo.com/view/journals/bile/49/1/article-p57.xml
11. Nieto AB, Galindo MP, Leiva V, Vicente-Galindo P. Una metodología para biplots basada en bootstrapping con R. Rev Colomb Estad. 2014;37(2):367–97.
12. Gallego-Álvarez I, Galindo-Villardón MP, Rodríguez-Rosa M. Analysis of the Sustainable Society Index Worldwide: A Study from the Biplot Perspective. Soc Indic Res. 2015;120(1):29–65.
13. Delgado Álvarez JF, Villardon PG. A proposal for spatio-temporal analysis of traffic matrices using HJ-biplot. 2015 IEEE Int Work Meas Networking, M N 2015 - Proc. 2015;(1):88–93.
14. Patino-Alonso MC, Recio-Rodríguez JI, Magdalena-Belio JF, Giné-Garriga M, Martínez-Vizcaino V, Fernández-Alonso C, et al. Clustering of lifestyle characteristics and their association with cardio-metabolic health: The Lifestyles and Endothelial Dysfunction (EVIDENT) study. Br J Nutr. 2015 Aug 13;114(6):943–51.
15. Hernández Suárez M, Molina Pérez D, Rodríguez-Rodríguez E, Díaz Romero C, Espinosa Borreguero F, Galindo-Villardón P. The Compositional HJ-Biplot—A New Approach to Identifying the Links among Bioactive Compounds of Tomatoes. Int J Mol Sci [Internet]. 2016 Nov 2 [cited 2020 Sep 16];17(11):1828. Available from: http://www.mdpi.com/1422-0067/17/11/1828
16. Ruiz NC, Egido J, Galindo-Villardón P, Del-Río P. Advantages of using HJ-Biplot analysis in executive functions studies. Psicol Teor e Pesqui. 2018;34:1–8.
17. Oliveira Da Silva A, Freitas A. The HJ-Biplot Visualization of the Singular Spectrum Analysis Method. 2019.
18. Jaramillo Feijo LE, Galindo Villardon MP, Real Cotto JJ. Análisis clúster para big data: una aplicación con variables demográficas en provincias del Ecuador Cluster analysis for big data: an application with demographic variables in provinces of Ecuador. Vol. 6, J. health med. sci. 2020.
19. Everitt BS, Hothorn T. A handbook of statistical analyses using R. 2nd ed. 2010.
20. Everitt BS, Landau S, Leese M, Stahl D. Cluster Analysis. 2011.
21. Saraçli S, Do- an N, Do- an I. Comparison of hierarchical cluster analysis methods by cophenetic correlation. J Inequalities Appl [Internet]. 2013 Apr 23 [cited 2020 Sep 24];2013(1):1–8. Available from: https://link.springer.com/articles/10.1186/1029-242X-2013-203
22. Milligan GW, Cooper MC. An examination of procedures for determining the number of clusters in a data set. Psychometrika [Internet]. 1985 Jun [cited 2020 Sep 25];50(2):159–79. Available from: https://link.springer.com/article/10.1007/BF02294245
23. Langfelder P, Zhang B, Horvath S. Defining clusters from a hierarchical cluster tree: The Dynamic Tree Cut package for R. Bioinformatics [Internet]. 2008 Mar 1 [cited 2020 Sep 25];24(5):719–20. Available from: https://academic.oup.com/bioinformatics/article/24/5/719/200751
24. Oldham MC, Horvath S, Geschwind DH. Conservation and evolution of gene coexpression networks in human and chimpanzee brains. Proc Natl Acad Sci U S A [Internet]. 2006 Nov 21 [cited 2020 Sep 25];103(47):17973–8. Available from: www.pnas.orgcgidoi10.1073pnas.0605938103
25. Zhang J, Cao Y, Tan G, Dong X, Wang B, Lin J, et al. Clinical, radiological, and laboratory characteristics and risk factors for severity and mortality of 289 hospitalized COVID- 19 patients. Allergy [Internet]. 2020 Aug 24 [cited 2020 Sep 19];all.14496. Available from: https://onlinelibrary.wiley.com/doi/abs/10.1111/all.14496

26. José Luis Vicente Villardón. MULTBIPLOT: A apackage for Multivariate Analysis using Biplots. [Internet]. 2016. Available from: http://biplot.usal.es/ClassicalBiplot/index.html
27. González Cabrera JM, Fidalgo Martínez MR, Martín Mateos EJ, Vicente Tavera S. Study of the evolution of air pollution in Salamanca (Spain) along a five-year period (1994-1998) using HJ-Biplot simultaneous representation analysis. Environ Model Softw. 2006 Jan 1;21(1):61–8.

Received: 10 November 2020
Accepted: 15 February 2021

RESEARCH / INVESTIGACIÓN

A Spatio-temporal distribution analysis of vesicular stomatitis outbreak in Ecuador, 2018

María Teresa Salinas[1], Euclides José De La Torre[2], Paola Katerine Moreno[3], Andrés Alejandro Vaca[3] and Rubén Alexander Maldonado[4]

DOI. 10.21931/RB/2021.06.02.19

Abstract: Vesicular stomatitis (VS) is a viral disease primarily affecting cattle, swine, and equine causing economic losses. It is of particular interest because its outward signs are similar to those of foot-and-mouth disease. Outbreaks of VS occurred in several herds in Ecuador in 2018, affecting principally bovines. In this sense, the present study was conducted to characterize the temporal and spatial dynamics of Vesicular stomatitis occurrence between January and December 2018. During the study period, 583 animals with symptoms of VS were reported. In this way, tissue samples were collected, VS was diagnosed, and outbreaks were defined as herds with a confirmed positive test for the disease. Outbreaks were georeferenced, and Space-time clusters were used to determine zones where the number of reported outbreaks was more significant than expected. A space-time permutation scan statistic (STPSS) was used to identify hot spots of space-time interaction within patterns of the cases reported. Standard Monte Carlo Critical Value was used to test for the cluster's significance. A total of 399 outbreaks were presented in 18 provinces. Spatial scan statistics allowed the detection of four significant space-time clusters of VS outbreaks. The highest incidence was reported around week 35 and week 44, which were observed outbreaks increase in the country's north region. In this sense, clusters coincided with the areas with the highest incidence of outbreaks. Besides, maps showed places where the disease is not shared. The information showed in the present study may contribute to prevents VS spread into regions of Ecuador that is only sporadically affected by the disease. Monitoring in affected zones may lead to quick responses to possible outbreaks issuing alerts when there is a greater than typical risk of spreading the disease.

Key words: Spatio-temporal analysis, outbreak, vesicular stomatitis virus.

Introduction

Spatio-temporal is a type of clustering in which data values, including the time dimension, are introduced into spatial data. Accordingly, the objects are grouped as per their spatial and temporal similarity[1]. Vesicular stomatitis (VS) is a disease of livestock commonly observed in adult animals caused by vesicular stomatitis virus (VSV) belonging to *Rhabdoviridae*, genera *Lyssavirus* and *Vesiculovirus*[2,3]. VSV affects cattle, swine, and equine. However, it also can affect sheep, goats, camelids, and buffalo. Natural infection in sheep and goats is rare but has been demonstrated in experimental conditions. The incubation period is between 2 to 8 days. The morbidity rate varies from 5 up to 90 percent[4]. How VS spreads is not fully understood; once the disease is introduced into a herd, it may move from animal to animal. VSV's can spread quickly under natural conditions. The most common transmission routes are vector-borne, direct contact, or exposure to saliva or fluid from ruptured vesicles[5]. However, the virus can infect animals by the transcutaneous or transmucosal route[6]. VSV has an important economic impact resulting in quarantine, animal movement restrictions, and decreases in meat and milk production[7]. Also, VSV denotes extensive regulatory responses by government agencies, including trade restrictions and market closures[8]. For this reason, it has become a disease of interest. Its clinical signs are similar to those of foot-and-mouth disease, vesicular exanthema of swine, or swine vesicular disease. However, generally less severe[9,10]. There are two serotypes of VSV, Vesicular stomatitis New Jersey (VSV-NJ) and Vesicular stomatitis Indiana (VSV-IND). Both serotypes have similar morphological characteristics and pathology with the difference of the neutralizing antibodies generation in infected animals[11]. Indiana serotype is subtyped serologically into 3 groups. VSV-IND belongs to the Indiana 1 subtype, Cocal virus to the Indiana 2 subtype, and VSV-AV to Indiana 3. Deaths are sporadic in cattle and horses, but higher mortality is observed with VSV-NJ infection in swine[12]. Confirmed VSV infection is limited to the Americas. The virus is thought to have originated in equatorial America and spread north during two separate colonizing events[3]. This disease is seasonal, although cases may occur throughout the year. Outbreaks caused by VSV-NJ or VSV-IND usually occur each year. They are particularly common at the end of the rainy season or early in the dry season. In endemic areas, both explosive epidemics and outbreaks of slow dissemination can be seen with a relatively small number of cases[11]. Specifically, VSV-NJ and IND-1 are endemic in Ecuador and other countries in South America[3]. The samples used for diagnosis include vesicle fluid, epithelium covering unruptured vesicles, or epithelial flaps of freshly ruptured vesicles. Recommended tests by World Organization for Animal Health for vesicular stomatitis include IS-ELISA (Indirect Sandwich), CFT (Complement Fixation test), RT-PCR (Reverse transcriptase-polymerase chain reaction), LP-ELISA (liquid phase blocking ELISA), c-ELISA (competitive ELISA), and V.N. (virus neutralization)[13]. In 2018, an outbreak of Vesicular stomatitis in Ecuador occurred. The outbreaks distribution included 18 provinces in which different livestock premises were investigated. Therefore, this study aimed to characterize the temporal-spatial distribution of Vesicular stomatitis outbreaks reported in Ecuador in 2018.

[1] Laboratorio de Virología. Agencia de Regulación y Control Fito y Zoosanitario – Agrocalidad, Pichincha, Ecuador.
[2] Dirección de Diagnóstico Animal. Agencia de Regulación y Control Fito y Zoosanitario – Agrocalidad, Pichincha, Ecuador.
[3] Dirección de Control Zoosanitario. Agencia de Regulación y Control Fito y Zoosanitario – Agrocalidad, Pichincha, Ecuador.
[4] Laboratorio de Cultivo Celular. Agencia de Regulación y Control Fito y Zoosanitario – Agrocalidad, Pichincha, Ecuador.

Corresponding author: ruben.maldonado@agrocalidad.gob.ec

Methods

Animal samples

Tissue samples (vesicles or lesions on the inner surfaces of the foot, lips, tongue, udder, gums, and dental pad) (n=583) were collected by field technicians as information about the suspected animals. VS was diagnosed through *IS-ELISA Differential Typing Kit* (PANAFTOSA-OPAS/OMS) (n=568). Molecular diagnosis (n=15) was performed using *Transcriptor First Strand cDNA Synthesis Kit* (Roche) and *GoTaq® Hot Start Green Master Mix* (Promega Corporation). The diagnosis was performed at the Animal Diagnosis Laboratories at Agrocalidad.

Data collection

Information and laboratory results corresponding to all livestock premises attended for VS between January and December 2018 were registered in databases. The information registered for each outbreak included: identification of cases and samples, date of the case reported, animal species, livestock premise activity, geographic location, number of samples collected, and diagnosis results.

Outbreak information

Outbreaks were assumed to have started on the date when clinical signs compatible with VS were first observed in the herd and were notified to the agency. Cases were defined as animals with compatible clinical signs of VS. Outbreaks were defined as herds with at least 1 animal with a confirmed positive test result for VSV. Livestock premises, where results were negative for testing, were considered negative for VSV infection. Cases were aggregated into 7-day groups to account for week variations. These variations were based on calendar week. Each outbreak was georeferenced using the geographic coordinates of the herd and QGIS software. To analyze outbreaks, these were georeferenced by use of the centroid of the municipalities. The centroid data were obtained from databases of the Instituto Geografico Militar - IGM. Outbreaks caused by VSV-NJ and VSV-IND were used in the analyses reported here.

Data analysis and Spatio-temporal distribution

The space-time was analyzed using SaTScan software, in which the number of cases was compared to the expected cases of outbreaks within each cluster. Outbreaks were mapped using the same software. Space-time clusters were used to determine zones where the number of reported outbreaks was more significant than expected based on the population size. A space-time permutation scan statistic (STPSS) was used to identify hot spots of space-time interaction within patterns of the cases reported. In this sense, a retrospective Space-Time analysis was used for clusters with high rates. Standard Monte Carlo Critical Value was used to test for the cluster's significance. The clusters were determined as statistically significant when its test statistic was greater than the critical value, which is the significance level ($P<0.001$).

Results

Cases started from January 5th through December 19th, 2018. During this period, 583 cases from different livestock premises were reported to Agrocalidad in different provinces. Cases were presented as follows: 561 cattle, 11 equines, 8 swine, and 3 caprines. From the total presented cases, 399 (68.44%) were confirmed outbreaks with VS. In this regard, about 60% of the reported cases were confirmed outbreaks. There was an increase in the number of outbreaks starting in August that continued through November. Outbreaks were present in three regions of Ecuador (Highlands, Coast, and Amazon). Bovines were the most affected with 391 (98.00%) outbreaks, followed by 5 (1.25%), 2 (0.50%), and 1 (0.25%) outbreaks in swine, equines, and caprines, respectively. Outbreaks were presented in 18 provinces. Consequently, Santo Domingo was the province with the highest number of outbreaks, presenting 93 (23.31%) outbreaks to VS, followed by Imbabura 75 (18,80%) and Napo 65 (16.29%). The remaining 184 (31.56%) cases were confirmed as a negative for VS. Furthermore, Santo Domingo de Los Tsáchilas presented outbreaks in 61.11% of its municipalities, followed by Imbabura (57.14%), Pastaza (47.62%), and Napo (39.13%). The distribution and the total outbreaks per province and municipalities are detailed in Table 1, in which the distribution of outbreaks by quarter can be observed. Thereby it is possible to visualize the months that arose a significant increment thereof. For a better appreciation, the outbreaks distributed by quarters are shown in Figure 1. From 399 outbreaks, 372 (93.23%) belong to VSV-NJ, 22 (5.52%) belong to VSV-IND, and 5 (1.25%) presented results for both virus serotypes. The serotype which had prevailed for most of the provinces during the outbreak was VSV-NJ. For the other hand, VSV-IND serotype was located in Morona Santiago, Pastaza, Orellana, Sucumbíos, Zamora Chinchipe, Pichincha, Santo Domingo de Los Tsáchilas, Esmeraldas and Guayas provinces. The distribution map of the serotypes is shown in Figure 2. Heat maps (Figure 3) were provided by the Directorate of Zoosanitary Surveillance of Agrocalidad and represent the alert notifications for vesicular diseases; this means that vesicular stomatitis and other diseases are included in the maps. Thus, heat maps show the distribution of alert notifications of vesicular diseases presented in 2017 and 2018. There was an increase in the number of outbreaks starting in August (Week 31) that continued through the last week of November; in this period, 509 cases were reported of which 351 outbreaks were confirmed. After week 37 of the recorded outbreaks, it went 2 weeks before new outbreaks were recorded, and after that, it was never more than 1 week between a recorded outbreak and another recorded outbreak. The highest incidence was reported in week 44, in which 76 outbreaks from 114 cases were confirmed (Figure 4). Spatial scan statistics allowed the detection of four significant space-time clusters ($P < 0.001$) of VS outbreaks (Table 2). The circular base represents the significant clusters corresponding to the outbreaks' geographical area (Figure 5).

Discussion

Due to the increase of vesicular stomatitis outbreaks presented during 2018 in Ecuador, this study analyzed the reported cases. Our approach through Spatio-temporal analysis enabled us to determine the sites of the outbreaks which have epidemiological importance. Literature mention that space-time scan statistics allow identifying statistically significant hotspots. The hotspots are evaluated by a significance value[1] and are helpful for pattern understanding[14]. In this manner, the space-time scan statistic of this study identified the locations of the most-significant clusters.

Consequently, these clusters coincided with the areas with the highest incidence of the outbreaks. Thus, the study revealed that the increase in VS outbreaks reported during 2018, compared with cases in 2017, was associated with four significant

Province	Quarter				No. of municipalities	No. of municipalities with VSV outbreaks	Municipalities with VSV outbreaks (%)	VSV outbreaks per province (%)
	1st	2nd	3rd	4th				
Coast Region								
Esmeraldas			17	2	64	7	10.94	4.76
Guayas	2	4			54	2	3.70	1.50
Los Rios		1	7		28	4	14.29	2.01
Santo Domingo de Los Tsáchilas		3	80	10	18	11	61.11	23.31
Highlands Region								
Azuay		1			77	1	1.30	0.25
Carchi				25	32	10	31.25	6.27
Cotopaxi			15		40	7	17.50	3.76
Imbabura			4	71	42	24	57.14	18.80
Loja	2	3	2		92	7	7.61	1.75
Pichincha		2	36	1	60	11	18.33	9.77
Tungurahua	1				53	1	1.88	0.25
Amazon Region								
Morona Santiago				4	60	6	10.00	1.00
Napo	4			61	23	9	39.13	16.29
Orellana				10	33	8	24.24	2.51
Pastaza	3			18	21	10	47.62	5.26
Sucumbios	1			4	33	6	18.18	1.25
Zamora Chinchipe		2		3	36	5	13.89	1.25
Total	13	16	161	209	-	-	-	100.00

Table 1. Distribution of outbreaks of Vesicular stomatitis per municipality confirmed in Ecuador in 2018.

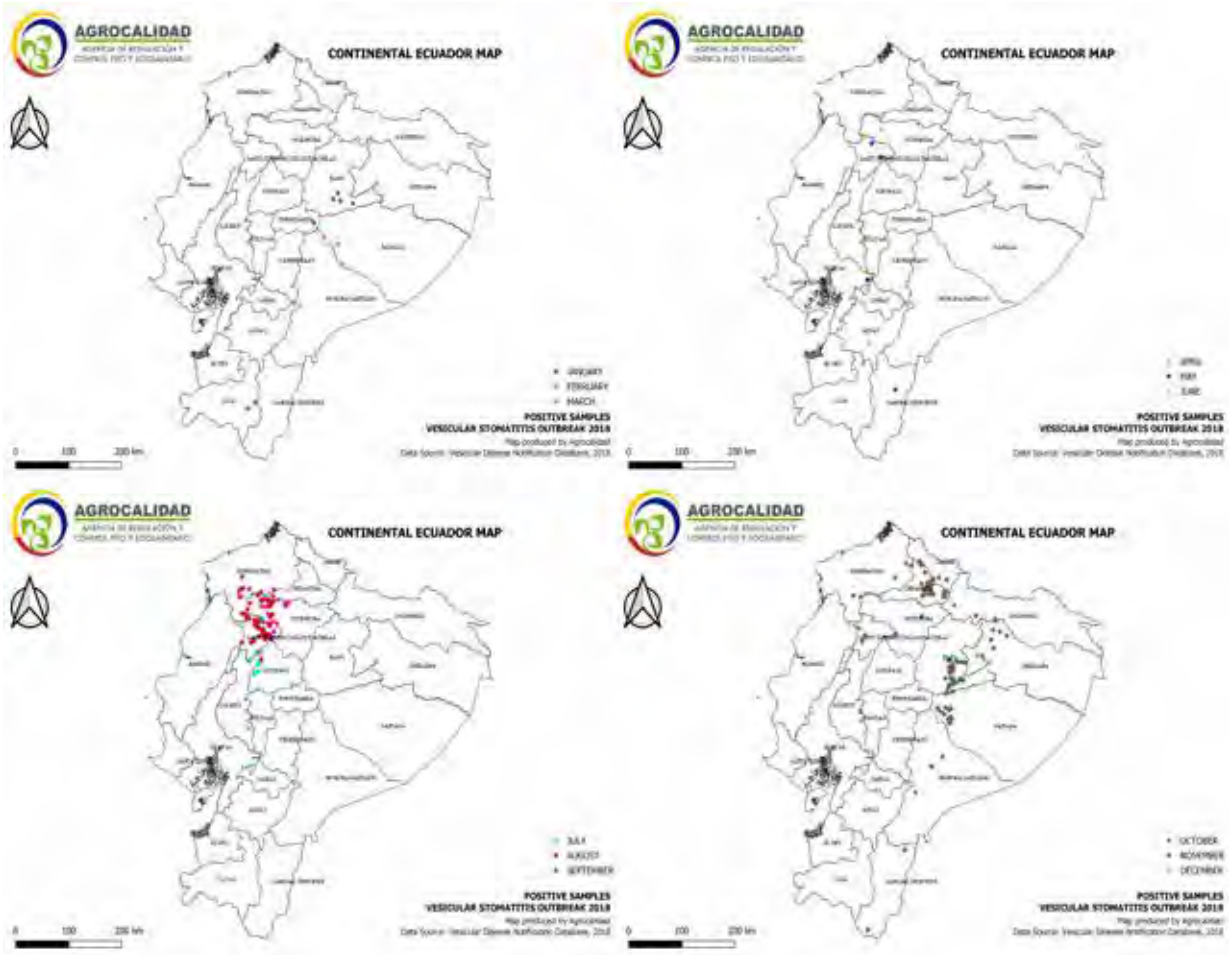

Figure 1. Distribution by quarters of outbreaks of Vesicular stomatitis confirmed in Ecuador in 2018.

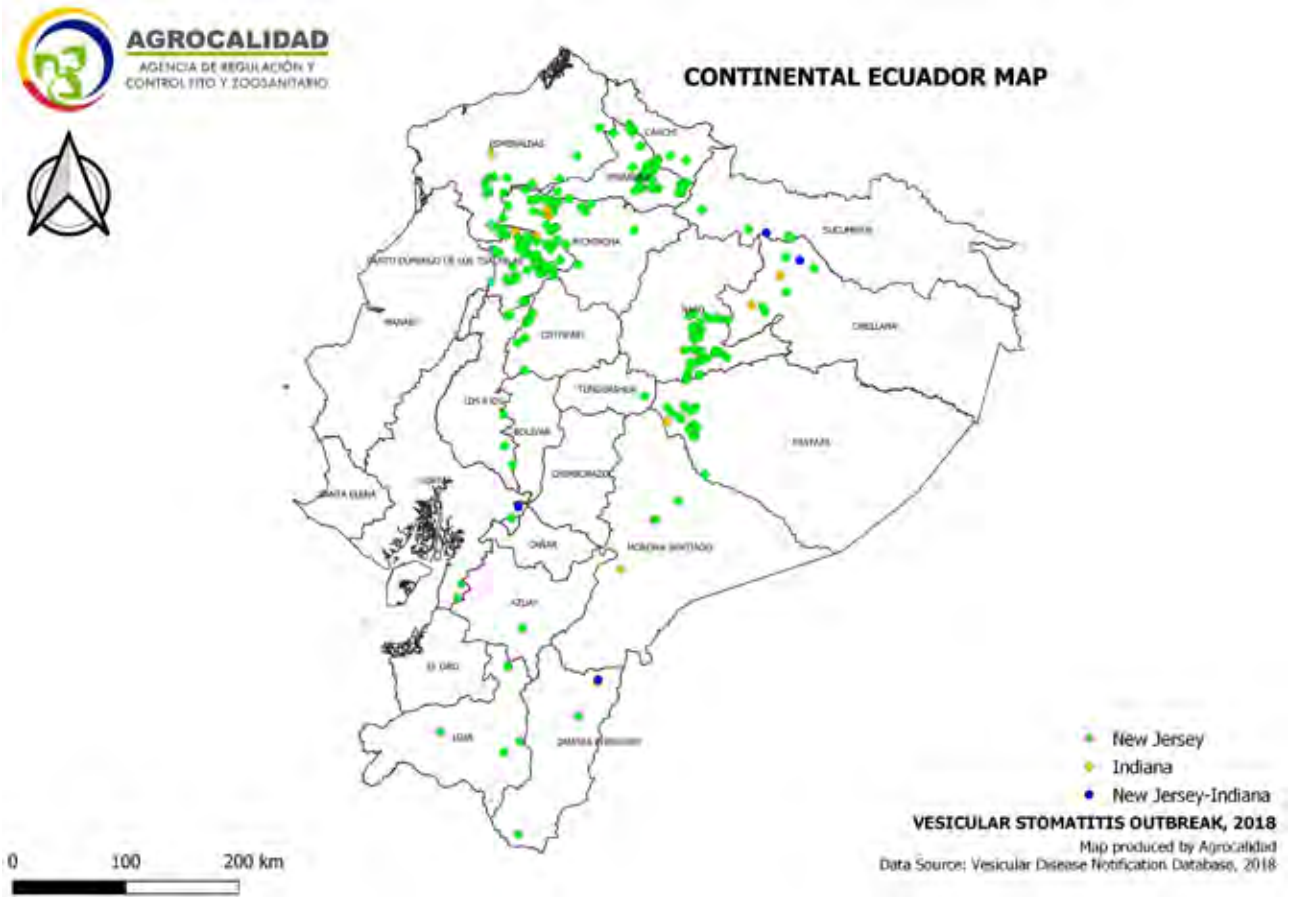

Figure 2. Distribution by serotype of outbreaks of Vesicular stomatitis confirmed in Ecuador in 2018.

	Date	Radius (km)	Number of Cases	Expected Cases	Observed/Expected	p-value[a]
1st Cluster Cotopaxi, Guayas, Los Rios, Santo Domingo de Los Tsáchilas	2018/5/21 to 2018/8/3	102.38	24	2.04	11.79	$<10^{-17}$
2nd Cluster Cotopaxi, Esmeraldas, Imbabura, Pichincha, Santo Domingo de Los Tsáchilas	2018/8/6 to 2018/9/26	62.78	122	43.99	2.77	$<10^{-17}$
3rd cluster Carchi, Imbabura	2018/10/3 to 2018/10/19	23.09	46	7.67	6.00	$<10^{-17}$
4th Cluster Morona Santiago, Napo, Pastaza, Tungurahua	2018/10/31 to 2018/11/20	99.78	72	27.69	2.60	$2.3*10^{-11}$

Table 2. Geographic Analysis of Vesicular Stomatitis Rates, using the Space-time Statistic: Ecuador, 2018.

space-time clusters. Some of the outbreaks were not included in any of the fourth clusters; this is due to common cases filed each year and are not representative.

The highest incidence was reported around week 35 and week 44, which were observed outbreaks increase in the country's north region (Figure 3). In this sense, the cluster closes to the municipality of Ibarra indicated the highest incidence rate, suggesting that the rate of transmission between herds was higher within this area than the other clusters in which the rate was similar. It was also observed that outbreaks increase began at the end of the summer or dry season and the beginning of the rainy season. This observation matches a monitoring study in Costa Rica in which all episodes of disease occurred at the beginning of the dry season[15]. Another study mention that VS outbreaks incidence from year to year varies according to the region. For example, in frostless areas, the disease is encountered every year[16].

Factors that caused outbreaks still are not determined; however, studies suggest climate change may have favored the increase of vectors in affected areas, promoting disease transmission. A study in Mexico suggested that a change in climatic conditions could favor the vectors' spread into areas in which they are usually absent[17]. Also, another study indicates an apparent relationship between climatic zones and the frequency of occurrence of vesicular stomatitis. However, it appears that limitations are imposed on the spread of the disease by particular physical features of the land or by habitat conditions within these zones[16]. Environmental conditions and climate variables play an essential role in the dynamics, distribution, and transmission of vector-borne diseases. In this way, when compared with pre-

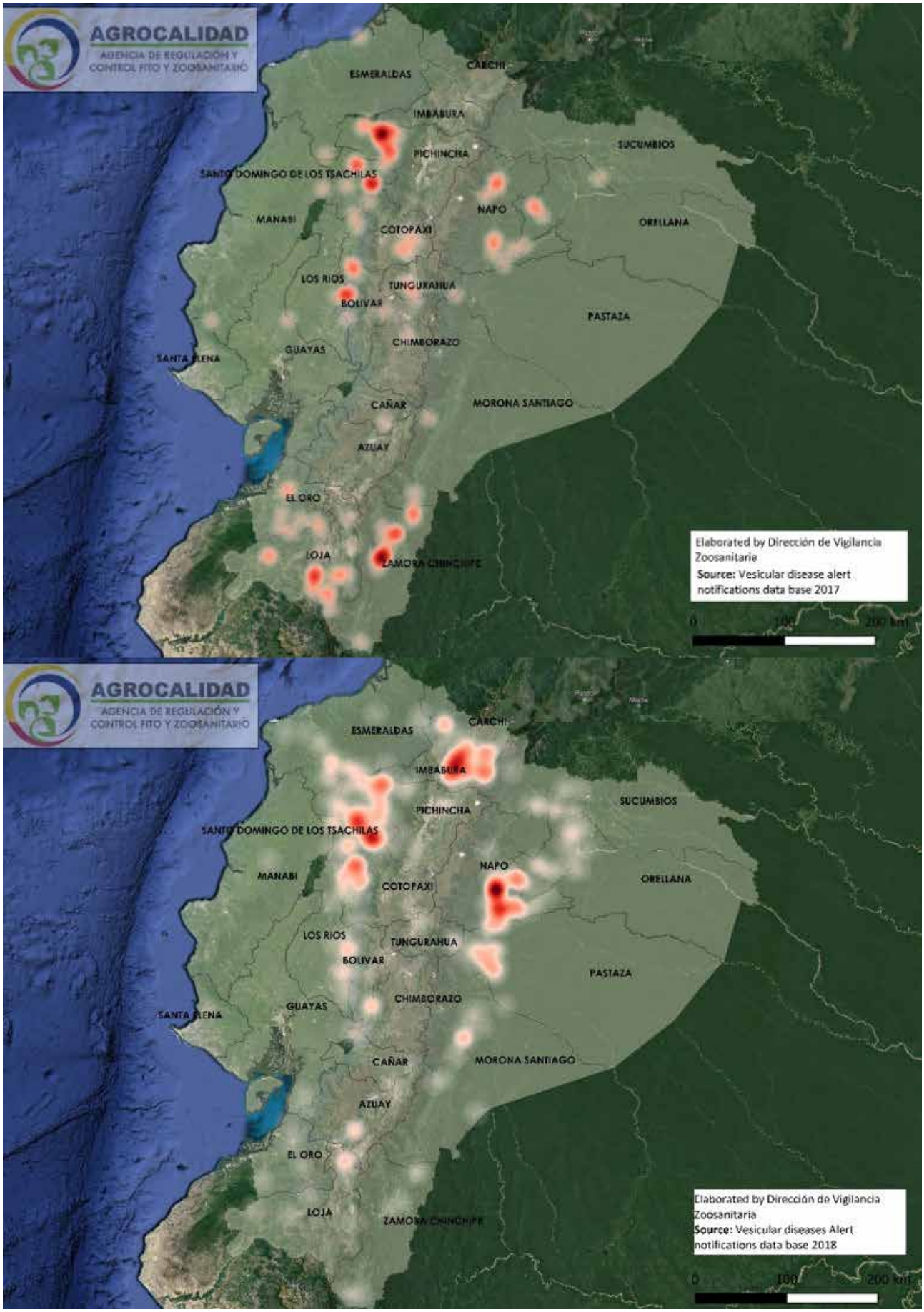

Figure 3. Heat maps of alert notifications for vesicular diseases in 2017 (3a) and 2018 (3b).

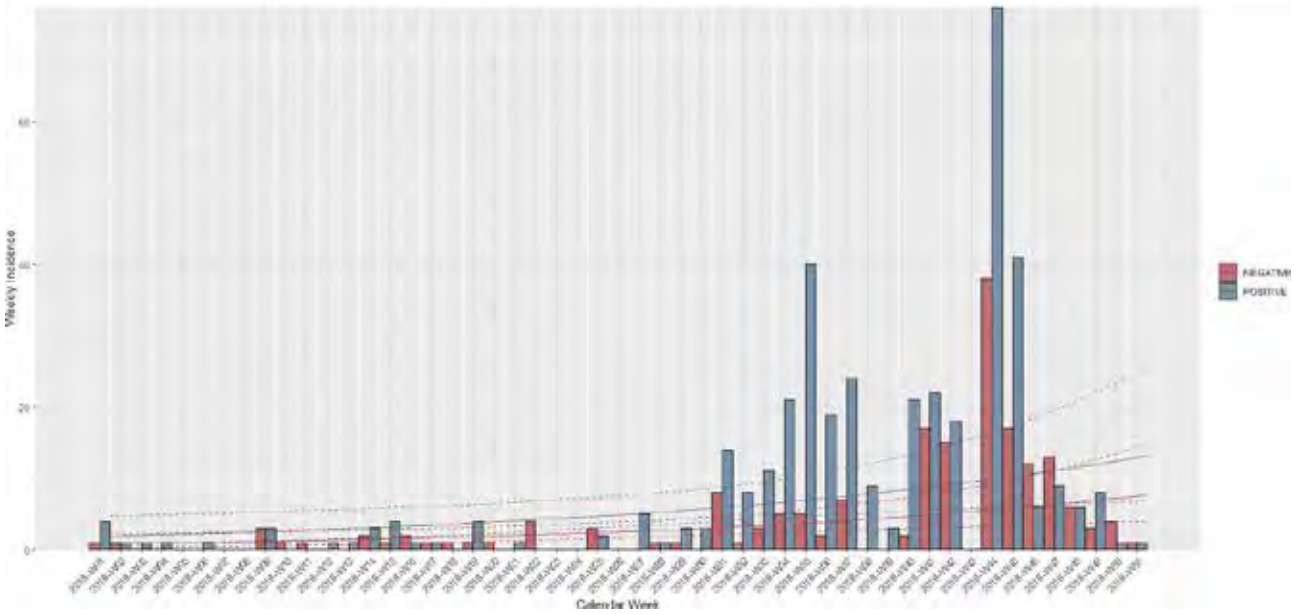

Figure 4. Weekly incidence of VS in Ecuador in 2018. Positive (blue) and negative cases (red).

Figure 5. Spatial distribution of outbreaks of Vesicular stomatitis confirmed in Ecuador in 2018.

vious years, it is possible to notice a change that triggered the outbreaks, suggesting that environmental and epidemiological factors may have influenced VSV spread. Even when the heat maps group all the vesicular disease alert notifications, it can be appreciated a difference in the distribution of cases between 2017 and 2018. In this manner, in the 2018 map, it can be seen an increment in the number of cases compared to the 2017 map, which represents the average number of alert notifications in provinces for each year. Likewise, the 2018 map shows places where the disease is not shared.

South and Central America have ecologic niches where outbreaks appear annually. The prevalence of the virus is established in the places where the disease is constantly being enzootic in those areas[18]. For instance, Costa Rica presents two zones where the virus's activity is high considerably, one is located in the highlands (premontane tropical forest), and another is located in the lowlands (tropical dry forest)[19]. Ecuador also shows enzootic zones for VS, it is so every year common cases are presented in provinces like Carchi, Guayas, Manabí, Pichincha, Loja, Los Ríos and Zamora Chinchipe. Moreover, the disease has repeatedly spread along waterways in certain zones in the USA. Woodland pastures, rivers, and lakes are common in most epizootic regions and absent in the regions where the disease is self-limiting[16]. In this way, water bodies in the country, in conjunction with environmental factors, could have been another factor of the spread of the virus. Additionally, increased attack rates in pastured animals suggest insect vectors' role in the transmission of VSV[20]. Investigations reports VSV transmission routes involve insect vectors, such as mosquitoes, sand flies[21, 22], black flies, and biting midges. In this way, VSV has been isolated

from multiple arthropods collected in enzootic areas and during epizootics. Similarly, they have been found in high abundance, vectors causing agricultural pests like black flies and *Culicoides* midges when outbreaks occur[5]. In Ecuador has been found sand flies in some provinces (Azuay, El Oro, Esmeraldas, Guayas, Morona Santiago, Pastaza, Pichincha, Sucumbíos, and Zamora Chinchipe)[23], being places that coincide with the presence of VS cases, so, the presence of vectors could have been a factor for the spread of the virus in the country.

Many places in South America are considered endemic zones for VSV, such as northeastern and northern Brazil[24]. In 1986, Ecuador recognized Loja province as an endemic area for VSV-N.J. Guayas, Los Rios, and Pichincha are recognized as endemic zones for VSV- N.J. at a low level, and Manabí, Cotopaxi, El Oro, and Zamora Chinchipe are considered as endemic zones at an occasional level. For VSV-I, there is not a specific place in Ecuador considered as an endemic, but it constantly appears in Loja, Zamora Chinchipe, Guayas, and Pichincha[25]. This is consistent with the distribution of VSV-NJ and VSV-I serotypes in Ecuador during the cases filed in 2018. However, the VSV-I serotype was found also in Esmeraldas, Santo Domingo de Los Tsáchilas, Sucumbíos, Orellana, Pastaza, and Morona Santiago.

The comparison with the distribution of the virus of previous years could help found an association of the expected virus each year and the virus found in new places.

Conclusions

Comprehend the temporal-spatial distribution is key to understanding VS epidemiology and improving and enforcing the responses of outbreaks when it appears, taking with regard that vesicular stomatitis presents similar symptoms with foot and mouth disease considered as a significant disease into animal health, economy, and business relationships. Viewed in this way, knowing the places where the farms are affected by the disease seasonally allows the prevention and control of the virus. For instance, in the USA, the outbreaks appear in intervals of 10 years in which the losses are estimated at around $200 per individual and around $15.565 per farm with the virus[5]. Further studies about vesicular stomatitis and its epidemiology will help better understand the disease and its behavior to changes that may cause new outbreaks. Accordingly, processes of regulation, control, and animal health surveillance headed to maintain the sanitary status in Ecuador could be supported based on the present study results. Monitoring in affected zones may lead to quick responses to possible outbreaks issuing alerts when there is a greater than typical risk of spreading the disease, in areas that are not affected by the disease, or present minimal cases that are expected every year.

Acknowledgments

We acknowledge field technicians of the Agencia de Regulación y Control Fito y Zoosanitario – Agrocalidad. They attend case notifications in the different Ecuador and Animal Health Coordination provinces because they manage animal health processes to increase animal health standards in the country.

Bibliographic references

1. Ansari MY, Ahmad A, Khan SS, Bhushan G, Mainuddin. Spatiotemporal clustering: a review. Artif Intell Rev 2020; 53: 2381–2423.
2. Letchworth GJ, Rodriguez LL. Review Vesicular Stomatitis. Control 1999; : 239–260.
3. McCluskey BJ. Vesicular Stomatitis. Second Edi. Elsevier Inc., 2013 doi:10.1016/B978-1-4557-0891-8.00024-5.
4. SHIC. Swine Health Information Center, Vesicular Stomatitis Virus. Encycl Virol 2015; : 291–299.
5. Rozo-Lopez P, Drolet BS, Londoño-Renteria B. Vesicular stomatitis virus transmission: A comparison of incriminated vectors. Insects 2018; 9: 1–16.
6. Jr JLR, Mead D, Rodriguez LL, Brown CC. Transmission and pathogenesis of vesicular stomatitis viruses. Brazilian J Vet Pathol 2009; 2: 49–58.
7. APHIS. Animal and Plant Health Inspection Service, Vesicular Stomatitis. US Dep Agric 2012; : 2.
8. Cornish TE, Stallknecht DE, Brown CC, Seal BS, Howerth EW. Pathogenesis of Experimental Vesicular Stomatitis Virus (New Jersey Serotype) Infection in the Deer Mouse (Peromyscus maniculatus). Vet Pathol 2001; 38: 396–406.
9. MacLachlan NJ, Dubovi EJ. Chapter 18 – Rhabdoviridae. Fenner's Vet Virol 2017; : 357–372.
10. Veterinary N, Program A. Module 5 : Vesicular Diseases. 2014.
11. McCluskey BJ, Pelzel-McCluskey AM, Creekmore L, Schiltz J. Vesicular stomatitis outbreak in the southwestern United States, 2012. J Vet Diagnostic Investig 2013; 25: 608–613.
12. Timoney P. Vesicular stomatitis. Vet Rec 2016; 179: 119–120.
13. رسولی چ. No Titleرساله ی دکترای دانشگاه شهید بهشتی. .
14. Shi Z, Pun-Cheng LSC. Spatiotemporal data clustering: A survey of methods. ISPRS Int J Geo-Information 2019; 8. doi:10.3390/ijgi8030112.
15. Rodriguez LL, Vernon S, Morales AI, Letchworth GJ. Serological Monitoring of Vesicular Stomatitis New Jersey Virus in Enzootic Regions of Costa Rica. Am J Trop Med Hyg 1990; 42: 272–281.
16. Hanson RP. The natural history of vesicular stomatitis. Bacteriol Rev 1952; 16: 179–204.
17. Arroyo M, Perez AM, Rodriguez LL. Characterization of the temporal and spatial distribution and reproductive ratio of vesicular stomatitis outbreaks in Mexico in 2008. Am J Vet Res 2011; 72: 233–238.
18. Rodriguez LL, Bunch TA, Fraire M, Llewellyn ZN. Re-emergence of vesicular stomatitis in the western United States is associated with distinct viral genetic lineages. Virology 2000; 271: 171–181.
19. Rodríguez LL, Fitch WM, Nichol ST. Ecological factors rather than temporal factors dominate the evolution of vesicular stomatitis virus. Proc Natl Acad Sci U S A 1996; 93: 13030–13035.
20. Stallknecht DE, Nettles VF, Fletcher WO, Erickson GA. Enzootic Vesicular stomatitis New Jersey Type in an insular feral swine population. Am J Epidemiol 1985; 122: 876–883.
21. Nettles VF, Comer JA, Erickson GA, Corn JL. Isolation of Vesicular Stomatitis Virus New Jersey Serotype from Phlebotomine Sand Flies in Georgia. Am J Trop Med Hyg 1990; 42: 476–482.
22. Tesh RB, Chaniotis BN, Johnson KM. Vesicular Stomatitis Virus (Indiana Serotype): Transovarial Transmission by Phlebotomine Sandflies. Science (80-) 1972; 175: 1477–1479.
23. Alexander JB, Takaoka H, Eshita Y, Gomez EA, Hashiguchi Y. New records of phlebotomine sand flies (Diptera: Psychodidae) from Ecuador. Mem Inst Oswaldo Cruz 1992; 87: 123–130.
24. Cargnelutti JF, Olinda RG, Maia LA, de Aguiar GMN, Neto EGM, Simões S V.D. et al. Outbreaks of Vesicular stomatitis Alagoas virus in horses and cattle in northeastern Brazil. J Vet Diagnostic Investig 2014; 26: 788–794.
25. Vicente, A. Estupiñan, J. Rosenberg, F. da Silva, A. Dora J. Epidemiological Study of Vesicular stomatitis in South America. Ser Monogr Científicas y Técnicas - Pan Am Foot-and-Mouth Dis Cent 1986; 15: 1–107.

Received: 12 December 2020
Accepted: 22 February 2021

RESEARCH / INVESTIGACIÓN

Protective potential of *Cynara scolymus* extract in thioacetamide model of hepatic injury in rats

Deena El-Deberky[1], Manar Rizk[1], Faten Elsayd[1], Aziza Amin[2], Abubakr El-Mahmoudy[1*]
DOI. 10.21931/RB/2021.06.02.20

Abstract: Hepatic injury is a worldwide health problem. This study aimed to evaluate the possible hepatoprotective potential of Artichoke (*Cynara scolymus*) extract (CSE) in albino rats using the thioacetamide (TAA) a model of liver injury. Acclimatized 42 rats were divided randomly into seven groups, each consists of six rats, and subjected to different treatments. Hepatic injury model was induced by administration of TAA at a dose of 100 mg per kg, intraperitoneally, twice weekly for 8 weeks (+ve control); test groups rats received CSE at doses of 100 or 200 mg/kg BW, orally, daily for 8 weeks adjunct with TAA; standard group rats received Silymarin at a dose of 100 mg per kg, orally, daily for 8 weeks adjunct with TAA; other 2 groups of rats received only CSE at the same dose levels; while -ve control rats received only the vehicles. Blood and liver tissue samples were collected at the end of the experimental course for different assessments. Results revealed that CSE exhibited dose-dependent hepatoprotection indicated by nearly normalized parameters, including enzymatic liver function parameters (AST, ALT, GGT & ALP with potential % of 94.06, 86.96, 85.93, 64.85, respectively, after large dose when standardized by Silymarin); non-enzymatic parameters (total protein, albumin, globulins, total bilirubin, conjugated bilirubin, unconjugated bilirubin, TAGs, Cholesterol, HDL, LDL & VLDL with potential % of 83.42, 85.9, 83.44, 98.1, 77.41, 91.5, 97.51, 97.46, 81.41, 88.52 & 89.4, respectively, after large dose when standardized by Silymarin). The underlying mechanism of the observed hepatoprotection of CSE was attributed to impeding the oxidative stress-mediated by TAA, indicated by reduced hepatocyte lipid peroxidation product MDA (95.96 % of Silymarin), and improved antioxidative enzymes in liver homogenate, namely, GPx, Catalase & SOD with potentials of 95.44, 87.02 & 81.48 % of Silymarin, respectively. Macroscopic and microscopic pathological pictures were supportive to the biochemical findings, where the pathological lesions caused by TAA as congestion and dilatation of central and portal veins with perivascular fibrous connective tissue proliferation admixed with few mononuclear leukocytes plus necrotic hepatocytes and hyperplastic biliary epithelium, were ameliorated dose-dependently when CSE was administered together with TAA. The present study's data may suggest CSE as a natural source for promising hepatoprotective and antioxidant drug preparations.

Key words: *Cynara scolymus*, Artichoke, Liver injury, Antioxidant, Phytomedicine.

Introduction

The liver is considered one of the large body organs that play significant roles in metabolizing absorbed food and dealing with toxic substances easily excreted from the body.

The liver's health problem (hepatic) disease has a high rate of incidence all over the world. Various factors may cause it as viruses, alcohol, obesity, drugs, or genetic. Upon the prolonged exposure to one or more of these factors, liver damage occurs in the form of fibrosis or scarring, or cirrhosis, which finally may result in hepatic failure, which is severe and life-threatening[1].

Drugs, in particular, are a significant cause of liver disease with different mechanistic pathways. Some drugs directly affect liver cells, while others are non-injurious by themselves; however, after being transformed by the liver into metabolites, the latter may cause injury to hepatic cells either with direct or indirect mechanisms. From another aspect, the liver cells' toxicity may be dose-dependent or idiosyncratic, or allergic[2].

The Incidence of hepatic adverse drug reactions (ADRs) remains unknown in the general population[3]. reported that the main drugs implicated in ADRs were anti-infectious, psychotropic, hypolipidemic agents, and nonsteroidal anti-inflammatory drugs (NSAIDs).

Health professionals as physicians, veterinarians, dentists, and pharmacists use chemical drugs for controlling and treating disease conditions, including liver diseases. However, although beneficial, these chemicals may have harmful side effects on the body organs, including the liver, especially in chronic states. Therefore, many researchers are looking for safe source derived from natural products as medicinal plants in the treatment of liver diseases and drug-induced liver injury.

Among medicinal plants, artichoke is a good source of natural antioxidants such as vitamin C, hydroxycinnamic acids, and flavones. It produces a concentration-dependent inhibition of oxidative stress when cells are stimulated with agents that generate reactive oxygen species (ROS): hydrogen peroxide, phorbol-12-myristate-13-acetateN-formyl-methionyl-leucyl-phenylalanine[4].

However, there is relatively little research on artichoke as a medicine. Studies on animals revealed that administration of root and leaf liquid extracts of artichoke exhibited good hepatoprotective results and helped hepatocytes regenerate. Although research is not yet conclusive, scientists were optimistic that its long-standing use in humans for digestive and bowel problems was justified. The plant also may have a hypocholesterolemic effect and thus may help protect against heart disease. Boiled wild artichoke reduced postprandial glycemic and insulinemic responses in normal subjects but did not affect metabolic syndrome patients[5].

Therefore, the present study aims to evaluate the possible hepatoprotective potential of artichoke and its antioxidant properties in thioacetamide-induced liver injury. To achieve this aim, the following assessments have been performed: liver function biomarkers, oxidative stress markers, and pathological examination in diseased and artichoke-treated rats as experimental models for humans.

[1] Department of Pharmacology, Faculty of Vet. Medicine, Benha University, Egypt.
[2] Department of Pathology, Faculty of Vet. Medicine, Benha University, Egypt.

Corresponding author: a.elmahmoudy@fvtm.bu.edu.eg

Methods

Plant part and its identification

The plant is a traditional vegetable crop of the Mediterranean basin. The cultivated variety: *Cynara cardunculus* L. var. *scolymus* L (globe artichoke) is grown for its fleshy capitula. It belongs to the family of *Asteraceae*[6]. The leaves of *Cynara scolymus* were purchased from a medicinal plants farm, Faculty of Agriculture, Benha University, Egypt. The leaves were collected in September 2019.

The plant was identified by Dr. Mostafa Hamza Mohamed, Assistant professor of vegetable crops, Horticulture department, Faculty of Agriculture, Benha University, Voucher number 96647 (Figure 1).

Preparation of plant extract

Leaves around the stems of *C. scolymus* were obtained, cut into smaller pieces, and dried at room temperature. The extraction was done by maceration of chopped leaves with 70% v/v (ethanol/distilled H_2O). The mixture was left for 72 hr. in the refrigerator with intermittent shaking. The extract was filtered with muslin mesh, concentrated in shaking water pass at 70°C for 3 days to determine the weight of crude extract, and then stored at 4 °C until preparation for administration. It was re-constituted by dissolving 4 g in 200 ml of isosaline (0.9%) for high dose extract and dissolving 2 g in 200 ml of isosaline (0.9%) for low dose extract to give concentrations of 40 mg/ml and 20 mg/ml, respectively. The prepared extracts were used to evaluate the hepatoprotective effect of artichoke extract at high (200 mg/kg) and small (100 mg/kg) doses in rats[7]. This method of extraction was repeated every week to prepare fresh extracts. Percentage of yield was determined using the formula:

$$\text{Yield \%} = \frac{\text{wt.of extract}}{\text{wt.of plant}} \times 100 \qquad (1)$$

Chemicals, reagents, and Kits

Thioacetamid

It is widely used as an antipyretic and analgesic. However, the major complication reported is hepatotoxicity. It is used for experimental induction of liver injury in animal studies[8]. It was obtained from Alamia company, Benha, Qalubia governorate, Egypt.

Thioacetamide powder was dissolved in saline at a concentration of 40 mg/ml. The standard hepatotoxic dose of thioacetamide is 100 mg/kg[9]. A rat weighing 200 gm was injected intraperitoneally with 0.5 ml of the prepared solution (40 mg/ml), equivalent to 100 mg/kg B. Wt.

Silymarin

It is traditionally used as a raw extracted from the seeds of *Silybum marianum* or milk thistle and used to treat liver diseases but is currently available as a standard mixture of 4 flavonolignane isomers: silibinin, isosilibinin, silidianin and silichristin[10]. Silymarin used in this study was produced by MUP (Medical Union Pharmaceuticals), Abu sultan, Ismailia, Egypt, under the commercial name Hepaticum®. It is presented as 50 mg / 5 ml suspension. Silymarin was used as such without dilution, where a rat weighing 200 g receives 2 ml of Hepaticum® suspension, equivalent to 100 mg/kg B.Wt[9].

Kits

The diagnostic kits for estimating aspartate aminotransferase (AST), alanine aminotransferase (ALT), gamma-glutamyl transferase (GGT), alkaline phosphatase level (ALP), total protein, albumin, total bilirubin, and conjugated bilirubin in plasma were supplied from Centronic GmbH Company, Am Kleinfeld, Wartenberg, Germany. The diagnostic kits for estimating triglycerides, cholesterol, HDL, and LDL in plasma were supplied

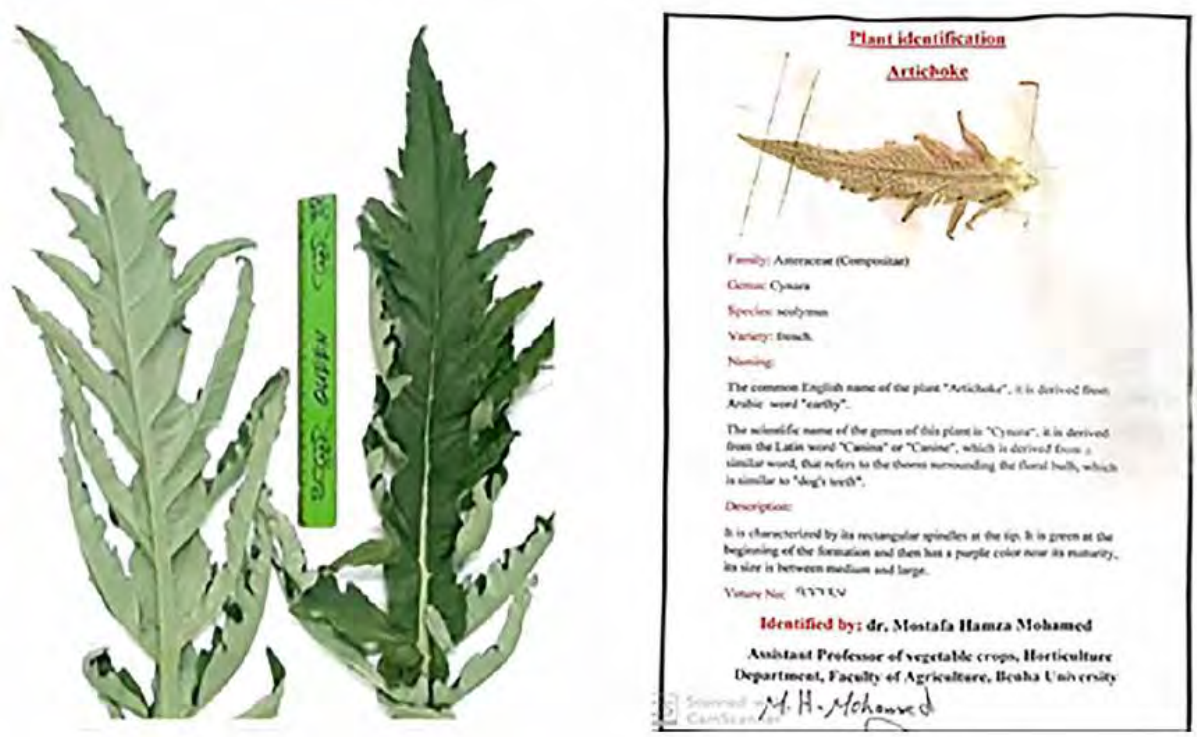

Figure 1. Leaves of *Cynara scolymus* used for extraction and its identification.

from BioDiagnostic Company, Dokki, Giza, Egypt. The diagnostic kits of estimating oxidative stress markers, Malondialdehyde (MDA), Glutathione peroxidase (GPx), superoxide dismutase (SOD), and Catalase (CAT) in liver tissue homogenate were also from BioDiagnostic Company, Dokki, Giza, Egypt.

Experimental animals and design

The study was performed on (42) male albino rats weighing 150-200 g, obtained from Animal house, Faculty of Veterinary Medicine, Benha University, Egypt. The animals were kept in controlled standard environmental conditions of temperature, humidity, and light/dark exposure. All experimental animals were supplied with a balanced maintenance diet, while water was provided *ad libitum*. Animals were housed in stainless steel wire mesh cages with bedding of groundwood chips. They were fed fresh pelleted food in a standard diet (vegetable feed containing 19 % protein). Rats were cared for at constant environmental and nutritional conditions for 15 days for acclimatization before the experiment. The research was conducted following the experimental animal care and procedure (Faculty of Veterinary Medicine, Benha University, Benha, Egypt).

Acclimatized rats were divided into seven groups; each consists of six rats. To assess the aim of the present work, groups were treated differently as follows:

- Group I: Rats received no drugs (only vehicles, saline orally and intraperitoneally) and were kept as a negative control group.
- Group II: Rats were subjected to induction of liver injury by administering TAA at a dose of 100 mg per kg, intraperitoneally, twice weekly for 8 weeks; the rats were kept as a positive control group (or diseased group).
- Group III: Rats were subjected to liver injury as those of group II and treated with Silymarin (100 mg per kg, orally, daily for 8 weeks) and kept as a standard group.
- Group IV: Rats were subjected to liver injury as those of group II and treated with artichoke extract (100 mg/kg BW, orally, daily for 8 weeks) and kept as group treated with a small dose of artichoke.
- Group V: Rats were subjected to liver injury as those of group II and treated with artichoke extract (200 mg/kg BW, orally, daily for 8 weeks) and kept as group treated with a large dose of artichoke.
- Group VI: Rats received only a small dose of artichoke extract (100 mg/kg).
- Group VII: Rats received only a large dose of artichoke extract (200 mg/kg).

Samples and assessments

Blood samples

Blood for plasma was collected after 8 weeks (2 months) from the experiment's start for biochemical assessments. Samples were collected from the venous plexus located at the eye's medial canthus using heparinized capillary tubes. Each blood sample was collected in a sampling tube with an anticoagulant to avoid clotting at room temperature. Clear plasma was separated by centrifugation at 900*Xg* for 10 minutes and then collected in Eppendorf's tubes using automatic pipettes. Plasma samples were kept in a deep freezer (-20 °C) for analysis.

Tissue samples

On the last day of feeding and administration and after blood sampling, rats of each group were sacrificed, and liver specimens were taken and preserved in formalin (10 %) solution for histopathological examination.

Other specimens from the liver were taken in sterile tubes for homogenate preparation. Liver tissues were rapidly removed, washed in ice-cooled saline, dried, weighed, and kept in buffer saline, then homogenized by an electric homogenizer. Then the homogenate was centrifuged in a cooling centrifuge for excluding debris from the clear supernatant. The clear supernatant was used for the assessment of oxidative stress markers[11].

Assessments

The estimation of some biochemical parameters such as enzymes' activities in blood, tissues, and body fluids plays a major role in assessing drug safety[12]. AST, ALT, GGT, and ALP activities in plasma were determined spectrophotometrically by specific kits as mentioned above according to methods described by (13-16) respectively, following the instructions of the manufacturer.

Total protein, albumin, total bilirubin, conjugated bilirubin, TAGs, Cholesterol, HDL, and LDL, were determined spectrophotometrically using specific kits according to principles of (17-23), respectively, following the instructions of the manufacturer.

Three parameters in plasma were calculated mathematically, namely, globulins, unconjugated bilirubin, and VLDL. The total globulin fractions were determined by subtracting the albumin value from the total protein, according to (24). Unconjugated bilirubin level was determined by subtracting the conjugated value from the total bilirubin, according to (25). VLDL concentration was calculated by dividing the triglyceride value by 5 to be the value in mg/dL according to (26).

Oxidative and antioxidative parameters in liver homogenate were determined spectrophotometrically using specific kits according to (27 (MDA)), (28 (GPx)), (29 (Catalase)), and (30 (SOD)), following the instructions of the manufacturer. Histopathological examination was done according to (31).

Data management and statistical analysis

Data are expressed as mean ± standard error of the mean of 6 samples/group. The one-way analysis of variance (ANOVA) followed by Tukey's post hoc test was performed on the data for intergroup comparisons. Database management and statistical analysis were performed using GraphPad Prism software v. 6. The significance level was set at a 0.05 probability value.

Results and Discussion

Liver disease of drug origin is common as many drugs have variable hepatic adverse effects that are, if not controlled, may cause a potential health hazard and enormous economic impact on health care expenditures. Numerous efforts and studies are, thus, have been conducted to establish reliable and early biomarkers to predict liver pathologies caused by drugs, especially the newly introduced and the chronically used ones. Classical informative candidates included serum aminotransferase markers that had been available for 30 years. Afterward, additional candidates have been used to evaluate hepato-safety of drugs like newer liver enzymes, total protein, lipid profile, and oxidation markers[32].

Pharmacological approaches to protect the liver need liver disease models to be the playground of the protection trial. The hepatotoxicity of TAA has been known since 1948.

In rats, single doses cause centrilobular necrosis accompanied by increases in plasma transaminases and bilirubin. To elicit these effects, TAA requires oxidative bioactivation by CYP450 oxidative enzymes, leading first to its S-oxide and then to its chemically reactive S, S-dioxide, which ultimately modifies amino acids, lipids, and proteins of hepatocytes[33,34]. Because of its relative specificity and availability, many researchers, including us, have used TAA as a model of experimental liver injury upon thinking about and evaluating various liver protection and treatment remedies.

As the pathogenesis of TAA depends mainly on oxidative stress on hepatocytes; so, antioxidants are considered as a therapeutic target for hepatoprotection. Silymarin is now an available standardized extract of the milk thistle (*Silybum marianum*) that exerts membrane-stabilizing and antioxidant activities, promotes hepatocyte regeneration; furthermore, it reduces the inflammatory reaction and inhibits the fibrogenesis in the liver[35,36].

There are many attempts made to find a natural substance like Silymarin or better for treating liver diseases. This study aimed to study the hepatoprotective effect of hydroethanolic *Cynara scolymus* leaves extract (CSE) on TAA-induced liver injury. CSE was selected as it is well growing in Egypt, and it has been reported elsewhere to have good antioxidant properties that have also been investigated here.

According to our extraction procedure described in the methodology section, the plant part's yield was 10.5 % that was used in the present investigation that revealed the findings presented and discussed below.

Liver function parameters

TAA elevated enzymatic markers (AST, ALT, GGT, ALP), as shown in Table 1 that were restored by co-administration of CSE in a dose-dependent manner, 85%, 94%, 86%, 86%, respectively, when standardized against Silymarin. This restoration potential of CSE could be attributed to its antioxidant effect that was proven in the present study (discussed later). Our data might be consistent with those of (37) who approved the hepatoprotective effects of CSE (0.5 g/kg/day) on carbon tetrachloride-induced liver injury (1 ml/kg) in broiler chickens. The present study's results may also be consistent with those of (38) who showed that artichoke extract (0.4, 0.8, and 1.6 g/kg body weight) decreased elevated liver enzymes in acute alcohol-induced liver injury (12 mL/kg body weight) in mice. On the other hand, our results may be inconsistent with those of (39) who reported the ineffectiveness of different *Cynara scolymus* preparations (1 and 2 g/kg) on liver injury induced by CCL4 (2.5 ml/kg, per os) in rats. Again, our data might be inconsistent with those of (40) who found that artichoke leave extracts (for 12 weeks with 3200 mg per day) seemed not to be adequate to improve liver enzyme levels in patients with chronic hepatitis C. This discrepancy between our results and the above mentioned two studies may be attributed to environmental and methodological differences, namely, different liver injury models, different doses of artichoke extract, different extraction procedures, and different course of diseases and species.

In the present study, TAA decreased total protein, albumin, and globulins as shown in table (2) that were restored by co-administration of CSE in a dose-dependent manner; being approximately (83%, 85%, 84%), respectively, when standardized against Silymarin. Decreased amounts of either albumin and globulins result in hypoproteinemia. Restoring liver function, even partly, may restore the levels of various protein fractions to their average level as exhibited by CSE in the present study. This restoration potential of artichoke could be attributed to its hepatoprotective effect based on its protection against oxidative radicals of TAA. These results of our study may be consistent with those of (41) who reported that pre-treatment of rats with artichoke leaves aqueous extract (200, 400 mg/kg for 6 weeks) protected against the dramatic decrease in albumin, globulin, and total protein upon subcutaneous injection of CCl4 (2 ml/kg diluted 1:1 by liquid paraffin). Also, the results are consistent with those of (42) who showed the prophylactic role of CSE (500 mg/kg) on doxorubicin-induced toxicity (10 mg/kg) intraperitoneally in rats indicated by a significant increase of both serum albumin and total protein

Group / Parameter	AST activity (IU/L)	ALT activity (IU/L)	GGT activity (IU/L)	ALP activity (IU/L)
Control: (saline, po)	44.7 ± 3.02 (d)	25.27 ± 1.44 (d)	1.93 ± 0.11 (d)	98.67 ± 6.12 (c)
Diseased: (TAA, 100 mg/kg, ip)	198.2 ± 10.05 (a)	96 ± 2.54 (a)	6.41 ± 0.28 (a)	462.5 ± 36.6 (a)
Standard: (TAA, 100 mg/kg + Sil, 100 mg/kg, po)	69 ± 3.42 (c)	41.13 ± 2.49 (c)	3.2 ± 0.14 (c)	176 ± 11.08 (c)
DSD: (TAA, 100 mg/kg + CSE, 100 mg/kg)	99.7 ± 4.01 (b)	69.93 ± 2.97 (b)	4.65 ± 0.13 (b)	430.3 ± 20.37 (a)
DLD: (TAA, 100 mg/kg + CSE, 200 mg/kg)	76.67 ± 3.27 (c)	48.28 ± 2.13 (c)	3.67 ± 0.14 (c)	276.7 ± 12.82 (b)
SD: (CSE, 100 mg/kg, po)	42.5 ± 3.94 (d)	25.83 ± 1.3 (d)	1.95 ± 0.08 (d)	103.3 ± 5.45 (c)
LD: (CSE, 200 mg/kg, po)	42.3 ± 3.91 (d)	24.67 ± 1.45 (d)	1.8 ± 0.12 (d)	101.5 ± 6.11 (c)
Potential % from standard (SD)	**76.24 %**	**47.51 %**	**55.21 %**	**11.23 %**
Potential % from standard (LD)	**94.06 %**	**86.96 %**	**85.93 %**	**64.85 %**

Table 1. Effects of *Cynara scolumus* extract (CSE) on liver enzyme activities (IU/L) in plasma of thioacetamide-intoxicated rats. The values in the same column with different letters are significantly different.

in the dox-CS groups, as compared to the doxorubicin group.

In the present study, TAA significantly increased total, conjugated and unconjugated bilirubin as shown in table (3) that were restored by co-administration of artichoke extract in a dose-dependent manner, being approximately (98 %, 77%, and 91%), respectively, when standardized against Silymarin. The restorative effect of CSE could be attributed to the maintained liver function of conjugation and albumin synthesis. Our results may be consistent with those of (43) who reported that the artichoke extracts prepared from either outer part or edible part of the plant (1.5 g/kg daily, for 2 months) significantly decreased serum bilirubin in the TAA hepatocarcinogenesis model (400 mg/kg, intraperitoneally, once weekly, for 3 months); and attributed this effect to the high phenolic content of artichoke.

Regarding the lipid profile in the present study, TAA has significantly increased total cholesterol, TAGs, and the risky lipoproteins (LDL, VLDL), but decreased the beneficial lipoprotein (HDL) as shown in table (4); such abnormalities have been protected by co-administration of CSE in a dose-dependent manner; being (97%, 97%, 81%, 86%, 86%) when standardized against Silymarin. This restoration potential of CSE could be attributed to its hypocholesterolemic and antihyperlipidemic effects that is proven in the present study based on its antioxidative and hepatoprotective properties. Moreover, CSE might decrease lipogenic enzyme activities in the liver and decrease lipid concentration in blood[44]. Our data may be consistent with those of (45) who reported antihyperlipidemic activity of artichoke leaves extract (200 mg/kg and 400 mg/kg during 8 weeks) against high fat diet-induced obesity in rats. In contrast, the data may disagree with those of Rodriguez et al. (2002), who found that repeated (twice a day for 7 consecutive days) oral administration of aqueous artichoke leaf extract (100, 200, and 400 mg/kg) to rats produced no significant differences in cholesterol, TG and phospholipids. The data are also not in agreement with (46) who reported insufficiency of cynarin, the active ingredient of artichoke (250 mg before meals either once or 3 times daily) as a therapeutic regimen in patients with familial type 2 hyperlipoproteinemia. The mean serum cholesterol and triglyceride concentrations in patients with Type II hyperlipoproteinemia had not significantly changed within 3 months, neither with 250 mg nor 750 mg Cynarin daily. These differences may be explained based on methodological and environmental differences, namely, different models of liver injury, different doses of artichoke extract, different extraction procedure, course of diseases and species.

Group / Parameter	Total protein (g/dL)	Albumin (g/dL)	Globulins (g/dL)
Control: (saline, po)	5.76 ± 0.21 (a)	3.91 ± 0.16 (a)	1.81 ± 0.14 (a)
Diseased: (TAA, 100 mg/kg, ip)	1.86 ± 0.13 (d)	1.45 ± 0.11 (d)	0.5 ± 0.06 (c)
Standard: (TAA, 100 mg/kg + Sil, 100 mg/kg, po)	5.33 ± 0.14 (ab)	3.56 ± 0.1 (ab)	1.56 ± 0.06 (ab)
DSD: (TAA, 100 mg/kg + CSE, 100 mg/kg)	3.31 ± 0.14 (c)	2.24 ± 0.1 (c)	0.89 ± 0.02 (c)
DLD: (TAA, 100 mg/kg + CSE, 200 mg/kg)	4.76 ± 0.14 (b)	3.26 ± 0.1 (b)	1.38 ± 0.03 (b)
SD: (CSE, 100 mg/kg, po)	5.79 ± 0.18 (a)	3.91 ± 0.16 (a)	1.9 ± 0.13 (a)
LD: (CSE, 200 mg/kg, po)	5.88 ± 0.25 (a)	3.92 ± 0.16 (a)	1.92 ± 0.14 (a)
Potential % from standard (SD)	**41.64 %**	**37.76 %**	**36.61 %**
Potential % from standard (LD)	**83.42 %**	**85.9 %**	**83.44 %**

Table 2. Effects of *Cynara scolumus* extract (CSE) on total protein, albumin and globulins levels (g/dL) in plasma of thioacetamide-intoxicated rats.
The values in the same column with different letters are significantly different.

Group / Parameter	Total bilirubin (mg/dL)	Conjugated bilirubin (mg/dL)	Unconjugated bilirubin (mg/dL)
Control: (saline, po)	0.58 ± 0.03 (c)	0.125 ± 0.008 (d)	0.38 ± 0.02 (c)
Diseased: (TAA, 100 mg/kg, ip)	2.07 ± 0.11 (a)	0.262 ± 0.008 (a)	1.71 ± 0.17 (a)
Standard: (TAA, 100 mg/kg + Sil, 100 mg/kg, po)	0.75 ± 0.01 (c)	0.138 ± 0.004 (d)	0.51 ± 0.02 (c)
DSD: (TAA, 100 mg/kg + CSE, 100 mg/kg)	0.97 ± 0.01 (b)	0.192 ± 0.002 (b)	1.03 ± 0.04 (b)
DLD: (TAA, 100 mg/kg + CSE, 200 mg/kg)	0.77 ± 0.01 (c)	0.166 ± 0.001 (c)	0.61 ± 0.02 (c)
SD: (CSE, 100 mg/kg, po)	0.56 ± 0.02 (c)	0.124 ± 0.003 (d)	0.38 ± 0.02 (c)
LD: (CSE, 200 mg/kg, po)	0.56 ± 0.01 (c)	0.132 ± 0.001 (d)	0.41 ± 0.02 (c)
Potential % from standard (SD)	82.94 %	56.45 %	61.69 %
Potential % from standard (LD)	98.1 %	77.41 %	91.5 %

Table 3. Effects of *Cynara scolumus* extract (CSE) on total bilirubin, conjugated bilirubin, and unconjugated bilirubin levels (mg/dL) in plasma of thioacetamide-intoxicated rats.
The values in the same column with different letters are significantly different.

Group / Parameter	TAGs (mg/dL)	Cholesterol (mg/dL)	HDL (mg/dL)	LDL (mg/dL)	VLDL (mg/dL)
Control	63.89 ± 2.26 (c)	69.3 ± 3.11 (d)	23.67 ± 0.56 (a)	42.58 ± 1.22 (d)	12.36 ± 0.46 (d)
Diseased	212.3 ± 10.56 (a)	167.7 ± 4.61 (a)	7.08 ± 0.68 (d)	124.2 ± 5.4 (a)	52.83 ± 2.35 (a)
Standard	74.41 ± 2.05 (c)	86.56 ± 0.58 (c)	18 ± 0.27 (b)	55.07 ± 1.03 (c)	15.72 ± 0.48 (cd)
DSD	98.27 ± 1.18 (b)	113.4 ± 1.37 (b)	12.17 ± 0.32 (c)	82.38 ± 0.84 (b)	30.5 ± 1.18 (b)
DLD	77.83 ± 1.81 (c)	88.62 ± 0.98 (c)	15.97 ± 0.15 (b)	63 ± 1.16 (c)	19.65 ± 0.72 (c)
SD	62 ± 2.02 (c)	70.5 ± 3.23 (d)	24.17 ± 0.92 (a)	44.33 ± 0.77 (d)	13.33 ± 0.37 (d)
LD	62.83 ± 2.71 (c)	70 ± 2.99 (d)	25.78 ± 0.84 (a)	44.85 ± 0.6 (d)	14.43 ± 0.36 (d)
SD Pot. %	82.69 %	66.92 %	45.78 %	60.49 %	60.17 %
LD Pot. %	97.51 %	97.46 %	81.41 %	88.52 %	89.4 %

Table 4. Effects of *Cynara scolymus* extract (CSE) on lipid parameters (mg/dL) in plasma of thioacetamide-intoxicated rats. The values in the same column with different letters are significantly different.

Oxidative stress parameters

In the present study, TAA significantly increased MDA from one hand and decreased GPx, SOD, and CAT from the other hand, as shown in figure (2); such abnormalities have been restored to a large extent by co-administration of CSE in a dose-dependent manner; being approximately (96%, 96%, 86%, 81%) when standardized against Silymarin. This restoration potential of artichoke could be attributed to its antioxidant effect proven in the present study; however, active principles in the extract responsible for such effect need to be investigated.

The antioxidant effect recorded in the present study may be consistent with (47) who reported a protective effect of the artichoke leaf extract (300 mg/kg BW) against cadmium (100 mg/L)-induced oxidative stress in rats. Artichoke leaf extract significantly improved the antioxidant system and hepatorenal function with a significant decline in MDA and elevation of GSH, GPX, SOD, and catalase. Moreover, our data are consistent with those of (48) who reported hepato-curative effects of aqueous artichoke leaf extract (1.5 g/kg orally for 14 days) on hepatic damage and oxidative stress generated by alpha-amanitine (3 mg/kg single dose ip) in male rats.

However, our data may be inconsistent with those of (39) who reported non-efficacy of different *Cynara scolymus* preparations (1 and 2 g/kg) on CCl4-induced liver injury in rats. Pre-treatment with either of those extracts or chlorogenic acid did not reduce significantly the production of MDA. This difference may happen because of environmental and methodological variations, namely, liver injury models, doses and types of artichoke extracts, and practical courses.

Pathological findings in the present study come parallel to biochemical data. Macroscopically, no gross changes were detected in these rats' examined livers, which received only the vehicles of drugs used (normal saline orally and parenterally). The liver showed standard, smooth, soft, and shiny brown surfaces, with no irregularities on the surface. Livers dissected from rats treated with TAA (100 mg/Kg, IP, twice weekly for 8 weeks) showed hepatic enlargement with multiple nodular irregularities, pale red color, rough surface. Livers dissected from rats treated with silymarin (100 mg/Kg, PO, daily for 8 weeks) and thioacetamide showed apparent recovery signs as red-brown color, smooth and shiny brown surface, with no or much fewer irregularities. Livers dissected from rats treated with low dose (100 mg/kg, orally) of CSE for 8 weeks and TAA showed hepatic enlargement with multiple nodular irregularities, pink color, rough surface. Livers obtained from rats of group 5, treated with CSE high dose (200 mg/kg, orally) for 8 weeks along with TAA, revealed good restoration of the hepatic architecture with almost normalized shape (smooth with no irregularities). Livers dissected from rats treated with either low or large CSE doses (100 or 200 mg/Kg, PO, daily, respectively) for 8 weeks showed normal liver with deep red color, soft, smooth, with no irregularities on the surface (Fig. 3 a-f).

Microscopically, the standard histological structure was detected in the examined livers of these rats as the liver showed standard histological criteria of blood vessels, bile ducts, and hepatic cords (Fig. 4a).

The microscopical examination of livers obtained from thioacetamide-treated rats revealed extensive congestion and dilatation of central and portal veins, dilatating hepatic blood sinusoids, and activation of Kupffer cells in association with perivascular fibrous connective tissue proliferation admixed with few mononuclear leukocytes. Fibrin thrombi were occasionally seen in portal veins. Obvious hydropic degeneration and fatty changes characterized by swollen, pale, vacuolated cytoplasm were commonly demonstrated in the hepatocytes (Fig. 4b). The proliferation of fibrous connective tissue was frequently seen around the central vein and in portal areas with occasional bridging from the central vein to central vein (Fig. 4c) and from the central vein to adjacent portal areas. The portal areas were moderately expanded by fibrous connective tissue proliferation with few mononuclear leukocytic cellular infiltration, prominent lymphocytes with mild hyperplasia of the biliary epithelium peri-ductal fibrous connective tissue proliferation (Fig. 4d). Multifocally, there were strands of fibrous connective tissue infiltrated by mononuclear inflammatory cells and replacing the hepatic parenchyma with a distinct nodular pattern with the formation of pseudo-lobulation; the hepatic parenchyma was also noticed as well as fibrous connective tissue proliferation was also demonstrated adjacent to degenerated and necrotic hepatocytes (Fig. 4e). Multifocally and randomly, there were small focal areas of lytic necrosis characterized by replacing the hepatic parenchyma with eosinophilic cellular and karyorrhectic debris, admixed with fibrin, and fewer lymphocytes (Fig. 4f). Occasionally, large areas of lytic necrosis, with the vacant space's replacement by erythrocytes and few inflammatory cells, were demonstrated.

Meanwhile, the histopathological examination of the liver of rats treated with Silymarin for 8 weeks revealed diffuse degeneration of the hepatocytes, characterized by marked enlargement of the cells by multiple variably sized discrete empty

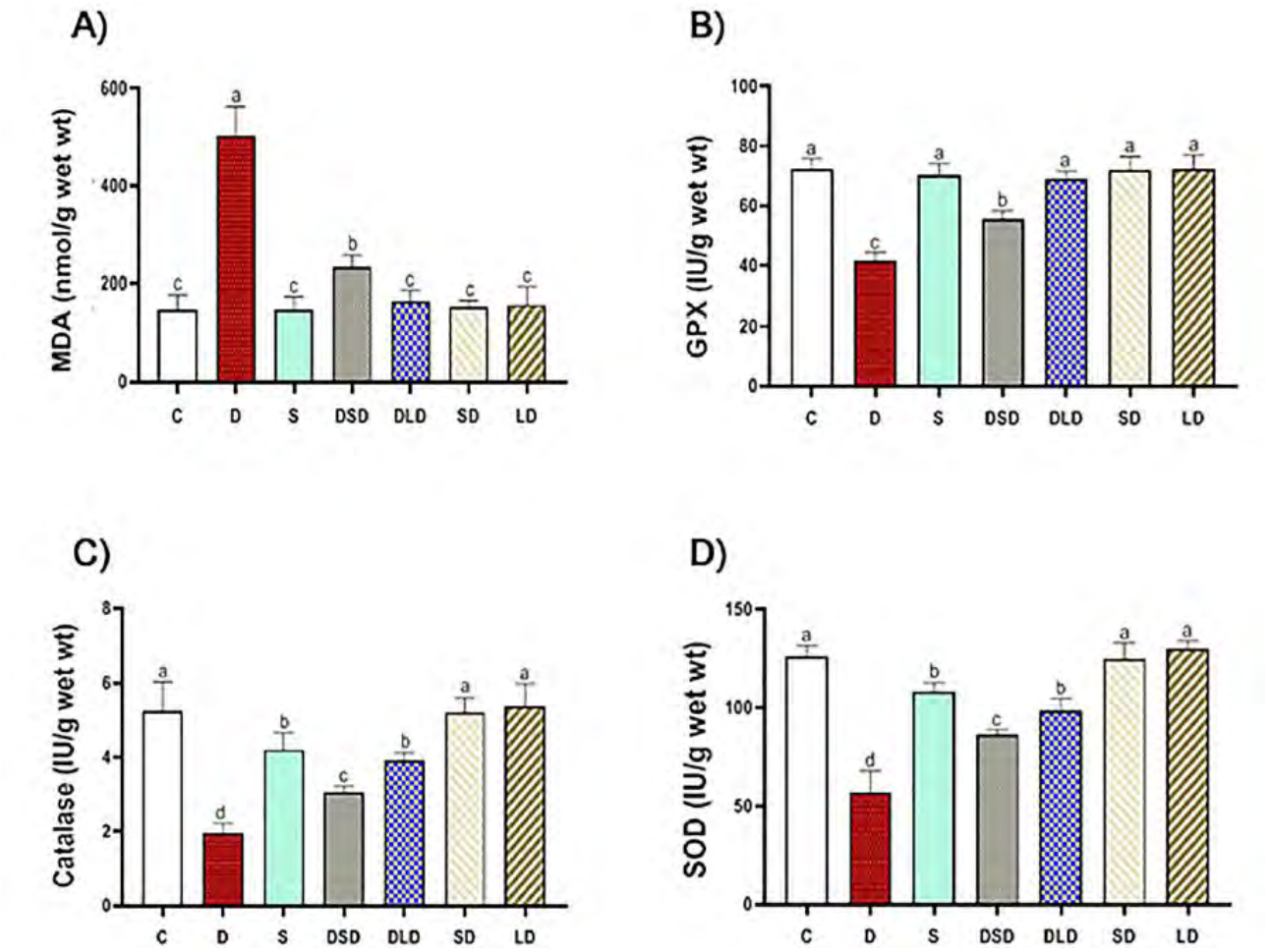

Figure 2. Effects of *Cynara scolymus* extract (CSE) on oxidative and antioxidative parameters in liver homogenate of thioacetamide-intoxicated rats: Bar-graph showing the effects of CSE on thioacetamide-induced hepatic oxidative stress evaluated by MDA (Malonyl-di-aldehyde, nmol/g wet wt, A), GPx (Glutathione peroxidase, IU/g wet wt, B), Catalase (IU/g wet wt, C) and SOD (Superoxide dismutase, IU/g wet wt, D) in different treatment groups. C (Control: saline, po); D (Diseased: thioacetamide, 100 mg/kg, ip), S (Standard: diseased rats treated with Silymarin, 100 mg/kg, po), DSD (diseased rats treated with a small dose of CSE, 100 mg/kg, po); DLD (diseased rats treated with a large dose of CSE, 200 mg/kg, po); SD (normal rats treated with a small dose of CSE); LD (normal rats treated with a large dose of CSE). The results represent the mean ± SE of 6 rats/group. The bars with different letters are significantly different at $P \leq 0.05$ (Tukey's after ANOVA).

vacuoles that distend the cell cytoplasm were observed. The liver's prominent microscopical findings were a noticeable reduction in the intensity and spreading of fibrous tissue proliferation that appeared as thin strands in between hepatic lobules in most examined sections was detected (Fig. 5a). Multifocally, mild periportal fibrous connective tissue proliferation effacing, separating, and surrounding the adjacent hepatic parenchyma (Fig. 5b).

However, the microscopical examination of the liver of animals treated for 8 weeks with a low dose of CSE showed less prominent histopathological changes when compared with the group treated with TAA for the same period. Mild vacuolar and hydropic degeneration in the hepatocytes with the expansion of the portal areas with edema admixed with a few inflammatory cells, mainly lymphocytes and fewer macrophages. Furthermore, the bile ducts were ecstatic and revealed mild periductal fibrosis infiltrated by few mononuclear inflammatory cells (Fig. 5c). Multifocally, there were variably small-sized discrete strands of fibrous connective tissue proliferation in the hepatic parenchyma, mainly adjacent to the degenerated hepatocytes (Fig. 5d). The proliferated fibrous tissue was infiltrated and rimmed by mononuclear inflammatory cells. Mild periportal fibrous connective tissue proliferation (Fig. 5e).

Concerning liver obtained from rats of group 5 treated with TAA and a high dose of CSE for 8 weeks revealed good restoration of the hepatic parenchymal cells as mild congestion of the central vein and hepatic sinusoid. Mild degenerative changes in the hepatocytes with Kuepfer cells' activation as the hepatocytes have small intracytoplasmic vacuoles were demonstrated. Meanwhile, the portal area nearly showed typical histological structures except for a few mononuclear leukocytic cellular infiltration. However, a marked reduction in the intensity and spreading of fibrous tissue proliferation appeared as thin strands of the fibrous connective tissue between hepatic lobules were noticed in most examined sections (Fig. 5f). Liver specimens from rats of 6 and 7 treated only with CSE revealed normal-like findings (not shown).

This study's above-mentioned pathological findings may be partially consistent with those of (43) who found that TAA (400 mg/kg, IP)-induced multilobular liver cirrhosis with the trabecular arrangement of hepatocytes with dilatation of hepatoportal blood vessel revealing criteria of malignancy. However, these criteria were regressed by artichoke extract (1.5 g/kg for 2 months), and the liver showed cirrhosis with focal vacuolation of the hepatocytes, dilatation of hepatoportal

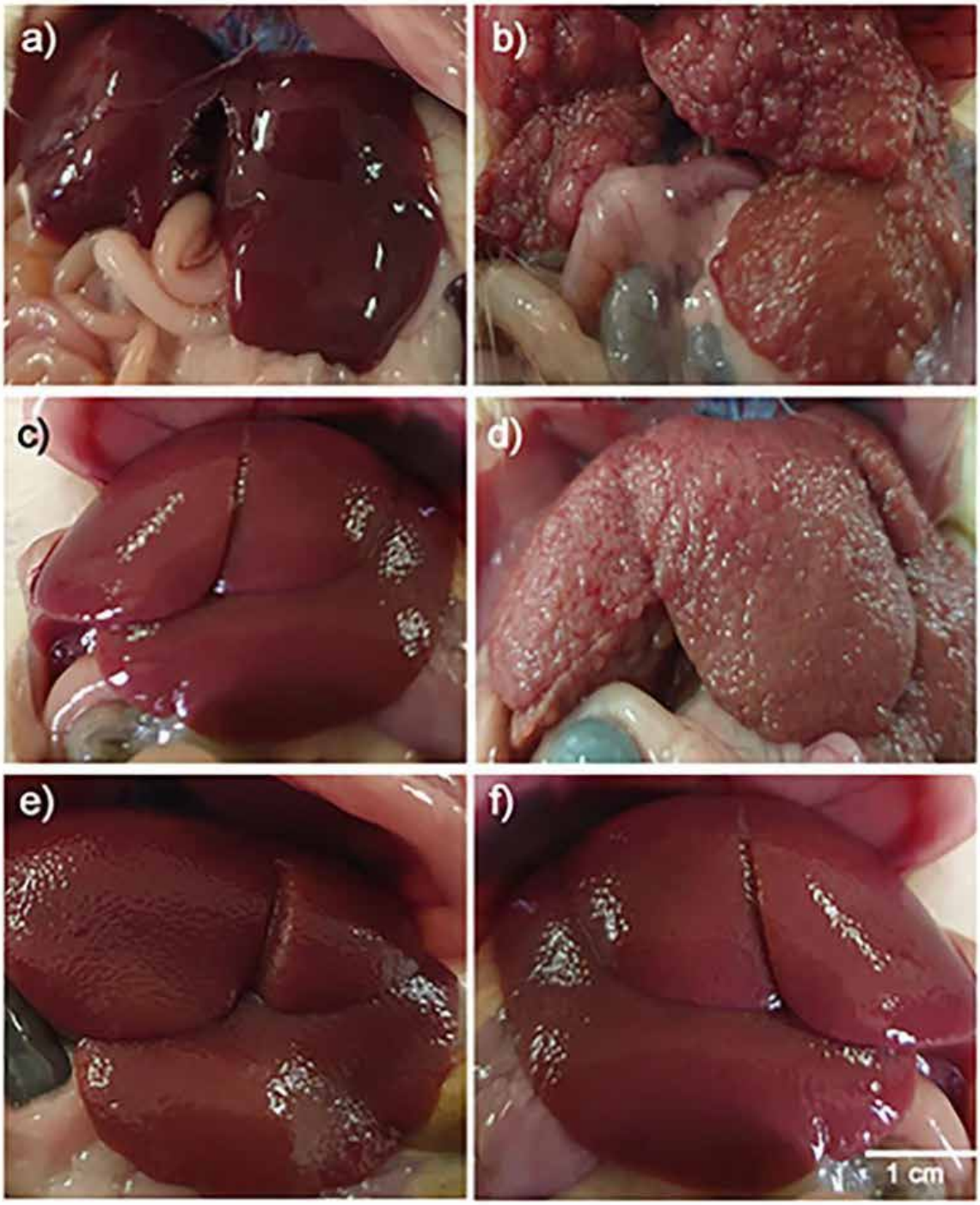

Figure 3. Macroscopic picture of livers obtained from rats of control (a), TAA-treated (b), TAA + Silymarin treated (c), TAA + CSE SD treated (d), TAA + CSE LD treated (e), CSE LD (f), showing (a) typical obvious signs of red-brown color, smooth and shiny brown surface, with no irregularities on the surface, (b) hepatic enlargement with multiple nodular irregularities, pale red color and rough surface, (c) signs of recovery as red color, smooth and shiny brown surface, with no irregularities, (d) hepatic enlargement with multiple nodular irregularities, pale color, rough surface, and edges, (e) good restoration of the hepatic architecture like normal appearance (smooth, soft, with no irregularities on the surface), (f) normal liver with deep red color, soft, smooth, with no irregularities on the surface.

blood vessel with regression of the trabecular arrangement of the hepatocytes. Our study's pathological findings may also be partially consistent with those of (49) who reported that di-ethyl-nitrosamine (100 mg/kg) affected the liver cells through the occurrence of hepatic cellular degeneration and necrosis. Simultaneously, treatment with artichoke heads or leaves (0.5, 1 g) for 25 days led to significant amelioration of such changes in the liver's histological architecture. Moreover, our results are partially consistent with those of (38) who reported the protective effects of ethanolic extracts from artichoke (0.4, 0.8, and 1.6 g/kg body weight) by gavage once daily, an edible herbal medicine, against acute alcohol-induced liver injury (12 mL/kg body weight) orally in mice for 10 days. Histopathological examination showed that artichoke attenuated degeneration, inflammatory infiltration and necrosis of hepatocytes.

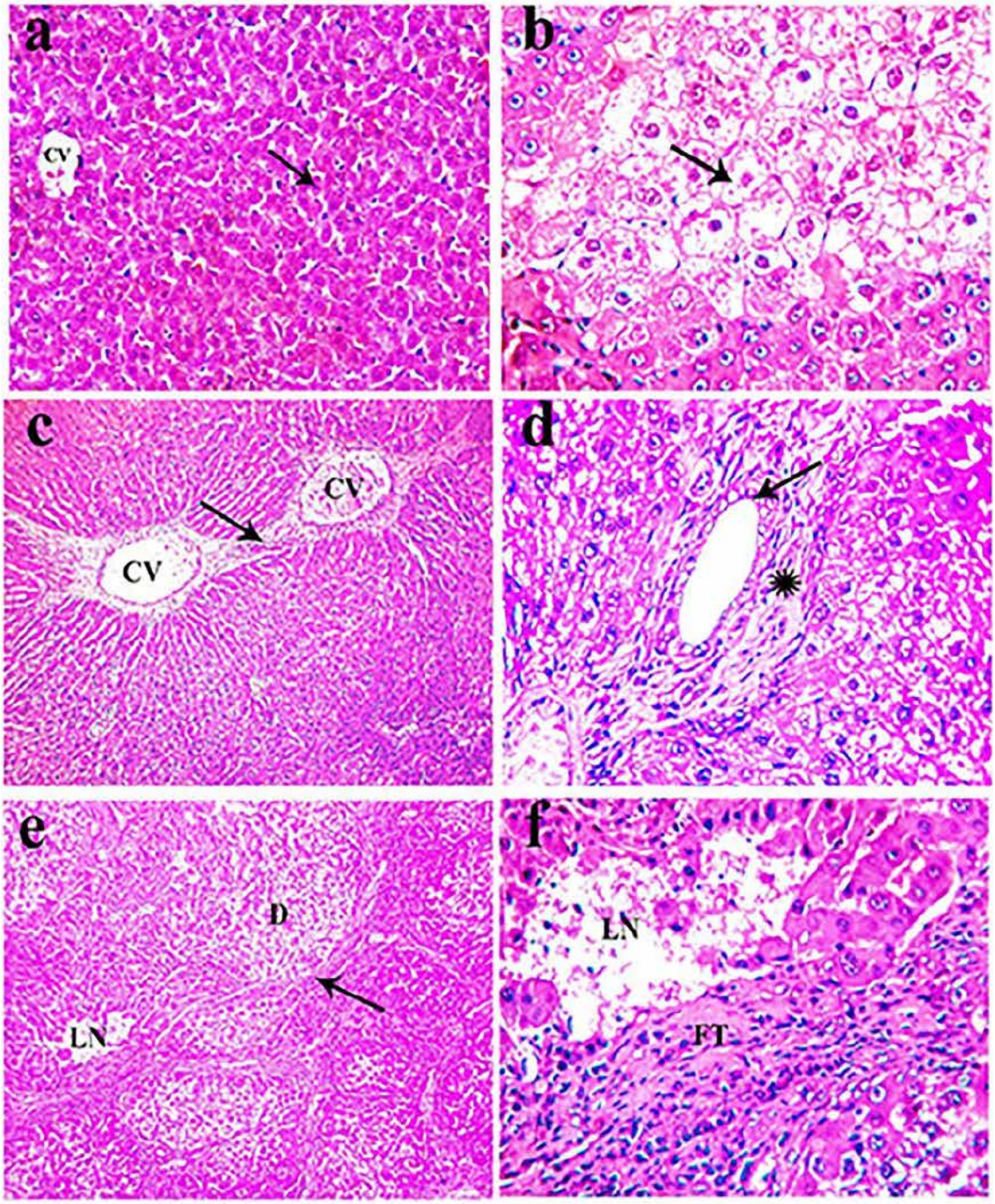

Figure 4. H&E stained section of liver obtained from rats of the control group (a) and intoxicated group that received 100 mg/kg TAA, twice a week for 8 weeks (b-f), showing: (a) standard histological criteria of blood vessels (CV) and hepatocyte (arrow, x 200), (b) extensive hydropic degeneration (arrow) of hepatocytes characterized by swollen, pale, vacuolated cytoplasm (arrow, x400), (c) fibrous connective tissue bridging (arrow) from the central vein (CV) to the central vein (CV, x100), (d) mild hyperplasia of the lining epithelium of bile duct (arrow) with peri-ductal fibrous connective tissue proliferation (asterisk, x400), (e) strands of fibrous connective tissue proliferation (arrow) in the hepatic parenchyma forming pseudo-lobulation adjacent to degenerated hepatocytes (D) and necrotic tissue (LN, x 100), (f) discrete foci lytic necrosis (LN) with fibrous connective tissue proliferation (FT) in the hepatic parenchyma (x 400).

Conclusions

It could be concluded that Artichoke extract has a significant hepatoprotective potential indicated by: i) It reduced elevated levels of enzymatic markers (AST, ALT, GGT & ALP); ii) It increased the levels of total protein, albumin, globulins and decreased levels of bilirubin; iii) It decreased high TAGs, cholesterol & risky lipoproteins (LDL & VLDL) while increased the level of beneficial lipoprotein (HDL), iv) It increased GPx, SOD, CAT, while decreased MDA in thioacetamide-induced liver injury rat model.

Overall, a large dose of artichoke could be a useful adjuvant in the prevention of liver injury. We highly recommend using artichoke extract as a supplement drug with the treatment of liver injury. However, the active constituents and molecular bases of the artichoke effect need further investigation.

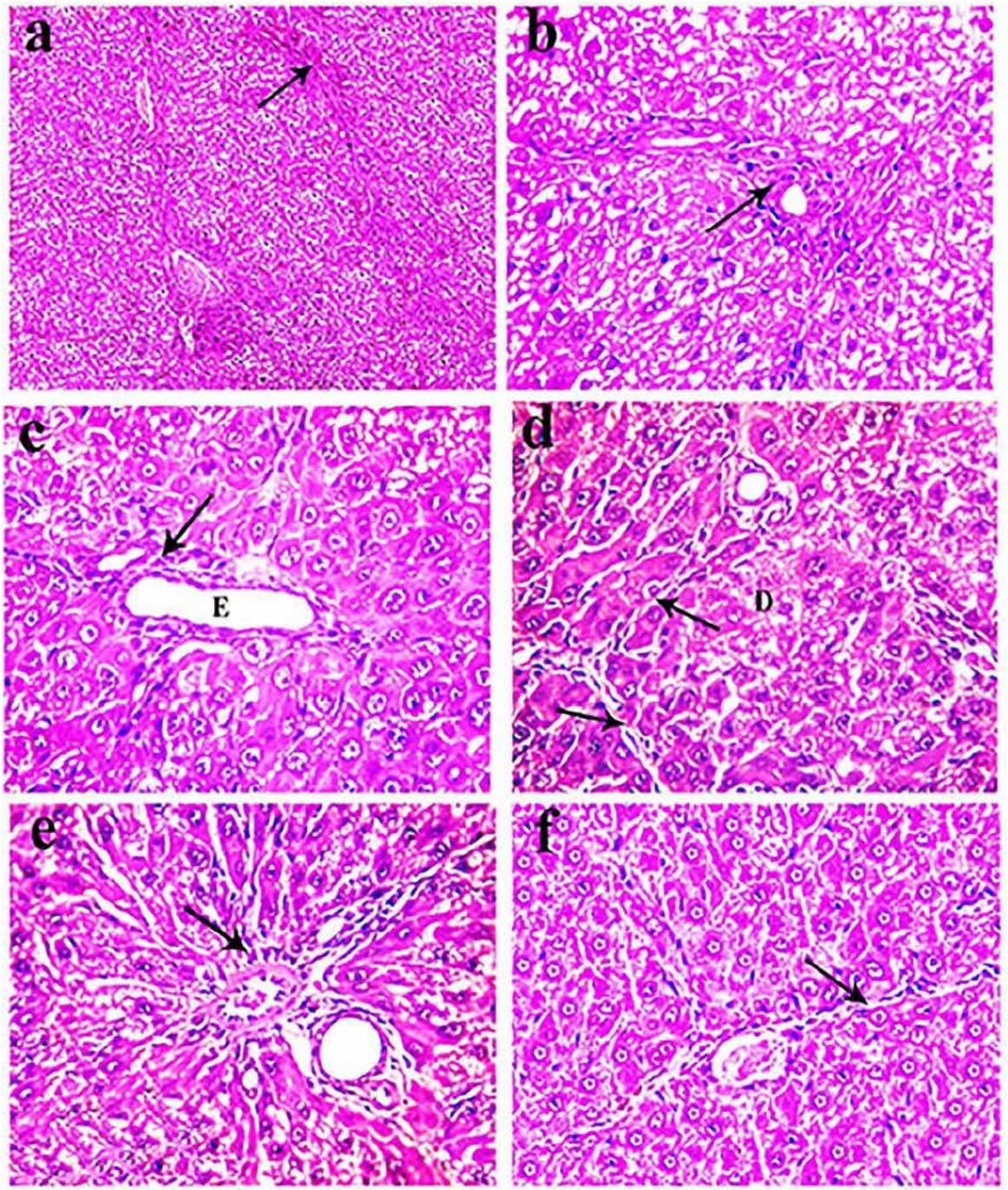

Figure 5. H&E stained sections of livers obtained from rats of group 3 (a-b), group 4 (c-e), and group 5 (f), showing (a) fine strands of fibrous connective tissue in the hepatic parenchyma (arrow, x 100), (b) mild peri-portal fibrous connective tissue proliferation (arrow, x400), (c) ectatic bile duct (E) with mild periductal fibrosis infiltrated by few mononuclear inflammatory cells (arrow, x400), (d) fine strands of fibrous connective tissue (arrow) adjacent to the degenerated hepatocytes (D, x400), (e) mild peri-portal fibrous connective tissue proliferation (arrow, x400), (f) thin strands of the fibrous connective tissue in the hepatic parenchyma (arrow, x400).

Acknowledgments

Not applicable.

Conflict of interest

There is no actual or potential conflict of interest in relation to this article.

Bibliographic references

1. Schuppan D, Afdhal NHJTL. Liver cirrhosis. 2008;371(9615):838-851.
2. Zimmerman HJ. Drug-induced liver disease. Clinics in liver disease 2000;4(1):73-96.
3. Sgro C, Clinard F, Ouazir K, et al. Incidence of drug- induced hepatic injuries: a French population- based study. Hepatology 2002;36(2):451-455.

4. Pérez-García F, Adzet T, Cañigueral S. Activity of artichoke leaf extract on reactive oxygen species in human leukocytes. Free Radical Research 2000;33(5):661-665.
5. Salem MB, Affes H, Ksouda K, et al. Pharmacological studies of artichoke leaf extract and their health benefits. 2015;70(4):441-453.
6. Giorgi D, Pandozy G, Farina A, et al. Karyotype of globe artichoke (Cynara cardunculus var. scolymus): preliminary studies to define its chromosome morphology. VIII International Symposium on Artichoke, Cardoon and their Wild Relatives 9832012:133-138.
7. Zhu X, Zhang H, Lo R. Phenolic compounds from the leaf extract of artichoke (Cynara scolymus L.) and their antimicrobial activities. Journal of Agricultural and Food Chemistry 2004;52(24):7272-7278.
8. Bernacchi A, De Castro C, de Toranzo E, et al. Pyrazole prevention of CC14-induced ultrastructural changes in rat liver. British journal of experimental pathology 1980;61(5):505.
9. Yan-Yu X, Yun-mei S, Zhi-peng C, Qi-neng P. Preparation of silymarin proliposome: a new way to increase oral bioavailability of Silymarin in beagle dogs. International journal of pharmaceutics 2006;319(1-2):162-168.
10. Gillessen A, Schmidt HH-J. Silymarin as supportive treatment in liver diseases: A narrative review. Advances in Therapy 2020:1-23.
11. Del Maestro R, McDonald W. Oxidative enzymes in tissue homogenates. Handbook of methods for oxygen radical research 1985:291-296.
12. Gheith I, El-Mahmoudy A, Elmajdoub A, Awidat S. Pharmacovigilance of tilmicosin in mice. Acta Scientiae Veterinariae 2015;43:1-10.
13. Reitman S, Frankel S. Colorimetric methods for aspartate and alanine aminotransferase. Am J Clin Pathol 1957;28:55-60.
14. Casillas E, Sundquist J, Ames W. Optimization of assay conditions for, and the selected tissue distribution of, alanine aminotransferase and aspartate aminotransferase of English sole, Parophrys vetulus Girard. Journal of Fish Biology 1982;21(2):197-204.
15. Sato K, Tsukamasa Y, Imai C, Ohtsuki K, Shimizu Y, Kawabata M. Improved method for identification and determination of. epsilon.-(. gamma.-glutamyl) lysine cross-link in protein using proteolytic digestion and derivatization with phenyl isothiocyanate followed by high-performance liquid chromatography separation. Journal of Agricultural and Food Chemistry 1992;40(5):806-810.
16. Haussament T. Quantitative determination of serum alkaline phosphatase. Clin Chem Acta 1977;35:271-273.
17. Gornall AG, Bardawill CJ, David MM. Determination of serum proteins by means of the biuret reaction. Journal of biological chemistry 1949;177(2):751-766.
18. Doumas BT, Peters Jr T. Origins of dye-binding methods for measuring serum albumin. Clinical Chemistry 2009;55(3):583-584.
19. Coolidge TBJJoBC. Chemistry of the van den Bergh reaction. 1940;132(1):119-127.
20. Fossati P, Prencipe L. Serum triglycerides determined colorimetrically with an enzyme that produces hydrogen peroxide. Clinical chemistry 1982;28(10):2077-2080.
21. Richmond W. Enzymatic determination of total serum cholesterol. Clin Chem 1973;20:470-475.
22. Lopes-Virella MF, Stone P, Ellis S, Colwell JA. Cholesterol determination in high-density lipoproteins separated by three different methods. Clinical chemistry 1977;23(5):882-884.
23. Wieland H, Seidel D. A simple specific method for precipitation of low density lipoproteins. Journal of Lipid Research 1983;24(7):904-909.
24. Pool JG, Robinson J. Assay of plasma antihaemophilic globulin (AHG). British journal of haematology 1959;5(1):17-23.
25. Walter M, Gerade H. Determination of the" Total" bilirubin and its conjugated" Direct" fraction. Microchem J 1970;15:231-240.
26. Wilson PW, Abbott RD, Garrison RJ, Castelli WP. Estimation of very-low-density lipoprotein cholesterol from data on triglyceride concentration in plasma. Clinical chemistry 1981;27(12):2008-2010.
27. Ohkawa H, Ohishi N, Yagi K. Assay for lipid peroxides in animal tissues by thiobarbituric acid reaction. Analytical biochemistry 1979;95(2):351-358.
28. Paglia DE, Valentine WN. Studies on the quantitative and qualitative characterization of erythrocyte glutathione peroxidase. The Journal of laboratory and clinical medicine 1967;70(1):158-169.
29. Aebi H. Catalase in vitro Methods Enzymol 105: 121–126. Find this article online 1984.
30. Nishikimi M, Roa N, Yogi K. Determination of superoxide dismutase in tissue homogenate. Biochem Bioph Res Common 1972;46:849-854.
31. Banchroft D, Cook C, Stirling R, Turner D. Manual of histopathological techniques and their diagnostic application. Chuchill Livingston. Edinburg; 1996.
32. Wang K, Zhang S, Marzolf B, et al. Circulating microRNAs, potential biomarkers for drug-induced liver injury. Proceedings of the National Academy of Sciences 2009;106(11):4402-4407.
33. Hajovsky H, Hu G, Koen Y, et al. Metabolism and toxicity of thioacetamide and thioacetamide S-oxide in rat hepatocytes. Chemical research in toxicology 2012;25(9):1955-1963.
34. Singh G, Bhatia D. Chemicals/drugs-hepatotoxicants: an overview. Der Pharma Chem 2015;7:164-8.
35. Feher J, Lengyel G. Silymarin in the prevention and treatment of liver diseases and primary liver cancer. Current pharmaceutical biotechnology 2012;13(1):210-217.
36. Freitag AF, Cardia GFE, da Rocha BA, et al. Hepatoprotective effect of Silymarin (Silybum marianum) on hepatotoxicity induced by acetaminophen in spontaneously hypertensive rats. Evidence-Based Complementary and Alternative Medicine 2015;2015.
37. Nateghi R, Samadi F, Ganji F, Zerehdaran S. Hepatoprotective effects of Cynara scolymus L. extract on CCl4 induced liver injury in broiler chickens. International Journal of AgriScience 2013;3(9):678-688.
38. Tang X, Wei R, Deng A, Lei T. Protective effects of ethanolic extracts from artichoke, an edible herbal medicine, against acute alcohol-induced liver injury in mice. Nutrients 2017;9(9):1000.
39. Speroni E, Cervellati R, Govoni P, Guizzardi S, Renzulli C, Guerra M. Efficacy of different Cynara scolymus preparations on liver complaints. Journal of ethnopharmacology 2003;86(2-3):203-211.
40. Huber R, Müller M, Naumann J, Schenk T, Lüdtke R. Artichoke leave extract for chronic hepatitis C–a pilot study. Phytomedicine 2009;16(9):801-804.
41. Shalaby M, Hammoda A. Hepatoprotective effect of artichoke leaves aqueous extract in ccl4 intoxicated rats. World Journal of Pharmacy and Pharmaceutical Sciences 2014;4(1):138-154.
42. Mustafa HN, El Awdan SA, Hegazy GA, Jaleel GAA. Prophylactic role of coenzyme Q10 and Cynara scolymus L on doxorubicin-induced toxicity in rats: Biochemical and immunohistochemical study. Indian journal of pharmacology 2015;47(6):649.
43. El-Mesallamy AM, Abdel-Hamid N, Lamis Srour SA. Identification of Polyphenolic Compounds and Hepatoprotective Activity of Artichoke (Cynara Scolymus L.) Edible Part Extracts in Rats. Egyptian Journal of Chemistry 2020;63(6):2273-2285.
44. El-Mahmoudy AM, Abdel-Fattah FA, Abd El-Mageid AD, Gheith IM. Effect of the growth promotant mannan-oligosaccharide on the lipogram and organ function profile in hyperlipidemic albino rats. Am J Phytomed Clin Ther 2014;2:334-347.
45. Ben Salem M, Ksouda K, Dhouibi R, et al. LC-MS/MS analysis and hepatoprotective activity of artichoke (Cynara Scolymus L.) leaves extract against high fat diet-induced obesity in rats. BioMed research international 2019;2019.
46. Heckers H, Dittmar K, Schmahl F, Huth K. Inefficiency of cynarin as therapeutic regimen in familial type II hyperlipoproteinaemia. Atherosclerosis 1977;26(2):249-253.
47. El-Boshy M, Ashshi A, Gaith M, et al. Studies on the protective effect of the artichoke (Cynara scolymus) leaf extract against cadmium toxicity-induced oxidative stress, hepatorenal damage, and immunosuppressive and hematological disorders in rats. Environmental Science and Pollution Research 2017;24(13):12372-12383.
48. Kaymaz MB, Kandemir FM, Pamukcu E, Eröksüz Y, Özdemir N. Effects of aqueous artichoke (Cynara scolymus) leaf extract on hepatic damage generated by alpha-amanitine. Kafkas Univ Vet Fak Derg 2017;23(1):155-160.
49. Metwally N, Kholeif T, Ghanem K, Farrag A, Ammar N, Abdel-Hamid A. The protective effects of fish oil and artichoke on hepatocellular carcinoma in rats. European review for medical and pharmacological sciences 2011;15(12):1429-1444.

Received: 15 January 2021
Accepted: 16 February 2021

RESEARCH / INVESTIGACIÓN

Fermentation study of *Cassava bagasse* starch hydrolyzed's using INIAP 650 and INIAP 651 varieties and a strain of *Lactobacillus leichmannii* for the lactic acid production

Shirley Inguillay[1], Felipe Jadán[2] and Pedro Maldonado-Alvarado[1*]

DOI. 10.21931/RB/2021.06.02.21

Abstract: Ecuador is an agricultural country, which has an actual production of starch obtained from cassava. Tuber processing residues do not have an economic impact; for example, the cassava bagasse, only used for plant fertilization and animal feeding. This project aimed to study the influence of the fermentation variables (pH and agitation), on the lactic acid production. Enzymatic hydrolysis of cassava bagasse starch for the varieties INIAP 650 and INIAP 651 was performed using α-amylase and glucoamylase. Then, glucose was fermented by *Lactobacillus leichmannii* ATCC 7830 strains, varying conditions such as agitation (150 *rpm* and absence) and pH (4.5, 5.0, and 5.5). Finally, the determination of lactic acid was performed by potentiometric and FTIR analysis. Conversions of cassava bagasse to reduced sugars were 71.66 and 85.05 % for INIAP 650 and INIAP 651 varieties. The best lactic acid concentrations were 27.62 and 33.48 g/L, obtained at pH 5.5 and agitation, for INIAP 650 and INIAP 651 varieties. Qualitative analysis conducted by FTIR spectrophotometry confirmed the presence of lactic acid in the reacted products. Lactic acid production from cassava bagasse starch could contribute to the Manabí and Esmeraldas provinces of Ecuador's economic development.

Key words: Cassava, Ecuador, bagasse starch, fermentation, *Lactobacillus leichmannii*, lactic acid.

Introduction

In 2016, the global market required 1 220 kton of lactic acid, with growing demand at a rate of 16.2 % per year. It is estimated that by 2025 these requirements will reach 2 000 kton, this would represent approximately 9.8 billion dollars of revenue for the global lactic acid-producing market[1].

Nowadays, green methods take advantage of residues, or by-products of agroindustry, for their conversion to fuels or industrial interest products is on the rise. Lactic acid is used in food, pharmaceutical, chemical, and cosmetic industries[2]. The production of lactic acid obtained from biomass rich in sugars, starch, or lignocellulosic material is relevant throughout the world due to its low production cost since the raw material used as a substrate comes from abundant and renewable resources[3,4]. The production of biofuels and compounds of industrial interest, such as lactic acid, presents a limitation, the recovery of first-generation biomass to obtain these products, which is why it seeks to take advantage of the second generation biomass of various food species such as cassava, potato, corn, among others[2].

Starch is a polymer made up of two types of molecules, amylose, and amylopectin. Amylose is a linear polymer made up of about 500 - 2 000 glucose units assembled by - 1-4 glucosidic bonds. Amylopectin is a branched polymer made up of approximately 1 000 000 glucose units, grouped by - 1-4 glucosidic bonds and 5 % α 1-6 bonds in the branches. The proportion of each of these polymers depends on the starch's origin; for corn and cassava the amylose values range from 20 to 30 % and for amylopectin from 80 to 70 %, respectively[5,6].

Lactic fermentation is an anaerobic metabolic process that involves the use of lactic microorganisms. This process can be batch or fed-batch types. In fermentation, the temperature and pH conditions are specific for each microorganism. However, lactic acid production is not affected by the initial pH due to neutralizing agents such as calcium carbonate and ammonium nitrate.

The fungi and bacteria that are used in the fermentation of sugars and production of lactic acid are strains of homofermentative microorganisms that belong to the genera *Kluyveromyces*, *Saccharomyces*, *Lactobacillus*, and *Rhizopus*[7]. Another study reports that *Lactobacillus*-type bacteria are appropriate for fermenting substrates rich in glucose, lactose, sucrose, and maltose[8]. *Lactobacillus delbrueckii* is a homofermentative bacterium that does not develop spores, has tolerance to acidity and its fermentative metabolic route is strictly directed to the formation of D (-) lactic acid. The optimal growth conditions for the *Lactobacillus delbrueckii* strain, contained in *Lactobacillus leichmannii* ATCC 7832, are 37 ºC and a pH of 4 to 6[9]. For processes with homofermentative bacteria, the conversion is 1 to 1 in g/L, respectively. The fermentation efficiency also depends on the initial concentration of carbohydrates, concentration of nitrogenous material, and the fermentation medium's agitation with ranges of 100 - 200 *rpm*[1,7].

Lactic acid or 2-hydroxypropanoic acid is a compound that has alcohol and carboxyl groups in its structure; it is obtained by chemical or biotechnological means[10]. To chemically obtain the acid, a reaction occurs between acetaldehyde and hydrocyanic acid[11]. There are two optical isomers: L (+) lactic acid, which is harmful because its consumption generates decalcification in living beings but is used for the production of polylactic acid, and D (-) lactic acid, which is considered as GRAS (food additive recognized as safe by the FDA (Food and Drug Administration)[12]. Titration methods with detection carry out the quantification of lactic acid ranges from 8.10 to 20.83 g/L, by colorimetry analysis with detection thresholds from 0.3 to 10 g/L and gas chromatography with detection limits of 0.02 - 1.37 g/kg[13].

Studies have been carried out to obtain lactic acid with bakery waste using *T. aotearoense*, with yields of 78.4 g/L[14]. Likewise, with the use of whey and *L. delbrueckii* and *S. thermophillus*, a production of 36.7 g/L of this acid was obtained[15].

[1] Department of Food Science and Biotechnology, Escuela Politécnica Nacional (EPN), Quito, Ecuador.
[2] Departament of chemical processes, Universidad Técnica de Manabí (UTM). Portoviejo, Ecuador.

Corresponding author: pedro.maldonado@epn.edu.ec

On the other hand, a lactic acid production of 19.17 g/L was achieved with sugarcane bagasse and *L. pentosus*[16]. In another study, a production of 97.6 g/L of lactic acid was obtained using corn stubble and *B. coagulans*[17]. Finally, with coffee mucilage, a fermentation efficiency of 68 % of this compound was obtained using a strain of *L. bulgaricus*[18].

Cassava (*Manihot esculenta* Crantz) is a tuber rich in complex carbohydrates, which grows mainly in tropical climates. In Ecuador, it is grown in the provinces of Manabí, Esmeraldas, Santo Domingo de los Tsáchilas, among others. For 2018, Manabí produced 13 819 000 kg of cassava of the INIAP 650 and INIAP 651 varieties[19]. In Ecuador cassava is consumed fresh and in the form of starch[20]. The root is 80 % made up of the tuber and 20 % of the cassava bagasse made up of the husk and bark. Cassava bagasse has a starch content of 50 to 60 %, cellulose 34 %, hemicellulose 15 %, and lignin 7 %[21–23].

Studies carried out in Colombia analyzed lactic acid production with 120 g/L of cassava starch and *Lactobacillus* strains grown from yogurt. In 3 days of fermentation at 37 ºC with the agitation of 100 *rpm* and pH of 5.0, was reached 51.15 g/L of lactic acid[24].

In April 2016, Ecuador suffered one of the strongest earthquakes in its history, with 7.6 on the Ritcher scale. The Technical Committee for the Reconstruction of the Manabí and Esmeraldas provinces was formed, focused on the productive reactivation of these areas (Unidad Digital de Pública FM, 2019)[25]. PREDU 2016-015 project "Sustainable development of modified starches and products of industrial interest from cassava as an alternative for the productive reactivation of the Manabí and Esmeraldas provinces", contemplates the production of lactic acid from a hydrolyzed cassava bagasse starch of the varieties INIAP 650 and INIAP 651, with the use of a strain of *Lactobacillus leichmannii* ATCC 7830 in the fermentation process. For the first time in Ecuador, it seeks to generate residues from the benefit of cassava, for the production of lactic acid by a biotechnological way.

Methods

Evaluation of the effect of pH and agitation in the fermentation process of starch hydrolyzate from cassava bagasse varieties INIAP 650 and INIAP 651

Raw material

The obtaining of cassava bagasse starch was carried out at the artisanal "Rallandería Bijahual" in the "Las Balsas" sector, located in Manabí. 90 kg of roots of the INIAP 650 and INIAP 651 varieties were extracted from the INIAP Portoviejo Experimental Station. The INIAP 650 variety comes from the MCol 2215 clone; it has a dry matter content of 37 % with a yield of 17 to 35 t/ha of fresh roots and a conversion rate from fresh to dry matter of 2 - 2.5 : 1 26. The variety INIAP 651 comes from the clone CM 1335-4; it has a dry matter content of 35.5% with a yield of 29 to 40 t/ha, and a conversion rate of 6 - 7.5 : 1[27].

The cassava root barks were separated and placed in a needle rack for grinding. With the help of a canvas-type cloth, the ground material was washed until the starch was released. The precipitate was collected and sun-dried at the extraction site's temperature (29 ºC) for 24 h[28].

Characterization of cassava bagasse starch

The properties of bagasse starch were determined employing a proximal analysis. The standardized norms indicated in Table 1. were used.

Component	Standardized regulation
Moisture	AOAC 925.10
Ashes	AOAC 923.03
Fiber	AOAC 920.86
Protein	AOAC 976.13
Lipids	AOAC 923.05
Amylose	ISO 1742:1980

Table 1. Standards used in the proximal analysis.

Cassava bagasse starch was stored at temperatures between 0 - 4 ºC[29], for later use.

Hydrolysis of cassava bagasse starch

A 10 % of the starch/water (w/v) solution was prepared. The solution was heated at 65 ºC for 1 h at 150 *rpm* in a thermostatic bath[30]. Subsequently, a liquefaction process was carried out with α-amylase from pig pancreas A3176-500KU, SIGMA-ALDRICH (USA) in a proportion of 5 µg of enzyme/mg of starch, dissolved in a phosphate buffer solution 400 mM at pH 7.1. Then, it was added NaN3 (0.02 %), CaCl2 (0.25 %), NaCl (0.013%)[31], it was allowed to react in a thermostatic bath for 24 h at 37 ºC and 100 *rpm*[32]. Finally, a saccharification process was carried out with the amyloglucosidase enzyme from *Aspergillus niger* A7095-50ML, SIGMA-ALDRICH (USA), in a proportion of 0.025 µg of enzyme/mg of starch in 10 mL of a 0.5 M acetate buffer solution and pH 4.8[33]. It was heated in a thermostatic bath for 48 h at 65 °C and 150 *rpm*[34].

After that, the hydrolyzate was stirred at 50 *rpm* for 12 h and 20 °C. Finally, it was centrifuged at 3000 *rpm* for 20 min[35].

Determination of reducing sugars in cassava bagasse starch hydrolyzate

The reducing sugars were determined with the colorimetric method by DNS (3.5-Dinitrosalicylic acid)[36]. 0.5 mL of the hydrolyzed sample and 0.5 mL of the DNS reagent were placed in a test tube. It was stirred manually and heated in a boiling thermostatic bath for 5 min. Then, it was cooled at 18 °C, and 3.5 mL of distilled water was added. The absorbance was analyzed in a spectrophotometer (Shimadzu, UV-160 A (Brazil)), at a wavelength of 540 nm, and finally, the concentration of reducing sugars was calculated.

Inoculum activation and preparation

A *Lactobacillus leichmannii* ATCC 7830 strain from Microbiologics Company (USA) was used. A pellet of the microorganism was taken and placed in 10 mL of sterilized MRS agar at 121 ºC for 15 min (Microbiologics, 2018). The agar with the pellet was incubated in a thermostatic bath for 24 h at 37 ºC and 1 mL of this was taken and seeded deeply on MRS agar. The Petri dish with the sowing was incubated for 72 h at 37 ºC[37]. To finish, a colony was taken from the agar, placed in 10 mL of MRS agar, vortexed, and incubated similarly at 37 ºC for 18 h[38].

Lactic fermentation

100 mL of cassava bagasse starch hydrolyzate were taken, and enriched with yeast extract 0.5 % (w/v), NH4Cl 0.5 % (w/v) and $CaCO_3$ 2.5 % (w/v). The pH was adjusted to 4.5, 5.0 and 5.5 with NaOH 4 % w/v or HCl 5 % w/v. Then, a volume of nitrogen was introduced at a rate of 2 cm^3/s for 1 min, and fi-

nally, the inoculum at 2 % (v/v) previously prepared was added. The flasks with the substrate to be fermented were placed in an incubator and a thermostatic bath at 37 ºC, with and without shaking, for 120 h[15].

The input variables were: pH (4.5, 5.0, and 5.5) and agitation (150 *rpm* or absence), while the output variable was the lactic acid content. The performed treatments are detailed in Table 2.

Treatment (T)	Variety	Agitation	pH
T1	INIAP 650	150 *rpm*	4.5
T2	INIAP 650	150 *rpm*	5.0
T3	INIAP 650	150 *rpm*	5.5
T4	INIAP 650	Absence	4.5
T5	INIAP 650	Absence	5.0
T6	INIAP 650	Absence	5.5
T7	INIAP 651	150 *rpm*	4.5
T8	INIAP 651	150 *rpm*	5.0
T9	INIAP 651	150 *rpm*	5.5
T10	INIAP 651	Absence	4.5
T11	INIAP 651	Absence	5.0
T12	INIAP 651	Absence	5.5

Table 2. Treatments for the production of lactic acid.

Evaluation of the yield and the final composition of lactic acid obtained from fermentation processes

Recovery of lactic acid

The lactic acid recovery was carried out by a hydrolysis and acidification process. All the fermented was filtered with a canvas. For all fermentation, H_2SO_4 1 M was added until reaching a pH of 2.0, pH at which $CaSO_4$ precipitates and liberates lactic acid. This mixture was stirred for 30 min and centrifuged at 8000 *rpm* for 15 min. Lactic acid was contained in the supernatant and the $CaSO_4$ precipitated[39]. The following section specifies how the lactic acid content was determined.

Determination of lactic acid content by acid-base titration

Aliquots of 20 mL were taken from the supernatant once the acidification process was finished. The content of lactic acid was measured by titration with NaOH 1 N. Finally, with this information, the concentration of lactic acid present in the solution was calculated using the equation (1):

$$C_{a.l} = \frac{C_{NaOH} * V_{NaOH} * PM_{a.l}}{V_{a.l}} \quad (1)$$

Where:
: Lactic acid content (g/L)
: Caustic soda concentration (mol/L)
: Caustic soda volume (mL)
: Lactic acid molecular weight (g/mol)
: Sample volume used for titration (mL)

Determination of the fermentative efficiency and characterization of lactic acid

The lactic acid solution density was measured with a Mettler Toledo (USA)[40] densimeter and the pH of the final solution containing lactic acid using a Hanna (USA) pH meter. The real fermentative yield was determined by the relationship between the lactic acid obtained and the amount of starch used as a substrate. A conversion of 1 glucose molecule to 2 lactic acid molecules was estimated for the theoretical fermentative yield.

Furthermore, the comparison between the spectrogram obtained by FTIR of the experimentation with a 98 % of lactic acid spectrogram was analyzed. The infrared spectrophotometry equipment used was a Perkin Elmer (USA) brand, Spectrum One 2370 model with a diamond cell. Three repetitions for each simple were performed.

Statistical analysis

The proximal analysis results, lactic acid concentration, optical density, fermentation efficiency, and pH were statistically analyzed with the StatGraphics Centurion XVIII X64 program using a multifactorial ANOVA followed by a Fisher test with a 95 % confidence level to determine statistically significant differences. Three repetitions were made for each treatment.

Results and Discussion

Evaluation of the effect of pH and agitation in the fermentation process of starch hydrolyzate from cassava bagasse varieties INIAP 650 and INIAP 651

Characterization of cassava bagasse starch

For this study, cassava bagasse starch was used, the by-product of the cassava grating process, of INIAP 650 and INIAP 651 varieties. Table 3. shows the moisture, ash, fiber, protein, lipids, and amylose contents. The carbohydrates content was calculated as the difference in content with these parameters. It is understood that carbohydrates are mainly made up of amylopectin[41].

Parameter (%)	Variety	
	INIAP 650	INIAP 651
Moisture	11.30 ± 0.16^a	14.50 ± 0.12^b
Ash	1.40 ± 0.10^b	1.32 ± 0.30^a
Fiber	4.30 ± 0.09^a	6.00 ± 0.09^b
Protein	1.20 ± 0.07^a	2.10 ± 0.14^b
Lipids	1.90 ± 0.04^b	1.50 ± 0.03^a
Amylose	24.34 ± 0.08^a	26.50 ± 0.06^b
^{a,b} Different letters, within row, show statistical differences between varieties for each parameter using an LSD test with 95 % of confidence		

Table 3. Physicochemical characteristics of cassava bagasse starch INIAP 650 and INIAP 651 varieties.

INIAP 650 and INIAP 651 varieties moisture content was 11.30 % (w/w) and 14.50 % (w/w), respectively. A previous study reported the cassava tuber starch had a moisture content in a range of 11 - 13 %[42]. The INIAP 650 variety was found within the indicated range, but the INIAP 651 variety surpassed these values, due to higher hygroscopy, at a rate of 3.30 g of water/g of starch.

The ash content in the cassava bagasse starch was 1.40 and 1.32 % for INIAP 650 and INIAP 651 varieties. A study showed the range for ash in cassava bagasse starch from 0.9 to 1.50 %[43]. Another work points out values of 0.05 % (w/w) for cassava bagasse starch[42], 28 times less ash content concerning the amount obtained in our study. Conversely, previous work reported that cassava starch had 7 times less ash con-

tent than bagasse[44], due to minerals present in its composition[45].

The fiber present in the cassava bagasse starch was 4.30 and 6.00 % for INIAP 650 and INIAP 651 varieties, respectively. No data on the fiber content of bagasse starch was found.

However, the bibliography shows that the amount of fiber present in the cassava tuber starch is 0.30 %. This is due to the high concentration of cellulose present in cassava bagasse, ranging from 15 to 51 %. It is mainly considered a soluble fiber[43,46].

In lipid content, bagasse starch presented values of 1.90 and 1.50 % for INIAP 650 and INIAP 651 varieties, respectively. These values were similar to the range established for cassava starch's lipid material, which is 0.53 - 1.60 %[47]. The average value of lipids of the tubers presented ranges from 2 to 5 %, and the lipid material of the cassava starch from the experimentation was lower but not far compared to the average value of cassava lipids. This may be due to different substrates being compared[22].

The amylose content presented 26.50 and 24.34 % values, respectively, for INIAP 651 and INIAP 650 varieties. The range of amylose in bagasse starch varies from 15.9 to 22.4 %, as reported by the literature[48]. The varieties of the present study had high values compared to those mentioned in the bibliography. These varieties are species improved by the Center for Agricultural Research (INIAP) for starch production and the tuber's consumption, respectively[26,27].

Hydrolysis of cassava bagasse starch and determination of reducing sugars

Enzymatic hydrolysis using α-amylase and glucoamylase showed conversion levels of cassava bagasse starch to reducing sugars of 71.66 and 85.05 % for INIAP 650 and INIAP 651 varieties, respectively. It should be noted that part of these reducing sugars is the glucose chains that Lactobacillus used. Similar results to this study were reported by the literature[49], with conversion yields from 81 to 109 %, from starch to reducing sugars. Another study stated 95 % conversion from starch to reducing sugars with α-amylase and glucoamylase[8].

Conversions greater than 100 % are standard because the enzymatic hydrolysis process adds one molecule of water for each broken bond and increases the hydrolyzed starch weight. Besides, amylose and amylopectin long chains have n glucose chains. When these chains are hydrolyzed, they break into n glucose, maltose, and dextrins that increase quantification concentration, reducing sugars[24].

Evaluation of the yield and final composition of lactic acid obtained from fermentation processes

Determination of lactic acid content

The multifactorial ANOVA statistical analysis determined that the agitation and the pH within the fermentation of the hydrolyzed cassava bagasse starch of INIAP 650 and INIAP 651 varieties presented significant influence in the response variable (Value-P < 0,05), the lactic acid produced.

Table 4. shows the results of the lactic acid concentration, quantified by titration. Statistically significant differences between the studies treatments were found. Treatment T9 presented higher lactic acid production (33.48 ± 1.87 g/L), which corresponds to the fermentation of the hydrolyzed cassava bagasse starch of INIAP 651 variety pH 5.5 with stirring of 150 *rpm*.

Table 4. Lactic acid production from cassava bagasse starch varieties INIAP 650 and 651 quantified by titration.

Treatment (T)	Lactic acid (g/L)
T1	22.89 ± 0.57^{d}
T2	24.17 ± 1.58^{d}
T3	27.62 ± 0.69^{e}
T4	4.43 ± 0.47^{a}
T5	6.76 ± 1.56^{b}
T6	8.41 ± 1.45^{b}
T7	26.87 ± 0.52^{e}
T8	29.88 ± 0.26^{f}
T9	33.48 ± 1.87^{g}
T10	7.06 ± 1.37^{b}
T11	10.81 ± 0.78^{c}
T12	12.76 ± 0.52^{c}
$^{a-g}$ Different letters show statistical differences between treatments using an LSD test with 95% confidence	

Table 4. Lactic acid production from cassava bagasse starch varieties INIAP 650 and 651 quantified by titration.

In T1, the stoichiometric content of H_2SO_4 was 6.83 mL, but the real volume used was 5.89 mL until reaching pH 2.0. It is then verified that there is a lack of H2SO4, so it reacted with all the calcium lactate, releasing lactic acid and calcium sulfate[50], so that all the lactic acid produced is quantified. This lactic acid was retained as calcium lactate in the precipitate.

The fermentation treatments, T4 to T6 and T10 to T12, carried out without stirring of the fermentation broth, presented the lowest lactic acid production compared with the other treatments. The lowest lactic acid production was obtained with T4, with a value of 4.43 ± 0.47 g/L at pH 4.5 conditions and without stirring from the fermentation of a hydrolyzed bagasse starch of cassava INIAP 650 variety. The main reason that would explain this is the lack of agitation of the system, which hinders the transfer of nutrients from the medium to the cells[51].

In this study, the lactic acid production rate increased by 80.65 % for the treatments with agitation compared to the treatments without agitation, as seen in T1 and T4, in 120 h of fermentation.

Other studies report an increase in lactic acid production by 42 %, when stirred from 0 to 300 *rpm* was reached in 36 h, with the formation of alcohol at pH between 4.5 and 5.5 at 37 ºC with a *Rhizopus oryzae* strain[52,53].

It can be noticed that the production of lactic acid increases as the pH increases in the range of 4.5 to 5.5. In values outside this range, there is an inhibition of the microorganisms that act in transforming glucose to lactic acid[51]. Besides, there are statistically significant differences between the treatments T3 and T9, the latter with the highest production of lactic acid.

The *Lactobacillus delbrueckii* strain develops in the pH range of 4.0 to 6.0, but its growth occurs at pH 5.0 for optimal

lactic acid production[54]. However, in this work, the *Lactobacillus leichmannii* developed better and obtained higher lactic acid production at pH 5.5 (33.48 ± 1.87 g/L) than at pH 5.0 (27.62 ± 0.69 g/L). This is due to the accumulation of lactic acid within the fermentation process that creates an environment not suitable for developing microorganisms, an acidic medium that reduces microbial growth, and therefore the low transformation of glucose to lactic acid. Furthermore, when the initial pH of the solution approaches the pKa of lactic acid (3.8), the undissociated form of this acid has a high inhibitory effect compared to the dissociated lactate form[7,52].

Studies performed with *Lactobacillus* strains indicate high lactic acid productions for pH ranges from 5.0 to 6.5. The literature reports lactic acid productions of 74.01 g/L from a hydrolyzed cassava starch with a starch concentration of 120 g/L at pH 5.0 with a 61.67 % degree of conversion[24]. This is a higher production than the major content of lactic acid obtained in our study (33.48 %), because cassava bagasse starch has non-hydrolyzed lignocellulosic matter that generates interference in fermentation.

A previous study showed lactic acid production from cassava bagasse starch with a *Lactobacillus delbrueckii* strain reaching 136.8 and 196.4 mg/g of lactic acid at pH 4.0 and 5.0, respectively[50]. In our study, a yield of 334.80 and 276.20 mg of lactic acid was obtained for each gram of cassava bagasse starch at pH 5.5 and pH 5.0, respectively, so higher contents of lactic acid than those mentioned in the literature. This is because, in the experimentation, cassava bagasse starch was used and not directly the bagasse.

The substrate plays a significant role in fermentation. Cassava bagasse starch presented a lignocellulosic fiber content that was not hydrolyzed by lactic acid bacteria. On the other hand, cassava starch, in general, does not contain this lignocellulosic material. Thus, cassava bagasse presented lower yields than starch because it presented a high degree of lignocellulosic matter without hydrolyzing; therefore, lactic acid production was lower.

Evaluation of the fermentation efficiency of Lactobacillus leichmannii of a starch hydrolyzate from cassava bagasse starch

The stoichiometric relationship was used under the microorganism's ideal conditions to perform the calculations for the theoretical production of lactic acid from glucose (pH 5.0 at 37 ºC)[51]. However, it should be considered the conditions of pH, temperature, and agitation are the essential variables in fermentation. As seen in Figure 1., there is low production of natural lactic acid compared to the theoretical one that should reach 71.66 g/L and 85.95 g/L of lactic acid for INIAP 650 INIAP 651 varieties, respectively. Thus, maximum values of 27.62 ± 0.69 g/L and 33.48 ± 1.87 g/L were obtained at pH 5.5 with agitation at 150 *rpm* for INIAP 650 and INIAP 651 varieties, respectively. This may be because the theoretical production will always be greater than the production that was reached experimentally. Due to the type of microorganisms for fermentation, fermentation times, pH, temperature, and agitation, the medium and substrate are not considered.

Furthermore, the theoretical yield was determined, assuming that reducing sugars correspond entirely to glucose. The determining factors were pH and substrate. Moreover, the microorganism used in the fermentation specifically consumes glucose for the production of lactic acid, and in the hydrolysis of starch, reducing sugars were obtained that include maltose, dextrins, and glucose. Therefore, the conversion of reducing sugars to lactic acid will not reach the total.

Characterization of the final lactic acid solution

The characterization of the purified lactic acid solution in the different treatments is presented below. The parameters to be evaluated were pH and density. Furthermore, the samples were characterized by FTIR with the representative lactic acid spectrograms.

Physicochemical characterization of lactic acid solutions

The physical properties, density, and pH were evaluated in lactic acid solution. In Table 5. the density and final pH of the

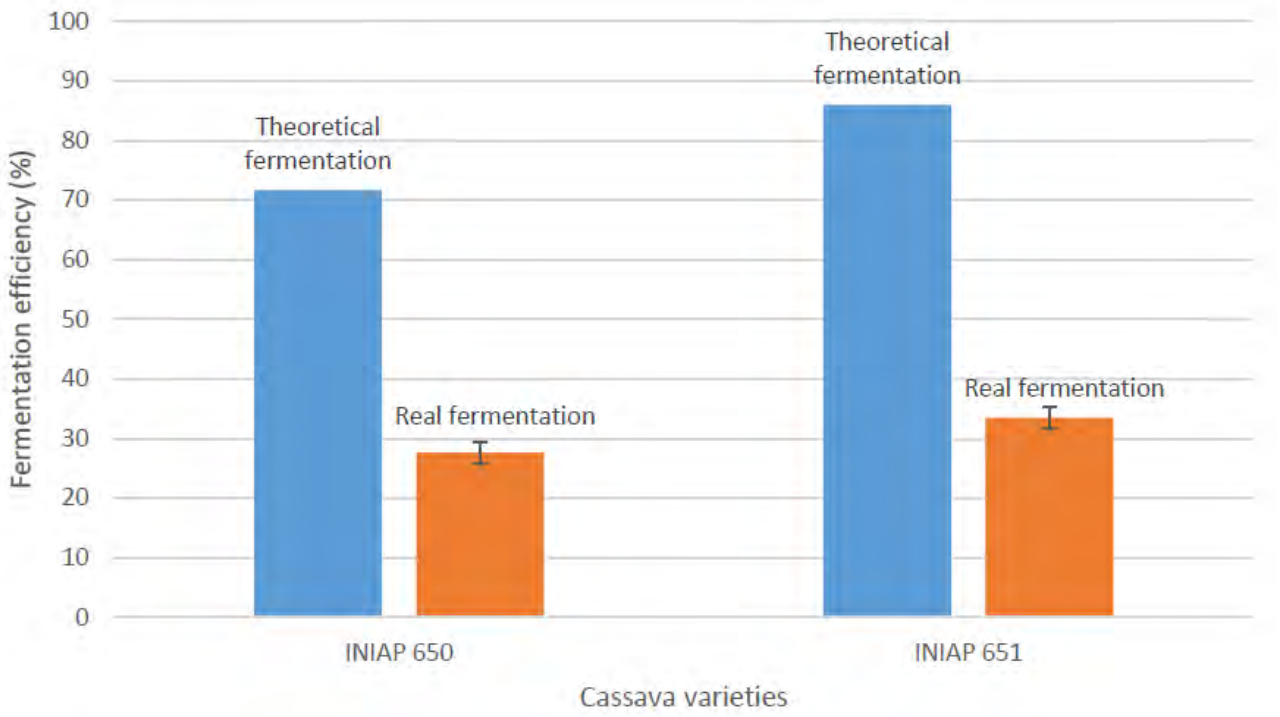

Figure 1. Theoretical (blue bars) and real (orange bars) fermentation efficiency at pH 5.5 with cassava varieties' agitation.

lactic acid solutions are presented. The density in treatments T7, T8, and T9 reached the highest values because they present the highest lactic acid concentration. The highest lactic acid production was at pH 5.5, stirring the hydrolyzed cassava bagasse starch of INIAP 651 variety. Therefore, the density directly relates to lactic acid concentration with a correlation coefficient of $R^2 = 0.961$. The higher the concentration, the higher the density because the water concentration decreases, and the density takes the value of pure lactic acid.

Treatment (T)	Density (g/mL)	pH
T1	1.065 ± 0.00306^{e}	3.73 ± 0.12^{c}
T2	1.074 ± 0.00306^{f}	3.98 ± 0.07^{d}
T3	1.099 ± 0.00058^{g}	4.01 ± 0.02^{d}
T4	1.007 ± 0.00208^{a}	4.22 ± 0.05^{e}
T5	1.014 ± 0.00153^{b}	4.60 ± 0.05^{f}
T6	1.026 ± 0.00306^{c}	5.02 ± 0.04^{h}
T7	1.110 ± 0.00100^{h}	3.05 ± 0.05^{a}
T8	1.117 ± 0.00458^{i}	3.41 ± 0.08^{b}
T9	1.133 ± 0.00351^{j}	3.84 ± 0.13^{c}
T10	1.011 ± 0.00058^{ab}	4.11 ± 0.06^{de}
T11	1.021 ± 0.00954^{c}	4.50 ± 0.10^{f}
T12	1.034 ± 0.00208^{d}	4.86 ± 0.11^{g}
$^{a-j}$ Different letters, within a column, show statistical differences between treatments through an LSD test with 95 % confidence.		

Table 5. Physico-chemical characteristics of the final lactic acid solution.

Within this work, density values were obtained in the range of 1.007 g/mL to 1.133 g/mL. The literature reports density in 98 % lactic acid of 1.215 g/mL[55]. The value is not within the range obtained in our work because the final lactic acid concentration reached a maximum of 33.48 g/L. The pH of all the treatments decreased due to the presence of lactic acid in the solution. This varies according to the initial pH for fermentation[51].

Evaluation of the organic compounds present in the final lactic acid samples

FTIR analysis was carried out to verify the presence of lactic acid in the samples obtained after fermentation. Figure 2. showed the FTIR spectrogram of the lactic acid sample that presented the best production, T9 of INIAP 651 variety, pH 5.5, and stirring, in which the characteristic bands of this organic compound appear, and the spectrogram of a commercial lactic acid. All the treatments presented similar characteristics of lactic acid spectrograms.

The experimental spectrogram shows the OH stretch bands at 3392.2 cm^{-1}, alcohol and carboxyl groups at 2940.9 and 2989.1 cm^{-1}. For the COOH group, the bond presented a tension at 1715.4 cm^{-1} , typical of the acid group. Groups *CH*3 and *CH* showed symmetric flexures at 1375 and 1456 cm^{-1}. The C-O stretches of the alcohol and acid groups at 1210.1, 1119.3, and 1040.4 cm^{-1}. The characteristics of the commercial lactic acid spectrogram are linked to OH stretches at 3338 cm^{-1}, alcohol and carboxyl groups at 2944 and 2995 cm^{-1}. For the COOH group, the bond presented a tension at 1716 cm^{-1}, typical of the acid group. Groups showed symmetric flexures at 1376 and 1432 cm^{-1}. The C-O stretches of the alcohol and acid groups at 1220, 1120, and 1070 cm^{-1} [56]. Thus, the bands of the spectra resulting from the lactic acid analysis of this work compared to those of the commercial one were similar. The resulting spectra showed the characteristic bands of this compound. Therefore, lactic acid was confirmed in all the final samples, with approximately 99% accuracy, compared to the characteristics bands' values.

In our research, the characteristic spectrogram presented a band at the level of 2635 cm^{-1}, because of the formation of amino compounds, due to protein in the initial substrate. Besides, the spectrograms of this work did not present peaks own of other substances. It is worth mentioning that the samples did not present the characteristic band of water that ranges from 3600 to 4000 cm^{-1}, because the samples were pre-treated by evaporation at 65 ºC and thus, there was no interference in the sample scanning with the equipment.

Conclusions

Lactic acid production from INIAP 650 and INIAP 651 varieties of cassava made of bagasse starch hydrolyzate reached relevant yields. The highest production of lactic acid was obtained at pH 5.5 with stirring. Thereby, it could be thought that at higher pH, the microorganism works better in the production of lactic acid. Agitation maximizes the production of lactic acid in the fermentation processes of hydrolyzed cassava bagasse starch. So, the pH-agitation system significantly affects lactic acid production in the fermentation processes of hydrolyzed cassava bagasse starch. The infrared spectrogram showed the characteristic of lactic acid bands for all the treatments analyzed. Finally, the quality of lactic acid from cassava by-products was verified and could have significant market value for Ecuador's sustainable development.

Further research to improve the quality and yield of lactic acid from a cassava bagasse starch is essential. Thus, to analyze the pH in ranges from 6 to 7, evaluate if there is a greater production of lactic acid and determine the optimal pH condition. The influence of enzymatic hydrolysis with cellulases to degrade all the cellulosic matter present in the cassava bagasse starch should be studied. The quantification of the initial amount of glucose and its consumption in the fermentation process is relevant for subsequent investigations. Evaluating the incidence of agitation of the fermentation broth at different levels until reaching 300 *rpm* is also in perspective. The work with cassava bagasse directly for the enzymatic hydrolysis process and thus evaluate lactic acid production with cellulase enzymes in the hydrolysis process of the lignocellulosic material present in the residue is relevant.

Acknowledgments

This research was supported economically by EPN through the project PREDU-2016-015. The authors thank H. Caballero (UTM) for their collaboration in collecting samples, starch extraction and information on the provenance of study cassava varieties. And I. Chango (CIAP - EPN) for assistance in analysis, recording, and interpreting spectra.

Bibliographic references

1. Alves de Oliveira R, Komesu A, Vaz Rossell CE, Maciel Filho R. Challenges and opportunities in lactic acid bioprocess design-From economic to production aspects. Biochem Eng J. 2018;133:219–39.

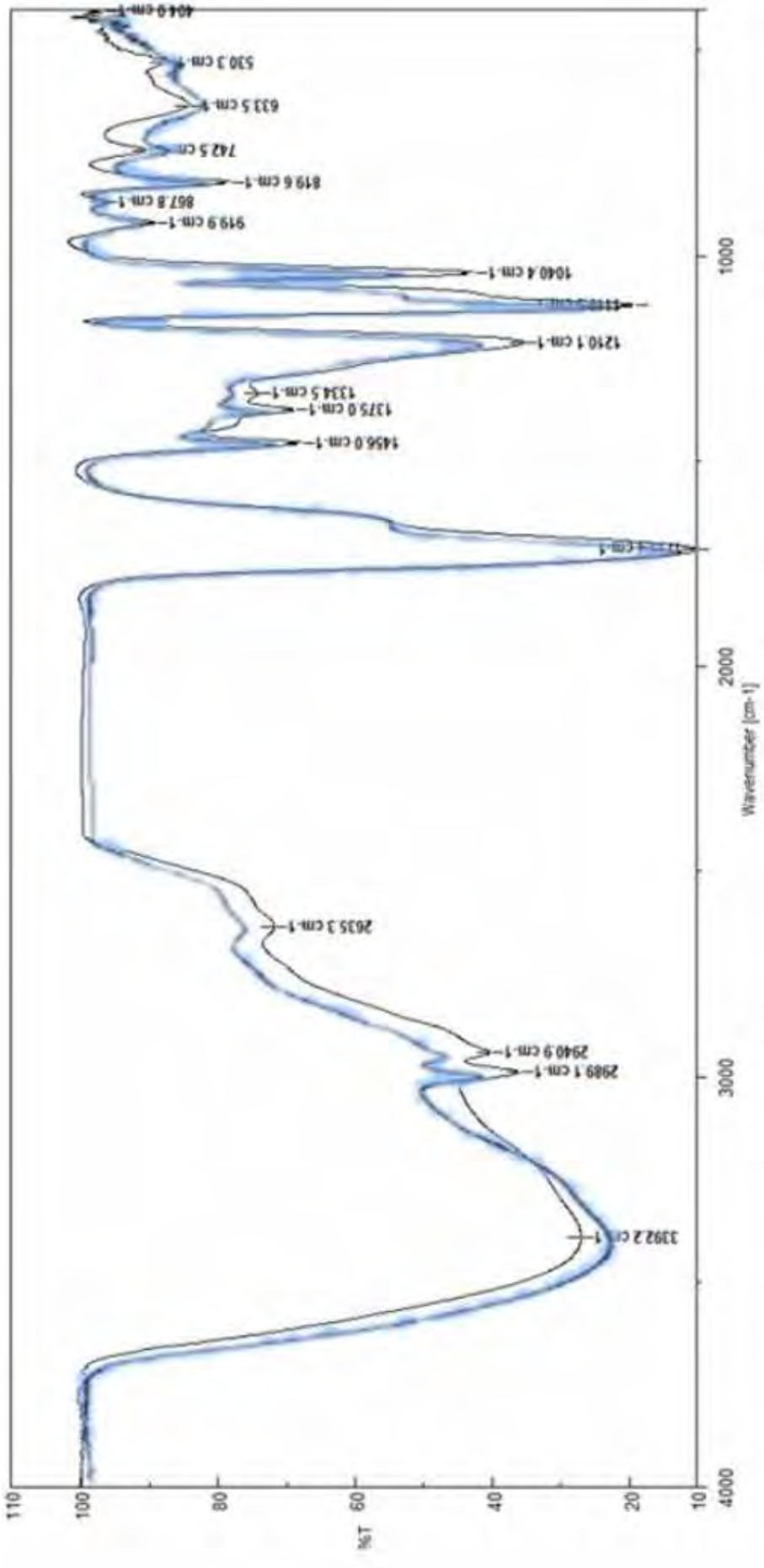

Figure 2. FTIR spectrogram of lactic acid obtained from T9 of INIAP 651 variety, pH = 5.5 with stirring (blue line) and FTIR spectrogram of commercial lactic acid (black line) (Carlo Erba brand, Pharmacopeia grade)[15].

2. Alves de Oliveira R, Komesu A, Vaz Rossell CE, Wolf Maciel MR, Maciel Filho R. A study of the residual fermentation sugars influence on an alternative downstream process for first and second-generation lactic acid. Sustain Chem Pharm. 2020;15(December 2019):100206.
3. Ge L, Wang P, Mou H. Study on saccharification techniques of seaweed wastes for the transformation of ethanol. Renew Energy. 2011;36(1):84–9.
4. Kwon EE, Yi H, Jeon YJ. Sequential co-production of biodiesel and bioethanol with spent coffee grounds. Bioresour Technol. 2013;136(March):475–80.
5. Bertoft E. Understanding starch structure: Recent progress. Agronomy. 2017;7(3).
6. Omoregie H. Chemical Properties of Starch and Its Application in the Food Industry. In: Chemical properties of starch. Intechopen; 2019. p. 13.
7. Ghaffar T, Irshad M, Anwar Z, Aqil T, Zulifqar Z, Tariq A, et al. Recent trends in lactic acid biotechnology: A brief review on production to purification. J Radiat Res Appl Sci. 2014;7(2):222–9.
8. Chen H, Chen B, Su Z, Wang K, Wang B, Wang Y, et al. Efficient lactic acid production from cassava bagasse by mixed culture of Bacillus coagulans and Lactobacillus rhamnosus using stepwise pH controlled simultaneous saccharification and co-fermentation. Ind Crops Prod. 2020;146(15):112175.
9. Kundrat L. October 2010 Dear Microbiologics Customer, The name of Microbiologics product 0235 (ATCC Licensed Derivative® ATCC® 7830TM*) is [Internet]. 2010. Available from: https://www.microbiologics.com/core/media/ media.nl?id=900&c=915960&h=c860a1caa7f78e5ebf50&_xt=.pdf
10. Abdel-Rahman MA, Tashiro Y, Sonomoto K. Recent advances in lactic acid production by microbial fermentation processes. Vol. 31, Biotechnology Advances. Elsevier; 2013. p. 877–902.
11. Tejada R. Obtención de ácido láctico por fermentación de almidón de ñame espino mediante el Lactobacillus delbrueckii ssp. bulgaricus y el Streptococcus thermophilus para su uso en la producción de ácido poliláctico (Proyecto de titulación previo a la obtención del [Internet]. Universidad de Cartagena –Universidad Nacional de Colombia sede Medellín; 2015. Available from: https://repositorio.unal.edu.co/handle/unal/55489
12. Delgado Troya J, Realpe Ortega P. Producción de ácido láctico por fermentación de la bacteria (Lactobacillus casei) utilizando cáscara de cacao (Theobroma cacao). Tesis [Internet]. Universidad de Guayaquil; 2019. Available from: http://repositorio.ug.edu.ec/handle/redug/40005
13. Torres MG, Gómez SL. Lactic Acid : a Review on Determination and Purification. Biociencias. 2019;14(2):149–75.
14. Yang X, Zhu M, Huang X, Lin CSK, Wang J, Li S. Valorisation of mixed bakery waste in non-sterilized fermentation for l-lactic acid production by an evolved Thermoanaerobacterium sp. strain. Bioresour Technol. 2015;198:47–54.
15. Rojas AM, Bastidas MJ. Producción de ácido láctico a partir del lactosuero utilizando Lactobacillus delbrueckii subsp. bulgaricus y Streptococcus thermophilus. Rev Colomb Química. 2015;44(3):5–10.
16. Wischral D, Jr NP. Statistical optimization of lactic acid production by Lactobacillus pentosus using hemicellulose hydrolysate from sugarcane bagasse. Rev Ing. 2018;29(1):41–51.
17. Caballero Salinas JC, Moreno Reséndez A, Reyes Carrillo JL, García Valdez JS, López Báez W, Jiménez Trujillo JA. Competencia del uso del rastrojo de maíz en sistemas agropecuarios mixtos en Chiapas. Rev Mex Ciencias Agrícolas. 2017;8(1):91.
18. Arias Zabala M, Henao Navarrete L, Castrillón Gutiérrez Y. Lactic acid production by fermentation of coffee mucilage with Lactobacillus bulgaricus NRRL-B548. DYNA. 2009;76(158):147–53.
19. INEC. Superficie según producción y ventas de yuca (Raíz), por región y provincia. https://www.ecuadorencifras.gob.ec › web-inec › espac › espac-2018,. 2018;
20. Zambrano JL, Ph D, D VBP, Sc IMHM, Domínguez JM, Ph D. Plan Estratégico De Investigación Y Desarrollo Tecnológico Del Iniap 2018 - 2022 [Internet]. Guayaquill: INIAP; 2018. 76 p. Available from: https://www.iniap.gob.ec/pruebav3/wp-content/uploads/2018/03/281-iniap-OK-baja.pdf
21. Tang Y, Li X, Chen PX, Zhang B, Hernandez M, Zhang H, et al. Characterisation of fatty acid, carotenoid, tocopherol/tocotrienol compositions and antioxidant activities in seeds of three Chenopodium quinoa Willd. genotypes. Food Chem. 2015;174(5):502–8.
22. Román Y, Techeira N, Yamarte J, Ibarra Y, Fasendo M. Caracterización físico-química y funcional de los subproductos obtenidos durante la extracción del almidón de musáceas, raíces y tubérculos. Interciencia. 2015;40(5):350–6.
23. Sivamani S, Baskar R. Process design and optimization of bioethanol production from cassava bagasse using statistical design and genetic algorithm. Prep Biochem Biotechnol [Internet]. 2018 Oct 21;48(9):834–41. Available from: https://doi.org/10.1080/10826068.2018.1514512
24. Ortíz C, Ospina L, Sánchez S. Producción de ácido Láctico a partir de almidón de yuca por bacterias acidolácticas del género Lactobacillus. UJTL. 2014;10.
25. Comité de Reconstrucción y Reactivación Productiva. Plan de Reconstrucción y Reactivación Productiva post terremoto [Internet]. 2017. p. 76. Available from: https://www.reconstruyoecuador.gob.ec/wp-content/uploads/2018/02/Plan-de-Reconstrucción-y-Reactivación-Productiva-post-terremoto.pdf
26. INIAP. INIAP 650- Estación Experimental Portoviejo [Internet]. Ecuador: SENECYT; 2012. p. 1–2. Available from: https://repositorio.iniap.gob.ec/bitstream/41000/1199/1/INIAP PORTOVIEJO-650.pdf
27. INIAP. INIAP 651- Estación Experimental Portoviejo [Internet]. Ecuador; 2012. p. 1–2. Available from: https://repositorio.iniap.gob.ec/bitstream/41000/1115/1/INIAP PORTOVIEJO-651.pdf
28. Vargas Aguilar P. Obtención de almidón fermentado a partir de yuca (Manihot esculenta crantz) variedad valencia, factibilidad de uso en productos de panadería. Tecnol en Marcha. 2010;23(3):15–23.
29. INEN 1529-2. Control Microbiológico de los Alimentos. Toma, envío y preparación de muestras para el análisis microbiológico [Internet]. Vol. Primera ed. 2013. p. 7–12. Available from: http://normaspdf.inen.gob.ec/pdf/ntel1529-2-1R.pdf
30. Chookietwattana K. Lactic Acid Production from Simultaneous Saccharification and Fermentation of Cassava Starch by Lactobacillus Plantarum MSUL 903. APCBEE Procedia [Internet]. 2014;8:156–60. Available from: http://www.sciencedirect.com/science/article/pii/S2212670814000992
31. Hofvendahl K, Hahn–Hägerdal B. Factors affecting the fermentative lactic acid production from renewable resources. Enzyme Microb Technol [Internet]. 2000 Feb [cited 2015 Mar 27];26(2–4):87–107. Available from: http://www.sciencedirect.com/science/article/pii/S0141022999001556
32. Gómez MB, Cárdenas ON, Santa C, Carpio C, Román G. Purificación Parcial y Caracterización de Alfa Amilasa de granos germinados de Chenopodium quinoa (Quinua). Rev ECIPeru. 2018;52–8.
33. Maldonado-Alvarado P. Facteurs déterminants du pouvoir de panification de l'amidon de manioc modifié par fermentation et irradiation UV. Université Montpellier 2. PhD thesis. 190 pag.; 2014.
34. Mera I, Cataño JC. Obtención de glucosa a partir de almidón de yuca (Manihot Sculenta). Fac Ciencias Agropecu [Internet]. 2005;3:54–63. Available from: file:///C:/Users/PEDROM~1.1-1/AppData/Local/Temp/Dialnet-ObtencionDeGlucosaAPartirDeAlmidonDeYucaManihotScu-6117970.pdf
35. Bomrungnok W, Sonomoto K, Pinitglang S, Wongwicharn A. Single Step Lactic Acid Production from Cassava Starch by Lactobacillus plantarum SW14 in Conventional Continuous and Continuous with High Cell Density. APCBEE Procedia. 2012;2:97–103.
36. Bello Gil D, Carrera B. E, Diaz M. Y. Determinación de azúcares reductores totales en jugos mezclados de caña de azúcar utilizando el método del ácido 3,5 dinitrosalicílico. ICIDCA obre los Deriv la Caña Azúcar. 2006;40:45–50.
37. Alonso L, Poveda A. Estudio comparativo en técnicas de recuento rápido en el mercado y placas petrifilm. Proyecto de titulación previo a la obtención del título de Microbiólogo Industrial). Pontificia Universidad Javeriana, Bogotá, Colombia. Comercial Experimental. 2008.

38. Cardona M, Larrosa-Fuentes J. Manual para la observación de medios [Internet]. 1st ed. ITESO; 2014. Available from: http://www.jstor.org/stable/j.ctvdmwzct
39. Miller C, Fosmer A, Rush B, McMullin T, Beacom D, Suominen P. Industrial Production of Lactic Acid. 2nd Ed. Vol. 3, Comprehensive Biotechnology. Elsevier B.V.; 2011. 179–188 p.
40. ASTM -D7777. Standard Test Method for Density, Relative Density, or API Gravity of Liquid Petroleum by Portable Digital Density Meter. 2016;1–8.
41. Vargas Aguilar P, Hernández Villalobos D. Harinas y almidones de yuca, ñame, camote y ñampí: propiedades funcionales y posibles aplicaciones en la industria alimentaria. Rev Tecnol en Marcha. 2013;26(1):37.
42. López JA, Rodríguez E, Sepúlveda JU. Evaluación de características fisicas y texturales de pandebono. Acta Agron. 2012;61(3):273–81.
43. Pandey A, Soccol CR, Nigam P, Soccol VT, Vandenberghe LPS, Mohan R. Biotechnological potential of agro-industrial residues. II: cassava bagasse. Bioresour Technol. 2000;74(1):81–7.
44. Montilla J, Arcila J, Aristizábal M, Montoya EC, Puerta GI, Oliveros CE, et al. Propriedades Físicas y Factores de Conversión del Café en el Proceso de Beneficio. Av Técnicos Cenicafé. 2008;370.
45. Vargas y Vargas M de L, Figueroa Brito H, Tamayo Cortez JA, Toledo López VM, Moo Huchin VM. Aprovechamiento de cáscaras de frutas: análisis nutricional y compuestos bioactivos. Cienc ergo sum. 2019;26(2):1–11.
46. Arroyo P, Mazquiaran L, Rodriguez P, Valero T, Ruiz E, Ávila JM, et al. Frutas y hortalizas: Nutrición y Salud en la España del SXXI. Fund Española la Nutr. 2018;198.
47. Woiciechowski AL, Nitsche S, Pandey A, Soccol CR. Acid and enzymatic hydrolysis to recover reducing sugars from cassava bagasse: An economic study. Brazilian Arch Biol Technol. 2002;45(3):393–400.
48. Hernández-Medina M, Torruco-Uco JG, Chel-Guerrero L, Betancur-Ancona D. Caracterización fisicoquímica de almidones de tubércules cultivados en Yucatán, México. Cienc e Tecnol Aliment. 2008;28(3):718–26.
49. Souto LRF, Caliari M, Soares Júnior MS, Fiorda FA, Garcia MC. Utilization of residue from cassava starch processing for production of fermentable sugar by enzymatic hydrolysis. Food Sci Technol. 2017;37(1):19–24.
50. John RP, Nampoothiri KM, Pandey A. Solid-state fermentation for L-lactic acid production from agro wastes using Lactobacillus delbrueckii. Process Biochem. 2006;41(4):759–63.
51. Eiteman MA, Ramalingam S. Microbial production of lactic acid. Biotechnol Lett. 2015;37(5):955–72.
52. Bahry H, Abdalla R, Pons A, Taha S, Vial C. Optimization of lactic acid production using immobilized Lactobacillus Rhamnosus and carob pod waste from the Lebanese food industry. J Biotechnol. 2019;306(September):81–8.
53. Bai DM, Jia MZ, Zhao XM, Ban R, Shen F, Li XG, et al. L(+)-lactic acid production by pellet-form Rhizopus oryzae R1021 in a stirred tank fermentor. Chem Eng Sci. 2003;58(3–6):785–91.
54. Ai Z, Lv X, Huang S, Liu G, Sun X, Chen H, et al. The effect of controlled and uncontrolled pH cultures on the growth of Lactobacillus delbrueckii subsp. bulgaricus. LWT - Food Sci Technol. 2017;77:269–75.
55. Farmaquímica. Ficha técnica de Ácido Láctico. [Internet]. 2013. Available from: http://archivosdemedicinadeldeporte.com/articulos/upload/Revision_acido_lactico_270_120.pdf
56. Rojas AM, Montaño L, Bastidas MJ. Producción de ácido láctico a partir del lactosuero utilizando Lactobacillus delbrueckii subsp. bulgaricus y Streptococcus thermophilus. Rev Colomb Química. 2015;44(3):5–10.

Received: 23 November 2020
Accepted: 16 February 2021

RESEARCH / INVESTIGACIÓN

The behavior of Mean Platelet Volume in Sepsis in critical patients with and without sepsis

Pablo Andrés Vélez[1], Lucy Baldeón R.[2], Jorge Luis Vélez-Paez[3]

DOI. 10.21931/RB/2021.06.02.22

Abstract: The mean platelet volume is an anatomical biomarker that has shown its usefulness in various cardiovascular and metabolic pathologies; in sepsis, it has been positioning itself as an indicator of mortality, easily accessible and immediately applicable when reported in the routine blood count. This study demonstrates the mean platelet volume's biological behavior in critical patients with sepsis compared with non-septic patients. An observational, longitudinal, prospective, monocentric cohort study was conducted in 250 patients treated at the intensive care unit of the Pablo Arturo Suárez Hospital, Quito- Ecuador, from January 2019 January 2020. A group of patients with sepsis (n = 125) and without infectious pathologies (n = 125) were studied. The inclusion criteria were patients over 18 years of age of both genders, diagnosed with sepsis or septic shock using SEPSIS 3 criteria, and patients without septic pathology. The mean platelet volume (MPV) of days 1, 2, and 3 were studied. Septic patients had a mean APACHE (18.74 SD 9.52) higher than the non-septic ones (11.93 SD 7.01) (p = < 0.000). The MPV was consistently higher in patients with sepsis than non-septic patients, but it reached statistical significance on day 3 (9.13 SD 1.55 vs. 8.66 SD 1.34, p=0.042). The MPV on day 3 presented a significant area under the curve (AUC =0.580) (CI. 0.500-0.661), where the cut-off point according to Youden's index was positive for sepsis if MPV≥ 9.85 femtoliter (fL) with OR=3.30 and p-value= 0.005. Likewise, lactate on admission showed an AUC of 0.625 (CI. 0.555-0.694), with a cut-off point ≥of 1.15 mmol / L, OR=2.51, and p=0.007. Age and hypertension did not show a multivariate relationship with the presence of sepsis. It was shown that MPV is higher in patients with sepsis compared to non-septic ones. This observation reaches significance on day 3. Additionally, elevated lactate at admission was also associated with a septic state. On the other hand, platelet count did not show the expected behavior.

Key words: Mean Platelet Volume, sepsis, mortality.

Introduction

Sepsis is defined as the unregulated response of the body to an infectious disease. Nowadays, this pathology is one of the main reasons for admission to the intensive care unit. There are still few strategies described to face it; however, it is known that an early antibiotic therapy, together with the adequate support of organ failure, are measures that reduce its pathophysiological impact and, therefore, its mortality[1].

Various biochemical markers (procalcitonin, C-reactive protein, and interleukin 6) and prognostic scales such as APACHE II and SOFA can determine this entity's severity. However, they are not always available in the daily clinical requirement, or their high economic value does not allow their routine use in low-income countries. Therefore, a new biomarker, such as the mean platelet volume (MPV), could become a practical and easily accessible tool to predict septic states.

Platelets are cell fragments from megakaryocytes, which are essential for blood clotting. The MPV is the measurement of platelet size and has an inverse relationship with the number of these; it is also an indicator of platelet activation[2,3].

There is no fixed cut-off point for MPV because the values change and vary from population to population. They also vary according to the technique used to measure it (impedance or laser scattering), the type of anticoagulant used (EDTA or citrate), and the test time. However, it is established that values greater than 9.5 femtoliters (fL) are correlated with diseases related to inflammation, endothelial dysfunction, and pro-thrombotic states[1]. Additionally, increased MPV has been reported to be associated with poor prognosis in patients with metabolic syndrome, diabetes mellitus, cardiovascular diseases, pulmonary embolism, smoking, and immuno-inflammatory diseases[2,4,5].

Van der Lelie *et al.* in 1983 reported that MPV increases in invasive infectious septic disease, but not in local infection and that this biomarker normalizes when controlling the disease[1]. There are no studies that demonstrate that platelet size is higher in sepsis compared to other critical pathologies. Therefore, this study's objective is to demonstrate that mean platelet volume (MPV) is higher in critical patients with sepsis than non-septic patients.

Materials and methods

An observational, longitudinal, prospective, monocentric cohort study was conducted. The sample consisted of 250 patients treated in the intensive care unit of the Pablo Arturo Suárez Hospital in Quito, Ecuador, in the period January 2019 - January 2020. The sample consisted of two groups, patients with sepsis (n = 125) and patients with other non-infectious pathologies (n = 125). The inclusion criteria were patients of both genders, older than 18 years with a diagnosis of sepsis or septic shock who met the criteria of SEPSIS 3 [6] and patients with non-septic pathology such as preeclampsia, eclampsia, HELLP syndrome, acute pancreatitis, or cardiovascular diseases. Patients with neoplasms or acute bleeding states that can alter MPV were excluded. Patient data were coded, and the results of the routine tests requested were documented in the clinical history for the required variables (lactate, MPV, leukocyte count, platelet count, and procalcitonin) on days 1, 2, 3. The difference in MPV between patients with and without sepsis and the value that determined the progression to septic states was evaluated. The MPV was measured in a femtoliter by impedance in a

[1] Servicio de Medicina Crítica-Hospital Pablo Arturo Suárez.
[2] Facultad de Ciencias Médicas-Universidad Central del Ecuador e Instituto de Investigación en Biomedicina Universidad Central del Ecuador.
[3] Servicio de Medicina Crítica-Hospital Pablo Arturo Suárez y Facultad de Ciencias Médicas-Universidad Central del Ecuador.

Corresponding author: pavelez@uce.edu.ec

Siemens machine, in venous blood collected in EDTA tubes. The data was coded and entered into a database, to which only the researcher has access. Analyzes were carried out with R and SPSS version 22 software. Qualitative variables were reported using tables and graphs representing absolute and relative values. Quantitative variables were represented as measures of central tendency and variability.

Inferential statistics were performed to compare the clinical characteristics and laboratory parameters between the sepsis and non-sepsis groups (bivariate analyzes). For categorical variables, the chi-square test was applied to compare proportions. For the analysis of quantitative variables, the assumption of normality was first verified. Thus, for variables that presented normality, a t-test was used. For the variables that do not meet the normality criteria, Mann Whitney test was used. Using the ROC Curve, the cut-off points for MPV and lactate significant in the bivariate analysis were determined, which were expressed as area under the curve (AUC). Besides, sensitivity, specificity, positive predictive value (PPV), negative predictive value (NPV), and Odds Ratio (OR) were determined for each cut-off point. A multivariate logistic regression analysis was performed to determine the relationship of sepsis using the OR. Statistical significance was established for the value of $p < 0.05$; the OR was considered significant, observing the limits of the 95% confidence interval. It was considered a risk factor if the lower limit was more significant than one.

Ethical considerations

Researchers have followed the bioethical principles of human research. The data were obtained from medical records (secondary data), the identification of patients will not be disclosed, and they have been recorded to avoid their recognition. The authors obtained the authorization for publication.

Results

The average age of patients with sepsis was 60.73 years, and 45.21 years of patients without sepsis. Differences in age between groups showed significance (p=0.000). In gender, no significant differences were observed; the predominant ethnic group was mestizo in sepsis and the non-infectious group (93.60% and 95.20%, respectively), without significant differences. Significant differences were observed for APACHE (p= 0.000), in patients with sepsis (18.74 points) and without sepsis (11.93 points). High blood pressure (HBP) presented significant differences between the groups (p= 0.011). The percentage of non-survivors was 26.40% in the sepsis group and 5.60% in the non-sepsis group, showing significance between groups (p= 0.000). The patients who required mechanical ventilation were 76.80% in the group of patients with sepsis and 52.80% in the patients without sepsis, showing significant differences (p=0.000). Patients who required sedation were 64.23% in the group sepsis and 35.54% in the group without sepsis, showing significant differences (p=0.000). The average days of hospitalization were 6.96 days in the sepsis group compared with 4.12 days without the sepsis group (p= 0.000) (see table 1).

When comparing laboratory parameters such as MPV in the sepsis (3 9.13 fL) and non-sepsis (8.66 fL) groups, significant differences were observed on day 3 (p= 0.042) and at discharge (p=0.035). Differences were also observed in leukocyte values on day 1 (p=0.007) and on day 3 (p= 0.001). Mean lactate in the sepsis group was 2.85 mmol/L and 2.05 mmol/L in the non-sepsis group, showing significant differences (p=0.005). The mean of procalcitonin in the sepsis group was 26.21 ng/ml and 3.37 ng/ml in the non-sepsis group showing significant differences (p-value 0.000) (see table 2).

Also, a graph was made to compare MPV values in survivors and non-survivors patients with and without sepsis, in whom platelet size superiority is evidenced in all measurements. (Figure 1).

For the variables MPV on day 3, at discharge, and lactate at admission, which were significant in comparing the sepsis and non-sepsis groups, the cut-off point was determined using the ROC curve.

The MPV at day 3 presented a significant area under the curve (AUC) of 0.580 (CI 0.500-0.661), where the cut-off point according to Youden's index was positive for sepsis if MPV ≥9.85 fL. Similarly, lactate on admission was significant with AUC 0.625 (CI 0.555-0.694), with cut-off points 1.15 and 1.25 to predict sepsis. Of these points, the one that showed relevance in the statistical tests and was positive for sepsis was lactate ≥1.15 mmol / L. (see Figure 2.)

The following values of sensitivity and specificity for sepsis were observed for the cut-off points determined by the ROC curve. MPV on day 3 presented a sensitivity of 30.48%, a specificity of 88.76%, PPV of 76.20%, NPV of 52.00%, the OR was significant for the cut-off point. Patients with MPV at day 3 ≥9.85 fL are 3.46 times more likely to present sepsis than those with values lower than this cut-off point.

Lactate on day 3 presented a sensitivity of 80, 80%, a specificity of 42, 40%, PPV of 58, 40%, NPV of 68, 80%, the OR was significant for the cut-off point. Patients with lactate on admission ≥1, 15 mmol/L are 3.10 times more likely to present sepsis than those with values lower than this cut-off point.

Logistic regression was used to determine the multivariate relationship of sepsis with the cut-off points of the MPV on day 3 and lactate at admission and the clinical characteristics of age (median 55 years) and comorbidity due to HBP, which were significant in the bivariate analysis.

The results showed that the MPV (≥9.85 fL) on day 3 (p = 0.005) and lactate at admission ≥1.15 mmol /L presented a multivariate relationship with sepsis. Patients with MPV on day 3 ≥9.85 fL are 3.30 times more likely to present sepsis, while patients with lactate on admission ≥1.15 mmol / L are 2.51 times more likely to present sepsis. Age and HBP did not show a relationship with the presence of sepsis.

Discussion

This study shows that platelet MPV is higher in critically ill patients with sepsis than non-septic patients. Similarly, it was observed that a higher lactate value on admission to intensive care was related to progression to septic states, establishing significant cut-off points and ORs for both variables.

In systemic processes with a high probability of organic impact, the coagulation system is frequently activated[6,7]. It has been shown that coagulation and platelet activation occur in early stages in pathologies with a different pathophysiological context, such as sepsis, ischemic heart disease, brain infarction, preeclampsia, and eclampsia[1,4,8].

The increase in platelet size and decrease in its count is due to pro-inflammatory cytokines, thrombopoietin, and other substances that stimulate the massive production of spherical and poorly functional young platelets due to the action of spherical and poorly functional young platelets to the severity of the septic shock. All this process leads to the formation of thrombi, almost always culminating in unfavorable outcomes[9,10].

Several studies have demonstrated the predictive utility

Clinic Characteristics	Group		p-value
	Sepsis	Non-Sepsis	
Age (mean (SD))[1/] years	60,73 (21,00)	45,21 (21,27)	0,000*
Gender (n (%))[2/]			
Male	47 (37,60)	54 (43,20)	0,367
Female	78 (62,40)	71 (56,80)	
Ethnicity (n (%))[2/]			
Mestizo	117 (93,60)	119 (95,20)	0,973
Afroamerican	4 (3,20)	3 (2,40)	
Indígenous	2 (1,60)	1 (0,80)	
Black	1 (0,80)	1 (0,80)	
White	1 (0,80)	1 (0,80)	
APACHE admission (mean (SD))[1/]	18,74 (9,52)	11,93 (7,01)	0,000*
Comorbidities (n (%))[2/]			
High Blood Pressure	43 (34,40)	25 (20,00)	0,011**
T2D	23 (18,40)	24 (19,20)	0,871
Liver disease	0 (0,00)	3 (2,40)	0,247
COPD	3 (2,40)	2 (1,60)	1,000
Discharge Condition (n (%))[2/]			
Non survivor	33 (26,40)	7 (5,60)	0,000**
Survivor	92 (73,60)	118 (94,40)	
Mechanical Ventilation (n (%))[2/]	96 (76,80)	66 (52,80)	0,000**
Sedation (n (%))[2/]	79 (64,23)	43 (35,54)	0,000**
Hospitalization days (mean (SD))[1/]	6,96 (5,16)	4,12 (3,24)	0,000*

Table 1. Distribution of demographic and clinical characteristics by sepsis and non-sepsis group.

of MPV in sepsis[9,11-24] however;, there is little reported bibliography that compares platelet kinetics in critically ill patients with and without sepsis, a critical situation to be demonstrated since several non-infectious diseases can also potentially increase platelet size.

Our findings indicate that the platelet is more significant in patients with sepsis than those without sepsis, but this difference is significant at day 3, marking a significant cut-off point of ≥9.85 fL. Simultaneously, we observed statistical significance in the ROC curve with relevant AUC for lactate at admission with a cut-off point of ≥1.15 mmol / L, which significantly marked septic states' progression. Although no bibliography contrasts these results in patients without sepsis, in patients with sepsis, some studies, for example, two large meta-analyses[25,26] show that the MPV increases at 72 hours, with cut-off points that differ in these studies and is associated with septic states and even higher mortality. When the host's inflammatory response has not been controlled, it has a strong impact, inducing greater clinical severity and unfavorable outcomes.

Although age and HBP were significant variables in the bivariate analysis, they did not present a multivariate relationship, meaning that they do not intervene in the outcome of presenting or not presenting septic states. Something striking was that the platelet count, which is a point to be evaluated in sepsis-induced multi-organ dysfunction, which is more severe than the lower number of platelets, was not significantly different from non-septic pathologies. This observation was unexpected and can be explained by the enrollment of patients with hypertensive pathology of pregnancy (preeclampsia, eclampsia, and HELLP) in the non-septic group; these pathologies also decrease the platelet count due to a different pathophysiological mechanism[27,28].

Our findings' relevance lies in the fact that we were able to show significant differences in MPV between patients with and without sepsis. This study is the basis for the execution of future studies investigating this biomarker in specific populations; Furthermore, taking into account that this biomarker is routinely reported in the common blood count, it makes it desirable for its immediate applicability.

Among the study's limitations, we can name the potential increase in MPV when using EDTA, which generates an increase in size not attributable to the underlying pathology since it is a post-analytical phenomenon and enhanced by the delay in the processing of the sample. Taking into account that this

Laboratory parameters	Group		p-value
	Sepsis	Non-Sepsis	
MPV (mean (SD))[1/] fL			
Day 1	8,98 (1,53)	8,66 (1,13)	0,135
Day 2	8,90 (1,53)	8,70 (1,20)	0,372
Day 3	9,13 (1,55)	8,66 (1,34)	0,042*
Platelets/mm3 (mean (SD))[1/]			
Day 1	225.416 (129,380)	261.168 (320.053)	0,248
Day 2	211.406 (134.634)	216.945 (113.608)	0,731
Day 3	206.067 (125.439)	218.696 (110.944)	0,463
Leukocytes /mm3 (mean (SD))[1/]			
Day 1	14984,40 (9833,36)	12214,64 (5781,67)	0,007*
Day 2	13978,74 (7140,80)	2505,77 (11887,44)	0,246
Day 3	13254,52 (6945,27)	10236,63 (5319,80)	0,001*
Lactate (mean (SD))[1/] mmol/L	2,85 (2,61)	2,05 (1,71)	0,005*
O2 Sat.VC admission (mean (DE))[1/] %	65,00 (14,29)	66,42 (12,15)	0,635
Procalcitonin (media (DE))[1/] ng/ml	26,21 (41,16)	3,37 (10,30)	0,000*

Table 2. Comparison of laboratory parameters by sepsis and non-sepsis group.

Parameters	MPV día 3	Lactate admission
Cut-off	≥9,85 fL	≥1,15 mmol/L
Sensitivity	30,48%	80,80%
Specificity	88,76%	42,40%
PPV	76,20%	58,40%
NPV	52,00%	68,80%
OR (CI95%)	3,46 * (1,59-7,54)	3,10* (1,75-5,47)
* OR= Odds Ratio significantly inferior limit >1		

Table 3. MPV kinetics from day 1 to day 3 in septic patients that survive and no-survive.

phenomenon could affect both groups (septic and non-septic); and that K3 tubes were also used, which preserve platelet morphology, and that the processing time was less than 30 minutes (samples from intensive care unit), we consider that this bias plays a minor role in our results. Agustino et al. described similar findings and gave little relevance to this bias in their studies that compared EDTA with citrate[29].

Another essential point to take into account is that, in our work, a high MPV was associated with septic states, but there is no generalized cut-off point reported. Perhaps ethnicity is an important variable to consider since the values reported in eastern countries show MPV cut-off points higher than 11 fL[30-32] compared to western countries like ours, where we obtained a cut-off point somewhat lower but no less significant. Besides, our study was carried out in the city of Quito at 2800 meters above sea level. Evidence shows that at high altitudes, hypoxia in non-acclimatized people could generate hyperreactivity and more significant platelet aggregation in response to adenosine diphosphate (ADP), which could also increase other cytometric indicators such as MPV, which indicates the need for more studies to clarify this theory[33,34].

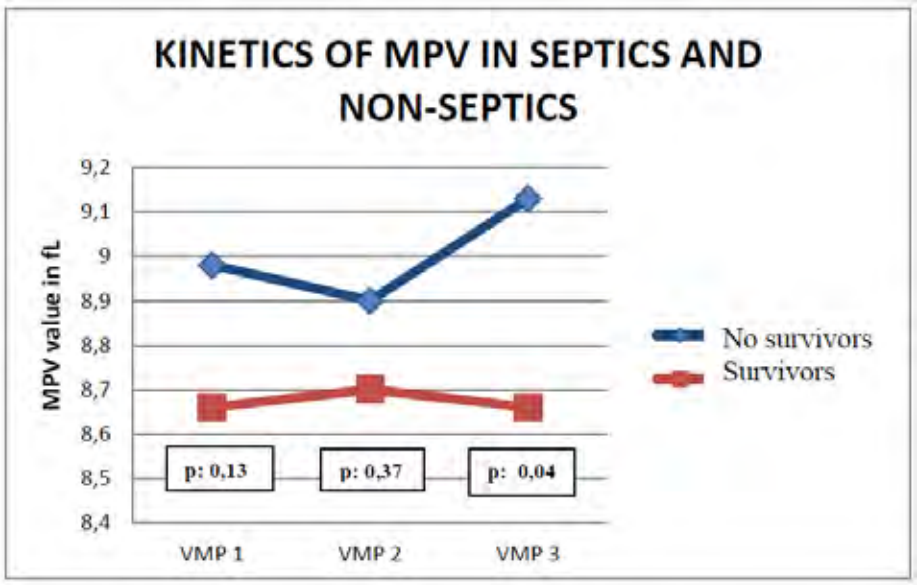

Figure 1. MPV kinetics from day 1 to day 3 in septic patients that survive and no-survive.

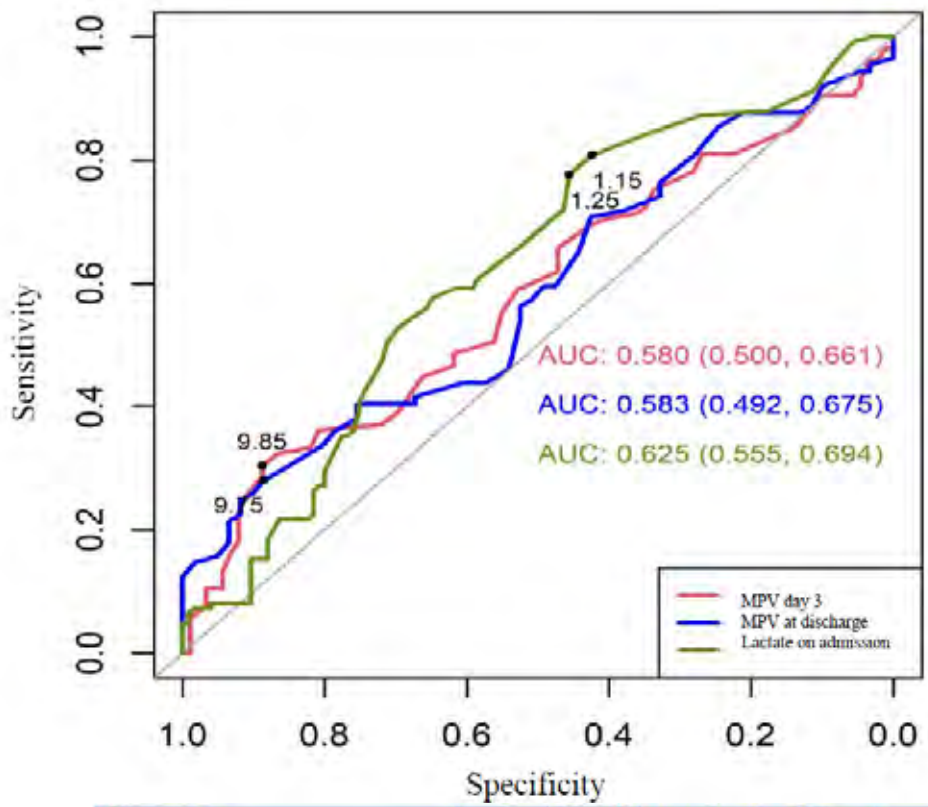

Figure 2. ROC curve for MPV at day 3 and lactate on admission to estimate sepsis.

Variables	B	Wald	p-valor	OR_{adj}	CI-OR 95%	
					Inferior	Superior
MPV día 3 ≥9,85 fL	1,19	7,87	0,005*	3,30**	1,43	7,59
Age >55 años	0,47	1,97	0,160	1,61	0,83	3,11
HBP present	0,72	3,59	0,058	2,04	0,98	4,28
Lactate admission ≥1,15 mmol/L	0,92	7,21	0,007*	2,51**	1,28	4,90

Based on Logistic regression; * variable significant p-value<0,05, ** OR=odds ratio significant Li >1;

Table 4. A multivariate relationship for sepsis.

Conclusions

This study demonstrated that the mean platelet volume is higher in patients with sepsis than in non-septic patients, findings that are accentuated and become significant on day 3. Likewise, lactate measured at the admission time is a biomarker whose elevation is associated with septic states. On the contrary, the platelet count did not show the expected behavior.

Bibliographic references

1. J.Van der Lelie and A. E. G. K.Von dem Borne, "Increased mean platelet volume in septicemia," Journal of Clinical Pathology, vol. 36, no. 6, pp. 693–696, 1983
2. Gutierrez-Romero A, Gutierrez-Grobe Y, Cariilo-Esper R. Volumen Plaquetario Medio: el tamaño sí importa. Med Int Mex. 2013; 29: 3017-310.
3. Greco E, Lupia E, Bosco O. Platelets and Multi-Organ Failure in Sepsis. Int. J. Mol. Sci. 2017, 18, 2200; doi:10.3390/ijms18102200
4. Takatoshi K, Yusuque Y, Keita T. Changes in the Mean Platelets Volume Levels after bloodstream infections have prognostic value. Intern Med. 52: 1487-1493, 2013.
5. Pabón P, Ballesteros F, Moríñigo JL. Influencia del volumen plaquetario medio sobre el pronóstico a corto plazo del infarto agudo de miocardio. Revista Española de Cardiología. 1998. 51 (10): falta números de páginas.
6. Singer M, Deutschman CS, Seymour CW, Shankar-Hari M, Annane D, Bauer M, et al. The Third International Consensus Definitions for Sepsis and Septic Shock (Sepsis-3). JAMA. 2016; 315: 801–10. https://doi.org/10.1001/jama.2016.0287 PMID: 26903338
7. Ates S, Okzus H, Dogu B. Can mean platelet volume and mean platelet volume/platelet count ratio be used as a diagnostic marker for sepsis and systematic inflammatory response syndrome?. Saudi Med J. 2015 Oct;36(10):1186-90. doi: 10.15537/smj.2015.10.10718.
8. Yun S, Sim F, Goh R. Platelet Activation: The Mechanisms and Potential Biomarkers. BioMed Research International Volume 2016, Article ID 9060143, http://dx.doi.org/10.1155/2016/9060143.
9. Machlus KR, Thon JN, Italiano JE. Interpreting the developmental dance of the megakaryocyte: a review of the cellular and molecular processes mediating platelet formation. Br J Haematol. 2014; 165: 227–236. https://doi.org/10.1111/bjh.12758 PMID: 24499183
10. Nishimura S, Nagasaki M, Kunishima S, Sawaguchi A, Sakata A, Sakaguchi H, et al. IL-1- induces thrombopoiesis through megakaryocyte rupture in response to acute platelet needs. J Cell Biol. 2015; 209: 453–466. https://doi.org/10.1083/jcb.201410052 PMID: 25963822.
11. Hampton T. Platelets' role in adaptative immunity may contribute to sepsis and shock. JAMA, abril 2018, vol 319, num 13, págs 1311. doi:10.1001/jama.2017.12859 https://jamanetwork.com/journals/jama/article-abstract/2677421
12. Monares-Zepeda E, Ríos-Ayala MA. Clinical evaluation of hematic cytometry in critical ill patient. The intensivist point of view. Rev Mex Patol Clin Med Lab. 2019; 66 (2): 100-106.
13. Pattraporn Tajarernmuang, Arintaya Phrommintikul, Atikun Limsukon, Chaicharn Pothirat, and Kaweesak Chittawatanarat, "The Role of Mean Platelet Volume as a Predictor of Mortality in Critically Ill Patients: A Systematic Review and Meta-Analysis," Critical Care Research and Practice, vol. 2016, Article ID 4370834, 8 pages, 2016. https://doi.org/10.1155/2016/4370834.
14. Patel SR, Hartwig JH, Italiano JE. The biogenesis of platelets from megakaryocyte proplatelets. J Clin Invest. 2005; 115: 3348–3354. https://doi.org/10.1172/JCI26891 PMID: 16322779
15. Thon JN, Montalvo A, Patel-Hett S, Devine MT, Richardson JL, Ehrlicher A, et al. Cytoskeletal mechanics of proplatelet maturation and platelet release. J Cell Biol. 2010; 191: 861–874. https://doi.org/10.1083/jcb.201006102 PMID: 21079248
16. Machlus KR, Thon JN, Italiano JE. Interpreting the developmental dance of the megakaryocyte: a review of the cellular and molecular processes mediating platelet formation. Br J Haematol. 2014; 165: 227–236. https://doi.org/10.1111/bjh.12758 PMID: 24499183
17. Nishimura S, Nagasaki M, Kunishima S, Sawaguchi A, Sakata A, Sakaguchi H, et al. IL-1- induces thrombopoiesis through megakaryocyte rupture in response to acute platelet needs. J Cell Biol. 2015; 209: 453–466. https://doi.org/10.1083/jcb.201410052 PMID: 25963822.
18. Grunewald T, et al. Tamaño de plaquetas predice mortalidad en sepsis. Revista Hospimedica. Disponible en: www.hospimedica.es/cuidados-criticos/articles/294742277/tamano-de-plaquetas-predice-mortalidad-en-sepsis.html.
19. Vélez JL, Bucheli R, Ramírez V. Volumen medio plaquetario: predictor de mortalidad en sepsis de pacientes críticos. Revista Metrociencia. 2015; 23: 40-43.
20. Vélez JL, Jara A, Vélez P. ¿Es el volumen medio plaquetario un predictor de mortalidad en sepsis de pacientes críticos? Revista de la Facultad de Ciencias Médicas. 2017; 42 (1); 84-90.
21. Vélez JL. ¿El volumen medio plaquetario es un es un predictor de mortalidad en pacientes sépticos? Revisión de la literatura.Rev Med Hered. 2018; 29:116-119. http://www.scielo.org.pe/pdf/rmh/v29n2/a10v29n2.pdf
22. Sànchez-Calzada A, Navarro JL, Delgado L. Mean platelet volume a marker of sepsis in patients admitted to intensive therapy. Intensive Care Medicine Experimental. 2015; 3(suppl 1):A871.
23. Ates S, Okzus H, Dogu B. Can mean platelet volume and mean platelet volume/platelet count ratio be used as a diagnostic marker for sepsis and systematic inflammatory response syndrome?. Saudi Med J. 2015 Oct;36(10):1186-90. doi: 10.15537/smj.2015.10.10718.
24. Fogagnolo A, Taccone F. Predictive values of platelets morphological indices analysis in septic and non-septic critically ill patients. Minerva Anestesiol-14528. 23 February, 2020
25. Pattraporn Tajarernmuang, Arintaya Phrommintikul, Atikun Limsukon, Chaicharn Pothirat, and Kaweesak Chittawatanarat, "The Role of Mean Platelet Volume as a Predictor of Mortality in Critically Ill Patients: A Systematic Review and Meta-Analysis," Critical Care Research and Practice, vol. 2016, Article ID 4370834, 8 pages, 2016. https://doi.org/10.1155/2016/4370834.
26. J.L. Vélez-Paez, et al. Volumen plaquetario medio como predictor de la mortalidad en pacientes con sepsis: revisión sistemática y metanálisis. Infectio 2020; 24(3): 162-168.
27. Cines DB, Devine LD. Thrombocytopenia in pregnancy. Hematology Am Soc Hematol Educ Program. 2017; 1: 144-151.
28. Myers B. Diagnosis and management of maternal thrombocytopenia in pregnancy. British Journal of Hematology. 2012; 158: 3-15
29. Agustino, AM. et al. Recuento de plaquetas y volumen plaquetario medio en una población sana. Rev Diagn Biol [online]. 2002, vol.51, n.2 [cited 2019-11-17], pp.51-53. Available from: <http://scielo.isciii.es/scielo.php?script=sci_arttext&pid=S0034-79732002000200002&lng=en&nrm=iso>. ISSN 0034-7973
30. Gao Y, Li L, Li Y, Yu X, Sun T, Lan C. [Change of platelet parameters in septic shock patients]. Zhonghua Wei Zhong Bing Ji Jiu Yi Xue. 2014;26(1):28-32.
31. Z. Zhang, X. Xu, H. Ni, and H. Deng, "Platelet indices are novel predictors of hospital mortality in intensive care unit patients," Journal of Critical Care, vol. 29, no. 5, pp. 885.e1–885.e6, 2014.
32. S. Zhang, Y. L. Cui, M. Y. Diao,D. C. Chen, and Z. F. Lin, "Use of platelet indices for determining illness severity and predicting prognosis in critically ill patients," ChineseMedical Journal, vol.128, no. 15, pp. 2012–2018, 2015.
33. Figallo M. Estudios sobre plaquetas. Tesis Doctoral. Lima: Universidad Peruana Cayetano Heredia. 1972.
34. Rocke AS, Paterson GG, Barber MT, et al. Thromboelastometry and Platelet Function during Acclimatization to High Altitude [published correction appears in Thromb Haemost. 2018 Apr;118(4):801. MacInnis, Martin [added]; Main, Shona [corrected to Main, Shona E]; Horne, Elizabeth H [corrected to Horn, Elizabeth H]]. Thromb Haemost. 2018;118(1):63-71. doi:10.1160/TH17-02-0138.

Received: 10 November 2020
Accepted: 15 February 2021

RESEARCH / INVESTIGACIÓN

Predicción temporal del número de muertes por lesiones causadas por tránsito en Estados Unidos

Temporal prediction of the number of deaths from traffic accidents in the United States

Javier Rodríguez-Velásquez[1], María Alejandra González-Bernal[2], Adiela Ruiz-Gómez[2], Esmeralda Guzmán-de la Rosa[1], Daniel Pallejá-Lopez[1], Freddy Barrios-Arroyave[3], Oscar Valero-Alvarado[4], Ribká Soracipa-Muñoz[1], Nathalia López-Sardoth[1,5], Jorge Rodríguez-Hernandez[6]

DOI. 10.21931/RB/2021.06.02.23

Resumen: Los estudios realizados hasta el momento sobre el comportamiento de los accidentes de tráfico han sido descriptivos; sin embargo, este comportamiento al ser estudiado como un sistema dinámico cuya evolución es predecible en el tiempo ha llevado al diseño de una nueva metodología matemática la cual establece órdenes a una aparente imprevisibilidad, el objetivo del presente estudio es predecir mediante la dinámica probabilística de caminata aleatoria y probabilidad. de la tasa de mortalidad por accidentes de tránsito en los Estados Unidos al 2013. El comportamiento de la tasa de mortalidad por accidentes de tránsito en los Estados Unidos se analiza para el período 1994-2012 desde un contexto físico y matemático, estableciendo longitudes de análisis probabilístico y probabilístico de cuatro espacios, para determinar relativo un aumento anual consecutivo y disminuciones que es la tasa de fatalidades probable tránsito 2013. En el 2013 Estados Unidos informó que la tasa de mortalidad por accidentes de tránsito fue de 10,35 por 100.000 habitantes, el valor previsto fue de 10,6, logrando una tasa de éxito del 98% del valor real. El comportamiento dinámico de las víctimas mortales de tráfico en Estados Unidos, según un orden matemático de causalidad en el que fue posible predecir la tasa de víctimas mortales de tránsito para 2013.

Palabras clave: Mortalidad, accidentes de tránsito, trauma, lesiones.

Abstract: Studies so far to the behaviour of traffic accidents have been descriptive; however, this behaviour to be studied as a dynamic system whose evolution is predictable over time has led to the design of new mathematical methodology which establishes orders to an apparent unpredictability, the objective of the present study is to predict by probabilistic random walk dynamics and probability of death rate from traffic accidents in the United States by 2013. The behaviour of the death rate from traffic accidents in the United States is analysed for the period between 1994-2012 from a physical and mathematical context, by setting lengths probabilistic and probabilistic analysis of four spaces, to determine relative a consecutive annual increase and decreases which is the rate of fatalities likely 2013 transit. 2013 United States reported that the death rate from traffic accidents was 10.35 per 100,000 inhabitants, the predicted value was 10.6, achieving a success rate of 98% of the actual value. The dynamic behaviour of traffic fatalities in the United States, according to a mathematical acausal order in which it was possible to predict the rate of traffic fatalities by 2013.

Key words: Mortality, traffic accidents, trauma, injuries.

Introducción

De acuerdo a la teoría de la probabilidad, en un experimento, la totalidad de posibles resultados se denomina espacio muestral; la probabilidad es un concepto que permite calcular que tan posible es un resultado respecto al espacio muestral[1,2]. Para el cálculo de la probabilidad de sucesos equiprobables se utiliza generalmente la Regla de Laplace[3], el cálculo de la probabilidad se basa en su definición axiomática[4] que establece que la probabilidad presenta valores entre 0 y 1, la probabilidad del espacio muestral es igual a 1 y la probabilidad de ocurrencia dos o más eventos independientes es igual al producto de sus probabilidades individuales. La probabilidad permite estudiar fenómenos que son variables pero que son en promedio consistentes[2].

Otro de los conceptos aplicados a fenómenos con un comportamiento irregular y que está asociado con la probabilidad, es la caminata al azar, término acuñado por Karl Pearson en 1905[5], este término puede entenderse en su forma más simple si imaginamos un caminante en un sistema coordenado, que inicia su movimiento en el origen[6], desplazándose aleatoriamente hacia valores positivos o negativos dando un paso de longitud también aleatoria, por lo algunas veces retrocederá y otras avanzará; lo que podríamos decir acerca del movimiento del caminante es cuál es el cuadrado de su desplazamiento medio, el cual está en función del número (N) de pasos dados[2]. Con la caminata al azar se puede acotar un movimiento probabilista, encontrando rangos de valores numéricos que permitan establecer predicciones, este concepto ha sido aplicado a diversos campos como la ecología, biología, economía entre otros[7-13].

De acuerdo al reporte mundial de seguridad vial de la WHO[14] las lesiones de tránsito han sido declarados como un problema de salud pública. De acuerdo a estimaciones hechas por la misma entidad, a nivel mundial más de 1,2 millones de personas fallecen por esta causa y alrededor de 50 millones

[1] Grupo Insight, Asociación Colombiana de Neurocirugía, Bogotá, Colombia.
[2] Universidad Cooperativa de Colombia, Bogotá, Colombia.
[3] Fundación Universitaria Autónoma de las Américas, Pereira, Colombia.
[4] Escuela de Ciencias de la Salud, Universidad Nacional Abierta y a Distancia, Bogotá, Colombia.
[5] Centro de Investigaciones Clínica del Country. Bogotá, Colombia.
[6] Instituto de Salud Pública, Pontificia Universidad Javeriana, Bogotá, Colombia.

Corresponding author: grupoinsight2025@gmail.com

quedan afectadas[14], se destaca que las tasas de mortalidad por inseguridad vial por 100.000 habitantes son recurrentemente inversamente proporcionales a los ingresos de los países[15]. Este fenómeno se ha asociado a diferentes factores de riesgo: beber y conducir, el exceso de velocidad y el no uso de cascos en las motocicletas, no portar cinturones de seguridad y sistemas de retención infantil, sumándose recientemente a estos el uso de dispositivos móviles[16].

Como consecuencia al gran número de información que se debe manejar en estudios de tipo, descriptivo, geográfico, demográfico y de revisión documental para el análisis de las variables se hace uso de metodologías estadísticas de corte prospectivo y retrospectivo[17,18]. En un estudio retrospectivo realizado para el análisis de muertes relacionadas con el vehículo todo terreno (ATV), durante el periodo comprendido entre los años 1985-2006[19], consideraron para el estudio todo análisis de información descriptiva y multivariada, encontrando que la disminución del uso de este tipo de vehículos en carretera podría ser una manera eficaz de reducir las muertes.

Por otro lado, estudios realizados para medir el impacto que tiene las lesiones causadas por el tránsito (LCT)[18] y su asociación con mortalidad, han evaluado la posible contribución de los sistemas organizados de atención de trauma, en la disminución de la mortalidad por accidentes causadas por el tránsito[20]. Han concluido que la disminución muertes causadas por el tránsito, se debe a la contribución de los protocolos de atención aplicados en traumatología, sin dejar de lado los planes de prevención realizados por otras instituciones.

Otro tipo de epidemias como el dengue y la malaria han sido estudiadas a partir de metodologías desarrolladas en el contexto de la física y la matemática, logrando evaluar la complejidad de su comportamiento como sistemas dinámicos predecibles[21-25], estableciendo ordenes matemáticos a causales, que permiten la predicción de la epidemia. A partir de la probabilidad y la entropía se desarrollaron predicciones de brotes de malaria en 810 municipios de Colombia, encontrando un porcentaje de precisión del 99,86%. También, a partir de una analogía con la caminata al azar probabilista, se desarrolló un método predictivo de la dinámica de dengue en Colombia, estableciendo predicciones superiores al 90%[22], de igual forma esta metodología se ha utilizado también para establecer predicciones y proyecciones del comportamiento de la obesidad infantil en Estados Unidos[25].

El presente estudio tiene como propósito predecir el número de muerte causadas por lesiones tránsito en Estados Unidos para el año 2013, mediante la caminata al azar probabilista[22], valor que será posteriormente comparado con el reportado para este año por el NHTSA (National Highway Traffic Safety Administration).]

Materiales y métodos

Longitud de la tasa de muertes por lesiones causadas por tránsito

Representa el valor de la tasa de muertes por lesiones causadas por tránsito la cual se calcula mediante la siguiente ecuación[22]:

$$L = \sqrt{(X_0 - X_1)^2 + (Y_0 - Y_1)^2} \quad \text{Ecuación 1}$$

Siendo,y las coordenadas para el año inicial y son las coordenadas para el año siguiente.

Longitud probabilista de la tasa de muertes por lesiones causadas por tránsito

Es el primer espacio de probabilidad que considera cada variación anual de la longitud L de muertes por lesiones causadas por tránsito como un evento mediante la siguiente ecuación:

$$P(L) = \frac{\text{Longitud variación anual de muertes por accidente de tránsito}}{\text{Total longitudes de muertes por accidente de tránsito}} = \frac{L}{TL} \quad \text{Ecuación 2}$$

Probabilidad de la tasa de muertes por lesiones causadas por tránsito

Se calcula en el segundo espacio de probabilidad y es el cociente entre la tasa de muertes por accidente de tránsito y la suma total de la tasa de muertes reportadas durante el periodo comprendido entre los años 1994-2012 mediante la siguiente ecuación:

$$P(N) = \frac{\text{Tasa anual de muertes por accidente de tránsito}}{\text{Total muertes por accidente de tránsito}} \quad \text{Ecuación 3}$$

Desviación media cuadrática

Para evaluar si en el segundo espacio de probabilidad existen probabilidades cargadas de la tasa de muertes por accidente de tránsito se usa la siguiente fórmula:

$$P(Rn) = \frac{\text{Tasa anual de muertes por accidente de tránsito}}{\text{Total de las tasas de muertes por accidente de tránsito}} \pm \frac{1}{2\sqrt{N}} \quad \text{Ecuación 4}$$

Siendo N la suma total de las tasas de muertes por accidente de tránsito registradas durante el periodo comprendido entre los años 1994-2013 en Estados Unidos, que en términos probabilistas lo que se está analizando es la totalidad de eventos del espacio muestral.

Ecuación de segundo grado para la predicción de muertes por lesiones causadas por tránsito

Para la predicción se tomó los valores de las longitudes hallada con la ecuación 1 de los tres años anteriores al año 2013, construyendo de esta manera un tercer espacio de probabilidad. Luego fue remplazado el promedio aritmético de la probabilidad hallado para estos tres últimos años y el valor de la suma de las tres longitudes (TL) en la siguiente ecuación:

Para determinar cuál de los dos valores de la predicción hallados para el 2013 con la ecuación 5 es el evento más probable en relación a de si hay una disminución (D) o aumento (A) de la tasa de muertes por accidente de tránsito respecto al año 2012, se construyó un cuarto espacio de probabilidad para estudiar el comportamiento de períodos consecutivos de dos y tres años.

Procedimiento

Se tomaron los valores anuales de la tasa de muertes de tránsito en Estados Unidos del periodo comprendido entre los años 1994-2012 de la base de datos de NHTSA[2].

Se evaluó la dinámica del comportamiento de la tasa de muertes por accidente de tránsito en Estados Unidos graficando estos valores en un plano cartesiano, ubicando en el eje x los años y en el eje y la tasa de muertes por accidente de tránsito, para luego analizar su comportamiento en analogía a una caminata al azar probabilista (ver figura 1).

Primero se calculó todas las longitudes de todas las variaciones anuales de la tasa de muertes por lesiones causadas por tránsito en Estados Unidos, con la ecuación 1. Para esta ecuación los valores del eje x que corresponde a la variación de cada año el cual toma valores de cero.

Halladas la tasa de longitudes con la ecuación 1, se calculó la probabilidad de cada tasa de longitud mediante la ecuación 2, que corresponde a los valores del primer espacio de probabilidad. Para ello se dividió la longitud para cada año

$$Y_{(año\ a\ predecir)} = \frac{2Y_{(año\ anterior)} \pm \sqrt{(-2Y_{(año\ anterior)})^2 - 4\{Y^2_{(año\ anterior)} + (X_0 - X_1)^2 - [(P(L)^2 \times (TL)^2]\}}}{2} \quad \text{Ecuación 5}$$

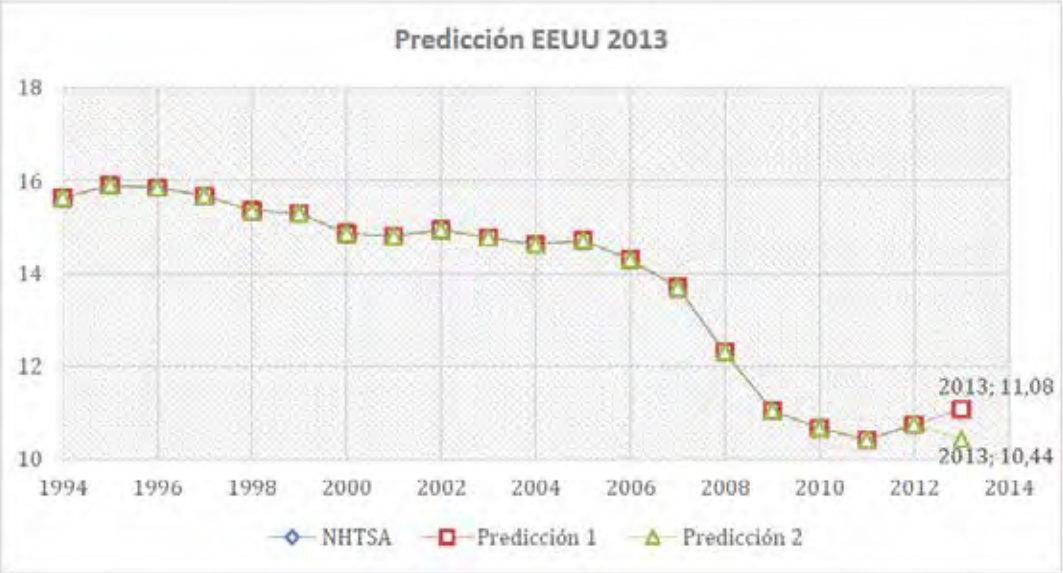

Figura 1. Superposición de los dos valores predichos para la tasa de muertes por accidente de tránsito en Estados Unidos para el año 2013. Trazado continuo corresponde al valor 11,08, y el trazado discontinuo, corresponde al valor 10,44. Todos los valores antes del 2013, corresponden al periodo comprendido entre1994-2012, tomados de la base de datos NHTSA.

entre la suma total de longitudes comprendidas del periodo comprendido entre 1994-2012. Seguidamente se halló la proporción entre la variación anual de cada una de las longitudes respecto al menor valor hallado en dicho periodo.

El segundo espacio de probabilidad se estableció a partir del calculó de la probabilidad de la tasa de muertes por lesiones causadas por tránsito para cada año reportada por la base de datos NHTSA, mediante la ecuación 3 dividiendo la tasa de muertes por lesiones causadas por tránsito reportado en un año entre la suma total de estas tasas de muerte en el periodo comprendido entre los años 1994-2012. Para determinar si existe un cargamiento en las probabilidades hacia valores específicos, al ser comparados los valores del segundo espacio de probabilidad con su valor esperado, se calculó la desviación media cuadrática de la tasa de muertes por accidente de tránsito en Estados Unidos.

Para predecir la tasa de muertes por lesiones causadas por tránsito para el 2013 en Estados Unidos, se estableció un tercer espacio de probabilidad, calculando primero el promedio aritmético de los valores de las longitudes halladas con la ecuación 1 para el período comprendido entre los años 2010-2012, para luego con este valor calcular la probabilidad de cada uno de estos tres periodos con la ecuación 2. Luego, el valor promedio de las longitudes probabilistas y la suma total de las tres longitudes comprendidas entre los años 2010-2012, fueron remplazados en la ecuación 5, incluyendo el valor de la longitud del año 2012; obteniendo como solución dos valores que corresponden a los rangos con los que determina la predicción.

El cuarto espacio de probabilidad compuesto por dos eventos disminución (D) y aumento (A) de muertes por lesiones causadas por tránsito, el cual permitió estudiar el comportamiento de períodos consecutivos de dos y tres años. El análisis hecho en este último espacio permite determinar cuál de los dos valores cuantitativos hallados con la ecuación 5 es más probable, y de este modo determinar con certeza el valor predictivo para el año 2013.

Resultados

La tasa de muertes por accidente tránsito para el periodo comprendido entre los años 1994-2012 en Estados Unidos varió entre 10,42 y 15,91. Los valores de las longitudes halladas para este periodo variaron entre 0,05 y 1,39. Los valores de la probabilidad de la tasa de longitudes de muertes por accidente de tránsito se encontraron entre 0,008 y 0,212. Los valores de la proporción de las distancias respecto a la distancia mínima encontrada para este periodo estuvieron entre 1 y 27,80 (valores no se muestran). La probabilidad de la tasa anual de muertes por lesiones causadas por tránsito en Estados Unidos para este mismo periodo varió entre 0,039 y 0,060. La desviación media cuadrática para los valores de la tasa de muertes por accidente de tránsito osciló entre un rango de 0,009 y 0,091, encontrando que la diferencia entre estos últimos y el valor esperado varía en un rango de 0,031 y -0,031 (Tabla 1). El cálculo de probabilidades halladas para la tasa anual de muertes por lesiones causadas por tránsito en Estados Unidos y los valores de la desviación media cuadrática para el periodo comprendido entre los años 1994-2012, muestran que no son equiprobable, presentándose probabilidades cargadas que determinan la predicción para el año 2013 (tabla 1).

Por otra parte, con el análisis realizado al tercer espacio de probabilidad que corresponde al periodo comprendido entre los años 2010-2012 de muertes por lesiones causadas por tránsito, así como la aplicación de la ecuación 5, se hallaron los dos valores de predicción para el año 2013 los cuales fueron de 10,44 y 11,8 (ver tabla3 y figura 1).

Para determinar el evento más probable para el año 2013 con relación a los aumentos (A) o disminuciones (D), se analizó la frecuencia y probabilidad de los valores consecutivos de los A o D (Tabla 2). Para ello, se analizó el tercer y cuarto espacio de probabilidades que contiene el número de posibles combinaciones entre A y D para un periodo de tres años consecutivos de muertes por LCT en Estados Unidos, encontrando que es

más probable que haya una disminución de lesiones causadas por tránsito (ver tabla 3).

Considerando como hecho más probable que haya una disminución, el establecimiento del valor predictivo fue realizado mediante el cálculo del promedio aritmético entre los dos valores predichos para el 2013 con la ecuación 5, tomando este resultado y el menor valor predicho para este año el cual fue de 10,44, nuevamente fueron promediados hallado como resultado 10,6, valor que al ser comparado con el reportado por NHTSA[2] el cual corresponde a una tasa del 10,35 por cada 100.000 habitantes para el año 2013, se halló un porcentaje de acierto del 98 %. Al estudiar el espacio de probabilidad de aumentos y disminuciones se observa que las diferentes triplas presentan probabilidades que se diferencian, mostrando que por ejemplo la tripla DDD se presenta la mitad de las veces. (ver tabla 4).

Año		L	P(L)	P(N)	DMC+	DMC-	DMC+ P	DMC- P
1994	15,64			0,059	0,090	0,028	0,031	-0,03
1995	15,91	0,27	0,07	0,060	0,091	0,029	0,031	-0,03
1996	15,86	0,05	0,01	0,060	0,090	0,029	0,031	-0,03
1997	15,69	0,17	0,03	0,059	0,090	0,028	0,031	-0,03
1998	15,36	0,33	0,05	0,058	0,088	0,027	0,031	-0,03
1999	15,30	0,06	0,01	0,058	0,088	0,027	0,031	-0,03
2000	14,87	0,43	0,07	0,056	0,087	0,025	0,031	-0,03
2001	14,81	0,06	0,01	0,056	0,086	0,025	0,031	-0,03
2002	14,95	0,14	0,02	0,056	0,087	0,026	0,031	-0,03
2003	14,78	0,17	0,03	0,056	0,086	0,025	0,031	-0,03
2004	14,63	0,15	0,02	0,055	0,086	0,024	0,031	-0,03
2005	14,72	0,09	0,01	0,055	0,086	0,025	0,031	-0,03
2006	14,31	0,41	0,06	0,054	0,085	0,023	0,031	-0,03
2007	13,70	0,61	0,09	0,052	0,082	0,021	0,031	-0,03
2008	12,31	1,39	0,21	0,046	0,077	0,016	0,031	-0,03
2009	11,05	1,26	0,19	0,042	0,072	0,011	0,031	-0,03
2010	10,67	0,38	0,06	0,040	0,071	0,009	0,031	-0,03
2011	10,42	0,25	0,04	0,039	0,070	0,009	0,031	-0,03
2012	10,76	0,34	0,05	0,040	0,071	0,010	0,031	-0,03

Tabla 1. Valores de la tasa de muertes por tránsito en Estados Unidos entre periodo comprendido en los años 1994-2012. Donde L: es la longitud de la tasa de muertes de tránsito, P(L): la longitud probabilista de la tasa de muertes de tránsito, (+/-) DMC: valores de la desviación media cuadrática de la tasa de muertes de tránsito.

Años consecutivos	1994 a 2012	Aumentos		Disminuciones	
		V	P	V	P
1		4	0,22	0	0
2		0	0	1	0,11
6		0	0	2	0,67
Total	18	4	0,22	14	0,78

Tabla 2. Frecuencia y probabilidad de los aumentos y disminuciones consecutivas para el periodo comprendido entre los años 1994-2012, en relación a la tasa de muertes tránsito en Estados Unidos, donde V: representa el valor total de cada tipo de variación y P: la probabilidad de esta variación.

Años consecutivos	1994 a 2012	Aumentos		Disminuciones	
		V	P	V	P
1		4	0,22	0	0
2		0	0	1	0,11
6		0	0	2	0,67
Total	18	4	0,22	14	0,78

Tabla 3. Valores de los tres últimos años que corresponden a la tasa y L: longitud de muertes por lesiones causadas por tránsito para hacer la predicción del año 2013. Valor real tomado de la base de datos NHTSA.

Combinaciones	V	P
DDD	8	0,50
DDA	3	0,19
DAD	2	0,13
DAA	0	0,00
ADD	3	0,19
ADA	0	0,00
AAD	0	0,00
AAA	0	0,00
Total	16	1

Tabla 4. Número de posibles combinaciones de aumentos (A) y disminuciones (D) para un periodo de tres años consecutivos de muertes por tránsito en Estados Unidos, observada durante el periodo comprendido durante los años 1994-2012.

Discusión

Este es el primer trabajo en el que se predice el número de muertes por LCT en Estados Unidos para el año 2013, analizando este comportamiento como si fuera una caminata al azar probabilista y el establecimiento de un espacio total de probabilidades. Se analizó el comportamiento de la dinámica de las longitudes probabilistas durante el periodo comprendido entre los años 2010-2012 respecto al promedio más probable, se consideró el comportamiento de aumentos y disminuciones durante el mismo periodo, estableciendo que el hecho más probable para el 2013 es que haya una disminución en la tasa de muertes por lesiones causadas por tránsito en Estados Unidos, logrando un 98% de predicción. Evidenciando así que la dinámica es un fenómeno determinista, contrariamente a la aleatoriedad e impredecibilidad que se le ha asociado convencionalmente.

Al analizar la dinámica del comportamiento de las LCT como una caminata al azar probabilista se pueden hacer proyecciones a futuro que contribuyan a optimizar los planes de acción orientados a la prevención y sensibilización de muertes por lesiones causadas por tránsito. También mediante la aplicación de esta metodología es posible hacer seguimientos del impacto que tienen los planes de acción para disminuir las lesiones causadas por tránsito, en el marco de la década de la seguridad vial (2011-2020) declarada por la WHO[14], que busca impulsar acciones que permitan obtener disminuciones del 50% en las muertes por causa de la violencia vial en los países más afectados.

Estudios realizados para evaluar el impacto que tienen las muertes por lesiones causadas por tránsito se han centrado en encontrar las causas, identificando por ejemplo el actor vial más vulnerable[26,27], como son los peatones, ciclista y motociclistas[18,27]. Así mismo las lesiones más frecuentes por este tipo de accidentes[18]. Por ejemplo, se ha establecido que, para el departamento de Valledupar, los motociclistas son los más afectados por las LCT, y se puede observar un continuo aumento en las LCT[28]. En este trabajo se encontró un patrón matemático de estas lesiones y en la presente investigación se logran hacer predicciones a partir de patrones probabilistas. Otros estudios en cambio han identificado como posibles causantes de lesiones causadas por tránsito, los mecanismos de distracción del conductor[16],concluyendo después de analizar la literatura que trata del tema que los sistemas que integren contramedidas son los que pueden dar solución al problema[29].

La dinámica de LCT a partir de la caminata al azar probabilista, permitió establecer predicciones a partir de una perspectiva acausal, considerando únicamente los aumentos y disminuciones propios de la dinámica, constituyéndose en una herramienta de ayuda para la toma de decisiones de salud pública, pues es más simple ya que permite abstraer los múltiples factores causales que has sido asociados a las LCT. Desde esta perspectiva acausal se han desarrollado metodologías para evaluar el comportamiento de epidemias, estableciendo predicciones del número de infectados de malaria y dengue en Colombia[21-24], estableciendo porcentajes de acierto de 90,4%[22] para la epidemia de dengue y de 99,86% en la predicción de brotes semanales de malaria[21], permitiendo que los rangos de tiempo que usualmente son necesarios para el análisis de este tipo de dinámicas que son de 5 a 7 años[29] se reduzca a tres semanas.

Órdenes matemáticos acausales se han encontrado en múltiples fenómenos de la medicina, permitiendo establecer predicciones en áreas como la cardiología de adulto[30], de mortalidad en pacientes de la Unidad de Cuidados Intensivo[31], en la fetal y neonatal, en inmunología y biología molecular, infectología. También, se han desarrollado metodologías de análisis y diagnóstico de imágenes de arterias coronarias, de células de cuello uterino y estructuras eritrocitarias.

Conclusiones

El contexto en el que se desarrolló la metodología para evaluar la dinámica de muertes por lesiones causadas por tránsito en Estados Unidos, aparte de predecir la tasa de muertes por lesiones causadas por tránsito en un año especifico puede también predecir la tasa de muertes por lesiones causadas por tránsito de diferentes zonas de Estados Unidos, independiente de factores causales, análisis estadísticos y epidemiológicos.

Agradecimientos

Esta investigación hace parte del proyecto INV2288 financiado por la Universidad Cooperativa de Colombia.

Agradecemos a la Asociación Colombiana de Neurocirugía, especialmente a su presidente, el doctor Marco Fonseca y al doctor Germán Forero, Director de Investigaciones, por su apoyo a nuestras investigaciones.

Conflictos de Interés

Los autores declaran no tener conflictos de interés.

Referencias bibliográficas

1. Spiegel M.R, Schiller J.J, Srinivasan RA. Probabilidad y estadística. Bogotá: Mc Graw Hill; 2003.
2. Feynman RP, Leighton RB, Sands M. Probabilidad. En: Feynman RP, Leighton RB, Sands M. Física. Wilmington: Addison-Wesley Iberoamericana, S. A; 1964; p. 6-1, 6-16.
3. Laplace P. Ensayo filosófico sobre las probabilidades. Barcelona: Altaza, 1995. p. 12-15
4. Blanco L. Probabilidad. 1a ed. Bogotá: Unibiblos; 2004
5. Pearson K. The Problem of the Random Walk. Nature. 1905; 72: 294.
6. Cattoni D, Ozu M, Chara O. Ruidos en la naturaleza An AFA. 2004; 16: 294-99. Disponible en: https://www.academia.edu/30624724/Ruidos_en_La_Naturaleza
7. Van Kampen N.G. Stochastic Processes in Physics and Chemistry. 3a ed. North-Holland, Amsterdam; 2007.
8. Redner S.A Guide to First-Passage Process. Cambridge. Cambridge University Press; 2001.
9. Goel N.S, Richter N. Stochastic Models in Biology. 1a ed. New York, Academic Press; 1974.
10. Doi M, Edwards S. The Theory of Polymer Dynamics. 1a ed. Oxford, Clarendon Press; 1986.
11. De Gennes P.G. Scaling Concepts in Polymer Physics. Ithaca, N.Y: Cornell University Press; 1979.
12. Risken H, Frank T. The Fokker–Planck Equation. 2a ed. Berlin, Springer; 1984.
13. Weiss, G. Aspects and Applications of the Random Walk. Amsterdam: North-Holland, 1994.
14. World Heath Organization. Global status report on road safety. Luxembourg City Luxembourg, 2013.
15. Organización Mundial de la Salud. Informe sobre la situación mundial de la seguridad vial: es hora de pasar a la acción. Ginebra, Suiza, 2013 [Citado el 1 Diciembre 2018]. Disponible en: www.who.int/violence_injury_prevention/publications/road_tra€c/en/index.html.
16. Centers for Disease Control and Prevention (CDC). Mobile device use while driving--United States and seven European countries, 2011. [Ciado 17 dic 2018]. Disponible en: https://www.cdc.gov/mmwr/preview/mmwrhtml/mm6210a1.htm

17. Híjar M. Utilidad del análisis geográfico en el estudio de las muertes por atropellamiento. Salud publica Mex. 2000; 42:188-193. Disponible en: https://www.scielosp.org/article/spm/2000.v42n3/188-193/
18. Dultz L, Foltin G, Simon R, Wall S, Levine D, Bholat O, et al. Vulnerable roadway users struck by motor vehicles at the center of the safest, large US city. Journal of Trauma and Acute Care Surgery. 2013; 74(4): 1138–1145. Disponible en: https://insights.ovid.com/pubmed?pmid=23511157
19. Denning G, Harland K, Ellis D, Jennissen C. More fatal all-terrain vehicle crashes occur on the roadway than off: increased risk-taking characterises roadway fatalities. Inj Prev 2013; 19:250-256. Disponible en: https://injuryprevention.bmj.com/content/19/4/250
20. Nathens A, Jurkovich G, Cummings P, Rivara F, Maier R. The Effect of Organized Systems of Trauma Care on Motor Vehicle Crash Mortality. JAMA. 2000; 283(15):1990-1994. Disponible en: https://jamanetwork.com/journals/jama/fullarticle/192607
21. Rodríguez J. Método para la predicción de la dinámica temporal de la malaria en los municipios de Colombia. Rev Panam Salud Pública 2010; 27(3):211-218. Disponible en: http://iris.paho.org/xmlui/bitstream/handle/123456789/9708/a08v27n3.pdf?sequence=1&isAllowed=y
22. Rodríguez J, Correa C. Predicción temporal de la epidemia de dengue en Colombia: dinámica probabilista de la epidemia. Rev. Salud pública. 2009; 11 (3): 443-453. Disponible en: https://revistas.unal.edu.co/index.php/revsaludpublica/article/view/37041/39046
23. Rodríguez J. Dinámica probabilista temporal de la epidemia de malaria en Colombia. Rev Fac Med. 2009; 17(2):214-221. Disponible en: http://www.scielo.org.co/pdf/med/v17n2/v17n2a05.pdf
24. Rodríguez J, Prieto S, Farjardo E, Correa C, López F, Castro J, Soracipa Y. Predicción de la dinámica temporal de egresos hospitalarios por obesidad en niños y jóvenes en Estados Unidos. Rev Chil Nutr 2015; 42(4):345-350. Disponible en: http://www.redalyc.org/toc.oa?id=469&numero=43554
25. Otte D, Jänsch M, Haasper C. Injury protection and accident causation parameters for vulnerable road users based on German In-Depth Accident Study GIDAS. Accident Analysis & Prevention. 2012; 44(1): 149-153. Disponible en: https://www.sciencedirect.com/science/article/abs/pii/S0001457510003830
26. Rodríguez J, Peñalosa R, Ariza L, Flórez C, Armindo F, Montoya S, et al. Factores de riesgo asociados a lesiones causadas por el tránsito y propuestas de intervenciones para el contexto colombiano. 1a ed. Universidad Javeriana. Bogotá: Ecoe ediciones. 2015.
27. Rodríguez JM, Peñaloza RE, Moreno Montoya J. Road traffic injury trends in the city of Valledupar, Colombia. A time series study from 2008 to 2012. PLoS ONE. 2015; 10(12): e0144002. Disponible en: https://journals.plos.org/plosone/article?id=10.1371/journal.pone.0144002
28. Young K, Salmon P. Examining the relationship between driver distraction and driving errors: A discussion of theory, studies and methods. Safety Science. 2012; 50(2):165-174. Disponible en: https://www.sciencedirect.com/science/article/pii/S092575351100155X
29. Bortman M. Elaboración de corredores o canales endémicos mediante planillas de cálculo. Rev Panam Salud Publica. 1999; 5(1):1–8. Disponible en: https://scielosp.org/pdf/rpsp/1999.v5n1/1-8/es
30. Rodríguez J, Prieto S, Correa C, Bautista J, Velasco A, Méndez, et al. Mathematics physical assessment of cardiac dynamics based on theory of probability and proportions of entropy in the intensive care unit for patients with arrhythmia. J Nucl Med Radiat Ther. 2015;6:4. Disponible en: https://www.omicsonline.org/2155-9619/2155-9619.S1.002-012.pdf
31. Rodríguez J. Dynamical systems applied to dynamic variables of patients from the intensive care unit (ICU): Physical and mathematical mortality predictions on ICU. J. Med. Med. Sci. 2015; 6(8): 102-108. Disponible en: http://dx.doi.org/10.14303/jmms.2015.115

Received: 30 Octubre 2020
Accepted: 30 Enero 2021

RESEARCH / INVESTIGACIÓN

Uso de aguas residuales de porcicultura y faenamiento para el crecimiento y obtención de biomasa algal de *Chlorella vulgaris*

Slaughtering and piggery wastewater for cultivation and biomass generation of *Chlorella vulgaris*

Johanna Medrano-Barboza[1], Alberto Alejandro Aguirre-Bravo[1], Paula Encalada-Rosales[1], Roberto Yerovi[1], José Rubén Ramírez-Iglesias[2]

DOI. 10.21931/RB/2021.06.02.24

Resumen: Diversas investigaciones respaldan el uso de microalgas como fuente de productos de interés biotecnológico, pero aún existen limitaciones para su implementación; como el uso de aguas residuales como medio de cultivo y la generación de biomasa en presencia de otros microorganismos que compiten por los nutrientes. En este estudio se compararon 3 métodos de desinfección para aguas residuales de porcicultura y faenamiento, y se evaluó su aplicabilidad para el cultivo de *Chlorella vulgaris*. Se probaron tres métodos de pretratamientos: irradiación UV, hipoclorito de sodio (NaClO) y ácido peracético (CH_3CO_3H) y se compararon los resultados con agua no tratada. Se determinó la generación de biomasa (g/L) y el consumo de nitratos, ortofosfatos y demanda química de oxígeno, durante 13 días de cultivo con pretratamiento y en agua sin tratar. La desinfección por UV durante 30 minutos eliminó completamente las bacterias, mientras que los tratamientos químicos con las concentraciones empleadas en este estudio lograron reducir parcialmente la carga bacteriana. El agua residual con pretratamiento por UV generó una biomasa de *C. vulgaris* de 0,2 g/L con elevados porcentajes de remoción de nutrientes del medio (97 y 89 % para nitratos y ortofosfatos), valores de remoción superiores a los presentados por la condición sin pretratamientos. Estos resultados sugieren la necesidad de desinfectar las aguas residuales para su implementación como medio de cultivo, además de indicar la factibilidad de su uso como medio de crecimiento complejo, con el objetivo de generar biomasa.

Palabras clave: Cultivo, desinfección, microalgas, pretratamiento, remoción de nutrientes.

Abstract: Several studies support the use of microalgae as source of products of biotechnological interest, but there are limitations for their implementation, such as the use of wastewater as a culture medium and the generation of biomass in presence of other microorganisms that compete for nutrients. In this study, 3 disinfection methods for slaughtering and piggery wastewater were compared, and their applicability for the cultivation of *Chlorella vulgaris* was evaluated. Three pretreatment methods were tested: UV irradiation, sodium hypochlorite (NaClO) and peracetic acid (CH_3CO_3H), and the results were compared with untreated water. The generation of biomass (g / L) and the consumption of nitrates, orthophosphates and chemical oxygen demand was determined, during 13 days of culture with pretreatment and in untreated water. UV disinfection for 30 minutes completely eliminated the bacteria, while chemical treatments with the concentrations used in this study managed to partially reduce the bacterial load. The residual water with UV pretreatment generated a *C. vulgaris* biomass of 0,2 g / L with high percentages of removal of nutrients from the medium (97 and 89% for nitrates and orthophosphates), removal values higher than those presented in the condition without pretreatments. These results suggest the need to disinfect wastewater for its implementation as a culture medium and support the feasibility of its use as a complex growth medium, to generate biomass.

Key words: Culture, disinfection, microalgae, nutrients removal, pretreatment.

Introducción

Las algas son un amplio grupo de organismos fotosintéticos cuyas formas de organización varían de unicelulares a pluricelulares, siendo las microalgas una de las formas de vida más primitivas del planeta junto con las cianobacterias procariotas y algas eucariotas[1]. El interés biotecnológico orientado al crecimiento y la obtención de biomasa a partir de estos microorganismos está asociado a la generación de diversos productos y aplicabilidades entre las cuales se encuentran su uso como biofertilizadores en la industria agrícola, como fuente de proteínas y ácidos grasos para la alimentación humana y animal, y para la generación de energía a partir de la producción de biodiesel y biocombustibles[2]. La producción de biocombustibles a través de microalgas se reconoce como una fuente potencial para reemplazar los derivados del petróleo, sin afectaciones en la alimentación humana[2,3]. Se estima que la misma área de campo usada para el cultivo de microalgas es 200 veces más productiva que el mismo campo sembrado con cultivos energéticos para la obtención de aceites vegetales[4].

Los componentes lipídicos de las microalgas sirven de base para diferentes usos bioenergéticos: biodiesel, bioetanol, biogás y biohidrógeno[5]. Los triacilglicéridos (TAG) sirven como reserva de energía en las algas. Estas grasas neutras están formadas de una cadena triple de ésteres, unidas a una molécula de glicerol. Estos lípidos pueden ser convertidos en biodiesel con facilidad mediante transesterificación, cambiando el glicerol por alcohol (por ejemplo, metanol). Los productos obtenidos por este medio son glicerol y éster-metílico de ácidos grasos (biodiesel)[6].

Algunas limitaciones que se presentan en el cultivo de microalgas son los elevados costos de los nutrientes que hay que aportar para el crecimiento de estos microorganismos. Sin embargo, alternativas como cultivar las microalgas en lugares donde ya existen los nutrientes adecuados puede reducir en un 50% los costos, comparado con el cultivo en biorreactores, los

[1] Universidad Internacional SEK, Facultad de Ingeniería y Ciencias Aplicadas, Quito, Ecuador.
[2] Universidad Internacional SEK, Facultad de Ciencias de la Salud, Quito, Ecuador.

Corresponding author: jose.ramirez@uisek.edu.ec

cuales requieren de energía eléctrica, fertilizantes e infraestructura[7]. En este contexto, las aguas residuales provenientes de desechos de porcicultura y/o faenamiento poseen características químicas potencialmente adecuadas, como alto contenido de fósforo y nitrógeno[8], pero su implementación como medio de cultivo para microalgas presenta escasos estudios de aplicabilidad. El uso de microalgas no sólo contribuye a la disminución de nitrógeno y fósforo en los cuerpos de aguas en las cuales sean empleadas, también permite reducir el contenido de metales pesados y componentes orgánicos tóxicos, por lo cual puede obtenerse un doble beneficio, al facilitar el cultivo de microalgas y generar efectos de biorremediación[4].

Sin embargo, la alta carga bacteriana presente en aguas residuales puede impedir el crecimiento de las microalgas. La proliferación bacteriana puede estar en contraposición al de las microalgas, lo que vuelve necesario el pretratar el agua para reducir o eliminar estas bacterias[8]. Las bacterias presentan una mayor capacidad de obtención de nutrientes, como el fósforo, en comparación con las microalgas, incluso bajo condiciones limitadas del mismo[9]. Para poder eliminar la mayor cantidad de estas bacterias, sin dañar los componentes necesarios para las microalgas, se deben emplear alternativas de desinfección al uso de autoclaves, los cuales generan altos costos de inversión y operación a escala industrial. La luz ultravioleta de 254 nm de longitud de onda (UV-C) se ha usado eficazmente para la desinfección de aguas residuales. Los microorganismos absorben la energía emitida por esta luz y las reacciones fotoquímicas alteran los componentes moleculares esenciales (ARN y ADN) resultando en efectos germicidas[10]. Por otra parte, el hipoclorito de sodio en concentraciones de 0,2 a 2 mg/L ha demostrado una buena desinfección, siendo recomendable 1,9 mg/L. Esta dosis permite desinfección y a la vez residuos de cloro de menos de 0,2 mg/L, al cabo de 24 horas[11]. Por último, el ácido peracético es un oxidante fuerte que actúa sobre las proteínas, enzimas y otros metabolitos, degradándolos, debido a la liberación de oxígeno activo. También actúa sobre las uniones dobles, impidiendo su función molecular, además de incidir de igual manera sobre las lipoproteínas citoplasmáticas[12].

Debido a que varios estudios están orientados hacia el empleo de aguas residuales para disminuir costos derivados del uso de medios de cultivo definidos, es indispensable asegurar un adecuado rendimiento en la obtención de biomasa algal y que esta no se vea afectada por la carga bacteriana propia del agua empleada. Con base en lo anterior, el objetivo del presente estudio fue comparar métodos de desinfección de aguas residuales procedentes de granjas de faenamiento y porcicultura, y evaluar la factibilidad del uso de este tipo aguas pretratadas para el cultivo de *Chlorella vulgaris*, microalga conocida por su potencial para la remoción de nutrientes, la generación de lípidos y su posterior conversión a biocombustibles.

Métodos

Agua residual

Posterior a la autorización por parte de los propietarios del complejo industrial, aproximadamente 5000 mL de agua residual fueron colectados de una industria de cría y faenamiento de cerdos ubicada en la provincia de Cotopaxi, en la ciudad de Latacunga, Ecuador, y llevados a los laboratorios de la Universidad Internacional SEK para ser usada como medio de cultivo de microalgas. Para su caracterización, se determinó el contenido de nitrógeno en forma de nitratos, el contenido de fósforo en forma de ortofosfatos y la demanda química de oxígeno. Los parámetros fisicoquímicos se determinaron en un espectrómetro HACH DR5000.

Métodos y protocolos de desinfección

En este estudio se trabajó con tres métodos para la desinfección del agua residual como pretratamiento previo al cultivo de microalgas; los métodos de desinfección seleccionados fueron: exposición a luz UV y uso de desinfectantes químicos, como hipoclorito de sodio (NaClO) y ácido peracético (CH_3CO_3H). También se realizaron ensayos empleando el agua residual sin pretratamiento, como muestra control. Los diferentes ensayos de desinfección se realizaron por triplicado, usando volúmenes de 50 mL de agua residual depositados en placas Petri.

Los tratamientos de desinfección por UV se llevaron a cabo con una lámpara de arco de mercurio a baja presión de 18 W y 253 nm (UV-C). La irradiación UV en la superficie de la muestra fue de 3,5 mW cm^{-2}. Los protocolos se realizaron de acuerdo a lo descrito por Bolton y otros (2003)[13] y Qin y otros (2014)[14], con modificaciones. Para ello, las muestras de agua fueron colocadas a 53 cm de distancia de la luz UV-C y expuestas a 10, 30 y 60 minutos de radiación.

El tratamiento con NaClO y la neutralización del excedente de cloruros se realizó de acuerdo a lo descrito por Koivunen & Heinonen-Tanski (2005)[15]. En resumen, se usó NaClO a concentraciones finales de 10, 30 y 60 ppm. Posteriormente, las muestras se incubaron por 12 horas en oscuridad y 12 horas en presencia de luz solar. Por último, se agregó Tiosulfato de Sodio ($Na_2S_2O_3$), en concentraciones de 2,3 ppm por cada ppm de NaClO para neutralizar el cloruro sobrante.

La desinfección con ácido peracético se realizó empleando concentraciones finales similares a las descritas por Rossi y otros (2007)[16] (5; 12,5 y 50 ppm) de CH_3CO_3H. Posteriormente, se dejaron las muestras en reposo durante 10 minutos.

El conteo de unidades formadoras de colonias (UFC) para determinar la desinfección e inactivación de la carga bacteriana, se realizó siguiendo protocolos generales para la determinación de la calidad de aguas[17]. A partir de las muestras de agua residual pretratadas con los diferentes métodos de desinfección, se realizaron diluciones de 10-1, 10-2, 10-3, 1-4, 10-5 y 10-6; se tomaron 25 µL de cada una y fueron sembradas en placas de agar Levine al 1,5% y expandidas con asa Digralsky, por triplicado. Las placas se incubaron a 37 °C durante 24 horas. Para el conteo de colonias se tomó en cuenta únicamente las placas que presentaron entre 25 a 250 colonias, ya que este que este número de bacterias es estadísticamente representativo[18] y el conteo se expresó como UFC por cada 100 mL.

Análisis de crecimiento de microalgas

Luego de analizar los resultados de los tratamientos de desinfección, se seleccionó el método que arrojó los mejores resultados de desinfección para el pretratamiento de aguas destinadas a los cultivos. El tipo de microalga utilizada fue *Chlorella vulgaris*, adquirida del Banco Español de Algas. Partiendo de un inóculo de las microalgas en Basal Bold Medium (BBM) en fase exponencial, con densidad celular de 2,75E6 y densidad óptica de 1,106 a 680 nm; en fotobiorreactores de vidrio (PBR) de 1 L, por duplicado. Los cultivos se mantuvieron durante 13 días expuestos a luz blanca artificial de 40 W e intensidad de luz de 3000 luxes, con fotoperiodo de 12:12 de luz:oscuridad y aireación constante de 4,2 L/min. La temperatura se mantuvo controlada en 21 ± 2°C. También se prepararon cultivos de microalgas en agua residual autoclavada y sin ningún pretratamiento (control).

Para la estimación de la biomasa se extrajo diariamente 5 mL de cada cultivo, los cuales se hicieron pasar por un filtro de jeringa, previamente pesado, y se secó usando una estufa durante la noche, hasta alcanzar peso constante. La diferencia entre el peso del filtro antes y después de aplicar el volumen de cultivo se usó para determinar el peso seco de la biomasa algal (g/L).

Análisis de parámetros fisicoquímicos

Se efectuaron análisis de nitratos, ortofosfatos, demanda química de oxígeno (DQO) y pH con el agua antes de ser tratada y durante el tiempo de cultivo de las microalgas en cada uno de los tratamientos. Los protocolos para realizar los análisis se efectuaron mediante espectrofotometría; el análisis de nitratos de rango bajo, medio y alto se realizó por el método de reducción de cadmio; la determinación de ortofosfatos o fósforo reactivo empleó el método con Molibdovanadato; mientras que la determinación de la DQO adaptado al método de digestión USEPA, acorde a los procedimientos estandarizados HACH, con espectrofotómetro HACH DR5000. El porcentaje de remoción de nutrientes (PRN) se calculó a partir de la siguiente fórmula:

$$PRN = (Co - Ci) / Co \times 100\% \qquad \text{Ecuación 1}$$

Donde C_o y C_i son definidos como los valores promedios de concentración de nutrientes al inicio y al final del ensayo, respectivamente.

Análisis estadístico

Los parámetros asociados al conteo de UFC y análisis de nutrientes fueron expresados como el valor ± desviación estándar (X ± DE), y se realizó una comparación de medias de los diferentes grupos de experimentación a través de la prueba Kruskal Wallis. Las diferencias de medias entre cada grupo se consideraron estadísticamente significativas al presentar valores de $p<0,05$.]

Resultados

Evaluación de los métodos de desinfección

La Figura 1 muestra el conteo de las UFC por cada 100 mL pre y post tratamiento, a partir de los diferentes métodos de desinfección evaluados. El conteo para el agua del grupo control (sin tratamiento) presentó $4,12E^7 \pm 3,59E^6$ UFC. El tratamiento de radiación por luz UV-C durante 10 minutos no generó una disminución significativa ($p>0,05$) de UFC, respecto al grupo control. Sin embargo, no se observaron UFC en las condiciones de exposición a 30 y 60 minutos de radiación UV-C ($p<0,05$), siendo los únicos tratamientos que lograron la completa eliminación de la carga bacteriana en las diferentes muestras de agua pretratadas. La desinfección usando NaClO en la concentración de 10 ppm no tuvo reducciones de UFC significativas ($p>0,05$), mientras que a las concentraciones de 30 y 60 ppm se observó disminución en el número de UFC en rango cercano a 1 orden de magnitud. En el caso del tratamiento con CH_3CO_3H se presentaron reducciones de 2 log, estadísticamente significativas, para las concentraciones de 5 y 12,5 ppm y cerca de 3 log para la concentración de 50 ppm.

La Tabla 1 muestra los tipos de bacterias detectadas en el agua residual de porcicultura y su eliminación a través de los métodos de desinfección aplicados. El agar Levine mostró una mayor presencia de bacterias entéricas seguido de bacterias no fermentadoras de lactosa y *Escherichia coli* en el agua residual control. Este número de UFC se redujo parcialmente en el tratamiento de 10 min UV-C, mientras que en los tratamientos 30 y 60 minutos de radiación se observó inactivación total (IT) para estas colonias. En el caso de los tratamientos de mayor concentración de NaClO y CH_3CO_3H, se observó una mayor resistencia a la desinfección por parte de las colonias de bacterias no fermentadoras de lactosa. A pesar de la disminución significativa de las diferentes UFC, los tratamientos químicos no lograron la IT bajo ninguna de las concentraciones usadas en los ensayos.

Tratamiento	Bacterias entéricas	*E. coli*	Bacterias no fermentadoras de lactosa	Total
	(UFC 100 mL^{-1})			
Control	$2,81E^7 \pm 2,14E^6$	$4,98E^6 \pm 2,53E^6$	$8,16E^6 \pm 4,42E^6$	$4,12E^7 \pm 3,59E^6$
UV-C				
10 min	$2,63E^7 \pm 3,23E^6$	$4,67E^6 \pm 3,17E^6$	$7,73E^6 \pm 4,42E^6$	$3,87E^7 \pm 3,57E^6$
30 min	IT	IT	IT	IT
60 min	IT	IT	IT	IT
NaClO				
10 ppm	$4,67E^6 \pm 1,89E^5$	$8,00E^6 \pm 3,86E^5$	$2,17E^7 \pm 2,34E^6$	$3,44E^7 \pm 1,44E^6$
30 ppm	$1,64E^6 \pm 3,12E^5$	$6,80E^5 \pm 8,00E^4$	$5,81E^6 \pm 3,59E^5$	$8,13E^6 \pm 1,22E^5$
60 ppm	$2,24E^6 \pm 2,08E^5$	$3,73E^5 \pm 2,01E^4$	$2,43E^6 \pm 7,51E^5$	$5,04E^6 \pm 4,87E^5$
CH_3CO_3H				
5 ppm	$1,75E^5 \pm 6,11E^4$	$3,87E^4 \pm 4,62E^3$	$4,39E^5 \pm 8,49E^4$	$6,52E^5 \pm 1,42E^5$
12,5 ppm	$1,05E^5 \pm 2,44E^4$	$4,13E^4 \pm 1,29E^4$	$2,31E^5 \pm 4,20E^4$	$3,77E^5 \pm 1,01E^4$
50 ppm	$4,13E^4 \pm 1,85E^4$	$8,00E^3 \pm 4,00E^3$	$5,60E^4 \pm 6,93E^3$	$1,05E^5 \pm 8,33E^3$

IT: inactivación total

Tabla 1. Recuento de unidades formadoras de colonias de bacterias heterótrofas en las muestras de aguas residuales pretratadas.

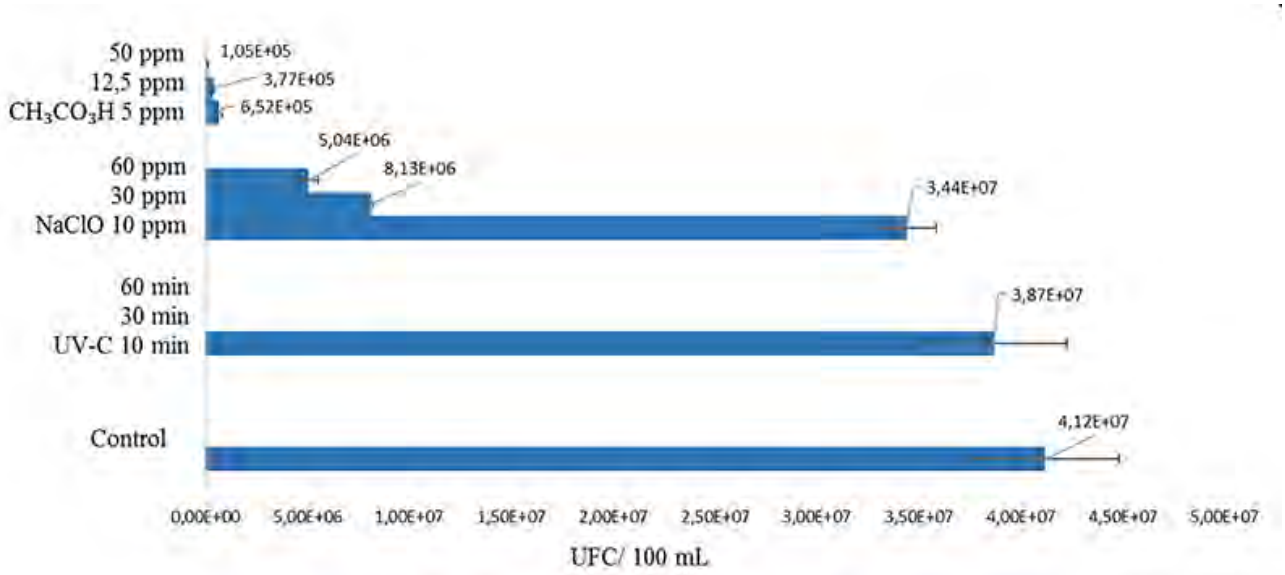

Figura 1. Conteo de UFC en las muestras de agua pretratadas bajo diferentes condiciones de desinfección. Las barras representan promedios de tres ensayos independientes, junto con la desviación estándar asociada (media ± DE).

Evaluación del crecimiento de microalgas

Con base en los resultados de los métodos de desinfección se seleccionó el pretratamiento con UV-C 30 min, el cual combinó la IT de bacterias junto con un menor tiempo de desinfección. Este tratamiento fue utilizado para desinfectar el agua destinada al cultivo de *C. vulgaris*; también se empleó agua residual esterilizada por ciclos estándar de autoclave, ya que el uso de este método es tradicionalmente empleado como garantía de esterilidad para los medios de cultivo. La Figura 2 muestra la curva de concentración de biomasa (g/L) de *C. vulgaris* cultivada en medio comercial BBM, en agua residual con el tratamiento UV-C 30 min, agua residual autoclavada y agua sin pretratamiento (control). El mayor crecimiento de microalgas determinado a partir de las aguas residuales se obtuvo con los tratamientos de autoclave y de UV-C, con valores finales de biomasa de 0,22 ± 0,03 g/L y 0,21 ± 0,04 g/L, respectivamente. Estos valores son estadísticamente superiores a la biomasa total generada en el agua sin pretratamiento, la cual generó un valor final promedio de 0,11 ± 0,05 g/L (p<0,05). Como era de esperarse para un medio comercial, la biomasa generada en el medio BBM alcanzó valores de 0,61 ± 0,06 g/L, superiores a los demás cultivos con agua residual. Durante el tiempo de cultivo no se hizo reposición de medio o de nutrientes en ninguno de los casos de estudio.

Evaluación de parámetros fisicoquímicos

La Tabla 2 muestra los valores iniciales y finales de los parámetros fisicoquímicos evaluados en el agua de faenamiento usada para el cultivo de *C. vulgaris*, previamente sometida a diferentes métodos de desinfección. Posterior a los 13 días de cultivo, se observó una notoria reducción en el contenido de nitratos evaluados, en las muestras de los tratamientos con autoclave y luz UV-C, lo cual representa hasta un 97,6 % de PRN.

Estos valores fueron estadísticamente superiores (p<0,05) en comparación a los mostrados por el cultivo en el agua sin pretratar (control), cuyo porcentaje de remoción de

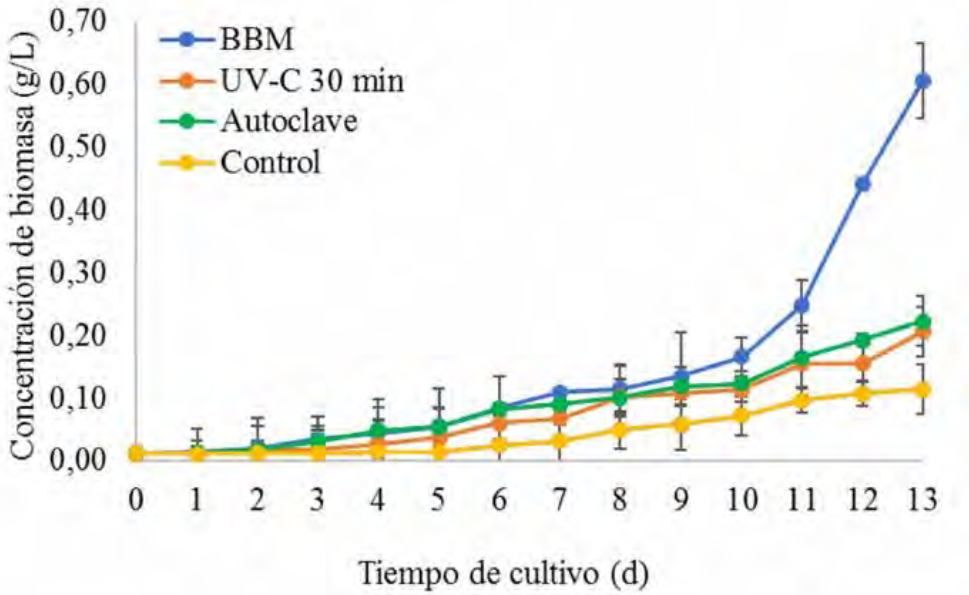

Figura 2. Concentración de biomasa de *C. vulgaris* en 13 días (d) de cultivo empleando un medio comercial y agua de porcicultura pretratada y sin tratar. Se muestra cada punto de medición registrado, junto con su desviación estándar asociada (media ± DE).

Tratamiento	Parámetro (mg/L)	Nitratos	Ortofosfatos	DQO
Sin tratar	C_o	60,5 ± 0,9	11 ± 1,1	833,8 ± 7,3
	C_i	5,9 ± 0,4	1,6 ± 0,6	243,7 ± 3,8
	PRN (%)	90,2	85,5	71
UV-C 30 min	C_o	62,4 ± 1,4	10,3 ± 0,4	826,3 ± 7,3
	C_i	1,4 ± 0,5	1,1 ± 0,5	158,8 ± 2,7
	PRN (%)	97,2	89,3	81
Autoclave	C_o	61,1 ± 1,6	11,1 ± 1,5	824 ± 6,9
	C_i	1,5 ± 0,5	1,2 ± 0,8	161,1 ± 4,6
	PRN (%)	97,6	89,1	80
BBM	C_o	180 ± 2	5,2 ± 0,8	N/A
	C_i	9,1 ± 0,7	0,6 ± 0,3	N/A
	PRN (%)	98,9	88,5	N/A

Co y Ci: valores promedios de concentración de nutrientes al principio y al final del ensayo N/A: no determinado.

Tabla 2. Porcentaje de remoción de nutrientes en el cultivo de *C. vulgaris* para el agua residual con y sin pretratamiento.

nitratos alcanzó el 90,2 %. Los ortofosfatos también presentaron una reducción general, con diferencias significativas entre los grupos con y sin pretratamiento de desinfección. Finalmente, los valores de DQO presentaron la menor reducción de los tres parámetros evaluados, con valores máximos de PRN de 80 y 81 % en el caso del tratamiento con UV y en el agua autoclavada. Estos valores representan alrededor de 7 % más de PRN en comparación con el agua sin pretratar.

Las cinéticas de remoción de nutrientes muestran una disminución drástica de los tres parámetros evaluados durante los primeros 5-6 días posterior al inicio de los cultivos con *C. vulgaris* (Figuras 3 a, b y c). A partir de los días 6-7, la remoción de nitratos, ortofosfatos y DQO se estabilizó hasta el final de la experimentación. A diferencia de las condiciones de cultivo con el agua pretratada, *C. vulgaris* en el agua sin pre tratamiento presentó una menor capacidad de remoción de nutrientes durante el tiempo de cultivo.

Discusión

En el presente estudio, se demostró que la luz UV fue capaz de lograr la IT de la carga bacteriana presente en el agua residual de faenamiento, a diferencia de los tratamientos químicos con NaClO y CH_3CO_3H. Una de las particularidades del uso de aguas residuales destinadas al cultivo de microalgas y a la generación de biomasa, es que cada tipo de agua presenta características propias y retos asociados tanto a la disponibilidad de nutrientes como a la presencia de inhibidores de crecimiento, entre los cuales se ubican los microorganismos presentes[19]. Comúnmente, la esterilización por autoclave se ha empleado para la eliminación de bacterias, hongos y protozoarios presentes en aguas residuales para su posterior uso en ensayos a escala de laboratorio, pero los costos derivados de escalar dicho método obligan a la búsqueda de pretratamientos más económicos y que logren la eliminación de microorganismos predadores[20]. En los ensayos realizados, el pretratamiento por 30 min de luz UV logró eliminar por completo la carga bacteriana presente en las muestras de agua. Otros estudios han descrito la inactivación de microorganismos presentes en aguas procedentes de granjas lecheras, con tiempos de exposición a la radiación tan bajos como 15 min[14]. Estas diferencias en los tiempos de exposición para la desinfección podrían estar asociadas a la variabilidad de microorganismos presentes entre los diferentes tipos de aguas, así como a la intensidad de la luz UV empleada, volúmenes de muestra y contenedores usados para las desinfecciones. Lo anterior, confirma la necesidad de estandarizar los procedimientos de desinfección a emplear junto con la evaluación de las características biológicas de las muestras de aguas residuales a emplear como medios de cultivo. Adicionalmente, estudios han demostrado que la aplicación de luz UV-C (longitud de onda λ: 200 - 280 nm), como la empleada en este estudio, presenta una mejor capacidad para la desinfección en comparación con la luz UV-B (λ: 280 - 320 nm)[21,22]. Sin embargo, para que la luz UV pueda ejercer efectos desinfectantes es necesario que la longitud de onda sea absorbida con la finalidad de generar alteraciones en los ácidos nucleicos, como la formación de dímeros de pirimidina, para la interrupción de procesos como la replicación celular en los microorganismos contaminantes. Con base en lo anterior, es necesaria la implementación de reactores de pre tratamiento de luz UV que permitan maximizar la exposición del agua a la radiación y evitar problemas asociados con compuestos que absorban la luz y disminuyan su capacidad de desinfección[23]. Con respecto a los tratamientos químicos, las máximas concentraciones empleadas en este estudio no lograron eliminar por completo la carga bacteriana, a pesar de presentar disminuciones de UFC significativas, en comparación con el agua sin pre tratar. Con relación a esto, una aproximación alternativa es el empleo de aguas residuales sin pre tratamientos de desinfección, en las cuales se ha demostrado la viabilidad de las microalgas para crecer en un medio con microorganismos[24,25]. No obstante, la aplicación de pretratamientos de desinfección sobre los diversos tipos de aguas residuales destinadas para el crecimiento microalgas son procesos recomendados con la finalidad eliminar agentes competitivos, como los microor-

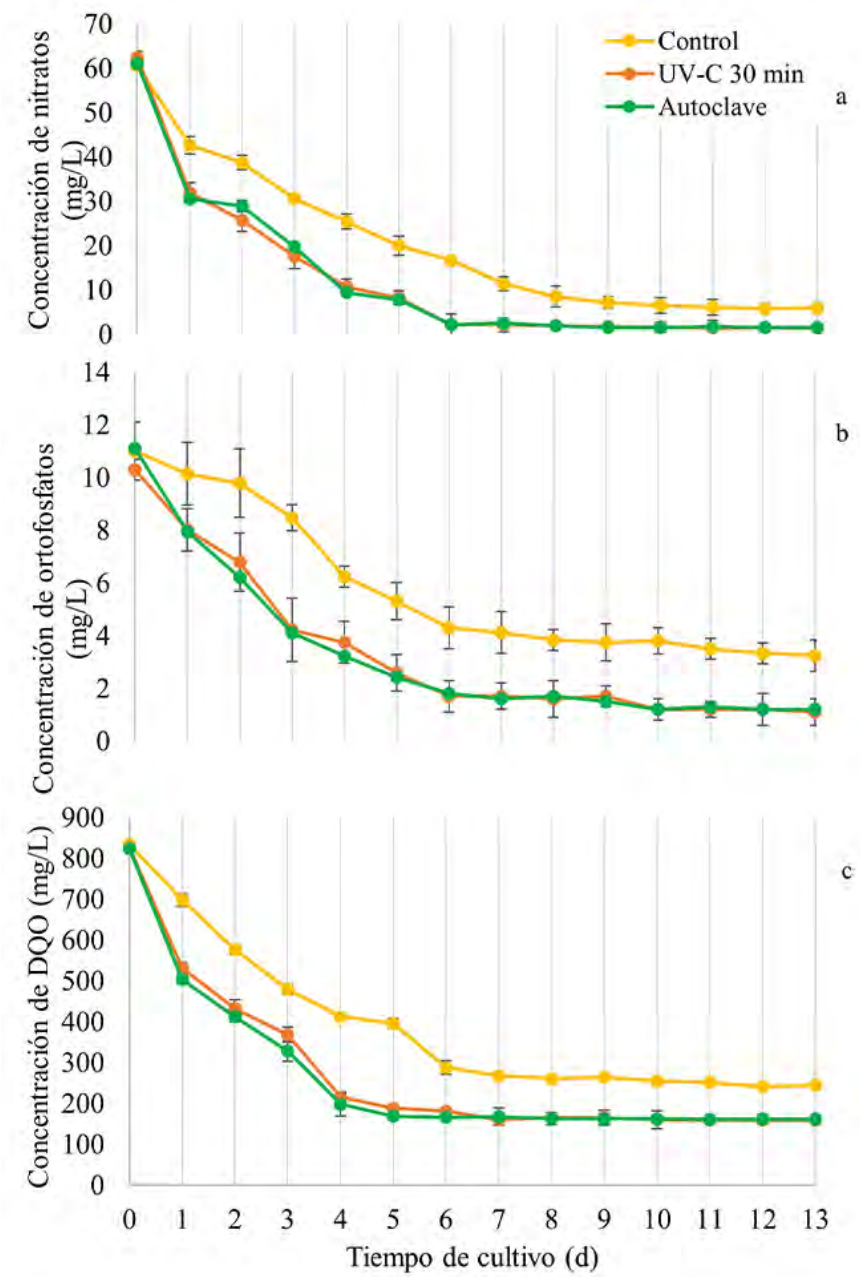

Figura 3. Cinética de remoción de nutrientes. Se muestran los cambios de concentración de diferentes parámetros químicos, durante 13 días de cultivo de *C. vulgaris* en agua de porcicultura con y sin pretratamiento: a) remoción de nitratos; b) remoción de ortofosfatos y c) remoción de DQO. Se muestra cada punto de medición registrado, junto con su desviación estándar asociada (media ± DE).

ganismos autóctonos presentes en las aguas, y asegurar una mayor generación de biomasa[4,26,27]. Otro tipo de tratamientos químicos, como el uso de 5 M NaOH junto con 5 M HCl son capaces de disminuir una elevada carga bacteriana hasta valores de 100 UFC/mL[27]. A pesar de esto, en general, los métodos de desinfección químicos suelen tener como una mayor desventaja frente a la luz UV la presencia de cloro o sustancias químicas residuales o la necesidad de aplicar tratamientos posteriores a la desinfección del agua empleada[23,28]. En el caso del CH_3CO_3H, no se presentan compuestos tóxicos o mutagénicos residuales en el agua pretratada, lo cual constituye una ventaja sobre los procesos de cloración. A pesar de ser un desinfectante alternativo, es posible que la incapacidad del CH_3CO_3H para lograr la IT de bacterias, mostrada en este estudio, está relacionada a la composición química del agua residual de faenamiento empleada. Bajo este punto, se ha reportado que la disponibilidad y velocidad de descomposición del CH_3CO_3H depende de la presencia de compuestos tanto orgánicos como inorgánicos en el agua, lo cual comprometería su capacidad de desinfección y obliga realizar un estudio más detallado para detectar las dosis óptimas de este ácido, con la finalidad de evitar efectos de sub o sobre dosis del desinfectante[29].

El crecimiento de microalgas está determinado por la disponibilidad de nutrientes del medio, las condiciones del medio (luz, temperatura, pH, etc.) y la densidad celular inicial[2]. Una vez que las microalgas se inocularon en los medios de agua residual con pretratamiento y sin tratamiento alguno, se apreció el periodo de adaptación a las nuevas condiciones y el posterior crecimiento de la microalga a partir del quinto día, como muestra la Figura 2. Aunque *C. vulgaris* pudo sobrevivir en todas las condiciones de pretratamientos analizados, incluyendo en el agua sin tratamiento; la concentración de biomasa de la microalga fue menor en el agua sin tratamiento respecto de las muestras pretratadas. Exámenes microscópicos mostraron una abundante presencia de bacterias y otros microorganismos en las aguas residuales sin pretratamiento (no mostrado), que pudieron limitar y amenazar el crecimiento de *C. vulgaris*. El tratamiento con UV-C 30 min inactivó estos microorganismos casi tan efectivamente como el tratamiento de autoclave, de acuerdo con el crecimiento de biomasa en

ambos casos. La biomasa en el tratamiento con autoclave tuvo mejores resultados que el de UV-C, pero sin diferencias significativas.

Investigaciones en microalgas de diferentes cepas han presentado producción de biomasa en el rango de 0,218± 0,06 g/L a 2,91 ± 0,02 g/L en una amplia diversidad de aguas residuales, tales como: urbana, efluentes primarios y secundarios de plantas de tratamientos de aguas residuales, industrial, agrícola, láctea, sintética, en condiciones mixotróficas y heterotróficas[2,26,30]. Las microalgas del género *Chlorella* son además muy usadas por su capacidad de remoción de nutrientes de éste tipo de aguas; se trata de una especie robusta y comúnmente utilizada en estudios de biomasa por su gran adaptabilidad a diferentes medios, incluyendo los de origen residual, sin requerimiento adicional de nutrientes[31]. Varios estudios reportan resultados de especies de *Chlorella* cultivadas en aguas residuales; uno de ellos es Gouveia y otros (2016)[25], cultivaron *C. vulgaris*, *S. obliquus* y un consorcio de microalgas en aguas residual urbana colectada luego del tratamiento primario de la planta de Águas da Figueira da Foz, en Portugal con fines de obtención de biocombustibles. Luego de 12 días de cultivo en fotobiorreactor vertical de 150 L y sin adición de ningún suplemento o reposición de nutrientes, la máxima productividad de biomasa de *C. vulgaris* se obtuvo al quinto día, reportando 0,11 g/L[25]. Li y otros (2011)[3], emplearon agua residual municipal cruda y autoclavada para el cultivo de *Chlorella. sp* con fines de remoción de nutrientes y producción de biodiesel. Al cabo de 14 días, del cultivo original de 25 L encontraron una productividad de biomasa de 0,12 g/ L.

Qin y otros (2014)[14], obtuvieron resultados similares a los encontrados en la presente investigación sobre crecimiento microalgal en medios residuales de empresas lácteas tratado con luz UV y desinfección química con NaOCl. En el pretratamiento realizado, a pesar de usar la luz UV por 15 min y obtener inactividad total comprobada al microscopio, la productividad de biomasa fue de 0,45 g/ L d para *C. vulgaris* en agua pretratada; un crecimiento superior al agua sin tratar con productividad de 0,198 g/ L d[14].

Las bacterias son más eficientes en la obtención de fósforo en condiciones adversas, esto coadyuvaría a que las algas carezcan de nutrientes y no tengan los niveles de reproducción que existen en las aguas pretratadas[9]. Otro factor que limitaría el crecimiento de las microalgas es el cambio en el ambiente debido a bacterias. El pH sufre variaciones a través de la producción de ácidos orgánicos y de la oxidación de varios componentes como el amonio[32]. Estos cambios en pH pueden afectar la disponibilidad de carbono para la fotosíntesis de las algas[8].

Por otra parte, los resultados de este estudio demuestran que el pretratamiento (a través de UV-30 minutos o autoclavado) de aguas residuales porcinas, y el posterior cultivo de *C. vulgaris* en ellas mejoró la remoción de algunos parámetros fisicoquímicos (principalmente nitrato y DQO) de este tipo de aguas residuales.

Respecto a la remoción de nitratos, comparando la remoción de este parámetro usando agua residual sin pretratamiento (tratamiento control) y agua residual pretratada, es posible identificar que *C. vulgaris* fue la principal responsable de la remoción de este parámetro en presencia o ausencia de pretratamiento, principalmente porque las condiciones de cultivo empleadas en este estudio (condiciones aerobias) no fueron adecuadas para favorecer procesos de desnitrificación bacteriana. Adicionalmente, las concentraciones finales de nitratos obtenidas en el cultivo de C. vulgaris utilizando pretratamiento de agua residual (con UV-30 minutos o autoclavado) se encuentran dentro de un rango de concentración de NO_3- muy cercano al reportado para concentraciones de NO_3- reportadas para aguas superficiales (igual o menor a 1 mg/L)[33], lo cual confirma que el pretratamiento del agua residual es necesario para obtener un agua tratada de calidad.

Por otra parte, tanto con pretratamiento del agua residual o sin pretratamiento se obtuvieron altas remociones de PO_4^{3-} en el agua residual, lo cual sugiere que *C. vulgaris* fue quien aportó de mayor manera en la remoción de PO_4^{3-}. De hecho, varios estudios[34–36] han demostrado la capacidad de *C. vulgaris* para consumir altas cantidades de PO_4^{3-}, así como la limitada capacidad de las bacterias en sistemas convencionales de tratamiento de agua para consumir fósforo, salvo si se implementan sistemas biológicos especiales con microorganismos acumuladores de polifosfato (PAOS)[37,38].

Finalmente, la remoción de DQO demostró ser más eficiente utilizando los pretratamientos del agua residual, lo cual indica que para el caso de este tipo de agua residual un sistema mixto bacteria-microalga no sería adecuado para obtener buenas remociones de DQO, a diferencia de un sistema biológico con uso exclusivo de *C. vulgaris*. Es importante indicar que pese a que los pretratamientos de agua residual mejoraron la eficiencia de remoción de la DQO, aún después del tratamiento la DQO se mantuvo sobre los límites máximos permisibles (50 mg DQO L-1) para efluentes de plantas de tratamiento de agua residual[39], por lo que si se desea optar por este sistema de tratamiento será adecuado implementar sistemas adicionales de tratamiento (coagulación-floculación, sedimentación, filtración) aguas arriba que permitan eliminar la carga de DQO adicional que no se puede eliminar en el sistema biológico.

Por los antecedentes mencionados, para la remoción de NO_3-, PO_4^{3-} y DQO de este tipo de agua residual un sistema biológico por lotes formado sólo por *C. vulgaris* presentaría mejor eficiencia que un sistema mixto (bacteria-microalga). Sería importante también evaluar en futuros estudios la remoción de NO_3-, PO_4^{3-} y DQO en sistemas continuos que incluyan el agua residual pretratada y *C. vulgaris*, puesto que el tiempo requerido para alcanzar remociones altas de dichos parámetros en el sistema por lotes en este estudio fue extenso, lo cual limitaría la capacidad de eliminación de estos contaminantes si los caudales a tratar de esta agua residual en campo son elevados.

Conclusiones

En este trabajo se demostró la factibilidad del uso de aguas residuales procedentes de granjas de porcicultura y faenamiento, para el crecimiento y obtención de biomasa algal, previa aplicación de un tratamiento de desinfección. Con base en la inactivación total de UFC, se determinó que la radiación por UV fue el mejor método de desinfección, dependiendo, en gran medida, del tiempo de exposición. Una dosis de 30 minutos es el tiempo necesario para la IT bacteriana del agua residual empleada en este estudio. El cultivo de microalgas con aguas pretratadas generó una mayor cantidad de biomasa en comparación con el agua sin pretratar, lo cual indica que es posible usar este tipo de aguas residuales para el cultivo de especies como *C. vulgaris*, en especial bajo un ambiente carente de alta carga bacteriana. El uso de un tratamiento no químico como UV no afectó los nutrientes originales de las aguas residuales, al permitir el crecimiento sostenido de la microalga empleada. Evaluaciones posteriores tanto del perfil lipídico y de ésteres metílicos de ácidos grasos, permitirán indicar si este tipo de agua tiene el potencial para la generación de subproductos de interés biotecnológicos como biocombustibles. Finalmente, los resultados de este estudio también sugieren

que el uso de un sistema biológico formado exclusivamente por *C. vulgaris* resulta más eficiente que un sistema mixto (bacteria-microalga) para la remoción de nitratos y ortofosfatos de aguas residuales porcinas.

Agradecimientos

Los autores de este trabajo agradecen a la Dirección de Investigación e Innovación de la Universidad Internacional SEK por el aporte financiero dentro del proyecto P101617_2.2 Obtención de biocombustibles de origen microalgal y vegetal

Referencias bibliográficas

1. Osundeko, O., Ansolia, P., Gupta, S. K., Bag, P. & Bajhaiya, A. K. Promises and challenges of growing microalgae in wastewater. Water Conserv. Recycl. Reuse Issues Challenges 29–53 (2019) doi:10.1007/978-981-13-3179-4_2.
2. Guldhe, A. et al. Prospects, recent advancements and challenges of different wastewater streams for microalgal cultivation. J. Environ. Manage. 203, 299–315 (2017).
3. Li, Y. et al. Characterization of a microalga Chlorella sp. well adapted to highly concentrated municipal wastewater for nutrient removal and biodiesel production. Bioresour. Technol. 102, 5138–5144 (2011).
4. Chiu, S. Y. et al. Cultivation of microalgal Chlorella for biomass and lipid production using wastewater as nutrient resource. Bioresour. Technol. 184, 179–189 (2015).
5. Jones, C. S. & Mayfield, S. P. Algae biofuels: Versatility for the future of bioenergy. Curr. Opin. Biotechnol. 23, 346–351 (2012).
6. Meher, L. C., Vidya Sagar, D. & Naik, S. N. Technical aspects of biodiesel production by transesterification - A review. Renew. Sustain. Energy Rev. 10, 248–268 (2006).
7. Slade, R. & Bauen, A. Micro-algae cultivation for biofuels: Cost, energy balance, environmental impacts and future prospects. Biomass and Bioenergy 53, 29–38 (2013).
8. Mostafa, S. S. M., Shalaby, E. A. & Mahmoud, G. I. Cultivating Microalgae in Domestic Wastewater for Biodiesel Production. Not. Sci. Biol. 4, 56–65 (2012).
9. Currie, D. J. & Kalff, J. A comparison of the abilities of freshwater algae and bacteria to acquire and retain phosphorus. Limnol. Oceanogr. 29, 298–310 (1984).
10. Newman, S. E. & Ph, D. Disinfecting Irrigation Water for Disease Management. Plant Dis. 1–10 (2003).
11. Lantagne, D. S. Sodium hypochlorite dosage for household and emergency water treatment. J. / Am. Water Work. Assoc. 100, (2008).
12. Gehr, R., Wagner, M., Veerasubramanian, P. & Payment, P. Disinfection efficiency of peracetic acid, UV and ozone after enhanced primary treatment of municipal wastewater. Water Res. 37, 4573–4586 (2003).
13. Bolton, J. R. & Linden, K. G. Standardization of methods for fluence (UV Dose) determination in bench-scale UV experiments. J. Environ. Eng. 129, 209–215 (2003).
14. Qin, L. et al. Cultivation of chlorella vulgaris in dairy wastewater pretreated by UV irradiation and sodium hypochlorite. Appl. Biochem. Biotechnol. 172, 1121–1130 (2014).
15. Koivunen, J. & Heinonen-Tanski, H. Inactivation of enteric microorganisms with chemical disinfectants, UV irradiation and combined chemical/UV treatments. Water Res. 39, 1519–1526 (2005).
16. Rossi, S., Antonelli, M., Mezzanotte, V. & Nurizzo, C. Peracetic Acid Disinfection: A Feasible Alternative to Wastewater Chlorination. Water Environ. Res. 79, 341–350 (2007).
17. APHA. Standard methods for examination of water and wastewater, 20th ed. (1998).
18. Sutton, S. The limitations of CFU: compliance to CGMP requires good science. J. GXP compliance 16, 74–80 (2012).
19. Ji, M. K. et al. Effect of mine wastewater on nutrient removal and lipid production by a green microalga Micratinium reisseri from concentrated municipal wastewater. Bioresour. Technol. 157, 84–90 (2014).
20. Sriram, S. & Seenivasan, R. Microalgae Cultivation in Wastewater for Nutrient Removal. Algal Biomass Utln 3, 9–13 (2012).
21. Choi, Y. & Choi, Y. june. The effects of UV disinfection on drinking water quality in distribution systems. Water Res. 44, 115–122 (2010).
22. Cho, S., Luong, T. T., Lee, D., Oh, Y. K. & Lee, T. Reuse of effluent water from a municipal wastewater treatment plant in microalgae cultivation for biofuel production. Bioresour. Technol. 102, 8639–8645 (2011).
23. Gibson, J., Drake, J. & Karney, B. UV Disinfection of Wastewater and Combined Sewer Overflows. in Ultraviolet Light in Human Health, Diseases and Environment 996 (Springer, Cham, 2017).
24. Ding, J. et al. Cultivation of Microalgae in Dairy Farm Wastewater Without Sterilization. Int. J. Phytoremediation 17, 222–227 (2015).
25. Gouveia, L. et al. Microalgae biomass production using wastewater: Treatment and costs. Scale-up considerations. Algal Res. 16, 167–176 (2016).
26. Zhu, L. et al. Nutrient removal and biodiesel production by integration of freshwater algae cultivation with piggery wastewater treatment. Water Res. 47, 4294–4302 (2013).
27. Ramsundar, P., Guldhe, A., Singh, P. & Bux, F. Assessment of municipal wastewaters at various stages of treatment process as potential growth media for Chlorella sorokiniana under different modes of cultivation. Bioresour. Technol. 227, 82–92 (2017).
28. Song, K., Mohseni, M. & Taghipour, F. Application of ultraviolet light-emitting diodes (UV-LEDs) for water disinfection: A review. Water Res. 94, 341–349 (2016).
29. Henao, L. D., Delli, R. C., Turolla, A. & Antonelli, M. Influence of inorganic and organic compounds on the decay of peracetic acid in wastewater disinfection. Chem Eng J 337, 133–142 (2018).
30. Gupta, P. L., Lee, S. M. & Choi, H. J. Integration of microalgal cultivation system for wastewater remediation and sustainable biomass production. World J. Microbiol. Biotechnol. 32, (2016).
31. Rawat, I. et al. Microalgae Applications in Wastewater Treatment. Springer, Cham. 249–268 (2016) doi:10.1007/978-3-319-12334-9_13.
32. Cole, J. J. Interactions between bacteria and algae in aquatic ecosystems. Annu. Rev. Ecol. Syst. Vol. 13 291–314 (1982) doi:10.1146/annurev.es.13.110182.001451.
33. EPA. Water: Monitoring & Assessment. https://archive.epa.gov/water/archive/web/html/vms57.html. (2012).
34. Bunce, J. T., Ndam, E., Ofiteru, I. D., Moore, A. & Graham, D. W. A review of phosphorus removal technologies and their applicability to small-scale domestic wastewater treatment systems. Front. Environ. Sci. 6, 1–15 (2018).
35. Osorio, J. H. M. et al. Nutrient removal efficiency of green algal strains at high phosphate concentrations. Water Sci. Technol. 80, 1832–1843 (2020).
36. Zheng, M. et al. Simultaneous fixation of carbon dioxide and purification of undiluted swine slurry by culturing Chlorella vulgaris MBFJNU-1. Algal Res. 47, 101866 (2020).
37. Izadi, P., Izadi, P. & Eldyasti, A. Design, operation and technology configurations for enhanced biological phosphorus removal (EBPR) process: a review. Reviews in Environmental Science and Biotechnology vol. 0123456789 (Springer Netherlands, 2020).
38. Li, H. et al. Simultaneous nitrogen and phosphorus removal by interactions between phosphate accumulating organisms (PAOs) and denitrifying phosphate accumulating organisms (DPAOs) in a sequencing batch reactor. Sci. Total Environ. 744, 140852 (2020).
39. Zhou, Y., Duan, N., Wu, X. & Fang, H. COD discharge limits for urban wastewater treatment plants in China based on statistical methods. Water (Switzerland) 10, (2018).

Received: 29 Noviembre 2020
Accepted: 20 Febrero 2021

RESEARCH / INVESTIGACIÓN

Effect of *Plasmodium berghei* infection on fetuses in pregnant BALB/c mice at two periods of pregnancy

Andreina Gómez[2], Beatriz Pernía[3], Lizbeth Zamora[1] and Lilian M. Spencer[1,2*]

DOI. 10.21931/RB/2021.06.02.25

Abstract: Malaria is a disease caused by a protozoan of the genus *Plasmodium* in humans and vertebrates. It has a high morbidity and mortality rate, especially in pregnant women living in countries with high transmission rates. Murine models have been an excellent tool to evaluate the effects of malarial infection in the mother-fetus relationship. For this reason, we evaluated the effect of malarial infection on fetal development at the beginning and middle of the gestational period in BALB/c mice infected with *Plasmodium berghei* ANKA. Our results show that malarial infection at the beginning of pregnancy markedly affects the development of the fetus in size, weight, and development of its limbs so that the control of the pregnant mother is relevant at the beginning of gestation

Key words: Malaria, loss weight, rodent, gestational period.

Introduction

Malaria is an endemic tropical disease with a high incidence among women and children. It is therefore considered a significant public health problem. World Health Organization (WHO) reported pregnant women in sub-Saharan Africa to show high malarial infection[1]. In 2019, WHO estimates 12 million pregnancies with malaria infection and 822.000 children with low birth weight[2]. Reflecting a high morbidity and mortality rate after infection as medical complications such as anemia, intrauterine growth retardation, low birth weight (LBW), and neonatal death occur[3,4]. The vulnerability of pregnant women to malaria increases in the first and second trimesters of the gestation period. However, there is some debate as to whether hormonal and immunological changes increase malaria sensitivity in pregnancy[5]. As a result, prenatal diagnosis and control are complex. Besides, known drugs are less effective due to resistance generated by parasites[6].

Malaria infection in pregnant women occurs when intracellular *Plasmodium falciparum* parasites accumulate and interact with chondroitin sulfate A (CSA) receptors, resulting in placental malaria[5,6]. The malaria-infected placenta has a thickened trophoblastic basement membrane that acts as a protective measure for the baby against increased cytokines that damage the placental tissue. Therefore, morphological alterations of the membrane directly affect the pathological conditions of the fetus[7]. The placenta has parasites that express antigens on its surface, known as variant surface antigens (VSA)[5]. The VSA of the malaria parasites prevents them from being recognized by the human immune system as they belong to the *Plasmodium falciparum* erythrocyte membrane protein 1 (PfEMP1)[8].

Meanwhile, the VAR2CSA protein present in malaria-infected red blood cells recognizes CSA in pregnant women, causing it to accumulate in the placenta. The parasites infect other red blood cells that will accumulate in the placenta[9]. Chronic malaria infection is related to low birth weight by restricting space for development, while the acute infection is related to early termination of pregnancy[10].

Plasmodium falciparum infection is the type of malaria with the highest incidence in pregnant women because infected red blood cells bind more quickly to the placenta during the gestation period[11,12]. Several experimental models of malaria infection reproduce the immune responses of the disease. Rats and mice are infected with *Plasmodium vinckei*, *Plasmodium yoelii* and *Plasmodium berghei*, among others[13]. To study malaria in pregnant women, the *Plasmodium berghei* ANKA strain is used in murine animals because it mimics the infectious process of chronic malaria in the gestation stage that occurs with *Plasmodium falciparum* in humans[10]. Specifically, pregnant BALB/c mice infected with *Plasmodium berghei* develop complications such as decreased fetal size, premature birth, slowed uterine growth, and postnatal growth problems[13,14]. The factors presented above are related to the placenta's nutritional deficit, which is essential for a healthy pregnancy[15,16].

This work aimed to determine in which gestation period the malarial infection is more deleterious to fetal development at the beginning or middle of gestation. For this, we evaluated the weight, size, and limb development in fetuses from pregnant BALB/c female mice.

Materials and methods

Experimental infection and appearance of the female BALB/c mice

Mice reared under specific pathogen-free conditions and with food and water ad libitum in the animal laboratory at the Simón Bolívar University. Female mice of 12-week-old were mate with a young puberty male mouse. When the formation of the vaginal plug was verified the next day, the male was separated from females in each group17. In this study, pregnant females were divided into three experimental groups with six mice per group (Figure 1 presents the experiments with mice). One control group that was not infected with *Plasmodium berghei* ANKA strain and two groups that were infected with the parasite at the beginning (second day after of formation vaginal plug) of gestational and in the middle of the gestational period (eighth day after of formation vaginal plug).

The parasite used for the challenge was the lethal ANKA

[1] School of Biological Sciences and Engineering, Yachay Tech University, San Miguel de Urcuquí, Ecuador.
[2] Cell Biology Department, Simón Bolívar University, Valle de Sartenejas, Caracas, Venezuela.
[3] University of Guayaquil, Faculty of Natural Sciences, Guayaquil, Ecuador.

Corresponding author: spencerlilian@gmail.com

strain of *P. berghei*; the parasite was stored at -80°C and passaged once in a mouse before use in these experiments. When the parasitaemia was 40%, parasitized red blood cells (PRBCs) were isolated using a cellulose column (CF-11, Sigma, with NaCl 0.85% solution). After, the trophozoites and schizonts were isolated by a discontinuous Percoll column (60, 70, and 80% gradient in ascending order)[18].

The parasite challenge was administered by intravenous injection of five thousand PRBCs to two experimental groups at the 2nd and other at the 8th days of the gestational period. Six mice were placed for each group and the control group that were not pregnant but if infected with *P. berghei*. Erythrocytic stage parasitaemia was assessed daily on smears made from tail blood from infected mice and stained with Giemsa's reagent to determine percentage of parasitaemia. These experiments were carried out twice to evaluate the effect of parasite infection on the fetuses.

In summary, we conducted two experimental groups of pregnant and infected mice. One of them to determine parasitemia and the other to determine the conditions of the fetuses depending on the day of infection with the parasite.

Fetus extraction and evaluation in size and weight

At 7 days post-infection, pregnant mice of the groups infected with *P. berghei* on the 2nd and 8th day of gestation were sacrificed, and their uterine sacs were opened (using a longitudinal incision on the mesometrial side); each mouse pregnant had an average of 10±1 fetus. Then, we macroscopically evaluated the fetuses. Which were washed with a physiological solution and weighed to determine their weight on balance Sartorius Entris II model (g), fetal length with a calibrate Vernier (cm), and external anatomical characteristics such as the development of the extremities.

The experiments described in this study were carried out following the laboratory's standards and the Bioethics Committee of the Simón Bolívar University.

Statistical analysis

To analyze whether the data presented a normal distribution, both Anderson-Darling and Levene tests for homoscedasticity were applied. Subsequently, to compare the percentage of parasitaemia between treatments, a two-way ANOVA test ($p < 0.001$) was applied, followed by a Dunnet test. Then, to compare the fetuses' weight and length, a non-parametric Kruskall-Wallis test was applied ($p < 0.001$). The graphics were made using the R program version 4.0.2.

Results

Figure 2 shows the percentage of parasitaemia during the infection, where it is evident that pregnant mice presented higher percentages of parasitaemia than non-pregnant control mice. On day 7 after infection, a significant difference is clearly shown between the three groups of mice infected with the parasite ($F = 46.28$; $p \leq 0.001$). With a percentage of parasitaemia of 60.0 ± 10.0% (green line) in mice inoculated on day 8 and 33.3 ± 5.8% in those inoculated on the second day (pink line), compared to control 6.8 ± 2.0% (blue line).

A difference was also evident concerning the days of survival, which are represented with a white bar for the control group, light gray for the group infected at the beginning of pregnancy (2nd day), and dark gray for the group of mice infected at the middle of pregnancy (8th day of gestation). Mice in the control group survived until day 11 post-infection, while mice inoculated on the second and eighth day of gestation died on day 7 post-infection. However, in the control group, the highest parasitaemia was 39% on day 10 post-infection.

Figure 3A shows fetal length in pregnant mice with 9 to 12 fetuses per placenta. Regarding the length of the fetuses, it was affected by infection with *P. berghei*, and a decrease in the median was observed, corresponding to the fetuses where the

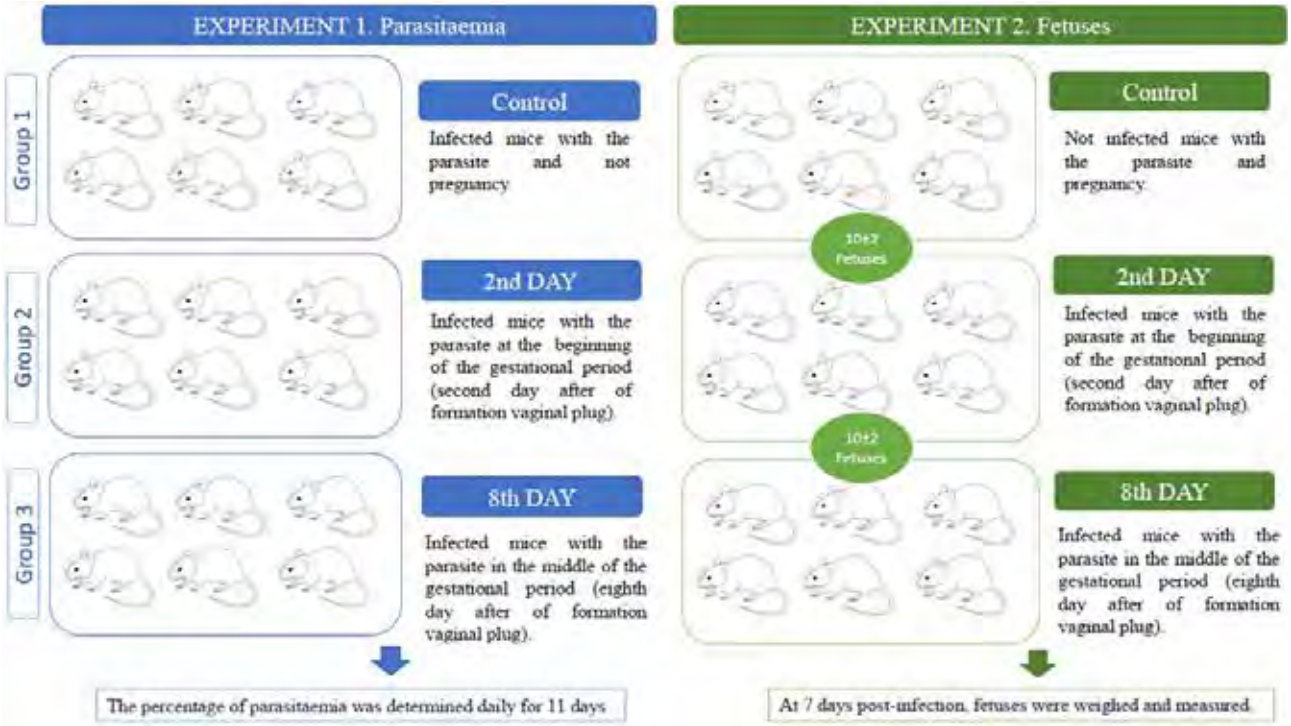

Figure 1. Experimental mice groups to evaluate the parasitaemia and physical conditions of fetuses. One control group was not infected with the ANKA strain of *Plasmodium berghei*, and two groups infected with the parasite at the beginning (second day) of gestational and in the middle of the gestational period (eighth day).

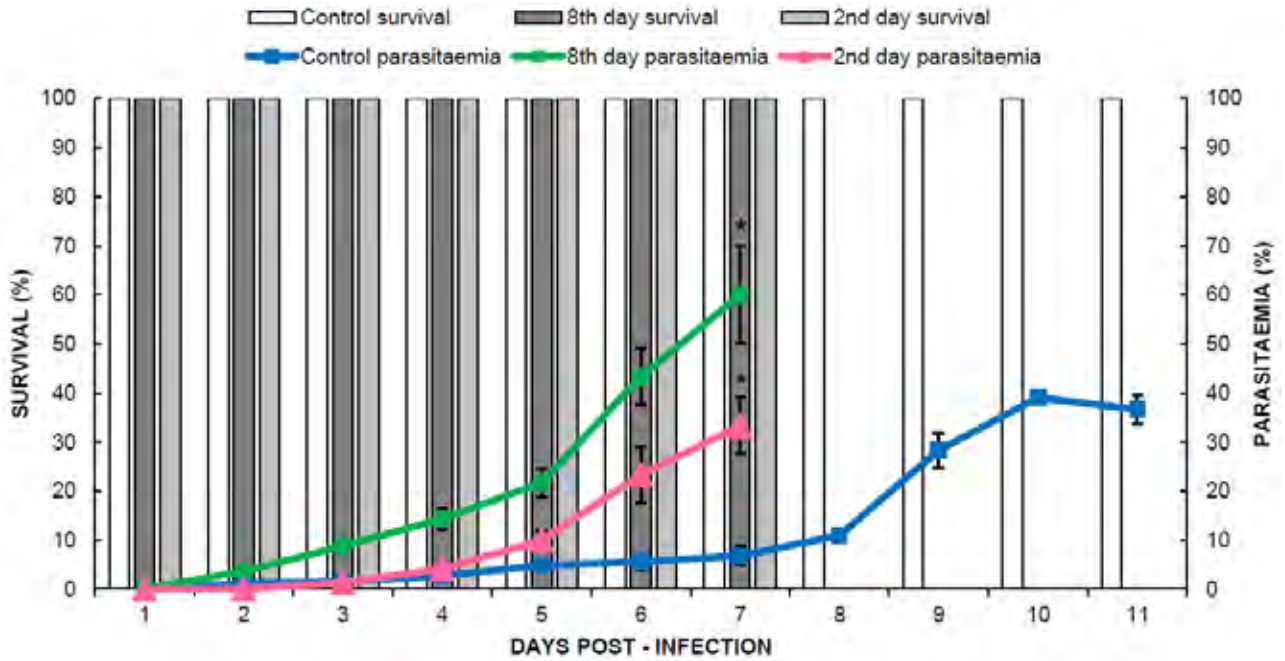

Figure 2. Percentage of parasitaemia over time and survival of control and pregnant mice inoculated on the 2nd and 8th day of gestation. Asterisks (*) indicate significant differences according to ANOVA and Dunnet a posteriori test ($p < 0.001$).

mothers were inoculated on the second day of pregnancy ($H = 16.04$; $p \leq 0.001$). The median fetal length in control fetuses was 1.5 cm, while fetuses from mice inoculated on the 2nd-day of pregnancy had a median fetal length of 1.2 cm, with a range of 0.9 to 1.5 cm.

Similarly, the fetus's weight was affected by infection with *P. berghei* (Figure 3B). The control group weighed 3.1 g, higher than the median of 2.6 g ($H = 16.76$; $p \leq 0.001$). However, the results showed no significant differences in fetal weight between inoculation day 8 and controls. Therefore, there is a marked influence on the effect of infection during pregnancy and the fetus's size.

Figure 3C shows images of fetuses from the three study groups. Apparent differences in the development of mouse fetuses can be observed between infected and non-infected pregnant mothers. The fetuses of mothers infected at the beginning of pregnancy have size and weight obviously below that of fetuses from the control group. The poor development of the hind limbs was also evidenced in comparison to the other two groups of fetuses of the mothers studied.

Consequently, the time at which malarial infection occurs during pregnancy is critical. The earlier in the pregnancy the infection occurs, the more significant the fetus's negative effects as evidenced by the results of weight, size, and development of the lower extremities.

Discussion

The murine model has always been a valuable tool to evaluate the pathogenicity of malaria infection[1,10]. Especially in the mother-fetus binomial, which for ethical reasons is very difficult to evaluate in humans. In the current work, we studied the time during pregnancy when infection by *Plasmodium berghei* is riskier for the fetus. This evidence will be helpful to in planning and implementing potential passive antibody therapy.

At the beginning of the infection, the parasitaemia curve was similar between mice infected on the second day of pregnancy and control non-pregnant mice at 4 days post-infection. On the contrary, pregnant mice infected on the eighth day of the gestational period developed a more significant infection from day 2 post-infection and reached a maximum parasitaemia of 60%. In comparison, the infected group on day 2 of pregnancy reached the maximum parasitaemia of 33% at 7 days post-infection. The control group survived until day 11 post-infection, and the maximum percentage of parasitaemia was 39% on day 10 post-infection (Figure 2). Pregnant mice are more susceptible to malarial infection, probably because their immune system is suppressed[19].

Based on the reports of clinical studies with pregnant mothers, such as Dobbs and Dent[24], who analyze the effect of antibodies on fetuses in pregnant women at the end of pregnancy and in the first years of the life of babies. They report that maternal antibodies effectively protect fetuses in the last trimester of pregnancy from infections against the parasite and babies in the first 6 months of life. Other studies in the 1960s showed that the effective recovery of children hospitalized by passive transfer of adult sera caused malaria[25,26].

Antibodies can block sporozoites to prevent the invasion of hepatocytes and merozoites to erythrocytes. Thus, as the opzonization of the infected erythrocytes and the Complement system's activation by the VSA molecules expressed on the infected erythrocytes (schizont stage). These antibodies recognize VSA and block interaction with its receptor in endothelial tissue of the placenta mediate the optimization process by monocytes and macrophages, which can engulf parasitized erythrocytes[27].

Malaria pregnancy has fatal consequences for both the fetus and the mother. The fact that parasite antigens can cross the syncytiotrophoblast barrier in the last trimester has resulted in the process of immunological tolerance, and consequently an inadequate immune response in the first years of life[28,29]. Therefore, poor immune response in the first months of life is reported to malaria in pregnancy.

Other studies by Megnekou and co-workers have shown in the BALB/c mice model a correlation between repeated infections of the parasite during pregnancy and concluded that cytokines such as IL-5, IL-12/70, IL -13, and IFN-γ are high.

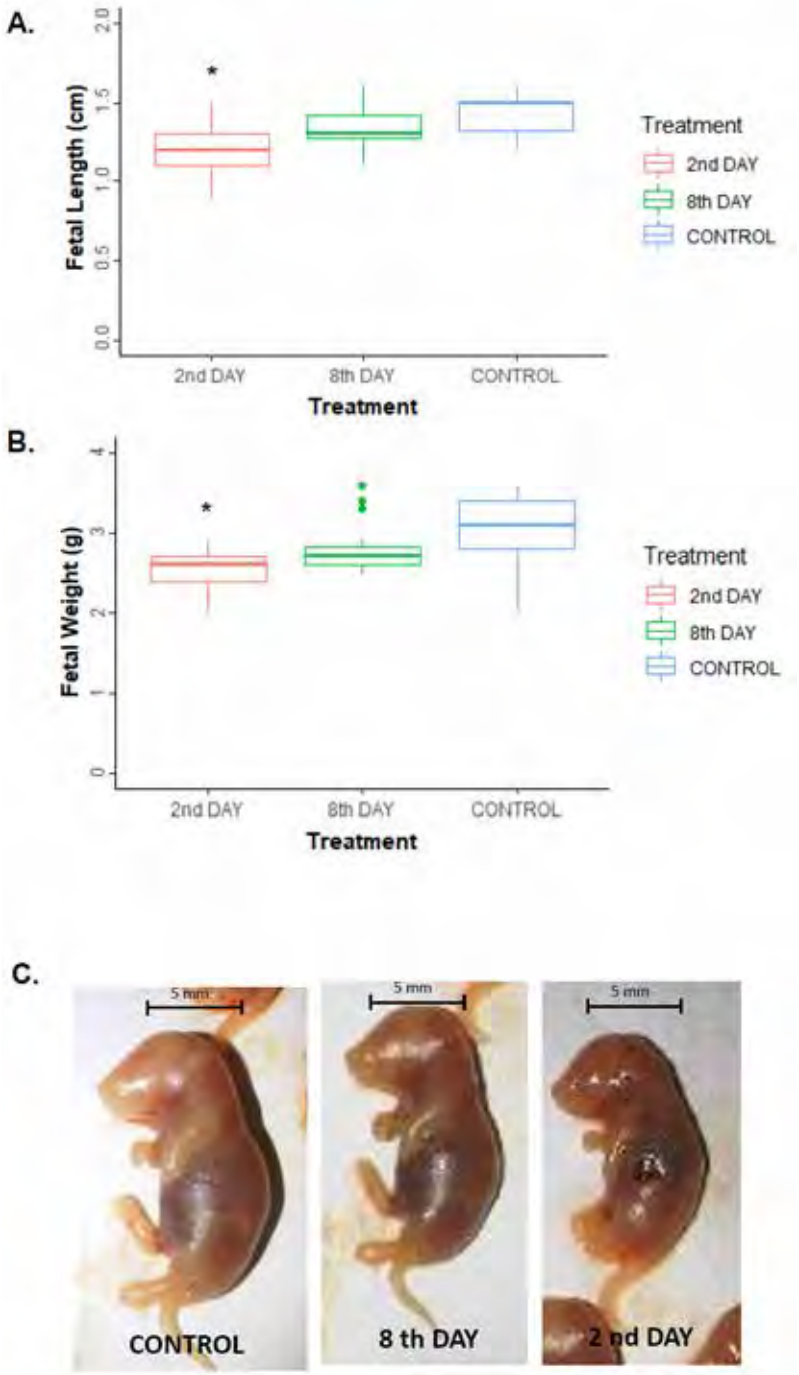

Figure 3. Length (A) and weight (B) of fetuses in control and pregnant mice inoculated with *P. berghei* on the 2nd and 8th day of gestation. Asterisks (*) indicate significant differences according to Kruskall-Wallis ($p < 0.001$). (C) Representative images of mouse fetuses at 9 days of gestation, which correspond to 7 days post-infection. The line corresponds to a 5 mm scale bar.

However, low levels of these cytokines were related to anemia and complicated pregnancies. At the same time, that high concentration of IL-10 levels in these pregnancies is correlated with anemia and complicated pregnancies due to the immune-suppression condition[20].

Consequently, the moment of infection is crucial in the fetus's development, as can be seen in figure 3, affecting the size and weight of the fetus[21]. Our results demonstrate that if the infection occurs early in pregnancy, there is a significant effect on the size reduction and LBW (Figures 3A and B). Reduced limb development was observed in the hind limbs of fetuses from pregnant and infected mice in early gestation (Figure 3C). Unlike this study, Akhabue and colleagues carried out the infection of pregnant mice at the end of the pregnancy on day 13 of gestation. They evaluated the litter's motor development and concluded that they presented changes in their behavior as anxiety and obesity. Nevertheless, it did not affect pups' locomotion when infection occurred during the final gestational period[22]. On the other hand, our results support the studies by Huynh and colleagues showing that early intake of sulfadoxine-pyrimethamine in pregnant women reduces the birth of children with low weight; this is correlated with our results infection at the beginning of pregnancy[23].

Hence, early treatment of the disease at the beginning of pregnancy by antimalarial drugs is recommended to avoid adverse effects in pregnancy and newborns.

However, fear of teratogenic effects restricts antimalarial drug options in the first trimester. In consequence of this situation, it is necessary to develop other strategies, such as vaccination of mothers and vector control. In this way, the risk of placental infection in early pregnancy could be reduced[30,31].

Conclusions

Our results showed that the level of parasitaemia in mice infected with *P. berghei* during the second day of pregnancy could strongly reduce litter size and pup weight than when infection occurs during the middle of the gestational period.

By knowing the time of pregnancy when malarial infections pose significant risks to the fetus, we could suggest alternative therapies for the mother, such as passive transfer of antibodies at the beginning of pregnancy or the use of antimalarial drugs in pregnant women at the beginning of their pregnancy, as reported by other authors. However, resistance to antimalarial drugs generates a problem in treating the disease, so the search for new drugs is necessary, and their studies in the animal model to evaluate teratogenic effects in the biological system of pregnancy.

Data Availability

The data used to support the findings of this study are included in the article.

Conflicts of Interest

The authors declare no conflict of interest regarding the publication of this paper.

Author's Contributions

Conceptualization, formal analysis of the results and writing the manuscript (LMS), experimental assays and analysis of the results (AG), performer of the statistical analysis (BP), writing the manuscript (LZ).

Funding Statement

This investigation was financed in part by a grant from FONACIT (Fondo Nacional de Ciencia, Innovación y Tecnología, No. 29407-2269), Venezuela and Yachay Tech University, Ecuador.

Acknowledgments

We want to thank the staff of the Simón Bolívar University animal house for their technical assistance. We thank Dr. Juan Carlos Piña Crespo for his critical review of this paper.

Bibliographic references

1. Boareto A, Gomes C, Centeno J, Golart J, Vergara F, Salum N, et al. Maternal and fetal outcome of pregnancy in Swiss mice infected with Plasmodium berghei ANKAGFP. Reprod Toxicol. octubre de 2019;89:107-14.
2. World Health Organization. World malaria report 2020: 20 years of global progress and challenges. [cited 2021 8 January]. Available from: https://www.who.int/publications/i/item/9789240015791
3. Ofori M, Ansah E, Agyepong I, Ofori-Adjei D, Hviid L, Akanmori B. Pregnancy-associated malaria in a rural community of ghana. Ghana Med J. marzo de 2009;43(1):13-8.
4. Menendez C, Ordi J, Ismail MR, Ventura PJ, Aponte JJ, Kahigwa E, et al. The impact of placental malaria on gestational age and birth weight. J Infect Dis. mayo de 2000;181(5):1740-5.
5. Mens PF, Bojtor EC, Schallig HDFH. Molecular interactions in the placenta during malaria infection. Eur J Obstet Gynecol Reprod Biol. 1 de octubre de 2010;152(2):126-32.
6. Fried M, Duffy PE. Malaria during Pregnancy. Cold Spring Harb Perspect Med. 1 de junio de 2017;7(6) a025551.
7. Kidima WB. Syncytiotrophoblast Functions and Fetal Growth Restriction during Placental Malaria: Updates and Implication for Future Interventions. BioMed Res Int. 2015;2015:451735.
8. Tuikue Ndam NG, Salanti A, Bertin G, Dahlbäck M, Fievet N, Turner L, et al. High level of var2csa transcription by Plasmodium falciparum isolated from the placenta. J Infect Dis. 15 de julio de 2005;192(2):331-5.
9. McLean ARD, Ataide R, Simpson JA, Beeson JG, Fowkes FJI. Malaria and immunity during pregnancy and postpartum: a tale of two species. Parasitology. julio de 2015;142(8):999-1015.
10. Hviid L, Marinho CRF, Staalsoe T, Penha-Gonçalves C. Of mice and women: rodent models of placental malaria. Trends Parasitol. agosto de 2010;26(8):412-9.
11. Umbers AJ, Aitken EH, Rogerson SJ. Malaria in pregnancy: small babies, big problem. Trends Parasitol. 1 de abril de 2011;27(4):168-75.
12. Rogerson SJ, Hviid L, Duffy PE, Leke RF, Taylor DW. Malaria in pregnancy: pathogenesis and immunity. Lancet Infect Dis. 1 de febrero de 2007;7(2):105-17.
13. Neres R, Marinho CRF, Gonçalves LA, Catarino MB, Penha-Gonçalves C. Pregnancy outcome and placenta pathology in Plasmodium berghei ANKA infected mice reproduce the pathogenesis of severe malaria in pregnant women. PloS One. 13 de febrero de 2008;3(2):e1608.
14. Marinho CRF, Neres R, Epiphanio S, Gonçalves LA, Catarino MB, Penha-Gonçalves C. Recrudescent Plasmodium berghei from pregnant mice displays enhanced binding to the placenta and induces protection in multigravida. PloS One. 20 de mayo de 2009;4(5):e5630.
15. Desai M, ter Kuile FO, Nosten F, McGready R, Asamoa K, Brabin B, et al. Epidemiology and burden of malaria in pregnancy. Lancet Infect Dis. febrero de 2007;7(2):93-104.
16. Barateiro A, Pereira MLM, Epiphanio S, Marinho CRF. Contribution of Murine Models to the Study of Malaria During Pregnancy. Front Microbiol. 2019;10:1369.
17. Mangels R, Young B, Keeble S, Ardekani R, Meslin C, Ferreira Z. Genetic and phenotypic influences on copulatory plug survival in mice. Hered Edinb. 2015;115(6):496-502.
18. Spencer L, Quintana D, Hidalgo L. Evaluation of the inhibition of invasion in vitro of P. yoelii strain with different monoclonal antibodies raised against MSP-119. Rev Bioméd. 2008;19(1):45-51.
19. Megnekou R, Hviid L, Staalsoe T. Variant-specific immunity to Plasmodium berghei in pregnant mice. Infect Immun. mayo de 2009;77(5):1827-34.
20. Megnekou R, Staalsoe T, Hviid L. Cytokine response to pregnancy-associated recrudescence of Plasmodium berghei infection in mice with pre-existing immunity to malaria. Malar J. 1 de noviembre de 2013;12:387.
21. Sharma A, Conteh S, Langhorne J, Duffy PE. Heterologous Infection of Pregnant Mice Induces Low Birth Weight and Modifies Offspring Susceptibility to Malaria. PloS One. 2016;11(7):e0160120.
22. Okojie AK, Rauf K, Iyare E. The Impact of Plasmodium berghei Exposure In-utero on Neurobehavioral Profile in Mice. Basic Clin Neurosci. abril de 2019;10(2):99-107.
23. Huynh B-T, Fievet N, Briand V, Borgella S, Massougbodji A, Deloron P, et al. Consequences of gestational malaria on birth weight: finding the best timeframe for intermittent preventive treatment administration. PloS One. 2012;7(4):e35342.
24. Dobbs, K. R. and Dent, A. E . Plasmodium malaria and antimalarial antibodies in the first year of life. Parasitology. 2016; 143(2):129-38.
25. Cohen, S., Mc, G. I. and Carrington, S. Gamma-globulin and acquired immunity to human malaria. 1961; Nature 192, 733–737.
26. McGregor, I. A. The passive transfer of human malarial immunity. American Journal of Tropical Medicine Hygiene.1964; 13(Suppl.), 237–239.
27. Hill, D. L., Eriksson, E. M., Li Wai Suen, C. S., Chiu, C. Y., Ryg-Cornejo, V., Robinson, L. J., Siba, P. M., Mueller, I., Hansen, D. S. and Schofield, L. Opsonising antibodies to P. falciparum merozoites associated with immunity to clinical malaria. 2016; PLoS ONE 8, e74627.

28. Malhotra, I., Dent, A., Mungai, Wamachi, A., Ouma, J.H, Narum,D.L., Muchiri,E., Tisch, D.J., King,C.L. Can prenatal malaria exposure produce an immune tolerant phenotype? A prospective birth cohort study in Kenya. 2009; PLoS medicine. 2009;6(7): e1000116.
29. Feeney, M.E. The immune response to malaria in utero. Immunol Rev. 2020; 293(1): 216–229.
30. Desai, M., Gutman, J., L'Lanziva, A., Otieno, K., Juma, E., Kariuki S., Ouma,P., Were,V., Laserson, K., Katana, A., Williamson A., Kuile, F. Intermittent screening and treatment or intermittent preventive treatment with dihydroartemisinin-piperaquine versus intermittent preventive treatment with sulfadoxine-pyrimethamine for the control of malaria during pregnancy in western Kenya: an open-label, three-group, randomised controlled superiority trial. Lancet. 2015; 386(10012):2507–2519.
31. Kakuru, A., Jagannathan, P., Muhindo, M.K., Natureeba, P., Awori, P., Nakalembe, M., Opira, B., Olwoch, P., Ategeka, J., Nayebare, P., Clark, T.D., Feeney, M.E., Charlebois, E.D., Rizzuto, G., Muehlenbachs, A., Havlir, D.V., Kamya, M.R., Dorsey, G. Dihydroartemisinin-Piperaquine for the Prevention of Malaria in Pregnancy. N Engl J Med. 2016; 374(10):928–939.

Received: 15 January 2021
Accepted: 30 March 2021

RESEARCH / INVESTIGACIÓN

Índices temporales del electrocardiograma en bovinos Holstein a diferentes edades y de uno y de otro sexo

Temporal indices of the electrocardiogram in Holstein cattle at different ages and of both sexes

Alberto Pompa Núñez[1] , Dania Yusimí Pompa Rodríguez[2]

DOI. 10.21931/RB/2021.06.02.26

Resumen: Esta investigación tuvo como objetivo establecer índices temporales entre los períodos de reposo y de actividad de cada porción cardíaca y del corazón en su conjunto, en bovinos Holstein a diferentes edades y de uno y de otro sexo. Para ello, se seleccionó una muestra de 150 ejemplares clínicamente sanos, de diferentes grupos etarios; muestreados durante la época de seca. Se empleó la derivación bipolar base-ápice (B-A) y el electrocardiógrafo fue calibrado con una señal de 1 mV/cm., con una velocidad de corrida del papel de 25 mm/s. Como resultado se obtuvo que los índices temporales, reposo/actividad del corazón (Rc), reposo/actividad de los ventrículos (Rv) y reposo actividad de las aurículas (RA), constituyen en los animales machos una fracción constante en las edades iniciales y sólo decrece el R_A en los sementales adultos. En las hembras los índices R_C y R_V se incrementan de terneras a novillas y en R_A no se producen diferencias, pero los tres disminuyen en las vacas lactantes ($p<0,05$). El índice reposo de las aurículas/reposo de los ventrículos (RAV), se mantiene constante, independientemente de la edad y del sexo. Se concluye que, entre las fracciones temporales reposo/actividad del electrocardiograma (ECG), se establecen proporciones relativamente constantes, las cuales se modifican por la edad y la producción láctea, excepto el R_{AV}, lo que permite emplear estos índices como referencia para diagnosticar alteraciones en la función cardíaca en la especie estudiada y para evaluar fármacos en los Biomodelos de animales destinados a estos fines.

Palabras clave: Índices temporales, ECG, bovinos, Holstein.

Abstract: This research aimed to establish temporal indices between the periods of rest and activity of each cardiac portion and the heart as a whole in Holstein cattle at different ages and both sexes. To do this, a sample of 150 clinically healthy specimens from different age groups was selected, sampled during the dry season. The base-apex bipolar lead (B-A) was used and the electrocardiograph was calibrated with a signal of 1 mV/cm., With a paper speed of 25 mm / s. As a result, it was obtained that the temporal indices, rest/activity of the heart (Rc), rest/activity of the ventricles (Rv), and rest-activity of the atria (RA), constitute in male animals a constant fraction in the initial ages and only R_A decreases in adult stallions. In females, the C_R and R_V indices increase from calves to heifers, and in R_A, there are no differences, but all three decreases in lactating cows ($p<0.05$). The resting ratio of the atria/resting ventricles (RAV) remains constant, regardless of age and sex. It is concluded that, between the rest/activity time fractions of the electrocardiogram (ECG), relatively constant proportions are established, which are modified by age and milk production, except for the RAV, which allows using these indices as a reference to diagnose alterations in cardiac function in the species studied and to evaluate drugs in Biomodels of animals for these purposes.

Key words: Temporary indexes, ECG, bovine, Holstein.

Introducción

En condiciones normales la actividad eléctrica del corazón debe considerarse como cíclica porque se repiten periódicamente las condiciones iniciales. El ciclo eléctrico es equivalente a la suma del período de actividad, que comprende desde que se inicia la onda P hasta que culmina la T, intervalo PT (IPT), más el periodo de reposo representado por el segmento TP denominado pausa cardíaca.

El ciclo eléctrico de los ventrículos y el de las aurículas puede ser analizado por separado. El primero es equivalente a la suma de los intervalos de actividad (IQT), que incluye desde el inicio de la onda Q hasta el final de la T y el de reposo (ITQ), desde el final de T al inicio de Q. En el segundo caso, como teóricamente la repolarización auricular ocurre en el instante en que se produce el complejo ventricular QRS quedando enmascarado por éste[1,2], puede considerarse como la suma del intervalo de actividad (IPS) cuya duración se mide desde el inicio de la onda P hasta la terminación del complejo QRS, más el período de reposo SP (ISP), equivalente a la suma del intervalo ST (IST) y el segmento TP.

En el análisis del proceso de excitación del corazón, es un indicador de gran valor las relaciones cuantitativas entre la duración de los períodos de reposo y los de actividad. Con la determinación de estas relaciones, es posible comparar la función cardíaca entre animales de la misma especie o entre los que pertenecen a especies diferentes; así como valorar los efectos de los medicamentos sobre el sistema cardiovascular durante su evaluación preclínica, obligatoria en al menos tres especies de animales, antes de ser utilizadas en el hombre. Una vez obtenido el valor normal de estas relaciones cuantitativas se pueden detectar también cuáles son las porciones del corazón que más se afectan en las situaciones mencionadas y en otras. Por eso, esta investigación tuvo como objetivo establecer índices temporales entre los períodos de reposo y de actividad de cada porción cardíaca y del corazón en su conjunto, en bovinos Holstein a diferentes edades y de uno y de otro sexo.

[1] Profesor de Biofísica y Fisiología, San José de Las Lajas, Mayabeque, Cuba.
[2] Hospital San Vicente de Paul. Ibarra. Ecuador.

Corresponding author: albertopompa1949@gmail.com

Materiales y métodos

Esta investigación se desarrolló en el Centro de Sanidad Agropecuaria (CENSA) ubicado en la provincia de Mayabeque. De una población de 200 bovinos del genofondo Holstein de Cuba, a los cuales se le habían registrado 20 derivaciones electrocardiográficas, se seleccionó una muestra de 150 ejemplares de uno y de otro sexo, pertenecientes a diferentes grupos etarios; todos muestreados durante la época de seca, de octubre a marzo. Para la medición de la duración de los segmentos e intervalos del ECG y para el establecimiento de los índices temporales se empleó la derivación bipolar base-ápice (B-A), en la que el electrodo negativo se colocó sobre la séptima vértebra torácica, o sea en la región de la base del corazón y el electrodo positivo o explorador sobre el apéndice xifoides del esternón, en la región apical cardíaca. Atendiendo a las variables edad y sexo, se trabajó con 6 categorías: 20 terneras con edades entre 7 y 60 días, con un peso promedio de 72 kg, 20 terneros con edades comprendidas entre 7 y 60 días y con un peso promedio de 75 kg, 40 novillas incorporadas al plan de reproducción, pero no gestadas, ni en celo, con edad promedio de 20 meses, y un peso de 302 kg, 25 sementales jóvenes incorporados al plan de extracción de semen con edad promedio de 21 meses y un peso de 546 kg, 25 sementales adultos con edad promedio de 7,8 años y un peso de 1007 kg, 20 vacas lactantes con producción y edad promedios de 13 litros de leche y 4,8 años, respectivamente. Se cumplió con las normas de aislamiento eléctrico de los animales durante la realización de los registros y la forma de conexión de los electrodos. El equipo empleado fue un electrocardiógrafo portátil de fabricación japonesa, HITACHI, calibrado con una señal de 1 mV/cm y velocidad de corrida del papel de 25 mm/s.

A partir de la ilustración de la figura 1, se calcularon los índices temporales para los que se emplearon las siguientes expresiones:

I. $R_C = \frac{\overline{TP}}{IPT}$ (Relación reposo/actividad del corazón) donde,

$\overline{TP}$ = Segmento TP

$IPT = IPQ + QRS + IST$ $\quad I \Rightarrow$ Intervalos = duración de ondas + la de los segmentos.

II. $R_V = \frac{ITQ}{IQT}$ (Relación reposo/actividad de los ventrículos) donde,

$ITQ = \overline{TP} + IPQ$ **e** $IQT = QRS + IST$.

III. $R_A = \frac{ISP}{IPS}$ (Relación reposo actividad de las aurículas) donde,

$ISP = IST + \overline{TP}$ **e** $IPS = IPQ + QRS$.

IV. $R_{AV} = \frac{ISP}{ITQ}$ (Relación reposo de las aurículas/reposo de los ventrículos).

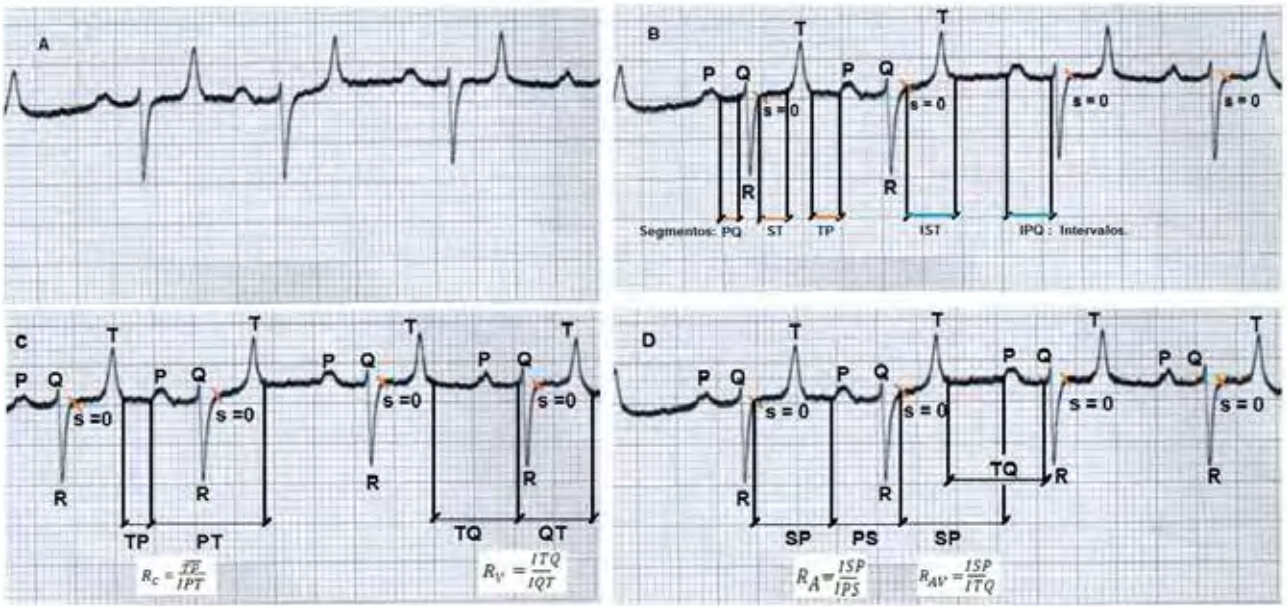

Figura 1. ECG normal en bovino en derivación BA (A), registros en los que se indican ondas, segmentos e intervalos (B) y las expresiones de los índices temporales (C y D).

Procesamiento estadístico

Los datos fueron compilados en una base de Excel y procesados con el paquete estadístico STATGHRAPHIC plus 5. Para la comparación de los valores de los índices temporales relacionados con la edad y con la influencia del sexo, se empleó un análisis de varianza simple con dócima de Duncan.

Resultados y discusión

En la tabla 1, se ilustran los valores de los segmentos e intervalos y la frecuencia cardíaca y en la tabla 2, los índices temporales del ECG en bovinos Holstein, calculados a partir de los mismos datos primarios. La derivación BA que se ha empleado en estas determinaciones es muy estable en morfología y polaridad[3,4] y posee características similares a la derivación estándar de extremidad DII, que también ha sido utilizada tanto en medicina veterinaria como en humana, sobre todo para evaluar alteraciones del ritmo[5-9].

El ECG es un medio de monitorización barato, fácil y no invasivo para dar seguimiento a la función cardíaca[10-12], detectar dilataciones miocárdicas[13] y otras patologías[14-16]. Constituye la herramienta de diagnóstico complementario más extensamente utilizada en cardiología[17-19]. Sin embargo, no se ha hecho ninguna referencia a los índices temporales que relacionan el período de reposo y el de actividad. Se plantea que si bien la repolarización ventricular se modifica, la mayoría de los índices comúnmente utilizados en la práctica clínica no incluyen el estudio simultáneo de las fases de despolarización y repolarización de cada porción del corazón por separado[20,21].

Existen diferentes alteraciones de la repolarización descritas en la población de atletas, entre ellas, las más frecuentemente reportadas en la literatura son: repolarización precoz, ondas T vagotónicas, ondas U, supradesnivelación del segmento ST y ondas T negativas[22]. Por eso, en la presente investigación se tienen en cuenta las interacciones entre el período de reposo y el de actividad cardíacas, en los que se valoran los procesos de despolarización y los de repolarización.

En la evaluación médico-deportiva del sistema cardiovascular de niños y adolescente, el consenso en Europa y en muchos países se basa en una anamnesis y exploración estandarizadas de 12 puntos de la *American Heart Association* (AHA), unidas a la lectura sistemática del ECG basal de 12 derivaciones[23]. La inclusión de los cuatro índices temporales, cuya importante significación fisiológica queda demostrada a lo largo de este artículo, resultaría de gran utilidad para evaluar la intensidad funcional del miocardio y cualquier hallazgo que se aleje de los valores normales justificaría la consulta con el cardiólogo pediátrico, desde muy temprana edad.

La comparación, para valorar los efectos de la edad sobre

Derivación	Segmentos e intervalos	Ternera (n =20)	Ternero (n = 20)	Novilla (n =40)	Semental Joven (25)	Semental Adulto (25)	Vaca Lactante (20)
B-A	TP	0,22 cd	0,25 bc	0,39 a	0,31 b	0,31b	0,15 c
	IPQ	0,14 c	0,14 c	0,21 b	0,21 b	0,23 a	0,22 ba
	IST	0,23 c	0,22 c	0,31 a	0,31 a	0,3 a	0,26 b
	IQT	0,29 c	0,3 c	0,38 ba	0,38 ba	0, 38a	0,36 b
	IPT	0,43 d	0,44 d	0,59 ba	0,59 ba	0, 61a	0,58 ba
	ITQ	0,36 c	0,39 c	0,60 a	0,52 b	0,54	0,37 b
	RR	0,65 c	0,69 bc	0,98 a	0,9 a	0, 92a	0,73 b
Frecuencia Cardiaca		92 a	87 a b	61 c	66 c	65 c	82 b

Letras desiguales difieren estadísticamente entre sí con $p < 0,05$.

Tabla 1. Duración (s) de los componentes electrocardiográficos y la frecuencia cardíaca (Latidos/min) en bovinos Holstein de diferentes categorías (n =150).

Índices Temporales	RC	RV	RA	RAV
Media ± desviación estándar.	$\bar{x} \pm sd$			
Categorías.				
Terneros	0,57± 0,05	1,3± 0,08	2,24± 0,03	1,2± 0,01
Sementales Jóvenes	0,52± 0,07	1,36± 0,06	2,21± 0,08	1,19± 0,03
Sementales Adultos	0,5± 0,03	1,42± 0,09	1,96± 0,10	1,13± 0,07
Terneras	0,51± 0,01	1,24± 0,15	2,25± 0,01	1,25± 0,01
Novillas	0,66± 0,02	1,58± 0,01	2,5± 0,06	1,16± 0,05
Vacas lactantes	0,25± 0,09	1,03± 0,04	1,28± 0,09	1,11± 0,09

Tabla 2. Índices Temporales del ECG (adimensionales) en distintas categorías de bovinos Holstein, calculados con la derivación base-ápice (n =150).

los índices temporales del ECG, fue efectuada: entre terneros, sementales jóvenes y sementales adultos (figura 2), entre terneras, novillas y vacas lactantes (Figura 3) y entre animales de uno y de otro sexo, pero pertenecientes al mismo grupo etario (Figura 4).

Los índices temporales R_C, R_V y R_A los cuales representan las relaciones reposo/actividad del corazón, de los ventrículos y de las aurículas respectivamente, constituyen en los animales machos una fracción constante en las edades iniciales y sólo decrece el R_A en los sementales adultos. El índice RAV que relaciona el periodo de reposo de las aurículas con el de los ventrículos se mantiene constante, independientemente de la edad. En las hembras (Gráfico 2), los índices R_C y R_V se incrementan de terneras a novillas y en R_A no se producen diferencias, pero los tres se acortan en las vacas lactantes ($p<0,05$). Para R_{AV} no se encontraron diferencias al comparar las tres categorías.

Las diferencias de los índices temporales entre los animales de uno y de otro sexo están determinadas, más por la producción que por el sexo en sí. En el gráfico 3, al comparar las novillas con los sementales jóvenes y los sementales adultos con las vacas lactantes, los menores valores de R_V corresponden a los animales que tienen mayor demanda energética y metabólica. Los sementales jóvenes se encontraban bajo el régimen de extracción de semen y al compararlos con las novillas, requieren de una actividad metabólica suplementaria. En la comparación de las vacas lactantes con los sementales adultos, está demostrado que en las primeras las transformaciones energéticas y las demandas en la circulación sanguíneas son mucho más elevada, lo que conlleva a una mayor cantidad de trabajo del corazón. Se plantea que para producir cada litro de leche deben pasar por la glándula mamaria de 400 a 600 litros de sangre[24]. Por esa causa, se obtuvieron valores mucho más bajos, además, para R_C y R_A en las vacas lactantes que en los sementales adultos ($p<0,05$). No se observan diferencias entre terneros y terneras porque presentan

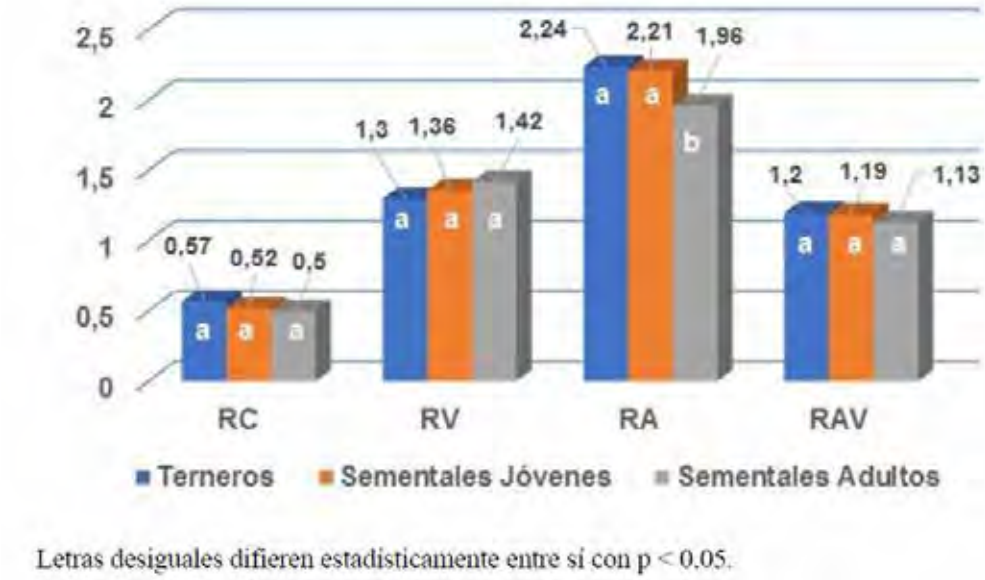

Letras desiguales difieren estadisticamente entre sí con $p < 0.05$.

Figura 2. Comportamiento de los índices temporales de bovinos Holstein machos con el avance de la edad.

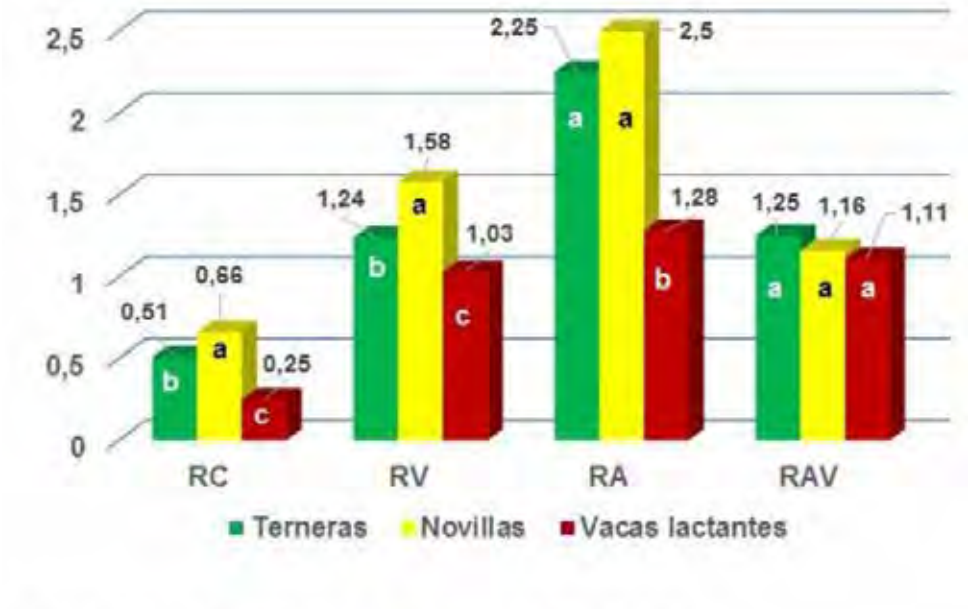

Letras desiguales difieren estadisticamente entre sí con $p < 0,05$.

Figura 3. Comportamiento de los índices temporales de bovinos Holstein hembras con el avance de la edad.

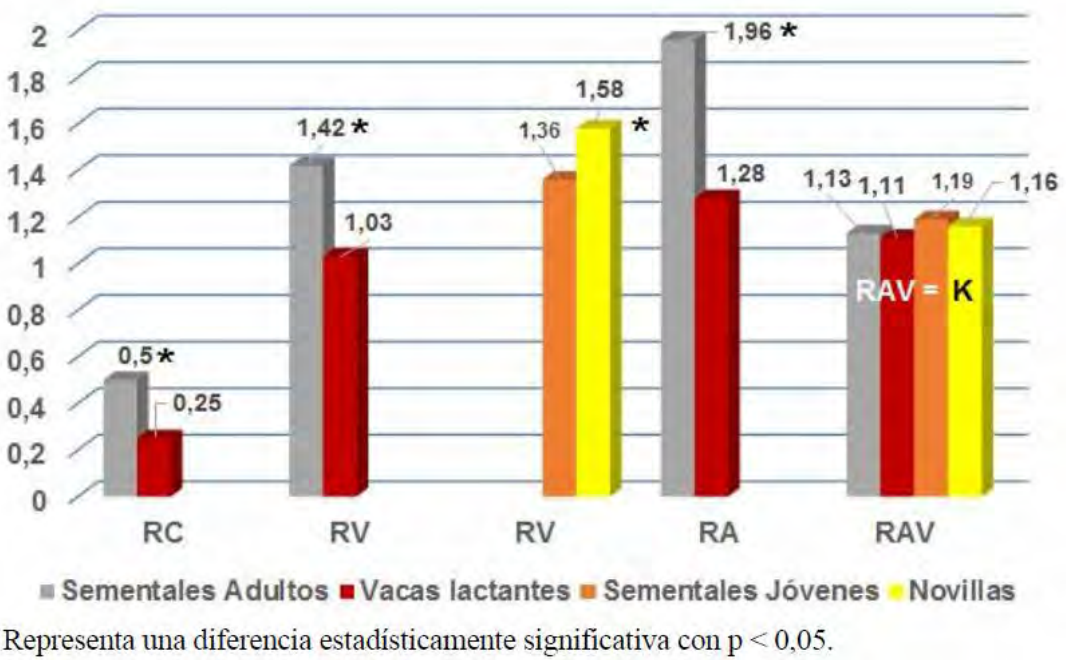

* Representa una diferencia estadísticamente significativa con $p < 0,05$.

Figura 4. Comparación de los índices temporales entre bovinos Holstein de uno y de otro sexo pertenecientes al mismo grupo etario.

demandas energéticas similares, en función del crecimiento y la relación reposo actividad del corazón es similar.

De los valores del segmento TP y del índice R_C obtenidos (tablas 1, 2 y Gráfico 3) se infiere que durante un período circadiano el tiempo de reposo del corazón de las vacas lactantes es de 4,8 horas y el de las restantes categorías es aproximadamente el doble, entre 8 y 9,6 horas. La frecuencia cardíaca de las vacas lactantes es significativamente superior a la de las novillas ($p< 0,05$), realizan 21 latidos más por cada minuto (82 vs. 61), lo que en un día representan 30 240 latidos y si se consideran 307 días de lactancia[25], la cifra sobrepasaría los 9 millones de latidos más. Esta sobrecarga conduce a una hipertrofia cardíaca fisiológica mucho más marcada que la que tiene lugar cuando hay una moderada actividad física[26] y tiene causas muy diferentes a las que se reportan en el hombre, asociadas a patologías[27-29].

El índice temporal R_{AV}, que establece la relación reposo de las aurículas/reposo de los ventrículos no se afecta por ninguno de los factores que se han analizado y de su constancia se deduce que entre los intervalos IST e IPQ existe una relación tal, que la variación normal en uno de ellos determina variaciones fijas y definidas en el otro. Esa relación puede plantearse como se detalla a continuación:

El IPQ está constituido por la suma de la duración de la

$$R_{AV} = \frac{ISP}{ITQ}$$

$$ISP = IST + \overline{TP}$$

$$ITQ = \overline{TP} + IPQ$$

$$R_{AV} = \frac{IST + \overline{TP}}{\overline{TP} + IPQ}$$

$$R_{AV}\left(\overline{TP} + IPQ\right) = IST + \overline{TP}$$

$$IST = R_{AV}\left(\overline{TP} + IPQ\right) - \overline{TP}$$

$$IST = R_{AV}\overline{TP} + R_{AV}IPQ - \overline{TP}$$

A partir de los datos de duración de la tabla 1 y de los valores de este índice (tabla 2), se puede establecer que para los animales más jóvenes la ecuación aproximada es:

$$IST = 1,20\,IPQ + 0,20\,\overline{TP}$$

y para las vacas lactantes y los sementales adultos:

$$IST = 1,12\,IPQ + 0,12\,\overline{TP}$$

onda P más la del segmento PQ, que es un trazado isoeléctrico provocado por el tiempo que demora el impulso eléctrico para atravesar el nodo Auriculoventricular[1,30,31]. Su valor se afecta por modificaciones de las propiedades de conducción eléctrica del tejido que conecta las aurículas con los ventrículos[32-34]. El IST comprende la duración del segmento ST más la duración de la onda T. El segmento es un período de inactividad que separa la despolarización ventricular de la repolarización ventricular y es normalmente isoeléctrico, pero puede desviarse por el infarto agudo del miocardio o alguna causa que afecte la repolarización ventricular[35-38] y por factores como el síndrome coronario agudo[39-41].

En la etapa inicial de la infección por SARS-COV-2 se diagnosticó que la patología provocada en sí misma, o los efectos colaterales de su tratamiento tienen manifestaciones cardiovasculares, como insuficiencia cardíaca, lesión miocárdica, isquemia y prolongación de QTc[42-45], del cual forma parte como el componente más vulnerable el IST. Por ello, sería recomendable que en los análisis electrocardiográficos se tengan en cuenta los índices temporales aquí evaluados, a los efectos de establecer un pronóstico evolutivo de la enfermedad.

Conclusiones

Entre las diferentes fracciones del ECG se establecen proporciones relativamente constantes que se expresan por los índices temporales, de los cuales en los animales machos sólo se afecta por la edad el R_A y en las hembras se modifican R_C, R_V y R_A, sobre todo por la producción láctea. R_{AV} no se modifica por ninguno de estos factores. Con el avance de la edad, el comportamiento de los índices temporales es diferente en los animales machos que en las hembras, lo que está determinado por las diferencias fisiológicas, humorales, productivas y por la constitución anatómica e histológica de cada sexo.

Referencias bibliográficas

1. Guyton A, Hall J. Tratado de Fisiología Médica. 13ma. Ed. Editorial ELSEVIER. [en línea] Mayo 2016. Disponible en: http:// www.meddics.com. [Consultada: 3 febrero de 2020].
2. Morán M. Relevancia de la interpretación del electrocardiograma de reposo en la evaluación pre- participativa de deportistas. Rev. Actuali. Clinic. Meds. 2018;2(1):8-12.
3. D´Roth L. Electrocardiographic parameters in the normal lactating Holstein cow. The Can Vet. J. 1980;21(10):271-277.
4. Matsui K, Sugano S. Species differences in the changes in heart and T- wave amplitude after autonomic blocade in thorrughbred horses,ponies, cows, pigs, goasts and chiquens. Japan Vet. Sci. 1987;49(4):637-644.
5. Dörner SMC, Godoy PA. Electrocardiografía en equinos fina sangre de carrera. Av. Cs. Vet. 2009;24(1 y 2):18-25.
6. Vargas PP, Galindo ZV, Pedraza Adriana. Efecto del entrenamiento en Agility en gran altitud en perros Border Collie en algunas variables electrocardiográficas: análisis preliminar. Rev Inv Vet Perú. 2018;29(1):41-54.
7. Rubio SJ. Papel de enfermería en el tratamiento de las principales alteraciones electrocardiográficas: bradiarritmias, taquiarritmias y fibrilación auricular. Enferm Cardiol. 2018;25(73):76-84..
8. Asenjo, R. Taquicardia de complejo ancho en paciente con fibrilación auricular permanente. Revista Chilena de Cardiología. 2017;36(1):53-56.
9. Paredes A, Bittner A, Vergara I. Compromiso de conciencia y bradicardia. Rev Chil Cardiol. 2018;37:55-57.
10. Battioni L, Costabel JP, Mondragón IL, Russo A, Sotelo V. Belén y Lamelas, P.M. Diferencias electrocardiográficas entre Takotsubo e infarto agudo de miocárdio. Rev Fed Arg Cardiol. 2015;44(1):51-54.
11. Moreno MG, Mejía MCS, Fernández NMI, Sánchez NR. Incidencia y manejo del infarto agudo miocárdico con elevación del segmento ST, Hospital José María Velasco Ibarra, 2014. Enfermería Investiga, Investigación, Vinculación, Docencia y Gestión. 2016;1(4):151-157.
12. Vesga B E. Estrategia en infarto agudo de miocardio con elevación del segmento ST con enfermedad multivaso. Acta Médica Colombiana 2016;41(2):98-99.
13. Costabel JP, Mandó F, Avegliano G. Miocardiopatía dilatada: ¿cuándo y cómo proceder a la investigación etiológica? Rev Urug Cardiol 2018;33:343-349.
14. Rendón GJA, Godoy PAL. Detección temprana de la falla cardiaca en pacientes diabéticos: Más allá de la fracción de eyección. Rev Colomb Cardiol. 2020;27(S2):17-21.
15. Martínez FC, Strada B. Reincidencia de eventos coronarios: disfunción endotelial como mediadora. Rev Urug Cardiol 2020; 35: 130-134
16. Cisneros JAI, Ugarte Palacios NA, Macias AJI, Suárez VEF. Cambios electrocardiográficos en hyperkalemia. RECIAMUC. 2020; 4(1):201-211.
17. Núñez A, Ortega M, Borgatta M, Cossio ME, Nuñez BJ, León de la Fuente R. Patrones electrocardiográficos en pacientes con enfermedad de Chagas en zona sur de la ciudad de Salta. Insuf Card. 2016;11(4):168-172.
18. Becerra PEN, Casillas TL, Becerra AF. Prevalencia del síndrome coronario agudo en primer nivel de atención. Revista ConaMed. 2020;25(1):16-22.
19. Roy T, Peralta GR, Gamarra CLC, Núñez VLM, Santacruz SMC, Alarcón MVB. Intervalo QTc prolongado en pacientes de Clínica Médica: estudio multicéntrico. Rev. virtual Soc. Parag. Med. Int. marzo 2020; 7 (1):10-19.
20. Bonomini, María Paula., Ingallina, F.J., Barone, Valeria., Antonucci, R., Arini, P.D. Nuevos marcadores electrocardiográficos de hipertrofia ventricular izquierda. Rev Fed Arg Cardiol. 2016; 45(1): 24-28.
21. Breijo MFR. Patrón electrocardiográfico Breijo. Rev. Arch Med Camagüey. 2018;22(3)277-271.
22. Cárdenes LA, García SJJ, Quintana CCA, Fernández AAM. Prevalencia y cambios dinámicos de las ondas T vagotónicas durante el ejercicio en una población futbolista de élite. Arch Med Deporte 2018;35(1):23-28.
23. Mónaco M, Pérez Martínez E, Sevilla Moya JC, Gutiérrez Rincón JA, Brotons CD, Schack M. Consejos y patología asociada a la práctica deportiva. En: AEPap (ed.). Curso de Actualización Pediatría 2018. Madrid: Lúa Ediciones 3.0; 2018. p.293-307.
24. Bobilev FI, Pigares NV, Potokin V, Lovedev V. Ganaderia. Editorial Mir. Moscú. 1979. p. 38 – 46.
25. Ponce P, Bell L. Estudio de la lactancia en vacas Holstein Friesian, Cebú y sus cruces en Cuba. Rev. Salud Anim.1986;8(1):73–78.
26. Vélez AC, Vidarte CJA. Efecto de un programa de entrenamiento físico sobre condición física saludable en hipertensos. Rev. Bras. Geriatr. Gerontol. 2016;19(2):277-288.
27. Denis PDA, Martínez GS, Figueredo GAR, Rodríguez VEC. Valor diagnóstico de la R de aVL en la hipertrofia ventricular izquierda. Univ Med Pinareña. 2020;16(1): e382.
28. Reyes CW, Trujillo P, Hartzell VS. Miocardiopatía hipertrófica: encare clínico y opciones de tratamiento. Rev Urug Cardiol 2020;35:109-129.
29. Amair MP, Arocha RI. El continuo cardiorrenal: una propuesta para la prevención de las enfermedades cardiovasculares y renales. Rev. Colomb. Nefrol. 2020;7(1):1-30.
30. De Micheli, A., Medrano, G.A. y Iturralde, T.P. Bases de las arritmias. Bloqueos miocárdicos periféricos no complicados y complicados. Arch Cardiol Mex 2009;79(Supl 2.):3-12.
31. Vogler J, Breithardt G, Eckardt L. Bradiarritmias y bloqueos de la conducción. Rev Esp Cardiol. 2012;65(7):656–667.
32. Forero GJE, Moreno JM, Agudelo CA, Rodríguez AEA, Sánchez MPA. Fibrilación auricular: enfoque para el médico no cardiólogo. IATREIA. 2017;30(4):404-422.
33. Serra JL, Figueroa JA, Fassano N. Taquicardia auricular focal y taquicardiomiopatía. Rev Fed Arg Cardiol. 2018;47(1):03-09.
34. Reyes CW. Alcohol, arritmias y enfermedad coronaria. Rev Urug Cardiol 2020;35:12-20.

35. Porras G, Quesada G. Reporte de un caso y Revisión Bibliográfica. Elevación transitoria del segmento ST en paciente víctima de trauma eléctrico en el hospital San Rafael de Alajuela. Revista Medicina Legal de Costa Rica - Edición Virtual. 2016;33(1)1-5.
36. Candiello, Alfonsina., Cigalini, I.M., Burgos, Lucrecia., Ortego, J.I., García, Z. S. y Godoy, A. Casandra. Hoja de ruta en el manejo del infarto agudo de Miocardio con elevación del segmento ST. Revista CONAREC 2017;33(138):13-14.
37. García FMA, Gómez DJJ. COVID-19 y afectación cardíaca Rev Chil Anest 2020;49: 397-400.
38. Solís SLD. Recomendaciones para prevención de Muerte Súbita y Arritmias asociadas a fármacos utilizados para COVID-19. Rev. Costarric. Cardiol. 2020;22 (Número especial):37-39.
39. Souto SP, Iglesias VJA, Santos LS. Evaluación de la actuación de los alumnos de tercer Grado en Enfermería de la USC en un escenario simulado de síndrome coronario agudo con elevación del segmento ST. Enferm Cardiol. 2019; 26 (78): 49-56.
40. Miranda PR, González SCM, Morales VY. Síndrome coronario agudo con elevación del segmento ST en el Centro de Diagnóstico Integral La Macandona. Rev Ciencias Médicas. 2020; 24(1): e4142:1-7.
41. Miró O, Martínez NG, Jiménez S, Gómez AE, Alonso JR, Antolín A, Salgado E, Perelló R, Gualandro DM, Strebel I, López AP, Rosselló X, Bragulat E, Sánchez M, Müller Ch, López BB. Asociación entre los datos clínicos y electrocardiográficos iniciales en pacientes con dolor torácico no traumático y la sospecha inicial y el diagnóstico final de síndrome coronario agudo. Emergencias 2020;32:9-18.
42. Figueroa TJF, Salas MDA, Cabrera SJS, Alvarado CCC, Buitrago SAF. COVID-19 y enfermedad cardiovascular. Revista Colombiana de Cardiología, Jornal Pre-proof. 2020;4(4):1-27.
43. Abuabara FE, Bohórquez RJ, Restom A, Sáenz LJ, Correa GJ, Mendoza PC. Consideraciones actuales de antimaláricos en la infección por SARS-COV-2 y su impacto. Rev. Colomb. Nefrol. 2020;7(Supl 2):1-39.
44. Kenar MR, Flores LA, Dante BL. Comité de Patología Crítica Cardiovascular. Sociedad Argentina de Terapia Intensiva (SATI). Informe cloroquina o hidroxicloroquina para el tratamiento del COVID-19. |en línea| 25 marzo 2020. Disponible en: https://www.google.com/search? [Consultada: 15 mayo 2020].
45. Torres A, Rivera A, García A, Arias C, Saldarriaga C, Gómez E, Mendoza F, González RG, Castellanos J, Esteban GJ, Echeverría LE, Rodríguez MJ, Navarrete S. Evaluación y tratamiento de la insuficiencia cardiaca durante la pandemia de COVID-19: resumen ejecutivo. Rev Colomb Cardiol. 2020. |en línea| 1 de abril 2020. Disponible en: http:// www.revcolcard.org. [Consultada: 11 de mayo 2020].

Received: 10 enero 2021
Accepted: 8 abril 2021

CASE REPORTS / REPORTE DE CASO

COVID-19 infected patients in a Hemodialysis facility in Ecuador, 2020

Mario Hernández[1], Emilio Fors[1], Fresia Massuht[1], Ingrid Figueredo[2], Raúl Caballero[2], Christian Berruz[2], Yinet Ramirez[2], Elsa Bernal[3] and Martha Fors[4]

DOI. 10.21931/RB/2021.06.02.27

Abstract: We retrospectively analyzed the data of 38 hemodialysis patients with COVID-19, including demographic and clinical characteristics were collected from the medical records of patients from Reynadial center from April to June 2020. Of 125 patients from the clinic, 38 (30.4%) were diagnosed with COVID-19. The third part of patients (12) died, the mortality rate was 31%. The mean (±SD) age of the patients was 61±13 years, 57.9% were men. The most common symptoms were shortness of breath and cough; 80% of patients had fever on admission, and more than 90% had hypertension. No significant differences were observed between survivors and non-survivors in demographic and epidemiological characteristics except for gender. We found statistically significant differences between blood pressure and weight before and after the infection by COVID-19. We found a high COVID-19 prevalence in our hemodialysis patients and a high rate of deaths among them, with non-significant statistical differences between survivors and non-survivors of the disease regarding most of the variables studied.

Key words: Clinical features; Coronavirus disease; Hemodialysis, COVID-19, epidemiology.

Introduction

Severe acute respiratory syndrome (SARS-CoV-2) emerged in Wuhan, China in December 2019 and was spread mainly by person-to-person transmission[1]. Symptoms associated with COVID-19 are nonspecific and may include fever, cough, muscle pain and fatigue among other[2].

One of a severe medical condition is the kidney failure which is associate with a high prevalence of concomitant diseases, such as diabetes and heart disease, severely affecting older adults[3,4].

In a few months, COVID-19 has gone from being a little-known respiratory infectious disease generated in China to a devastating pandemic that threatens the health and has changed action protocols worldwide. There are no health care areas that have not been affected by the COVID-19 pandemic, and the chronic kidney patient's management is no exception. Both healthcare professionals and these patients have been forced to adjust the workflow to minimize exposure to COVID-19 in this type of patient.

A mortality rate in hemodialysis (HD) patients of approximately 16%[5] have been reported internationally, and others report infection rates in the range of approximately 1%[6] to 30%[7]. Patients in the dialysis healthcare institutions are relatively mobile, and patients with uremia who require long-term hemodialysis make it more challenging to prevent and control infectious diseases than in general universe[8].

Also, patients in dialysis due to a non very efficient immune system are more likely to develop different and serious infectious diseases than the rest of the population[9,10].

Reynadial clinic in Guayaquil has developed a model for managing kidney patients in pandemic time according to national and international regulations. This institution is a care center dedicated to providing Hemodialysis Service to patients with chronic kidney disease grade V. We have followed recommendations from published interim guidance for the prevention and control of COVID-19 in outpatient hemodialysis facilities by the US Centers for Disease Control and Prevention (CDC)[11].

The clinic began to provide Services in 2016 (11/19/2016) and has been a faithful follower of the Treatment Protocols drawn up by the Ministry of Public Health and concerned about the incorporation of new techniques for the management of these patients. This institution has also taken all precautions and measures to avoid infection due to this disease, but there is always the risk that patients will acquire COVID-19. Since the development of COVID-19 may worsen kidney functions in this type of patient strict management protocols are followed in our institution to prevent the spread of COVID-19 among our patients. The study's objective was to describe the clinical characteristics and outcomes of patients with COVID-19 and determine the percentage of death among them.

Materials and methods

Study design

Retrospective observational cross-sectional study. Medical records were reviewed from patients treated from March to June of 2020.

Participants

Medical records of patients from both gender and ≥18 years old receiving hemodilysis treatment and with COVID-19 diagnosis.

Definitions

It was considered a suspected of COVID-19 clinical case a patient fulfilling: 1) a presence of at least one the these symptoms: fever; respiratory symptoms such as cough, fever or dyspnea; or radiographic evidence of pneumonia, 2) a recent close contact with confirmed COVID-19 persons within 14 days before illness onset or qRT-PCR result positive for COVID-19.

Fever was defined as a temperature of at least 37·3°C.

[1] Clinica Reynadial, Guayaquil, Ecuador. Hospital General IESS Babahoyo, Los Ríos, Ecuador.
[2] Clinica Reynadial, Guayaquil, Ecuador.
[3] Universidad Técnica de Babahoyo, Los Ríos, Ecuador.
[4] Universidad de las Américas, Quito, Ecuador.

Corresponding author: martha.fors@udlanet.ec

Variables

Demographic information, baseline comorbidities, and the use of antibiotics were extracted from electronic medical records and compared between survivors and non-survivors. According to the age, it was divided into the elderly group (≥60 years old) and the young and middle-aged group (<60 years old).

Ethics

None personally identifiable information was collected and guaranteed anonymity and confidentiality for this study. Informed consent for humans was hence not required as there was no data obtained directly from the subjects. Declaration of Istanbul regarding the traffic of organs and Declaration of Helsinki was observed during this study's performance. We followed STROBE guidelines for the report of the results.

Statistical analysis

Cuantitative variables were displayed as means and standard deviations. Confidence intervals at 95% were calculated for means. Categorical variables were expressed as number and relative frequencies (%).

Mann-Whitney U test, or Fisher's exact test to compare differences between survivors and non-survivors where appropriate were used (non-parametric methods). Nonparametric Paired T-test was used to compare each variable before and after the disease. A P-value less than 0.05 was considered statistically significant. SPSS, version 24.0 was used for Statistical analysis.

Results

The number of patients of this health institution who are receiving hemodialysis is 125, from them 38 patients were COVID-19 diagnosed for a general prevalence of the disease of 30.4%. Only 10. Real-time PCR confirmed 5%, the rest was clinically diagnosed.

The mean age of the 38 patients was 61.2 with an SD of 13.4 years (range, 18–83), while weight was 61.09 kilograms (range, 35–88.4). No statistical differences were found between survivors and non-survivors for most of the evaluated characteristics (p>0.05), except for the number of days from the beginning of the disease until curation or death. (Table 1).

The average value of the systolic blood pressure BP, diastolic pressure, and weight before COVID-19 infection was seen to be 160.5 mm/hg, 76.4 mm/hg, and 62.4 kg. At the end of the disease, the average values of blood pressures (BP) and weight were significantly lower when analyzed using the paired *t*-test (P-value < 0.01). (Table 2).

Among the 38 patients, 57.9% were male. There were significant differences according to gender for non-survivors and survivors (p=0.004). Regarding the group of age (≥60 years old and <60 years old), we did not find any differences between non-survivors and survivors.

Most of the patients presented comorbidities, being hypertension the most common comorbidity, followed by diabetes and chronic kidney disease. There were no patients with chronic obstructive lung disease. Non-statistical differences were found between survivors and non-survivors (p>0.05 (Table 3).

Characteristics	Non-survivors n= 12 (31.6)	Survivors N=26 (68.4)	Total	p value*
	Mean(CI95%)	Mean(CI95%)		
Age	64.8 (61.1-68.5)	59.5(58.8-62.2)	61.2	0.23
Weight	64.3(61.5-67.1)	59.5(56.8-62.2)	61.1	0.25
Diastolic pressure mm/hg	63.4(60.7-66.1)	64.3(62.1-66.5)	61.0	0.58
Systolic pressure mm/hg	127.2(122.5-132.5	122.5(118.4-126.6)	124.0	0.17
Time from illness onset to death or discharge, days	12.3 (9.6-15)	25.7 (23.8-27.6)	21.5	0.00

*Mann-Whitney U test

Table 1. Demographic findings. Comparison between means of the two groups and 95%confidence intervals.

	Before Disease	After disease	p value*
Systolic pressure	160.5 mm/hg	124.0 mm/hg	< .001
Diastolic pressure	76.4 mm/hg	64.0 mm/hg	< .001
Weight	62.4 kg	64.0 kg	0.002

* Wilcoxon signed-rank test

Table 2. Paired Samples test. Comparison between means in two points of time in the same patient.

	Non-survivors n= 12 (31.6)		Survivors N=26 (68.4)		Total	p value*
Comorbilities	No.	%	No.	%		
Hypertension						
Yes	12	100.0	25	96.2	37	0.492
No	0	0.0	1	3.8	1	
Diabetes Mellitus						
Yes	8	66.6	17	65.4	25	0.916
No	4	33.3	9	34.6	13	
Coronary heart disease						
Yes	1	8.4	3	11.5	4	0.763
No	11	91.6	23	88.5	34	
Chronic kidney disease						
Yes	12	100.0	25	96.2	37	0.491
No	0	0.0	1	3.8	1	
Use of antibiotics						
Yes	9	75.0	19	73.1	27	0.51
No	3	25.0	7	26.9	10	

*Fisher Test

Table 3. Comparison between proportions according comorbidities of the two groups.

The most common symptoms at the beginning of the infection were dyspnea (89.4%), fever, and cough with 78%, respectively, followed by diarrhea (23.6%) and headache (10.5%). Less common symptoms included myalgia, fatigue, and convulsions. Non-statistical differences were found between survivors and non-survivors (p>0.05) (Table 4).

Thirty-three patients had an arteriovenous fistula, and 5 patients had a permanent central venous catheter. In each session the convective volume ranged from 22 to 32 liters. All patients were receiving low molecular weight heparin anticoagulation therapy. The most used antibiotic was Cefazoline. (Table 5)

Discussion

To date, this report is the only case series of hemodialyzed patients with COVID-19 in Ecuador. Data of patients with COVID-19 in hemodialysis facilities are limited. Among 125 patients in the dialysis center Reynadial in Guayaquil, 38 patients had 2019-nCoV infection (30.4%). The mortality rate, 31.6%, was similar to the results obtained by Goicochea *et al.*[12] but much higher than that observed in the general population.

A university dialysis facility in Renmin Hospital reported that among 230 hemodialysis patients, 37 (16%) COVID-19 cases were diagnosed, and 7 hemodialysis patients died (18.9%) during a short period[13]. Another study reported that among 602 subjects receiving hemodialysis as renal replacement therapy, 7 patients (1.1%) were infected with SARS-CoV-2, and none died during the study[14].

Both studies have shown the disease much lower than what we are reporting in the current work.

Albalate at al. reported that from 90 HD patients, 37 (41.1%) had COVID-19 and 6 of them died (16,2%)[15]. At the moment of this study, the province of Guayas, where this clinic is located, reported 14728 confirmed cases with 1516 deaths in the general population[16].

We did not find any differences between survivors and non-survivors regarding age, arterial pressure, or weight. There were significant statistical differences between both arterial blood pressures before and after the disease. HD treatment generally reduces BP, and these reductions in BP

	Non-survivors n= 12 (31.6)		Survivors N=26 (68.4)		Total	p value*
	No.	%	No.	%		
Fever						
Yes	10	83.3	20	76.9	30	0.50
No	2	16.7	6	23.1	8	
Cough						
Yes	10	83.3	20	76.9	30	0.50
No	2	16.7	6	23.1	8	
Dyspnea						
Yes	11	91.7	23	88.5	34	
No	1	8.3	3	11.5	4	0.62
Headache						
Yes	1	8.3	3	11.5	4	0.62
No	11	91.7	23	88.5	34	
Diahrrea						
Yes	3	25,0	6	23,1	9	0.59
No	9	75,0	20	76,9	29	

*Fisher Test

Table 4. Comparison between proportions according symptoms of the two groups.

	No.	%
Amikacin	2	5.3
Cefazoline	11	28.9
Ceftiaxone	1	2.6
Ceftriaxone	4	10.5
Ciprofloxacine	8	21.1
Vancomicine	2	5.3
None	10	26.3
Total	38	100,0

Table 5. Antibiotics used during the disease. Frequencies and percentages of the most used antibotics.

are associated with intradialytic decreases in both body weight and plasma volume. These mild degrees of hypotension we have seen could be attributed to COVID-19 treatments as high doses of sedatives, positive pressure ventilation with high levels of positive end-expiratory pressure (PEEP), restrictive fluid management, and aggressive diuresis. Generally, weight gain is commonly observed in patients undergoing chronic hemodialysis; nevertheless, we observed decreased patients' weight after the disease.

We observed that more men than women get infected, consistent with some authors who have reported[17,18].

There was a statistically significant difference in the proportion of non survivors and survivors according to gender in our study. Older adults, men, and those with pre-existing comorbidities like hypertension and diabetes mellitus were highly prevalent. A similar pattern is reported from China[19].

We found that the most common symptoms at the beginning of the infection were dyspnea (89.4%), fever, and cough, with 78% consistent with other studies. In a retrospective study performed by Guan et al., including 1,099 patients with COVID19 respiratory disease, fever and cough were the most important symptoms, while vomiting and diarrhea were the less frequent[20]. Wang *et al.* reported that diarrhea (80%), fever (60%), and fatigue (60%) were the most common symptoms

in Hemodialysis five cases they studied[21]. The most common symptom reported were cough and dyspnea in a study performed by Jung *et al.*[22].

Some symptoms of COVID-19 disease may be difficult to distinguish from other symptoms common among patients receiving dialysis. According to Borges, hemodialysis patients have disorders of B- and T-cell function patients and they may have atypical presentations of the disease[23]. Freitas has appointed the same[24].

Hemodialysis population is vulnerable to COVID-19 pneumonia due to the presence of immunosuppression and the high prevalence of comorbid clinical conditions[25].

All our patients were receiving heparin, the most used anticoagulant during HD procedures, associated with a better prognosis in patients with COVID-19[26].

We initiated empiric therapy with antibiotics for possible co-infection, considering clinical judgment, the bacterial pathogens commonly isolated in our institution.

Limitations

Our study has some limitations; because it is a cross-sectional study, we cannot identify a causal relationship between the variables we have included in the study. Due to the retrospective study design, laboratory tests for diagnoses were not available in most patients. Small sample of patients.

Conclusions

Patients with SARS-CoV-2 infection were high in our institution as well as the mortality rate. Most of the infected patients were male. Further observational studies are required to clearly understand clinical evolution and the right diagnostic and treatment methods for COVID-19 disease in hemodialysis patients.

Author Contributions

MH, EF, MF, and FM worked on the design of the research. MH, FM, IF, YR, RC, CB, and EF were responsible for the data collection. MF, CB, EB, and EF were responsible for analyzing, interpreting, drafting, and revising the work. All authors participated in the interpretation and revision process of the manuscript. All authors gave their final approval of the version to be published.

Availability of data and materials

The datasets used and/or analyzed during the current study available from the corresponding author on reasonable request.

Conflict of Interest Statement

The authors declare that the research was conducted in the absence of any commercial or financial relationships that could be construed as a potential conflict of interest.

Funding

No funds received.

Bibliographic references

1. Perlman S. Another Decade, Another Coronavirus. N. Engl. J. Med. 2020 doi: 10.1056/NEJMe2001126.
2. Guan WJ, Zhong NS. Clinical Characteristics of Covid-19 in China. Reply.N Engl J Med. 2020 7 May; 382(19):1861-1862.
3. US Renal Data System. https://www.usrds.org/Default.aspx Accessed 3 March, 2020.
4. Saran R, Robinson B, Abbott KC, et al. US Renal Data System 2017 Annual Data Report: Epidemiology of Kidney Disease in the United States [published correction appears in Am J Kidney Dis. 2018 Apr;71(4):501]. Am J Kidney Dis. 2018;71(3 Suppl 1):A7. doi:10.1053/j.ajkd.2018.01.002
5. Meijers B, Messa P, Ronco C. Safeguarding the Maintenance Hemodialysis Patient Population during the Coronavirus Disease 19 Pandemic. Blood Purif. 2020;49(3):259- 264. doi:10.1159/000507537
6. Europa Press. El 1,3% de personas en diálisis o con trasplante renal están infectados de Covid-19. Infosalus (2020).
7. Sánchez-Álvarez JE, Pérez Fontán M, Jiménez Martín C, et al. SARS-CoV-2 infection in patients on renal replacement therapy. Report of the COVID-19 Registry of the Spanish Society of Nephrology (SEN) [published online ahead of print, 2020 16 April]. Situación de la infección por SARS-CoV-2 en pacientes en tratamiento renal sustitutivo. Informe del Registro COVID-19 de la Sociedad Española de Nefrología (SEN) [published online ahead of print, 2020 Apr 16]. Nefrologia. 2020;S0211-6995(20)30040-0. doi:10.1016/j.nefro.2020.04.002
8. Park HC, Lee YK, Lee SH, Yoo KD, Jeon HJ, Ryu DR, Kim SN, Sohn SH, Chun RW, Choi KB; Korean Society of Nephrology MERS-CoV Task Force Team: Middle East respiratory syndrome clinical practice guideline for hemodialysis facilities. Kidney Res Clin Pract 36: 111–116, 2017pmid:28680819
9. Syed-Ahmed M, Narayanan M. Immune dysfunction and risk of infection in chronic kidney disease. Adv Chronic Kidney Dis. 2019;26(1):8–15. [PubMed] [Google Scholar]
10. Betjes MG. Immune cell dysfunction and inflammation in end-stage renal disease. Nat Rev Nephrol. 2013;9(5):255–265
11. Centers for Disease Control and Prevention. Interim guidance for infection prevention and control recommendations for patients with suspected or confirmed COVID-19 in outpatient hemodialysis facilities. CDChttps://www.cdc.gov/coronavirus/2019-ncov/healthcare-facilities/dialysis.html (2020)
12. Goicoechea M, Sánchez Cámara LA, Macías N, Muñoz de Morales A, González Rojas Á, Bascuñana A, Arroyo D, Vega A, Abad S, Verde E, García Prieto AM, Verdalles U, Barbieri D, Felipe Delgado A, Carbayo J, Mijaylova A, Pérez de José A, Melero R, Tejedor A, Rodriguez Benitez P, de José AP, Rodriguez Ferrero ML, Anaya F, Rengel M, Barraca D, Luño J, Aragoncillo I. COVID-19: Clinical course and outcomes of 36 maintenance hemodialysis patients from a single center in Spain. Kidney Int. 2020 May 10;98(1):27–34. doi: 10.1016/j.kint.2020.04.031. Epub ahead of print. PMID: 32437770; PMCID: PMC7211728.
13. Ma Y, Diao B, Lv X, Zhu J, Liang W, Liu L, Bu W, Cheng H, Zhang S, Yng L, Shi M, Ding G, Shen B, Wang H. 2019 novel coronavirus disease in hemodialysis (HD) patients: Report from one HD center in Wuhan, China. medRxiv preprint 2020, doi: https://doi.org/https://doi.org/10.1101/2020.02.24.20027201-y.
14. Arslan H, Musabak U, Ayvazoglu Soy EH, et al. Incidence and Immunologic Analysis of Coronavirus Disease (COVID-19) in Hemodialysis Patients: A Single-Center Experience. Exp Clin Transplant. 2020;18(3):275-283. doi:10.6002/ect.2020.0194
15. Albalate M, Arribas P, Torres E, Cintra M, Alcázar R, Puerta M, Ortega M, Procaccini F, Martin J, Jiménez E, Fernandez I, de Sequera P; Grupo de Enfermería HUIL; Grupo enfermería HUIL. High prevalence of asymptomatic COVID-19 in haemodialysis: learning day by day in the first month of the COVID-19 pandemic. Nefrologia. 2020 May-Jun;40(3):279-286. English, Spanish. doi: 10.1016/j.nefro.2020.04.005. Epub 2020 Apr 30. PMID: 32456944; PMCID: PMC7190471.
16. Coronavirus COVID-19 – Ministerio de Salud Pública. https://www.salud.gob.ec/coronavirus-covid-19/.
17. Du X, Li H, Dong L, Li X, Tian M, Dong J. Clinical features of hemodialysis patients with COVID-19: a single-center retrospective study on 32 patients. Clin Exp Nephrol. 2020 May 27:1–7. doi: 10.1007/s10157-020-01904-w. Epub ahead of print. PMID: 32462378; PMCID: PMC7252511.

18. Trujillo H, Caravaca-Fontán F, Sevillano Á, Gutiérrez E, Caro J, Gutiérrez E, Yuste C, Andrés A, Praga M. SARS-CoV-2 Infection in Hospitalized Patients with Kidney Disease. Kidney Int Rep. 2020 May 1;5(6):905–9. doi: 10.1016/j.ekir.2020.04.024. Epub ahead of print. PMID: 32363253; PMCID: PMC7194060.
19. Zhou F, Yu T, Du R, et al. Clinical course and risk factors for mortality of adult inpatients with COVID-19 in Wuhan, China: a retrospective cohort study. Lancet. 2020;395(10229):1054-1062.
20. Guan W-j, Ni Z-y, Hu Y, et al; The China Medical Treatment Expert Group for Covid-19. Clinical characteristics of 2019 novel coronavirus infection in China. N Engl J Med. 2020;382: 1708-1720
21. Wang, Rui, Cong Liao, Hong He, Chun Hu, Zimeng Wei, Zixi Hong, Chengjie Zhang, Meiyan Liao, and Hua Shui. "COVID-19 in Patients: A Report of 5 Cases." American Journal of Kidney Diseases 76, no. 1 (2020): 141–43. https://doi.org/10.1053/j.ajkd.2020.03.009.
22. Jung H-Y, Lim J-H, Kang SH, Kim SG, Lee Y-H, Lee J, et al. Outcomes of COVID-19 among Patients on In-Center Hemodialysis: An Experience from the Epicenter in South Korea. Journal of Clinical Medicine 2020;9:1688.
23. Borges A, Borges M, Fernandes J. Apoptosis of peripheral CD4(+) T-lymphocytes in end-stage renal disease patients under hemodialysis and rhEPO therapies. Ren Fail. 2011;33(2):138–143.
24. Freitas GRR, da Luz Fernandes M, Agena F. Aging and end stage renal disease cause a decrease in absolute circulating lymphocyte counts with a shift to a memory profile and diverge in Treg population. Aging Dis. 2019;10(1):49–61
25. Tang B, Li S, Xiong Y, Tian M, Yu J, Xu L, Zhang L, Li Z, Ma J, Wen F, Feng Z, Liang X, Shi W, Liu S. Coronavirus Disease 2019 (COVID-19) Pneumonia in a Hemodialysis Patient. Kidney Med. 2020 12 March. doi: 10.1016/j.xkme.2020.03.001. Epub ahead of print. PMID: 32292904; PMCID: PMC7103984.
26. Tang N, Bai H, Chen X, Gong J, Li D, Sun Z. Anticoagulant treatment is associated with decreased mortality in severe coronavirus disease 2019 patients with coagulopathy. J Thromb Haemost. 2020;18:1094–9. http://dx.doi.org/10.1111/jth.14851.

Received: 30 December 2020
Accepted: 15 February 2021

REVIEW / ARTÍCULO DE REVISIÓN

Biorremediación de carbamazepina por hongos y bacterias en aguas residuales

Bioremediation of carbamazepine by fungi and bacteria in wastewater

Leslie Tatiana Morales[1], Gabriela Inés Méndez[2*]

DOI. 10.21931/RB/2021.06.02.28

Resumen: La carbamazepina (CBZ), un fármaco psiquiátrico, antiepiléptico; mayormente utilizado en la actualidad para tratar enfermedades como la epilepsia y neuralgia del trigémino; es un contaminante emergente, considerado como una fuente importante de contaminación de fuentes hídricas, al no ser totalmente metabolizado por el organismo y ser excretado por vía urinaria y fecal, sin cambios o en forma de metabolitos conjugados. Estos contaminantes pasan por tratamientos de aguas residuales, sin embargo, los tratamientos convencionales no son capaces de degradarlo, produciendo daños a los seres vivos que habitan y necesitan de este recurso natural para poder sobrevivir. Frente a este problema, el objetivo de esta revisión fue identificar tratamientos biológicos con la utilización de microorganismos (bacterias y hongos) para la degradación de este compuesto recalcitrante. Los microorganismos identificados con mayor porcentaje de degradación de carbamazepina fueron *Labrys portucalensis* F11 y *Trametes versicolor*; la primera una bacteria que se adapta a diferentes fuentes de carbono; y el segundo un hongo denominado de pudrición de la madera, que presenta enzimas oxidativas que le permiten degradar una amplia gama de contaminantes emergentes. *Trametes versicolor*, es el microorganismo mayormente estudiado para los procesos de degradación de carbamazepina, con porcentajes de degradación de hasta el 94% a una temperatura de 25°C y un pH de 4.5.

Palabras clave: Aguas residuales, degradación, carbamazepina, microorganismos.

Abstract: Carbamazepine (CBZ), a psychiatric, antiepileptic drug; currently mainly used to treat diseases such as epilepsy and trigeminal neuralgia, it is an emerging pollutant, considered an essential source of contamination of water sources because of it is not fully metabolized by the body and is excreted via the urinary and fecal routes, unchanged or in the form of conjugated metabolites. These pollutants go through wastewater treatment; however, conventional treatments cannot degrade them, causing damage to the living beings that inhabit and need this natural resource to survive. Faced with this problem, this review's objective was to identify biological treatments with the use of microorganisms (bacteria and fungi) for the degradation of this recalcitrant compound. The microorganisms with the highest percentage of carbamazepine degradation identified were *Labrys portucalensis* F11 and *Trametes versicolor*; the first a bacterium that adapts to different carbon sources; and the second a so-called wood rot fungus, which has oxidative enzymes that allow the degradation of a wide range of emerging pollutants. *Trametes versicolor*, is the microorganism most studied for carbamazepine degradation processes, with degradation percentages of up to 94% at a temperature of 25 ° C and a pH of 4.5.

Key words: Degradation, microorganisms, carbamazepine, sewage water.

Introducción

Los contaminantes emergentes son compuestos de alta persistencia y baja degradación en el medio ambiente; considerados de distinto origen y naturaleza química, por lo que han pasado desapercibidos, hasta hace poco. Sin embargo, estos contaminantes no son nuevos, han estado presentes en el medioambiente, pero no se les había dado la importancia necesaria ya que aún no eran evaluados y no se conocía sus efectos toxicológicos[1-2].

Existen dos grupos de sustancias catalogadas como contaminantes emergentes; los productos de aseo y cuidado personal; y los fármacos[3]. Los productos de aseo, empleados para desinfectar áreas o materiales inertes, pueden provocar alteraciones en el comportamiento y desarrollo de los organismos, incluso si se llegan a encontrar en pequeñas concentraciones en el medio ambiente; los fármacos por otra parte, son utilizados para combatir o prevenir enfermedades, los cuales se liberan al medio ambiente por excreción, vertido de productos caducados y residuos de procesos de fabricación; es por ello que pueden estar presentes en todas las etapas del ciclo de vida del agua[4].

La carbamazepina (CBZ), 5H-dibenzazepina-5-carboxamida, un producto farmacéutico, el cual es utilizado para el tratamiento de enfermedades como la epilepsia, neuralgia del trigémino, depresión y trastornos bipolares[5]; es un compuesto de difícil remoción, puesto que se ha encontrado que la carbamazepina es persistente y solo se logra remover valores menores[6]. Después de la administración de este medicamento a un paciente, se metaboliza en el hígado por la enzima CYP3A4 y es excretado del cuerpo vía urinaria y fecal[5]. "Aproximadamente el 72% de la carbamazepina administrada por vía oral es absorbida, mientas el 28% es descargado sin cambios a través de las heces"[6]. Una vez excretados ingresan a las plantas de tratamiento de aguas residuales, sin embargo, estos compuestos no son eliminados en su totalidad por tratamientos convencionales, lo que representa un alto riego, dado que al encontrarse presente en el ambiente se la ha asociado con la producción de efectos mutagénicos y teratogénicos en los seres vivos[7].

Procesos fisicoquímicos como la coagulación-floculación y flotación no han dado buenos resultados en cuanto a la degradación, obteniendo valores entre 20 a 35 %. Los procesos de oxidación avanzada (ozonización), la degradación fotolítica

[1] Universidad Politécnica Salesiana, Quito, Ecuador.
[2] Universidad Politécnica Salesiana, Grupo de investigación BIOARN, Quito, Ecuador.

Corresponding author: gmendez@ups.edu.ec

(UV- 29 H2O2) degradación fotocatalítica (TiO2) dan altos porcentajes de degradación (>90%), pero su principal limitante es el hecho que dan lugar a productos tóxicos, afectando de igual forma al medio ambiente[6].

Sin embargo, se ha observado que hongos y bacterias, tales como hongos de pudrición blanca y *Pseudomonas* están involucrados en la biodegradación de carbamazepina y otros compuestos recalcitrantes, por su versatilidad metabólica, con menor impacto ambiental[7].

Por todo lo anteriormente mencionado, la degradación de carbamazepina se ha convertido en un tema de preocupación para el medio ambiente, por lo que en esta revisión se plantea como objetivo identificar hongos y bacterias involucradas en la biorremediación de la carbamazepina, referenciados en la literatura científica, que sirva como guía para posteriores investigaciones sobre el tema.

Contaminación del agua con carbamazepina

El agua es un recurso natural imprescindible para la vida de los seres vivos, que se ha visto afectado por el rápido desarrollo humano, económico y por el uso inadecuado[8]. Por años toneladas de sustancias biológicamente activas, utilizadas en la medicina, han sido dispersadas al medio ambiente sin un tratamiento adecuado y sin pensar en las posibles consecuencias que esto trae en el presente y en el futuro a los seres vivos[9].

Los medicamentos cuya función es tratar, prevenir y mitigar enfermedades, también forman parte de los contaminantes del agua; por ello es un tema de preocupación, ya que no logran ser eliminados en las plantas de tratamientos de agua, por lo que pueden causar afectaciones a los seres vivos[8].

Los fármacos más empleados son los analgésicos, antinflamatorios y antiepilépticos; los cuales son eliminados en los excrementos e ingresan a las aguas residuales, donde se almacenan como contaminantes[9]. La carbamazepina (CBZ), un fármaco psiquiátrico, antiepiléptico, resistente a la biodegradación; no es metabolizado completamente por el hígado, por lo que es eliminado en la orina y las heces fecales, permaneciendo en el ambiente hasta 100 días, lo que lo ha convertido en un marcador de contaminación del agua[5].

Los tratamientos convencionales de depuración de aguas residuales no están diseñados para tratar contaminantes farmacéuticos, identificándose la presencia de estos al final del proceso, lo que indica que sus metabolitos son descargados al medio ambiente[2]. Gracias a tecnologías avanzadas se ha podido detectar y cuantificar este tipo de contaminantes que se encuentran en las fuentes de agua; encontrando concentraciones que varían entre los ng/L a los µg/L, lo cual muestra el carácter persistente y no biodegradable de estos fármacos[10,11].

En el caso de la carbamazepina un medicamente antiepiléptico y psiquiátrico, al estar presente en el agua, produce algunos efectos negativos, como son problemas ecotóxicos, mutágenos, teratogénicos, alteraciones del sistema reproductivo femenino y masculino, disrupción endocrina, alteración en los mecanismos de defensa inmunológica, entre otros, sobre las especies acuícolas y el ser humano[12]. Por todos los efectos mencionados anteriormente, es necesario estudiar e investigar microorganismos degradadores que reduzcan el impacto ambiental y el proceso más eficaz para llevar a cabo el mismo.

Microorganismos utilizados en biodegradación de carbamazepina

Existen varios microorganismos estudiados para la degradación de carbamazepina, que se resumen en la (Figura 1), como son: los de pudrición blanca que atacan a la madera y degradan la lignina (*Trametes versicolor, Ganoderma lucidum, Irpex lacteus, Stropharia rugosoannulata, Gymnopilus luteofolius y Agrocybe erebia, Pleurotus ostreatus y Phanerochaete chrysosporium, Trichoderma harzianum*). También se emplean bacterias como *Pseudomonax putida* y *Labrys portucalensis F11*, que se adaptan a varias condiciones del ambiente, por lo que son capaces de degradar hidrocarburos y otros compuestos aromáticos para su crecimiento y mantenimiento[13].

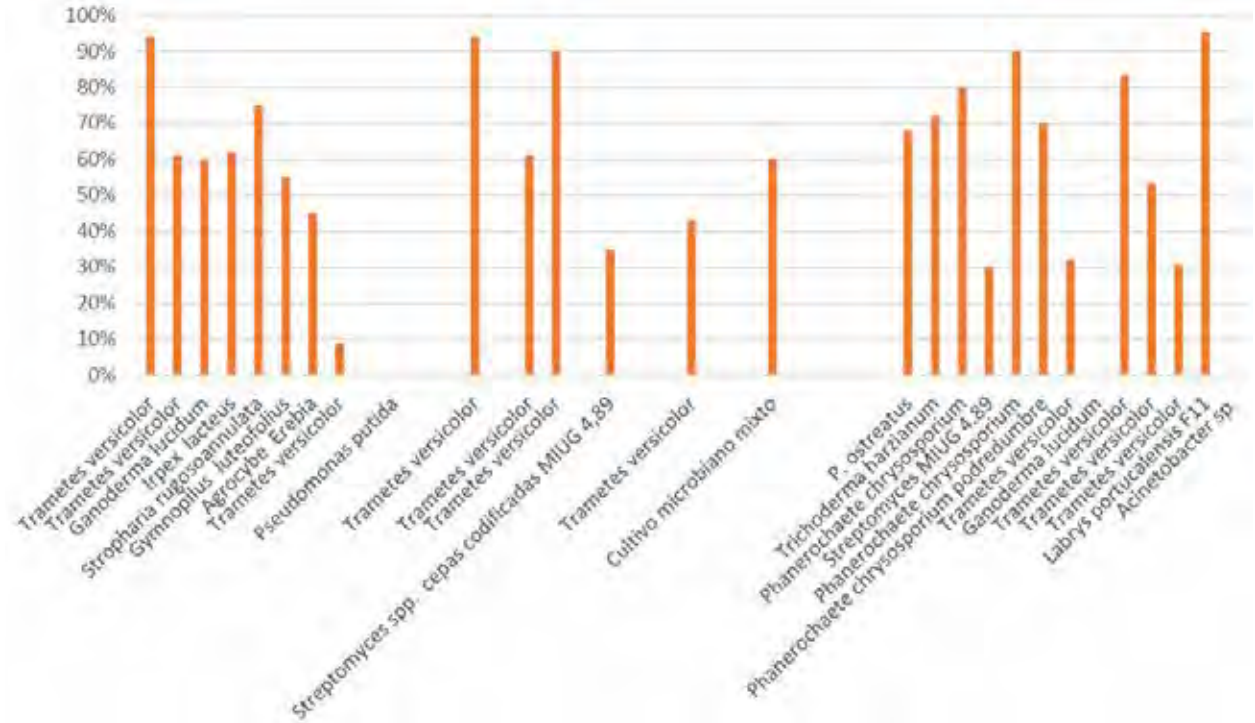

Figura 1. Microorganismos vs porcentaje de degradación. Fuente: tomado de Castellet-Rovira *et al*[28]; Rodríguez *et al*[36]; Forrez *et al*[29]; Jelic *et al*[37]; Cruz-Morató *et al*[38]; Popa *et al*[39]; Rodríguez-Rodríguez *et al*[40]; Ha *et al*[42,43,44,45,46,47]; Vasiliadou *et al*[48]; Cruz *et al*[49,50]; Bessa *et al*[27,30].

Hongos de pudrición blanca

Los hongos más importantes que han sido identificados con capacidad de degradación de carbamazepina, son *Trametes versicolor, Ganoderma lucidum, Irpex lacteus, Stropharia rugosoannulata, Gymnopilus luteofolius, Agrocybe erebia, Pleurotus ostreatus* y *Phanerochaete chrysosporium*. Estos hongos pertenecen a la clase Basidiomicetes, se localizan en tejidos vegetativos y poseen un grupo de enzimas conocidas como ligninasas o enzimas lignolíticas, capaces de degradar compuestos orgánicos persistentes como la lignina de la madera. La lignina es la encargada de darle el color marrón, que al ser degradada por estos hongos se va enriqueciendo en celulosa, cuyo color es blanco y de ahí el nombre de este tipo de pudrición 14 (Figura 2).

Figura 2. Hongo de pudrición blanca (*Trametes versicolor*).

Estos hongos presentan tres mecanismos de biodegradación, dos oxidativos y uno reductivo: el primero para degradar la lignina mediante ataques oxidativos por medio de enzimas ligninolíticas peroxidasas; en el segundo intervienen las enzimas citocromo P-450 monooxigenasas y en el reductivo las enzimas catalizan reacciones de conjugación[15]. Es decir, estos mecanismos no utilizan los contaminantes como sustratos, sino que los degradan por cometabolismo[15].

La lignina peroxidasa oxida compuestos aromáticos no fenólicos; el manganeso peroxidasa y la lacasa catalizan la oxidación de aminas y oxidan compuestos no fenólicos; en la madera su función es comenzar el ataque a la lignina mediante fuertes oxidaciones. Las reacciones que llevan a cabo estas enzimas son inespecíficas dado que se ha visto que pueden atacar no solo la lignina sino una amplia variedad de compuestos aromáticos, incluso varios de los que constituyen serios problemas de contaminación como la carbamazepina[16].

Trichoderma harzianum

Es un hongo Deuteromicete, perteneciente a los mohos, predomina en ecosistemas terrestres, bosques, pastizales, desiertos, y se caracteriza por poseer enzimas hidrolíticas y quitinolíticas[17].

Este hongo es metabólicamente versátil, ya que puede utilizar sucrosa, rafinosa, polisacáridos, y sustratos más complejos como compuestos orgánicos, lo que permite que contribuyan en la degradación de estos[18]. No se alimentan de la celulosa y lignina, por lo que no provocan daños en la madera, pero si crean un ambiente favorable para el desarrollo de los hongos de pudrición[18].

***Labrys portucalensis* F11**

Una bacteria aerobia de la clase Alphaproteobacteria, gram negativa, no es móvil y no presenta esporas. Sus colonias son circulares, convexas y de consistencia mucosa[19]. Esta bacteria es aislada de suelos contaminados, que puede utilizar varios compuestos orgánicos como fuentes de carbono y energía, como el benceno, fenol, citrato, metilamina, entre otros; por lo que puede ser empleada para estudios de degradación de contaminantes del ambiente[19]. Según Aparicio[20] se ha observado que el proceso de degradación es iniciado por las enzimas citocromo P450 mono y dioxigenasas.

Acinetobacter sp.

Es una bacteria gram negativa, aeróbica, inmóvil, no es fermentativa, y no esporulada[21], aprovecha una variedad de fuentes de carbono y energía, lo que le permite sobrevivir en la naturaleza; es resistente a múltiples fármacos, mediante la producción de β-lactamasas[22].

Pseudomonas putida

Es una bacteria gram negativa, aerobia, produce un pigmento azul, vive en suelos y aguas, y se adapta a varias condiciones del ambiente, por lo que son capaces de degradar hidrocarburos para su crecimiento y mantenimiento[13]. En cuanto a sus requerimientos nutricionales, utiliza diferentes fuentes de carbono y nitrógeno según el ambiente en donde se desarrolle y posee una gran capacidad degradadora de compuestos aromáticos y xenobióticos, que resultan tóxicos y contaminantes[23]; esta característica se debe a la presencia de enzimas como catalasa, proteasa, gelatinasa, celulasa y pectinasa[24]. Por ello esta bacteria se emplea en tareas de biorremediación de derivados del petróleo y de la industria química.

Streptomyces spp.

Bacteria del género actinobacterias, aerobia, gram positiva[25]. Forman un complejo micelio de sustrato que ayuda a eliminar compuestos orgánicos de sustratos. Reduce nitratos a nitritos y degrada sustratos poliméricos, por la presencia de enzimas celulolíticas. Se encuentra predominantemente en suelos y en la vegetación descompuesta[26].

Biodegradación de carbamazepina

En la (Tabla 1, Figura 1), se puede visualizar los porcentajes de degradación de carbamazepina de los microrganismos más utilizados; pudiendo identificar como uno de los mejores microorganismo a la bacteria *Labrys portucalensis*, con un porcentaje de degradación del 95%, utilizando a la carbamazepina como fuente de carbono principal[27]. Según Castellet-Rovira *et al.*[27] y Jelic *et al.*[28] el hongo *Trametes versicolor* también presenta un alto porcentaje de degradación, de hasta el 94%, utilizando la glucosa como fuente de carbono principal y la CBZ como co-metabolito. Por otro lado, los microorganismos *Pseudomonas putida* y *Acinetobacter sp*, presentan un bajo porcentaje de degradación, con valores del 0% según Forrez *et al.*[29] Wang[30].

El hongo *Trametes versicolor* es el microorganismo mayormente evaluado para la degradación de carbamazepina por tener una adecuada eficiencia en la remoción de este, demostrando altos porcentajes en estudios de degradación de contaminantes[31] (Tabla 2, Figura 3). Una característica morfológica destacable de este hongo es la envoltura hifal extracelulares, compuestas de membrana y β-1, 6-1, 3 glucanos; que son importantes en la degradación, pero su función específica aún no se conoce[32].

Su capacidad degradadora en la madera, es uno de los aspectos que sorprende en este tipo de hongos; puesto que la madera no es un material de fácil degradación; esta resistencia se debe a la composición química: celulosa (40-50%), hemicelulosa (25-40%) y lignina (20-35%); estos hongos al encontrarse en la madera primero degradan la lignina para ob-

Microorganismo degradador	Porcentaje de degradación	País	Fuente
Trametes versicolor	94% - 9 mg/L	España	[28]
Trametes versicolor	61% - 50 mg/L		
Ganoderma lucidum	60%		
Irpex lacteus	62%		
Stropharia rugosoannulata	75%		
Gymnopilus luteofolius	55%		
Agrocybe Erebia	45%		
Trametes versicolor	9%	España	[36]
Pseudomonas putida	No hubo cambios	España	[29]
Trametes versicolor	94% - 9 mg/L	España	[37]
Trametes versicolor	61% - 50ug/L		
Trametes versicolor	80-100%	España	[38]
Streptomyces spp. cepas codificadas MIUG 4,89	35%	Romania	[39]
Trametes versicolor	43%	España	
Cultivo microbiano mixto (*Acinetobacter sp. US1, Bacillus halodurans, Micrococcus sp. SBS-8, Pseudomona sp. Putida*)	60%	España	[42]
P. ostreatus	68%	Italia	[43]
Trichoderma harzianum	72%		
Phanerochaete chrysosporium	80%	China	[44]
Streptomyces MIUG 4.89	30%	Romania	[45]
Phanerochaete chrysosporium	90%	China	[46]
Phanerochaete chrysosporium podredumbre	60-80%	Germany	[47]
Trametes versicolor	32%	España	[48]
Ganoderma lucidum			
Trametes versicolor	Biorreactor estéril: 83,2%	España	[49]
Trametes versicolor	Biorreactor no estéril: 53,3%		
Trametes versicolor	30,70%	España	[50]
Labrys portucalensis F11	95%	Portugal	[27]
Acinetobacter sp.	No puede degradar	China	[30]

Tabla 1. Microorganismos y porcentaje de degradación.

Microorganismo degradador	Porcentaje de degradación	Fuente
Trametes versicolor	94%	[28]
Trametes versicolor	61%	
Trametes versicolor	9%	[36]
Trametes versicolor	94%	[37]
Trametes versicolor	61%	
Trametes versicolor	90%	[38]
Trametes versicolor	43%	[40]
Trametes versicolor	32%	[48]
Trametes versicolor	83%	[49]
Trametes versicolor	53%	
Trametes versicolor	30,70%	[50]

Tabla 2. *Trametes versicolor* y porcentaje de degradación.

tener energía y fuente de carbono para su desarrollo, y de esta forma acceder a la hemicelulosa y celulosa[32]. La hemicelulosa y la celulosa mantienen la producción de enzimas en procesos de biorremediación; todo esto ha conllevado a pensar que es capaz de degradar compuestos recalcitrantes, gracias a la presencia de enzimas oxidativas y reductivas no específicas; lo que le da una inespecificidad al sustrato, permitiendo utilizar estos microorganismos para degradar una amplia gama de contaminantes orgánicos[15].

Trametes versicolor ha sido empleado en procesos de degradativos con diferentes modos de operación; algunos estudios utilizan biorreactores de escala industrial y otros se realizan a nivel de laboratorio, es decir a pequeña escala en cajas Petri con medios de cultivo apropiados. Entre estos se ha observado algunos estudios, que obtienen un 94-95% de degradación empleando un biorreactor fluidizado[26,28]. El biorreactor fluidizado, empleado en los estudios investigativos, se maneja ampliamente en las industrias de procesos químicos; el cual permite una mezcla homogénea entre las partículas y el fluido, a velocidades superiores a la de fluidización; este proceso da lugar a ventajas con respecto a otros, puesto que permite tener mezclas sólidas rápidas, uniformidad en cuanto a la temperatura y composición; por estas características mencionadas, se asume que permite una apropiada degradación de contaminantes; a más de presentar los condiciones adecuadas para el desarrollo y mantenimiento de los microorganismos[33].

Otro aspecto de gran relevancia son las condiciones del medio de cultivo y parámetros ambientales utilizados durante los ensayos de degradación. Para *Trametes versicolor* en la mayoría de los ensayos se utiliza el medio Kirk, según Márquez[34], es un medio limitante en nitrógeno, que provoca un estrés en el hongo y hace que expulse al medio extracelular enzimas lignolíticas para degradar los nutrientes.

La temperatura y el pH son factores primordiales para el correcto desarrollo del microorganismo, para *Trametes versicolor*, las condiciones ambientales identificadas por varios estudios (Tabla 3) como las más adecuadas son: temperatura de 25°C y 4.5 de pH. En otras investigaciones, los rangos óptimos para este hongo son de 22-30°C[34] y el pH menor a 3.5, lo que produce repulsión electrostática entre los iones de la pared del hongo y el contaminante; si es superior a 4 y menor a 6, da paso al acercamiento de la pared con el contaminante[35]. La variación de estos valores puede influir en la producción de enzimas ligninolíticad, el pH inadecuado altera la estructura tridimensional de la enzima y la variación de temperatura perturba el metabolismo del microorganismo causando la inhibición en el crecimiento y la generación de enzimas[32].

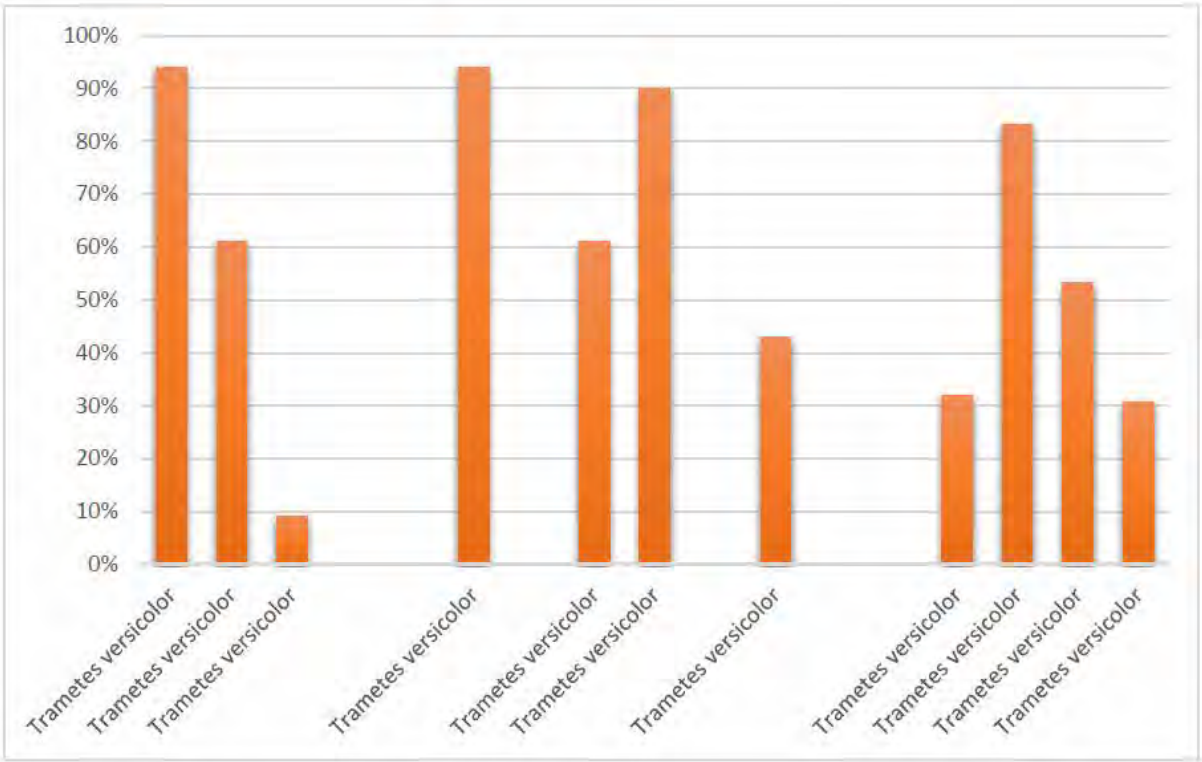

Figura 3. Porcentajes de degradación de carbamazepina (CBZ) mediante el uso de *Trametes versicolor*. Fuente: tomado de Castellet-Rovira *et al*[28]; Rodríguez *et al*[36]; Jelic *et al*[37]; Cruz-Morató *et al*[38]; Rodríguez-Rodríguez *et al*[40]; Vasiliadou *et al*[48]; Cruz *et al*[49,50].

Conclusiones

Los tratamientos de aguas residuales no son capaces de disminuir la concentración de los contaminantes emergentes, como la carbamazepina; por lo que se ha optado por tratamientos alternativos con microorganismos.

Labrys portucalensis F11 y *Trametes versicolor* muestran un elevado porcentaje de degradación frente a la carbamazepina, con 95% y 94% respectivamente; siendo *Trametes versicolor* el microorganismo mayormente estudiado para los procesos de degradación de carbamazepina, presentando mejores resultados a una temperatura de 25°C y un pH de 4.5. Por otro lado, los microorganismos identificados con una menor degradación son *Acinetobacter sp.* a un pH de 7 y *Pseudomonas putida* con un pH de 6,8; sin resultados positivos.

Referencias bibliográficas

1. Castillos J, Caixach J. Contaminantes emergentes en el siglo XXI. Rev Digit Univ [Internet]. 2016;Volumen 10:1067–6079. Available from: http://www.ecorfan.org/spain/researchjournals/Ciencias_Ambientales_y_Recursos_Naturales/vol2num5/Revista_de_Ciencias_Ambientales_y_Recursos_Naturales_V2_N5_1.pdf
2. Arbeláez P. Contaminantes emergentes en aguas residuales y de río y fangos de depuradora [Internet]. Universitat Rovira i Virgili; 2015. Available from: https://www.tdx.cat/bitstream/handle/10803/334397/Tesi Paula.pdf?sequence=1
3. Salibián A. Los Fármacos como Contaminantes Emergentes de los Ambientes Acuáticos. Rev Farm. 2014;156(1–2):76–92.
4. Quesada I, Jáuregui U, Wilhelm A-M, Delmas H. Contaminación de las aguas con productos farmacéuticos . Estrategias para enfrentar la problemática. Rev CENIC Ciencias Biológicas [Internet]. 2009;40(3):173–80. Available from: http://www.scielosp.org/pdf/bwho/v78n9/v78n9a05.pdf
5. González A. Alteraciones bioquímicas y fisiológicas causadas por ibuprofeno y carbamazepina en juveniles de Solea senegalensis : efecto modulador de la temperatura [Internet]. Universidad de Valencia; 2017. Available from: https://core.ac.uk/download/pdf/84751237.pdf
6. Martínez A. Cuantificación de carbamazepina en efluentes hospitalarios por cromatografía de líquidos de alta resolución y determinación de la cinética de degradación [Internet]. Universidad Autónoma del Estado de México; 2013. Available from: https://core.ac.uk/reader/55519035
7. Rubio J. Avances en el metabolismo del ácido fenilacético en ´´Pseudomonas sp. Y2´´: aproximación genética y proteómica. [Internet]. Universidad Complutense de Madrid; 2009. Available from: https://dialnet.unirioja.es/servlet/tesis?codigo=91575
8. Hernando N. Estudio de la eliminación de Diclofenaco en aguas residuales mediante fotocatálisis heterogénea con TiO2 [Internet]. Repositorio insitucional: uvadoc.uva.es. Universidad de Valladolid; 2017. Available from: http://uvadoc.uva.es/handle/10324/26959
9. Barceló D, López M. Contaminación y calidad química del agua: el problema de los contaminates emergentes. Inst Investig Químicas y Ambient [Internet]. 2007;4(2):125–8. Available from: https://fnca.eu/phocadownload/P.CIENTIFICO/inf_contaminacion.pdf
10. Varo P, López C, Cases V, Ramírez M. Presencia contaminantes emergentes en aguas naturales [Internet]. Universidad d' Alacant; 2016. Available from: http://www.agroambient.gva.es/documents/163005665/163975683/UA_Presencia+contaminantes+emergentes+en+aguas+naturales.pdf/bd71c431-e80b-4810-9870-03fad0420fa4
11. Gil M, Soto M, Usma J, Gutiérrez D. Contaminantes emergentes en aguas, efectos y posibles tratamientos. 2012;7(2):52–73. Available from: http://www.scielo.org.co/pdf/pml/v7n2/v7n2a05.pdf
12. Moreno V, Martínez J, Kravzov J, Pérez L, Moreno C, Altagracia M. Los medicamentos de receta de origen sintético y su impacto en el medio ambiente. Rev Mex Ciencias Farm [Internet]. 2013;44(4):17–29. Available from: http://www.scielo.org.mx/scielo.php?pid=S1870-01952013000400003&script=sci_abstract
13. González R. Salicylic acid biodegradation by Pseudomonas putida : Effect of particulate materials, microorganisms and other substrates [Internet]. University of Oviedo; 2016. Available from: http://digibuo.uniovi.es/dspace/bitstream/10651/38783/1/TD_RosanaGonzalezCombarros.pdf
14. Camacho R, Gerardo J, Navarro K, Sánchez J. Producción de enzimas ligninolíticas durante la degradación del herbicida paraquat por hongos de la pudrición blanca. Rev Argent Microbiol [Internet]. 2017;(xx):4–11. Available from: http://dx.doi.org/10.1016/j.ram.2016.11.004
15. Quintero J. Revisión : Degradación de Plaguicidas Mediante Hongos de la Pudrición Blanca de la Madera. 2011;64(1):5867–82. Available from: http://www.scielo.org.co/pdf/rfnam/v64n1/a12v64n01.pdf
16. Simbaña C. Biorremediación de suelos contaminados con hidrocarburos de la parroquia Taracoa en Francisco de Orellana, mediante el hongo Pleurotus ostreatus [Internet]. Universidad Politécnica de Chimborazo; 2016. Available from: http://dspace.espoch.edu.ec/bitstream/123456789/4916/1/236T0192.pdf
17. Argumedo R, Alarcón A, Ferrera R, Peña J. El género fúngico Trichoderma y su relación con contaminantes orgánicos e inorgánicos. 2009;25(4):257–69. Available from: http://www.scielo.org.mx/pdf/rica/v25n4/v25n4a6.pdf
18. Hernández D, Ferrera R, Alarcón A. Trichoderma: Importancia agrícola, biotecnológica y sistemas de fermentación para producir biomasa y enzimas de interés industrial. 2019; Available from: https://scielo.conicyt.cl/pdf/chjaasc/v35n1/0719-3890-chjaasc-00205.pdf
19. Carvalho M, Marco P, Duque A, Pacheco C, Janssen D, Castro P. Labrys portucalensis sp . nov ., a fluorobenzene- degrading bacterium isolated from an industrially contaminated sediment in northern Portugal. 2008;692–8. Available from: https://www.semanticscholar.org/paper/Labrys-portucalensis-sp.-nov.%2C-a-bacterium-isolated-Carvalho- Marco/e441a260d006ad1067cffe438c4fba3b87d1afda
20. Aparicio M. Aislamiento de microorganismos capaces de crecer en presencia de diclofenaco a partir de suelo de humedales artificiales [Internet]. Vol. 4, Insitituto de Ciencias. Benemérita Universidad Autónoma de Puebla; 2019. Available from:https://repositorioinstitucional.buap.mx/bitstream/handle/20.500.12371/4808/845319T.pdf?sequence=1
21. Rodriguez R, Bustillo D, Caicedo D, Cadena D, Castellanos C. Acinetobacter baumannii : patógeno multirresistente emergente. 2016;29(2). Available from: http://www.scielo.org.co/pdf/muis/v29n2/v29n2a11.pdf
22. Rada J. Acinetobacter un patógeno actual. 2016;55(1):29–48. Available from: http://www.scielo.org.bo/pdf/rbp/v55n1/v55n1_a06.pdf
23. Lacal J. Caracterización bioquímica y moloecular del sistema de dos componentes TODS/TODT de Pseudomonas putida DOT-T1E [Internet]. Universidad de Granada; 2008. Available from: https://dialnet.unirioja.es/servlet/tesis?codigo=71636
24. Vertus D, Ruíz M, Henriquéz J, Ortíz V. Blodegradación bacteriana de Polietileno y propuesta de aplicación en Cerro Patacón. 2017;1(1):1–6. Available from: https://www.researchgate.net/publication/318315747_Biodegradacion_bacteriana_de_polietileno_y_propuesta_de_aplicacion_para_Cerro_Patacon
25. Tarazona U. Caracterización de actinomicetos de sedimento marino y su potencial actividad antagonista frente a Vibrio sp . aislados de Litopenaeus vannamei [Internet]. 2017. Available from: http://cybertesis.unmsm.edu.pe/bitstream/handle/cybertesis/5704/Tarazona_ju.pdf?sequence=3&isAllowed=y
26. Gutierrez C. Aislamiento , caracterización y evaluación de la capacidad antimicrobiana de actinomicetos asociados a hormigas cortadoras de hojas (Formicidae : Myrmicinae : Attini) [Internet]. Universidad Nacional Mayor San Marcos; 2017. Available from: http://cybertesis.unmsm.edu.pe/bitstream/handle/cybertesis/7092/Gutierrez_ec.pdf?sequence=1
27. Bessa V, Moreira I, Murgolo S, Mascolo G, Castro P. Carbamazepine is degraded by the bacterial strain Labrys portucalensis F11. Sci Total Environ [Internet]. 2019;690:739–47. Available from: https://doi.org/10.1016/j.scitotenv.2019.06.461

28. Castellet-Rovira F, Lucas D, Villagrasa M, Rodríguez-Mozaz S, Barceló D, Sarrà M. Stropharia rugosoannulata and Gymnopilus luteofolius: Promising fungal species for pharmaceutical biodegradation in contaminated water. J Environ Manage [Internet]. 2018;207:396–404. Available from: http://www.sciencedirect.com/science/article/pii/S030147971730734X
29. Forrez I, Carballa M, Fink G, Wick A, Hennebel T, Vanhaecke L, et al. Biogenic metals for the oxidative and reductive removal of pharmaceuticals, biocides and iodinated contrast media in a polishing membrane bioreactor. Water Res [Internet]. 2011;45(4):1763–73. Available from: https://www.scopus.com/inward/record.uri?eid=2-s2.0-78651468366&doi=10.1016%2Fj.watres.2010.11.031&partnerID=40&md5=6c4a128d6ecb39af2f4ec54521467005
30. Wang S, Hu Y, Wang J. Biodegradation of typical pharmaceutical compounds by a novel strain Acinetobacter sp. J Environ Manage [Internet]. 2018;217:240–6. Available from: https://doi.org/10.1016/j.jenvman.2018.03.096
31. Kuhar F, Castiglia V, Papinutti L. Reino Fungi : morfologías y estructuras de los hongos. Rev Boletín Biológica. 2013;28(January):11–8.
32. Chaparro D, Rosas D. Aislamiento y evaluación de la actividad enzimática de hongos descomponedores de madera en la Reserva natural La Montaña del Ocaso, Quimbaya - Quindío [Internet]. Vol. 30, Motivation and Emotion. 2006. Available from: https://repository.javeriana.edu.co/handle/10554/8268
33. Baxter R, Hastings N, Law A, Glass E. Biorreactores. Anim Genet. 2008;39(5):561–3.
34. Márquez S. Producción de lacasa a partir de hongos ligninolíticos utilizando vinazas y bagazo de origen mezcalero [Internet]. Universidad Tecnológica de la Mixteca; 2015. Available from: http://jupiter.utm.mx/~tesis_dig/12566.pdf
35. Colquier G. Evaluación de crecimiento de micelio de hongos de pudrición blanca con capacidad para biodegradar en condiciones de laboratorio [Internet]. 2017. Available from: https://www.unas.edu.pe/web/sites/default/files/web/archivos/actividades_academicas/EVALUACIÓN%2520DE%2520CRECIMIENTO%2520DE%2520MICELIO%2520DE%2520HONGOS%2520DE%2520PUDRICIÓN%25
36. Rodríguez C, Jelić A, Pereira M, Sousa D, Petrović M, Alves M, et al. Bioaugmentation of sewage sludge with Trametes versicolor in solid-phase biopiles produces degradation of pharmaceuticals and affects microbial communities. Environ Sci Technol [Internet]. 2012;46(21):12012–20. Available from: https://www.scopus.com/inward/record.uri?eid=2-s2.0-84868553742&doi=10.1021%2Fes301788n&partnerID=40&md5=a65b8345a8993372bbdddb70d2a498c6
37. Jelic A, Cruz-Morató C, Marco-Urrea E, Sarrà M, Perez S, Vicent T, et al. degradation of carbamazepine by Trametes versicolor in an air pulsed fluidized bed bioreactor and identification of intermediates. Water Res [Internet]. 2012;46(4):955–64. Available from: https://www.scopus.com/inward/record.uri?eid=2-s2.0-84856085194&doi=10.1016%2Fj.watres.2011.11.063&partnerID=40&md5=23c688b23e0f7973b1563162e533a86e
38. Cruz-Morató C, Ferrando-Climent L, Rodriguez-Mozaz S, Barceló D, Marco-Urrea E, Vicent T, et al. degradation of pharmaceuticals in non-sterile urban wastewater by Trametes versicolor in a fluidized bed bioreactor. Water Res [Internet]. 2013;47(14):5200–10. Available from: https://www.scopus.com/inward/record.uri?eid=2-s2.0-84883268061&doi=10.1016%2Fj.watres.2013.06.007&partnerID=40&md5=24657acaf21444bbfe5a897123ea8d50
39. Popa C, Favier L, Dinica R, Semrany S, Djelal H, Amrane A, et al. Potential of newly isolated wild Streptomyces strains as agents for the biodegradation of a recalcitrant pharmaceutical, carbamazepine. Environ Technol (United Kingdom) [Internet]. 2014;35(24):3082–91. Available from: https://www.scopus.com/inward/record.uri?eid=2-s2.0-84907883475&doi=10.1080%2F09593330.2014.931468&partnerID=40&md5=4679f7d24a7beaa1fd7d8bb4626b7711
40. Rodríguez-Rodríguez, C. E., Barón, E., Gago-Ferrero, P., Jelić, A., Llorca, M., Farré, M., ... Vicent, T. (2012). Removal of pharmaceuticals, polybrominated flame retardants and UV-filters from sludge by the fungus Trametes versicolor in bioslurry reactor. Journal of Hazardous Materials, 233–234, 235–243. https://doi.org/10.1016/j.jhazmat.2012.07.024
41. Ha H, Mahanty B, Yoon S, Kim C-G. Degradation of the long-resistant pharmaceutical compounds carbamazepine and diatrizoate using mixed microbial culture. J Environ Sci Heal - Part A Toxic/Hazardous Subst Environ Eng [Internet]. 2016;51(6):467–71. Available from: https://www.scopus.com/inward/record.uri?eid=2-s2.0-84958049873&doi=10.1080%2F10934529.2015.1128712&partnerID=40&md5=9cc7acdf7b6513d0be711ae9d11fb768
42. Buchicchio A, Bianco G, Sofo A, Masi S, Caniani D. Biodegradation of carbamazepine and clarithromycin by Trichoderma harzianum and Pleurotus ostreatus investigated by liquid chromatography – high-resolution tandem mass spectrometry. Sci Total Environ [Internet]. 2016;557–558:733–9. Available from: http://dx.doi.org/10.1016/j.scitotenv.2016.03.119
43. Li X, Xu J, Toledo R, Shim H. Bioresource Technology Enhanced removal of naproxen and carbamazepine from wastewater using a novel countercurrent seepage bioreactor immobilized with Phanerochaete chrysosporium under non-sterile conditions. Bioresour Technol [Internet]. 2015;197:465–74. Available from: http://dx.doi.org/10.1016/j.biortech.2015.08.118
44. Ungureanu C, Favier L, Bahrim G, Amrane A. Response surface optimization of experimental conditions for carbamazepine biodegradation by Streptomyces MIUG 4.89. N Biotechnol [Internet]. 2015;00(00). Available from: http://dx.doi.org/10.1016/j.nbt.2014.12.005
45. Li X, Xu J, Toledo R, Shim H. Enhanced carbamazepine removal by immobilized Phanerochaete chrysosporium in a novel rotating suspension cartridge reactor under non-sterile condition. Int Biodeterior Biodegradation [Internet]. 2016;115:102–9. Available from: http://dx.doi.org/10.1016/j.ibiod.2016.08.003
46. Zhang Y, Geißen S. Elimination of carbamazepine in a non-sterile fungal bioreactor. Bioresour Technol [Internet]. 2012;112:221–7. Available from: http://dx.doi.org/10.1016/j.biortech.2012.02.073
47. Vasiliadou I, Sánchez R, Molina R, Martínez F, Melero J, Bautista L, et al. Biological removal of pharmaceutical compounds using white-rot fungi with concomitant FAME production of the residual biomass. 2016;180:228–37.
48. Cruz C, Lucas D, Llorca M, Rodriguez S, Gorga M, Petrovic M, et al. Hospital wastewater treatment by fungal bioreactor : Removal ef fi ciency for pharmaceuticals and endocrine disruptor compounds. Sci Total Environ [Internet]. 2014;493:365–76. Available from: http://dx.doi.org/10.1016/j.scitotenv.2014.05.117
49. Rodríguez-Rodríguez, C. E., Barón, E., Gago-Ferrero, P., Jelić, A., Llorca, M., Farré, M., Vicent, T. (2012). Removal of pharmaceuticals, polybrominated flame retardants and UV-filters from sludge by the fungus Trametes versicolor in bioslurry reactor. Journal of Hazardous Materials, 233–234, 235–243. https://doi.org/10.1016/j.jhazmat.2012.07.024

Received: 18 enero 2021
Accepted: 10 marzo 2021

REVIEW / ARTÍCULO DE REVISIÓN

¿Cómo el Lactato tiene un efecto inmunosupresor en la sepsis?

How does Lactate have an immunosuppressor effect on sepsis?

Santiago Xavier Aguayo-Moscoso[1], Laisa Micaela Lascano-Cañas[2], Mario Montalvo-Villagómez[1], Fernando Jara González[1], Pablo Andrés Vélez-Paez[1], Gustavo Velarde-Montero[1], Pedro Torres-Cabezas[3], Jorge Luis Vélez-Paez[4]
DOI. 10.21931/RB/2021.06.02.29

Resumen: El sistema inmunitario es nuestro medio de defensa contra la sepsis, el cual mantiene la homeostasis a través de diversas funciones que requieren un control preciso de las vías celulares y metabólicas. Tal es así, que se han definido mejor estas vías metabólicas: las células inmunes dependen de la β-oxidación y la fosforilación oxidativa como fuentes de energía para la producción de ATP para conservar el equilibrio celular. Sin embargo, una vez estimulados, los leucocitos cambian su metabolismo a través del efecto Warburg, por lo que hay aumento en la glucólisis aeróbica seguido de la producción de lactato. Se ha determinado, como el lactato puede tener un efecto inmunosupresor en el microambiente y como estos cambios metabólicos conllevan a la supresión inmune y la progresión de la infección. Comprender los factores que intervienen en esta relación entre el sistema inmunitario y el lactato aportará nuevos conocimientos para modular la inflamación, la inmunidad celular, recuperación en los procesos sépticos y avances en la terapéutica.

Palabras clave: Lactato, inmunosupresión, sepsis, efecto Warburg. (DeCS-BIREME).

Abstract: The immune system is our means of defense against sepsis, which maintains homeostasis through various functions that require precise control of cellular and metabolic pathways. So much so, that these metabolic pathways have been better defined: Immune cells depend on β-oxidation and oxidative phosphorylation as sources of energy for ATP production to preserve cell balance. However, once stimulated, leukocytes change their metabolism through the Warburg effect, so there is an increase in aerobic glycolysis followed by lactate production. It has been determined how lactate can have an immunosuppressive effect on the microenvironment and how these metabolic changes lead to immune suppression and the progression of infection. Understanding the factors involved in this relationship between the immune system and lactate will provide new insights to modulate inflammation, cellular immunity, recovery in septic processes, and advances in therapy.

Key words: Lactate, immunosuppression, sepsis, Warburg effect. (MeSH-NIH).

Introducción

La sepsis es un problema clínico en donde su condición más grave, el shock séptico, conduce a una morbimortalidad alta a pesar de los tratamientos implementados. La sepsis se identifica por una respuesta inflamatoria sistémica no controlada del sistema inmune, como resultado de interacciones entre el huésped y los agentes infecciosos, por ello es esencial comprender los mecanismos moleculares asociados con el desarrollo de la sepsis[1–3].

En los pacientes con sepsis existe una fase inmunosupresora, en la cual contribuyen algunos factores: apoptosis, disminución de los progenitores linfoides y reducción de la producción de la médula ósea; uno de los puntos a destacar es el metabolismo de la glucólisis aeróbica y su relación con la activación del sistema inmune. Además, un grupo etario que merece atención, son los adultos mayores, debido a que poseen una inmunidad disminuida como resultado de la inmunosenescencia[4–8].

En los siguientes párrafos escribiremos los resultados de una búsqueda estructurada con las palabras clave lactato, inmunidad y sepsis en inglés y en español, en las bases medline, scopus, WoS, LILACS y LATINDEX. Antes de eso, veremos brevemente en qué consisten estos componentes.

Lactato

Medir el lactato es parte del manejo diario en la Unidad de Cuidados Intensivos, de manera particular en casos de sepsis, donde se evalúa: gravedad de la enfermedad, respuesta al tratamiento y el pronóstico[9,10].

El lactato se sintetiza como producto de la glucólisis anaeróbica una vez que la demanda de oxígeno se reduce hasta un punto crítico y no es viable la síntesis de ATP por la vía aerobia, esto se lleva a cabo debido a que el piruvato se reduce a lactato, gracias a la reacción por la enzima L-lactato deshidrogenasa, de esta manera se regenera el NAD+ y la glucólisis continúa. La hiperlactacidemia se da cuando la tasa de producción supera la tasa de eliminación, lo que ocasiona disfunción celular dando la acidosis láctica[7,11–14].

Sistema inmune

El sistema inmune es la defensa natural del cuerpo, donde su principal función actuar contra microorganismos, pero además cumple su papel en procesos tumorales, alérgicos o autoinmunes. Se lo clasifica en sistema innato y adquirido, pero hay que tomar en cuenta que ambos trabajan en conjunto, ya que el sistema inmune innato impulsa al sistema inmune adquirido en respuesta a las infecciones y por otro lado el sistema inmune adquirido utiliza los mecanismos efectores de la inmunidad innata para eliminar los patógenos[15].

El sistema innato es la primera línea de defensa del huésped, cuyos principales componentes son: barreras físicas y

[1] Hospital Pablo Arturo Suárez, Ecuador.
[2] Facultad de Medicina, Universidad de las Américas, Ecuador.
[3] Facultad de Ciencias de la Salud, Universidad Técnica del Norte y Hospital General Ibarra, Instituto Ecuatoriana de Seguridad Social, Ecuador.
[4] Hospital Pablo Arturo Suárez y Facultad de Ciencias Médicas, Universidad Central del Ecuador, Ecuador.

Corresponding author: jlvelez@uce.edu.ec

químicas (epitelios, enzimas), células fagocíticas (neutrófilos macrófagos), células Natural Killer (NK), sistema del complemento, citoquinas y receptores tipo Toll (TLRs)[15].

El sistema adaptivo se caracteriza por mejorar la capacidad defensiva frente exposiciones sucesivas. Los principales elementos son los linfocitos B y T que se activan frente a los antígenos, además posee dos tipos de respuestas inmunes: inmunidad humoral e inmunidad celular[15].

Las células inmunes, al llegar un agente externo requieren activar sus mecanismos, y en este contexto, también se ha estudiado como estas células producen lactato a través del metabolismo glucolítico aeróbico. Revisemos en que consiste la glucólisis aeróbica.

Glucólisis aeróbica

La molécula clave que proporciona energía para los procesos celulares es el ATP, ya que esta mantiene los niveles de ATP celular esenciales para la homeostasis y supervivencia de todas las células. La glucólisis y la fosforilación oxidativa (OxPhos) son las vías que convierten a la glucosa, en la principal fuente de energía: el ATP7(Figura 1).

Otto Warburg reconoció que el metabolismo de las células cancerosas era distinto al de los tejidos normales, ya que facilita el crecimiento y la proliferación de estas células. Las células malignas absorben grandes cantidades de glucosa que metabolizan al piruvato por una vía glucolítica altamente activa. Además, determinó que las células tumorales no tienen altas tasas de OxPhos y que el piruvato generado por la glucólisis se convierte en lactato, el cual es secretado por la célula[16].

Este es el tipo de metabolismo de la glucosa que adoptan las células en condiciones anaeróbicas donde no hay oxígeno disponible para facilitar la OxPhos. Sin embargo, las células cancerosas y otras células metabólicamente activas y proliferativas, también metabolizan la glucosa a lactato incluso en presencia de abundante oxígeno, esto se conoce como glucólisis aeróbica. Warburg también observó que los linfocitos activados se vuelven altamente glucolíticos produciendo grandes cantidades de lactato[17,18].(Figura 2)

En nuestro sistema inmune, las células T naïve tienen poca demanda de procesos biosintéticos. Sin embargo, los linfocitos efectores tienen demandas bioenergéticas y biosintéticas completamente diferentes por lo que adoptan una característica metabólica distinta. En respuesta a un agente patógeno, pequeñas cantidades de células T específicas deben experimentar una expansión clonal masiva para generar el conjunto de células T efectoras necesarias para combatir la infección. De manera que existe una gran carga biosintética en estas células y una demanda significativa de moléculas precursoras, por esto las células T efectoras activadas participan en la glucólisis aeróbica[19,20].

Inmunosupresión en sepsis

Durante la sepsis, se ha propuesto que puede existir una fase de inmunosupresión, porque tanto las respuestas proinflamatorias como las antiinflamatorias ocurren temprano y simultáneamente[21]. La demostración de inmunosupresión incluye el agotamiento de las células inmunes (células T más afectadas), funciones efectoras de las células T comprometidas, presentación de antígenos deteriorada, susceptibilidad a infecciones nosocomiales y reactivación de virus latentes[22].

En el estudio realizado por Boomer, se analizó las células inmunes esplénicas y pulmonares de pacientes con sepsis dentro de los 30 a 180 minutos del fallecimiento, se evidenció una producción disminuida de citocinas, expresión aumentada de receptores inhibitorios, expansión de células T reguladoras, poblaciones de células supresoras derivadas de mieloides y disminución de las vías de activación mediadas por CD28 y HLA-DR[23].

¿Cómo el lactato modula la respuesta inmune?

Leite realizó un estudio en donde examinó los efectos del lactato sobre la actividad enzimática de la piruvato quinasa (PK), fosfofructoquinasa (PFK) y hexoquinasa (HK) en diversos tejidos de ratones. Los resultados mostraron que el lactato inhibía tanto la actividad de PFK como de la HK, mientras que la actividad de la PK no se vio afectada por el lactato. La

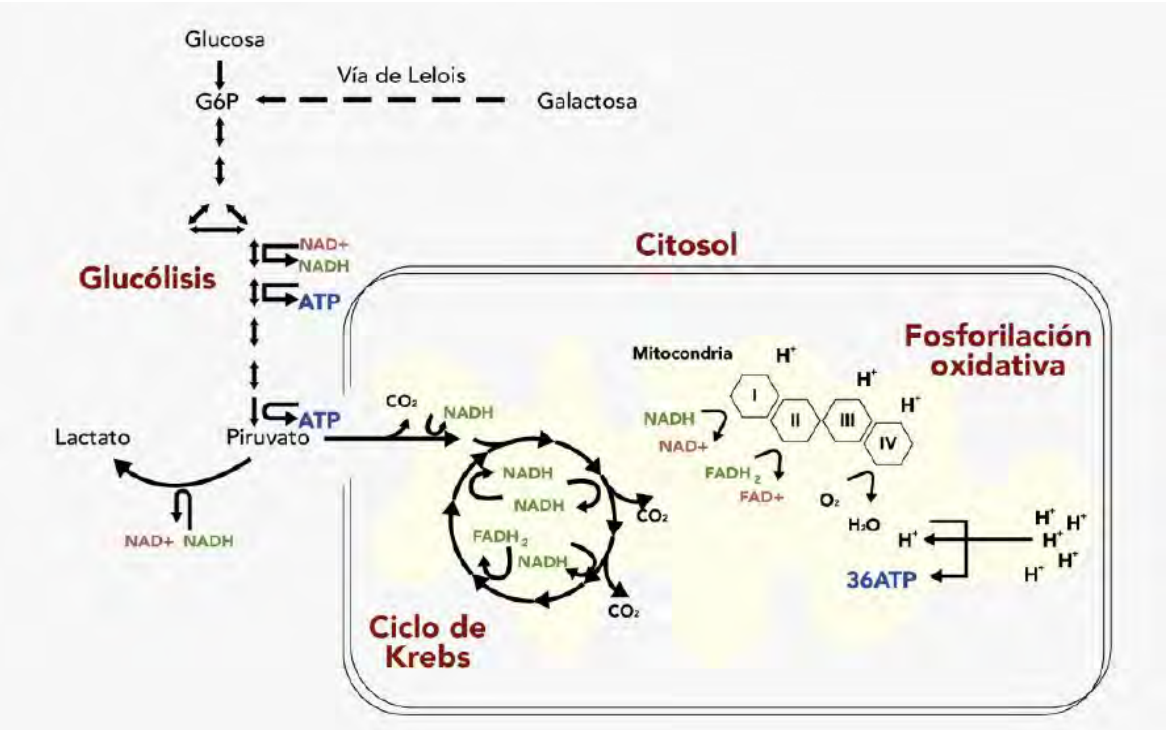

Figura 1. Producción de ATP por glucólisis y fosforilación oxidativa.

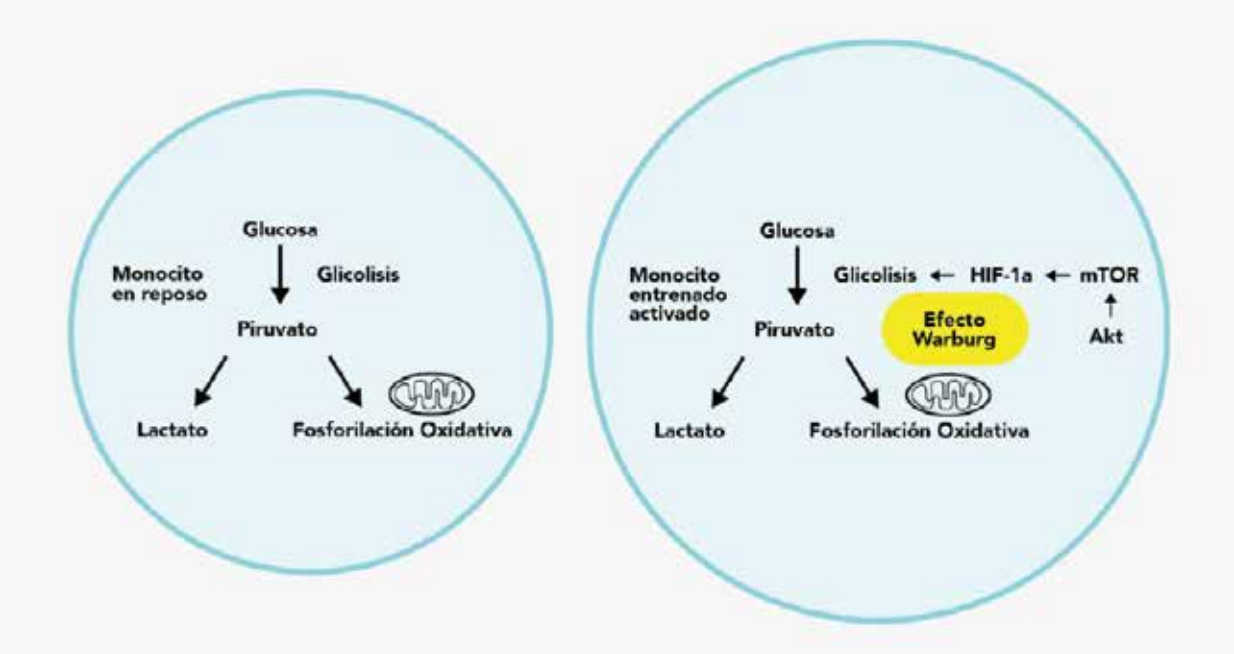

Figura 2. La glucólisis como base metabólica para la inmunidad.

actividad de HK y PFK está directamente relacionada con el metabolismo de la glucosa, por lo tanto, es razonable que la exposición al lactato pueda inducir la inhibición del consumo de glucosa en los tejidos[24].

Es necesario retomar el ejemplo de las células cancerosas, y recordar que derivan la energía de la glucosa a través de la glucólisis al ácido láctico, incluso en condiciones altamente aeróbicas[16].

Al tener un metabolismo energético alterado puede mejorar el crecimiento de los cánceres al promover la evasión tumoral de la destrucción inmune. Una célula inmunogénica transformada solo puede convertirse en un tumor si tiene la capacidad de evadir la respuesta inmune citotóxica que evoca. La respuesta inmune anticancerígena, está mediada por células T efectoras, las cuales son altamente dependientes de los componentes del microambiente y de igual manera está influenciado por el pH: un pH ácido dificulta la función de las células inmunes normales. Reducir el pH a 6.0-6.5, como se puede encontrar en las masas tumorales, conduce a la pérdida de la función de las células T en tumores humanos y murinos. (Figura 3)[25–27].

La causa principal responsable del pH ácido y del efecto supresor de la función de las células T dependientes del pH en un microambiente tumoral es secundaria al ácido láctico. Por lo tanto, durante la glucólisis aeróbica se evidencia una retroalimentación negativa que ajusta el pH pericelular en los tumores hacia un medio ácido mediante la producción y secreción de ácido láctico. Al inhibir la respuesta inmune, las células cancerosas pueden mejorar su supervivencia contra el cáncer al mantener un microambiente ligeramente ácido. Aparentemente pueden hacer esto alterando su metabolismo energético para regular su producción/secreción de ácido láctico[28–30].

Es evidente que los estudios se han enfocado en el ámbito de la oncología. De una manera más detallada veremos como el lactato interviene en la inmunidad innata y adaptativa.

Inmunidad innata y lactato

Las investigaciones se han enfocado en los efectos inmunomoduladores del lactato en las células inmunes innatas, principalmente las células dendríticas y macrófagos. Un papel importante en la respuesta tanto inmune innata como adaptativa es a través de las células dendríticas (DC). Las DC se originan a partir de células progenitoras hematopoyéticas y contribuyen a la inmunidad mediante el reconocimiento de señales patogénicas por medio de receptores de reconocimiento de patrones (PRRs) que son proteínas capaces de reconocer moléculas frecuentemente asociadas con patógenos (patrones moleculares asociados a patógenos, PAMP). La participación de PRRs en las células inmunes innatas induce señales coestimuladoras para las células inmunes adaptativas (particularmente los linfocitos T). De destacar, la "Teoría del peligro" planteada por Matzinger quien sugirió que, durante el estrés o daño tisular, las moléculas endógenas se liberan o activan e inician la respuesta inflamatoria, que capacita a las células presentadoras de antígeno para activar la respuesta inmune adaptativa. Estas moléculas se conocen como alarminas o DAMP (patrones moleculares asociados al daño)[31–34].

Las DC presentan antígenos al exponer al complejo mayor de histocompatibilidad moléculas a las células T específicas de antígeno que luego eliminan los patógenos, esta defensa contra los microorganismos es importante, pero también es esencial que el sistema inmunitario no responda a sí mismo, lo que se conoce como tolerancia. Las células dendríticas tolerogénicas son esenciales en la tolerancia central y periférica. Las células dendríticas junto con las células epiteliales tímicas medulares tienen un papel crítico en la inducción de tolerancia central en el timo mediante la eliminación de los timocitos autorreactivos con antígenos y la generación de células T reguladoras (Tregs). Aunque la selección tímica elimina eficazmente la mayoría de las células T autorreactivas, algunas permanecen y migran hacia la periferia. Por lo tanto, la tolerancia periférica es decisiva para el mantenimiento de la homeostasis inmune durante toda la vida[31,32,35].

En el ámbito de la sepsis, una característica destacada es el desarrollo inadecuado de la tolerancia inmunológica hacia los patógenos. Por ejemplo, las DC pasan a un fenotipo progresivamente tolerogénico y promueven la diferenciación de células Tregs inmunosupresoras. Las DC tolerogénicas muestran la expresión de moléculas inmunomoduladoras y producen factores inmunosupresores como IL-10, TGF-β, IL-35 e indo-

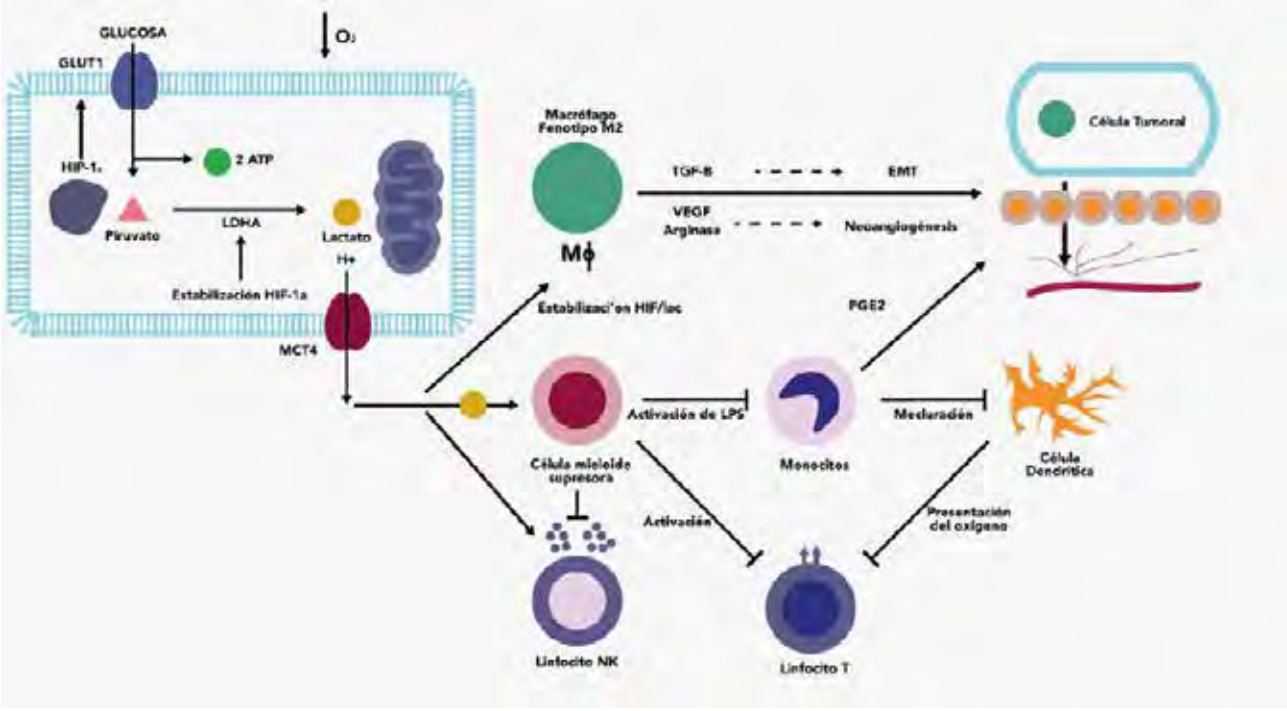

Figura 3. Descripción de los efectos inmunosupresores del lactato en el microambiente tumoral.

leamina 2,3-dioxigenasa, lo que produce anergia y apoptosis de células T e inducción de Tregs[31,32,35,36].

Por otro lado, tenemos a los macrófagos, los cuales pueden activarse por varios desencadenantes y diferenciarse en subtipos funcionalmente diferentes. Existen dos tipos funcionales de macrófagos: los M1 y los M2. Mientras los M1 fagocitan, atacan a células tumorales y presentan antígenos, los M2 son estimulados por complejos inmunitarios e interleucinas de carácter antiinflamatorio, además que son macrófagos asociados a tumores, ya que muestran patrones oncogénicos, facilitando la supervivencia, la proliferación y la diseminación de las células malignas[37].

El metabolismo es distinto en cada uno de estos macrófagos: mientras los M1 aumentan su metabolismo de la glucosa y la producción de lactato a través de la glucólisis, los M2 lo realizan a través de OxPhos y la β-oxidación por la absorción de ácidos grasos[38].

Pero, ¿qué sucede en la sepsis? En etapas tardías de la sepsis, los macrófagos tienen un fenotipo M2 predominantemente inmunosupresor que puede tener un papel en la patogénesis de la disfunción del sistema inmune. El lactato puede servir como responsable de promover la diferenciación inhibitoria M2. En experimentos in vitro con macrófagos derivados de la médula ósea, se ha determinado que el lactato es capaz de inducir una diferenciación de macrófagos similar a M2 mediante un mecanismo dependiente de la subunidad alfa del factor 1 inducible por hipoxia (HIF-1a). También se ha demostrado que cuando se coloca lactato al medio de crecimiento antes de la inducción de la diferenciación de las células madre de médula ósea da como resultado una producción mayor de células supresoras derivadas de mieloides (MDSC) en comparación con el control. Las MDSC son un grupo heterogéneo de células que tienen efectos inmunosupresores e intervienen en el desarrollo del cáncer y las enfermedades infecciosas crónicas. Además, el aumento de MDSC en la sepsis se vio implicado en la patogénesis de la disfunción inmune prolongada[38–41].

Los efectos supresores del lactato en los macrófagos se extienden más allá del ambiente del tumor, ya que la inducción de la glucólisis aeróbica durante la eferocitosis, un proceso principalmente inmunosupresor, da como resultado la liberación de lactato. El lactato inducido por eferocitosis actúa de manera parácrina y contribuye a un ambiente antiinflamatorio al aumentar la expresión de genes antiinflamatorios[42].

Inmunidad adaptativa y lactato

Ahora continuemos de la manera en que interviene el lactato en el sistema inmune adaptativo. La inmunidad adaptativa o adquirida es la segunda línea de defensa del sistema inmune contra los patógenos no propios, también conocida como inmunidad específica. Está mediado por linfocitos T y B y su función es reconocer y eliminar los antígenos no propios durante el proceso de presentación del antígeno, y desarrollar memoria inmunológica. Las células T tienen dos subconjuntos principales: CD4 (helper) y CD8 (citotóxicos)[15].

Las células T desempeñan un papel clave mediante sus actividades citolíticas y la producción de citocinas pro y antiinflamatorias. Tras el reconocimiento del antígeno por el receptor de células T, células naïve a través de señales conducen a la diferenciación en células T efectoras. Para mantener un suministro adecuado de macromoléculas durante el crecimiento, las células T experimentan un cambio metabólico de la OxPhos a la glucólisis aeróbica, lo que lleva a un aumento en el flujo glucolítico y la producción concomitante de lactato[44].

Dentro de las investigaciones realizadas, se ha determinado que el lactato se acumula en la sinovia de los pacientes con artritis reumatoide. El lactato de sodio extracelular y el ácido láctico inhiben la motilidad de las células CD4 y CD8. En las células CD4 el lactato de sodio también induce un cambio hacia el subconjunto Th17 que produce grandes cantidades de la citocina proinflamatoria IL-17, mientras que en las células CD8, el ácido láctico causa la pérdida de su función citolítica[44].

Es probable que las células T reguladoras sean menos dependientes de la glucólisis aeróbica y utilicen principalmente la OxPhos para su producción de energía. Por lo tanto, teóricamente pueden no ser susceptibles a este tipo de regulación metabólica[45].

Utilidad clínica actual

La función de las células inmunológicas se afecta de una u otra manera por la sepsis. En este contexto, se han investigado varios biomarcadores para ayudar a comprender si el paciente está en la fase hiperinflamatoria o hipoinflamatoria del trastorno, por lo tanto, se podrían usar para identificar pacientes inmunodeprimidos y beneficiarse de las inmunoterapias. Se los clasificará de acuerdo al tipo de inmunidad que queremos buscar (Tabla 1):

Enfoque traslacional

La sepsis mantiene una alta morbilidad que se ve intensificada por microorganismos multirresistentes, la cual induce numerosos defectos en la inmunidad innata y adaptativa del huésped de tal manera que, si los organismos invasores no se eliminan rápidamente, el huésped se vuelve más susceptible a la infección o a infecciones secundarias, por lo que es importante implementar terapéuticas guiadas para combatir a la infección, uso de antibióticos, soporte hemodinámico etc. Podemos dividir en dos grupos los fármacos en esta sección, por un lado los que actúan en la glucólisis y por otro los inmunomoduladores[46].

Se han realizado algunas investigaciones dentro del primer grupo:

Hay que recordar que la estimulación de macrófagos con LPS aumenta la expresión de piruvato quinasa M2 (PKM2), un modulador de la producción de IL-1b. Además, la activación de PKM2 atenúa el fenotipo de macrófago M1 proinflamatorio inducido por LPS y promueve al macrófago M2. La glucólisis mediada por PKM2 inicia la activación del inflamasoma y modula la fosforilación de EIF1AK2 en los macrófagos. En este contexto, en el estudio realizado por Xie, determinó que la inhibición farmacológica de la vía PKM2-EIF2AK2 protegió a los ratones de la endotoxemia letal y la sepsis polimicrobiana[47].

- La inhibición de la glucólisis aeróbica por el inhibidor de 2-desoxi-D-glucosa (2-DG) o inhibidor PKM2 mejoró la supervivencia en la sepsis polimicrobiana, y redujo los niveles de lactato sérico y la liberación de HMGB1[48].
- Se reportó de que la inhibición de la glucólisis aeróbica por 2-DG mejoró la supervivencia en la sepsis bacteriana y también hubo reducción de la inflamación inducida por LPS *in vivo*.[49,50].
- Por último, y no menos importante, Zheng destacó que la glucólisis aumentada por sepsis contribuyó a la miocardiopatía y mortalidad. Al inhibir la glucólisis con 2-DG ayudó a la función cardíaca y supervivencia, al mejorar la función mitocondrial y la respuesta inflamatoria[51].

Por otro lado, existen estrategias para aumentar la inmunidad del huésped. Los agentes inmunomoduladores tienen como objetivo mejorar las funciones inmunitarias durante la sepsis. Veamos a continuación algunos de estos:

Interleucina-7 humana recombinante (IL-7)

La IL-7 tiene efecto estimulante en las células B y T. En estas últimas tiene potencial para mejorar la homeostasis durante la sepsis. Las células estromales producen la IL-7 a través de los órganos linfoides periféricos, timo, piel, intestino y el hígado. Se considera que la IL-7 es una citocina pluripotente que es necesaria para el desarrollo de células T humanas. Se ha determinado que aumenta la producción de células T naïve, promueve la proliferación de células T, así como la activación y la diversidad de receptores de células T, disminuye la apoptosis de células T, incrementa células T que recluta neutrófilos al sitio de infección, aumenta la expresión de la molécula de adhesión en las células T[21,22].

Interleucina-15 (IL-15)

La glicoproteína IL-15 es producida por macrófagos, monocitos, células dendríticas, células endoteliales, células del estroma y células epiteliales renales. De igual forma, se han determinado algunos mecanismos de acción: estimula las células NK, NKT, CD8, prolifera y activa las células dendríticas; disminuye la apoptosis de células dendríticas y neutrófilos NK, T; provoca la secreción de citocinas de macrófagos y la fagocitosis; en las células NK y T aumenta la secreción de IFNγ[21,22].

Anticuerpo anti-PD-1 y anti-PD-L1

La expresión de receptores inhibitorios como PD-1 en células T y PD-L1 en células presentadoras de antígeno y células parenquimatosas disminuye las funciones de las células T durante la sepsis. De las funciones se destacan las siguientes: se une a los receptores PD-1 en las células T, bloquea la interacción PD-1 con PD-L1 y PD-L2, previene la inhibición de las células T a través de la vía PD-1 / PD-L[21,22].

Interferón gamma (IFN-γ)

Las células T CD4 y CD8 activadas, junto con las células NK, son la principal fuente de IFNγ. IFN-γ aumenta la expresión de HLA-DR en monocitos y es una de las citocinas clave responsables de la activación de monocitos y macrófagos, que son esenciales para la eliminación microbiana durante la sepsis. Se ha determinado que la producción de IFN-γ de células T disminuye durante la sepsis, además se ha demostrado que

Inmunidad innata:
↓ HLA-DR en monocitos.
↓ TNF por células estimuladas por LPS.
↑ PDL1 en monocitos.
Inmunidad adaptativa:
Linfopenia severa persistente
Reactivación de infecciones por citomegalovirus o herpes simple
↑ PD1 en CD4 o CD8
↑ Número de células T reguladoras circulantes
↓ IFNγ por las células T
↓ Proliferación de células T
Inmunidad innata/adaptativa:
Infecciones por *Enteroroccus*spp., *Acinetobacters*pp. o *Candida*spp.
↑ Relación IL-10:TNF
↓ Respuesta de hipersensibilidad de tipo retardado.

Tabla 1. Biomarcadores y hallazgos clínicos de laboratorio aplicado a la sepsis[21].

las terapias que restauran la producción de IFN-γ de células T mejoran la supervivencia en modelos animales de sepsis[21,22].

Conclusiones

El efecto Warburg también se ha demostrado en las células inmunes como los monocitos, macrófagos, células dendríticas y células T que utilizan un mecanismo similar para su activación.

Los monocitos/macrófagos activados cambian su metabolismo de la fosforilación oxidativa a la glucólisis, porque las células inmunes activadas necesitan una fuente de energía disponible para la fagocitosis y precursores biosintéticos para dividirse y producir citocinas.

La elevación del lactato es secundaria a una perfusión deficiente o trastornos microcirculatorios, pero probablemente indica un cambio fundamental en el metabolismo hacia una glucólisis más proinflamatoria.

La función general del lactato parece ser cambiar el equilibrio de la activación de los macrófagos de un fenotipo inflamatorio a un fenotipo reparador.

Identificar pacientes inmunosuprimidos con la ayuda de biomarcadores y administrar inmunomoduladores específicos tiene un potencial significativo para la terapia de sepsis en el futuro.

La inmunoterapia podría representar el próximo gran avance en el tratamiento de enfermedades infecciosas y sepsis.

Fuente de financiamiento

Autofinanciado.

Conflicto de interés

Los autores declaran no tener conflictos de interés con la publicación de este artículo.

Referencias bibliográficas

1. Rhodes A, Evans LE, Alhazzani W, Levy MM, Antonelli M, Ferrer R, et al. Surviving Sepsis Campaign: International Guidelines for Management of Sepsis and Septic Shock: 2016. Intensive Care Med. marzo de 2017;43(3):304-77.
2. Oberholzer A, Oberholzer C, Moldawer LL. Sepsis syndromes: understanding the role of innate and acquired immunity. Shock Augusta Ga. agosto de 2001;16(2):83-96.
3. Browne EP. Regulation of B-cell responses by Toll-like receptors. Immunology. agosto de 2012;136(4):370-9.
4. Martin GS, Mannino DM, Moss M. The effect of age on the development and outcome of adult sepsis. Crit Care Med. enero de 2006;34(1):15-21.
5. Ono S, Tsujimoto H, Hiraki S, Aosasa S. Mechanisms of sepsis-induced immunosuppression and immunological modification therapies for sepsis. Ann Gastroenterol Surg. septiembre de 2018;2(5):351-8.
6. Hotchkiss RS, Monneret G, Payen D. Immunosuppression in sepsis: a novel understanding of the disorder and a new therapeutic approach. Lancet Infect Dis. marzo de 2013;13(3):260-8.
7. Donnelly RP, Finlay DK. Glucose, glycolysis and lymphocyte responses. Mol Immunol. diciembre de 2015;68(2 Pt C):513-9.
8. Ventura MT, Casciaro M, Gangemi S, Buquicchio R. Immunosenescence in aging: between immune cells depletion and cytokines up-regulation. Clin Mol Allergy CMA [Internet]. 14 de diciembre de 2017 [citado 31 de mayo de 2020];15. Disponible en: https://www.ncbi.nlm.nih.gov/pmc/articles/PMC5731094/
9. Nguyen HB, Rivers EP, Knoblich BP, Jacobsen G, Muzzin A, Ressler JA, et al. Early lactate clearance is associated with improved outcome in severe sepsis and septic shock. Crit Care Med. agosto de 2004;32(8):1637-42.
10. Suetrong B, Walley KR. Lactic Acidosis in Sepsis: It's Not All Anaerobic: Implications for Diagnosis and Management. Chest. enero de 2016;149(1):252-61.
11. Vásquez-Tirado GA, García-Tello AV, Evangelista Montoya FE. Utilidad del lactato sérico elevado como factor pronóstico de muerte en sepsis severa. HorizMéd Lima. abril de 2015;15(2):35-40.
12. Jl Á-V, Ac G-G, Ej D-G, Fl W. Índices estáticos y dinámicos de la hiperlactatemia. Med Interna México. 2016;7.
13. Ramírez PG, García RD, Ortega AG, Campuzano EG, Malumbres S, Soria JLM, et al. Sociedad Española de Bioquímica Clínica y Patología Molecular Comité Científico Comisión Magnitudes Biológicas relacionadas con la Urgencia Médica1 Documento N. Fase 3. Versión 3. :5.
14. Srivastava A, Mannam P. Warburg revisited: lessons for innate immunity and sepsis. Front Physiol. 2015;6:70.
15. Paola TP. Visión panorámica del sistema inmune. Rev Médica Clínica Las Condes. julio de 2012;23(4):446-57.
16. Warburg O. On the Origin of Cancer Cells. Science. 24 de febrero de 1956;123(3191):309-14.
17. Vander Heiden MG, Cantley LC, Thompson CB. Understanding the Warburg effect: the metabolic requirements of cell proliferation. Science. 22 de mayo de 2009;324(5930):1029-33.
18. Warburg O, Gawehn K, Geissler AW. [Metabolism of leukocytes]. Z Naturforsch B. agosto de 1958;13B(8):515-6.
19. Pearce EL, Pearce EJ. Metabolic pathways in immune cell activation and quiescence. Immunity. 18 de abril de 2013;38(4):633-43.
20. Wang R, Dillon CP, Shi LZ, Milasta S, Carter R, Finkelstein D, et al. The transcription factor Myc controls metabolic reprogramming upon T lymphocyte activation. Immunity. 23 de diciembre de 2011;35(6):871-82.
21. Hotchkiss RS, Monneret G, Payen D. Sepsis-induced immunosuppression: from cellular dysfunctions to immunotherapy. Nat Rev Immunol. diciembre de 2013;13(12):862-74.
22. Patil NK, Bohannon JK, Sherwood ER. Immunotherapy: A promising approach to reverse sepsis-induced immunosuppression. Pharmacol Res. 2016;111:688-702.
23. Boomer JS, To K, Chang KC, Takasu O, Osborne DF, Walton AH, et al. Immunosuppression in patients who die of sepsis and multiple organ failure. JAMA. 21 de diciembre de 2011;306(23):2594-605.
24. Leite TC, Coelho RG, Da Silva D, Coelho WS, Marinho-Carvalho MM, Sola-Penna M. Lactate downregulates the glycolytic enzymes hexokinase and phosphofructokinase in diverse tissues from mice. FEBS Lett. 3 de enero de 2011;585(1):92-8.
25. Hanahan D, Weinberg RA. Hallmarks of cancer: the next generation. Cell. 4 de marzo de 2011;144(5):646-74.
26. Kellum JA. Metabolic acidosis in patients with sepsis: epiphenomenon or part of the pathophysiology? CritCareResusc J Australas Acad CritCareMed. septiembre de 2004;6(3):197-203.
27. Calcinotto A, Filipazzi P, Grioni M, Iero M, De Milito A, Ricupito A, et al. Modulation of microenvironment acidity reverses anergy in human and murine tumor-infiltrating T lymphocytes. Cancer Res. 1 de junio de 2012;72(11):2746-56.
28. Kellum JA, Song M, Li J. Lactic and hydrochloric acids induce different patterns of inflammatory response in LPS-stimulated RAW 264.7 cells. Am J PhysiolRegulIntegr Comp Physiol. abril de 2004;286(4):R686-692.
29. Goetze K, Walenta S, Ksiazkiewicz M, Kunz-Schughart LA, Mueller-Klieser W. Lactate enhances motility of tumor cells and inhibits monocyte migration and cytokine release. Int J Oncol. agosto de 2011;39(2):453-63.
30. Mazzio EA, Boukli N, Rivera N, Soliman KFA. Pericellular pH homeostasis is a primary function of the Warburg effect: inversion of metabolic systems to control lactate steady state in tumor cells. CancerSci. marzo de 2012;103(3):422-32.
31. Ueno H, Klechevsky E, Morita R, Aspord C, Cao T, Matsui T, et al. Dendritic cell subsets in health and disease. Immunol Rev. octubre de 2007;219:118-42.

32. Hasegawa H, Matsumoto T. Mechanisms of Tolerance Induction by Dendritic Cells In Vivo. Front Immunol. 2018;9:350.
33. Amarante-Mendes GP, Adjemian S, Branco LM, Zanetti LC, Weinlich R, Bortoluci KR. Pattern Recognition Receptors and the Host Cell Death Molecular Machinery. Front Immunol [Internet]. 16 de octubre de 2018 [citado 7 de junio de 2020];9. Disponible en: https://www.ncbi.nlm.nih.gov/pmc/articles/PMC6232773/
34. Matzinger P. Tolerance, danger, and the extended family. Annu Rev Immunol. 1994;12:991-1045.
35. Sim WJ, Ahl PJ, Connolly JE. Metabolism Is Central to Tolerogenic Dendritic Cell Function. Mediators Inflamm. 2016;2016:2636701.
36. Xing Y, Hogquist KA. T-Cell tolerance: Central and peripheral. Cold Spring HarbPerspect Biol. 1 de junio de 2012;4(6):1-15.
37. Macrófagos: ¿Aliados o enemigos del cáncer? | MiSistemaInmune [Internet]. [citado 31 de mayo de 2020]. Disponible en: https://www.misistemainmune.es/macrofagos-aliados-o-enemigos-del-cancer/
38. Arts RJW, Gresnigt MS, Joosten LAB, Netea MG. Cellular metabolism of myeloid cells in sepsis. J Leukoc Biol. 2017;101(1):151-64.
39. Pena OM, Pistolic J, Raj D, Fjell CD, Hancock REW. Endotoxin tolerance represents a distinctive state of alternative polarization (M2) in human mononuclear cells. J ImmunolBaltim Md 1950. 15 de junio de 2011;186(12):7243-54.
40. Colegio OR, Chu N-Q, Szabo AL, Chu T, Rhebergen AM, Jairam V, et al. Functional polarization of tumour-associated macrophages by tumour-derived lactic acid. Nature. 25 de septiembre de 2014;513(7519):559-63.
41. Husain Z, Huang Y, Seth P, Sukhatme VP. Tumor-derived lactate modifies antitumor immune response: effect on myeloid-derived suppressor cells and NK cells. J Immunol Baltim Md 1950. 1 de agosto de 2013;191(3):1486-95.
42. Ivashkiv LB. The hypoxia–lactate axis tempers inflammation. Nat Rev Immunol. febrero de 2020;20(2):85-6.
43. Haas R, Smith J, Rocher-Ros V, Nadkarni S, Montero-Melendez T, D'Acquisto F, et al. Lactate Regulates Metabolic and Pro-inflammatory Circuits in Control of T Cell Migration and Effector Functions. PLoS Biol. julio de 2015;13(7):e1002202.
44. Santos N, Pereira-Nunes A, Baltazar F, Granja S. Lactate as a Regulator of Cancer Inflammation and Immunity. Immunometabolism [Internet]. 16 de octubre de 2019 [citado 31 de mayo de 2020];1(2). Disponible en: https://ij.hapres.com/htmls/IJ_1118_Detail.html
45. Michalek RD, Gerriets VA, Jacobs SR, Macintyre AN, MacIver NJ, Mason EF, et al. Cutting edge: distinct glycolytic and lipid oxidative metabolic programs are essential for effector and regulatory CD4+ T cell subsets. J Immunol Baltim Md 1950. 15 de marzo de 2011;186(6):3299-303.
46. Palsson-McDermott EM, Curtis AM, Goel G, Lauterbach MAR, Sheedy FJ, Gleeson LE, et al. Pyruvate kinase M2 regulates Hif-1- activity and IL-1- induction and is a critical determinant of the warburg effect in LPS-activated macrophages. Cell Metab. 6 de enero de 2015;21(1):65-80.
47. Xie M, Yu Y, Kang R, Zhu S, Yang L, Zeng L, et al. PKM2-dependent glycolysis promotes NLRP3 and AIM2 inflammasome activation. Nat Commun. 25 de 2016;7:13280.
48. Yang L, Xie M, Yang M, Yu Y, Zhu S, Hou W, et al. PKM2 regulates the Warburg effect and promotes HMGB1 release in sepsis. Nat Commun. 14 de julio de 2014;5:4436.
49. Wang A, Huen SC, Luan HH, Yu S, Zhang C, Gallezot J-D, et al. Opposing Effects of Fasting Metabolism on Tissue Tolerance in Bacterial and Viral Inflammation. Cell. 8 de septiembre de 2016;166(6):1512-1525.e12.
50. Liu L, Lu Y, Martinez J, Bi Y, Lian G, Wang T, et al. Proinflammatory signal suppresses proliferation and shifts macrophage metabolism from Myc-dependent to HIF1- -dependent. ProcNatl Acad Sci U S A. 9 de febrero de 2016;113(6):1564-9.
51. Zheng Z, Ma H, Zhang X, Tu F, Wang X, Ha T, et al. Enhanced Glycolytic Metabolism Contributes to Cardiac Dysfunction in Polymicrobial Sepsis. J InfectDis. 01 de 2017;215(9):1396-406.

Received: 20 febrero 2021
Accepted: 27 abril 2021

REVIEW / ARTÍCULO DE REVISIÓN

A Competitive Analysis Of Top Ten Pharmaceutical Companies In India

Anupam Saha[1*], Arijit Das[1], Subhasish Dutta[2], Suprodip Mandal[3]

DOI. 10.21931/RB/2021.06.02.30

Abstract: Contemplating the activities and conduct of close contenders is fundamental. Competitive analysis is a significant piece of the vital arranging process, and the wellsprings of such Web data are enhanced, and the data are refreshed much of the time. This expansive intrigue has brought about different definitions and conceptualizations of recognizable contender proof just as different ways to deal with considering it, which disables the reconciliation of existing information planned for responding to fundamental inquiries regarding its revenue, procedures, and suggestions. To compete with the opposition organizations are against, it is essential to survey things that are genuinely working in the business. Inquire about rely upon measurable studying, which is limited most definitely and limit. There can be more recommendations, which can show profitability to the association. In this task, the top ten pharmaceutical organizations of India are firmly watched. The absolute positioning gives according to general income, i.e., overall revenue.

Key words: Pharmaceuticals, Pharma Companies, Strategic Analysis, Competitive Analysis, TopTen Pharma Companies, Indian Pharmaceuticals.

Introduction

India – The pharmacy of the world is one of the largest producers of pharmaceuticals. One out of three vaccines in the world is made in India. Every year India produces three billion of the vaccine. Its role in global polio eradication must be underlined. Jerome Kim, director-general of International Vaccine Institute, an eminent researcher, says, "Almost 70% vaccine used in the world is made in India. Almost every child in the world received a vaccine made in India"[1]. Competitive analysis is a method of get-together and analyzing information about adversaries, their practices, things, quality and deficiency, and business floats to assess our circumstance in the market and improve our things and publicizing strategies. In the current market, we ought to appreciate what opponents are doing and what to do to stay before the restriction. Various associations acknowledge they are giving a better than average thing to their customers, anyway don't have reliable information exhibiting how customers see their thing or what it looks like to the resistance[2].

A competitive analysis performed by a fair outsider is a priceless instrument since it can assist clients with recognizing approaches to draw in new clients, just as keep the ones happy with items[3].

Results of Competitive Analysis can assist us with deciding the accompanying strengths and weaknesses upon how item piles facing the opposition and in what regions it may have the edge over own item, and in what zones own items are un-rivaled. Identification of Competition, which is to verify who essential and auxiliary contenders are. Improvements on how and in what regions own items, procedure, and practices must be improved to fulfill advertising needs or remain in front of the opposition. Marketing approach which might need to feature why our item is in front of the opposition or the particular highlight that marketing. It upgrades what have to make in own clients want or desire[4].

Steps of competitive analysis

There are several significant components of competitive analysis, each of which should be painstakingly considered if one wants to change serious investigation exercises into business productivity[5]. Significant parts of Competitive Analysis incorporate the accompanying.

Characterizing competitors

The initial phase in a severe investigation is to characterize an organization's universe of rivals, cautioned that both unduly expansive definitions and unnecessarily restricted meanings of rivalry could bargain the adequacy of serious examination. The business directing the severe examination needs to choose whether rivalries are accidental or present a potential danger (either now or later on) to the business's money-related prosperity[6,7].

Investigation of competitors strengths and weaknesses

When an organization's universe of rivals has been characterized and recognized, it can begin the way toward distinguishing the qualities and shortcomings of those contenders. Abrams forewarned that numerous entrepreneurs are enticed to put undue load on the nature of the item or administration they offer or plan to offer on account of new organizations. This might be a soothing idea, conceded Abrams, however it double-crosses a central misconception of how business functions: The target highlights of your item or administration might be a generally little piece of the severe picture. All the segments of client inclination, including value, administration, and area, are just 50% of the serious investigation. The other portion of the condition is inspecting the interior quality of your rivals' organizations. Over the long haul, organizations with substantial monetary assets, exceptionally energetic or inventive workforce, and other operational resources will end up being intense, suffering rivalry[5,8-10].

Creating Business Strategies, David Aaker an eminent American Consultant, recommended that entrepreneurs should think their examination endeavors in four significant territories such as Studying the cause behind the successes and

[1] M.Pharm, Pharmacology, Nshm College Of Pharmaceutical Technology, NSHM Knowledge Campus, B.L. Rd, Kolkata.
[2] B.Pharm, School Of Pharmacy, Techno India University, Salt Lake Sec-V, Kolkata.
[3] Department Of Pharmacognosy, School Of Pharmacy, Techno India University, Salt Lake Sec-V, Kolkata.

Corresponding author: sahaanupam05@gmail.com

failures of competitive business, significant aspects that motivate customers, major element costs, and barriers to potency within the industry[5,11].

Investigation of internal strengths and weaknesses

Another significant component of a competitive analysis is figuring out what organizations' qualities and shortcomings are. The parts of the organization's activity pass on a bit of leeway in the commercial center. Business power is made out of splendid or aggressive people resulting in the organization has a propelled stock administration framework set up. Workers with the ability to promote and advertise when an organization has decided its qualities can approach using those qualities to improve its situation in the commercial centers. On the other hand, an assessment of interior shortcomings enlivened item introduction, headstrong work power, awful physical area, and so on, should spike activities intended to address those weaknesses[5,9,12–14].

Examination of customer needs and wants

Finding out about client needs and needs is a significant piece of serious investigation, too[15]. Client needs ought to turn into the organization's business needs. What's more, independent companies should take care that they do not limit their examination to needs that are now showed in the commercial center. Without a doubt, new item improvement and new advancements in administration are fundamental to business accomplishment in any industry. Entrepreneurs and chiefs need to study and foresee future client needs and needs and needs that are at present being tended to[16–18].

Examining impediments to market for own and competition

Organizations looking to enter new markets typically need to ponder a few unique obstructions. A portion of these can be overcome without unnecessary trouble, while others might be overwhelming to the point that they block propelling a battle. A few primary obstructions to section for new rivalry i.e., Patents[NSV4] which give some protection for brand protection for new products or processes. Then, High start-up costs-In many cases, that may be a barrier that's most daunting for tiny businesses. Followed by Lack of technical Knowledge, manufacturing, marketing, or engineering expertise can all be a significant obstacle to successful market entry.

Last but not least, market saturation may be a fundamental reality that makes it harder to carve out a distinct segment during a crowded market than to determine a presence during a market set apart by generally light rivalry. Not many obstructions to the section keep going exceptionally long, especially in new ventures. Indeed, even licenses don't live close to as much insurance as is commonly expected. In this way, you have to sensibly extend the timeframe by which new contenders will break this obstructions[5,11,19,20].

Building strategic plans to improve market place position

When an entrepreneur has taken care of the above prerequisites of serious investigation, the person in question can continue with the last component of the work, building a necessary arrangement that mirrors the discoveries. Vital plans should address all regions of business activity, including the creation of products and additional benefits, appropriation of those merchandise or potentially benefits, valuing of merchandise and additionally administrations, and advertising of products as well as administrations[5].

Advantages of competitive analysis

As the name proposes, competitive analysis is examining the associations in a given industry division or market claim to fame that are battling with your association's things or organizations for a bit of the pie. The examination may be a thorough and thorough examination of the best five contenders, or a more significant number of contenders could be investigated[21,22].

Understand the competition

The essential advantages of any severe investigation are a superior comprehension of what our rivals are doing, what they are offering to clients, and how to keep up our upper hand. The findings from this investigation are probably going to factor unequivocally into own organization's essential arranging. In any case, this is certainly not the only detract from the way toward breaking down contenders from the process of analyzing competitors[23].

Build domain knowledge

Another advantage of serious examination includes growing the information base of those taking a shot at our site or web application.

The examination offers data about substance and usefulness that they have presumably not thought of. This is particularly valid for newcomers to our industry and ought to be genuinely average; not every person will be a topic master. Looking longer-term, this instructive procedure benefits the present undertaking, yet in addition any future venture in that equivalent industry[21,24,25].

Identify best practices

Investigating contender sites offers the chance to find what is functioning admirably for them, just as what is usually being offered through the Web. For instance, if all the contenders offer explicit substance and usefulness, clients will probably anticipate that your site should offer comparable substance and usefulness. On the off chance that they are missing, clients may go to the contender site[21,26,27].

Expand the dialogue and the possibilities

The last advantage originates from extended discourse inside the improvement group, and with different units in our organization, about what serious information intends to our crucial bearing. Such exchange can open up new choices that would not, in any case, have been thought of. Contenders might be adopting different strategies to arriving at the client base, so various prospects exist. In this circumstance, a novel methodology may be ideal, since no standard is developing[21,28].

Criticism of competitive analysis

Competitive analysis that's incomplete or supported incorrect data can lead businesses to construct faulty business strategies, and analysts have also acknowledged that traditional competitive analysis has become more complex and potentially time-consuming. Other observers, meanwhile, argue that judging a company's performance strictly on the idea of performance against chief competitors can retard a business's profitability and cause a false sense of security. Finally, some experts contend that preoccupation with competitive analysis often leads companies to spend insufficient time looking ahead[5].

Basis of comparison

Headquarter, Therapeutic Segments, Industry location, and mainly Overall Revenue. Mainly this competitive ranking is based on two web databases. They are Market Research Reports (https://www.marketresearchreports.com/

blog/2019/04/11/top-15-pharma-companies-india) and INDIAN companies.in (https://indiancompanies.in/top-10-pharma-companies-in-india/). India is one of the largest producers of pharmaceuticals (Fig No. 1), here medicines, vaccines, and neutraceuticals of various types are manufactured in a magnificent quantity.

Based on the above criteria the analysis of comparison the rankings are:

1. Sun Pharma.
2. Aurobindo Pharma Ltd.
3. Lupin.
4. Cipla.
5. Dr. Reddy's.
6. Cadila Healthcare Ltd.
7. Intus Pharmaceuticals Ltd.
8. Glenmark Pharma Ltd.
9. Torrent Pharmaceuticals Ltd.
10. Mankind Pharma Ltd.

Overall Rankings and Company Profiles are given in Table No.1.

Pharmaceutical competitor analysis

Contender Intelligence for the pharmaceutical business is talked about, and the most significant sources are portrayed[46]. Contenders can just set various costs as a market procedure. Endeavoring to boost their benefit, firms will sell an item as long as its negligible income is higher than the minimal expense. With the new contender section, the cost will descend to the negligible expense over the long haul, making this a perfect circumstance for purchasers. The contention for the competitiveness of the pharmaceutical market can't be fully trusted because the pharmaceutical market is not a solitary market but a whole of an enormous number of individual sub-markets. This is because prescriptions utilized to treat a specific well-being condition can't be subbed with medications utilized to treat another well-being condition. The movements in a piece of the overall industry and value all occur within sight of whatever remedial rivalry is presented by other marked medications[6,46–49].

Challenges and Limitations

Since this field competition is very high, the information collected is very tough; no organization gives detailed information as they have their privacy rights. Available information is not enough, and in one of the sources, not more than two pieces of information are available. So, to collect one complete database, it is needed to visit 5-6 places once or even twice. Official websites do not reveal overall revenue. It is obtained by market research.

Recommendation

By emphasizing advertisement in career-related magazines, journals the ardent organization may probably increase its client. The company, by providing scholarships to bright and needy students, may attract more students. By improving the study place environment, ardent may help students in concentrating their programs. By participating in career-related fairs, ardent can improve its reputation and ability to attract more students. To attract more clients, ardent can provide its brochure in coaching centers, medical centers, specific campaigns which provide coaching to technical students and Pharmaceutical colleges. By making faculty more approachable to students, ardent can support its students in a better way. By hiring a suitable placement cell, ardent may give better support to students.

Conclusions

Above mentioned suggestions, recommendations, research depend on our statistical surveying, which is restricted as far as anyone is concerned and capacity. There can be more suggestions, which can demonstrate gainful to the organization. All the segments of customer preference, including value, administration, and area, are just 50% of the severe examination. Investigators have additionally brought up that conventional serious examination has gotten increasingly mind-boggling and possibly tedious. A serious investigation that is fragmented or dependent on off-base information can lead organizations to develop broken business procedures. Client needs ou-

Figure 1. India – One of the largest producer of pharmaceuticals.

Company name and Rank	Headquarter	Mumbai, Maharashtra	Reference
1st **Sun Pharma**	Therapeutic segments	Psychiatry, Anti-Infectives, Neurology, Cardiology, Orthopaedic, Diabetology, Gastroenterology, Ophthalmology, Nephrology, Urology, Dermatology, Gynaecology, Respiratory, Oncology, Dental and Nutritionals.	33, 34, 35
	Plant Location	• Halol, Gujrat • Baska, Gujrat • Dadra, Dadra & Nagar Haveli • Silvassa, Dadra & Nagar Haveli • Jammu, JK • Samba, JK • Baddi, Himachal Pradesh • Batamandi, Himachal Pradesh • Mohali, Punjab • Setipool, Sikkim • Madkai, Goa • Guwahati, Assam • Paonta Sahib, Himachal Pradesh • Dahej, Gujrat • Toansa, Punjab • Malanpur, Dewas,Madhya Pradesh • Ahmednagar, Maharashtra • Panoli, Gujrat • Ankleshwar, Karkhadi, Gujrat • Maduranthakam, Tamil Nadu	
	Overall Revenue	**INR 273.28 Billion**	
	Rankings	It is the number one in rank as per 2019 survey. It is present in many states in India and has wide range of therapeutic segments. Its Market Capital as per 2019 is **57,919** Cr.	
	Company Website	https://www.sunpharma.com/	
2nd **Aurobindo Pharma Ltd.**	Headquarter	Hyderabad	34, 35, 36
	Therapeutic Segments	Cephalosporins, Penams, Quinolones, Ace Inhibitors, Calcium Channel Blocker, Beta Blockers, Diuretics, Lipid Lowering Agents, Anti Platelets, NSAIDS, Anti-Fungal, Anti Diabetic, Anti-Viral, Anti-Depressants, Anti-Alzheimers, Drugs For Schizophrenia And Anti – Retroviral.	
	Plant Location	• Ranga Reddy, Andhra Pradesh • Srikakulam, Andhra Pradesh • Mahboobnaga, Andhra Pradesh • Vishakhapatnam, Andhra Pradesh • Nellore, Andhra Pradesh • Cuddalore, Tamil Nadu • Sangareddy, Telangana • Medak, Telangana • Mahbubnagar, Telangana • Medchal-Malkajgiri, Telangana • Bhiwad, Rajasthan	
	Overall Revenue	**INR 164.99 Billion**	
	Rankings	It is the number two in rank as per 2019 survey. It is present in some states in india and has wide range of therapeutic segments. Its Market Capital as per 2019 is **27,615** Cr.	
	Company Website	https://www.aurobindo.com/	
3rd **Lupin**	Headquarter	Mumbai	34, 35, 37
	Therapeutic Segments	Cardiovascular, Diabetology, Asthma, Pediatric, CNS, Anti-Infective and NSAIDS	
	Plant Location	• Jammu, J & K • Verna, Goa • Pune, Maharastra • Ankleshwar, Gujarat	

Table 1. Overall Rankings and Company Profiles.

		• Mandideep, Gujarat • Vadodara, Gujarat • Tarapur, Maharashtra • Bhasmey, Sikkim • Indore, Madhya Pradesh • Nagpur, Maharashtra	
		• Aurangabad, Maharashtra • Vizag, Andhra Pradesh	
	Overall Revenue	**INR 159.55 Billion**	
	Rankings	It is the number three in rank as per 2019 survey. It is present in many states in India and has wide range of therapeutic segments. Its Market Capital as per 2019 is **29,497** Cr.	
	Company Website	https://www.lupin.com/	
4th **Cipla**	Headquarter	Mumbai	34, 35, 38
	Therapeutic Segments	Myocardial infarction, Angina Pectoris, Heart Failure, Hypertension, Arrhythmia, Lipid Abnormalities, Diabetes, and Obesity.	
	Plant Location	• Patalganga, Maharashtra • Kurkumbh, Maharashtra • Satara, Maharashtra • Indore, Madhya Pradesh • Verna, Goa • Baddi, Himachal Pradesh • Rangpo , Sikkim • Bangalore, Karnataka • Virgonagar, Karnataka • Bommasandra, Karnataka	
	Overall Revenue	**INR 155.77 Billion**	
	Rankings	It is the number four in rank as per 2019 survey. It is present in many states in India and has wide range of therapeutic segments. Its Market Capital as per 2019 is **34,358** Cr.	
	Company Website	https://www.cipla.com/	
5th **Dr. Reddy's**	Headquarter	Hyderabad	34, 35, 39
	Therapeutic Segments	Gastrointestinal Ailments, Cardiovascular Disease, Pain Management, Oncology, Anti-Infective, Paediatrics And Dermatology	
	Plant Location	• Medchal-Malkajgiri, Telangana • Hyderabad, Telangana • Medak, Telangana • Sangareddy, Telangana • Ranga Reddy, Telangana • Srikakulam, Andhra Pradesh • Vishakapatnam, Andhra Pradesh • Solan District, Himachal Pradesh • Bengaluru, Karnataka	
	Overall Revenue	**INR 144.36 Billion**	
	Rankings	It is the number five in rank as per 2019 survey. It is present in some states in India and has wide range of therapeutic segments. Its Market Capital as per 2019 is **50,867** Cr.	
	Company Website	https://www.drreddys.com/	
6th **Cadila Healthcare Ltd.**	Headquarter	Ahmedabad	
	Therapeutic Segments	Gastroenterology, Cardiology, Cardiovascular, Gynaecology And Diabetology.	
	Plant Location	• Padra, Gujarat • Vadodara, Gujarat • Ahmedabad, Gujarat • Thane, Maharashtra • Mumbai, Maharashtra	

Table 1. Overall Rankings and Company Profiles.

		• Kundaim Industrial Estate, Goa • Baddi, Himachal Pradesh • Majitar, Sikkim	34, 35, 40
	Overall Revenue	**INR 120.50 Billion**	
	Rankings	It is the number six in rank as per 2019 survey. It is present in some states in India and has wide range of therapeutic segments. Its Market Capital as per 2019 is **26,228** Cr.	
	Company Website	https://zyduscadila.com/	
7th **Intus Pharmaceuticals Ltd.**	Headquarter	Ahmedabad	
	Therapeutic Segments	CNS, Cardiovascular, Diabetology, Gastroenterology, Urology and Oncology.	
	Plant Location	• Matoda, Rajasthan • Moraiya, Gujarat • Valia, Gujarat • Vatva, Ahmedabad, Gujarat • Sanand, Ahmedabad, Gujarat	
		• Ankeleshwar, Gujrat • Bageykhola, Sikkim • Dehradun, Uttarakhand	34, 41
	Overall Revenue	**INR 108.86 Billion**	
	Rankings	It is the number seven in rank as per 2019 survey. It is present in some states in India and has wide range of therapeutic segments.	
	Company Website	https://www.intaspharma.com/	
8th **Glenmark Pharma Ltd.**	Headquarter	Mumbai	
	Therapeutic Segments	Dermatology, Respiratory And Oncology	
	Plant Location	• Baddi, Himachal Pradesh • Nalagarh, Himachal Pradesh • Colvale, Goa • Samlik-Marchak, Sikkim • Nashik, Maharashtra • Aurangabad, Maharashtra • Raigad, Maharashtra • Pune, Maharashtra • Indore, Madhya Pradesh • Ankleshwar, Gujarat • Bharuch, Gujarat	34, 35, 42, 43
	Overall Revenue	**INR 91.86 Billion**	
	Rankings	It is the number eighth in rank as per 2019 survey. It is present in some states in India and has wide range of therapeutic segments. Its Market Capital as per 2019 is **7,505** Cr.	
	Company Website	https://www.glenmarkpharma.com/	
9th **Torrent Pharmaceuticals Ltd.**	Headquarter	Ahmedabad	
	Therapeutic Segments	Anti Diabetic, Anti Microbial Therapy, Cardiovascular Therapy, Dermatologic Therapy, Gastro Intestinal Therapy, Gynecology Therapy, Nephrology Therapy, Neuro Psychiatric, Nutritional, Oncology, Pain Therapy, Urology	
	Plant Location	• Indrad, Gujarat • Dahej, Gujarat • Baddi, Himachal Pradesh • Gangtok, Sikkim • Vizag, Andhra Pradesh • Pithampur, Madhya Pradesh	34, 35, 44
	Overall Revenue	**INR 63.01 Billion**	

Table 1. Overall Rankings and Company Profiles.

	Rankings	It is the number ninth in rank as per 2019 survey. It is present in some states in India and has wide range of therapeutic segments. Its Market Capital as per 2019 is **35,530** Cr.	
	Company Website	https://torrentpharma.com/	
10th	Headquarter	New Delhi	
	Therapeutic Segments	Cardiovascular, Antibiotics, Gastro-intestinal, Anti-allergic, Anti-fungal, Nutritional, NSAIDs, Ortho and Gynaecological.	
Mankind Pharma Ltd.	Plant Location	• Paonta Sahib, Himachal Pradesh • Bermiok Elaka, Sikkim • Vizag, Andhra Pradesh • Sotanala, Rajasthan	34, 43
	Overall Revenue	**INR 52.00 Billion**	
	Rankings	It is the number tenth in rank as per 2019 survey. It is present in some states in India and has wide range of therapeutic segments.	
	Company Website	https://www.mankindpharma.com/	

Table 1. Overall Rankings and Company Profiles.

ght to turn into the organization's business needs. Investigating customer needs and wants is about client needs and needs is a significant piece of serious examination. Examining internal strengths and weaknesses is another significant component of serious investigation, figuring out what organizations own qualities and shortcomings are. The discoveries from this investigation are probably going to factor unequivocally into our own organization's essential arranging. Steps of competitive analysis are a few significant components of serious investigation, every one of which should be deliberately considered on the off chance that one would like to change serious examination exercises into business productivity. Significant parts of serious investigation incorporate the business leading the serious examination to choose whether rivalries are coincidental or whether they present a potential danger, either now or later on, to the business' monetary prosperity.

Bibliographic references

1. Gravitas: India: The World's Vaccine Producer. INDIA: THE WORLD'S VACCINE PRODUCER. Published online 17 July, 2020. Accessed 17 July, 2020. https://www.youtube.com/watch?v=7_lwr1zjFqg&feature=youtu.be
2. Ensure that customers really do have different needs. Course Hero. Accessed 9 May, 2020. https://www.coursehero.com/file/p6jo00v/ensure-that-customers-really-do-have-different-needs-and-wants-in-other-words/
3. Competitor analaysis. SlideShare. Published 23 May, 2014. Accessed 9 May, 2020. https://www.slideshare.net/tousifirshad/competitor-analaysis
4. 19777594-Project-on-Competitive-Analysis-and-Scope-of-Placement-Consultancies. SCRIBD. Accessed 10 May, 2020. https://www.scribd.com/document/48477753/19777594-Project-on-Competitive-Analysis-and-Scope-of-Placement-Consultancies
5. COMPETITIVE ANALYSIS. Reference For Busiess. Accessed 10 May, 2020. https://www.referenceforbusiness.com/small/Bo-Co/Competitive-Analysis.html
6. Mitteness C, Sudek R, Cardon MS. Angel investor characteristics that determine whether perceived passion leads to higher evaluations of funding potential. Journal of Business Venturing. 2012;27(5):592-606. doi:10.1016/j.jbusvent.2011.11.003
7. National Cancer Institute. Serious Breach. In: Definitions. Qeios; 2020. doi:10.32388/1CUPHH
8. H Coronel M. Sbp4sample(Aca). SCRIBD. Accessed 10 May, 2020. https://www.scribd.com/document/237797640/Sbp4sample-Aca
9. Ck A. competitive analysis. SCRIBD. Accessed 10 May, 2020. https://www.scribd.com/document/431524350/competitive-analysis
10. Anderson D, ed. Survive Success: How to Overcome the Six Temptations of Successful Organizations. In: Up Your Business!. John Wiley & Sons, Inc.; 2015:203-242. doi:10.1002/9781119197720.ch6
11. The successful business plan rhonda abrams. Accessed 10 May, 2020. https://kalofyhizoci.omgmachines2018.com/the-successful-business-plan-rhonda-abrams-4549dx.html
12. Shanmuga P. mm. SCRIBD. Accessed May 10, 2020. https://www.scribd.com/document/179331354/mm
13. Shalhoub S. 101: Sizing up the competition. (WBJ) Worcester Business Journal. Published 10 November, 2014. Accessed 10 May, 2020. https://www.wbjournal.com/article/101-sizing-up-the-competition
14. Rahulingle. Projcet on Packaged Drinking Water Compny. SCRIBD. Accessed 10 May, 2020. https://www.scribd.com/doc/71550033/Projcet-on-Packaged-Drinking-Water-Compny
15. Wainwright P. Deciding What the Client Needs. In: Pro Apache. Apress; 2004:231-306. doi:10.1007/978-1-4302-0658-3_5
16. Customer Needs, Business Needs, and Government Requirements. In: Automotive Product Development. 1st ed. CRC Press; 2017:59-73. doi:10.1201/9781315119502-4
17. Marketing – from needs to wants. In: Scaling up Business Solutions to Social Problems. Palgrave Macmillan; 2015. doi:10.1057/9781137466549.0024
18. Gallaway GR. Delivering what your customer wants, needs, and/or can pay for . . In: IEEE Conference on Aerospace and Electronics. IEEE; 1990:875-877. doi:10.1109/NAECON.1990.112883
19. An Organization Of A Business Perspective : A Company That Has Fallen Behind The Competition With Other Companies. 123HELPME. Accessed 12 May, 2020. https://www.123helpme.com/essay/An-Organization-Of-A-Business-Perspective-A-534293
20. Material form color quantity description hdpe etc. Course Hero. Accessed 13 May, 2020. https://www.coursehero.com/file/p6hhajda/Material-Form-Color-Quantity-Description-HDPE-Baled-lumpsfluffpowder-etc-Natural/
21. Withrow J. Competitive Analysis: Understanding the Market Context. Boxes and Arrows. Published 27 February, 2006. Accessed 12 May, 2020. https://boxesandarrows.com/competitive-analysis-understanding-the-market-context/
22. The Main Contenders. In: Knowing What Is Good For You. Palgrave Macmillan; 2011. doi:10.1057/9780230359796.0005
23. A competitive analysis and study in Indian Telecom Sector (MBA Marketing). P2P Programmer 2 Programmer. Accessed 12 May, 2020. http://programmer2programmer.net/tips/mba/get_mba_project_idea.aspx?mba-marketing&projid=283
24. Westbrook J. Expanding Our D&U Knowledge Base. Published online 2001. doi:10.1037/e321802004-002
25. Sebastian T. Our Long-Term Strategic Outlook [Looking Forward]. IEEE Ind Appl Mag. 2015;21(1):141-142. doi:10.1109/MIAS.2014.2362035

26. Use competitor analysis to avoid situations that involve head on competition. Kegexelisujuj Tranceforming Nlp. Accessed 13 May, 2020. https://kegexelisujuj.tranceformingnlp.com/use-competitor-analysis-to-avoid-situations-that-involve-head-on-competition-11674pb.html
27. BHATTAD SM. COMPETITIVE ANALYSIS FOR SUHANA MASALA PRODUCTS IN SOLAPUR MARKET. SCRIBD. Accessed 12 May, 2020. https://www.scribd.com/document/68510218/Sonal-Project-Report
28. Competitive Analysis and Site Objectives. a flux state the journal of an enquiring mind at Brighton University. Published 19 November, 2011. Accessed 12 May, 2020. https://afluxstate.wordpress.com/2011/11/19/competitive-analysis-and-site-objectives/
29. Farhan M. Methodology. SCRIBD. Accessed 13 May, 2020. https://www.scribd.com/document/146866649/Methodology
30. Dori D. Object-Process Methodology. Springer Berlin Heidelberg; 2002. doi:10.1007/978-3-642-56209-9
31. Definition of methodology. Merriam Webster. Accessed 13 May, 2020. https://www.merriam-webster.com/dictionary/methodology
32. How can you explain these three words to me...? Yahoo!Answers. Accessed 13 May, 2020. https://answers.yahoo.com/question/index?qid=20090123211046AAIjQrX
33. Sun Pharma. Accessed 13 May, 2020. https://www.sunpharma.com/
34. Top 15 Pharma Companies in India. Market Research Reports. Published 11 April, 2019. Accessed 13 May, 2020. https://www.marketresearchreports.com/blog/2019/04/11/top-15-pharma-companies-india
35. Raveendran R. Top 10 Pharma Companies in India 2020. indiancompanies.in. Published 20 August, 2019. Accessed 14 May, 2020. https://indiancompanies.in/top-10-pharma-companies-in-india/
36. Aurobindo Pharma. Accessed 13 May, 2020. https://www.aurobindo.com/
37. Lupin. indiancompanies.in. Accessed 14 May, 2020. https://www.lupin.com/
38. Cipla. Accessed 13 May, 2020. https://www.cipla.com/our-offerings/our-therapies
39. Dr. Reddy's. Accessed 13 May, 2020. https://www.drreddys.com/
40. Zyduscadila. Accessed 14 May, 2020. https://zyduscadila.com/
41. Intas Pharma. Accessed 14 May, 2020. https://intaspharma.com/manufacturing/facilities/
42. Glenmark Pharma. Accessed 14 May, 2020. https://www.glenmarkpharma.com/
43. Money Control. Glenmark Pharma Ltd. Accessed 14 May, 2020. https://www.moneycontrol.com/company-facts/glenmarkpharma/locations/gp08
44. Torrent Pharma. Accessed 14 May, 2020. http://www.torrentpharma.com/
45. Mankind Pharma. Accessed 14 May, 2020. https://www.mankindpharma.com/
46. Desai BH, Bawden D. Competitor Intelligence in the pharmaceutical industry; the role of the information professional. Journal of Information Science. 1993;19(5):327-338. doi:10.1177/016555159301900501
47. Mehta A, Hasan Farooqui H, Selvaraj S. A Critical Analysis of Concentration and Competition in the Indian Pharmaceutical Market. Beck EJ, ed. PLoS ONE. 2016;11(2):e0148951. doi:10.1371/journal.pone.0148951
48. Frank RG, Hartman RS. The Nature of Pharmaceutical Competition: Implications for Antitrust Analysis. International Journal of the Economics of Business. 2015;22(2):301-343. doi:10.1080/13571516.2015.1045745
49. Garattini L, Padula A. Competition in pharmaceuticals: more product- than price-oriented? Eur J Health Econ. 2018;19(1):1-4. doi:10.1007/s10198-017-0932-4

Received: 10 February 2021
Accepted: 21 April 2021

REVIEW / ARTÍCULO DE REVISIÓN

Major epigenetic factors associated with the novel coronavirus disease-2019 (COVID-19) severity

Ahmed A Mhawesh[1], Daniah Muneam Hamid[2], Abdolmajid Ghasemian[3]

DOI. 10.21931/RB/2021.06.02.31

Abstract: The worldwide spread and high rate of viral transmission and related morbidity and mortality of Coronavirus disease-19 (COVID-19) is a crisis. Some epigenetic determinants predispose individuals to severe infection. Patients with prior chronic medical illnesses (hypertension, diabetes, lupus, and chronic obstructive lung disease) are highly susceptible to the infection. The aging and diabetes pandemic possibly exacerbate the COVID-19 or SARS-CoV-2 pandemic by enhancing COVID-19 associated comorbidities. COVID-19 utilizes several proteins for tackling the host immune response associated with enhancing comorbidities. The angiotensin-converting enzyme (ACE) is a significant receptor for SARS-CoV-2, which significantly expresses higher among individuals with comorbidities and under stress conditions. Patients with systemic lupus erythematosus are also prone to be susceptible to the disease. Viral infections cause a defect in the DNA methylation in lupus, causing further ACE2 hypomethylation and overexpression, leading to viral binding and cytokine storm and tissue damage during COVID-19 infection. The microRNAs (miRNAs) epigenetics regulations also play a critical role in the suppression of immune responses. Meanwhile, viral proteins interplays with the host cell are conferred primarily through TGF-β and HIF-1 signaling, endocytosis, autophagy, and Toll-like receptor signaling RIG-I signaling, Il-17 signaling, and fatty acid oxidation/degradation. Furthermore, the COVID19 patient's metabolic states determine the infection severity. Noticeably, ten human metabolic proteins, including SGTA, SPECC1, FGL2, PHB, STAT3, BCL2L1, CAV1, JUN, PPP1CA, and XPO1, interact with the SARSE-CoV-2. Interactions between SARSCoV's spike protein-containing lipid-rich membrane compartments and epigenetic modulations are considered targets to inhibit the viral infection. Therefore, it seems that epigenetics plays a substantial role in the COVID-19 severity. Future in-depth studies will be promising. Vaccine design, particularly regarding ACE viral receptor monoclonal antibodies, is a proposal alongside adhering to personal hygiene.

Key words: Coronavirus disease-19, epigenetics, severe respiratory disease.

Introduction

For fighting against every infection, a triangle including genetics, environment, and lifestyle is the primary determinant of triumph. The recent emergence and spread of novel *Coronavirus* disease known as COVID-19 or Severe Acute Respiratory Syndrome *Coronavirus*-2 (SARSE CoV-2, also coronavirus) in Wuhan in central China, has recently caused a pandemic scale of pneumonia in humans leading to concurrently and continuing high transmission, morbidity and mortality rat[1] *Coronavirus* subfamily is single-stranded positive-sense (+ssRNA) virus. The pandemic spread of novel coronavirus disease-19 (CoVID-19) in 2019-2020 originated from Wuhan, China, continues to affect human health and many life aspects and activities. The severity of infection increases with advancing age. Data suggests that very complex host-virus interplays occur during the SARS-CoV-2 infections (table1 and Figure 1).

Although the pathogenicity of SARSE-CoV-2 has not been entirely understood, extensive lung damage, enhanced infiltration of monocytes, macrophages, and neutrophils within the respiratory system and the blood storm of proinflammatory cytokines and chemokines are associated with the severity of infection[2,3]. Another mechanism of viral evasion includes delayed IFN type I transduction which stimulates the monocytes and macrophages and delays T-cells activation. Both the SARSE-CoV and SARSE-CoV-2 viruses bind to the angiotensin-converting enzyme receptor (ACE) via their spike protein receptor-binding domains which share 72% amino acid similarity[4,5]. Strikingly, the SARSE-CoV-2 domain has an incredibly higher receptor affinity. Higher expression of ACE among patients with comorbidities supposedly predisposes them to severe infection.

Moreover, it was stated that viral binding to the ACE downregulates its expression and leads to lower level biosynthesis of end-product vasodilator heptapeptide angiotensin 1-7. This, in turn, causes lung injury due to increased pulmonary vascular permeability. Another receptor for *Coronaviruses* includes a zinc peptidase known as aminopeptidase N (APN), which shares homology and membrane topological similarities with the ACE[4,6,7].

Those epigenetic factors mainly facilitating the viral attachment to host cells seem to enhance the death rate. These primarily include methylation or expression of angiotensin-converting enzyme 2 (ACE2), microRNAs regulation, metabolic conditions, individual behavior (such as smoking), and some environmental conditions (temperature and humidity)[37-39].

The genomic material released by its virus is mRNA, so it is prepared to stay translated into protein. In its genome range, its virus is complemented by using respecting 14 open reading frames (ORF), each of which encodes a variety concerning proteins, each structural yet non-structural, so move a function into its uplift so nicely as much virulence power. In its transformation section, the gene segments so encode non-structural polyproteins use this method to advance ORF1a yet ORF1b under production twins full-size overlapping polyproteins, pp1a and pp1ab utilizing contributing a ribosomal body shifting match[40] . The polyproteins are supplemented by using protea-

[1] Dept. of Med. and Mol. Biotech., College of Biotechnology, Alnahrain Univesirt, Baghdad, Iraq.
[2] DNA Forensic center for research and training, Alnahrain University, Baghdad, Iraq.
[3] Islamic Azad University, Central Tehran Branch, Tehran, Iran.

Corresponding author: alshammariahmed.a.m@gmail.com

nsps (range)	Functions	Ref.
nsp1 (1–180)	• The nsp1 is encoded by α-CoVs and β-CoVs but not by γ-CoVs and δ-CoVs • Blocks host cell translation • Cellular mRNA degradation • Chemokine Dysregulation • Highly divergent among CoVs • Inhibiting IFN signaling • Regulation of host and viral genes expression • Promotes cellular/host mRNA degradation • Potential virulence factor • Results in blocking the innate immune response Suppress of type I interferon • Suppress the host protein synthesis • Target for CoV vaccine development	8-11
nsp2 (181–818)	• Binds to prohibitin proteins • Dispensable for viral replication • Regulator of nsp3 gene function • Pivotal role in the viral life cycle • Viral infection	12, 13
nsp3 (819–2763)	• ADRP (ADP-ribose-1'-phosphate) activity promotes cytokine expression • Interacts with viral proteins and participates in viral assembly • Blocks host innate immune response • Blocking host innate immune response • Cleaves viral polyprotein • Key role in the replication/transcription of DNA • PLPro (papain-like proteinase) • PLPro/Deubiquitinase domain • Polypeptides cleaving • Promoting cytokine expression • The papain-like protease of Nsp3 as a target for therapy	13-17
nsp4 (2764–3263)	• Assembly of murine Coronavirus DMVs • Double-membrane vesicle (DMV) formation • Essential for viral multiplication by interaction with the nsp3 via H120&F121 • Potential transmembrane scaffold protein	18, 19
nsp5 (3264–3569)	• Cleaves viral polyprotein • Cysteine protease • Chymotrypsin-like protease (3CLpro) • Inhibiting IFN signaling • Main protease (Mpro) • Novel targets for non-active site inhibitors • Polypeptides cleaving	20, 21
nsp6 (3570–3859)	• Complex with nsp3 and 4: DMV formation • Potential transmembrane scaffold protein • Restricting autophagosome expansion	22
nsp7 (3860–3942)	• Cofactor with nsp8 and nsp12 • Complex with nsp8: primase • Hexadecameric complex with nsp8 • As a clamp for RNA polymerase	21, 23, 24

Table 1. Major *Coronavirus* non-structural proteins (nsps) and their pathogenicity capabilities.

nsp8 (3943–4140)	• Cofactor with nsp7 and nsp12 • Complex with nsp7: primase • Forms hexadecameric complex with nsp7 • May act as processivity clamp for RNA polymerase	21, 25
nsp9 (4141–4253)	• Dimerization and RNA binding • Replicase Protein • RNA binding protein	26
nsp10 (4254–4392)	• Cofactor for nsp16 and nsp14 • Complex with nsp14: replication fidelity • Enzymatic co-factor • Stimulates the ExoN and 2-O-MT via heterodimer forming • As the nsp14 and nsp16 scaffold protein	27-29
nsp11 (4393–5324)	• Endoribonuclease (EndoU) • Short peptide at the end of orf1a	30, 31
nsp12 (5325–5925)	• NiRAN, nidovirus RdRp-associated nucleotidyl transferase • Primer dependent RdRp • RNA-dependent RNA polymerase (RdRp)	32, 33
nsp13 (5926–6452)	• Exoribonuclease activity acting in a 3′ to 5′ direction and N7-guanine methyltransferase activity.	34
nsp14 (6453–6798)	• Mn(2+)-dependent endoribonuclease activity	34
nsp15 (6799–7096)	• Methyltransferase that mediates mRNA cap 2′-O-ribose methylation to the 5′-cap structure of viral mRNAs	35
nsp16 (4393-4405)	• **Avoiding MDA5 recognition and inhibit innate immunity regulation**	21, 36

Table 1. Major *Coronavirus* non-structural proteins (nsps) and their pathogenicity capabilities.

se enzymes, specifically papain-like proteases (PLpro), yet a serine kind Mpro (chymotrypsin-like protease (3CLpro)) protease as are encoded of nsp3 then nsp 5. Subsequently, burst occurs into pp1a yet pp1ab into non-structural proteins (nsps) 1–11 and 1–16. The nsps shed a vital role in deep approaches of viruses yet host cells, as shown in Table 1[21].

Angiotensin-converting enzyme as the CoVID-19 receptor

Several body compartments, such as respiratory and gastrointestinal systems, have cells that express the *ACE2* as the CoVID-19 receptor for its binding, entry (activation of the viral spike glycoprotein and *ACE2* C-terminal segment cleavage), replication, and shedding. Epigenetics surveys have suggested that the *ACE2* gene located on the X chromosome is regulated by DNA methylation[41-43]. It was postulated that the variability in D/I genotype distribution of the *ACE* gene is possibly associated with the variable prevalence of the COVID-19 infection[42].

Notably, methylation varies across tissue cell types, and at three CpGs (cg04013915, cg08559914, and cg03536816) was lowest in lung epithelial cells. This figure was significantly lower among females than males, which differs in the *ACE2* gene and protein expression and COVID-19 severity[44]. Interestingly, increased *ACE2* expression has been observed by staining lung tissue sections from patients with pulmonary hypertension. As the potential cause of *ACE2* gene expression, enzymes that modify histones (KDM5B, H3K27a, H3K4me1, and H3K4me3) are notable. However, significant differences in *ACE2* between racial groups, age groups, or gender groups were not verified in one study. Besides, smoking as an epigenome effector was not shown to have a role in COVID-19 infection risk. Also, *IL-6* and *INS* (encoding the insulin hormone) genes have been associated with significant comorbidities. NAD-dependent histone deacetylase Sirtuin 1 (SIRT1) can also epigenetically induce the *ACE* gene expression under stress conditions. Viral infections cause a defect in the DNA methylation in lupus disease, causing further *ACE2* gene hypomethylation and overexpression, leading to viral binding and cytokine storm and tissue damage COVID-19 infection[45,46]. The viral

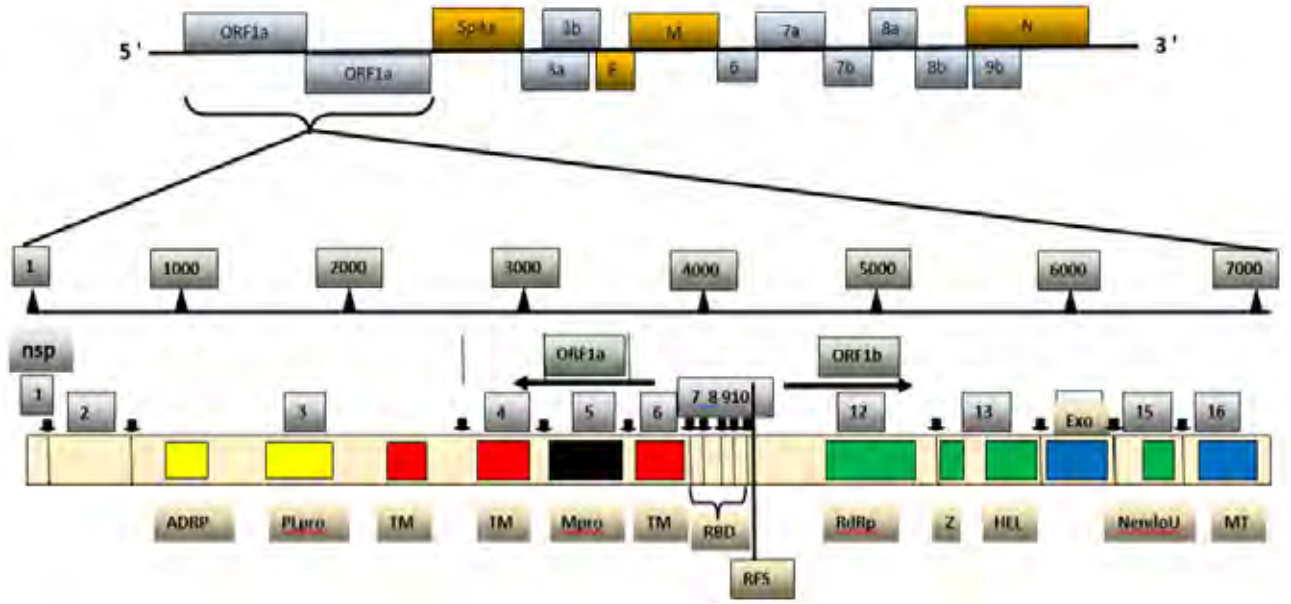

Figure 1. Genome and non-structural proteins of Severe Acute Respiratory Syndrome Coronavirus-2.

proteins exploit the host's genetic and epigenetic mediators, leading to viral evasion and determining disease pathophysiology (table1 and figure1). Besides, RAB1A gene was adequate for the COVID-19 infection development. Considering the ACE gene diffential expression, the age and sex of patients are also considered as risk factors for the COVID-19 infection[47].

Host and viral microRNAs epigenetic regulations

It has been revealed that epigenetics aspects of miRNA (small ncRNA molecules) mediated interactions with the host cells differ between SARSE-Cov and SARSE-Cov-2 (COVID-19). Hence, some viral miRNAs in a particular way affect several immune signaling pathways (IFN-I signaling, autophagy, etc.) that facilitate the prolonged latency. Moreover, COVID-19 modulates several critical cellular pathways resulting in the enhancement of anomalies in patients with comorbidities. The nucleocapsid protein from *Coronavirus* strain OC43 interacts with miR-9 and stimulates the NF-κB pathway. These findings are advantageous towards designing RNA therapeutics to mitigate the COVID-19 mediated comorbidities. Viral respiratory infections imposed by coronaviruses, influenza, adenovirus, rhinovirus, and RSV causes aberrant host miRNA expression mostly related to suppressing immune responses. Evidence has supposed that SARSE-Cov and SARSE-Cov-2 employ novel immune evasion strategies through utilizing host miRNA, but the exact mechanisms exerted by miRNA on the epigenetic interactions with the host have not been verified. It was hypothesized that genetic differences between SARSE-Cov and SARSE-Cov-2 and variations in binding to host miRNAs lead to differential pathogenesis[46].

Additionally, viral miRNAs differences and the fast mutation rate of SARSE-Cov2 in various regions have caused a higher pathogenicity rate. It was outlined that hsa-miR-20b-5p, hsa-miR-17-5p, and hsa-miR-323a-5p had anti-COVID-19 activities primarily targeting viral ORF1ab and S regions[44,48]. It is noteworthy that host miRNAs play a role like a double-edged sword and sometimes promote viral evasion, attachment, and replication. Patients suffering from underlying diseases (such as diabetes, cardiovascular diseases, and renal impairments) are more susceptible to SARS-CoV-2. It was revealed that host miRNA-mediated downregulated pathways disturb patients with the infection, making them more susceptible.

Viruses inflicting severe pulmonary illness can use three epigenetic-regulated approaches in the course of host-pathogen interaction: i. they execute affect host DNA methylation signatures then miRNAs regulating a cassette of genes underlying native yet adaptive antiviral responses; ii. those can encode because viral proteins up to expectation at once interact along with the host modified histones. Yet, iii. that may manipulate the host miRNA technology nuclear equipment in imitation of encoding viral non-canonical miRNA-like RNA fragments (v-miRNAs) regulating the viral life cycle or immune response[49]. Here, we center on epigenetic-sensitive mechanisms via who H5N1 and SARS-CoV-2 can also affect susceptibility in imitation of pulmonary sickness by interfering with both born yet adaptive immune responses into human beings, as shown in Figure 2.[50,51].

Mainly, T cells yet neutrophils execute bear deoxyribonucleic acid hypomethylation yet histone modifications, respectively, in COVID-19 patients. Otherwise, in vitro lung epithelial cells above H5N1 contamination can undergo adjustments of micro-ribonucleic sour taste (RNA) patterns yet histone tail marks, propulsion according to downregulation regarding antiviral defense. ACE, angiotensin-converting enzyme; AGO2, argonaute 2; CGI, CpG island; COVID-19, coronavirus disorder 2019; mRNA, messenger RNA; NET, neutrophil extracellular trap; NS1, non-structural protein 1; PCBP2, poly (RC)-binding protein 2; ROS, reactive oxygen species; SARS-CoV-2, severe acute respiratory indication coronavirus 2; SLE, systemic lupus erythematosus.

Patients'behavior, nutrition, and metabolic conditions

COVID19 patient's metabolic states determine the infection severity. Noticeably, ten human proteins, including SGTA, SPECC1, PHB, BCL2L1, FGL2, STAT3, JUN, PPP1CA, CAV1, and XPO1 interact with the SARSE-CoV-2. Interactions between SARSCoV's spike protein with lipid-rich membrane compartments and epigenetic modulations are considered targets to inhibit the viral infection[52]. It was revealed that obesity is a risk factor for the SARSE-CoV-2 infection[53]. Noticeably, ten human metabolic proteins, including SGTA, SPECC1, PHB, BCL2L1, FGL2, STAT3, JUN, PPP1CA, CAV1, and XPO1 interact with the SARSE-CoV-2. Interactions between SARSCoV's spi-

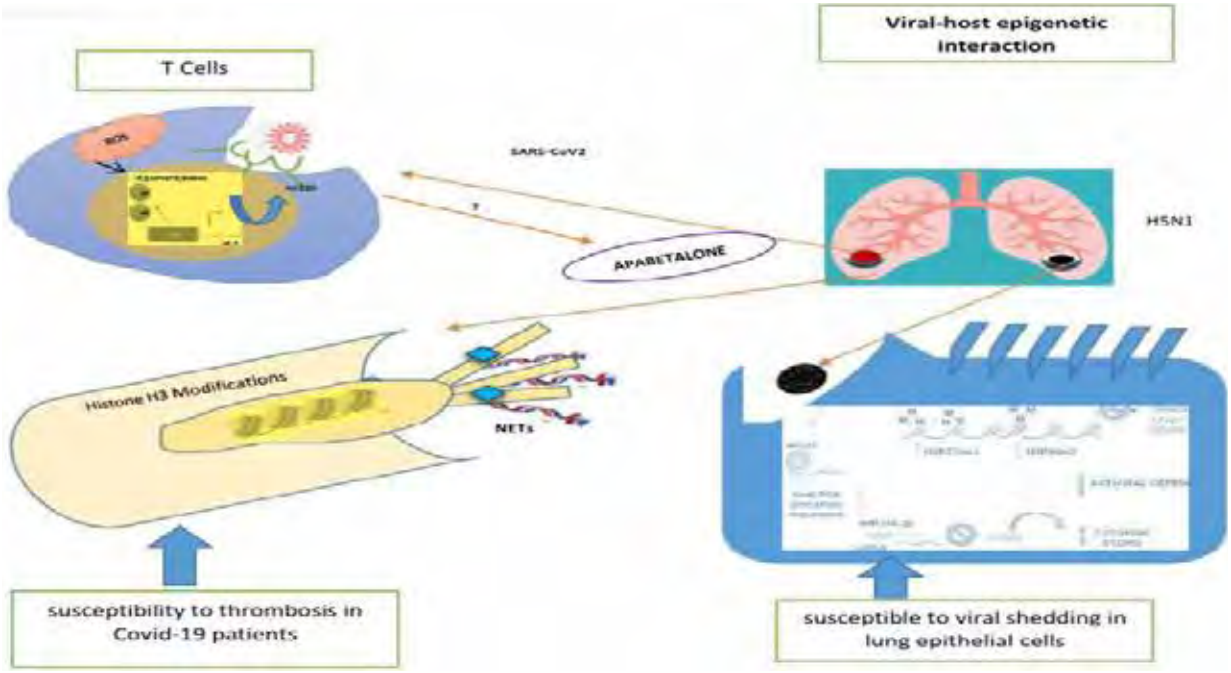

Figure 2. Viral–host epigenetic interactions. We illustrated that III putative cell-specific epigenetic-sensitive mechanisms using SARS-CoV-2 or H5N1 might also affect single sensitiveness according to severe pulmonary quintessential illness.

ke proteins, which have membranes rich in lipids components and epigenetic modulations, are considered targets to inhibit the viral infection. Some personal behaviors such as smoking or common personal behaviors that can reduce COVID-19 exposure are also notable, affecting the transmission, morbidity, and mortality rate[54,55].

Future perspectives

Owing to the lack of effective vaccination until now, investigations in this regard will be promising. Additionally, the application of lower toxic disinfectants and adherence to personal hygiene; particularly among individuals meeting healthcare and developing effective drugs, can be helpful towards reducing the burden of infection. More in-depth verifications regarding epigenetic factors and application inhibitors of the ACE and outcomes are also proposed.

Conclusions

Those epigenetic factors mainly facilitating the viral attachment to host cells seem to enhance the death rate. These primarily include methylation or expression of angiotensin-converting enzyme 2 (*ACE2*), microRNAs regulation, metabolic conditions, individual behavior (such as smoking), and some environmental conditions (temperature and humidity). The angiotensin-converting enzyme (*ACE*) is a significant receptor for SARS-CoV-2, which significantly expresses higher among individuals with comorbidities and under stress conditions. Patients with systemic lupus erythematosus are also prone to be susceptible to the disease. Viral infections cause a defect in the DNA methylation in lupus, causing further *ACE2* hypomethylation and overexpression, leading to viral binding and also cytokine storm and tissue damage during COVID-19 infection. The microRNAs (miRNAs) epigenetics regulations also play a critical role in the suppression of immune responses.

Meanwhile, viral proteins interplays with the host cell are conferred mainly through TGF-β and HIF-1 signaling, endocytosis, autophagy, and Toll-like receptor signaling RIG-I signaling, Il-17 signaling, and fatty acid oxidation/degradation. Furthermore, the COVID19 patient's metabolic states determine the infection severity. Noticeably, ten human metabolic proteins, including SGTA, SPECC1, PHB, BCL2L1, FGL2, STAT3, JUN, PPP1CA, CAV1, and XPO1 interact with the SARSE-CoV-2. Interactions between SARSCoV's spike structural proteins containing membranes rich in lipidic macromolecules and epigenetic modulations are considered targets to inhibit the viral infection. Therefore, it seems that epigenetics plays a substantial role in the COVID-19 severity. Future in-depth studies will be promising. Vaccine design, particularly regarding ACE viral receptor monoclonal antibodies, is a proposal alongside adhering to personal hygiene.

Conflict of interest

None to declare.

Acknowledgments

Ohe authors wrote this study.

Bibliographic references

1. Novel, CPERE, 2020. The epidemiological characteristics of an outbreak of 2019 novel coronavirus diseases (COVID-19) in China. Zhonghua liu xing bing xue za zhi= Zhonghua liuxingbingxue zazhi, 41(2), p.145.
2. Xu, Z., Shi, L., Wang, Y., Zhang, J., Huang, L., Zhang, C., Liu, S., Zhao, P., Liu, H., Zhu, L. and Tai, Y., 2020. Pathological findings of COVID-19 associated with acute respiratory distress syndrome. The Lancet respiratory medicine, 8(4), pp.420-422.
3. Rothan, H.A. and Byrareddy, S.N., 2020. The epidemiology and pathogenesis of coronavirus disease (COVID-19) outbreak. Journal of autoimmunity, p.102433.
4. Patel, A.B. and Verma, A., 2020. COVID-19 and angiotensin-converting enzyme inhibitors and angiotensin receptor blockers: what is the evidence? Jama, 323(18), pp.1769-1770.
5. Vaduganathan, M., Vardeny, O., Michel, T., McMurray, J.J., Pfeffer, M.A. and Solomon, S.D., 2020. Renin–angiotensin–aldosterone system inhibitors in patients with Covid-19. New England Journal of Medicine, 382(17), pp.1653-1659.

6. Fang, L., Karakiulakis, G. and Roth, M., 2020. Are patients with hypertension and diabetes mellitus at increased risk for COVID-19 infection? The Lancet. Respiratory Medicine, 8(4), p. e21.
7. Diaz, J.H., 2020. Hypothesis: angiotensin-converting enzyme inhibitors and angiotensin receptor blockers may increase the risk of severe COVID-19. Journal of Travel Medicine.
8. Narayanan, K., Ramirez, S.I., Lokugamage, K.G. and Makino, S., 2015. Coronavirus non-structural protein 1: Common and distinct functions in the regulation of host and viral gene expression. Virus research, 202, pp.89-100.
9. HUI, WH, 2012. Host-viral Interactions: Host factors in coronavirus replication and coronaviral strategies of immune evasion (Doctoral dissertation).
10. Sun, L., Xing, Y., Chen, X., Zheng, Y., Yang, Y., Nichols, D.B., Clementz, M.A., Banach, B.S., Li, K., Baker, S.C. and Chen, Z., 2012. Coronavirus papain-like proteases negatively regulate antiviral innate immune response through disruption of STING-mediated signaling. PloS one, 7(2), p. e30802.
11. Kamitani, W., Narayanan, K., Huang, C., Lokugamage, K., Ikegami, T., Ito, N., Kubo, H. and Makino, S., 2006. Severe acute respiratory syndrome coronavirus nsp1 protein suppresses host gene expression by promoting host mRNA degradation. Proceedings of the National Academy of Sciences, 103(34), pp.12885-12890.
12. Graham, R.L., Sims, AC, Baric, RS and Denison, M.R., 2006. The nsp2 proteins of mouse hepatitis virus and SARS coronavirus are dispensable for viral replication. In The Nidoviruses (pp. 67-72). Springer, Boston, MA.
13. Fehr, A.R. and Perlman, S., 2015. Coronaviruses: an overview of their replication and pathogenesis. In Coronaviruses (pp. 1-23). Humana Press, New York, NY.
14. Fehr, A.R., Athmer, J., Channappanavar, R., Phillips, J.M., Meyerholz, D.K. and Perlman, S., 2015. The nsp3 macrodomain promotes virulence in mice with coronavirus-induced encephalitis. Journal of virology, 89(3), pp.1523-1536.
15. Imbert, I., Snijder, E.J., Dimitrova, M., Guillemot, J.C., Lécine, P. and Canard, B., 2008. The SARS-Coronavirus PLnc domain of nsp3 as a replication/transcription scaffolding protein. Virus research, 133(2), pp.136-148.
16. Clementz, M.A., Kanjanahaluethai, A., O'Brien, T.E. and Baker, S.C., 2008. Mutation in murine coronavirus replication protein nsp4 alters assembly of double membrane vesicles. Virology, 375(1), pp.118-129.
17. Lei, J., Kusov, Y. and Hilgenfeld, R., 2018. Nsp3 of coronaviruses: Structures and functions of a large multi-domain protein. Antiviral research, 149, pp.58-74.
18. Sakai, Y., Kawachi, K., Terada, Y., Omori, H., Matsuura, Y. and Kamitani, W., 2017. Two-amino acids change in the nsp4 of SARS coronavirus abolishes viral replication. Virology, 510, pp.165-174.
19. Tomar, S., Johnston, M.L., John, S.E.S., Osswald, H.L., Nyalapatla, P.R., Paul, L.N., Ghosh, A.K., Denison, M.R. and Mesecar, AD, 2015. Ligand-induced dimerization of middle east respiratory syndrome (MERS) coronavirus nsp5 protease (3CLpro) implications for nsp5 Regulation and The Development of Antivirals. Journal of Biological Chemistry, 290(32), pp.19403-19422.
20. Qiu, Y. and Xu, K., 2020. Functional studies of the coronavirus non-structural proteins. STEMedicine, 1(2), pp. e39-e39.
21. Chen, Y., Liu, Q. and Guo, D., 2020. Emerging coronaviruses: genome structure, replication, and pathogenesis. Journal of medical virology, 92(4), pp.418-423.
22. Alexander, S.P., Ball, J.K. and Tsoleridis, T., 2020. SARS-CoV-2 proteins (version 2020.2) in the IUPHAR/BPS Guide to Pharmacology Database. IUPHAR/BPS Guide to Pharmacology CITE, 2020(2).
23. Subissi, L., Posthuma, C.C., Collet, A., Zevenhoven-Dobbe, J.C., Gorbalenya, A.E., Decroly, E., Snijder, E.J., Canard, B. and Imbert, I., 2014. One severe acute respiratory syndrome coronavirus protein complex integrates processive RNA polymerase and exonuclease activities. Proceedings of the National Academy of Sciences, 111(37), pp. E3900-E3909.
24. Zhai, Y., Sun, F., Li, X., Pang, H., Xu, X., Bartlam, M. and Rao, Z., 2005. Insights into SARS-CoV transcription and replication from the structure of the nsp7–nsp8 hexadecamer. Nature structural & molecular biology, 12(11), pp.980-986.
25. Egloff, M.P., Ferron, F., Campanacci, V., Longhi, S., Rancurel, C., Dutartre, H., Snijder, E.J., Gorbalenya, A.E., Cambillau, C. and Canard, B., 2004. The severe acute respiratory syndrome-coronavirus replicative protein nsp9 is a single-stranded RNA-binding subunit unique in the RNA virus world. Proceedings of the National Academy of Sciences, 101(11), pp.3792-3796.
26. Klosterman, S.J., Subbarao, K.V., Kang, S., Veronese, P., Gold, S.E., Thomma, B.P., Chen, Z., Henrissat, B., Lee, Y.H., Park, J. and Garcia-Pedrajas, M.D., 2011. Comparative genomics yields insights into niche adaptation of plant vascular wilt pathogens. PLoS pathog, 7(7), p. e1002137.
27. Bouvet, M., Lugari, A., Posthuma, C.C., Zevenhoven, J.C., Bernard, S., Betzi, S., Imbert, I., Canard, B., Guillemot, J.C., Lécine, P. and Pfefferle, S., 2014. Coronavirus Nsp10, a critical co-factor for activation of multiple replicative enzymes. Journal of Biological Chemistry, 289(37), pp.25783-25796.
28. Ma, Y., Wu, L., Shaw, N., Gao, Y., Wang, J., Sun, Y., Lou, Z., Yan, L., Zhang, R. and Rao, Z., 2015. Structural basis and functional analysis of the SARS coronavirus nsp14–nsp10 complex. Proceedings of the National Academy of Sciences, 112(30), pp.9436-9441.
29. Deng, X. and Baker, S.C., 2018. An "Old" protein with a new story: Coronavirus endoribonuclease is important for evading host antiviral defenses. Virology, 517, pp.157-163.
30. Woo, P.C., Huang, Y., Lau, S.K., Tsoi, H.W. and Yuen, K.Y., 2005. In silico analysis of ORF1ab in coronavirus HKU1 genome reveals a unique putative cleavage site of coronavirus HKU1 3C- like protease. Microbiology and immunology, 49(10), pp.899-908.
31. Posthuma, C.C., te Velthuis, A.J. and Snijder, E.J., 2017. Nidovirus RNA polymerases: complex enzymes handling exceptional RNA genomes. Virus research, 234, pp.58-73.
32. Snijder, E.J., Bredenbeek, P.J., Dobbe, J.C., Thiel, V., Ziebuhr, J., Poon, L.L., Guan, Y., Rozanov, M., Spaan, W.J. and Gorbalenya, A.E., 2003. Unique and conserved features of genome and proteome of SARS-coronavirus, an early split-off from the coronavirus group 2 lineage. Journal of molecular biology, 331(5), pp.991-1004.
33. Ahn, D.G., Choi, J.K., Taylor, D.R. and Oh, J.W., 2012. Biochemical characterization of a recombinant SARS coronavirus nsp12 RNA-dependent RNA polymerase capable of copying viral RNA templates. Archives of virology, 157(11), pp.2095-2104.
34. Ahmad Abu TurabNaqviaKisaFatimabTajMohammadaUroojFatimacIndrakant K. SinghdArchanaSinghеShaikh MuhammadAtiff-GururaoHariprasadgGulam MustafaHasanhMd. ImtaiyazHassana, 2020. Insights into SARS-CoV-2 genome, structure, evolution, pathogenesis and therapies: Structural genomics approach. Biochimica et Biophysica Acta (BBA) - Molecular Basis of Disease. Vol. 1866, Issue 10, 165878.
35. M. von Grotthuss, L.S. Wyrwicz, L. Rychlewski.mRNA cap-1 methyltransferase in the SARS genome, 2003.Cell, 113, pp. 701-702.
36. Shi P, Su Y, Li R, Liang Z, Dong S, Huang J., 2019. PEDV nsp16 negatively regulates innate immunity to promote viral proliferation. Virus Res.; 265:57- 66.
37. Brake, SJ, Barnsley, K., Lu, W., McAlinden, K.D., Eapen, MS and Sohal, SS, 2020. Smoking upregulates angiotensin-converting enzyme-2 receptor: a potential adhesion site for novel coronavirus SARS-CoV-2 (Covid-19).
38. Zhang, P., Zhu, L., Cai, J., Lei, F., Qin, J.J., Xie, J., Liu, Y.M., Zhao, Y.C., Huang, X., Lin, L. and Xia, M., 2020. Association of inpatient use of angiotensin converting enzyme inhibitors and angiotensin II receptor blockers with mortality among patients with hypertension hospitalized with COVID-19. Circulation research.
39. Wang, J., Tang, K., Feng, K. and Lv, W., 2020. High temperature and high humidity reduce the transmission of COVID-19. Available at SSRN 3551767.
40. Masters P.S. The molecular biology of coronaviruses. Adv Virus Res., 2006; 66:193–292.

41. Crackower, M.A., Sarao, R., Oudit, G.Y., Yagil, C., Kozieradzki, I., Scanga, S.E., Oliveira-Dos-Santos, A.J., da Costa, J., Zhang, L., Pei, Y. and Scholey, J., 2002. Angiotensin-converting enzyme 2 is an essential regulator of heart function. Nature, 417(6891), pp.822-828.
42. Delanghe, J., Speeckaert, M. and De Buyzere, M., 2020. The host's angiotensin-converting enzyme polymorphism may explain epidemiological findings in COVID-19 infections. Clinica Chemica Acta.
43. Rasmussen, E.R., Hallberg, P., Baranova, E.V., Eriksson, N., Karawajczyk, M., Johansson, C., Cavalli, M., Maroteau, C., Veluchamy, A., Islander, G. and Hugosson, S., 2020. Genome-wide association study of angioedema induced by angiotensin-converting enzyme inhibitor and angiotensin receptor blocker treatment. The Pharmacogenomics Journal, pp.1-14.
44. Corley, M.J. and Ndhlovu, L.C., 2020. DNA methylation analysis of the COVID-19 host cell receptor, angiotensin I converting enzyme 2 gene (ACE2) in the respiratory system reveal age and gender differences.
45. Pinto, B.G., Oliveira, A.E., Singh, Y., Jimenez, L., Gonçalves, A.N.A., Ogava, R.L., Creighton, R., Peron, J.P.S. and Nakaya, H.I., 2020. ACE2 expression is increased in the lungs of patients with comorbidities associated with severe COVID-19. MedRxiv.
46. Sawalha, A.H., Zhao, M., Coit, P. and Lu, Q., 2020. Epigenetic dysregulation of ACE2 and interferon-regulated genes might suggest increased COVID-19 susceptibility and severity in lupus patients. Clinical Immunology, p.108410.
47. Chai, P., Yu, J., Ge, S., Jia, R. and Fan, X., 2020. Genetic alteration, RNA expression, and DNA methylation profiling of coronavirus disease 2019 (COVID-19) receptor ACE2 in malignancies: a pan-cancer analysis. Journal of Hematology & Oncology, 13, pp.1-5.
48. Khan, M.A.A.K., Sany, M.R.U., Islam, M.S., Mehebub, M.S. and Islam, A.B., 2020. Epigenetic regulator miRNA pattern differences among SARS-CoV, SARS-CoV-2 and SARS-CoV-2 worldwide isolates delineated the mystery behind the epic pathogenicity and distinct clinical characteristics of pandemic COVID-19. bioRxiv.
49. Gómez-Díaz E., Jordà M., Peinado M.A., Rivero A. Epigenetics of host–pathogen interactions: the road ahead and the road behind. PLoS Pathog. 2012;8
50. Iwasaki A., Foxman E., Molony R. Early local immune defences in the respiratory tract. Nat Rev Immunol.2017; 17:7–20.
51. Chiu C., Openshaw P. Antiviral B cell and T cell immunity in the lungs. Nat Immunol.2015; 16:18–26.
52. Kamepalli, M.D. and FIDSA, C., 2020. How Immune T-Cell Augmentation Can Help Prevent COVID-19: A Possible Nutritional Solution Using Ketogenic Lifestyle. The University of Louisville Journal of Respiratory Infections, 4(1), p.7.
53. Petrakis, D., Margină, D., Tsarouhas, K., Tekos, F., Stan, M., Nikitovic, D., Kouretas, D., Spandidos, D.A. and Tsatsakis, A., 2020. Obesity-a risk factor for increased COVID-19 prevalence, severity and lethality. Molecular Medicine Reports, 22(1), pp.9-19.
54. Basch, C.H., Hillyer, G.C., Meleo-Erwin, Z.C., Jaime, C., Mohlman, J. and Basch, C.E., 2020. Preventive behaviors conveyed on YouTube to mitigate transmission of COVID-19: cross-sectional study. JMIR public health and surveillance, 6(2), p. e18807.
55. Vardavas, C.I. and Nikitara, K., 2020. COVID-19 and smoking: A systematic review of the evidence. Tobacco induced diseases, 18.

Received: 24 January 2021
Accepted: 12 March 2021

BOOK REVIEW / RESEÑA DEL LIBRO

Adaptation in Metapopulation: Book Review

Jordy José Cevallos-Chávez

DOI. 10.21931/RB/2021.06.02.32

The members of any family are not always living in the same region. Either for work, study or other reasons they are separated by distance. Although they live separately, they are related by blood and still interact with another family member to some extent. This phenomenon not only happens with humans. In the same way, we can see this pattern with any living organism in nature. For instance, we can see individuals of a forest bird species distributed among several separate forest patches, within which more or fewer stable populations are established, but that maintain migratory movements from one patch to another. At present, nature is increasingly fragmenting due to natural causes as well as a human activity. Therefore, since nature is patchy and becoming more so, biologists have become more interested in metapopulations[1]. Specifically, they have a particular interest in understanding how metapopulations adapt. *Adaptation in Metapopulations* addresses this topic, providing a varied, profoundly considered discussion of the current condition of the understanding of it.

Michael Wade (professor of Biology at Indiana University Bloomington) has synthesized decades of research in the lab and the field in a book both experimentally founded and supported by a solid conceptual framework. In this book, he has approached a diverse array of topics, from types of selection (group, kind, individual, and sexual), genetics (speciation and parent), to host-symbiont coevolution to assess *"How is the process of adaptation different if the members of a population live clustered in small groups instead of being homogeneously distributed like grass on a lawn?*" Wade presents a series of artificial group selection studies on flour beetles reinforced by natural experiments with willow leaf beetles, as well as additional experiments on the related issue of Wright's shifting balance theory. *Adaptation in Metapopulations* is a relevant contribution since it explores interaction as a critical factor for understanding this type of evolutionary mechanism.

Wade's work would be controversial if presented in an earlier stage of the understanding of evolution since interactions had primarily been overlooked. In that stage, researchers believed that individuals could be broken up into their parts (genes and environment), and conversely, the sum of them would represent the reality of the whole without considering the interaction between them. Therefore, the leading researchers' approach to comprehend evolution was understanding how adaptation works at the genetic level. If the adaptations were understood at the genetic level, then the higher-level units would be too, since they were merely an aggregate of lower levels. As our understanding of gene interactions improved, it prepared the way for Wade's work, e.g., Lewontin and Matsuo[2], and Michod[3], which are about interaction at the genetic level. The way that Wade compares evolution with a poker game to introduce interaction is mesmerizing. In his book, he presented experimental results using artificial metapopulations of flour beetles (genus *Tribolium*) and moving individuals among clusters to maintain gene flow.

Wade's experiments that imposed group selections generally got strong results with cannibalism, a group interaction that became the noticeable critical trait. Cannibalism in beetle clusters was helpful to understand the metapopulations' differences in growth rate. Some of the results derived from Wade's experimental research even exceeded his expectations. For instance, when he analyzes the size of the between-group variance and the strength of the group response in one of his experiments, he found it was more significant than expected. Wade, in his book, not only presents his findings but also explores possible explanations for them. Furthermore, *Adaptation in Metapopulation* contains discussions of Wade's results as evidence that strongly support and enforce other related theories such as Wright's shifting balance theory of selection. Based on his experimental work, Wade shows that Wright's theory is solid.

This book could look some dense in the content sense because of the wide theoretical framework. This is a book that offers a structured (chronologically) literature review of evolution. The reader could easily follow the history of the development of theories about the field. Furthermore, the author's attractive way explains some biological phenomena can help to understand the idea faster. Also, the book contains illustrations and clear diagrams to show their results graphically.

Adaptation in Metapopulations is a book that contributes meaningfully to the understanding of evolution due to the broad range of topics that the author addresses. Furthermore, he provides some explanations of his outlier findings which are insights that are worth considering. This book could be valuable and helpful for beginners to get involved in contemporary evolution theory, offering the reader an extensive background in the field with new approaches. I strongly encourage everyone to read this book to have a rich panorama of evolutionary phenomena. It is worth reading.

Acknowledgments

I thank professor James Collins for his comments and suggestions in developing this work during his Evolutionary Ecology class.

Bibliographic references

1. Hanski I. Metapopulation ecology. Oxford, England: Oxford University Press; 1999.
2. Lewontin and Yoshiro Matsuo R. Interaction of Genotypes Determining Viability in Drosophila Busckii. Proceedings of the National Academy of Sciences. 1963 Feb 1;49(2):270–8.
3. Michod RE. Evolution of interactions in family-structured populations: mixed mating models. genetics. 1980 Sep;96(1):275–96.

Received: 16 January 2021
Accepted: 20 March 2021

Simon A. Levin Mathematical, Computational and Modeling Sciences Center, Arizona State University, United States.

Corresponding author: hosseini.msalar@gmail.com

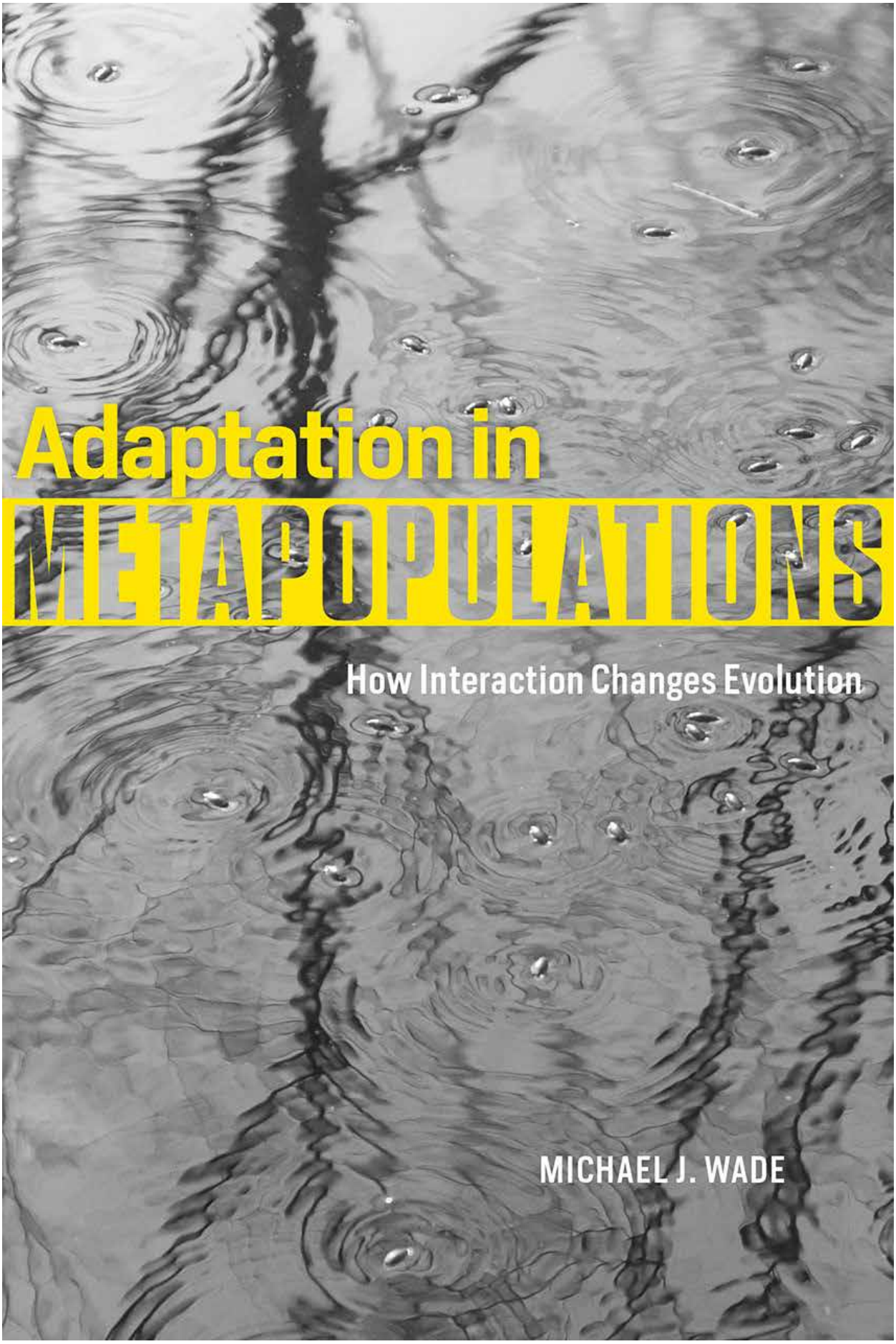
Adaptation in
METAPOPULATIONS
How Interaction Changes Evolution
MICHAEL J. WADE


UNIVERSIDAD
YACHAY
TECH
DE LA CURIOSIDAD ACADÉMICA
A LA INNOVACIÓN TECNOLÓGICA
ESCUELA DE
CIENCIAS MATEMÁTICAS
Y COMPUTACIONALES
ESCUELA DE
CIENCIAS FÍSICAS
Y NANOTECNOLOGÍA
ESCUELA DE
CIENCIAS QUÍMICAS
E INGENIERÍA
ESCUELA DE
CIENCIAS DE LA TIERRA,
ENERGÍA Y AMBIENTE
ESCUELA DE
CIENCIAS BIOLÓGICAS
E INGENIERÍA

ESCUELA DE CIENCIAS BIOLÓGICAS E INGENIERÍA

YACHAY TECH

www.yachaytech.edu.ec

YACHAY TECH
UNIVERSIDAD DE INVESTIGACIÓN DE TECNOLOGÍA EXPERIMENTAL

/YachayTech @YachayTech /YachayTech /YachayTech

Es el momento de los que se atreven a soñar y luchan por alcanzar sus metas.

En la UCO te acompañamos

UCO Universidad Católica de Oriente
Acreditación Institucional en ALTA CALIDAD

Vigilada Mineducación

Pregrados

Tecnología en Operaciones Financieras
SNIES 104841 Registro Calificado - Res. 12903 del 21-09-2015 M.E.N.
95 créditos - A distancia tradicional - Rionegro Ant.

Contaduría Pública
SNIES 13018 Registro Calificado - Res. 9256 del 07- 06- 2018
Acreditación de Alta Calidad 4610 del 21- 03 - 2018 M.E.N.
165 créditos Presencial - Rionegro

Comercio Exterior
SNIES 1854 Registro Calificado - Res.14314 del 11-12-2019 M.E.N.
159 créditos - Presencial - Rionegro Ant.

Administración de Empresas
SNIES 55096 Registro Calificado - Res. 7658 del 18-04-2017 M.E.N.
152 créditos - Presencial - Rionegro Ant.

Tecnología Agropecuaria
SNIES 1850 Registro Calificado - Res. 8684 del 10-07-2013 M.E.N.
113 créditos - Presencial - Rionegro Ant.

Agronomía
SNIES 4443 Registro Calificado - Res. 8087 del 17-05-2018
Acreditación de Alta Calidad Nº 29149 del 26-12-2017
157 créditos - Presencial - Rionegro Ant.

Zootecnia
SNIES 53037 Registro Calificado - Res. 14466 del 04-09-2014 M.E.N.
156 créditos - Presencial - Rionegro Ant.

Psicología
SNIES 8562 Registro Calificado - Res. 9902 del 31-07-2013 M.E.N.
Acreditación de Alta Calidad Nº 17227 del 24 - 10 - 2018
175 créditos - Presencial - Rionegro Ant.

Comunicación Social
SNIES 53045 Registro Calificado - Res. 14892 del 11-09-2014 M.E.N.
146 créditos - Presencial - Rionegro Ant.

Trabajo Social
SNIES 106586 Registro Calificado - Res. 26741 del 29-11-2017 M.E.N.
141 créditos - Presencial - Rionegro Ant.

Derecho
SNIES 53539 Registro Calificado - Res. 10542 del 14-07-2015 M.E.N.
166 créditos - Presencial - Rionegro Ant.

Nutrición y Dietética
SNIES 104601 Registro Calificado - Res. 7823 del 01-06-2015 M.E.N
166 créditos - Presencial - Rionegro Ant.

Gerontología
SNIES 1853 Registro Calificado - Res. 14839 del 22-10-2013 M.E.N.
138 créditos - A distancia con apoyo virtual - Rionegro Ant.

Enfermería
SNIES 91027 Registro Calificado- Res. 12600 del 03-08-2018 M.E.N.
166 créditos - Presencial - Rionegro Ant.

Licenciatura en Filosofía
SNIES 106542 Registro Calificado - Res. 22108 del 24 - 10 - 2017 M.E.N.
164 créditos - Presencial - Rionegro Ant.

Licenciatura en Lenguas Extranjeras con énfasis en Inglés
SNIES 106647 Registro Calificado - Res. 29529 del 29-12-2017 M.E.N.
164 créditos - Presencial - Rionegro Ant.

Licenciatura en Educación Física, Recreación y Deportes
SNIES 106436 Registro Calificado - Res. 17481 del 31-08-2017 M.E.N.
164 créditos - Presencial - Rionegro Ant.

Licenciatura en Educación para la Primera Infancia
SNIES 105359 Registro Calificado - Res. 02848 del 16-02-2016 M.E.N.
164 créditos - Presencial - Rionegro Ant.

Licenciatura en Ciencias Naturales
SNIES 105898 Registro Calificado - Res.19869 del 18-10-2016 M.E.N.
164 créditos - Presencial - Rionegro Ant.

Licenciatura en Educación Religiosa
SNIES 106705 Registro Calificado - Res. 2084 del 13 - 02 - 2018 M.E.N.
164 créditos - Presencial - Rionegro Ant.

Técnico Profesional en Programación Web
SNIES 103704 Registro Calificado - Res.14454 del 04-09-2014 M.E.N.
67 créditos - Presencial - Rionegro Ant.

Ingeniería Ambiental
SNIES 4361 Registro Calificado - Res. 3654 del 02-03-2018 M.E.N.
Acreditación de Alta Calidad No. 6543 del 18 - 04 - 2018
173 créditos - Presencial - Rionegro Ant.

Ingeniería de Sistemas
SNIES 1855 Registro Calificado - Res. 0178 del 05-01-2019 M.E.N.
164 créditos - Presencial- Rionegro Ant.

Ingeniería Industrial
SNIES 1856 Registro Calificado - Res. 1293 del 04-02-2019 M.E.N.
160 créditos - Presencial- Rionegro Ant.

Ingeniería Electrónica
SNIES 20271 Registro Calificado - Res. 24646 del 14-11-2017 M.E.N.
178 créditos - Presencial- Rionegro Ant.

Teología
SNIES 103450 Registro Calificado - Res. 10638 del 09-07-2014 M.E.N.
130 créditos - A distancia - Rionegro Ant.

¡HAGAMOS QUE PASE!

www.uco.edu.co @uconiano universidad catolica de oriente 322 569 90 90